ISSN 0386—5878
土木研究所資料第2847号

土 木 研 究 所 資 料

第5回日米橋梁ワークショップ論文集

平成2年1月

建 設 省 土 木 研 究 所

Copyright © (1990) by P.W.R.I.

All rights reserved. No part of this book may be reproduced by any means, nor transmitted, nor translated into a machine language without the written permission of the Director General of P.W.R.I.

この報告書は、土木研究所長の承認を得て刊行したものである。したがって、本報告書の全部又は一部の転載、複製は、土木研究所長の文書による承認を得ずしてこれを行ってはならない。

土木研究所資料
第2847号 1990年1月

第5回日米橋梁ワークショップ論文集

構造橋梁部長　佐　伯　彰　一

要　旨

1989年5月9日，10日の2日間にわたって，筑波研究学園都市にある建設省土木研究所において，第5回日米橋梁ワークショップが開催された。本資料は，同ワークショップに提出された論文および会議プログラム，討議内容，ワークショップ後に行われた視察旅行の内容をとりまとめたものである。

キーワード：橋梁工学，日米技術協力，耐風工学，耐震工学

まえがき

第５回日米橋梁ワークショップが平成元年５月９日，10日の２日間にわたり筑波研究学園都市にある建設省土木研究所において開催された。

会議には，米国側より11名，日本側から31名が参加し，橋梁の耐風設計や耐震設計，既設橋梁の維持管理や補修などの橋梁工学に関する課題について提出された23編の論文発表とこれらに関する討議が行われた。

日米橋梁ワークショップは，天然資源の開発利用に関する日米会議（ＵＪＮＲ）の耐風耐震構造専門部会における作業部会Ｊ（ＴＣ－Ｊ）「交通システムの耐風耐震技術」において橋梁に関連した課題をより深く論議することを目的に，昭和58年５月に筑波の土木研究所において第１回が開催されたのが最初であり，その後第２回のワークショップが昭和60年８月にサンフランシスコにおいて，第３回のワークショップが昭和62年５月に土木研究所において，第４回のワークショップが昭和63年５月にサンディアゴにおいてそれぞれ開催されている。

本報告書は，このように本ワークショップが継続的開催にある状況を考慮し，今後の参考に資するとともに，会議の成果を記録に残して有効に活用したいとの願いのもとにとりまとめたものである。

本ワークショップが日米両国のこの分野における研究活動の推進に役立つとともに，関係者の理解と協力を得て今後ますます発展していくことを期待している。

最後に，本ワークショップに参加された関係各位ならびに現地視察旅行を含め会議開催にあたり数々の御支援をいただいた関係各機関の皆様に厚く御礼申し上げます。

平成２年１月

佐　伯　彰　一
ＵＪＮＲ耐風耐震構造専門部会
作業部会(J)日本側部会長
土木研究所構造橋梁部長

目　　次

1. 日本橋梁ワークショップの概要 …… 1
　1.1　背景と過去の経緯 …… 3
　1.2　目　　的 …… 3
　1.3　全体計画 …… 3
　参考資料　UJNR耐風耐震構造専門部会の概要 …… 4

2. 会議プログラム …… 9

3. 会議参加者 …… 17

4. 論文および討議 …… 75
　(1)　Session 1 …… 77
　(2)　Session 2 …… 79
　(3)　Session 3 …… 139
　(4)　Session 4 …… 179
　(5)　Session 5 …… 235
　(6)　Session 6 …… 297
　(7)　Session 7 …… 347
　(8)　Session 8 …… 395
　(9)　Session 9 …… 429
　(10)　討議録 …… 431

5. 視察旅行記 …… 441

あとがき …… 449

付属資料

(1)　第5回日米橋梁ワークショップ結論（英文） …… 455

(2)　UJNR耐風耐震構造専門部会
　第21回合同部会におけるワークショップ報告（英文） …… 461

(3)　UJNR耐風耐震構造専門部会
　第21回合同部会におけるJ部会 部会報告（英文） …… 467

(4)　UJNR耐風耐震構造専門部会
　第21回合同部会におけるJ部会 部会報告（和文） …… 473

1．日米橋梁ワークショップの概要

1. 日本橋梁ワークショップの概要

1.1 背景と過去の経緯

わが国とアメリカ合衆国との間には政府間ベースの技術協力プログラムを有しており，活発な活動が種々の分野で行われている。UJNR耐風耐震構造専門部会の活動はその1つであり，建設省土木研究所と米国商務省国立標準技術研究所を中心として，約20年にわたる会議や共同研究の実績がある。UJNR耐風耐震構造専門部会の詳しい説明は本章末の参考資料に譲ることにするが，同部会は10の作業部会を有しており，その1つが作業部会(J)，「交通システムの耐風耐震技術」であり，作業部会長は日本側が建設省土木研究所の佐伯彰一構造橋梁部長，米国側が連邦道路局研究開発技術部門のJ.D. Cooper 次長が務めている。

作業部会(J)は主として道路橋の耐風耐震技術に関する研究をテーマにしており，昭和58年5月に土木研究所で開催されたUJNR耐風耐震構造専門部会の第15回合同部会において，作業部会(J)は道路橋の耐風耐震技術に関する研究協力を推進するために，日米橋梁ワークショップの実施を提案し，同専門部会で承認された。これを受けて第1回のワークショップが筑波で昭和59年2月に開催された。その後，第2回のワークショップが昭和60年8月にサンフランシスコにおいて，第3回のワークショップが昭和62年5月に土木研究所において，第4回のワークショップが昭和63年5月にサンディアゴにおいてそれぞれ開催されている。

1.2 目　的

第5回橋梁ワークショップは前4回のワークショップの成果を踏まえ，道路橋の耐風耐震技術に加えて設計・施工一般および既設橋梁の維持管理に関する研究にまで幅広く範囲を広げ，これらの課題について日米両国間でより深く論議することを目的に実施されたものである。具体的な課題としては以下のとおりである。

(1) 橋梁の耐震設計
(2) 橋梁の耐風設計
(3) 橋梁の設計・施工一般
(4) 既設橋梁の維持・管理
(5) 既設橋梁の補修・補強
(6) 既設橋梁の非破壊検査
(7) 橋梁の計測・監視

1.3 全体計画

全体計画は，今回の米国側窓口となった南カリフォルニア大学A.M. Abdel-Ghaffar 教授と連絡を取りながら，土木研究所構造橋梁部橋梁研究室が事務局となって検討された。

全体日程を表－1に示す。ワークショップには2日間があてられ，その後，首都高速道路，阪神高速道路，関西国際空港連絡橋，本州四国連絡橋等への視察旅行に3日間があてられた。

表－1　第5回橋梁ワークショップ全体日程

月　日	曜　日	行　　程	宿　　泊
5/9	火	ワークショップ（土木研究所）	筑　　波 （建設省研修会館）
10	水	ワークショップ（土木研究所） 筑波 ⇨ 東京	東　　京 （農林年金会館）
11	木	首都高速道路（横浜ベイブリッジ） 東京 ⇨ 大阪	大　　阪 （大阪後楽園ホテル）
12	金	阪神高速道路（安治川橋梁，北港ＪＣ） 関西国際空港連絡橋，本四 明石海峡大橋	岡　　山 （サンルート岡山）
13	土	本四　瀬戸大橋　　岡山 ⇨ 東京	東　　京 （農林年金会館）

ワークショップの参加者は，米国側については11名，日本側については土木研究所，公団などからの31名，計42名であった。

論文発表については，日本側からの13編，米国側からの10編，計23編であった。これらの論文は3ないし4編ごとにグループ分けし，それぞれセッションを構成することとし，1つの論文発表に対して20分，および1セッション全体での討議に対して15分をわりあてた。会議は英語によることとし，通訳を付けずに行った。各セッションは，日米両国双方から選任された各1名，計2名の議長の進行のもとに行われた。

参考資料　UJNR耐風耐震構造専門部会の概要

1. UJNR

天然資源の開発利用に関する日米会議（U.S.－Japan Conference on Development and Utilization of Natural Resources＝U.J.N.R.）の設立については，昭和39年1月27日東京で開催された第3回日米貿易経済合同委員会第1回全体会議の席上，米国側から提案され，日米科学委員会及び日米貿易経済合同委員会のいずれにも属さないものとして，同年から発足しました。そのとき提案された主旨は「日米が両国の利益のために人的及び天然資源の分野で技術要因と調査結果の交換を，新たに政府レベルで行いたい。また，本計画を実現するために日米両国の政府職員による会議を早い機会に開催してはどうか。」というもので，日本側もこの旨を了解し，科学技術庁を中心として活動が開始されました。

この会議の目標は，世界の天然資源の有効利用と保全及び人間の居住環境問題の解決のために日米両国がお互いの協力を通じて，可能な限り学びとることにあります。

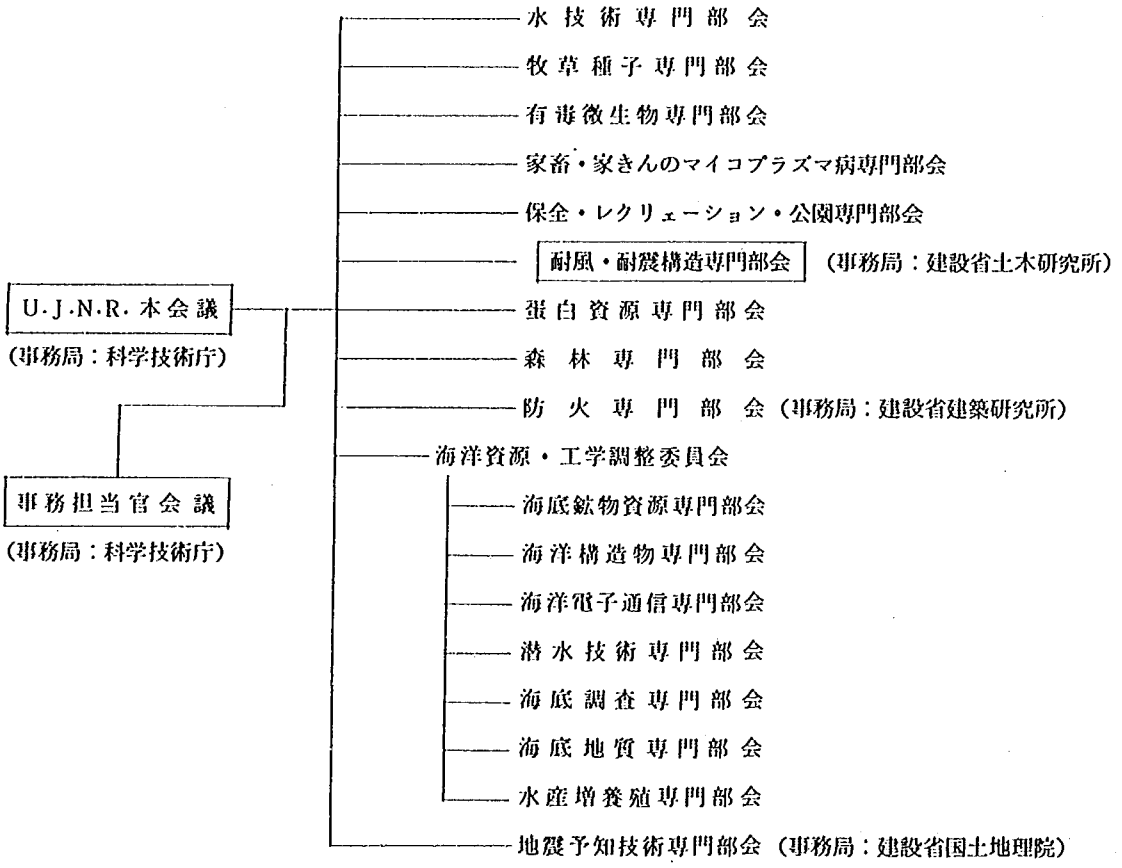
昭和39年5月に，日米両国の最高責任者が会合する本会議の第1回が開催されて以来，既に20年以上を経過し，その間「試行と組織化」の段階から「実施と拡充」の段階へと発展したこの会議は，技術研究情報の交換，研究者の交流だけでなく，共同研究も実施され，ますます重要性を増しつつあります。

この会議の運営組織は，本会議，事務担当官会議並びに日米両国に置かれた17の専門部会，その他の海洋に関係する7つの専門部会を調整する海洋資源工学調整委員会から成り立っています。

本会議は両国の担当行政部局の最高責任者が会合するものであり，およそ1年半毎に東京又はワシントンで交互に開催されています。事務担当官会議は本会議の円滑な運営を図るために両国の事務担当官が会合するものであり，本会議の間に開催されています。また両国の専門部会が合同して行う合同部会はおよそ1年に1回開催され，情報交換，成果の検討，意見交換等を行っています。

なお，専門部会の組織図を参考として以下に示します。

天然資源の開発利用に関する日米会議（ＵＪＮＲ）
専門部会の組織



2. 耐風・耐震構造専門部会

○目　　的

耐風・耐震構造専門部会は，昭和42年東京で開かれた第3回本会議の席上で新しい協力活動として取り上げられました。このプログラムは，日米両国が互いに地震，強風，高潮，津波の被害国である実情に鑑

み，従来別々に行われてきた構造物の耐風耐震設計法等の開発研究の成果を持ち寄り，意見を交換する機会をもたらすことに主眼が置かれています。その後活動範囲は拡大され，設計基準の改正上の問題点に関連して実施された調査研究の成果の交換，さらには強風，地震，高潮，津波により生ずる災害から人命及び財産の損失を防止するための総合的対策，技術分野の開拓を目標としています。

○組　　織

日米と米国の双方に設置され，日本側の部会は，建設省土木研究所長を部会長として，同土木研究所，同建築研究所，同国土地理院，運輸省港湾技術研究所，同気象研究所，科学技術庁国立防災科学技術センターから選ばれた計29名の委員で構成され，部会事務局は土木研究所企画部企画課に置かれています。

米国側の部会は，国立標準技術研究所建築技術センター所長のR.N.ライト博士を部会長として，同標準技術研究所，地質調査所，住宅都市開発省，連邦道路局，国立海洋気象庁，内務省開拓局，陸軍工兵隊，海軍土木工学研究所等の機関より選出された計35名の委員で構成されています。

○現在の活動方針

1. 災害防除を考慮した構造物や地域社会の設計・計画に関連する研究協力及び技術情報や研究資料の交換
2. 実施した最近の調査研究の相互検討
3. 都市の再開発に関連する災害の防除対策の調査研究の成果
4. 開発途上国に対する技術援助の現況紹介
5. 科学者・技術者の人材交流の促進
6. 両国保有の大型実験施設を使用する日米共同研究の実施の推進
7. 両国保有の実験施設の利用を含む共同研究計画の推進

○作業部会

耐風・耐震構造専門部会の活動をより緊密にするため下記の作業部会を設け，研究情報の交換，作業部会ごとのワークショップ等を実施しています。

作業部会名	作業部会長（日本）	作業部会長（米国）
A．強震計配置計画と強震記録	土田　肇（港湾研）	A.G.Brady　(USGS)
B．大型実験計画	大谷圭一（防災センター）	H.S.Lew　(NIST)
C．既存構造物の補修及び補強	広沢雅也（建研）	K.J.Eggenberger　(NSF)
D．構造物の性能評価	岡本　伸（建研）	G.R.Fuller　(HUD)
E．自然災害予測と国土利用計画による自然災害軽減	川島一彦（土研）	S.T.Algermissen (USGS)
F．ライフライン施設の災害防止法	佐々木康（土研）	S.C.Liu　(NSF)
G．風の特性と構造物の応答	蔵重　清（気象研）	R.D.Marshall　(NIST)
H．地震時における地盤の挙動と安定	常田賢一（土研）	A.G.Franklin　(WES)
I．高潮及び津波	宇多高明（土研）	H.Meyers　(NOAA)
J．交通システムの耐風耐震技術	佐伯彰一（土研）	J.D.Cooper　(FHWA)

○将来の計画

耐風・耐震構造専門部会は，強風，強震，高潮，津波による災害を防ぐため技術的諸問題の解決を図るものであり，そのためには従来から実施してきたこれらの自然現象を的確に把握することのほかに，さらにそれらに対する構造物の挙動を明確に把握すること，人命や財産の損失を最小限にするための総合的対策を追及することが必要となります。これらの目的を達成するためには，従来の活動に加えて以下の諸事項について，より具体的な計画の立案及び実施の強化が緊要とされています。

1. 試験機・実験装置の共同利用，資料，模型の相互交換を含む共同研究計画を推進すること。
2. 上記目的のための科学者・技術者の相互交換を推進すること。
3. 関連分野からの広汎な協力を求め，活動分野を拡大すること。
4. 作業部会において各分野の研究ニーズを明確にし，各作業部会間で連絡・調整を図り，今後の研究計画を作成すること。
5. 国際防災旬年の計画に注意し，専門部会の活動がより有意義なものとなる方向を模索すること。

2. 会議プログラム

WORKSHOP PROGRAM

5th U.S.-JAPAN BRIDGE WORKSHOP

(Workshop on Bridge Engineering)

May 9 and 10, 1989

Tsukuba Science City, Japan

Tuesday, May 9, 1989 Place: International Conference Room (8F) PWRI

SESSION 1: OPENING SESSION
(Chairman: Shoichi Saeki) 9:00am~9:15am

Welcome Remarks: Nobuyuki Narita (Director General, PWRI)
Remarks: A. M. Abdel-Ghaffar (For U.S. Chairman, T/C(J))

SESSION 2: SEISMIC DESIGN(1) 9:15am~10:30am
(Co-Chairman: T. Iwasaki, D.A. Foutch)

(1) Y. Sasaki, K. Tamura※ and K. Aizawa: Attenuation Characteristics of Ground Motions in the Period Range of 2 to 20 Seconds
(9:15am~9:35am)

(2) E. Maragakis※ and B. Douglas: On the Estimation of Longitudinal Linear and Nonlinear Abutment Stiffnesses
(9:35am~9:55am)

(3) B. Douglas※ and E. Maragakis: New Aspects Regarding the Use of Quick-Release Dynamic Tests for the Experimental Analysis of Bridge Structures
(9:55am~10:15am)

DISCUSSION(2)
(10:15am~10:30am)

COFFEE BREAK
(10:30am~10:45am)

SESSION 3: SEISMIC DESIGN(2) 10:45am~ 0:00pm
(Co-Chairman: K. Kawashima, B. Douglas)

(4) K. Kawashima, K. Hasegawa※ , T. Yoshida and T. Ikeuchi: Hysterestic Behavior of Steel Bridge Piers by Shaking Table Tests
(10:45am~11:05am)

(5) H. Shinohara, A. Hasegawa and T. Oishi※ : Aseismic study of kawasaki Man-made Island in Trans-Tokyo Bay Highway Project
(11:05am~11:25am)

(6) D. Foutch※ , T. Havenar and S. Pezeshk: Considerations for the Seismic Design of the Clark Cable-Stayed Bridge
(11:25am~11:45am)

DISCUSSION(3)
(11:45am~0:00pm)

LUNCH (8F, International Conference Room)
(0:00am~1:30pm)

PHOTOGRAPH (Entrance of Main Building)
(1:30pm~1:45pm)

SESSION 4: WIND RESISTANT DESIGN(1) 1:45pm~3:20pm
(Co-Chairman: K. Yokoyama, H.R. Bosch)

(7) K. Yokoyama※ and H. Sato: Experiment on the Effects of Turbulence on Wind-induced Vibrations of Long-span Bridges
(1:45pm~2:05pm)

(8) K. Wada, H. Takano※ and H. Makuta : Study on Suppressing Wind-induced Vibration in Plane for Tower of Yokohama Bay Bridge under Construction (Design and On-site Testing of a Dynamic Damper for Cable Suspension Bridge)
(2:05pm~2:25pm)

(9) F. Ehsan and R. H. Scanlan※ : Damping Stay Cables with Ties
(2:25pm~2:45pm)

(10) T. T. Baber※ , F. W. Barton, M. Mohr, and D. Ramsey: Field Instrumentation of the I-295 Cable-Stayed Box Girder Bridge
(2:45pm~3:05pm)

DISCUSSION(4)
(3:05pm~3:20pm)

COFFEE BREAK
(3:20pm~3:35pm)

SESSION 5: WIND RESISTANT DESIGN(2) 3:35pm~5:10pm
(Co-Chairman: K. Yokoyama, R. H. Scanlan)

(11) M. Tatsumi, K. Hata※ and M. Takeuchi: Wind Resistant Design of Akashi Kaikyo Bridge
(3:35pm~3:55pm)

(12) H. Bosch※ : Structural Modification for Enhanced Aerodynamic Behavior of of a Suspension Bridge
(3:55pm~4:15pm)

(13) H. Kosaka※ , H. Hanno and Y. Fujino: Wind Tunnel Test on Tokyo Port Bridge
(4:15pm~4:35pm)

(14) S. Motoyama, M. Hoshino, N. Takahashi※ and T. Maruyama: Aerodynamic Stability of Three Parallely Located Box-Girder Bridges
(4:35pm~4:55pm)

DISCUSSION(5)
(4:55pm~5:10pm)

RECEPTION BY DIRECTOR GENERAL OF PWRI

Place: Heian no Ma of GRAND SHINONOME (TEL: 0297-55-2211)
Time: 6:00pm~8:00pm
Traffic: Bus of GRAND SHINONOME starts from Entrance of Main Building at 5:30pm

Wednesday, May 10, 1989 Place: International Conference Room (8F) PWRI

SESSION 6: BRIDGE CONSTRUCTION(1) 9:00am~10:15am
(Co-Chairman: M. Okahara, H. Seible)

(15) H. J. Farran※ : Current Research on Cable-Stayed Bridges at Caltrans
(9:00am~9:20am)

(16) N. Yoshikawa, I. Sugiyama and F. Hakamada※ , and S. Kaneko: Design and Experiments on Shin-Hamadera Oohashi Bridge
(9:20am~9:40am)

(17) H. E. Waldner and J. M. Kulicki: Quality Control Testing for Construction of Cable-Stayed Bridge at Quency, Illinois
(9:40am~10:00am)

DISCUSSION(6)
(10:00am~10:15am)

COFFEE BREAK
(10:15am~10:30am)

SESSION 7: BRIDGE CONSTRUCTION(2) 10:30am~11:45am
(Co-Chairman: M. Fujiwara, H. E. Waldner)

(18) M. Okahara※ , S. Takagi, H. Obata and H. Mori : Large-scale Plane Strain Bearing Capacity Test of Shallow Foundation on Sand
(10:30am~10:50am)

(19) F. Seible※ : Evaluation of Tendon Coupling Joints in Continuous Post-Tensioned Concrete Bridges
(10:50am~11:10am)

(20) M. Fujiwara, K Minosaku※ , M. Adachi and T. Yamashita: Application of Carbon Fiber Reinforced Plastics to Prestressed Concrete Bridges
(11:10am~11:30am)

DISCUSSION(7)
(11:30am~11:45am)

LUNCH (8F, International Conference Room)
(11:45am~0:45pm)

SESSION 8: BRIDGE MAINTENANCE 0:45pm~2:00pm

(Co-Chairman: M. Fujiwara, A. M. Abdel-Ghaffar)

(21) M. S. Agbabian and S. F. Masri※ , M.I Traina and O. Waqfi: Detection of Structural Changes in a Bridge Model
(0:45pm~1:05pm)

(22) S. Katoh, S. Utoh, S. Motomura※ and M. Ishizuka: A Program and Evaluation of Inspection System for Road Structures on Hanshin Expressway
(1:05pm~1:25pm)

(23) Y. Ito and Y. Oka※ : An Experimental Study on Deterioration of Bridge Deck Slabs and Their Repair Method
(1:25pm~1:45pm)

DISCUSSION(8)
(1:45pm~2:00pm)

SESSION 9: CLOSING SESSION 2:00pm~2:25pm

(Co-Chairman: M. Fujiwara, A. M. Abdel-Ghaffar)
Remarks: Harold R. Bosch (U.S. Representative,T/C(J))
Remarks: Shoichi Saeki (Japanese Chairman, T/C(J))

3. 会 議 参 加 者

5th U.S.-JAPAN BRIDGE WORKSHOP
LISTS OF PARTICIPANTS

May 9 and 10, 1989

Tsukuba Science City, Japan

-U.S. SIDE-

(1) Dr.Hani J. Farran

Position: Professor and Consultant
State of California, Department of Transportation
Division of Structures
Address: Box 942874
Sacramento, California 94274-0001
Tel: (714)-869-2643

(2) Professor Ahmed M. Abdel-Ghaffar

Position: Department of Civil Engineering,
University of Southern California
Address: University Park, Los Angeles, California 90089-0242
Tel: (213)743-6915
※Representative of U.S. side of the Workshop

(3) Professor Robert H. Scanlan

Position: Department of Civil Engineering
The Johns Hopkins University
Address: Baltimore, MD 21218-2699
Tel: (301)338-7138

(4) Professor Sami F. Masri

Position: Department of Civil Engineering,
University of Southern California
Address: Los Angeles, California 90089-0242
Tel: (213)743-6209

(5) Professor Frieder Seible

Position: Department of Applied Mechanics and Engineering Sciences B010
University of California
Address: San Diego, La Jolla, California 92093
Tel: (619)534-4640

(6) Professor Emmanuel Maragakis

Position: Civil Engineering Department, College of Engineering
University of Nevada
Address: Reno, Nevada 89557
Tel: (702)784-6937

(7) Professor Bruce Douglas

Position: Civil Engineering Department, College of Engineering
University of Nevada
Address: Reno, Nevada 89557
Tel: (702)784-6937

(8) Professor Thomas T. Baber

Position: Department of Civil Engineering
University of Virginia
Address: Charlottesville, Virginia 22901
Tel: (804)924-6360

(9) Mr. H. Eugene Waldner

Position: Modjeski and Masters Consulting Engineers
Address: 4713 Carlisle Pike, Mechanicsburg, PA 17055
Tel: (717)761-1891

(10) Mr. Harold Bosch

Position: Structure Division, Fed. Admin/Res Div&Tech
US DOT., Turner-Fairbank Highway/Res Center
Address: 6300 Georgetown Pike HNR 10, McLean, VA 22101-2296
Tel: (703)285-2446
※Tentative Chairman of U.S.-side of J task committee
(for Mr. James D. Cooper)

(11) Professor Douglas A. Foutch

Position: Civil Engineering Department
University of Illinois
Address: 208 No. Romaine, Urbana,Illinois 61801
Tel: (217)333-6359

-JAPAN SIDE-

(Public Works Research Institute)

Address: 305, 1-chome, Asahi-machi, Tsukuba-shi, Ibaraki-ken

Tel: (0298)64-2211

(1)Nobuyuki Narita

Position: Director General

(2)Toshio Iwasaki

Position: Deputy Director General

(3)Yoshio Adachi

Positon: Director, Planning and Research Adiministration Dep.

(4)Shoichi Saeki

Position: Director, Structure and Bridge Dep.

※Chairman of Japanese-side of J task committee

(5)Yasushi Sasaki

Position: Director, Earthquake Disaster Prevention Dep.

(6)Junzo Inoue

Position: Bridge Instructor, Planning and Research Adiministration Dep.

(7)Michio Okahara

Position: Head, Foundation Engineering Div.
Structure and Bridge Dep.

(8)Shoji Takagi

Position: Senior Research Engineer, Foundation Engineering Div.
Structure and Bridge Dep.

(9)Shoichi Nakatani

Position: Research Engineer, Foundation Engineering Div.
Structure and Bridge Dep.

(10)Atsushi Hatamoto

Position: Research Engineer, Foundation Engineering Div.
Structure and Bridge Dep.

(11)Yoshitomi Kimura

Position: Research Engineer, Foundation Engineering Div.
Structure and Bridge Dep.

(12)Koichi Yokoyama

Position: Head, Structure Div.
Structure and Bridge Dep.

(13)Takaaki Kusakabe

Position: Research Engineer, Structure Div.
Structure and Bridge Dep.

(14)Minoru Fujiwara

Position: Head, Bridge Div.
Structure and Bridge Dep.

(15)Koichi Minosaku

Position: Research Engineer, Bridge Div.
Structure and Bridge Dep.

(16)Jun Murakoshi

Position: Research Engineer, Bridge Div.
Structure and Bridge Dep.

(17)Kenichi Tokita

Position: Head, Ground Vibration Div.
Earthquake Disaster Prevention Dep.

(18)Keiichi Tamura

Position: Research Engineer, Ground Vibration Div.
Earthquake Disaster Prevention Dep.

(19)Tetsuro Kuwahara

Position: Research Engineer, Ground Vibration Div.
Earthquake Disaster Prevention Dep.

(20)Hideo Matsumoto

Position: Research Engineer, Ground Vibration Div.
Earthquake Disaster Prevention Dep.

(21)Kazuhiko Kawashima

Position: Head, Earthquake Engineering Div.
Earthquake Disaster Prevention Dep.

(22)Kinji Hasegawa

Position: Research Engineer, Earthquake Engineering Div.
Earthquake Disaster Prevention Dep.

(23)Hideki Sugita

Position: Research Engineer, Earthquake Engineering Div.
Earthquake Disaster Prevention Dep.

(Research Institute)

(1)Tokunosuke Fujitani

Position: Head, Second Lab. Applied Meteorological Div.
Meteorological Research Institute
Address: 305, Nagamine-machi 1-1, Tsukuba-shi, Ibaraki-ken
Tel: (0298)51-7111

(Highway Pub. Corp. etc.)

(1)Osamu Nakano

Position: Head, Structure Div. Civil Engineering Research Institute,
Hokkaizo Developement Bureau
Address: 062, 3-chome, 1-jyo, Hiragishi-cho, Toyohira-ku, Sapporo-shi
Hokkaido
Tel: (011)841-1111

(2)Atsuo Ogawa

Position: Assistant Manager, Structual Engineering Div.
Engineering Department, Japan Highway Public Corporation
Address: 100, Kasumigaseki 3-3-2, Chiyoda-ku, Tokyo-to,
Tel: (03)506-0272

(3)Yoneo Oka

Position: Assistant Manager, Concrete Section, Laboratory
Japan Highway Public Corporation
Address: 194, Tadao 1-4-1, Machida-shi, Tokyo-to
Tel: (0427)91-1622

(4)Haruo Takano

Position: Deputy Head, Special Design Div. Kanagawa Construction Bureau,
Metropolitan Expressway Public Corporation
Address: 231, Masa-machi 2-25, Naka-ku, Yokohama-shi, Kanagawa-ken
Tel: (045)662-1151

(5)Hiromi Kosaka

Position: Acting Head, Design Div. Third Construction Department,
Metropolitan Expressway Public Corporation
Address: 104, Hachobori 2-14-4, Cyuoh-ku, Tokyo-to
Tel: (03)553-1231

(6)Shunichi Nakamura

Position: Section Chief, Second Design Div. Design Dep.,
Trans-Tokyo Bay Highway Co, Ltd.
Address: 102,Ichi-ban-cho NN Bld. Ichiban-cho 15-5, Chiyoda-ku, Tokyo-to
Tel: (03)239-6585

(7)Tsuguo Oishi

Position: Section Chief, Third Design Div. Design Dep.,
Trans-Tokyo Bay Highway Co, Ltd.
Address: 102,Ichi-ban-cho NN Bld. Ichiban-cho 15-5, Chiyoda-ku, Tokyo-to
Tel: (03)239-6585

(8)Masaaki Tatsumi

Position: Manager, First Design Div. Design Dep.,
Honshu-Shikoku Bridge Authority
Address: 105,Toranomon 45 Mori Bld., Toranomon5-1-5, Minato-ku, Tokyo-to
Tel: (03)434-7281

(9)Kensaku Hata

Position: First Design Div. Design Dep.,
Honshu-Shikoku Bridge Authority
Address: 105,Toranomon 45 Mori Bld., Toranomon5-1-5, Minato-ku, Tokyo-to
Tel: (03)434-7281

(10)Fumio Hakamada

Position: Design Section, Kobe Management Dep.
Hanshin Expressway Public Corporation
Address: 650, Shinminato-machi 16-1, Chuoh-ku, Kobe-shi, Hyogo-ken
Tel: (078)331-9801

(11)Shunichi Motomura

Position: Section Chief,
Hanshin Expressway Administration and Technology Center
Address: 541, Toa Bld., Karamono-machi 5-5, Higashi-ku, Osaka-Fu
Tel: (06)282-0171

(12)Mikitake Ishizuka

Position: Former Section Chief,
Hanshin Expressway Administration and Technology Center
Address: 541, Toa Bld., Karamono-machi 5-5, Higashi-ku, Osaka-Fu
Tel: (06)282-0171

(13)Mitsuru Hoshino

Position: General Manager, Second Engineering Dep.,
Kansai International Airport Co, Ltd.
Address: 542, Shisaibashi-Taiyo Bld., Minami-Senba 3-11-10,Minami-ku,
Osaka-Fu
Tel: (06)282-2271

(14)Noboru Takahashi

Position: Assistant General Manager, Second Engineering Dep.,
Kansai International Airport Co, Ltd.
Address: 542, Shisaibashi-Taiyo Bld., Minami-Senba 3-11-10,Minami-ku,
Osaka-Fu
Tel: (06)282-2271



Dr. Hani J. Farran
Professor and Consultant

AUTHOR'S PROFILE

Dr. Farran is Professor of Civil & Structural Engineering at the California State Polytechnic University in Pomona, California. He is a registered professional engineer in California and West Virginia. He has authored 30 papers in the area of structural analysis and design and two reports on prestressed concrete segmental bridges and cable stayed bridges. Dr. Farran is working on a Masters Degree in Aerospace Engineering at Cal Poly, Pomona and plans are under way for 2 post-doctoral fellowships in the future. Post-doctoral research in the area of Earthquake engineering is contemplated at the California Institute of Technology as well as a post - doctoral Mellon Fellowship at M.I.T. on the impact of technology on society. Dr. Farran has been awarded the Meritorious Performance and Professional Promise Award as well as the Golden Leaves Award for research and publications at Cal-Poly, Pomona. He is a member of 13 professional, technical, and honorary societies. He is a graduate professor for the Northrop Aircraft Corporation in Los Angeles, California.

EDUCATION

B.S. Civil Engineering June 1973, Tennessee Technological University
M.S. Civil Engineering June 1975, Tennessee Technological University
Ph.D. Civil Engineering August 1981, West Virginia University

Academic Doctoral & Research Major: Structural Engineering
Academic Doctoral Minors:
a. Transportation
b. Engineering Mechanics
c. Mathematics

PROFESSIONAL REGISTRATION

Registered Professional Engineer, California #C 039302
Registered Professional Engineer, West Virginia #7876

PROFESSIONAL SOCIETY MEMBERSHIP

ASCE American Society of Civil Engineers
ASHE American Society of Highway Engineers
ASEE American Society for Engineering Education
AAUP American Association of University Professors
SEAOC Structural Engineers Association of California
ITE Institute of Transportation Engineers
AIAA American Institute of Aeronautics and Astronautics

HONOR SOCIETY MEMBERSHIP

TAU BETA PI National Engineering Honor Society
CHI EPSILON Civil Engineering Honor Society
SIGMA XI Scientific Research Society of North America
PHI DELTA KAPPA Professional Education Honor Society
ORDER OF THE ENGINEER State of Tennessee
Outstanding Young Men of America

WORK EXPERIENCE

1. Construction Engineer in Saudi Arabia 1975-1976.
2. Professor Civil Engineering at West Virginia Tech and West Virginia University 1976-1985.
3. Professor of Civil Engineering at Cal Poly Pomona, 1985-Present.



AHMED M. ABDEL-GHAFFAR

Dr. Ahmed M. Abdel-Ghaffar is Professor of Structural Engineering in the Civil Engineering Department of the University of Southern California. Before joining USC he was a Professor at the Civil Engineering Department of Princeton University. Professor Abdel-Ghaffar earned his graduate degrees (M.S. and Ph.D) in Civil Engineering (Structural Dynamics and Earthquake Engineering) at the California Institute of Technology in 1973 and 1976, respectively. In general, Professor Abdel-Ghaffar's research interests include various aspects of earthquake engineering (particularly dynamic analysis and earthquake-response analysis of cable-supported bridges including cable-stayed and suspension bridges, and of earth dams), soil-structural interaction, dynamic tests of full-scale structures (such as cable-supported bridges and earth dams), strong-motion data processing and interpretation for engineering purposes and identification of structural properties from earthquake records. He is the author and co-author of several publications covering the above topics; one of the papers on suspension bridges received the 1982 ASCE Raymond C. Reese Research Prize while one of the papers on earth dams received the 1982 ASCE Thomas Al Middlebrooks Award. Finally, Professor Abdel-Ghaffar was among a group of U.S. bridge researchers and consultants who visited both New Zealand and Japan several times to participate in workshops on the Seismic Design of Highway Bridges and to develop joint-research efforts between the U.S. and New Zealand and the U.S. and Japan in this important area. In 1986 he was a recipient of a Fellowship from the Japan Society for the Promotion of Science; he spent three months in Japan to initiate the potential for a U.S.-Japan cooperative research program on bridge engineering. Professor Abdel-Ghaffar is a member of the Steering Committee that organized the First International Conference on the 1985 Mexican earthquakes.

For the last few years Professor Abdel-Ghaffar has investigated the dynamic characteristics and earthquake response of long-span suspension and cable-stayed bridges when subjected to multiple-support seismic response of earth dams. Both projects were supported by grants from the National Science foundation. He organized, in August 1985, via an NSF grant, the 2nd U.S.-Japan Workshop on Performance and Strengthening of Bridge Structures and the Research Needs. He is also the organizer of the 3rd U.S.-Japan Workshop on Bridge Engineering (Tsukuba Science City, Japan, May 8-9, 1987), 4th U.S.-Japan Workshop on Bridges (San Diego, California, May 1987) and the U.S. side of the 5th Workshop (Tsukuba, Japan, May 8-9, 1989).



April 12, 1989

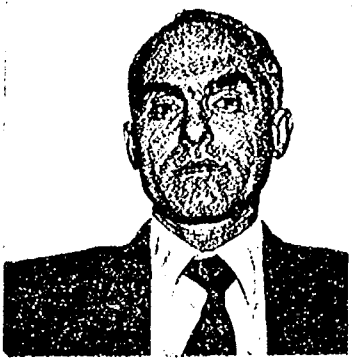
ROBERT H. SCANLAN
Professor and Principal Research Scientist
The Johns Hopkins University

Professor Scanlan, who joined the Department of Civil Engineering at The Johns Hopkins University in 1984, was born in Chicage, Illinois and received his early training there in the public schools, Armour Institute of the Illinois Institute of Technology, and the University of Chicago. He later did graduate studies at M.I.T. and the Sorbonne, Paris, receiving a doctoral degree from each of these institutions.

He has had a range of technical and research experience including industry, government, and the university. His university experience prior to accepting the professorship at Hopkins was as director of the program in Structures and Mechanics at Princeton University.

He is a member of the American Society of Mechanical Engineers and the American Society of Civil Engineers. His principal areas of interest include vibrations, stress, structural dynamics, and fluid-structure interaction, with emphasis on dynamic effects upon mechanical and civil engineering structures. He was formerly chairman of the ASCE Committee on Dynamics for the Engineering Mechanics Division and of the Task Committee on Wind Forces of the ASCE. He is presently chairman of the national Executive Committee for the Engineering Mechanics Division, ASCE. He is author of over 100 technical papers in his areas of interest and has been consultant in these areas to agencies of the U.S. and foreign governments, and to private firms. He was awarded the Higgins National Lectureship of the American Institute of Steel Construction in 1977, and has received several other prizes, from ASCE, for his work on the aeroelastic stability of bridges, most notably the State-of-the-Art in Civil Engineering, 1968; a Structural Division commendation in 1985; both the Wellington Prize and the Nathan M. Newmark Medal in 1986, and the James Croes medal in 1988. In 1982 he directed a two-week, on-site ambient vibration survey of the Golden Gate Bridge, the results of which appear in two ASCE papers. He is a registered professional engineer in the State of Ohio. Professor Scanlan was elected to membership in the National Academy of Engineering of the United States in 1987.

RESUME



Name	Sami F. Masri
Title	Professor, Civil and Mechanical Engineering
Address:	Department of Civil Engineering School of Engineering University of Southern California Los Angeles, CA 90008-0242
Telephone:	(213) 743-6209 (213) 743-2941

Education

B.S.	Aerospace Engineering, 1960, The University of Texas
M.S.	Aerospace Engineering, 1961, The University of Texas
M.S.	Mechanical Engineering, 1962, California Institute of Technology
Ph.D.	Mechanical Engineering, 1965, California Institute of Technology
1961 - 1966	California Institute of Technology Research Fellow in Mechanical Engineering, 1965-66; Research Assistant in Mechanical Engineering, 1961-65.
1966 - 1969	Assistant Professor, Department of Civil Engineering, U.S.C.
1969 - 1976	Associate Professor, Department of Civil Engineering, U.S.C.
1976 - present	Professor, Department of Civil Engineering, U.S.C.
1973 - 1981	Associate Chairman, Department of Civil Engineering, U.S.C.
1982 - 1985	Associate Chairman, Department of Civil Engineering, U.S.C.
1981 - present	Professor, Departments of Civil and Mechanical Engineering, U.S.C.

CURRICULUM VITAE

FRIEDER SEIBLE

Associate Professor of Structural Engineering

EDUCATION



Dipl. Ing.	University of Stuttgart, West Germany, 1976 (Civil Engineering)
M.Sc.	University of Calgary, Alberta, Canada, 1978 (Civil Engineering)
Ph.D.	University of California, Berkeley, 1982 (Civil Engineering)
P.E.	State of California, 1985 (Civil Engineering)

RESEARCH INTERESTS

Analysis and design of reinforced/prestressed concrete bridges. Evaluation and rehabilitation of existing bridge structures and buildings. Development of new computer models to predict dynamic and static nonlinear response of reinforced and prestressed concrete structures under service loads, overloads and failure loads. Verification of computer models by means of large or full scale experimental testing. Earthquake resistant design of reinforced concrete and concrete masonry structures. Development of new large-scale structural testing techniques.

PROFESSIONAL EXPERIENCE

1982-1983: Design Engineer, Philipp Holzmann AG, Frankfurt, West Germany

1983-1987: Assistant Professor of Structural Engineering, University of California, San Diego

1985- : Associate Director, Charles Lee Powell Structural Systems Laboratory, University of California, San Diego

I987- : Associate Professor of Structural Engineering, University of California, San Diego

HONORS, AWARDS, AND PROFESSIONAL RECOGNITION

Best Paper Award for "Non-linear Behavior and Failure Analysis of Multicell RC Box Girder Bridges," International Conference on Short and Medium Span Bridges, Canadian Society for Civil Engineering, 1982.

K.B. Woods Award in recognition of a paper of outstanding merit entitled "Response of a 45° Skew RC Girder Bridge Model to AASHTO Trucks and Overload Construction Vehicles," 62nd Annual Meeting of the Transportation Research Board, Washington, D.C., 1983.

Presidential Young Investigator Award, President Reagan, The White House, 1986.

Japanese Government Research Award for Foreign Research Specialists, Science and Technology Agency, Tokyo, Japan, 1987.

Research Scholarship, Japan Association for Building Research Promotion, Japan, 1987.

EMMANUEL A. MARAGAKIS
Associate Professor, Civil Engineering
University of Nevada Reno
Citizenship: Permanent resident of the U.S.



Education: B.S. Civil Engineering, National Technical University of Athens, June 1980 (5-year program)
M.S. (June 1981) and Ph.D. (Dec. 1984) Civil Engineering, California Institute of Technology, Pasadena, Thesis topic: "A Model for the Rigid Body Motions of Skew Bridges," supervised by Dr. P.C. Jennings

Society Memberships:

Associate Member of ASCE, Member of ASCE - Reno Chapter, Member of EERI, Member of National Technical Chamber of Greece, Registered Professional Engineer in Greece

Committee Membership:

Member of the ASCE Technical Committee of the Engineering Mechanics Division on the Dynamics of Structures, Member of the ASCE Technical Committee on the Methods of Analysis, Reviewer for ASCE and NSF

Major Research Interests:

Dynamic Response of Bridges, Nonlinear Behavior of Structures, Soil-Structure Interaction, Finite Element Modeling

Courses Taught at the University of Nevada:

CE 243 Computational Methods in Civil Engineering, CE 483/683 Structural Analysis II, CE 381 Structural Analysis, CE 731 Advanced Dynamics of Structures, CE 372 Strength of Materials, CE 704 Applied Finite Element Analysis, CE 726 Plates and Shells, CE 471/681 Mathematical Methods in Civil Engineering, CE 723 Advanced Reinforced Concrete

Current Research:

"An Improved Three-Layer Pavement Model and Granular Material Characterization," 12/87-12/89, NSF, $60,000
"Nonlinear Interaction Between the Bridge Deck and the Abutments During Earthquakes," 12/87-4/89, NSF, $53,347
"Analysis of the Response of Reinforced Concrete Building During the 1987 Whittier Earthquake," 2/88-7/89, NSF, $30,000
"Analysis of Highway Bridges for Transportation of Nuclear Materials" NWPO, $44,000, 4/89-8/89
"Analysis of Railway Bridge for Transportation of Nuclear Materials" NWPO, $25,000, 4/89-8/89

Publications:

Author of about 25 technical papers published in professional journals and conference proceedings.



BRUCE M. DOUGLAS, Director
Center for Civil Engineering
Earthquake Research
University Of Nevada-Reno
Reno, Nevada 89557

Dr. Douglas obtained his B.S.C.E. degree from the University of Santa Clara in 1959, and his M.S. and Ph.D. degrees in Engineering Mechanics from the University of Arizona in 1965. He has been at the University of Nevada-Reno since September of 1964 where he has served as assistant, associate and full professor of Civil Engineering. He served as the associate director of the Seismological Laboratory in the Mackay School of Mines from 1974 to 1976, and as the Chairman of the Civil Engineering Department in the College of Engineering from 1976 to 1984. Since then he has served as the director of the Center for Civil Engineering Earthquake Research and as professor of Civil Engineering.

His research interests have been primarily related to the lateral dynamic testing of full scale highway bridges at high amplitudes using the quick-release method. He has conducted these experiments in Nevada, California, and New Zealand. The focus of these studies has been the identification of the structural and foundation parameters which significantly affect the distribution of seismic loads.

Patents: Co-patentor U.S. Patent No. 3740301 June 1973. (Ski)
Co-patentor U.S. Patent Pending 1989. (Device to improve the efficiency of forming concrete decks on steel girder bridges)

Registered Civil Engineer: Nevada 07305

Committees: National Research Council, Transportation Research Board Committee A2C05-Dynamics and Field Testing of Bridges; Vice-Chairman ASCE Transportation Lifelines Committee of the Technical Council on Lifeline Earthquake Engineering; Earthquake Engineering Research Institute - Federal Highway Administration Task Force - Post Earthquake Seismic Damage Investigation and Evaluation of Bridges; Roster for National Research Council Committee on Natural Disasters - Post Disaster Investigations.

Professional Societies: American Society of Civil Engineers, President Nevada Section 1975; Seismological Society of America; Earthquake Engineering Research Institute; New Zealand Society for Earthquake Engineering; American Arbitration Society - Panel Member; and International Association of Bridge and Structural Engineering.

Recognition: Named Engineer of the Year by Nevada Society of Professional Engineers, 1983.



THOMAS T. BABER, PhD., P.E.
Associate Professor of Civil Engineering
The University of Virginia
Thornton Hall
Charlottesville, Virginia 22901
U.S.A.
Telephone: 804-924-6360
BITNET: TTB@Virginia

EDUCATION:

PhD, Civil Engineering, University of Illinois at Urbana-Champaign, 1980
M.E., Civil Engineering, Virginia Polytechnic Institute and State University, 1975
B.S., Civil Engineering, Virginia Polytechnic Institute and State University, 1969

EMPLOYMENT:

3/64-5/68	West Virginia Pulp and Paper Company, Covington, VA
6/69-1/70	Bechtel Corporation, Gaithersburg, MD.
1/70-12/71	Military Service, U. S. Army
7/74-7/77	Leo A. Daly Company, Washington, D. C.
9/77-12/79	University of Illinois, Urbana, Illinois
1/80-Present	University of Virginia, Charlottesville, VA.

TEACHING INTERESTS

Probabilistic Modeling, Reliability Theory, and Random Vibration
Earthquake Engineering
Finite Element and Numerical Methods in Solid Mechanics
Prestressed Concrete Design

RESEARCH INTERESTS

Structural Dynamics, and Random Vibration
Seismic Analysis of Structures
Dynamic Testing of Structures

PhD'S DIRECTED: 2

PUBLICATIONS

Nearly thirty publications in the areas of random vibration of hysteretic systems under seismic load, response of nonsymmetrical prestressed concrete beams, and field testing of bridges.



H. EUGENE WALDNER, P. E.

SUBJECT OF PRESENTATION

Quality Control Testing for Construction of the Cable-Stayed Bridge at Quincy, Illinois.

SUMMARY OF EXPERIENCE

Mr. Waldner is a Senior Associate with the Consulting Engineering firm of Modjeski and Masters.

He has 30 years of experience in all areas of bridge design, including long-span and movable bridges. As Project Engineer, he has had responsibility for the preparation of Conceptual Studies and Preliminary and Final Designs for numerous medium- and long-span highway and railway bridges. He supervised the preliminary and final design and construction advisory activities for the cable-stayed bridge crossing of the Mississippi River at Quincy, Illinois. His experience also includes supervision of the substructure design, the superstructure design review and design modifications for the cable-stayed Mississippi River Bridge at Luling, Louisiana, which was completed in 1983.

EDUCATION

Bachelor of Science in Civil Engineering, Bucknell University

PROFESSIONAL AFFILIATIONS

American Railway Engineering Assn.
American Society of Civil Engineers
Engineers Society of Pennsylvania
National Society of Professional Engineers
Structural Stability Research Council

Harold R. Bosch



Date of Birth: July 14, 1948

Birthplace: Callicoon, New York

Education: B.S. Degree, University of New Mexico
Civil Engineering, 1971
M.S. Degree, Colorado State University
Structures, in-progress

Position: Research Structural Engineer
Director, G.S. Vincent Aerodynamics Lab
Structures Division, HNR-10
Federal Highway Administration
U.S. Department of Transportation

In his position, Mr. Bosch is responsible for the planning, coordination, and conduct of a national program of wind engineering research aimed at ensuring the aerodynamic stability of long-span bridge structures. The wind engineering program involves analytical research, theoretical research, wind tunnel model studies in the Federal Highway Administration's Aerodynamics Laboratory, and field measurements on suspension and cable-stayed bridges.

In addition to being a program manager, Mr. Bosch is lab manager and principal investigator for the G.S. Vincent Memorial Aerodynamics Laboratory. The Aerodynamics Laboratory is located at the Federal Highway Administration's Turner-Fairbank Highway Research Center in McLean, Virginia. For more than 3 decades, this laboratory has been actively involved with investigating the aerodynamic stability of major highway bridge structures. The laboratory contains a number of unique features including a large-scale active turbulence simulation system, a high-frequency dual force-balance system, and a computer-controlled 3-D traverse. In parallel with the laboratory research, Mr. Bosch directs a program of field research which involves instrumenting and monitoring suspension and cable-stayed bridges.

Mr. Bosch has published more than 30 articles, technical papers, and research reports on bridge aerodynamic stability, bridge dynamics, wind tunnel model testing, full-scale structural testing, and automated instrumentation systems. He is an active member of the Wind Engineering Research Council (WERC) and serves as secretary of the Transportation Research Board (TRB) committee on Dynamics and Field Testing of Bridges.

Dr. Douglas A. Foutch
Professor of Civil Engineering
Department of Civil Engineering
3110 Newmark Civil Engineering Lab
205 North Mathews Avenue
Urbana, IL 61801 USA
Telephone: (217) 333-6359
FAX: (217) 333-9464



Biography:

Dr. Foutch received a B.S. degree in Civil Engineering from the University of Illinois at Urbana-Champaign in 1970, an M.S. degree from the University of Hawaii at Manoa in 1973, and his Ph.D. degree from the California Institute of Technology in 1976.

Dr. Foutch joined the faculty of Civil Engineering 1976 as an Assistant Professor. He was promoted to Associate Professor in 1982 and to Professor in 1988. Dr. Foutch's principal areas of research include dynamics of full-scale structures, behavior and design of bridges and buildings under dynamic loads, and behavior of steel members and connections. He has developed innovative techniques for the identification of dynamic characteristics of structures through field testing and analysis. He has also developed improved methods for computing the response of bridges and buildings to dynamic loads. Dr. Foutch has conducted investigations on the behavior of large size structures and subassemblies. He is currently the principal investigator on research projects on "The Effects of Vertical Earthquake Motions on the Response of Highway Bridges", "A Study of Two Buildings Shaken by the Mexico Earthquake", "Response of Steel Buildings to the Whittier Earthquake," and "Research for Evaluation, Rehabilitation and Design of Railway Bridges," sponsored by the National Science Foundation. Dr. Foutch has also consulted on the design and analysis of numerous major steel and concrete structures, including a major cable-stayed bridge crossing the Mississippi River.

Professional Societies and Activities:

Dr. Foutch has served on several committees of the American Society of Civil Engineers and is currently the chairman of the Committee on Seismic Effects of the Structural Division. He has also been active on the Seismological Society of America, Earthquake Engineering Research Institute, and the American Society for Engineering Education. He is also a registered structural engineer in the State of Illinois.

PERSONAL CAREER



NAME: Nobuyuki NARITA

POSITION: Director-General
Public Works Research Institute
Ministry of Construction

ADDRESS: 1, Asahi, Tsukuba-shi
Ibaraki-ken
305 Japan
Tel. 0298-64-2211 (Ext. 201)

DATE OF BIRTH: July 10, 1934

PERMANENT ADDRESS: Chiba Prefecture

EDUCATION: In Structural Engineering, Bridge Engineering, River Engineering and Concrete Engineering at Department of Civil Engineering, Faculty of Engineering, Tokyo University
In Structural Engineering and Bridge Engineering at Graduate Course, Faculty of Engineering, Tokyo University
Doctor of Engineering

SPECIALITY: Wind resistant design of civil engineering structures

MAJOR AREAS OF EXPERIENCE:

1960-1964	Research on earthquake engineering
1960-	Research on wind resistant design of bridges
1970-1980	Head, Structure Division, Structure and Bridge Department, Public Works Research Institute, Ministry of Construction
1980-1983	Director, Structure and Bridge Department, Public Works Research Institute, Ministry of Construction
1983-1985	Director, Planning and Research Administration Department, Public Works Research Institute, Ministry of Construction
1985-1986	Assistant Director-General, Public Works Research Institute, Ministry of Construction
1986-1988	Deputy Director-General, Public Works Research Institute, Ministry of Construction
1988-	Director-General,Public Works Research Institute, Ministry of Construction

MAJOR SUBJECT: Wind resistant design of bridges

TRAVEL ABROAD: United States, United Kingdom, Portugal, Burma, Tanzania and People's Republic of China

MAJOR PUBLICATION:
"Wind resistant design of a cable stayed bridge with solid bridge girder," March, 1978

PERSONAL CAREER

NAME: Toshio IWASAKI

POSITION: Deputy Director-General
Public Works Research Institute
Ministry of Construction

ADDRESS: 1, Asahi, Tsukuba-shi
Ibaraki-ken
305 Japan
Tel. 0298-64-2211



DATE OF BIRTH: March 30, 1939

PERMANENT ADDRESS: Oita Prefecture

EDUCATION: Bachelor of Engineering in Civil Engineering
Kyushu University (1961)
M.S. in Civil Engineering, University of Michigan, U.S.A. (1970)
Doctor of Engineering, Kyushu University (1981)

SPECIALITY: Civil Engineering

MAJOR AREAS OF EXPERIENCE:

1961-1973	Public Works Research Institute, M.O.C.
1973-1975	Head, Civil Engineering Section, IISEE Building Research Institute, M.O.C.
1975-1981	Head, Ground Vibration Division, Earthquake Disaster Prevention Department, PWRI, M.O.C.
1981-1984	Head, Earthquake Engineering Division, do.
1984-1987	Director, Earthquake Disaster Prevention Department, PWRI, M.O.C.
1987-1988	Director, Planning and Research Administration Department, PWRI, M.O.C.
1988-1989	Assistant Director-General, PWRI, M.O.C.
1989-	Deputy Director-General, PWRI, M.O.C.

MAJOR SUBJECT: Earthquake Engineering, Soil Dynamics

TRAVEL ABROAD: U.S.A., India, Peru, Mexico

MAJOR PUBLICATIONS:

1) "Estimation Procedure of Liquefaction Potential and Its Application to Earthquake Resistance Design," 14th Joint Meeting, Panel on Wind and Seismic Effects, UJNR, Washington D.C., May, 1982
2) "Dynamic Response Analysis of Shizunai Bridge Damaged by the Urakawa-oki Earthquake of March 21, 1982," 15th Joint Meeting, Panel on Wind and Seismic Effects, UJNR, Tsukuba, May, 1983
3) "A Case History of Bridge Performance during Earthquakes in Japan," International Conference on Case History in Geotechnical Engineering, St. Louis, Missouri, May, 1984
4) "Model Experiments on Dynamic Behavior of Reinforced Concrete Bridge Pier Columns," 16th Joint Meeting, Panel on Wind and Seismic Effects, UJNR, Washington D.C., May, 1984
5) "Soil Liquefaction Studies in Japan : State-of-the-Art," International Journal of Soil Dynamics and Earthquake Engineering, January, 1986
6) "Development of Manual For Repair Methods For Civil Engineering Structures Damaged by Earthquakes," 9th World Conference on Earthquake Engineering, August, 1988

PERSONAL CAREER



NAME: Yoshio ADACHI

POSITION: Director, Planning and Research
Administration Department
Public Works Research Institute
Ministry of Construction

ADDRESS: 1, Asahi, Tsukuba-shi
Ibaraki-ken
305 Japan
Tel. 0298-64-2211

DATE OF BIRTH: October 3, 1939

PERMANENT ADDRESS: Osaka

EDUCATION: Doctor of Engineering
Osaka City University

SPECIALITY: Civil Engineering

MAJOR AREAS OF EXPERIENCE:

1964-1973	Research Engineer, Bridge Foundation Engineering, PWRI
1974-1976	Deputy Director, Meishi National Highway Construction Office, M.O.C.
1976-1978	Head, Planning Section, Chubu Regional Construction Bureau, M.O.C.
1978-1984	Head, Traffic Environment Division, PWRI
1984-1986	Road Traffic Research Coordinator, PWRI
1986-1988	Director, Road Department, PWRI

MAJOR SUBJECT: Research on Road Design and Traffic Engineering

TRAVEL ABROAD: Canada, Italy, Kenya

MAJOR PUBLICATIONS:

"Settlement Characteristics of Sand-Gravel Layers"(1967)
"Present Status of Road Environmental Problems in Japan" (1979)
"Investigation on the Radiation of Low Frequency Sound from Highway Bridge"(1987)
"Dynamic Response in Infrasonic Frequency Range of Highway Bridge Deck Slab"(1983)
"New Development in Japan's Pavement Management Process" (1987)

PERSONAL CAREER



NAME : Shoichi SAEKI

POSITION: Director
Structure and Bridge Department
Public Works Research Institute
Ministry of Construction

ADDRESS: 1, Asahi, Tsukuba-shi
Ibaraki-ken
305 JAPAN
Tel. 0298-64-2211

DATE OF BIRTH: July 21, 1938

PERMANENT ADDRESS: Hyogo prefecture

EDUCATION: Bachelor of Civil Engineering
Nagoya Institute of technology

SPECIALITY: Civil Engineering

MAJOR AREAS OF EXPERIENCE:

1962-1966	Research Engineer, Bridge Division, PWRI
1967-1973	Office for Kanmon Bridge, Japan Highway Public corporation
1974-1975	Senior Research Engineer, Bridge Division PWRI
1975-1985	Head, Bridge Division, PWRI
1985-1987	Director, Tarumi Construction Office, First Construction Bureau, Honshu Shikoku Bridge Authority
1987-1988	Director, Construction Department, First Construction Bureau, Honshu Shikoku Bridge Authority
1988-	Director, Structure and Bridge Department, PWRI

MAJOR SUBJECT: Research on superstructure of Bridge

TRAVEL ABROAD: Indonesia, Thailand, Philippines, U.S.A. and China

MAJOR PUBLICATIONS:

"Handbook for the Bridge Design and Erection," (Joint Work), Society for Construction Works, 1978

"Erection of Long-Span Bridges," (Joint Work), Sankaido Publication, 1979

"Analysis of Cable-Stayled Bridge," Technical Memorandum of the PWRI, 1978

"Resistance of Concrete Beams subjected to Shear," Technical Memorandum of the PWRI, 1978

"Reliability Analysis of Steel Highway Bridges," Technical Memorandum of the PWRI, 1977

"Ultimate Resistance of Steel Piles Subjected to Bending," Annual Meeting of Japan Society for Civil Engineers, 1975

"Study on Hybrid Girders," 10th Congress of IABSE, 1977

"Design of Non-Composite Steel Girders Based on Load Factor Design Method," Technical Memorandum of the PWRI, 1976

"Erection of Suspension Bridges," Annual Meeting of the Japan Society for Civil Engineers, 1968

PERSONAL CAREER

NAME : Yasushi SASAKI

POSITION : Director, Earthquake Disaster Prevention Department
Public Works Research Institute
Ministry of Construction

ADDRESS : 1, Asahi, Tsukuba-shi
Ibaraki-ken
305 Japan
Tel. 0298-64-2211



DATE OF BIRTH : February 8, 1942

PERMANENT ADDRESS : Hiroshima Prefecture

EDUCATION : Master of Engineering (1966, Hiroshima Univ.)
Doctor of Engineering (1985, Hiroshima Univ.)

SPECIALITY : Civil Engineering

MAJOR AREAS OF EXPERIENCE :

1966-1972	Researcher, Soil Mechanics Division, PWRI
1972-1974	Assistant Chief, Planning Division, PWRI
1974-1975	Chief, Investigation Division Fukushima Construction Office Tohoku Regional Construction Bureau, M.O.C
1975-1976	Chief, Investigation Division Aomori Construction Office Tohoku Regional Construction Bureau, M.O.C
1976-1978	Senior Engineer, River Planning Division Hokkaido Development Bureau Prime Minister's Office
1978-1978	Head, Systems Division, PWRI
1978-1984	Head, Soil Dynamics Division, PWRI
1984-1989	Head, Ground Vibration Division, PWRI
1989-	Director, Earthquake Disaster Prevention Department, PWRI

MAJOR SUBJECTS AND SUMMARY :
Soil Mechanics and Foundation Engineering
Soil Dynamics
Aseismic Design of Soil Structure

TRAVEL ABROAD : U.S.A., Philippine, Peru, Mexico

MAJOR PUBLICATIONS :

"Damage to River Dykes Caused by the Miyagi-ken-oki Earthquake of June, 1978," Sept. 1979
"An Evaluation Method on Aseismicity of Earth Structures (Road Embankment)," May 1980
"Vibratory Cone Penetrometer to Assess the Liquefaction Potential of the Ground," May 1982
"Shaking Table Tests on Gravel Drains to Prevent Liquefaction of Sand Deposits," Sept. 1982
"Shaking Table Tests on the Remedial Measures to Improve Seismic Stability of Embankments," May 1983
"Dense Instrument Array Program by Public Works Research Institute for Observing Strong Earthquake-Motion", Feb. 1985



PERSONAL CAREER

NAME: Junzo Inoue

POSITION: Research Engineer, Structure Division,
Structure and Bridge Department,
Public Works Research Institute
Ministry of Construction

ADDRESS: Asahi 1, Tsukuba-shi, Ibaraki-ken,
305 Japan
Tel. 0298-64-2211

DATE OF BIRTH: February 28, 1960

PERMANENT ADDRESS: Hyogo Prefecture

EDUCATION: Bachelor of Engineering University of Tokyo, Japan
Master of Engineering University of Tokyo, Japan

SPECIALTY: Civil Engineering

MAJOR AREAS OF EXPERIENCE:

1984- Research on Bridge Vibration due to Traffic

1989- Bridge Instructor, PWRI

MAJOR SUBJECT: Bridge Engineering

TRAVEL ABROAD: None

MAJOR PUBLICATION:

1) Field Test and Simulation Analysis on Dynamic Design Load of Bridge, Technical Memorandum NO. 2258 Public Works Research Institute, December 1985 (in Japanese)
2) Field Test of Traffic Induced Vibration of the Viaducts in Urban Area, Technical Memorandum NO. 2428 Public Works Research Institute, January 1987 (in Japanese)

PERSONAL CAREER



NAME : Michio OKAHARA

POSITION : Head
Foundation Engineering Division
Public Works Research Institute
Ministry of Construction

ADDRESS : 1, Asahi, Tsukuba-shi
Ibaraki-ken
305 Japan
Tel. 0298-64-2211

DATE OF BIRTH : April 23, 1948

PERMANENT ADDRESS : Wakayama Prefecture

EDUCATION : Bachelor of Science, Kyoto University
Master of Science, Kyoto University
Degree of Civil Engineer, Columbia University

SPECIALITY : Civil Engineering

MAJOR AREAS OF EXPERIENCE :

1974-1977	Research Engineer, Foundation Engineering Division, PWRI
1977-1979	Graduate Student, Department of Civil Engineering, Columbia University
1979-1980	Research Engineer, Foundation Engineering Division, PWRI
1980-1981	Head, Investigation Division Ohmiya Road Construction office, MOC
1981-1983	Deputy Director, Planning Division, Science and Technology Agency
1983-1986	First Secretary, Embassy of Japan in Malaysia, Ministry of Foreign Affairs
1986-	Head, Foundation Engineering Division, PWRI

MAJOR SUBJECT AND SUMMARY :

Soil Mechanics, Foundation Engineering and Reliability Design of Substructures

TRAVEL ABROAD : U.S.A., Malaysia

MAJOR PUBLICATIONS :

"Studies on Characteristics and Design Method of Assembled Steel Pile Foundation," Journal of Research PWRI Vol 150, 1978
"Safety Evaluation for Bearing Capacity of Piles in Load and Resistance Factor Design Criteria," Journal of Research PWRI, Vol 20, 1979



NAME : Shoji TAKAGI

POSITION : Senior Research Engineer,
Foundation Engineering Division,
Structure and Bridge Department,
Public Works Research Institute,
Ministry of Construction

ADDRESS : Asahi-1 Tsukuba-shi Ibaraki-ken,
305 Japan
Tel. 0298-64-2211

DATE OF BIRTH : November 11, 1952

PERMANENT ADDRESS : Kumamoto Prefecture

EDUCATION : Master of Technology (Civil Engineering)
Saga University

SPECIALITY : Civil Engineering

MAJOR AREAS OF EXPERIENCE :

1977-1985 Kyusyu Regional Construction Bureau, M.O.C.
1985-1987 Chief of Bridge Section, Local Road Division, Road Bureau, M.O.C.
1987- Senior Research Engineer, Foundation Engineering Division, P.W.R.I.

MAJOR SUBJECT AND ITS SUMMAY :
Research on substructure of bridge

TRAVEL ABROAD :

MAJOR PUBLICATIONS :

NAME : Shoichi NAKATANI



POSITION : Foundation Engineering Division,
Structure and Bridge Department,
Public Works Research Institute,
Ministry of Construction

ADDRESS : Asahi-1 Tsukuba-shi Ibaraki-ken,
305 Japan
Tel. 0298-64-2211

DATE OF BIRTH : May 18, 1960

PERMANENT ADDRESS : Hyogo

EDUCATION : Master of Technology (Civil Engineering)
Kyoto University

SPECIALITY : Civil Engineering

MAJOR AREAS OF EXPERIENCE :
1985- Research Engineer, Foundation Engineering Division, PWRI

MAJOR SUBJECT AND ITS SUMMAY :
Research on substructure of bridge

TRAVEL ABROAD :

MAJOR PUBLICATIONS :

NAME : Atsushi HATAMOTO



POSITION : Research Engineer,
Foundation Engineering Division,
Structure and Bridge Department,
Public Works Research Institute,
Ministry of Construction

ADDRESS : Asahi-1 Tsukuba-shi Ibaraki-ken,
305 Japan
Tel. 0298-64-2211

DATE OF BIRTH : January 9, 1963

PERMANENT ADDRESS : Hokkaido

EDUCATION : Bachelor of Technology (Civil Engineering)
Hokkaido University

SPECIALITY : Civil Engineering

MAJOR AREAS OF EXPERIENCE :

1985-1987 Obihiro Development and Construction Division of Hokkaido Development Bureau

1988- Research Engineer, Foundation Engineering Division, PWRI

MAJOR SUBJECT AND ITS SUMMAY :
Research on substructure of bridges

TRAVEL ABROAD : None

MAJOR PUBLICATIONS :

NAME : Yoshitomi KIMURA



POSITION : Foundation Engineering Division,
Structure and Bridge Department,
Public Works Research Institute,
Ministry of Construction

ADDRESS : Asahi-1 Tsukuba-shi Ibaraki-ken,
305 Japan
Tel. 0298-64-2211

DATE OF BIRTH : September 26, 1962

PERMANENT ADDRESS : Shimane

EDUCATION : Master of Technology (Civil Engineering)
Technorogical University of Nagaoka

SPECIALITY : Civil Engineering

MAJOR AREAS OF EXPERIENCE :

1987 First Investigation Division, Meishi National Highway Construction Office, M.O.C.

1988 Investigation Division, Tenryugawa-Jyoryu Constraction Office, M.O.C.

1989- Research Engineer, Foundation Engineering Division, PWRI

MAJOR SUBJECT AND ITS SUMMAY :
Research on substructure of bridge

TRAVEL ABROAD :

MAJOR PUBLICATIONS :

PERSONAL CAREER



NAME : Koichi YOKOYAMA

POSITION : Head, Structure Division
Structure and Bridge Department
Public Works Research Institute
Ministry of Construction

ADDRESS : 1, Asahi, Tsukuba-shi
Ibaraki-ken
305 Japan
Tel. 0298-64-2211

DATE OF BIRTH : July 8, 1945

PERMANENT ADDRESS : Nagano Prefecture

EDUCATION : Master of Civil Engineering
Tokyo Institute of Technology

SPECIALITY : Structural Engineering

MAJOR AREAS OF EXPERIENCE :

1971-1979	Researcher, Structure Division Structure and Bridge Department, PWRI
1979-1980	Kyushu Regional Construction Bureau, M.O.C.
1980-1981	Technical Advisor, Prefectural Police Head-quarters, Fukuoka Prefecture
1982-1984	Colombo Plan Expert, Bridge Engineering Training Centre in Burma
1984-	Head, Structure Division Structure and Bridge Department, PWRI

MAJOR SUBJECT : Wind resistant design of bridges

TRAVEL ABROAD : U.K., Burma, Canada

MAJOR PUBLICATIONS :

1) "Aerodynamic Stability of a Long-span Suspension Bridge at Construction Stage," UJNR, 1977
2) "Field Observation of Aerodynamic Behavior of Long-span Bridges," 4th Int. Conf. on Wind Engineering, 1979

NAME: Takaaki Kusakabe



POSITION: Research Engineer, Structure Division
Structure and Bridge Department
Public Works Research Institute
Ministry of Construction

ADDRESS: Asahi-1, Tukuba-shi
Ibaraki-ken
305 JAPAN
Tel. 0298-64-2211

DATA OF BIRTH: January 28, 1962

PERMANENT ADDRESS: Hiroshima-chou, Sapporo-gun

EDUCATION: Master of Technology(Civil Engineering)
Hokkaido University

SPECIALITY: Civil Engineering

MAJOR AREAS OF EXPERIENCE:

1986- Research Engineer, Structure Division, PWRI

MAJOR SUBJECT: Research on Wind-Resistance of superstructure of Bridge

TRAVEL ABROAD: No Travel

MAJOR PUBLICATIONS: There are none

PERSONAL CAREER



NAME: Minoru FUJIWARA

POSITION: Head, Bridge Division
Structure and Bridge Department
Public Works Research Institute
Ministry of Construction

ADDRESS: 1, Asahi, Tsukuba-shi
Ibaraki-ken
305 Japan
Tel. 0298-64-2211

DATE OF BIRTH: April 11, 1942

PERMANENT ADDRESS: Chiba

EDUCATION: Master of Technology (Civil Engineering)
Nagoya University

SPECIALITY: Civil Engineering

MAJOR AREAS OF EXPERIENCE:

1967-1975	Research Engineer, Bridge Division, PWRI
1975-1976	Head, Planning Section, Hyogo National Highway Office, M.O.C.
1976-1978	Head, Traffic Safety Section, Osaka Prefectural Police Headquarters
1978-1979	Head, Planning Section, Kinki Regional Construction Bureau, M.O.C.
1979-1982	Deputy Director, National Highway 2nd Division, Road Bureau, M.O.C.
1982-1983	Director, Naniwa National Highway Office, M.O.C.
1984-1985	Team Leader, Japanese Expert Team, Bridge Engineering Training Centre Project in BURMA
1985-1986	Deputy Director for Environmental Engineering, Planning Division, Chugoku Regional Construction Bureau, M.O.C.
1986-	Head, Bridge Division, PWRI

MAJOR SUBJECT: Research on Superstructure of Bridge

TRAVEL ABROAD: U.K., Burma

MAJOR PUBLICATIONS:

"Design and Construction for Highway Bridges" (Joint Work), Sankaido Publication, May 1983

"Study on Ultimate Strength of Suspension Bridge Towers", Report of PWRI, November 1973

"Inelastic Lateral Buckling Tests on Welded Beams and Girders" (Joint Work), Proceedings of JSCE, May 1971

"Practical Design Method of Steel Plate Deck Bridges based on Theory of Orthotropic Plates", Report of PWRI, August 1969

PERSONAL CAREER



NAME: Koichi MINOSAKU

POSITION: Reseach Engineer, Bridge Division
Structure and Bridge Department
Public Works Research Institute
Ministry of Construction

ADDRESS: Asahi-1,Tsukuba-shi
Ibaraki-ken
305 JAPAN
Tel. 0298-64-2211

DATE OF BIRTH: August 27, 1957

PERMANENT ADDRESS: Hyogo Prefecture

EDUCATION: Master of Technology(Civil Engineering)
Tottori University

SPECIALITY: Civil Engineering

MAJOR AREAS OF EXPERIENCE:

1982- Research Engineer, Bridge Division,PWRI

MAJOR SUBJECT AND ITS SUMMARY:

Research on Superstructure of Concrete Bridge

TRAVEL ABROAD: U.S.A

MAJOR PUBLICATION:

"Loading Test on the Connection of Concrete Filled Steel Tubes", UJNR, 1986.

PERSONAL CAREER



NAME: Jun MURAKOSHI

POSITION: Reseach Engineer ,Bridge Division
Structure and Bridge Department
Public Works Research Institute
Ministry of Construction

ADDRESS: Asahi-1,Tsukuba-shi
Ibaraki-ken
305 JAPAN
Tel. 0298-64-2211

DATE OF BIRTH: January 14,1963

PERMANENT ADDRESS: Kanagawa

EDUCATION: Master of Technology(Civil Engineering)
Tokyo Institute of Technology

SPECIALITY: Civil Engineering

MAJOR AREAS OF EXPERIENCE:

1987- Research Engineer,Bridge Division,PWRI

MAJOR SUBJECT AND ITS SUMMARY:

Research on Superstructure of Steel Bridge

TRAVEL ABROAD: No

MAJOR PUBLICATION:

" A Report of Ultimate Strength Tests on Plate Girders",Report of PWRI, December 1987

PERSONAL CAREER



NAME : Ken-ichi TOKIDA

POSITION : Head, Ground Vibration Division
Earthquake Disaster Prevention Department
Public Works Research Institute
Ministry of Construction

ADDRESS : 1, Asahi, Tsukuba-shi
Ibaraki-ken
305 Japan
Tel. 0298-64-2211

DATE OF BIRTH : July 16, 1951

PERMANENT ADDRESS : Nagano Prefecture

EDUCATION : Master of Engineering, Osaka University

SPECIALITY : Soil Characteristics Engineering

MAJOR AREAS OF EXPERIENCE :

1976-1982	Researcher, Ground Vibration Division, Earthquake Disaster Prevention Department, PWRI
1982-1983	Takada Work Office, Hokuriku Regional Construction Bureau
1983-1985	Planning Division, Hokuriku Regional Construction Bureau
1985-1987	Engineering Division 2, Japan Institute of Construction Engineering (Foundation Juridical Person)
1987-1989	System Division, Planning and Research Administration Department, PWRI
1989-	Head, Ground Vibration Division, Earthquake Disaster Prevention Department, PWRI

MAJOR SUBJECTS AND SUMMARY :
Seismic Ground Motion and Dynamic Ground Characteristics

TRAVEL ABROAD : -

MAJOR PUBLICATIONS :
1)"A Practical Method for Assessing Soil Liquefaction Potential Based on Case Studies at Various Sites in Japan," 2nd Microzonation Conf., 1978

PERSONAL CAREER



NAME : Keiichi TAMURA

POSITION : Research Engineer
Ground Vibration Division
Earthquake Disaster
Prevention Department
Public Works Research Institute
Ministry of Construction

ADDRESS : 1 Asahi, Tsukuba-shi
Ibaraki-ken, 305 JAPAN
Tel. 0298-64-2211 Fax 0298-64-2840

DATE OF BIRTH : December 12, 1956

PERMANENT ADDRESS : Saitama Prefecture

EDUCATION : Bachelor and Master of Engineering
University of Tokyo, Japan

SPECIALTY : Civil Engineering

MAJOR AREAS OF EXPERIENCE :

1982 - Research Engineer, Ground Vibration Division,
Earthquake Disaster Prevention Department,
Public Works Research Institute

MAJOR SUBJECTS AND SUMMARY :

Earthquake Engineering

TRAVEL ABROAD : None

MAJOR PUBLICATIONS :

1) Finite Ground Strains Induced during Earthquake for Application to Seismic Design of Underground Structures, 5th International Conference on Numerical Methods in Geomechanics, April, 1985

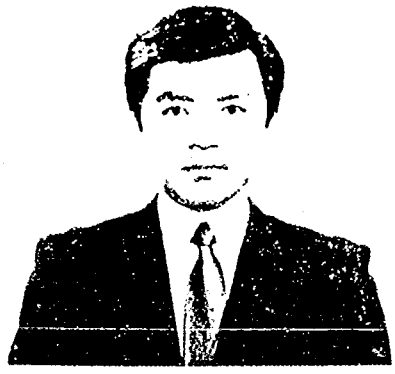
2) Recording Accuracy of Digital Strong-Motion Accelerograph with Independent Triggering and Recording System for Analysis of Finite Ground Strains Induced during Earthquakes, Proc. of Japan Society of Civil Engineers, April, 1988 (in Japanese)

3) Analysis on Phase Velocity of Ground Motion with Use of Array Records, 9th World Conference on Earthquake Engineering, August, 1988

PERSONAL CAREER

NAME: Tetsuro KUWABARA

POSITION: Research Engineer
Ground Vibration Division
Earthquake Disaster Prevention
Department
Public Works Research Institute
Ministry of Construction



ADDRESS: 1,Asahi,Tsukuba-shi,
Ibaraki-ken,
305 JAPAN
Tel.0298-64-2211(Ext.443)

DATE OF BIRTH: May 15,1958

PERMANENT ADDRESS: Gunma Prefecture

EDUCATION: Bachelor and Master Degree of Civil Engineering
Tohoku University

SPECIALITY: Civil Engineering

MAJOR AREAS OF EXPERIENCE:

1984- Research Engineer,Ground Vibration Division,
Earthquake Disaster Prevention Department,
Public Works Research Institute,
Ministry of Construction

MAJOR SUBJECTS AND SUMMARY:

Observation and Analysis of Strong Motion Earthquakes
Aseismic Design of Soil Structure

TRAVEL ABROAD: None

MAJOR PUBLICATION:

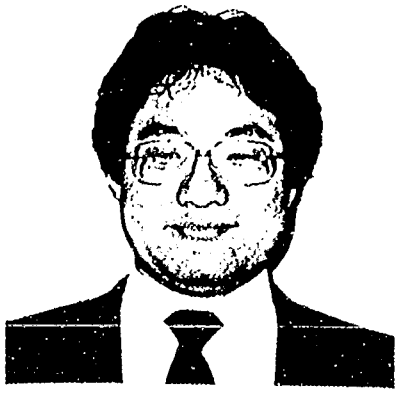
1)Strong Motion Observation System of P.W.R.I., U.S.-Japan Panel on Wind and Seismic Effects, UJNR, 19th Joint Meeting, May 1987
2)Shaking Table Test on the Ridge Response during Earthquake, UJNR, 20th Joint Meeting, May 1988
3)Behavior of the Nagara Dam during the Earthquake of December 17,1987, UJNR, 21th Joint Meeting, May 1989

PERSONAL CAREER

NAME : Hideo MATSUMOTO

POSITION : Research Engineer
Ground Vibration Division
Earthquake Disaster
Prevention Department
Public Works Research Institute
Ministry of Construction

ADDRESS : Asahi 1-banchi, Tsukuba-shi
Ibaraki-ken, 305 JAPAN
Tel. 0298-64-2211



DATE OF BIRTH : March 12, 1959

PERMANENT ADDRESS : Kagawa Prefecture

EDUCATION : Bachelor of Engineering
(Mechanical and Civil Engineering)
University of Ehime, Japan

SPECIALITY : Civil Engineering

MAJOR AREAS OF EXPERIENCE :

1983 - Research Engineer, Ground Vibration Division,
Earthquake Disaster Prevention Department, PWRI
Ministry Of Construction

MAJOR SUBJECTS AND SUMMARY :

Soil Dynamics (Liquefaction of Ground)

TRAVEL ABROAD : None

MAJOR PUBLICATIONS :

1) Experimental Study of Embankment on Sandy Layers During Earthquakes, -Characteristics of Reconstructed Embankment on Liquefied Layers-, 16th Joint Meeting, UJNR, 1984

2) Shaking Table Test on the Effects of Thickness of Liquefied Layer on Deformation of Embankments, 17th Joint Meeting, UJNR,1985

PERSONAL CAREER



NAME: Kazuhiko KAWASHIMA

POSITION: Head
Earthquake Engineering Division
Earthquake Disaster Prevention
Department
Public Works Research Institute
Ministry of Construction

ADDRESS: 1, Asahi, Tsukuba-shi
Ibaraki-ken
305 Japan
Tel. 0298-64-2211

DATE OF BIRTH: December 25, 1947

EDUCATION: Bachelor and Master Degree of Civil Engineering
Nagoya University
Doctor of Engineering, Nagoya University

SPECIALITY: Civil Engineering

MAJOR AREAS OF EXPERIENCE:

1972-1984	Ground Vibration Division, Earthquake Disaster Prevention Department, PWRI, M.O.C.
1984-	Head, Earthquake Engineering Division, do.

MAJOR SUBJECT: Earthquake Engineering

TRAVEL ABROAD: Argentina, Burma, Indonesia, Mexico, New Zealand, Peru, U.S.A., U.S.S.R., Venezuela

MAJOR PUBLICATIONS:

1) "Soil-Structure Interaction of a Highway Bridge with Use of Recorded Strong-Motion Accelerations," 7th WCEE, 1980
2) "Correlative Investigations on Theoretical and Experimental Behavior of a Curved Model Bridge Structure," Report NO.EERC 76-26, Earthquake Engineering Research Center, Univ. of California, Berkeley, 1976
3) "Attenuation of Peak Ground Acceleration, Velocity and Displacement Based on Multiple Regression Analysis of Japanese Strong Motion Records", Earthquake Engineering and Structural Dynamics, Vol.14, 1986
4) "Earthquake Response Spectra Taking Account of Number of Response Cycles," Earthquake Engineering and Structural Dynamics, Vol.14, 1986
5) "Effects of Cyclic Loading Hysteresis on Dynamic Behavior of Reinforced Concrete Bridge Piers" Proc. JSCE, 1988

PERSONAL CAREER

NAME : Kinji HASEGAWA

POSITION : Research Engineer
Earthquake Engineering Division
Earthquake Disaster Prevention Department
Public Works Institute
Ministry of Construction

ADDRESS : 1 Asahi, Tsukuba City,
Ibaraki Pref., JAPAN 305
Tel. 0298-64-2211



DATE OF BIRTH : October 5, 1958

PERMANENT ADDRESS : Okayama Pref.

EDUCATION : Bachelor and Master Degree of Civil Engineering,
University of Tokyo

SPECIALITY : Civil Engineering

MAJOR AREAS OF EXPERIENCE :
1983- Earthquake Engineering Division, Earthquake Disaster Prevention Department, PWRI, M.O.C.

MAJOR SUBJECT : Earthquake Engineering

TRAVEL ABROAD : U.S.A.

MAJOR PUBLICATIONS :

1)"Model Experiments on Dynamic Behavior of Reinforced Concrete Bridge Pier Columns", 16th Joint Meeting, Wind and Seismic Effects, UJNR, 1984
2)"Experimental Investigation on Hysteretic Behavior of Reinforced Concrete Bridge Pier Columns", 17th Joint Meeting, Wind and Seismic Effects, UJNR, 1985
3)"Hysteretic Behavior of Reinforced Concrete Bridge Piers by Dynamic Loading Tests and Shaking Table Tests", 3rd U.S.- Japan Bridge Workshop, 1987
4)"Effect of Number of Loading Cycles and Loading Velocity of Reinforced Concrete Bridge Piers", 19th Joint Meeting, Wind and Seismic Effects, UJNR, 1987
5)"Seismic Response of Base Isolated Highway Bridge by Shaking Table Tests", 4th U.S.- Japan Bridge Workshop, 1988
6)"Dynamic Strength and Ductility of Reinforced Concrete Bridge Piers", 20th Joint Meeting, Wind and Seismic Effects, UJNR, 1988
7)"Hysteretic Behavior of Reinforced Concrete Bridge Piers by Dynamic Loading Tests and Shaking Table Tests", 9th WCEE, 1988

PERSONAL CAREER



NAME : Hideki SUGITA

POSITION : Research Engineer
Earthquake Engineering Division
Earthquake Disaster Prevension Department
Public Works Research Institute
Ministry of Construction

ADDRESS : Asahi-1, Tsukuba-si
Ibaraki-ken
305 JAPAN
Tel. 0298-64-2211

DATE OF BIRTH : May 7, 1964

PERMANENT ADDRESS : Shizuoka

EDUCATION : Bachelor of Civil Engineering
Osaka University

SPECIALITY : Civil Engineering

MAJOR AREAS OF EXPERIENCE :

1987- Research Engineer, Earthquake Engineering Division, PWRI

MAJOR SUBJECT AND ITS SUMMARY :

Earthquake Engineering

TRAVEL ABROAD : None

MAJOR PUBLICATIONS :

"Loading Test of Shield Tunnel Specimen Subjected to Alternative Axial Loading", 3RD UJNR/WS on Lifeline Systems, May 1989

PERSONAL CAREER



NAME: Tokunosuke FUJITANI

POSITION: Chief, The Second Research Laboratory
Applied Meteorology Research Division
Meteorological Research Institute (MRI)
Japan Meteorological Agency

ADDRESS: 1-1 Nagamine, Tsukuba-shi
Ibaraki-ken, 305 JAPAN
Tel. 0298-51-7111

DATE OF BIRTH: October 4, 1945

PERMANENT ADDRESS: Osaka Prefecture

EDUCATION: Bachelor of Science, Kyoto University
Master of Science, Kyoto University

SPECIALITY: Meteorology

MAJOR AREAS OF EXPERIENCE:

1972-1974	Research Associate, Disaster Prevention Research Institute, Kyoto University
1974-1981	Research Staff, Physical Meteorology Research Division, MRI
1981-1988	Senior Research Staff, ditto

MAJOR SUBJECT AND ITS SUMMARY:
Research in the field of boundary layer meteorology

TRAVEL ABROAD: U.S.A., Canada and Korea

MAJOR PUBLICATIONS:

"Observational study of the spatial variability of statistics of turbulencein the atmospheric boundary layer", Sep. 1986.

"Seasonal variation of the structure of the atmospheric boundary layer over a suburban area", Oct. 1986.

Personal Career



NAME : Osamu NAKANO

POSITION : Head, Structure Division
Structure Department
Civil Engineering Research Institute
Hokkaido Development Burear

ADDRESS : 1-20-902, Minami6, Nishi17, Cyuou-ku
Sapporo, Hokkaido
064 JAPAN
Tel. 011-551-7604

DATE OF BIRTH : July 4, 1949

PERMANENT ADDRESS: Hokkaido

EDUCATION : Master of Technology (Civil Engineering)
Hokkaido University

SPECIALITY : Civil Engineering

MAJOR AREAS OF EXPERIENCE :
1974-1979 Engineer, Sapporo Construction Department
1979-1981 Section Head, Bridge Section, Sapporo Construction Department
1981-1982 Assistant Head, Structure Division, CERI
1982-1984 Assistant Director, Aid Policy Division, Ministory of Foreign Affairs
1984-1987 First Secretary, Embassy of Japan, KENYA
1987-1989 Director, Road Division, Otaru Construction Department
1989- Head, Structure Division, CERI

MAJOR SUBJECT AND ITS SAMMARY :
Research on Seismic Design of Bridge

TRAVEL ABROAD : U.S.A., U.K., South Africa, Spain, Portugal

PERSONAL CAREER



NAME: Atsuo OGAWA

POSITION: Assistant Manager
Structural Engineering Division
Engineering Department
JAPAN Highway Public Corporation

ADDRESS: Shin-kasumigaseki Bldg.
3-2,3-chome,Kasumigaseki,Chiyoda-ku,
100 TOKYO JAPAN
Tel. 03-506-0272

DATE OF BIRTH: September 8,1949

PERMANENT ADDRESS: KANAGAWA

EDUCATION: Bachelor of Civil Engineering
KYUSHU University

SPECIALITY: Civil Engineering

MAJOR AREAS OF EXPERIENCE:

1972-1976	Civil Engineer,SUWA Construction Work-office
1976-1979	Bridge Engineer,Structural Engineering Division, TOKYO 1st Construction Bureau
1979-1983	Bridge Engineer,Structural Engineering Division, Head Office
1983-1986	Assistant Manager,Structural Engineering Division, SENDAI Construction Bureau
1986-1989	Head,Structural Engineering Section, MATSUDA Construction Work-office
1989-	Assistant Manager,Structural Engineering Division, Engineering Department,Head Office

MAJOR SUBJECT AND ITS SUMMARY:
Research and Design of Bridge

TRAVEL ABROAD: Saudi Arabia,Indonesia

MAJOR PUBLICATIONS:
"Design and Construction for Superstructure of Steal Bridge,New Civil Engineering" (Joint Work), Gihodo Publication,March 1988



PERSONAL CAREER

NAME: Yoneo OKA

POSITION: Assistant Manager
Concrete Section, Laboratory
Japan Highway Public Corporation

ADDRESS: The Laboratory of Japan Highway Public Corporation
1-4-1 Tadao, Machda
Tokyo JAPAN 194
phone 0427-91-1625

DATE OF BIRTH: Nov.19,1953

PERMANENT ADDRESS: 1070-5-203 Ichigao Midori-ku
Yokohama
JAPAN 227
phone 045-973-7669

EDUCATION: Master of Engineering (Civil Engineering)
Saitama University

SPECIALITY: Civil Engineering

MAJOR AREA OF EXPERIENCE:

1979-1982	Engineer, Structural Division Sendai Construction Bureau, JHPC
1982-1985	Engineer,Owani Construction Office, JHPC
1985-1986	Engineer,Management and Economic Office, JHPC
1986-1988	Study in Abroad,Ohio State University U.S.A.
1988-	Assistant Manager,Concrete Section,JHPCL

MAGER SUBJECT AND ITS SUMMARY:
Structural Eng. and Geotechnical Engineering

TRAVEL ABROAD: U.S.A.,Canada and Korea

MAJOR PUBLICATION:

"Foundations of SUGOHATA Bridge" Annual Meeting,
JHPC 1981
"Design of Friction Piles" Annual Meeting,
JHPC 1982
"Water Treatment for Tunnel Excavation"
Annual Meeting,JHPC 1984



PERSONAL CAREER

NAME: Haruo Takano

POSITION: Deputy Head
Special Structural Design Division
Kanagawa Construction Bureau
Metropolitan Expressway Public Corporation

ADDRESS: 2078-4, 304 Tozuka-machi
Tozuka-ku, Yokohama
244 JAPAN
Tel. 045-862-0708

DATE OF BIRTH: June 27, 1949

PERMANENT ADDRESS: Kanagawa

EDUCATION: Master of Science (Civil Engineering)
Oregon State University

SPECIALITY: Structural Engineering

MAJOR AREAS OF EXPERIENCE:

1973-1977 Survey and Design Division
Bay Shore Line
Construction Bureau

1977-1980 Research and Design Division
Head Office of MPPC

1980-1982 Field Office of Kanagawa
Construction Office

1982-1985 Design Division of Second
Construction Office

1985-1986 Engineering Management Division
Head Office of MPPC

1986- Special Structural Design
Division, Kanagawa Construction
Bureau

MAJOR SUBJECT AND ITS SUMMARY:

Design of Cable Stayed Bridge

TRAVEL ABROAD: U. S. A., CANADA, FRANCE,
GERMANY, KENYA

PERSONAL CAREER



NAME : Hiromi Kosaka

POSITION : Acting Head of Design Division, Third Construction Department, Metropolitan Expressway Public Corporation

ADDRESS : 2-14-4 Hacchobori, Chuo-ku, Tokyo 104 JAPAN
(03) 553-1231

DATE OF BIRTH : April 9,1948

PERMANENT ADDRESS : Chiba Prefecture

EDUCATION : Master of Civil Engineering
Tokyo Institute of Technology

SPECIALITY : Bridge Engineering

MAJOR AREAS OF EXPERIENCE:

1975-1978	First Planning Division, Planning Department
1978-1981	Design Division, Second Construction Depaertment
1982-1983	Institute of Massivbau, Technical University of Darmstadt, West Germany
1984-1985	Chief of Shimura Construction Office, Second Construction Department
1986-1988	Chief of Design Section, Engineering Department
1988-	Acting Head of Design Division, Third Construction Department

MAJOR SUBJECT AND ITS SUMMARY
Aseismic design of bridges

TRAVEL ABROAD:
West Germany, Switzerland, Czechoslovakia, Thailand, East Germany and France

MAJOR PUBLICATION:
"Foundation Works for Yokohama Bay Bridge Utilizing Large-Scale Precast Members", 5th U.S.-Japan Seminar on Precast Concrete Construction in Seismic Zones, Tokyo, 1986
"An Active Control of Traffic Vibrations on the Urban Viaducts", 3rd U.S.-Japan Bridge Workshop, Tsukuba 1987

PERSONAL CAREER



NAME: Shunichi NAKAMURA

POSITION: Assistant Manager
Design Section No.3, Design Division
Trans-Tokyo Bay Highway Corporation

ADDRESS: NN-BLDG, 15-5 Ichibancho
Chiyodaku, Tokyo 102
Tel 03-239-6585

DATE OF BIRTH: October 5, 1950

PERMANENT ADDRESS: Gifu City

EDUCATION: BEng, Kyoto University (Civil Engineering), 1974
MEng, Kyoto University (Civil Engineering), 1976
PhD, Imperial College of Science & Technology
University of London (Civil Engineering), 1987
PE (Construction Division), 1989

SPECIALITY: Civil Engineering

MAJOR JOB EXPERIENCES:

1976-1979	Offshore Structure Design & Construction Division Nippon Steel Corporation (NSC)
1979-1984	Bridge Design & Construction Division, NSC
1984-1986	Post Graduate Study at Imperial College, UK
1986-1989	Assistant Manager, Bridge Design & Construction Division, NSC
1989-	Assistant Manager, Trans-Tokyo Bay Highway Corporation

MAJOR SUBJECTS: Design and Research on Steel Structures

OVERSEAS EXPERIENCE: UK, INDIA, MALAYSIA, CHINA, WEST GERMANY, FRANCE
ITALY, DENMARK, FINLAND, SWEDEN, AUSTRIA

MAJOR PUBLICATION:

'Economical Computation of Stress Histories in Suspension Bridge Element, with Special Reference to Inclined Hangers', Proceedings of the International Conference on Steel and Aluminium Structures, Cardiff, UK, 1987.

'On the Cable-fatigue Sensitivity of Multi-stayed Bridges', International Conference on Cable-stayed Bridges, Bangkok, November 1987.

'A Parametric Study on Cable-stayed Bridges by the Limit States Design', Structural Eng./ Earthquake Eng., Vol.5, No.2, 265s-273s, October 1988

PERSONAL CAREER



NAME: Tsuguo Oishi

POSITION: Assistant Manager,Second Design Div.
Design Dep.
Trans-Tokyo Bay Highway Corporation (TTB)

ADDRESS: Ichiban-cho 15-5,
Chiyoda-ku,Tokyo-to, 102 Japan
Tel. 03-239-6585

DATE OF BIRTH:October 30,1954

PERMANENT ADDRESS:Shizuoka

EDUCATION: Master of Technology (Civil Engineering)
Kyoto University

MAJOR AREA OF EXPERIENCE:

1987-1981 Construction Engineer,Ishioka Construction Office,Japan Highway Pubric Corporation (JHPC)

1981-1984 Design Engineer,Bridge Division, Tokyo First Construction Bureuw,JHPC

1984-1987 Reseach Engineer,Trans-Tokyo Bay Highway Research Division,JHPC

1987- Assistant Manager,Second Design Division,TTB

MAJOR SUBJECT AND ITS SUMMARY:

Design of Kawasaki Manmade Island

TRAVEL ABROAD:None

MAJOR PUBRICATIONS:

"Geotechnical problem in construction of Manmade Islands for Trans-Tokyo Bay Highway Project"(Joint Work),TSUCHI-TO-KISO JSSMFE,Ser.No.336,Vol.34,No.1

"Trans-Tokyo Bay Highway"(Joint Work),TSUCHI-TO-KISO JSSMFE,Ser.No.348,Vol.35,No.1

PERSONAL CAREER



NAME: Masaaki TATSUMI

POSITION: Head, Design Division,
Design Department,
Honshu-Shikoku Bridge Authority

ADDRESS: Torano-mon 45th Mori Building
5-1-5 Torano-mon
Minato-ku,
Tokyo 105 JAPAN

DATE OF BIRTH: April 18, 1944

PERMANENT ADDRESS: Yokohama, JAPAN

EDUCATION: Master of Technology (Civil Engineering)
Kyoto University, Kyoto, JAPAN

SPECIALITY: Civil Engineering

MAJOR AREAS OF EXPERIENCE:

1969-1972	Consultant Engineer
1972-1978	Deputy Head, Design Division, 3rd Construction Bureau, HSBA
1978-1981	Head, Construction Division, Mukaijima Construction Office, 3rd Construction Bureau, HSBA
1981-1983	Deputy Manager, Construction Office of President Mobutu Sese Seko Bridge in Zaire
1983-1984	Deputy Head, Design Division, Design Department,HSBA
1984-1985	Head, Construction Division, 1st Construction Bureau, HSBA
1985-1988	Head, Planning Division, 2nd Construction Bureau, HSBA
1988-	Head, Design Division, Design Department,HSBA

MAJOR SUBJECT AND ITS SUMMARY:
Design for superstructure of Bridges

TRAVEL ABROAD: Austrailia, Indonesia, U.S.A., Zaire

MAJOR PUBLICASION:
"Honshu-Shikoku Bridge Project" (Joint Work)
Japan Society of Civil Engineers, October, 1988

PERSONAL CAREER



NAME: Kensaku HATA

POSITION: Engineer, Design Division,
Design Department,
Honshu-Shikoku Bridge Authority

ADDRESS: Torano-mon 45th Mori Building
5-1-5 Torano-mon
Minato-ku,
Tokyo 105 JAPAN

DATE OF BIRTH: January 7, 1957

PERMANENT ADDRESS: Okayama, JAPAN

EDUCATION: Master of Engineering (Civil Engineering)
Waseda University, Tokyo, JAPAN

SPECIALITY: Civil Engineering

MAJOR AREAS OF EXPERIENCE:

1981-1982	Engineer, Construction Division, 2nd Construction Bureau, HSBA
1982-1984	Engineer, Planning Division, Planning and Development Department, HSBA
1984-1985	Engineer, Construction Division, Naruto Construction Office, 1st Construction Bureau, HSBA
1986	Graduate Student (Masters Candidate) Department of Civil Engineering, Oregon State University, Corvallis, Oregon
1987-	Engineer, Design Division, Design Department,HSBA

MAJOR SUBJECT AND ITS SUMMARY:
Design for superstructure of Bridges

TRAVEL ABROAD: Korea, U.S.A.

MAJOR PUBLICASION:
"Design and Construction of the Highway-Railroad Combined Bridges on the Kojima-Sakaide Route of Honshu-Shikoku Bridges" (Joint Work)
11th IRF International Meeting, April, 1989

PERSONAL CAREER



Name : Fumio HAKAMADA

Position: Kobe Construction Division,
Hanshin Expressway Public
Corporation,
16-1 Shinkou-chou, Chuou-ku,
Kobe-shi, Hyogo 650 Japan.
(phone) 078-331-9801

Date of Birth : Nov. 3, 1955.

Permanent Address : Shizuoka Japan.

Education : Master of Engineering at Kyoto University
Mar. 1980.

Master of Engineering,
University of California, Berkeley
May, 1986.

membership : Member of Japanese Society of Civil Engineers
Associate Member of American Society of Civil
Engineers.

Major Subjects of Experience :
. Design Specification
. Structural Analysis of Long Bridges
. Maintenance of Highway Bridges

Travel Abroad : Thailand, US, European countries.

Major Publications :
Technical papers published are,
seismic risk analysis, design of prefabricated
prestressed concrete slab, design and experiments
of composite steel column, design of steel columns
with curved corner, replacement of defected steel
bearing, and design and analysis of arch bridge.

PERSONAL CAREER

NAME: Shunnichi . MOTOMURA

POSITION: Manager of Research and Development.
Hanshin Expressway Administration and
Technology Center.

ADDRESS: Toa Bld., Minamihon-machi 4-5-7,Chuo-ku
Osaka-shi, 541 JAPAN.
Tel. 06-282-0171



DATE OF BIRTH: April 21, 1938

PERMANENT ADDRESS: Hyogo

EDUCATION: Bachelor of Technology (Civil Engineering)
Nagoya Technology College.

SPECIALITY: Civil Engineering.

MAJOR AREAS OF EXPERIENCE:

1966-1968 Design Engineer,Engineering Division,Hanshin Expressway Public Corporaion.
1968-1970 Inspector,Fist Osaka Construction Division, H.E.P.C.
1970-1971 Design Engineer,Engineering Division, H.E.P.C.
1971-1973 Chief,Planning Section,Hanshin National Highway Oaffice, M.O.C.
1973-1980 Chief,Design Engineer,First Osaka Constraction Division, H.E.P.C.
1980-1985 Chief,Design Engineer,Maintenace Design Division, H.E.P.C.
1985-1989 Deputy Director, Osaka Maintenace Office, H.E.P.C.
1989- Manager of Research and Development, H.E.A.T.C.

MAJOR SUBJECT AND ITS SUMMARY:

Design on Superstructure of P.C. Bridge.

TRAVEL ABROAD: U.S.A

MAJOR PUBLICATIONS:

"Test of Welding Technique for Repair of Steel Highway Bridges "
Second Bridge Engineering Confevence,Volume 1, TRB.(WASHINGTON,D.C,1984).

PERSONAL CAREER



NAME: Mikitake ISHIZUKA

POSITION: Counselor,
International Engineering
Reseach Institute
International Engineering
Consultant Association (IECA)

ADDRESS: 5-3-23, Kojimachi, Chiyoda-ku,
Tokyo, 102 JAPAN
Tel. 03-263-4821~5

DATE OF BIRTH: February 15, 1941

PERMANENT ADDRESS: Takatsuki-city, Osaka

EDUCATION: Master of Technology (Civil Engineering)
Nagoya Institute Technology

SPECIALITY: Civil Engineering

MAJOR AREAS OF EXPERIENCE:

1968-1975 Bridge Engineer, Construction Division
Hanshin Expressway Public Corporation (HEPC)

1975-1981 Head, Design Section,
Kobe Construction Division, HEPC

1981-1983 Head, Maintenance Engineering Section
Maintenance Planning and Facility Design Division, HEPC

1983-1987 Advisor to Expressway and Bridge Construction,
Expressway and Rapid Trasit Authority of Thailand
under Technical Assistanct Program dispatched by
Japan International Coporation Agency (JICA)

1987-1989 Director, Development and Reseach Division
Hanshin Expressway Administration and Technology Center

1989- Councelor, IECA

MAJOR SUBJECT AND ITS SUMMARY:

Bridge Construction and its Maintenance

TRAVEL ABROAD: EC, Thailand, Nepal, Australia, Korea, U.S.A.,

MAJOR PUBLICATION:

〃The Activities of the Expressway and Rapid Transit Authority of Thailand〃 April 1985

〃Deterioration and Repair of Road Structures on Hanshin Expressways〃 October 1987

〃Characteristics of Road Structures Damaged by AAR on the Hanshin Expressway by Continuous Observation〃 November 1988

PERSONAL CAREER



NAME: Mituru HOSHINO

POSITION: General Manager
Engineering Department 2
Kansai International Airport Company Ltd.

ADDRSS: 11-10 Minamisenba 3-Chome, Chuo-ku
Osaka 542 JAPAN
TEL.06-282-2271

DATE OF BIRTH: December 1, 1943

PERMANENT ADDRESS: Osaka

EDUCATION: Master of Technology (Civil Engineering) 1969
Kyoto University

MAJOR AREAS OF EXPERIENCE:

1977-1980 Highway Engineer, Consultant,
Transport & Communications Division,
United Nations ESCAP (in Thailand)
1980-1982 Head, Planning Section, Road Division, Kinki Regional
Construction Bureau, M.O.C.
1982-1983 Deputy Director, National Highway 2nd Division,
Road Bureau, M.O.C.
1983-1985 Director, Naniwa National Highway Office, in Osaka M.O.C.
1985-1987 Deputy Director, Planning Division, Kinki Regional Construction
Bureau, M.O.C.
1987-1988 Deputy Director, Local Road Division, Road Bureau, M.O.C.
1988- Present Position

MAJOR SUBJECTS: Bridge & Highway Construction

MAJOR PUBLICATIONS:

"Explanation of Road Structure Ordinance" (Joint Wark), Japan Road Association, January 1983
"Guide for Cost Estimation of Civil Works" (Joint Work),Japan Construction Engineer's Association, July 1974
"Explanation of Specifications for Highway Bridges"(Joint Work), Japan Road Association, February 1973

PERSONAL CAREER



NAME: Noboru TAKAHASHI

POSITION: Special Assistant to General Manager
Engineering Department 2
Kansai International Airport Company Ltd.

ADDRESS: 11-10 Minamisenba 3-Chome, Chuo-ku
Osaka 542 JAPAN
TEL.06-282-2272

DATE OF BIRTH: October 23, 1945

PERMANENT ADDRESS: Yokohama

EDUCATION: B.S.Civil Engineering 1968
Tokyo Institute of Technology

MAJOR AREAS OF EXPERIENCE:

1972-1975	Chief, Planning Section, Tokyo Bureau of Shinkansen Construction, Japan Railway Construction Public Corporation
1975-1978	Director, Gunma Shinkansen Construction Office, J.R.C.P.C.
1978-1980	Head, Construction Section, Morioka Bureau, J.R.C.P.C.
1980-1985	Senior Assistant, Shinkansen Division, J.R.C.P.C. Tokyo
1985-1987	Head, Construction Division, Sapporo Bureau, J.R.C.P.C.
1987-1988	Adviser, General Affairs Division, J.R.C.P.C.Tokyo
1988-	Present Position

MAJOR SUBJECTS: Bridge & Railway Construction

MAJOR PUBLICATIONS:

"A Treatment of Boundary Condition as Resultant Forces on Finite Element Substructure Models" (Joint Work)
Proceedings of JSCE, Aug. 1978
"The Omotogawa Bridge, a Prestressed Concrete Cable-Stayed Bridge for Railway" (Joint Work)
The Ninth International Congress of the FIP, June 1982

4. 論文および討議

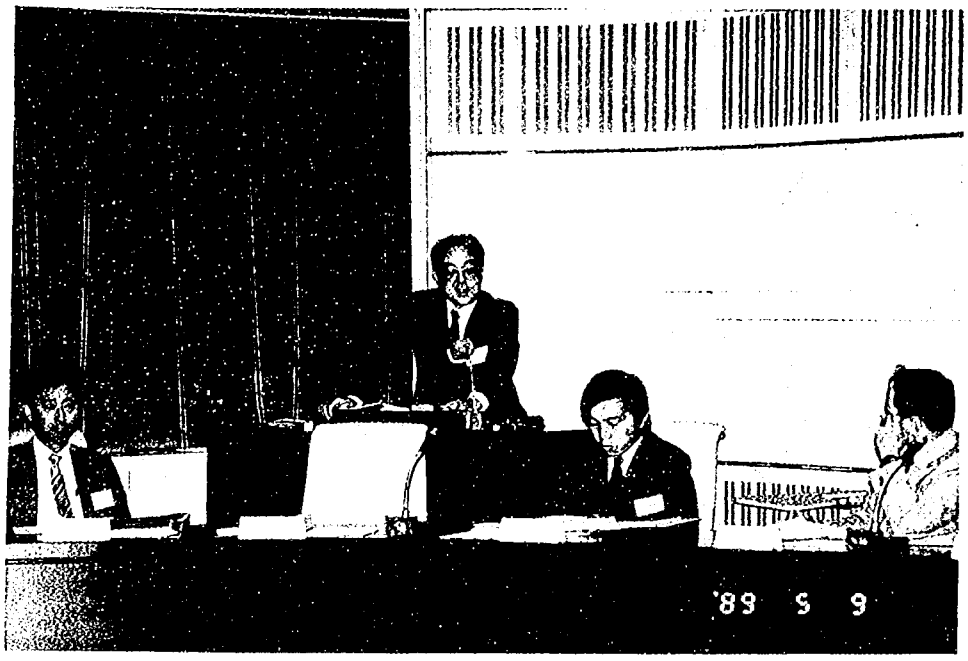
(1) Session 1

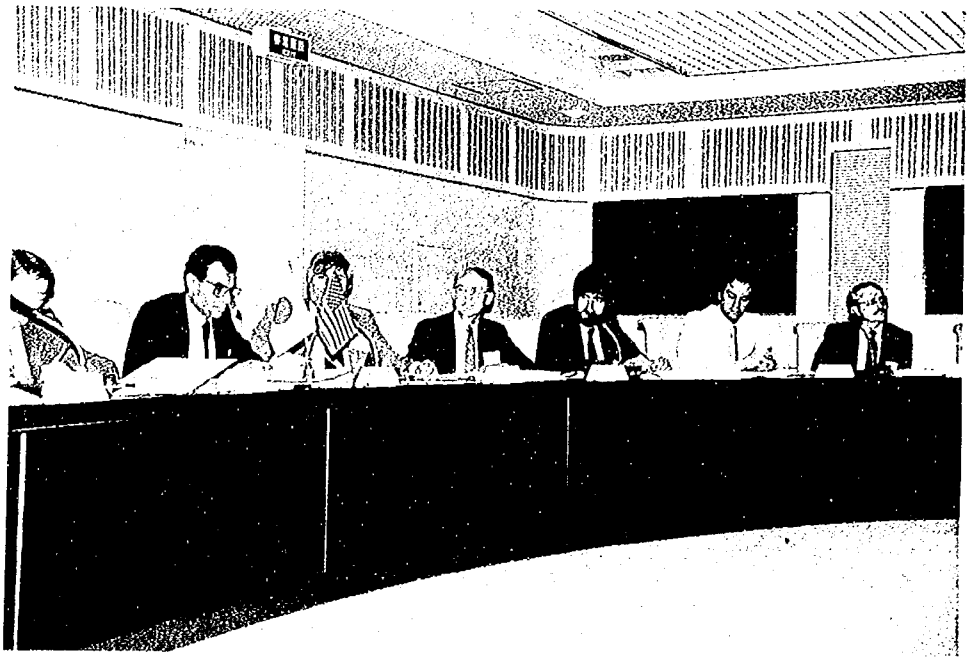
Tuesday, May 9, 1989 Place: International Conference Room (8F) PWRI

SESSION 1: OPENING SESSION
(Chairman: Shoichi Saeki) 9:00am~9:15am

Welcome Remarks: Nobuyuki Narita (Director General, PWRI)
Remarks: A. M. Abdel-Ghaffar (For U.S. Chairman, T/C(J))




'89 S 9



(2) Session 2

SESSION 2: SEISMIC DESIGN(1) 9:15am~10:30am
(Co-Chairman: T. Iwasaki, D.A. Foutch)

(1) Y. Sasaki, K. Tamura※ and K. Aizawa: Attenuation Characteristics of Ground Motions in the Period Range of 2 to 20 Seconds
(9:15am~9:35am)

(2) E. Maragakis※ and B. Douglas: On the Estimation of Longitudinal Linear and Nonlinear Abutment Stiffnesses
(9:35am~9:55am)

(3) B. Douglas※ and E. Maragakis: New Aspects Regarding the Use of Quick-Release Dynamic Tests for the Experimental Analysis of Bridge Structures
(9:55am~10:15am)

DISCUSSION(2)
(10:15am~10:30am)



ATTENUATION CHARACTERISTICS OF GROUND MOTIONS IN THE PERIOD RANGE OF 2 TO 20 SECONDS
- FOR APPLICATION TO THE SEISMIC DESIGN OF LARGE-SCALE STRUCTURES -

Yasushi SASAKI[1], Keiichi TAMURA[2] and Koh AIZAWA[3]

1 Director, Earthquake Disaster Prevention Department, Public Works Research Institute, Ministry of Construction, Tsukuba-shi, Ibaraki-ken, Japan
2 Research Engineer, Ground Vibration Division, ditto
3 Ground Vibration Division, ditto

INTRODUCTION

Not a few studies on ground motion characteristics from the engineering point of view have been conducted with the records obtained by SMAC accelerograph in Japan[1,2,3]. As a result, attenuation equations of peak ground motions and earthquake response spectra have been proposed and they are applied to the seismic design of structures[4]. The fundamental natural period of civil engineering structures is generally short and few exceed 2 or 3 seconds. However, the natural period of large-scale structures such as long-span suspension bridge exceeds 2 or 3 seconds. The reliable period range of the records provided by SMAC accelerograph, which is a mechanical type accelerograph with natural frequency of pendulum of 7.14 Hz and with critical damping, is limited to 0.08 to 3 seconds[5]. For determining appropriate seismic input motion to be applied to the design of large-scale structures, it is indispensable to consider the characteristics of ground motions in the long period range carefully.

In this paper, records of the Japan Meteorological Agency (JMA) low-magnification seismograph were digitized and the characteristics of ground motions in the long period range are discussed. The empirical formulae of attenuation equation of absolute acceleration response spectra are proposed by multiple regression analysis of 97 horizontal JMA low-magnification seismograph records. Considering the continuity with acceleration response spectra derived from SMAC accelerogram, a modified attenuation equation of acceleration response spectra is also presented and a design spectrum for the seismic design of long suspension bridge is proposed.

GROUND MOTION RECORDS ANALYZED

217 horizontal components and 108 vertical components of JMA low-magnification seismograms were digitized in this study[6]. They were obtained during 7 earthquakes with JMA magnitude of 7.1 to 7.9 (see Table 1). The method of digitization is same with the case of SMAC accelerogram by a manually operated digitizer[5].

The subsoil ground conditions at recording sites were classified into three groups as shown in Table 2. This classification depends on a point-by-point evaluation of amplification characteristic of subsoil structure around the JMA observatory sites[7]. A ground characteristic index was derived from the statistical analysis of the amplitude of JMA low-magnification seismograph records. This index is thought to reflect the characteristic of the deep soil deposits at a site. An index of 1.0 means that the amplification characteristic of the site is average one in Japan. An index more than 1.0 or less than 1.0 means that the amplification characteristic of the site is large or small from the average, respectively. Fig.1 shows a distribution of ground characteristic indexes. The records obtained at sites whose subsoil conditions are unknown, were not included in this analysis. The number of record corresponding to ground groups 1, 2 and 3 are 29, 46 and 22, respectively.

JMA low-magnification seismograph is a mechanical type seismograph with natural period of pendulum of 6 seconds and with damping of 0.55 to the critical. Since the sensitivity of the seismograph in the long period range, such as longer than 10 seconds, is substantially suppressed, the instrumental correction is necessary to use the records for the long period range. The ground velocity and acceleration were calculated by differentiating the corrected displacement in the frequency domain. The procedure of instrumental correction and calculation of velocity and acceleration are as follows[8].

The Fourier transform $F_o(f)$ of the original displacement $d_o(t)$ is written as

$$F_o(f)=\int_{-\infty}^{\infty} d_o(t)\cdot\exp(-i2\pi ft)dt \qquad (1)$$

Introducing correction filter $F_c(f)$, the corrected displacement $d(t)$, velocity $v(t)$ and acceleration $a(t)$ are obtained as

$$d(t)=\int_{-\infty}^{\infty} F(f)\cdot\exp(i2\pi ft)df \qquad (2)$$

$$v(t)=\int_{-\infty}^{\infty} i2\pi fF(f)\cdot\exp(i2\pi ft)df \tag{3}$$

$$a(t)=\int_{-\infty}^{\infty} -4\pi^2 f^2 F(f)\cdot\exp(i2\pi ft)df \tag{4}$$

where

$$F(f)=F_0\cdot F_c(f) \tag{5}$$

$$F_c(f)=[\exp\{i\phi(f)\}/R(f)]\cdot A(f) \tag{6}$$

$R(f)$ and $\phi(f)$ in Eq.(6) are the amplitude and phase characteristic function of the seismograph, and are written as

$$R(f)=1/[\{(f_0/f)^2-1\}^2+4h^2(f_0/f)^2]^{1/2} \tag{7}$$

$$\phi(f)=\tan^{-1}[2h(f_0/f)/\{(f_0/f)^2-1\}] \tag{8}$$

where f_0 and h represent natural frequency and damping ratio to the critical, respectively. $A(f)$ in Eq.(6) is the envelope function of correction filter and is expressed in terms of period T as

$$A(T)=\begin{cases} 0 & T<T_{LL} \\ [1-\cos\{(T-T_{LL})\pi/(T_{LU}-T_{LL})\}]/2 & T_{LL}\leqq T\leqq T_{LU} \\ 1 & T_{LU}<T<T_{UL} \\ [1+\cos\{(T-T_{UL})\pi/(T_{UU}-T_{UL})\}]/2 & T_{UL}\leqq T\leqq T_{UU} \\ 0 & T_{UU}<T \end{cases} \tag{9}$$

where T_{LU} and T_{UL} represent lower cut-off period and upper cut-off period, respectively, and T_{LL} and T_{UU} are the periods at which amplitude of correction filter becomes 0 at short and long period range, respectively. Referring to the result of a study on the recording accuracy of JMA low-magnification seismograph[9], cut-off periods were set up as

$$T_{LL}=1.3[s],\ T_{LU}=2[s],\ T_{UL}=20[s],\ T_{UU}=30[s] \tag{10}$$

Consequently, it is necessary to note that the ground motion characteristics discussed in this paper are limited to the characteristics in the period range of 2 to 20 seconds.

Fig.2 shows an example of corrected displacement, velocity and acceleration waveform. It is seen from Fig.2 that big amplitude of displacement is caused by long period component. Fig.3 shows absolute acceleration response spectra derived from the acceleration shown in Fig.2, where damping ratios to the critical were taken as 0.0, 0.01, 0.02 and 0.05.

Resultant of two horizontal orthogonal components of the ground

motion was not considered in this analysis, because the two components of JMA low-magnification seismograph are not synchronous. Larger one of the spectral values calculated from two horizontal components was considered for this study.

ATTENUATION OF ACCELERATION RESPONSE SPECTRA

In the past analyses on attenuation characteristics of maximum peak ground motions and absolute acceleration response spectra, based on accelerograph records, the following empirical formula is often used[3].

$$X=a\times 10^{bM}\times(\Delta+\Delta_0)^c \tag{11}$$

where

X: Maximum acceleration, velocity and displacement / Absolute acceleration response spectral amplitude

M: Magnitude of earthquake

Δ : Epicentral distance [km]

Δ_0: Constant to adjust X for small Δ

a, b, c: Coefficient

The same expression with Eq.(11) was assumed to represent the attenuation characteristics of absolute acceleration response spectra derived from JMA low-magnification seismograph records. Δ_0 in Eq.(11) was assumed to be 30 km. Acceleration response spectral amplitude $S_A(T_i)$[gal] with damping ratio of 0.02 and 0.05 to the critical at 13 discrete natural periods T_i(i=1,2, $\cdots$,13) from 2 to 20 seconds, was assumed to be represented as

$$S_A(T_i,GC)=a(T_i,GC)\times 10^{b(T_i,GC)M}\times(\Delta+30)^{c(T_i,GC)} \tag{12}$$

where coefficients $a(T_i,GC)$, $b(T_i,GC)$ and $c(T_i,GC)$ are the constants to be determined by multiple regression analysis for each natural period T_i, and are dependent on subsoil conditions.

Table 3 shows the coefficients $a(T_i,GC)$, $b(T_i,GC)$ and $c(T_i,GC)$ together with the correlation coefficient $R(T_i,GC)$. The variation of coefficient b in accordance with natural period is almost same for the cases of damping ratio of 0.02 and 0.05 to the critical. It is the same with the variation of coefficient c. These facts indicate that the response spectral shape of the damping ratio of 0.02 to the critical and that of 0.05 are similar for an arbitrary combination of earthquake magnitude and epicentral distance. Fig.4 shows the coefficients $a(T_i,GC)$, $b(T_i,GC)$ and $c(T_i,GC)$ for the case of damping ratio of 0.05 to

the critical. Fig.5 shows the coefficients a, b and c of the attenuation equation of acceleration response spectra derived from SMAC accelerograph records[3]. Comparing Figs.4 and 5, the followings are pointed out.

1)The coefficient b obtained from JMA low-magnification seismograph records, which represents the effect of earthquake magnitude on the absolute acceleration response spectral amplitude, shows variation with natural period. The coefficient b of attenuation equation of acceleration response spectra based on SMAC accelerograms, which is obtained for the natural period of 0.1 to 3 seconds, increases almost monotonously with natural period. The maximum values of coefficient b for SMAC accelerograph records is 0.45 to 0.65, whereas the coefficient b derived from JMA low-magnification seismograms is relatively large.
2)As for ground group 1, the coefficient c derived from JMA low-magnification seismograph records, which represents the attenuation rate of spectral amplitude with epicentral distance, increases almost monotonously with natural period. This signifies that the attenuation of long period component of ground motion is small. As for ground groups 2 and 3, the coefficient c takes peak value at natural period of 10 seconds.

Fig.6 shows an example of acceleration response spectra predicted from Eq.(12) for a combination of earthquake magnitude of 8.0 and epicentral distance of 150 km. As seen from Fig.6, response spectral amplitude becomes large in the order of ground group 1, 2 and 3.

APPLICATION TO THE SEISMIC DESIGN OF LARGE-SCALE STRUCTURES

The input ground motion considered in the seismic design of substructure of the Akashi-Kaikyou bridge, one of the Honsyu-Shikoku bridges with a span of 1990 m, is derived from an earthquake of magnitude 8.5 with epicentral distance of 150 km. In this paper, the design spectrum for the seismic design of superstructure of the Akashi-Kaikyou bridge is proposed, using the attenuation equation of acceleration response spectra derived from JMA low-magnification seismograph records. Since it is considered consistent that the design spectra for the substructure and superstructure of a bridge are derived from same earthquake, the design spectrum for the superstructure of the Akashi-Kaikyou bridge is proposed for the same combination of earthquake magnitude and epicentral distance with the substructure.

Fig.7 shows a comparison of acceleration response spectra derived from SMAC accelerograph records and JMA low-magnification seismograph records, in which earthquake magnitude is 7.0, 8.0 and 8.5, and epicentral distance is 150 km. The subsoil condition was considered as ground group 1 for both attenuation equations of SMAC accelerograph records[3] and JMA low-magnification seismograph records. It is seen from Fig.7 that the acceleration response spectrum for magnitude of 8.5 derived from JMA low-magnification seismograms is considerably larger than the extension of the response spectrum derived from SMAC accelerograms. This is mainly due to the fact that the coefficient b of the attenuation equation of JMA low-magnification seismograph records is large and the spectral amplitude estimated from Eq.(12) with a large magnitude of 8.5 shows large value.

Considering the continuity with the attenuation equation of SMAC accelerograms, a modified attenuation equation for JMA low-magnification seismograph records was proposed. As seen from Fig.5, the coefficient b of the attenuation equation of SMAC accelerograph records for ground group 1 changes almost lineally with a logarithm of natural period T[s]. This relation is expressed by least squares fit as

$$b(T)=0.367+0.177\ \log T \tag{13}$$

Assuming that Eq.(13) is effective for the natural period range of 2 to 20 seconds, the coefficient b of the attenuation equation of JMA low-magnification seismograph records was determined at first. Then the coefficients a and c were determined by regression analysis. Table 4 shows the coefficient a(T), b(T) and c(T) together with correlation coefficient R(T). Fig.8 shows acceleration response spectra estimated from the coefficients shown in Table 4. It is seen from Fig.8 that the acceleration response spectra derived from JMA low-magnification seismograms locate on the extensions of response spectra derived from SMAC accelerograms. The acceleration response spectra with damping ratio of 0.02 to the critical are also shown in Fig.8. The acceleration response spectrum with damping ratio of 0.02 to the critical calculated for the combination of earthquake magnitude of 8.5 and epicentral distance of 150 km was proposed as the base of design spectrum for the superstructure of Akashi-Kaikyou bridge.

CONCLUSION

The Japan Meteorological Agency low-magnification seismograph

records obtained during 7 earthquakes were digitized and processed in the period range of 2 to 20 seconds. Results of multiple regression analysis on absolute acceleration response spectra are presented. Attenuation equation of acceleration response spectra in terms of earthquake magnitude and epicentral distance is proposed for three subsoil conditions. As an application of the results, the design spectrum for the seismic design of superstructure of Akashi-Kaikyou bridge is proposed. The result of presenting study might be expected to provide a fundamental information for assessing the ground motion characteristics in the long period range.

ACKNOWLEDGEMENT

The authors would like to express their sincere thanks to the personnel of the Japan Meteorological Agency for allowing the use of the data for this analysis.

REFERENCES

[1]Public Works Research Institute, "A Proposal for Earthquake Resistant Design Method", Technical Memorandum of PWRI, No.1185, March, 1977(in Japanese)

[2]Katayama T., Iwasaki T. and Saeki M., "Statistical Analysis of Earthquake Acceleration Response Spectra", Proc. of Japan Society of Civil Engineers, No.275, July, 1978(in Japanese)

[3]Kawashima K., Aizawa K. and Takahashi K., "Attenuation of Peak Ground Motion and Absolute Acceleration Response Spectra", Proc. of Eighth World Conference on Earthquake Engineering, July, 1984

[4]Japan Society of Civil Engineers, "Earthquake Resistant Design for Civil Engineering Structures in Japan", 1988

[5]Kawashima K., Takagi Y. and Aizawa K., "Procedure of Instrument Correction and Displacement Calculation for SMAC-B2 Accelerograph Records with Considering Accuracy of Digitization", Proc. of Japan Society of Civil Engineers, No.325, September, 1982(in Japanese)

[6]Sasaki Y., Tamura K. and Aizawa K., "Analysis of Long-Period Ground Motions based on Displacement Seismograph Records by JMA", Technical Memorandum of PWRI, No.2664, August, 1988(in Japanese)

[7]Okada S. and Kagami H., "A Point-by-Point Evaluation of Amplification Characteristics in Japan on 1 to 10 sec Seismic Motions in relation to

Deep Soil Deposits", Transactions of the Architectural Institute of Japan, No.267, May, 1978(in Japanese)
[8]Japan Society of Civil Engineers, "A Survey on Displacement Characteristics of Input Ground Motions for the Seismic Design of Storage Tanks", December, 1982(in Japanese)
[9]Sasaki Y., Tamura K., Aizawa K. and Takahashi K., "Experimental Study on Recording Accuracy of JMA Seismograph", Technical Memorandum of PWRI, No.2386, June, 1986(in Japanese)

Table 1 Earthquakes and Records Analyzed

Earthquake	Date	M	Number of Components		
			Horizontal	Vertical	Total
Niigata	1964.6.16	7.5	50	22	72
Hyuganada	1968.4. 1	7.5	33	18	51
Tokachi-Oki	1968.5.16	7.9	27	14	41
Tokachi-Oki(AS)	1968.5.16	7.5	6	3	9
Miyagiken-Oki	1978.6.12	7.4	38	19	57
Nihonkai-Chubu	1983.5.26	7.7	43	21	64
Nihonkai-Chubu(AS)	1983.6.21	7.1	20	11	31
Total			217	108	325

AS : Aftershock

Table 2 Classification of Subsoil Conditions

Group	Ground Characteristic Index	Number of Records
1	～0.67	29
2	0.67～1.50	46
3	1.50～	22
Total		97

Table 3(1) Coefficients of Attenuation Equation

(a) Damping Ratio h=0.05

Natural Period T[s]	Ground Group	Coefficient a(T)	Coefficient b(T)	Coefficient c(T)	Correla. Coeffi. R(T)
T= 2.0	All Data	9.494E+00	0.4318	-1.2711	0.5021
	Group 1	1.929E-01	0.7799	-1.7577	0.7082
	Group 2	9.123E-01	0.6910	-1.6414	0.6712
	Group 3	1.159E+00	0.8552	-2.0462	0.7567
T= 2.5	All Data	1.519E+01	0.3905	-1.2486	0.4941
	Group 1	6.614E-01	0.7487	-1.9005	0.7415
	Group 2	2.130E+00	0.6306	-1.6296	0.6707
	Group 3	3.019E-01	0.8364	-1.7766	0.7037
T= 3.0	All Data	2.446E+00	0.4029	-0.9995	0.4555
	Group 1	4.485E-01	0.6892	-1.6756	0.7518
	Group 2	1.037E-01	0.6904	-1.3175	0.6568
	Group 3	1.865E-01	0.7707	-1.5353	0.6204
T= 4.0	All Data	3.151E+00	0.2655	-0.6801	0.3336
	Group 1	1.692E-01	0.6499	-1.4393	0.7743
	Group 2	7.097E-02	0.5775	-0.9675	0.5401
	Group 3	5.900E+00	0.4403	-1.1908	0.5312
T= 5.0	All Data	1.854E-01	0.4027	-0.6374	0.3421
	Group 1	2.316E-03	0.8109	-1.2132	0.7645
	Group 2	8.325E-03	0.6727	-0.9179	0.5118
	Group 3	3.835E-01	0.6861	-1.4791	0.6291
T= 6.0	All Data	1.407E-01	0.3830	-0.5719	0.3563
	Group 1	1.882E-03	0.7764	-1.0993	0.7754
	Group 2	8.305E-03	0.6193	-0.8002	0.5017
	Group 3	8.836E-01	0.5490	-1.2725	0.6495
T= 7.0	All Data	1.835E-01	0.3413	-0.5129	0.3317
	Group 1	3.475E-02	0.6342	-1.1848	0.7279
	Group 2	1.138E-03	0.6896	-0.6942	0.5091
	Group 3	7.026E+00	0.3192	-0.9765	0.5171
T= 8.0	All Data	2.412E-02	0.4263	-0.4344	0.3447
	Group 1	4.598E-02	0.6002	-1.1382	0.6692
	Group 2	1.665E-05	0.8899	-0.5873	0.5909
	Group 3	3.457E+00	0.3237	-0.8894	0.4319
T= 9.0	All Data	5.453E-03	0.4918	-0.3851	0.3534
	Group 1	2.493E-01	0.4853	-1.0816	0.6057
	Group 2	1.934E-06	0.9938	-0.5414	0.5923
	Group 3	4.946E-02	0.4910	-0.6756	0.3592
T=10.0	All Data	3.769E-04	0.6052	-0.2734	0.3796
	Group 1	4.344E-02	0.5372	-0.9398	0.5678
	Group 2	3.065E-07	1.0463	-0.3885	0.5759
	Group 3	3.340E-04	0.7559	-0.6174	0.3978
T=13.0	All Data	1.313E-05	0.8431	-0.4804	0.5129
	Group 1	2.157E-05	0.9448	-0.9041	0.7086
	Group 2	2.278E-08	1.2197	-0.5275	0.6229
	Group 3	2.759E-02	0.5032	-0.7390	0.3161
T=16.0	All Data	6.150E-07	1.0558	-0.6509	0.6185
	Group 1	6.059E-06	1.0523	-1.0641	0.7867
	Group 2	1.264E-09	1.4059	-0.6360	0.6650
	Group 3	6.864E-04	0.7069	-0.8006	0.4050
T=20.0	All Data	7.179E-08	1.1800	-0.7236	0.6707
	Group 1	1.995E-07	1.1756	-0.9143	0.8201
	Group 2	7.790E-11	1.6106	-0.8402	0.7112
	Group 3	3.646E-04	0.7558	-0.9078	0.4830

Attenuation Equation : $S_A(T) = a(T) \times 10^{b(T)M} \times (\Delta+30)^{c(T)}$

Table 3(2) Coefficients of Attenuation Equation

(b) Damping Ratio h=0.02

Natural Period T[s]	Ground Group	Coefficient a(T)	Coefficient b(T)	Coefficient c(T)	Correla. Coeffi. R(T)
T= 2.0	All Data	8.673E+00	0.4500	-1.2500	0.4848
	Group 1	1.049E-01	0.7924	-1.6345	0.6708
	Group 2	3.285E-01	0.7964	-1.7195	0.6811
	Group 3	3.934E+00	0.8014	-2.0344	0.7705
T= 2.5	All Data	1.469E+01	0.4139	-1.2609	0.4863
	Group 1	1.631E+00	0.7469	-2.0075	0.7447
	Group 2	1.418E+00	0.6760	-1.6372	0.6419
	Group 3	2.190E-01	0.8512	-1.7191	0.7113
T= 3.0	All Data	1.224E+00	0.4481	-0.9650	0.4481
	Group 1	1.069E-01	0.7510	-1.5579	0.7485
	Group 2	5.245E-02	0.7386	-1.2963	0.6468
	Group 3	1.902E-01	0.7985	-1.5685	0.6075
T= 4.0	All Data	2.674E+00	0.2506	-0.5565	0.2851
	Group 1	1.618E-01	0.6435	-1.3646	0.7666
	Group 2	5.636E-02	0.5735	-0.8646	0.5072
	Group 3	4.134E+00	0.4045	-0.9719	0.4731
T= 5.0	All Data	1.982E-01	0.4014	-0.5957	0.3170
	Group 1	4.581E-03	0.7845	-1.2047	0.7379
	Group 2	6.735E-03	0.6767	-0.8436	0.4685
	Group 3	2.687E-01	0.7516	-1.5589	0.6381
T= 6.0	All Data	9.605E-02	0.3939	-0.4935	0.3234
	Group 1	5.829E-04	0.8218	-0.9901	0.7474
	Group 2	1.545E-02	0.5733	-0.7239	0.4459
	Group 3	1.977E-01	0.6492	-1.2628	0.6402
T= 7.0	All Data	3.377E-01	0.3010	-0.4568	0.2814
	Group 1	1.608E-02	0.6727	-1.1319	0.7209
	Group 2	2.363E-03	0.6341	-0.6142	0.4530
	Group 3	5.331E+01	0.2549	-1.0851	0.5176
T= 8.0	All Data	2.581E-02	0.4175	-0.3802	0.3121
	Group 1	3.582E-02	0.6040	-1.0682	0.6447
	Group 2	4.735E-06	0.9597	-0.5434	0.5988
	Group 3	3.659E+01	0.2283	-0.9644	0.4310
T= 9.0	All Data	4.204E-03	0.5014	-0.3260	0.3349
	Group 1	3.051E-01	0.4852	-1.0727	0.5547
	Group 2	5.465E-07	1.0512	-0.4552	0.6049
	Group 3	1.370E-01	0.4468	-0.6735	0.3299
T=10.0	All Data	2.465E-04	0.5911	-0.1094	0.3452
	Group 1	1.308E-01	0.4706	-0.8863	0.5138
	Group 2	7.665E-08	1.0759	-0.1896	0.5775
	Group 3	1.304E-04	0.8025	-0.5386	0.3687
T=13.0	All Data	3.297E-06	0.9251	-0.4521	0.5325
	Group 1	4.973E-06	1.0667	-0.9842	0.7382
	Group 2	6.639E-09	1.2755	-0.4472	0.6288
	Group 3	1.007E-02	0.5591	-0.6974	0.3177
T=16.0	All Data	1.473E-07	1.1287	-0.5901	0.6286
	Group 1	1.402E-06	1.1355	-1.0251	0.8019
	Group 2	3.623E-10	1.4541	-0.5316	0.6673
	Group 3	2.973E-04	0.7333	-0.7097	0.3875
T=20.0	All Data	2.473E-08	1.2334	-0.6694	0.6774
	Group 1	4.275E-08	1.2410	-0.8109	0.8228
	Group 2	2.810E-11	1.6677	-0.8048	0.7136
	Group 3	2.888E-04	0.7335	-0.7776	0.4605

Attenuation Equation : $S_A(T) = a(T) \times 10^{b(T)M} \times (\Delta+30)^{c(T)}$

Table 4 Coefficients of Modified Attenuation Equation for Ground Group 1

(a) Damping Ratio h=0.05

Natural Period T[s]	Coefficient			Correla. Coeffi. R(T)
	a(T)	b(T)	c(T)	
2.0	5.890E+01	0.4200	-1.6551	0.6172
2.5	9.378E+01	0.4370	-1.8116	0.6747
3.0	1.980E+01	0.4510	-1.6077	0.6867
4.0	2.818E+00	0.4730	-1.3888	0.7050
5.0	3.800E-01	0.4900	-1.1217	0.5926
6.0	1.429E-01	0.5040	-1.0217	0.5982
7.0	2.276E-01	0.5160	-1.1511	0.6350
8.0	1.496E-01	0.5260	-1.1171	0.5813
9.0	1.132E-01	0.5350	-1.0958	0.5540
10.0	3.960E-02	0.5430	-0.9415	0.4749
13.0	9.175E-03	0.5640	-0.7955	0.3982
16.0	1.122E-02	0.5790	-0.9292	0.4751
20.0	1.968E-03	0.5970	-0.7493	0.3939

(b) Damping Ratio h=0.02

Natural Period T[s]	Coefficient			Correla. Coeffi. R(T)
	a(T)	b(T)	c(T)	
2.0	3.906E+01	0.4200	-1.5283	0.5632
2.5	2.250E+02	0.4370	-1.9192	0.6858
3.0	1.259E+01	0.4510	-1.4724	0.6510
4.0	2.432E+00	0.4730	-1.3160	0.6908
5.0	4.945E-01	0.4900	-1.1207	0.5757
6.0	9.108E-02	0.5040	-0.8995	0.5122
7.0	1.942E-01	0.5160	-1.0872	0.6011
8.0	1.238E-01	0.5260	-1.0459	0.5427
9.0	1.382E-01	0.5350	-1.0869	0.5027
10.0	4.135E-02	0.5430	-0.9070	0.4432
13.0	1.470E-02	0.5640	-0.8409	0.3942
16.0	9.747E-03	0.5790	-0.8664	0.4348
20.0	1.194E-03	0.5970	-0.6273	0.3220

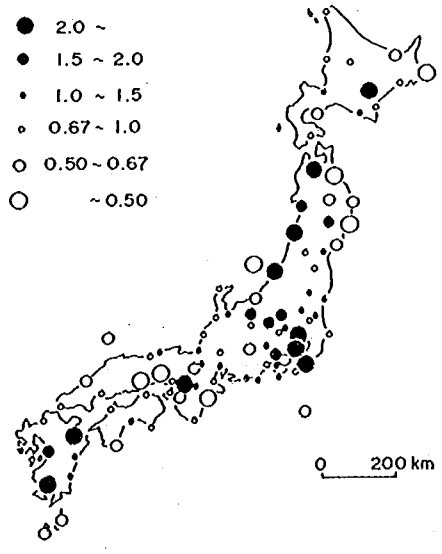


Fig.1 Distribution of Ground Characteristic Indexes[7]

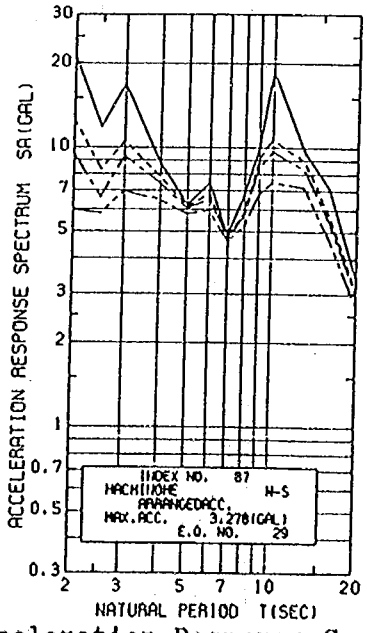


Fig.3 Acceleration Response Spectra of Hachinohe Record (h=0, 0.01, 0.02, 0.05)

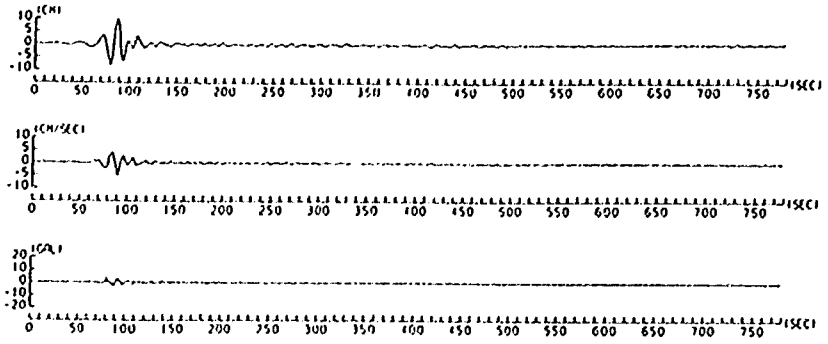
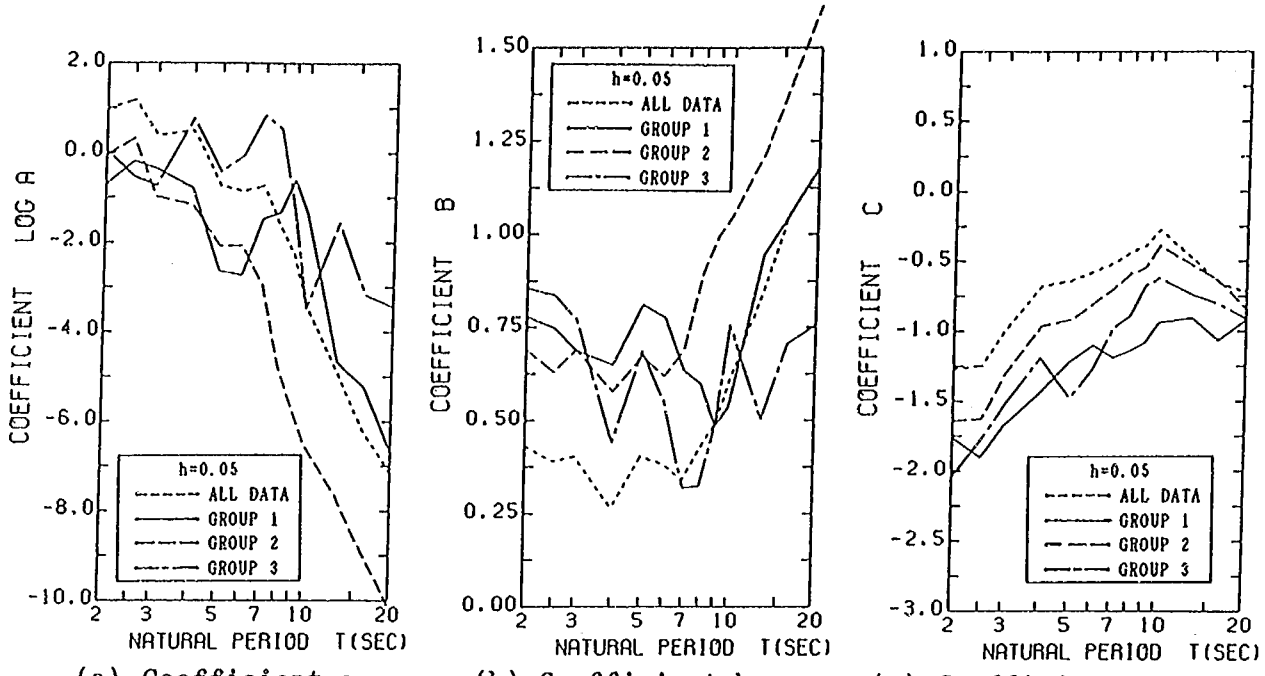
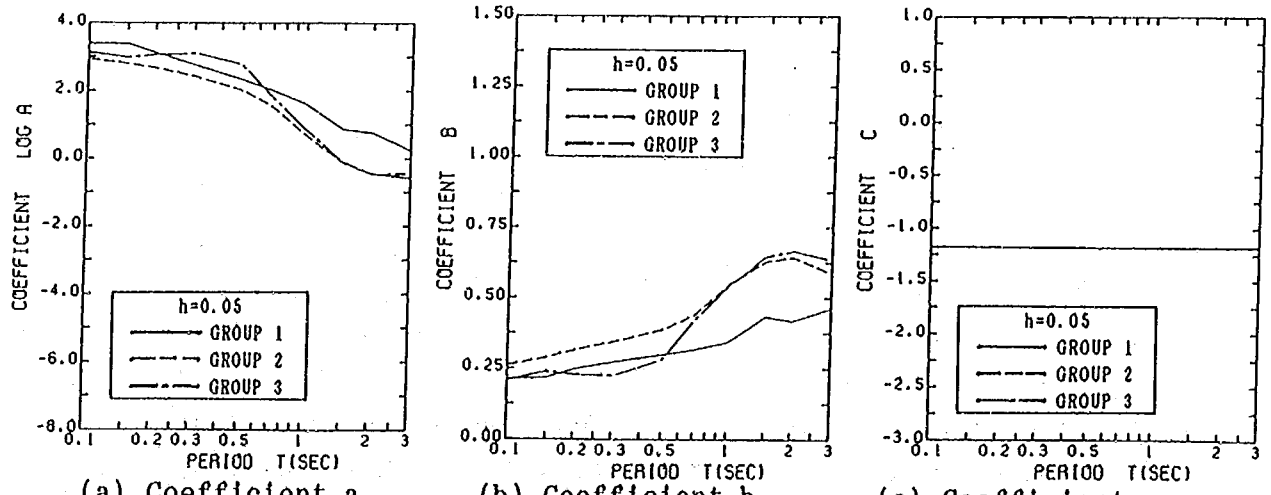


Fig.2 Displacement, Velocity and Acceleration Recorded at Hachinohe during Nihonkai-Chubu Earthquake of 1983



(a) Coefficient a (b) Coefficient b (c) Coefficient c

Fig.4 Coefficients of Attenuation Equation Derived from JMA Seismograms



(a) Coefficient a (b) Coefficient b (c) Coefficient c

Fig.5 Coefficients of Attenuation Eq. Derived from SMAC Accelerograms

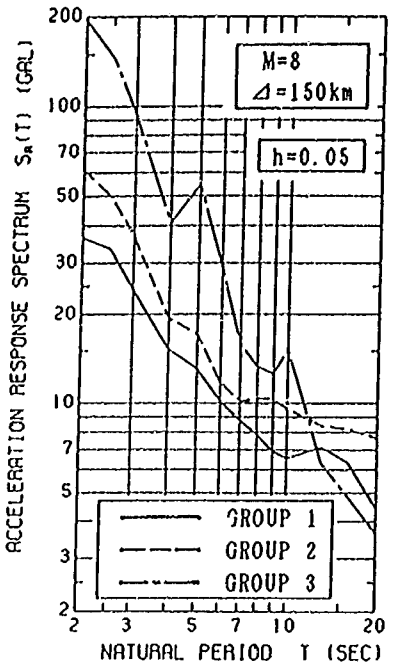


Fig.6 Acceleration Response Spectra Predicted by Attenuation Equation

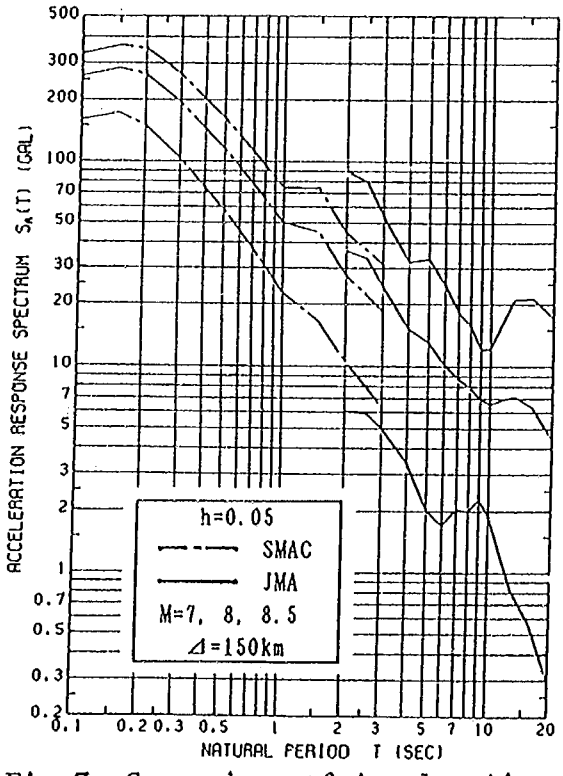


Fig.7 Comparison of Acceleration Response Spectra Predicted by Attenuation Equation of JMA Seismograms and SMAC Accelerograms (Damping Ratio h=0.05)

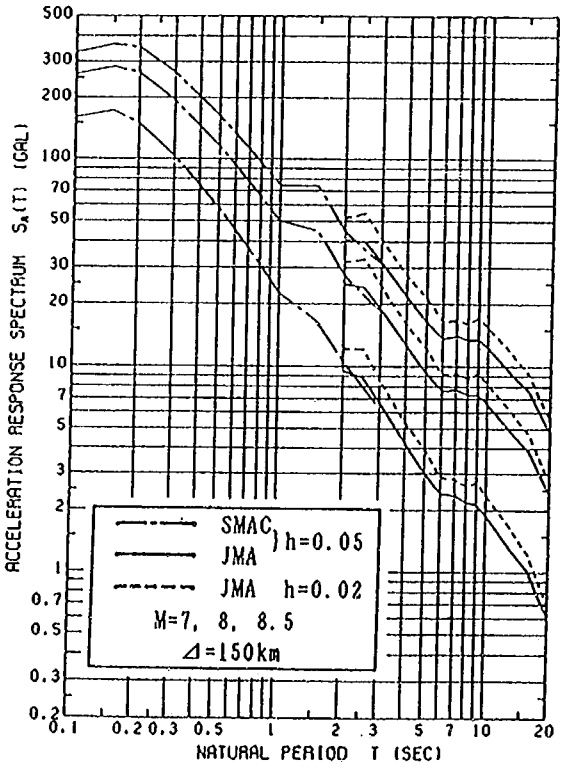


Fig.8 Acceleration Response Spectra Predicted by Modified Attenuation Equation of JMA Seismograms with Damping Ratio h=0.05, 0.02

ATTENUATION CHARACTERISTICS OF GROUND MOTIONS IN THE PERIOD RANGE OF 2 TO 20 SECONDS - FOR APPLICATION TO THE SEISMIC DESIGN OF LARGE-SCALE STRUCTURES -

Yasushi SASAKI[1], Keiichi TAMURA[2] and Koh AIZAWA[3]

1 Director, Earthquake Disaster Prevention Department, Public Works Research Institute, Ministry of Construction, Tsukuba-shi, Ibaraki-ken, Japan
2 Research Engineer, Ground Vibration Division, ditto
3 Ground Vibration Division, ditto

INTRODUCTION

Not a few studies on ground motion characteristics from the engineering point of view have been conducted with the records obtained by SMAC accelerograph in Japan[1,2,3]. As a result, attenuation equations of peak ground motions and earthquake response spectra have been proposed and they are applied to the seismic design of structures[4]. The fundamental natural period of civil engineering structures is generally short and few exceed 2 or 3 seconds. However, the natural period of large-scale structures such as long-span suspension bridge exceeds 2 or 3 seconds. The reliable period range of the records provided by SMAC accelerograph, which is a mechanical type accelerograph with natural frequency of pendulum of 7.14 Hz and with critical damping, is limited to 0.08 to 3 seconds[5]. For determining appropriate seismic input motion to be applied to the design of large-scale structures, it is indispensable to consider the characteristics of ground motions in the long period range carefully.

In this paper, records of the Japan Meteorological Agency (JMA) low-magnification seismograph were digitized and the characteristics of ground motions in the long period range are discussed. The empirical formulae of attenuation equation of absolute acceleration response spectra are proposed by multiple regression analysis of 97 horizontal JMA low-magnification seismograph records. Considering the continuity with acceleration response spectra derived from SMAC accelerogram, a modified attenuation equation of acceleration response spectra is also presented and a design spectrum for the seismic design of long suspension bridge is proposed.

GROUND MOTION RECORDS ANALYZED

217 horizontal components and 108 vertical components of JMA low-magnification seismograms were digitized in this study[6]. They were obtained during 7 earthquakes with JMA magnitude of 7.1 to 7.9 (see Table 1). The method of digitization is same with the case of SMAC accelerogram by a manually operated digitizer[5].

The subsoil ground conditions at recording sites were classified into three groups as shown in Table 2. This classification depends on a point-by-point evaluation of amplification characteristic of subsoil structure around the JMA observatory sites[7]. A ground characteristic index was derived from the statistical analysis of the amplitude of JMA low-magnification seismograph records. This index is thought to reflect the characteristic of the deep soil deposits at a site. An index of 1.0 means that the amplification characteristic of the site is average one in Japan. An index more than 1.0 or less than 1.0 means that the amplification characteristic of the site is large or small from the average, respectively. Fig.1 shows a distribution of ground characteristic indexes. The records obtained at sites whose subsoil conditions are unknown, were not included in this analysis. The number of record corresponding to ground groups 1, 2 and 3 are 29, 46 and 22, respectively.

JMA low-magnification seismograph is a mechanical type seismograph with natural period of pendulum of 6 seconds and with damping of 0.55 to the critical. Since the sensitivity of the seismograph in the long period range, such as longer than 10 seconds, is substantially suppressed, the instrumental correction is necessary to use the records for the long period range. The ground velocity and acceleration were calculated by differentiating the corrected displacement in the frequency domain. The procedure of instrumental correction and calculation of velocity and acceleration are as follows[8].

The Fourier transform $F_o(f)$ of the original displacement $d_o(t)$ is written as

$$F_o(f)=\int_{-\infty}^{\infty} d_o(t)\cdot\exp(-i2\pi ft)dt \qquad (1)$$

Introducing correction filter $F_c(f)$, the corrected displacement $d(t)$, velocity $v(t)$ and acceleration $a(t)$ are obtained as

$$d(t)=\int_{-\infty}^{\infty} F(f)\cdot\exp(i2\pi ft)df \qquad (2)$$

$$v(t)=\int_{-\infty}^{\infty} i2\pi fF(f)\cdot\exp(i2\pi ft)df \tag{3}$$

$$a(t)=\int_{-\infty}^{\infty} -4\pi^2 f^2 F(f)\cdot\exp(i2\pi ft)df \tag{4}$$

where

$$F(f)=F_D\cdot F_o(f) \tag{5}$$

$$F_o(f)=[\exp\{i\phi(f)\}/R(f)]\cdot A(f) \tag{6}$$

R(f) and $\phi(f)$ in Eq.(6) are the amplitude and phase characteristic function of the seismograph, and are written as

$$R(f)=1/[\{(f_D/f)^2-1\}^2+4h^2(f_D/f)^2]^{1/2} \tag{7}$$

$$\phi(f)=\tan^{-1}[2h(f_D/f)/\{(f_D/f)^2-1\}] \tag{8}$$

where f_D and h represent natural frequency and damping ratio to the critical, respectively. A(f) in Eq.(6) is the envelope function of correction filter and is expressed in terms of period T as

$$A(T)=\begin{cases} 0 & T<T_{LL} \\ [1-\cos\{(T-T_{LL})\pi/(T_{LU}-T_{LL})\}]/2 & T_{LL}\leqq T\leqq T_{LU} \\ 1 & T_{LU}<T<T_{UL} \\ [1+\cos\{(T-T_{UL})\pi/(T_{UU}-T_{UL})\}]/2 & T_{UL}\leqq T\leqq T_{UU} \\ 0 & T_{UU}<T \end{cases} \tag{9}$$

where T_{LU} and T_{UL} represent lower cut-off period and upper cut-off period, respectively, and T_{LL} and T_{UU} are the periods at which amplitude of correction filter becomes 0 at short and long period range, respectively. Referring to the result of a study on the recording accuracy of JMA low-magnification seismograph[9], cut-off periods were set up as

$$T_{LL}=1.3[s],\ T_{LU}=2[s],\ T_{UL}=20[s],\ T_{UU}=30[s] \tag{10}$$

Consequently, it is necessary to note that the ground motion characteristics discussed in this paper are limited to the characteristics in the period range of 2 to 20 seconds.

Fig.2 shows an example of corrected displacement, velocity and acceleration waveform. It is seen from Fig.2 that big amplitude of displacement is caused by long period component. Fig.3 shows absolute acceleration response spectra derived from the acceleration shown in Fig.2, where damping ratios to the critical were taken as 0.0, 0.01, 0.02 and 0.05.

Resultant of two horizontal orthogonal components of the ground

motion was not considered in this analysis, because the two components of JMA low-magnification seismograph are not synchronous. Larger one of the spectral values calculated from two horizontal components was considered for this study.

ATTENUATION OF ACCELERATION RESPONSE SPECTRA

In the past analyses on attenuation characteristics of maximum peak ground motions and absolute acceleration response spectra, based on accelerograph records, the following empirical formula is often used[3].

$$X=a\times 10^{bM}\times(\Delta+\Delta_0)^{c} \tag{11}$$

where

X: Maximum acceleration, velocity and displacement / Absolute acceleration response spectral amplitude

M: Magnitude of earthquake

Δ : Epicentral distance [km]

Δ_0: Constant to adjust X for small Δ

a, b, c: Coefficient

The same expression with Eq.(11) was assumed to represent the attenuation characteristics of absolute acceleration response spectra derived from JMA low-magnification seismograph records. Δ_0 in Eq.(11) was assumed to be 30 km. Acceleration response spectral amplitude $S_A(T_i)$[gal] with damping ratio of 0.02 and 0.05 to the critical at 13 discrete natural periods $T_i(i=1,2,\cdots,13)$ from 2 to 20 seconds, was assumed to be represented as

$$S_A(T_i,GC)=a(T_i,GC)\times 10^{b(T_i,GC)M}\times(\Delta+30)^{c(T_i,GC)} \tag{12}$$

where coefficients $a(T_i,GC)$, $b(T_i,GC)$ and $c(T_i,GC)$ are the constants to be determined by multiple regression analysis for each natural period T_i, and are dependent on subsoil conditions.

Table 3 shows the coefficients $a(T_i,GC)$, $b(T_i,GC)$ and $c(T_i,GC)$ together with the correlation coefficient $R(T_i,GC)$. The variation of coefficient b in accordance with natural period is almost same for the cases of damping ratio of 0.02 and 0.05 to the critical. It is the same with the variation of coefficient c. These facts indicate that the response spectral shape of the damping ratio of 0.02 to the critical and that of 0.05 are similar for an arbitrary combination of earthquake magnitude and epicentral distance. Fig.4 shows the coefficients $a(T_i,GC)$, $b(T_i,GC)$ and $c(T_i,GC)$ for the case of damping ratio of 0.05 to

the critical. Fig.5 shows the coefficients a, b and c of the attenuation equation of acceleration response spectra derived from SMAC accelerograph records[3]. Comparing Figs.4 and 5, the followings are pointed out.

1)The coefficient b obtained from JMA low-magnification seismograph records, which represents the effect of earthquake magnitude on the absolute acceleration response spectral amplitude, shows variation with natural period. The coefficient b of attenuation equation of acceleration response spectra based on SMAC accelerograms, which is obtained for the natural period of 0.1 to 3 seconds, increases almost monotonously with natural period. The maximum values of coefficient b for SMAC accelerograph records is 0.45 to 0.65, whereas the coefficient b derived from JMA low-magnification seismograms is relatively large.
2)As for ground group 1, the coefficient c derived from JMA low-magnification seismograph records, which represents the attenuation rate of spectral amplitude with epicentral distance, increases almost monotonously with natural period. This signifies that the attenuation of long period component of ground motion is small. As for ground groups 2 and 3, the coefficient c takes peak value at natural period of 10 seconds.

Fig.6 shows an example of acceleration response spectra predicted from Eq.(12) for a combination of earthquake magnitude of 8.0 and epicentral distance of 150 km. As seen from Fig.6, response spectral amplitude becomes large in the order of ground group 1, 2 and 3.

APPLICATION TO THE SEISMIC DESIGN OF LARGE-SCALE STRUCTURES

The input ground motion considered in the seismic design of substructure of the Akashi-Kaikyou bridge, one of the Honsyu-Shikoku bridges with a span of 1990 m, is derived from an earthquake of magnitude 8.5 with epicentral distance of 150 km. In this paper, the design spectrum for the seismic design of superstructure of the Akashi-Kaikyou bridge is proposed, using the attenuation equation of acceleration response spectra derived from JMA low-magnification seismograph records. Since it is considered consistent that the design spectra for the substructure and superstructure of a bridge are derived from same earthquake, the design spectrum for the superstructure of the Akashi-Kaikyou bridge is proposed for the same combination of earthquake magnitude and epicentral distance with the substructure.

Fig.7 shows a comparison of acceleration response spectra derived from SMAC accelerograph records and JMA low-magnification seismograph records, in which earthquake magnitude is 7.0, 8.0 and 8.5, and epicentral distance is 150 km. The subsoil condition was considered as ground group 1 for both attenuation equations of SMAC accelerograph records[3] and JMA low-magnification seismograph records. It is seen from Fig.7 that the acceleration response spectrum for magnitude of 8.5 derived from JMA low-magnification seismograms is considerably larger than the extension of the response spectrum derived from SMAC accelerograms. This is mainly due to the fact that the coefficient b of the attenuation equation of JMA low-magnification seismograph records is large and the spectral amplitude estimated from Eq.(12) with a large magnitude of 8.5 shows large value.

Considering the continuity with the attenuation equation of SMAC accelerograms, a modified attenuation equation for JMA low-magnification seismograph records was proposed. As seen from Fig.5, the coefficient b of the attenuation equation of SMAC accelerograph records for ground group 1 changes almost lineally with a logarithm of natural period T[s]. This relation is expressed by least squares fit as

$$b(T)=0.367+0.177\ \log T \tag{13}$$

Assuming that Eq.(13) is effective for the natural period range of 2 to 20 seconds, the coefficient b of the attenuation equation of JMA low-magnification seismograph records was determined at first. Then the coefficients a and c were determined by regression analysis. Table 4 shows the coefficient a(T), b(T) and c(T) together with correlation coefficient R(T). Fig.8 shows acceleration response spectra estimated from the coefficients shown in Table 4. It is seen from Fig.8 that the acceleration response spectra derived from JMA low-magnification seismograms locate on the extension of response spectra derived from SMAC accelerograms. The acceleration response spectra with damping ratio of 0.02 to the critical are also shown in Fig.8. The acceleration response spectrum with damping ratio 0.02 to the critical calculated for the combination of earthquake magnitude of 8.5 and epicentral distance of 150 km was proposed as the base of design spectrum for the superstructure of Akashi-Kaikyou bridge.

CONCLUSION

The Japan Meteorological Agency low-magnification seismograph

records obtained during seven earthquakes were digitized and processed in the period range of 2 to 20 seconds. Results of multiple regression analysis on absolute acceleration response spectra are presented. Attenuation equation of acceleration response spectra in terms of earthquake magnitude, epicentral distance are proposed. As an application of the results, the design spectrum for the seismic design of superstructure of long suspension bridge is proposed. The result of presenting study might be expected to provide a fundamental information for assessing the ground motion characteristics in the long period range.

ACKNOWLEDGEMENT

The authors would like to express their sincere thanks to the personnel of the Japan Meteorological Agency for allowing the use of the data for this analysis.

REFERENCES

[1]Public Works Research Institute, "A Proposal for Earthquake Resistant Design Method", Technical Memorandum of PWRI, No.1185, March, 1977(in Japanese)

[2]Katayama T., Iwasaki T. and Saeki M., "Statistical Analysis of Earthquake Acceleration Response Spectra", Proc. of Japan Society of Civil Engineers, No.275, July, 1978(in Japanese)

[3]Kawashima K., Aizawa K. and Takahashi K., "Attenuation of Peak Ground Motion and Absolute Acceleration Response Spectra", Proc. of Eighth World Conference on Earthquake Engineering, July, 1984

[4]Japan Society of Civil Engineers, "Earthquake Resistant Design for Civil Engineering Structures in Japan", 1988

[5]Kawashima K., Takagi Y. and Aizawa K., "Procedure of Instrument Correction and Displacement Calculation for SMAC-B2 Accelerograph Records with Considering Accuracy of Digitization", Proc. of Japan Society of Civil Engineers, No.325, September, 1982(in Japanese)

[6]Sasaki Y., Tamura K. and Aizawa K., "Analysis of Long-Period Ground Motions based on Displacement Seismograph Records by JMA", Technical Memorandum of PWRI, No.2664, August, 1988(in Japanese)

[7]Okada S. and Kagami H., "A Point-by-Point Evaluation of Amplification Characteristics in Japan on 1 to 10 sec Seismic Motions in relation to

Deep Soil Deposits", Transactions of the Architectural Institute of Japan, No.267, May, 1978(in Japanese)
[8]Japan Society of Civil Engineers, "A Survey on Displacement Characteristics of Input Ground Motions for the Seismic Design of Storage Tanks", December, 1982(in Japanese)
[9]Sasaki Y., Tamura K., Aizawa K. and Takahashi K., "Experimental Study on Recording Accuracy of JMA Seismograph", Technical Memorandum of PWRI, No.2386, June, 1986(in Japanese)

Table 1 Earthquakes and Records Analyzed

Earthquake	Date	M	Number of Components		
			Horizontal	Vertical	Total
Niigata	1964. 6. 16	7. 5	50	22	72
Hyuganada	1968. 4. 1	7. 5	33	18	51
Tokachi-Oki	1968. 5. 16.	7. 9	27	14	41
Tokachi-Oki(AS)	1968. 5. 16	7. 5	6	3	9
Miyagiken-Oki	1978. 6. 12	7. 4	38	19	57
Nihonkai-Chubu	1983. 5. 26	7. 7	43	21	64
Nihonkai-Chubu(AS)	1983. 6. 21	7. 1	20	11	31
Total			217	108	325

AS : Aftershock

Table 2 Classification of Subsoil Conditions

Group	Ground Characteristic Index	Number of Records
1	～0. 67	29
2	0. 67～1. 50	46
3	1. 50～	22
Total		97

Table 3(1) Coefficients of Attenuation Equation

(a) Damping Ratio h=0.05

Natural Period T[s]	Ground Group	Coefficient a(T)	Coefficient b(T)	Coefficient c(T)	Correla. Coeffi. R(T)
T= 2.0	All Data	9.494E+00	0.4318	-1.2711	0.5021
	Group 1	1.929E-01	0.7799	-1.7577	0.7082
	Group 2	9.123E-01	0.6910	-1.6414	0.6712
	Group 3	1.159E+00	0.8552	-2.0462	0.7567
T= 2.5	All Data	1.519E+01	0.3905	-1.2486	0.4941
	Group 1	6.614E-01	0.7487	-1.9005	0.7415
	Group 2	2.130E+00	0.6306	-1.6296	0.6707
	Group 3	3.019E-01	0.8364	-1.7766	0.7037
T= 3.0	All Data	2.446E+00	0.4029	-0.9995	0.4555
	Group 1	4.485E-01	0.6892	-1.6756	0.7518
	Group 2	1.037E-01	0.6904	-1.3175	0.6568
	Group 3	1.865E-01	0.7707	-1.5353	0.6204
T= 4.0	All Data	3.151E+00	0.2655	-0.6801	0.3336
	Group 1	1.692E-01	0.6499	-1.4393	0.7743
	Group 2	7.097E-02	0.5775	-0.9675	0.5401
	Group 3	5.900E+00	0.4403	-1.1908	0.5312
T= 5.0	All Data	1.854E-01	0.4027	-0.6374	0.3421
	Group 1	2.316E-03	0.8109	-1.2132	0.7645
	Group 2	8.325E-03	0.6727	-0.9179	0.5118
	Group 3	3.835E-01	0.6861	-1.4791	0.6291
T= 6.0	All Data	1.407E-01	0.3830	-0.5719	0.3563
	Group 1	1.882E-03	0.7764	-1.0993	0.7754
	Group 2	8.305E-03	0.6193	-0.8002	0.5017
	Group 3	8.836E-01	0.5490	-1.2725	0.6495
T= 7.0	All Data	1.835E-01	0.3413	-0.5129	0.3317
	Group 1	3.475E-02	0.6342	-1.1848	0.7279
	Group 2	1.138E-03	0.6896	-0.6942	0.5091
	Group 3	7.026E+00	0.3192	-0.9765	0.5171
T= 8.0	All Data	2.412E-02	0.4263	-0.4344	0.3447
	Group 1	4.598E-02	0.6002	-1.1382	0.6692
	Group 2	1.665E-05	0.8899	-0.5873	0.5909
	Group 3	3.457E+00	0.3237	-0.8894	0.4319
T= 9.0	All Data	5.453E-03	0.4918	-0.3851	0.3534
	Group 1	2.493E-01	0.4853	-1.0816	0.6057
	Group 2	1.934E-06	0.9938	-0.5414	0..5923
	Group 3	4.946E-02	0.4910	-0.6756	0.3592
T=10.0	All Data	3.769E-04	0.6052	-0.2734	0.3796
	Group 1	4.344E-02	0.5372	-0.9398	0.5678
	Group 2	3.065E-07	1.0463	-0.3885	0.5759
	Group 3	3.340E-04	0.7559	-0.6174	0.3978
T=13.0	All Data	1.313E-05	0.8431	-0.4804	0.5129
	Group 1	2.157E-05	0.9448	-0.9041	0.7086
	Group 2	2.278E-08	1.2197	-0.5275	0.6229
	Group 3	2.759E-02	0.5032	-0.7390	0.3161
T=16.0	All Data	6.150E-07	1.0558	-0.6509	0.6185
	Group 1	6.059E-06	1.0523	-1.0641	0.7867
	Group 2	1.264E-09	1.4059	-0.6360	0.6650
	Group 3	6.864E-04	0.7069	-0.8006	0.4050
T=20.0	All Data	7.179E-08	1.1800	-0.7236	0.6707
	Group 1	1.995E-07	1.1756	-0.9143	0.8201
	Group 2	7.790E-11	1.6106	-0.8402	0.7112
	Group 3	3.646E-04	0.7558	-0.9078	0.4830

Attenuation Equation : $S_A(T) = a(T) \times 10^{b(T)M} \times (\Delta+30)^{c(T)}$

Table 3(2) Coefficients of Attenuation Equation

(b) Damping Ratio h=0.02

Natural Period T[s]	Ground Group	Coefficient a(T)	Coefficient b(T)	Coefficient c(T)	Correla. Coeffi. R(T)
T= 2.0	All Data	8.673E+00	0.4500	-1.2500	0.4848
	Group 1	1.049E-01	0.7924	-1.6345	0.6708
	Group 2	3.285E-01	0.7964	-1.7195	0.6811
	Group 3	3.934E+00	0.8014	-2.0344	0.7705
T= 2.5	All Data	1.469E+01	0.4139	-1.2609	0.4863
	Group 1	1.631E+00	0.7469	-2.0075	0.7447
	Group 2	1.418E+00	0.6760	-1.6372	0.6419
	Group 3	2.190E-01	0.8512	-1.7191	0.7113
T= 3.0	All Data	1.224E+00	0.4481	-0.9650	0.4481
	Group 1	1.069E-01	0.7510	-1.5579	0.7485
	Group 2	5.245E-02	0.7386	-1.2963	0.6468
	Group 3	1.902E-01	0.7985	-1.5685	0.6075
T= 4.0	All Data	2.674E+00	0.2506	-0.5565	0.2851
	Group 1	1.618E-01	0.6435	-1.3646	0.7666
	Group 2	5.636E-02	0.5735	-0.8646	0.5072
	Group 3	4.134E+00	0.4045	-0.9719	0.4731
T= 5.0	All Data	1.982E-01	0.4014	-0.5957	0.3170
	Group 1	4.581E-03	0.7845	-1.2047	0.7379
	Group 2	6.735E-03	0.6767	-0.8436	0.4685
	Group 3	2.687E-01	0.7516	-1.5589	0.6381
T= 6.0	All Data	9.605E-02	0.3939	-0.4935	0.3234
	Group 1	5.829E-04	0.8218	-0.9901	0.7474
	Group 2	1.545E-02	0.5733	-0.7239	0.4459
	Group 3	1.977E-01	0.6492	-1.2628	0.6402
T= 7.0	All Data	3.377E-01	0.3010	-0.4568	0.2814
	Group 1	1.608E-02	0.6727	-1.1319	0.7209
	Group 2	2.363E-03	0.6341	-0.6142	0.4530
	Group 3	5.331E+01	0.2549	-1.0851	0.5176
T= 8.0	All Data	2.581E-02	0.4175	-0.3802	0.3121
	Group 1	3.582E-02	0.6040	-1.0682	0.6447
	Group 2	4.735E-06	0.9597	-0.5434	0.5988
	Group 3	3.659E+01	0.2283	-0.9644	0.4310
T= 9.0	All Data	4.204E-03	0.5014	-0.3260	0.3349
	Group 1	3.051E-01	0.4852	-1.0727	0.5547
	Group 2	5.465E-07	1.0512	-0.4552	0.6049
	Group 3	1.370E-01	0.4468	-0.6735	0.3299
T=10.0	All Data	2.465E-04	0.5911	-0.1094	0.3452
	Group 1	1.308E-01	0.4706	-0.8863	0.5138
	Group 2	7.665E-08	1.0759	-0.1896	0.5775
	Group 3	1.304E-04	0.8025	-0.5386	0.3687
T=13.0	All Data	3.297E-06	0.9251	-0.4521	0.5325
	Group 1	4.973E-06	1.0667	-0.9842	0.7382
	Group 2	6.639E-09	1.2755	-0.4472	0.6288
	Group 3	1.007E-02	0.5591	-0.6974	0.3177
T=16.0	All Data	1.473E-07	1.1287	-0.5901	0.6286
	Group 1	1.402E-06	1.1355	-1.0251	0.8019
	Group 2	3.623E-10	1.4541	-0.5316	0.6673
	Group 3	2.973E-04	0.7333	-0.7097	0.3875
T=20.0	All Data	2.473E-08	1.2334	-0.6694	0.6774
	Group 1	4.275E-08	1.2410	-0.8109	0.8228
	Group 2	2.810E-11	1.6677	-0.8048	0.7136
	Group 3	2.888E-04	0.7335	-0.7776	0.4605

Attenuation Equation : $S_A(T) = a(T) \times 10^{b(T)M} \times (\Delta+30)^{c(T)}$

Table 4 Coefficients of Modified Attenuation Equation for Ground Group 1

(a) Damping Ratio h=0.05

Natural Period T[s]	Coefficient			Correla. Coeffi. R(T)
	a(T)	b(T)	c(T)	
2.0	5.890E+01	0.4200	-1.6551	0.6172
2.5	9.378E+01	0.4370	-1.8116	0.6747
3.0	1.980E+01	0.4510	-1.6077	0.6867
4.0	2.818E+00	0.4730	-1.3888	0.7050
5.0	3.800E-01	0.4900	-1.1217	0.5926
6.0	1.429E-01	0.5040	-1.0217	0.5982
7.0	2.276E-01	0.5160	-1.1511	0.6350
8.0	1.496E-01	0.5260	-1.1171	0.5813
9.0	1.132E-01	0.5350	-1.0958	0.5540
10.0	3.960E-02	0.5430	-0.9415	0.4749
13.0	9.175E-03	0.5640	-0.7955	0.3982
16.0	1.122E-02	0.5790	-0.9292	0.4751
20.0	1.968E-03	0.5970	-0.7493	0.3939

(b) Damping Ratio h=0.02

Natural Period T[s]	Coefficient			Correla. Coeffi. R(T)
	a(T)	b(T)	c(T)	
2.0	3.906E+01	0.4200	-1.5283	0.5632
2.5	2.250E+02	0.4370	-1.9192	0.6858
3.0	1.259E+01	0.4510	-1.4724	0.6510
4.0	2.432E+00	0.4730	-1.3160	0.6908
5.0	4.945E-01	0.4900	-1.1207	0.5757
6.0	9.108E-02	0.5040	-0.8995	0.5122
7.0	1.942E-01	0.5160	-1.0872	0.6011
8.0	1.238E-01	0.5260	-1.0459	0.5427
9.0	1.382E-01	0.5350	-1.0869	0.5027
10.0	4.135E-02	0.5430	-0.9070	0.4432
13.0	1.470E-02	0.5640	-0.8409	0.3942
16.0	9.747E-03	0.5790	-0.8664	0.4348
20.0	1.194E-03	0.5970	-0.6273	0.3220

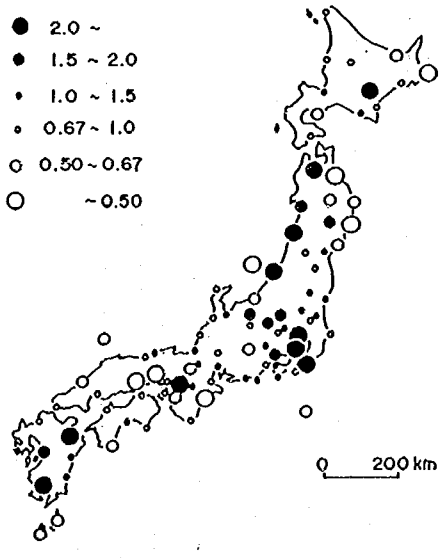


Fig.1 Distribution of Ground Characteristic Indexes[7]

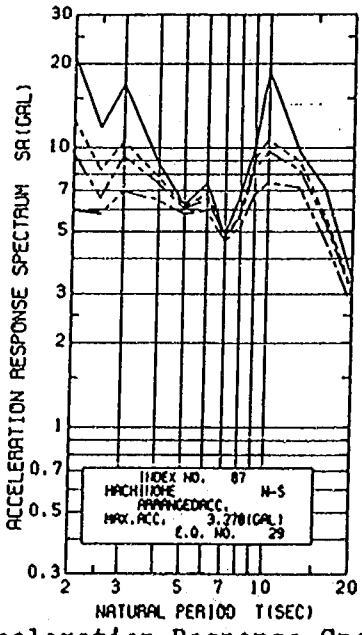


Fig.3 Acceleration Response Spectra of Hachinohe Record (h=0, 0.01, 0.02, 0.05)

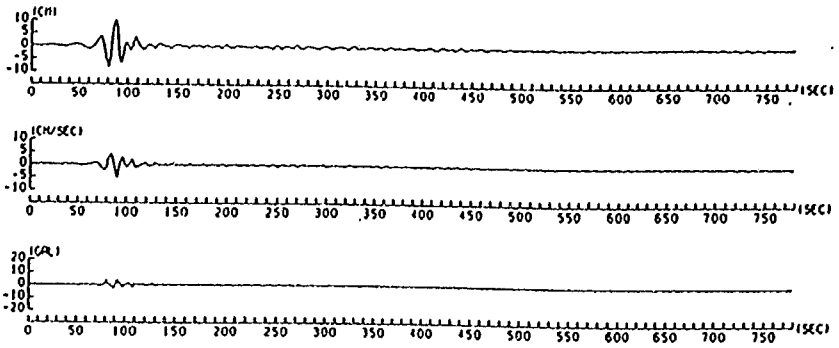
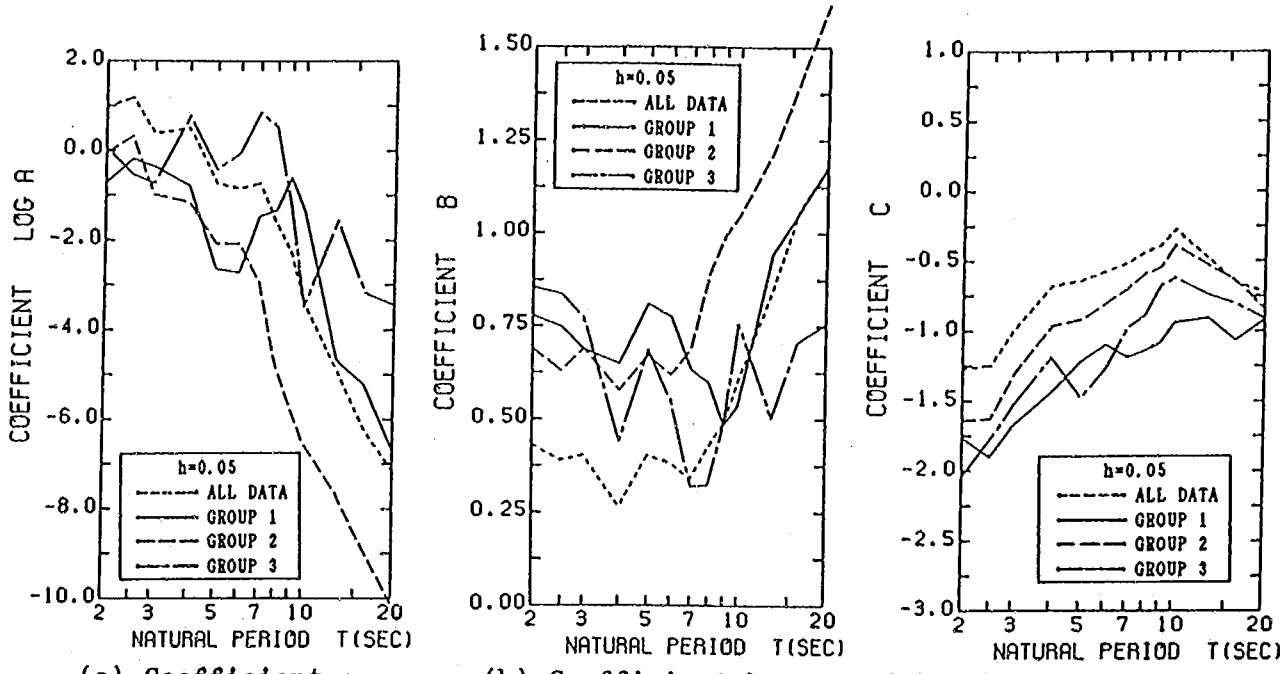
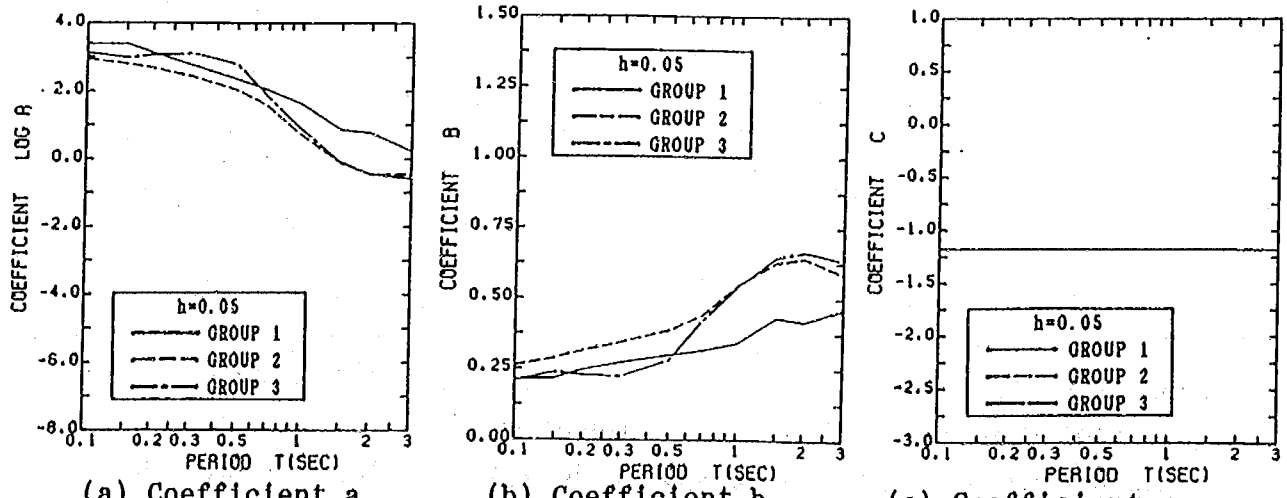


Fig.2 Displacement, Velocity and Acceleration Recorded at Hachinohe during Nihonkai-Chubu Earthquake of 1983



(a) Coefficient a (b) Coefficient b (c) Coefficient c

Fig.4 Coefficients of Attenuation Equation Derived from JMA Seismograms



(a) Coefficient a (b) Coefficient b (c) Coefficient c

Fig.5 Coefficients of Attenuation Eq. Derived from SMAC Accelerograms

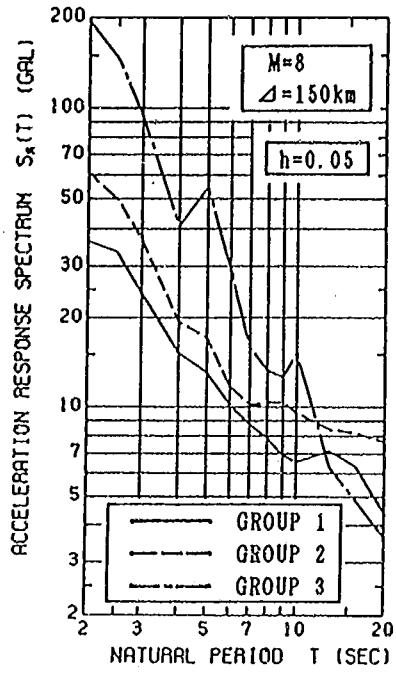


Fig.6 Acceleration Response Spectra Predicted by Attenuation Equation

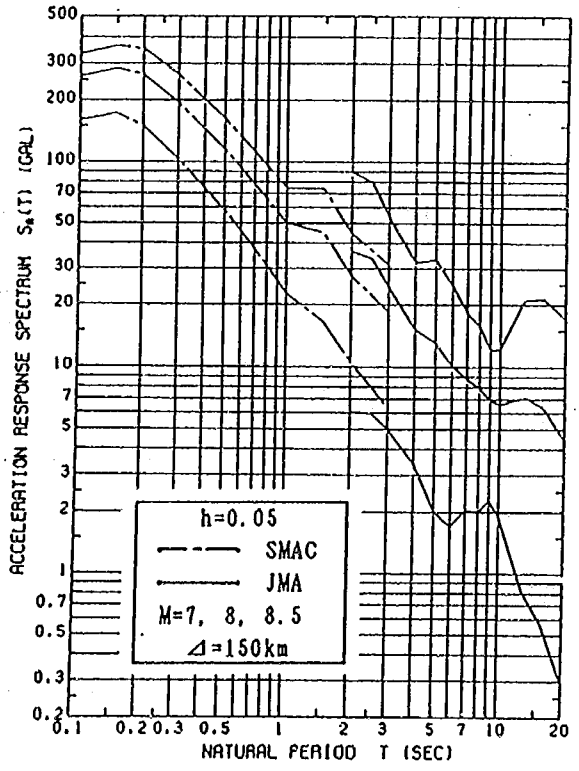


Fig.7 Comparison of Acceleration Response Spectra Predicted by Attenuation Equation of JMA Seismograms and SMAC Accelerograms (Damping Ratio h=0.05)

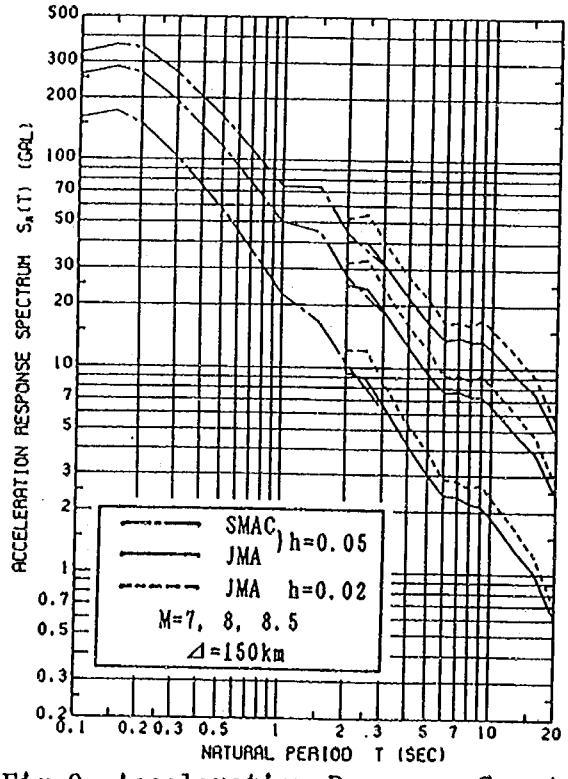


Fig.8 Acceleration Response Spectra Predicted by Modified Attenuation Equation of JMA Seismograms with Damping Ratio h=0.05, 0.02

ON THE ESTIMATION OF LONGITUDINAL LINEAR AND NONLINEAR ABUTMENT STIFFNESSES

by

Emmanuel Maragakis and Bruce Douglas
University of Nevada, Reno

Abstract

The longitudinal stiffness of the bridge abutments is a parameter extensively used for the dynamic analysis of bridges since it affects the longitudinal vibration of the bridge deck. In this paper a simple method is presented for the evaluation of a force displacement diagram of bridge abutments. For the development of the method it was assumed that the abutment can be represented as a uniform rigid plate, and the soil deposits on the two sides of the abutment as Winkler foundation with elastic springs linearly varying with depth. For the evaluation of the yielding of the abutment springs the Rankine Theory of Active Thrust and Passive Resistance was used. The application of the method is demonstrated with the evaluation of the force-displacement diagram of the abutments of a bridge located in Riverside, California.

Introduction

One of the most important parameters for the dynamic analysis of bridges is the stiffness of the abutments. In recent studies by Maragakis, 1984, 1986 (Refs. 1,2), and Maragakis and Jennings, 1987 (Ref. 3), it has been shown that the abutment stiffness is a crucial parameter for modeling the rigid body motions of skew bridges. Also in recent studies by Maragakis et al. (Ref. 4) the influence of the longitudinal vibration of bridges was studied. Some of the results of these studies are shown in fig. 1,2. In Fig. 1 one can see the variation of the in plane rotation of a skew bridge with the abutment stiffness for two values of the angle of skewness. This rotation occurs in the case of bridges with seat type abutments after the closure of the abutment gap during strong earthquake shakings. In Fig. 2 the variation of the maximum displacement is shown with the abutment stiffness for various gap values. In both cases the abutment stiffness is expressed in terms of the parameter KR which is the ratio between the abutment stiffness and the bridge pier stiffness.

The calculation of a precise value of abutment stiffness would involve very difficult calculations since an accurate representation of the abutment-soil system would be very complicated involving complex three-dimensional geometry, many degrees of freedom, and the nonlinear constitutive relation for the properties of the soil. However, for most cases of dynamic bridge modeling, a reasonable estimation of the abutment stiffness is sufficient.

[1]Assistant Professor, Civil Engineering Department, University of Nevada, Reno, Nevada 89557
[2]Assistant Professor, Civil Engineering Department, University of Nevada, Reno, Nevada 89557

The purpose of this paper is the presentation of a simplified method by which one can construct the force-displacement diagram of a bridge abutment. In this method, the soil is modeled as a Winkler foundation with springs that can either be constant or vary linearly with depth. The soil springs are considered to be linearly elastic, but the soil deposits on the left and right sides of the abutment are allowed to yield. The yielding criterion used for the soil deposits is based on the Rankine theory of active thrust and passive resistance and is discussed in the section containing the basic assumptions of the analysis.

Rankine Theory

The Rankine theory is one of two classical theories of earth pressure (the other one is due to Coulomb). Relative to the Rankine states of active thrust and passive resistance, the following relations about the active and passive stress can be derived.

$$\sigma_a = K_A \gamma Z - 2c\sqrt{K_A} \tag{1}$$

$$\sigma_p = K_p \gamma Z + 2c\sqrt{K_p} \tag{2}$$

where K_A and K_p, the active and passive pressure coefficients, respectively, are

$$K_A = \frac{1 - \sin\phi_o}{1 + \sin\phi_o} \tag{3}$$

$$K_p = \frac{1 + \sin\phi_o}{1 - \sin\phi_o} \tag{4}$$

In the above equations γ and ϕ_o are the unit weight and the angle of internal friction of the soil, respectively. The active and passive stress distributions are shown in Fig. 3. The forces per unit width of the wall due to the active and passive stresses are referred to as total active thrust, P_A, and total passive resistance, P_p, respectively. For a vertical wall of height ℓ, these forces (along with the length of the tension zone, Z_o) are given by the following formulas.

$$Z_o = \frac{2c}{\gamma K_A} \tag{5}$$

$$P_A = \int_{Z_o}^{\ell} \sigma_a \, dZ = 1/2 \, K_A \gamma (\ell^2 - Z_o^2) - 2c K_A (\ell - Z_o) \tag{6}$$

$$P_p = \int_{o}^{\ell} \sigma_p dZ = 1/2 \, K_{p\gamma} \ell^2 + 2c \, K_p \ell \tag{7}$$

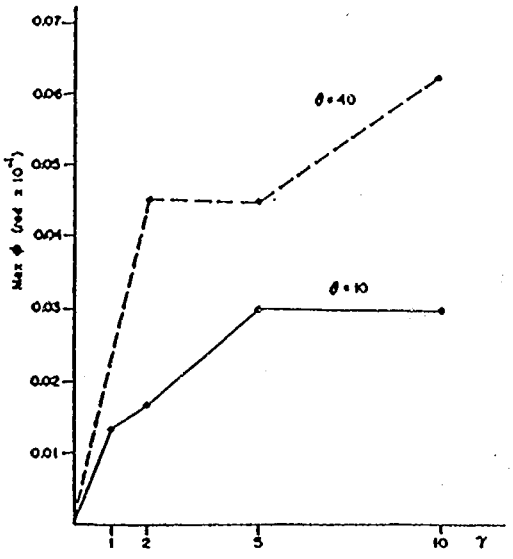


Fig. 1 Variation of Maximum In Plane Rotation with Abutment Stiffness

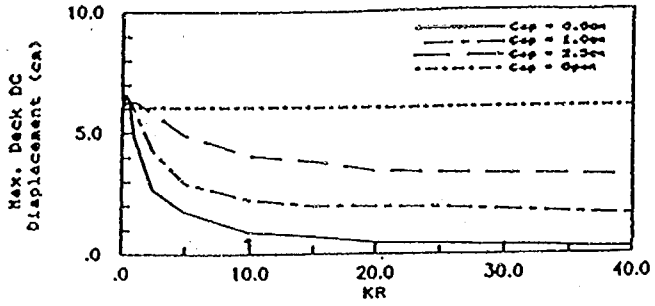


Fig. 2 Variation of Maximum Longitudinal Deck Translation With Abutment Stiffness

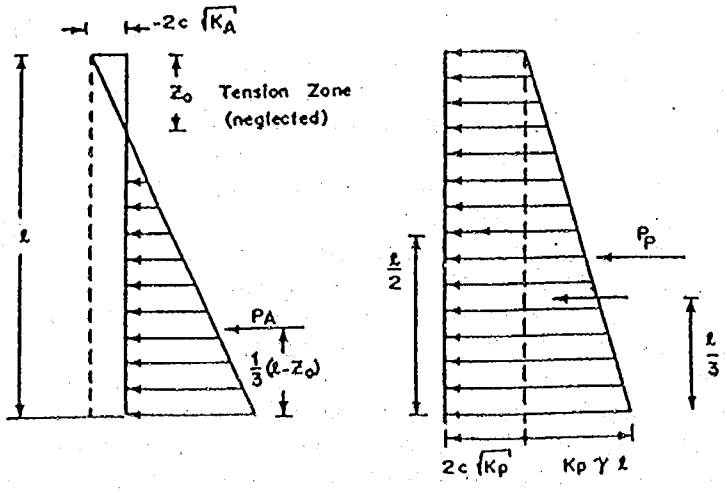


Fig. 3 Active and Passive Stress Distributions

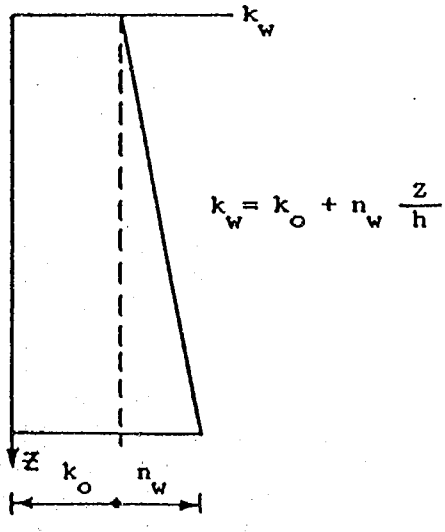


Fig. 4 Variation of K_w with Depth

More details regarding the Rankine theory are provided by Lambe and Whitman, 1979 (Ref. 5).

Fundamental Assumptions

The approach presented below is based on the following simplifying assumptions:

(a) The problems to be solved are static; consequently, no inertia forces are included in the analysis;

(b) The abutment is assumed to behave as a uniform, rigid plate, i.e., deformations due to bending and shear are neglected;

(c) When elastic, the soil is assumed to behave as a Winkler foundation.

Thus, the pressure, p, exerted by the ground at a point, is assumed to depend only on the displacement, W, of that point through a proportionality factor k_w.

$$p = k_w W \tag{8}$$

The factor k_w is called the horizontal subgrade reaction coefficient. In the first part of the analysis, k_w is assumed to vary linearly with depth according to the relation:

$$k_w = n_w \frac{Z}{h} + k_o \tag{9}$$

where h is the total depth of the soil deposit, Z is the depth, and n_w and k_o are constants (Fig. 4). Note that for the application of equation (9) h has to be adjusted, depending on the deposit for which this equation is applied. Thus, for the deposit on the right of the abutment the total depth of the deposit, h, is equal to the total height of the abutment, while for the deposit on the left of the abutment the height of the deposit is equal to ℓ-d, where d is the distance of the top of the left deposit from the top of the abutment. The application of equation (9) for each of the soil deposits is clearly demonstrated in Fig. 5. From this figure one can see that at the top of each deposit the soil stiffness is equal to k_o, while at the bottom of each deposit it is equal to $k_o + n_w$. Equation (9) includes both a uniform subgrade coefficient ($n_w = 0$) and triangular distribution of resistance with depth ($k_o = 0$), which are the two most frequently used expressions for the factor k_w. More information about the subgrade reaction coefficient is provided by Scott, 1981 (Ref. 6). The resistance of the soil at the bottom of the abutment is modelled by a torsional spring which resists the rigid body rotation of the abutment.

The contact between the abutment and the soil is assumed to be frictionless.

(d) When no force or displacement is imposed on the soil by the

bridge, the system of the soil and the abutment is in equilibrium under the initially applied forces (weight and geostatic forces). Thus, in the analysis, only the equilibrium of the forces applied beyond the initial equilibrium state will be examined.

(e) It will be seen later that the soil deposits on both sides of the abutment are divided into two regions. A region is considered to yield if the total force imposed on the region equals to its active or passive resistance. It is assumed that when the total compressive force is between these values, the soil deposit behaves elastically. This means that the "yielding criterion" used is global in nature and thus does not take into account local yielding at any point in the region. For the purpose of the present analysis, this assumption is considered to be acceptable.

(f) A soil deposit cannot assume tensile stresses. The deposit is said to be "tensioned" only in the sense that its initial compressive stresses are decreased. The maximum level of the decrease is specified by (e).

Statement of the Problem

The problem to be solved can be briefly summarized as follows: Let W_a be the deflection imposed by the bridge deck on the soil through the abutment and let P_t equal the reaction of the soil on the bridge. The problem is to find an equivalent stiffness k_{ab} such that

$$P_t = k_{ab}W_a \tag{10}$$

Solution of the Problem - Consider a strip of the abutment of unit width loaded by a load, P, per unit width applied at a distance a from the top (see Fig. 5). Let the displaced position of the abutment be that shown in Fig. 6, and let W_o and W_1 be the displacements of the top and bottom of the abutment, respectively. If $W(Z_1)$ is the displacement at a depth Z_1, and the rotation of the abutment, then:

$$W(Z_1) = W_o - \frac{W_o - W_1}{\ell} Z_1$$

$$\phi = \frac{W_o - W_1}{\ell} \tag{11}$$

Note that in the above equation the displacement is measured positive to the right. The stress between the soil and the abutment can be expressed as a function of depth as follows:

$$p_r(Z_1) = W(Z_1)k_w(Z_1) \qquad 0 \le Z_1 \le \ell \quad \text{(on the right side of the abutment)}$$

$$p(Z_1) = W(Z_1)k_w(Z_1) \qquad d \le Z_1 \le \ell \quad \text{(on the left side of the abutment)} \tag{12}$$

The equation of force equilibrium requires that:

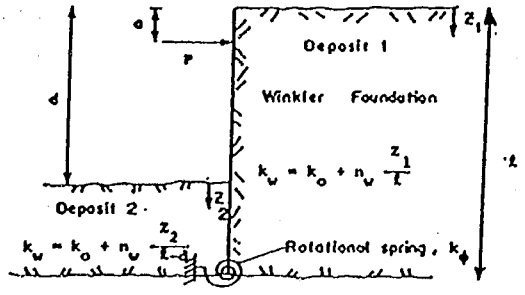


Fig. 5 Initial Position of the Abutment with the Soil Deposits and the Load Applied by the Bridge Deck

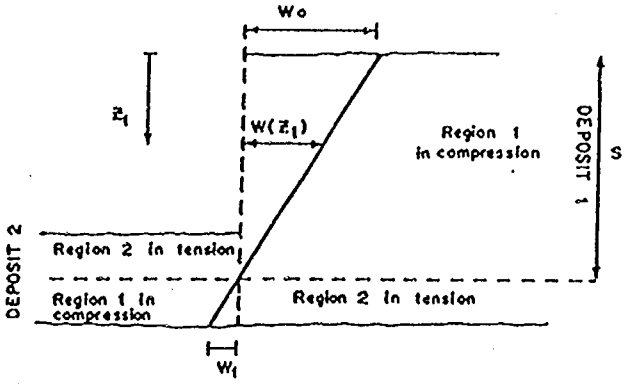
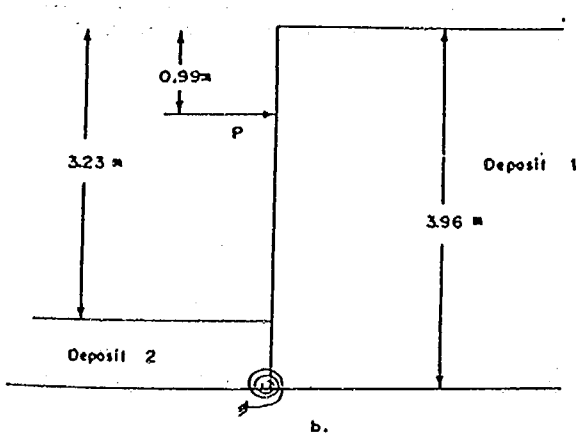


Fig. 6 Displaced Position of the Abutment



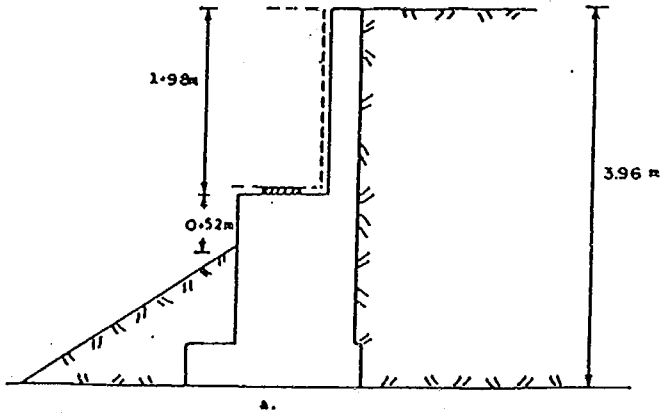


Fig. 7 a. Abutment of Nichols Road Overcrossing
b. Model

$$P = \int_0^{\ell} p_r(Z_1)dZ_1 + \int_d^{\ell} p_\ell(Z_1)dZ_1 \tag{13}$$

From the equation of moments about $Z_1 = \ell$:

$$P(1 - a) = \int_0^{\ell} p_r(Z_1)(\ell - Z_1)dZ_1 + \int_d^{\ell} p_\ell(Z_1)(\ell - Z_1)dZ_1 + k_\phi\phi \tag{14}$$

From (12), (13) and (14), one gets:

$$\begin{aligned} P &= R_o W_o + R_1 W_1 \\ P(\ell - a) &= T_o W_o + T_1 W_1 \end{aligned} \tag{15}$$

where:

$$R_o = -\frac{n_w\ell}{3} + \frac{(n_w - k_o)\ell}{2} + k_o\ell - \frac{n_w(\ell^3 - d^3)}{3\ell(\ell - d)}$$

$$+ \frac{\ell^2 - d^2}{2}\left(-\frac{k_o}{\ell} + \frac{n_w}{\ell - d} + \frac{n_w d}{(\ell - d)}\right) +$$

$$\left(k_o - \frac{n_w d}{\ell - d}\right)(\ell - d)$$

$$R_1 = \frac{n_w\ell}{3} + k_o\frac{\ell}{2} + \frac{n_w(\ell^3 - d^3)}{3\ell(\ell - d)} +$$

$$\left(\frac{k_o}{\ell} - \frac{n_w d}{\ell(\ell - d)}\right)\frac{\ell^2 - d^2}{2}$$

$$T_o = -\frac{n_w\ell^2}{12} + (n_w - k_o)\frac{\ell^2}{6} + \frac{k_o\ell^2}{2} + \tag{16}$$

$$\frac{n_w}{\ell - d}\left(\frac{\ell^4 - d^4}{4} - \frac{\ell^3 - d^3}{3}\right) +$$

$$\left(-\frac{k_o}{\ell} + \frac{n_w}{\ell - d} + \frac{n_w d}{\ell(\ell - d)}\right)\left(\frac{\ell^2 - d^2}{2} - \frac{\ell^3 - d^3}{3}\right) +$$

$$(k_o - \frac{n_w d}{\ell - d})(\ell(\ell - d) - \frac{\ell^2 - d^2}{2}) + \frac{k_\phi}{\ell}$$

$$T_1 = \frac{n_{w1}^2}{12} + \frac{k_o \ell^2}{6} + \frac{n_w}{\ell - d}(\frac{\ell^3 - d^3}{3} - \frac{\ell^4 - d^4}{4}) +$$

$$+ (\frac{k_o}{\ell} - \frac{n_w d}{(\ell - d)})(\frac{\ell^2 - d^2}{2} - \frac{\ell^3 - d^3}{3}) - \frac{k_\phi}{\ell}$$

Solving the system of equations (15) for the displacements gives:

$$W_o = PA_o$$

$$W_1 = PA_1$$

where:
$$A_o = \frac{R_1(\ - a) - T_1}{R_1 T_o - R_o T_1} \qquad (17)$$

$$A_1 = \frac{\qquad\qquad}{R_o T_1 - R_1 T_o}$$

From equations (11) and (17), one gets

$$W(Z_1) = P(A_o - \frac{A_o - A_1}{\ell} Z_1) \qquad (18)$$

For $Z_1 = a$, equation (18) gives:

$$P = \frac{W_a}{A_o \frac{A_o - A_1}{\ell} a} \qquad (19)$$

The total force P_t is found by multiplying by the foundation width, b.

$$P_t = \frac{b}{A_o - \frac{A_o - A_1}{\ell} a} W_a \qquad (20)$$

So, the desired stiffness coefficient is

$$k_{ab} = \frac{b}{A_o - \frac{A_o - A_1}{\ell} a} \qquad (21)$$

Equation (21) provides an expression for the equivalent abutment stiffness when the soil behaves elastically.

Yielding of regions of the two soil deposits - As shown in Fig. 6, in the general case each soil deposit is divided into two regions: region 1, which in both deposits is compressed by the abutment, and region 2, which in both deposits is in tension in the sense that it was defined earlier. The distance s, which defines the point of zero displacement, can be found from equations (11) and (17):

$$s = \ell \frac{A_o}{A_o - A_1} \tag{22}$$

The yield criterion stated earlier in this paper (assumption (e)) can now be used to identify the displacement W_a, which is required to cause yielding of each of the four regions. Each region will yield when the total force imposd on it by the geostatic stresses and the movement of the abutment equals either the passive resistance or the active thrust depending on whether the region is in compression or tension respectively. Based on that, the following expressions can be derived for the yielding displacements.

Yielding of the regions of deposit 1

(i) Region 1 (in compression)

$$W^{Y}_{a,11} = \frac{1}{\alpha_1}\left[\ell \frac{A_o}{A_o - A_1}\left(1/2\, K_p \gamma \ell \frac{A_o}{A_o - A_1} + 2c \quad K_p\right) - 1/2\, K_o \gamma \ell^2 \frac{A_o^2}{(A_o - A_1)^2}\right] \tag{23}$$

where

$$\alpha_1 = \frac{k_{ab}}{b} \frac{A_o}{A_o - A_1} \ell \left\{n_w \frac{A_o^2}{3(A_1 - A_o)} + \left[A_o(n_w - k_o) + A_1 k_o\right] \frac{A_o}{2(A_o - A_1)} + k_o A_o\right\} \tag{24}$$

(ii) Region 2 (in tension)

For this region the length of the tension zone is found from (5):

$$z_1^o = \frac{2c}{\gamma\sqrt{K_A}} \tag{25}$$

Then the yielding displacements are provided by the following expressions.

$$\text{If } Z_1^o > \ell : \quad W_{a,12}^Y = -\frac{1}{\alpha_2} 1/2 K_o \gamma \ell^2 \left(1 - \frac{A_o^2}{(A_o - A_1)^2}\right)$$

$$\text{If } s < Z_1^o < \ell: \quad W_{a,12}^Y = \frac{1}{\alpha_2}\left[1/2\, K_A\, (\ell^2 - Z_1^{o2}) - \right.$$

$$\left. 2c\, K_A (\ell - Z_1^o) - 1/2\, K_o \gamma \ell^2 \left(1 - \frac{A_o^2}{(A_o - A_1)^2}\right)\right] \qquad (26)$$

$$\text{If } Z_1^o < s: \quad W_{a,12}^Y = \frac{1}{\alpha_2}\left[1/2 K_A \gamma \ell^2 \left(1 - \frac{A_o^2}{(A_o - A_1)^2}\right) - \right.$$

$$\left. 2c\, K_A \left(\ell - \frac{A_o}{A_o - A_1}\right) - 1/2\, K_o \gamma \ell^2 \left(1 - \frac{A_o^2}{(A_o - A_1)^2}\right)\right]$$

where $\alpha_2 =$

$$\alpha_2 = \frac{k_{ab}}{b} \ell \left\{(A_1 - A_o) n_w \frac{1 - \frac{A_o^3}{(A_o - A_1)^3}}{3} + \right. \qquad (27)$$

$$\left. [A_o (n_w - k_o) + A_1 k_o] \frac{1 - \frac{A_o^2}{(A_o - A_1)^2}}{2} + k_o A_o \left(1 - \frac{A_o}{A_o - A_1}\right)\right.$$

Yielding of the regions of deposit 2

For region 1:

$$W_{a,21}^Y = \frac{1}{\beta_1}\left\{1/2\gamma \left[(\ell - d)^2 - \left(\ell \frac{Ao}{A_o - A_1} - d\right)^2\right](K_p - K_o)\right. \qquad (28)$$

$$\left. + 2c\, K_p \ell \left(1 - \frac{A_o}{A_o - A_1}\right)\right\}$$

where:

$$\beta_1 = -\frac{k_{ab}}{b} \ell \left\{(A_1 - A_o) \frac{n_w \ell}{3(\ell - d)} \left(1 - \frac{A_o^3}{(A_o - A_1)^3}\right)\right.$$

$$+ [A_o \left(- \frac{k_o}{\ell} - \frac{n_w}{\ell - d} + \frac{n_w d}{\ell(\ell - d)}\right) +$$

$$+ A_1 \left(\frac{k_o}{\ell} - \frac{n_w d}{\ell(\ell - d)}\right)] \frac{\ell}{2}\left(1 - \frac{A_o^2}{(A_o - A_1)^2}\right) \qquad (29)$$

$$+ A_o\left(k_o \frac{n_w d}{\ell - d}\right) \left(1 - \frac{A_o}{A_o - A_1}\right)$$

For region 2:

$$\text{If } Z_1^o > s: \quad W^Y_{a,22} = - \frac{1}{\beta_2} 1/2\, K_o \gamma \left(\ell \frac{A_o}{A_o - A_1} - d\right)^2$$

$$\text{If } d < Z_1^o < s: \quad W^Y_{a,22} = \qquad (30)$$

$$\frac{1}{\beta_2}\{1/2\, K_A \gamma [\left(\ell \frac{A_o}{A_o - A_1} - d\right)^2 - (Z_1^o - d)^2$$

$$-2c\, K_A \left(\ell \frac{A_o}{A_o - A_1} - Z_1^o\right) - 1/2\, K_o \gamma \left(\ell \frac{A_o}{A_o - A_1} - d\right)^2$$

where:

$$\beta_2 = - \frac{k_{ab}}{b}\{(A_1 - A_o) \frac{n_w}{\ell(\ell - d)} \frac{\ell^3 \frac{A_o^3}{(A_o - A_1)^3} - d^3}{3} \qquad (31)$$

$$+ [A_o \left(- \frac{k_o}{\ell} + \frac{n_w}{\ell - d} + \frac{n_w d}{(\ell - d)}\right) +$$

$$A_1 \left(\frac{k_o}{\ell} - \frac{n_w d}{\ell(\ell - d)}\right)] \frac{\ell^2 \frac{A_o^2}{(A_o - A_1)^2} - d^2}{2} +$$

$$A_o\left(k_o - \frac{n_w d}{\ell - d}\right) \left(\ell \frac{A_o}{A_o - A_1} - d\right)$$

Estimation of the force-deflection diagram - From the analysis presented above, it is obvious that the region which requires the smallest displacement W_a in order to yield will yield first. After a region has

yielded, it stops contributing additional force to the resistance to the abutment motion. Consequently, after the yielding of a region, a redistribution of stresses and displacements will take place and a new problem has to be solved in order to find the new expression for the equivalent abutment stiffness. Therefore, the whole problem can be divided into phases. The end of one phase and the beginning of the next one are marked by the yielding of a soil region. The stress and displacement conditions at the beginning of a phase can be found from the stress and displacement conditions at the end of the previous phase.

The procedure for the calculation of the equivalent abutment stiffness and the yielding displacement in each phase is identical to the procedure described in the preceeding part of this paper.

The estimated values of the abutment stiffness and the yield displacement in each phase can be used for the estimation of the force displacement diagram of the abutment. The slope of this diagram will be changing from one phase to the next. The whole procedure is described and illustrated in the following example.

Example

Consider the abutment shown in Fig. 7a. This is a section of one of the abutments of the Nichols Road Overcrossing (bridge No. 56-725) located in Riverside County, California). This is a two span bridge, with a total length of 91.4 m, and is skew at an angle of 20° and has a set of two columns located 0.63 m left of the center of the mass of the deck. The bridge has been used in the study of rigid body motion of skew bridges. More details are provided by Maragakis, 1984 (Ref. 1) and Maragakis and Jennings, 1987 (Ref. 3). The model used to estimate the stiffness of this abutment is shown in Fig. 7b. The height of deposit 2 in the model is the average height of the deposit on the left hand side of the abutment. The values of the soil springs were estimated based on the properties of stiff soil (Ref. 1).

During the first phase the soil deposits on both sides of the abutment provide resistance to the movement of the abutment. Therefore, using formulas (22), (28), (36), (37) and (38) one can estimate the elastic stiffness of the abutment and the displacements required to cause yielding of the regions of each soil deposit. More specifically, the abutment stiffness during this phase was estimated to be equal to 21676 t/m, while the analysis of the yielding produced the following values for the required yielding displacement for the first phase:

Region 1, Deposit 1: $W_{a,11} = 0.092m$
Region 2, Deposit 1: $W_{a,12} = 0.0658m$
Region 1, Deposit 2: $W_{a,12} = 0.53m$
Region 2, Deposit 2: $W_{a,22} = 0.0051m$

From these results, it is clear that region 2 of deposit 2 will yield first. The yielding of this region marks the end of the first phase and the beginning of the second phase. During the second phase the region 2 of deposit 2, that yielded at the end of the previous phase, will stop

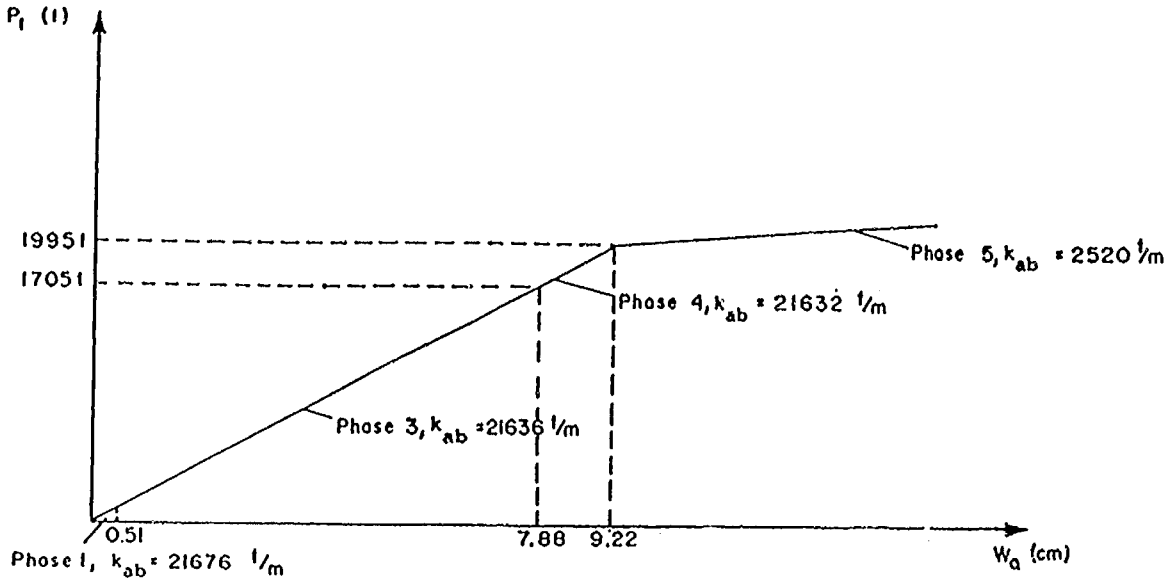


Fig. 8 Force-displacement Diagram of the Abutment Shown in Fig. 7

TABLE 1: RESULTS OF THE EXAMPLE

Phase	Estimation of Abutment Stiffness				Examination of Yielding		
	A_0	A_1	k_{ab} (t/m)	S (m)	Required Yielding Displacement W_a (m)	Critical Region R*	D*
1	9.1×10^{-4}	4.6×10^{-5}	21676	3.76	0.005	2	2
2	9×10^{-4}	-3.7×10^{-5}	21636	3.8	0.0052	2	2
3	9×10^{-4}	3.77×10^{-5}	21636	3.8	0.073	2	1
4	9×10^{-4}	4×10^{-5}	21632	3.8	0.013	1	1
5	6.66×10^{-3}	3×10^{-3}	2526.4				

NOTE: R* Region
D* Deposit

contributing to resistance of the abutment motion. Therefore, the center of rotation of the abutment, defined by the distance s (formula (23)) will change. The procedure for estimation of the abutment stiffness and the analysis of yielding during this phase is similar to the procedure used during the first phase. The results of the analysis for all the phases are shown in Table 1.

From this table one can see that the differences in the values of the abutment stiffness among the first four phases are insignificant, because the depths of the yielding regions are small compared to the height of the abutment. However, at the end of the fourth phase region 1 of deposit 1 yields. This region has a depth equal to 3.80m and therefore its yielding results in a significant reduction of the abutment stiffness. Examination of the yielding during phase 5 is of no practical importance since a total displacement of about 0.53m is required to cause yielding of the remaining active soil. The resulting force deflection diagram is shown in Fig. 9.

Summary - Conclusions

A simple method has been presented for the construction of the force-displacement diagram for the longitudinal motions of bridge abutments. In this method the abutment was modeled as a uniform rigid plate and deformations due to bending and shear have been neglected. When elastic, the soil was assumed to behave as a Winkler foundation with elastic springs varying linearly with depth. For the estimation of the yield level a global yielding criteria based on the Rankine Theory of Active Thrust and Passive Resistance was used. The application of the method is demonstrated through an illustrative example in which the force displacement diagram of the abutment of the Nichols Road Overcrossing in Riverside, California is constructed. From this example it is obvious that the method provides a useful tool for the designer or the researcher since it is relatively simple and can be applied even with the use of only a common table programable calculator.

It is believed that the method provides a reasonable estimate of the initial elastic abutment stiffness. However, the yield point is probably overestimated. This is because the used "yielding criterion" was global in nature and, therefore, the total active thrust or passive resistance of a soil deposit have to be reached before yielding occurred. However, the yielding stress for each soil element will depend on its depth. More research on this particular aspect of the problem is recommended.

References

1. Maragakis, E.A. (1984), "A Model for the Rigid Body Motions of Skew Bridges," Report No. EERL 85-02, California Institute of Technology, Pasadena, CA.

2. Maragakis, E.A. (1986). "Parametric Studies on a Simple Model for the Rigid Body Rotation of Skew Bridges" Proceedings of the Third U.S. National Conference on Earthquake Engineering, Volume III, pp. 2237-2248, Charleston, South Carolina, August 1986.

3. Maragakis, E.A., Jennings, P.C. (1987). "Analytical Models for the Rigid Body Motions of Skew Bridges," Journal of Earthquake Engineering and Structural Dynamics, Vol. 15, pp. 923-944, 1987.

4. Maragakis, E.A., Thornton, G., Saiidi, M., Siddharthan, R., "A Simple Non-Linear Model for the Investigation of the Effects of the Gap Closure at the Abutment Joints of Short Bridges" accepted for publication at the Journal of Earthquake Engineering and Structural Dynamics.

5. Lambe, T.W. and Whitman, R.V. (1979) Soil Mechanics, John Wiley and Sons, Inc. New York, NY.

6. Scott, R.F. (1981). Foundation Analysis. Prentice-Hall, Civil Engineering and Engineering Mechanics Series.

NEW ASPECTS REGARDING THE USE OF QUICK-RELEASE DYNAMIC TESTS FOR THE EXPERIMENTAL ANALYSIS OF BRIDGE STRUCTURES

by

Bruce Douglas[1] and Emmanuel Maragakis[2]

ABSTRACT

The paper outlines a new method for performing baseline corrections on accelerograms generated by the quick-release method. These accelerograms are produced when highway bridges are subjected to dynamic excitations by initially deforming the bridge structure and subsequently quick-releasing the loads causing the deformation. The baseline correction method is developed such that the step function character of the quick-release baseline is preserved. It is this feature which allows the complete static deformation state to be recovered by integrating the accelerograms. The power of the method is illustrated by applying it to quick-release data obtained during full scale field tests of the Meloland Road Overcrossing located near El Centro, California.

INTRODUCTION

The quick-release method (Douglas, 1976; Douglas and Reid, 1982; Douglas and Richardson, 1984) has been used extensively in the past for the detailed analysis of the modal characteristics and the dynamic response of bridge structures. Both hydraulic rams and cables pulled by heavy tractors have been used to deform the structures prior to quick-release. The hydraulic ram method of loading is the superior procedure when experimental conditions permit its use. In this case, the experimental load level is controlled by reading a pressure gage attached to the pump. Even with this method, slight load variations can occur in reaching the target load during a series of repetitive loadings because of the difficulty of holding the load absolutely steady with hand operated pumps. After the desired load is imposed on the structure, the imposed load is then quick-released, causing the structure to vibrate starting from its initial deformed position. Appropriately placed accelerometers measure the acceleration response at various parts of the structure. By analyzing the recorded accelerograms the dynamic characteristics of the structure can be studied.

The quick-release method was recently used in a full-scale dynamic test of the Meloland Road Overcrossing, which was conducted May 23-26, 1988. This bridge is located in a very active seismic zone near El Centro, in Southern California. The bridge has been permanently instrumented with an extensive strong motion recording system, which has recorded significant earthquake response data (Rojahn, 1982). In the 1979 Imperial Valley earthquake, the peak transverse acceleration recorded on the bridge deck was about 50% of gravity while the peak acceleration in the transverse direction recorded at the nearby field station was about

[1]Professor of Civil Engineering, University of Nevada Reno
[2]Assoc. Professor of Civil Engineering, University of Nevada Reno

30% of gravity (Rojahn, et al., 1982). No observable damage was suffered by the bridge during this strong shaking.

The Meloland Road Overpass is a two span reinforced concrete box girder bridge. with a 208 ft. long deck monolithically connected to the abutments. The single central pier and the abutments are supported with pile foundations. An elevation and a section of the bridge are shown in Fig. 1 along with the location of some of the permanent accelerometer instrumentation. During the May experiments, the bridge was loaded with a single hydraulic ram which induced the quick-release motions at the central pier. A photograph of the bridge and the hydraulic loading ram is shown in Fig. 2.

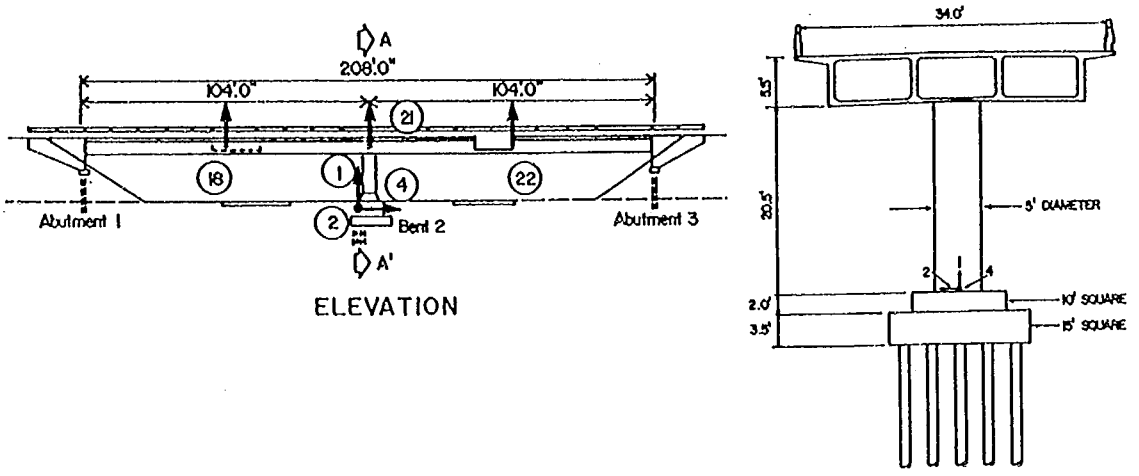


Figure 1. Elevation and Section of the Meloland Road Overpass (Rojahn et al., 1982)

The bridge was completely instrumented with accelerometers in a sequential way so as to measure the transverse and rotational response of the bridge deck, the foundations, and abutments. The accelerometers at the deck were placed at stations which were 20.67 feet apart. In addition, measurements were made to estimate the extent to which the soils in the approach fills and central pier foundation participated in the response of the structure. Two levels of ram load were used, 21.2 kips and 141 kips. The shaking amplitudes achieved during the experiments were representative of earthquake caused motions. At the highest load levels, the peak transverse deck acceleration was about 200 cm/sec^2 or 20% of gravity. The peak vertical accelerations at the edges of the bridge deck during these experiments were about 30% of gravity.

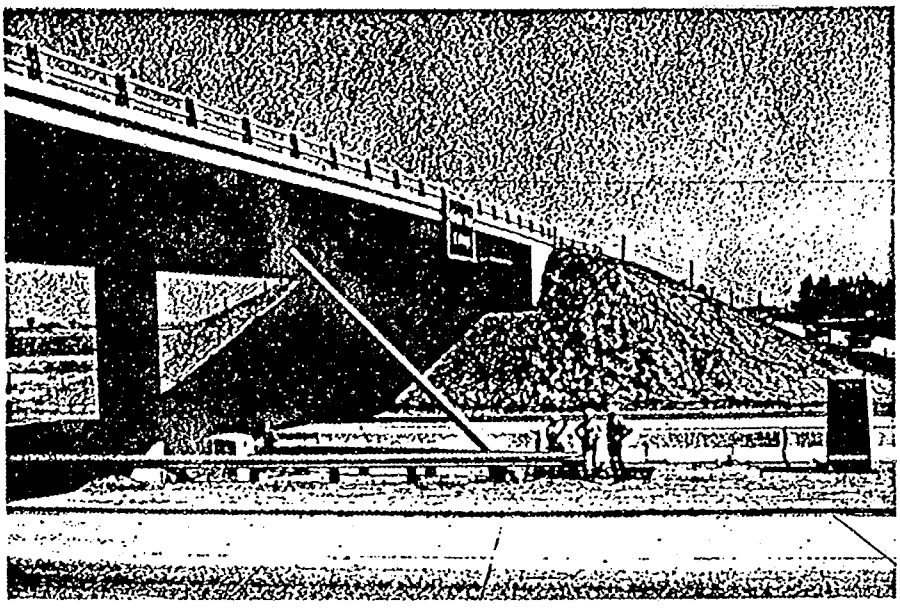


Figure 2. Photograph of the Bridge and Loading Ram

Recently, at the University of Nevada Reno, an algorithm was produced for integrating accelerograms obtained from quick-release experiments to velocity and displacement records (Douglas, et al., 1989). In addition to producing the displacement time histories, the algorithm provides reliable estimates of the offset or release displacement of the structure. The reliability of the results of this integration method has been tested using an experimental structure at the Dynamics Laboratory of the University of Nevada, Reno (Douglas, et al., 1989). The main objective of this paper is to demonstrate the application of the algorithm on the acceleration records obtained from the full scale test of the Meloland overpass. In the Meloland example, the complete static deformation states of the bridge deck, foundations, abutments, and approach fills were obtained by using the initial release displacements calculated by the double integration of the aforementioned accelerograms. It should be noted that this information was obtained as a by-product of the full scale dynamic tests and includes both translation and rotation components of the static deformations.

REVIEW OF INTEGRATION METHODOLOGY

In general, the integration of acceleration time histories to velocity and displacement records is a classically difficult problem which has been addressed by many researchers in the past (Brady, 1966;

Hudson, 1979; Iwan et al., 1985; Trifunac and Lee, 1973). It is the poor signal to noise ratio associated with the long period part of the accelerograms that generates the serious baseline-shift problems arising from the double integration of acceleration records.

A review of the available literature regarding this problem, reveals that most of the researchers in the past concentrated their efforts in recovering displacement time histories from strong motion accelerograms (Hudson, 1979). Recently, at the University of Nevada, Reno, a method was developed for the double integration of accelerograms obtained from quick-release experiments (Douglas et al., 1989). This method consists of a baseline correction algorithm, which is a generalization of a method developed earlier by Brady (1966). In brief, this algorithm is developed by applying a polynomial baseline correction on the acceleration record and evaluating the unknown coefficients of this polynomial by minimizing the mean square of the displacement record, which is found from the double integration of the adjusted acceleration record. This, in effect, makes baseline of the corrected displacement record flat after the initial step caused by quick-releasing the structure, which is true for the case of quick-release experiments. This method produces directly and reliably the offset or release displacement of the structure (Douglas et al., 1989). This feature allows for the complete and detailed calculation of the static deformations caused by the quick release loads as a by-product of a dynamic quick-release experiment.

MATHEMATICAL FORMULATION OF CORRECTION ALGORITHM

The measured acceleration record was adjusted by applying a polynomial base line correction of order n. The need for the application of this baseline correction has been addressed by other researchers in the past. The scheme used in this paper is an extension and generalization of the work by Brady (1966).

After the polynomial baseline correction is applied to the measured acceleration trace, the following formula is obtained for the corrected acceleration.

$$a^*(t) = a(t) - (C_0 + C_1 t + C_2 t^2 + \cdots + C_n t^n) = a(t) - \sum_{m=0}^{n} C_m t^m \qquad (1)$$

In the above expression and the Cm's and n are coefficients and the order of the polynomial correction respectively. The coefficients and the order to the polynomial will be evaluated using methods which will be described later in this section.

Integrating Eq. (1) to velocity and then to displacement yields:

$$V^*(t) = V(t) - \sum_{m=0}^{n} \frac{C_m}{m+1} t^{m+1} + C_{n+1} \qquad (2)$$

$$d^*(t) = d(t) - \sum_{m=0}^{n} \frac{C_m}{(m+1)(m+2)} t^{m+2} + C_{n+1} t + C_{n+2} \qquad (3)$$

In the above expressions $v^*(t)$, $d^*(t)$ are the corrected velocity and displacement respectively, $v(t)$, $d(t)$ are the velocity and displacement obtained by integrating the measured acceleration record without any correction and C_{n+1}, C_{n+2} are constants of integration.

The unknown coefficients in the above expressions now need to be determined. Previously, Brady (1966) required that the velocity have a minimum mean aquare value. This procedure had some merit in this application because it was known that the original and final velocity was zero and minimizing the mean square of velocity gave the resulting velocity trace a flat baseline consistent with the physical problem. The mean square of displacement could also be minimized, but this clearly would only be applicable to those cases where it was known that the final baseline of the displacement trace was flat. It should be observed here, however, that minimizing either the mean square of the velocity or the displacement will not give correct results for the case where the actual displacement baseline will have arbitrary permanent offsets. This is true because the equivalent effect of either of the above procedures is to apply a high pass filter to either the velocity or the displacement traces. In both cases, the long period content of the record, which is necessary to describe the general case, is altered in such a way as to tend to distort the final displacement baseline.

However, in the case of the quick release problem it is known a priori that the baseline of the displacement is going to be a horizontal straight line shifted by an amount equal to the release displacement. Therefore, in this case the unknown coefficients of equation (3) can be determined by operating directly on displacement. Furthermore, operation on displacement will directly produce the value of the constant C_{n+2}, which, as can be seen from (3) is the value of the release or offset displacement.

In order that the displacement $d^*(t)$ have a minimum mean square value, the following equations must hold:

$$\frac{\partial}{\partial C_i}\int_0^S [d^*(t)]^2 dt = 0\,, \quad i = 0, 1, 2, \ldots, n+2 \qquad (4)$$

In the above equations, S is the total length of the record. Substituting the expression of $d^*(t)$ from expression (3) in expression (4) and performing all the necesssary complicated algebraic calculations yields the following system of equations.

$$\sum_{m=0}^{n} \frac{1}{(m+1)(m+2)(m+r+3)} C_m S^{r+m+3} - \frac{1}{r+2} C_{n+1} S^{r+2} - \frac{1}{r+1} C_{n+2} S^{r+1} = I_r \qquad (5)$$

$$\text{where: } I_r = \int_0^S d(t)\, t^r dt \qquad r = 0, 1, \ldots, n+2$$

Equation (5) is the condensed form of a system of n+2 equations with unknowns the n+2 coefficients which appear in expression (3). Solution of this system will obviously produce the values of the unknown coefficients.

To demonstrate the application and the reliability of the integration technique, a three story experimental frame was built in the University of Nevada-Reno Dynamics Laboratory (Douglas et al., 1989).

The frame was instrumented with accelerometer and LVDT displacement transducers, and was excited by quick-release hooks which are attached at each story. The displacements measured by the LVDT transducers were compared to the displacements obtained by integrating the corresponding acceleration records.

An example of this comparison is shown in Fig. 3. From this Figure it can be seen that the measured and the estimated displacement time histories, as well as the measured and estimated release displacement are very close. Similar comparisons were made for several quick-release excitations at various levels of this structure, in order to demonstrate the reliability of the method.

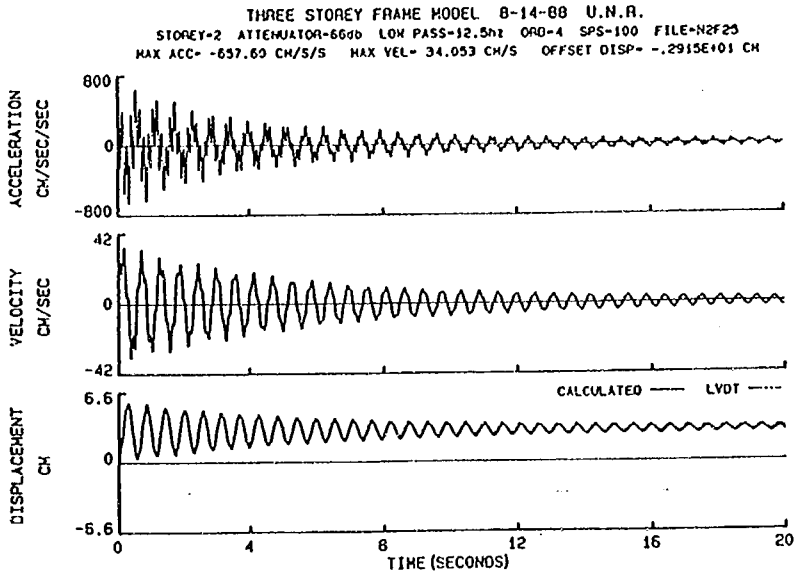


Figure 3. Example acceleration, calculated velocity, and displacement traces along with the directly measured displacement trace obtained from the laboratory frame.

The integration technique was applied on the data obtained from the full scale quick-release excitation of Meloland Bridge. As was mentioned in the introduction, the bridge was excited at two levels of ram load. In each case several acceleration records were obtained from the accelerometers placed on the deck of the bridge and on the foundation.

By applying the integration technique to these acceleration records the offset displacements were calculated, which are the static deformations of the bridge caused by the applied ram loads. Therefore, the complete static deformations of the bridge and the foundation were obtained as a by-product of the study of its dynamic response to the quick-release excitation.

Examples of the measured acceleration records and their corresponding calculated velocity and displacement traces at the deck and the foundation level are shown in Fig. 4 and Fig. 5 respectively. The load for both cases in these figures was the high amplitude ram loading (141 kips).

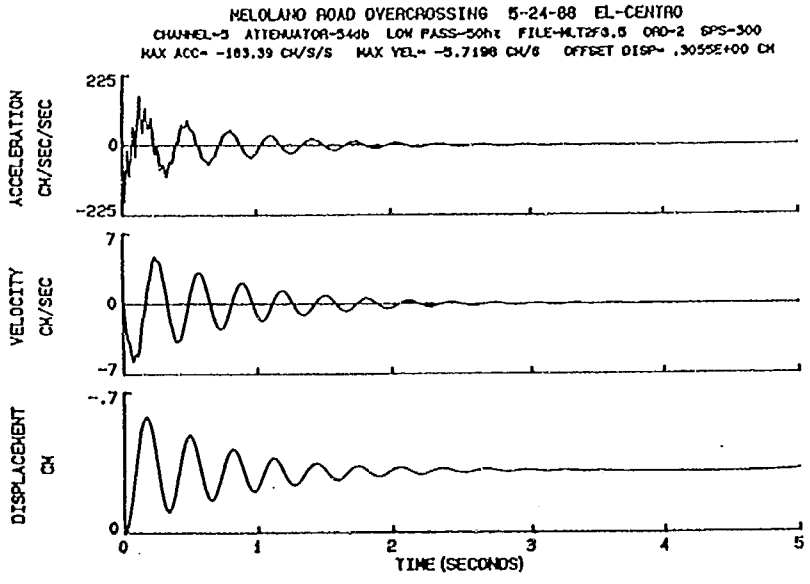


Figure 4. High ampltude deck level center pier transverse acceleration, velocity, and displacement traces from the May 1988 field tests.

MELOLAND STATIC DISPLACEMENT RESULTS

In the previous section, two sample accelerograms obtained from the field tests were discussed to illustrate the type of dynamic response data that can be obtained from quick-release experiments. It was shown that reliable acceleration, velocity, and displacement time histories can be produced if a suitable baseline correction algorithm is used. In addition, reliable offset displacements caused by the quick-release loads can be obtained as a by-product of the analysis. The purpose of this section will be to illustrate the detail with which the complete static deformation of the test structure can be described by using the offset displacements obtained from all of the quick-release accelerograms obtained during the Meloland field tests. It should be noted that all static deformations shown in Figures 6 through 13 are in centimeter units.

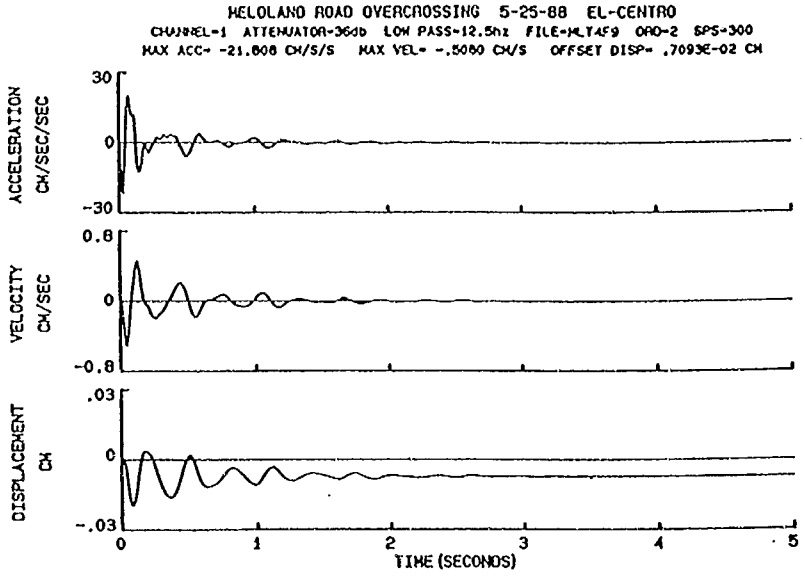


Figure 5. High amplitude center pier foundation transverse acceleration, velocity and displacement traces from the May 1988 field tests.

Figure 6 shows the transverse static displacements (positive to the West) of the south approach fill and the bridge deck caused by the low amplitude 21.2 kip ram load. The approach fill measurements were taken at roadway level at stations 1 and 2. The bridge deck measurements at stations 3 through 13 were taken on top of the concrete barrier rail at the edges of the deck 17 inches above pavement level. This is also the case for all subsequent figures. All stations are 20.67 feet apart.

A word should be said about how the displacement diagrams were developed from a number of different quick-release loading cases. In order to make all the measurements shown in this and subsequent figures the accelerometers had to be relocated several times to cover all the cases. The ram load was controlled by reading the pressure gage on the hand pump, giving rise to the fact that the release loads were not always equal to the target value of 21.2 kips, but only as close as the pump operator could get to that value. The average lateral displacement at station 8, the center of the bridge, of all seven load cases in Fig. 6 was 0.0363 cm with a standard deviation of 0.00113 cm. This indicates that the load repeatability was adequate. For presentation purposes, all deflections for a given release were normalized such that central deflection at station 8 was adjusted slightly to the average value of 0.0363 cm. By inspection of Fig. 6 it can be seen that the displacement pattern is quite consistent with the exception of the value at station 10. As was pointed out in the paper (Douglas, et al., 1989) where the

baseline correction technique was developed, individual displacement estimates may have errors as large as 10%, but a statistical estimate of the displacement configuration will, of course, improve the accuracy.

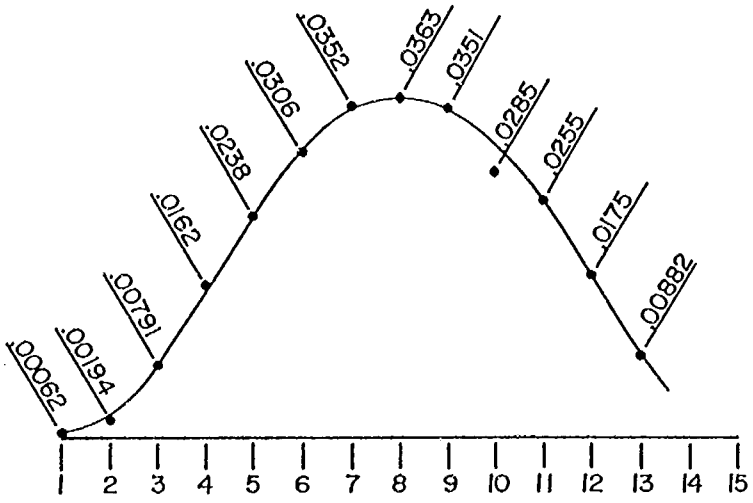


Figure 6. Transverse bridge/roadway release displacement configuration caused by the low amplitude 21.1 kip ram load.

Figure 7 shows the vertical displacements of both the West and East edges of the bridge deck and the approach fill. Positive numbers indicate up. As can be seen from this figure, there is a net upward displacement of the bridge deck because of the difference in the amplitudes of the West and East side vertical displacements. This of course makes sense, because there was a 15 kip upward force component applied by the ram.

One of the advantages of simultaneous digital recording is that time history traces are easily combined to give mean value traces or traces proportional to rotation. In Fig. 8, the mean difference of the East and West vertical accelerograms was produced to give an accelerogram which was proportional to deck rotation. These accelerograms were integrated to displacement traces using the same correction technique mentioned above. Actual rotation in radians can be obtained by dividing the resulting bridge traces by 503 cm, the half distance between the barrier rails. The half distance between the approach fill accelerometers was only 442 cm. Figure 8 shows the rotation release configuration of the bridge deck and approach fill. The units are in centimeters and true rotation of the deck in radians can be obtained by the procedure noted above. It is of interest to note that there is significant rotation of the monolithic abutments at stations 3 and 13. This will have an impact on the gross torsional resistance of the deck.

The next figure shows the result of producing mean value accelerograms from the vertical accelerograms pairs at the edges of the deck. These were integrated and the net upward displacement of the deck

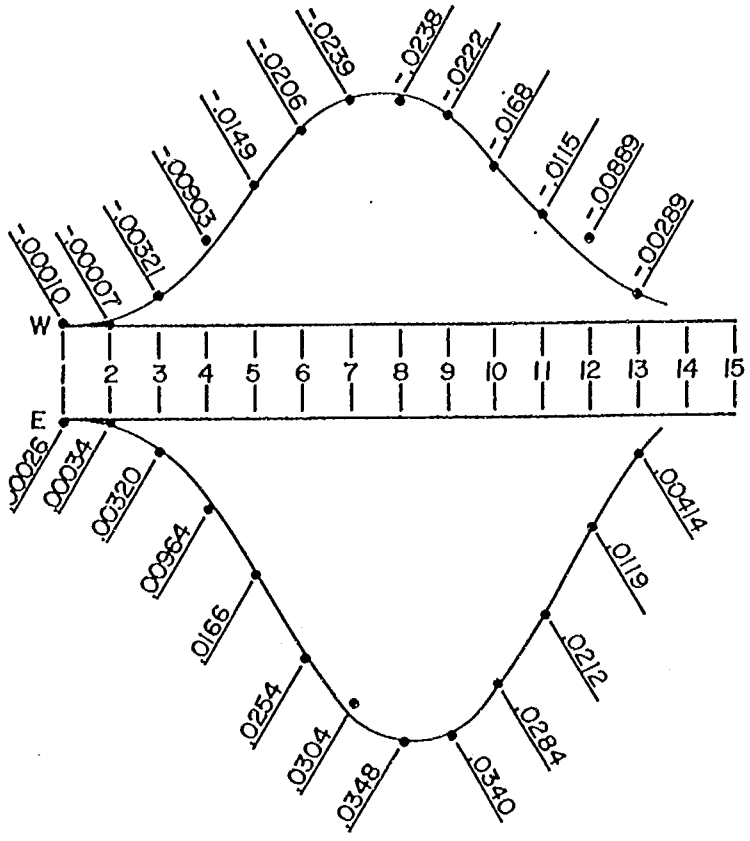


Figure 7. Vertical release displacement configuration at both the East and West sides of the bridge/roadway caused by the low amplitude 21.2 kip ram load.

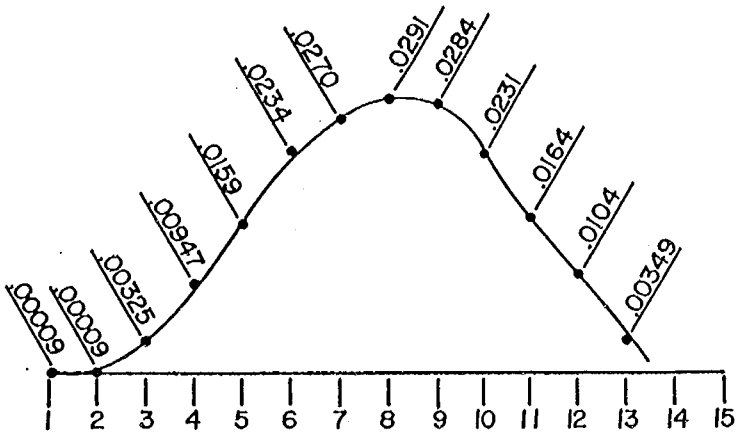


Figure 8. Rotation release displacement configuration of the bridge/roadway caused by the low amplitude 21.E kip ram load.

centerline is shown in Fig. 9. The maximum value of 0.00612 cm is 17% of the largest lateral displacement of the deck in Fig. 6, and this indicates a quite soft central pier foundation.

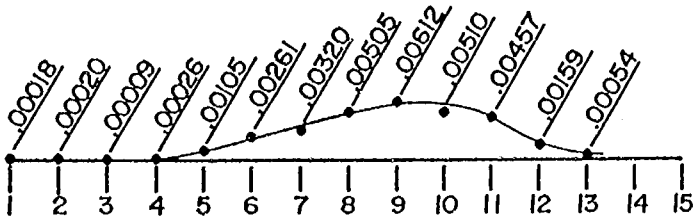


Figure 9. Vertical release displacement configuration of the bridge/roadway centerline caused by the low amplitude 21.2 kip ram load.

Figures 10 and 11 show the release configuration of the hammerhead, central pier, and pier foundation at low and high amplitudes respectively. By comparing the two figures it can be seen that the pier is in single curvature bending at low amplitude, while it is in double curvature bending at high amplitude. If the behavior of the bridge was linear these two diagrams would be proportional. Examination of Fig. 15 reveals that the deck rotation has been restrained more in this case relative to the low amplitude result. Investigation of this phenomenon awaits further study.

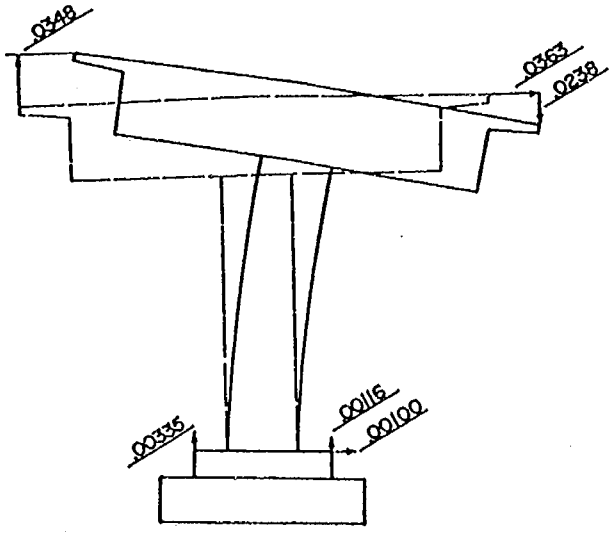


Figure 10. Release configuration of pier section including foundation displacements caused by the low amplitude 21.2 kip ram load.

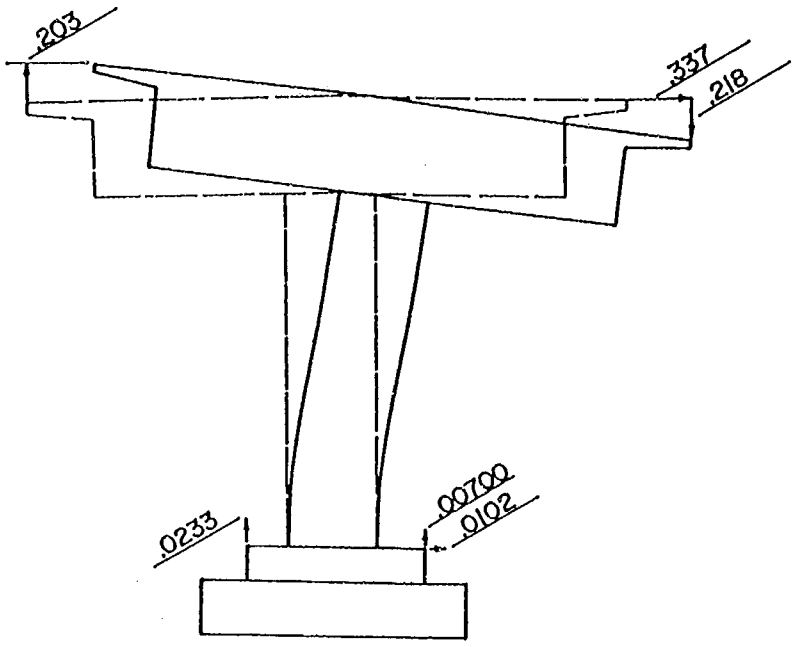


Figure 11. Release configuration of pier section including foundation displacements caused by the high amplitude 141 kip ram.

Figure 12 shows a plot of ram load versus the lateral deflection of the deck at the central pier. There are three data points at ram loads of 0, 21.2 and 141 kips. The straight line is the initial slope, and the curve is a parabola fitted to the three points. This clearly shows the nonlinear behavior over the experimental load range. This is attributed to the soil structure interaction effects of the foundations, whose responses are always strain dependent at all reasonable levels of response.

Finally, Fig. 13 shows the extent of soil involvement at the central pier foundation. The lower curve shows the transverse release displacement configuration out to 47.5 feet away from the edge of the upper pile cap. It can be seen that significant involvement occurs out to a distance of 10 or 15 feet. This is about one pile cap diameter, which is 15 feet in width. Also shown in the curve is a plot of the first arrival times for the accelerograms in question. The slope of the curve is about 1250 feet per second for the apparent wave velocity. As these were first arrivals, it is presumed that they measure the p wave velocity at these close distances. A shear wave velocity of about one third of this p wave velocity would be consistent with the soft soils at the site.

CONCLUSIONS

1. The benefits of a method of calculating the complete static deformation of structures by using quick release dynamic test data has been illustrated for the Meloland Road Overcrossing bridge.

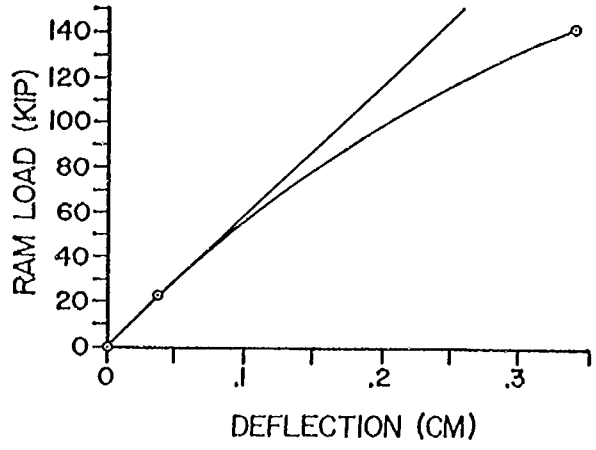


Figure 12. Ram load versus transverse pier displacements at the deck level.

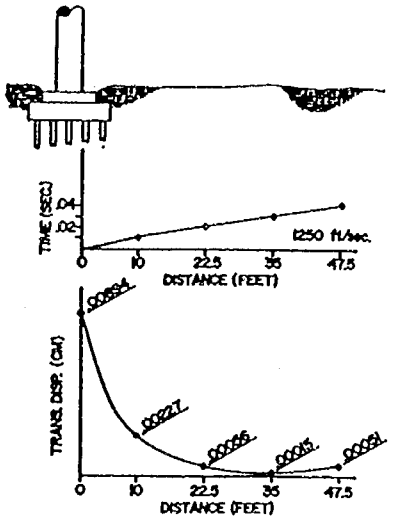


Figure 13. Vertical release displacement configuration of the soils adjacent to the pier foundation caused by the high amplitude ram load and the associated travel time curve developed from the first arrival times.

2. This method greatly enhances the use of data obtained by the quick-release dynamic test method. Now complete acceleration, velocity, and displacement time histories can be generated as well as the offset dis placements used herein.

3. With this method detailed foundation and abutment displacements and rotations can be obtained, which would be extremely difficult to measure with fixed reference frames and displacement transducers. These, of course, are very important in developing accurate soil/structure interaction models of the structural foundations.

4. With respect to the Meloland bridge data, it has been possible to observe nonlinear response characteristics by using the calculated static deformations at two different load levels. It should be remembered that the foundations of bridges always respond in a displacement dependent manner in the usual range of earthquake and test loads. This causes the overall nonlinearities observed in the response of this bridge.

ACKNOWLEDGEMENTS

The authors gratefully acknowledge the support of the National Science Foundation (NSF) and the California Department of Transportation (CALTRANS). The support of our colleagues C.B. Crouse, Mehdi Saiidi, and Stu Werner are also gratefully acknowledged. Our thanks also go to B. Nath. Finally we want to acknowledge the special support of Kinemetric's Inc., and especially the advice of Robert Nigbor.

REFERENCES

1. Brady, A.G., (1966), "Studies of Response to Earthquake Ground Motion," Earthquake Engineering Research Laboratory, California Institute of Technology, Pasadena, CA.

2. Brady, A.G., Perez, V., Mark, P.M., (1982) "Digitization and Processing of Main-Shock Ground-Motion Data from the U.S. Geological Survey Accelerograph Network," Professional Paper 1254, U.S. Geological Survey, Menlo Park, CA.

3. Douglas, B.M., (1976) "Quick-release Pullback Testing and Analytical Seismic Analysis of a Six Span Composite Girder Bridge," Report No. FHWA-RD-76-173, Federal Highway Administration, Office of Research and Development, Washington, D.C., 73 pp.

4. Douglas, B.M., E.A. Maragakis and B. Nath, (1989) "Integration of Bridge Quick-Release Accelerograms to Displacements," submitted to ASCE Journal of Structural Engineering for possible publication (companion paper).

5. Douglas, B.M., and J. Richardson, (1984) "Maximum Amplitude Tests of a Highway Bridge," Proceedings of 8th World Conference on Earthquake Engineering, San Francisco, CA, July 21-28, 1984, 8 pp.

6. Douglas, B.M., and W.H. Reid, (1982) "Dynamic Tests and System Identification of Bridges," Journal of the Structural Division, ASCEVol. 108, No. ST. 10, Proc. Paper 17412, 2295-2312.

7. Hudson, D.E., (1979) Reading and Interpreting Strong Motion Accelerograms, Earthquake Engineering Research Institute, 1979.

8. Iwan, W.D., Moser, M.A., Peng, C.Y., (1985) "Some Observations on Strong-Motion Earthquake Measurement Using a Digital Accelerograph," Bulletin of the Seismological Society of America, Vol. 75, 1225-1246.

9. Rojahn, C., J.T. Ragsdale, J.D. Ragget and J.H. Gates, 1982) "Mainshock Strong-Motion Records from Meloland Road-Interstate Highway 8 Overcrossing, The Imperial Valley California, Earthquake of Oct. 15, 1979," Geological Survey Professional Paper 1254, pp 337-383.

10. Trifunac, M.D., and V. Lee, (1973) "Routine Computer Processing of Strong Motion Accelerograms," Report No. 73-03, Earthquake Engineering Research Laboratory, California Institute of Technology, Pasadena, CA.

(3) Session 3

SESSION 3: SEISMIC DESIGN(2) 10:45am~ 0:00pm
(Co-Chairman: K. Kawashima, B. Douglas)

(4) K. Kawashima K. Hasegawa※ T. Yoshida and T. Ikeuchi: Hysterestic Behavior of Steel Bridge Piers by Shaking Table Tests
(10:45am~11:05am)

(5) H. Shinohara, A. Hasegawa and T. Oishi※ : Aseismic study of kawasaki Man made Island in Trans-Tokyo Bay Highway Project
(11:05am~11:25am)

(6) D. Foutch※ , T. Havenar and S. Pezeshk: Considerations for the Seismic Design of the Clark Cable-Stayed Bridge
(11:25am~11:45am)

DISCUSSION(3)
(11:45am~0:00pm)



HYSTERETIC BEHAVIOR OF STEEL BRIDGE PIERS BY SHAKING TABLE TESTS

Kazuhiko KAWASHIMA[1], Kinji HASEGAWA[2] and Takehumi IKEUCHI[3]

1: Head, Earthquake Engineering Division, Public Works Research Institute, Ministry of Construction, Japan
2: Research Engineer, ditto
3: Chief of Research and Design Section, Engineering Department, Tokyo, Metropolitan Expressway Public Corporation, Japan

INTRODUCTION

A number of steel piers have been adopted for highway bridges constructed in densely populated area like Tokyo and Osaka. Steel piers have high stiffness even with small sections, and therefore they have been adopted at city area in which there are many restrictions for space. As the number of the steel piers increases, considerations for seismic vulnerability is being increasingly concentrated to the steel piers subjected to a significant earthquake ground motion.

There have been few investigations on seismic performance of steel piers in inelastic range. A comprehensive investigation was initiated to study seismic strength, ductility and failure mode of steel piers. This paper presents a shaking table test which was made to study seismic vulnerability of steel piers.

TEST SPECIMEN AND EXPERIMENT PROCEDURE

Test specimens of steel piers used in the shaking table test are shown in Fig. 1. The specimen has a box type section with 40 cm X 40 cm. It was fabricated by welding four main plates (two flange plates and two web plates) with thickness of 4.5 mm. The main plates are stiffened by vertical stiffeners with thickness of 3.5 mm and height of 2.5 m. They are also stiffened by diaphragms placed 35 cm interval. Structural steel (SS41) was used to fabricate the main plates, vertical stiffeners and diaphragms. Yielding stress of the main plates determined by the tension test was 2,130 kgf/cm^2.

The specimen was designed and fabricated in accordance with the Specifications for Highway Bridges [1]. The dimensions of the specimen were determined so that they satisfy the following requirements stipulated in the specifications.

1) stress developed at any part of the specimen subjected to the seismic force as well as weight of super and substructures should be less the allowable stress.

2) cross section area A_ℓ and moment of inertia I_ℓ of the vertical stiffener should be more than the minimum value stipulated by the following equations.

$$I_l \geqq \frac{bt^3}{11} \cdot \gamma_{l \cdot req}$$

$$A_l \geqq \frac{bt}{10n}$$

$$\gamma_{l \cdot req} = 4\alpha^2 n \left(\frac{t_0}{t}\right)^2 (1 + n\delta_l) - \frac{(\alpha^2 + 1)^2}{n}$$

where,

t : thickness of main plate (cm)
b : width of main plate (cm)
n : number of panel divided by vertical stiffener
α : ratio of interval of diaphragm to width of main plate
δ_ℓ : ratio of cross section area of stiffener to cross section of main plate
t_0 : thickness calculated by the equation of $t_0 = b/28n$ (cm)

Yielding displacement corresponding δy to one displacement ductility factor was determined as the displacement at loading point (refer to Fig. 1) at which the steel plates (flange plates) at the bottom of pier reached yielding strain[2]. The yielding displacement δy and lateral force corresponding to δy (yield strength) are 12 mm and 7.83 tf, respectively.

Set-up used for the test is shown in Fig. 2 and Photos 1 and 2. The pier specimen was anchored at the center of a shaking table, and two-span simply supported girders with total weights of 40 ts and length of 17 m were placed on the specimen. Because the other end of the girders could not be supported on the shaking table, it was supported by a steel frame placed outside the table. The steel pier and girder was connected by a fixed support, while the other side of the girder being connected by a movable support with the steel frame outside the table . Therefore, all inertia force developed during excitation is to be supported by the specimen. Because the yielding strength of the specimen is 7.83 tf, the acceleration which causes the yielding of the specimen is 7.83/40 = 0.196 G. It should be noted that the stress developed by the superstructure is 234 kgf/cm^2. Because the allowable stress specified for a combination of principal load and seismic load is approximately equal to the yielding stress, the specimen can be considered that it is designed for the design seismic coefficient of 0.2, in accordance with the current Specification for Highway Bridges.

The shaking table was excited along the axis of model bridge. An acceleration record obtained at Hachiro-gata during the Nihonkai-chubu Earthquake of 1983 was used as an input motion. The time axis was, however, reduced to one half to adjust the predominant frequency of the records. The intensity was scaled to two times, three times and four times as large as the original as a parameter to be investigated. They were designated herein as Test A (peak table acceleration a_{max} = 0.18 G), Test B (a_{max} = 0.29 G) and Test C (a_{max} = 0.44 G), respectively.

Extensive instrumentation was used to measure the basic parameters, such as accelerations at the bottom of the specimen as well as at the girder, strain of main plates, and displacement of the girder relative to

the shaking table.

TEST RESULTS

Figs. 3, 4 and 5 show response accelerations at the footing and the girder as well as the relative response displacement of the girder for Tests A, B and C, respectively. Peak accelerations developed at the footing, which is recognized as peak input acceleration to the pier-superstructure system, is 0.18G, 0.29G and 0.44G for Tests A, B and C, respectively. Local buckling of main plates occurred as shown in Photos 4 and 5 at the bottom of the column in Tests B and C. In Test C, the maximum out-of-plain deformation amounted to 6 cm at the bottom. The specimen tilted with an amount of 24cm at the pier crest after excitation as shown in Photo 3. It is interesting to note that such drift of a response displacement seems to be developed at the first large excursion which exceeded the yield displacement, i.e., accumulation of a response displacement after the first large excursion seems small.

Table 1 shows the peak response values of response accelerations and relative displacements. Nonlinear response of steel bridge piers can be clearly seen in comparison between a peak response acceleration and a peak relative response displacement at the girder, i.e., a relative response displacement of the girder increases with increasing an input acceleration while a peak response acceleration of the girder takes almost the same value which is independent of the intensity of an input motion.

The hystersis loops of the inertia force and relative displacement relation in Tests A, B and C are shown in Fig. 6, 7 and 8, respectively. It can be seen from these figures that the biased vibration was developed, in particular in Tests B and C after the first significance movement with larger displacement than the yield displacement. Maximum force developed during the Tests B and C is about 16 tf, which is 2 times as large as the yield strength of 7.83 tf. The degradation of the tangential stiffness in accordance with nonlinear response is less significant.

CONCLUDING REMARKS

For aiming to study inelastic behavior of steel bridge piers, a shaking table test was conducted by varying intensity of table motion. The following conclusions may be deduced from these tests:

1) Significant out-of-plane deformation followed by the local buckling developed in the main plate at bottom causes a considerable deterioration of bearing capability of the model steel piers.
2) Maximum force of the model steel pier is approximately two times as large as the yielding strength. Significant deterioration of the bearing capability developed over the maximum force.
3) Once the relative displacement of the pier exceeds the displacement corresponding to the maximum force, the model pier is likely to show a biased response to one side. Thus, large residual displacement remained after excitation in Tests B and C.

REFERENCE

1) Japan Road Association : Specifications for Highway Bridges, Part I Common Part, Part II Steel Bridges, Part IV Foundation and Part V Seismic Design, 1980

2) Kawashima, K. and Koyama, T. : Effects of Cyclic Loading Hysteresis on Behavior of Reinforced Concrete Bridge Piers, Structural Eng. / Earthquake Eng., Vol. 5, No. 2, pp. 343 - 350, 1988. 10

3) Kawashima, K., Hasegawa, K., Koyama, T., and Yoshida, T. : Hysteretic Behavior of Reinforced Concrete Bridge Piers by Dynamic Loading Tests and Shaking Table Tests, Proc. 9th WCEE, Tokyo / Kyoto, Japan, 1988.8

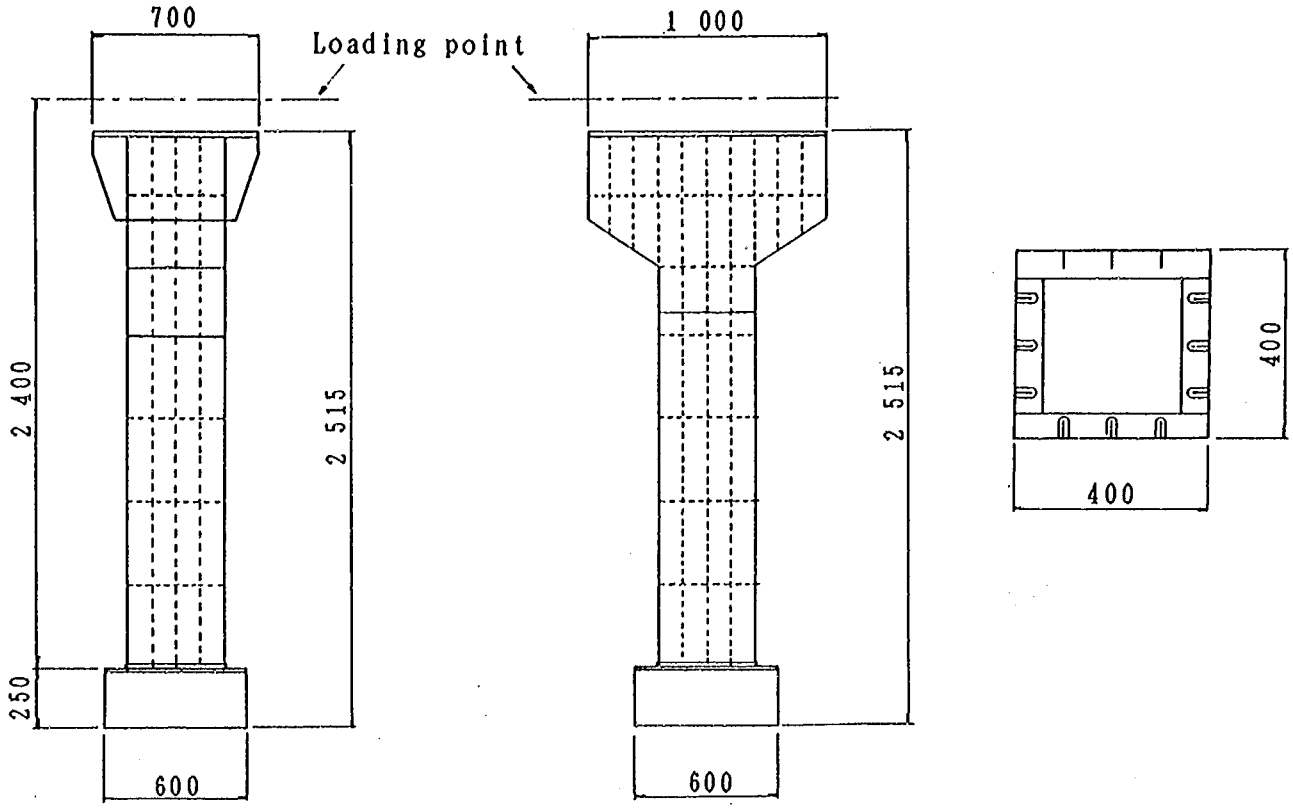


Fig. 1 Test Specimen of Steel Bridge Pier

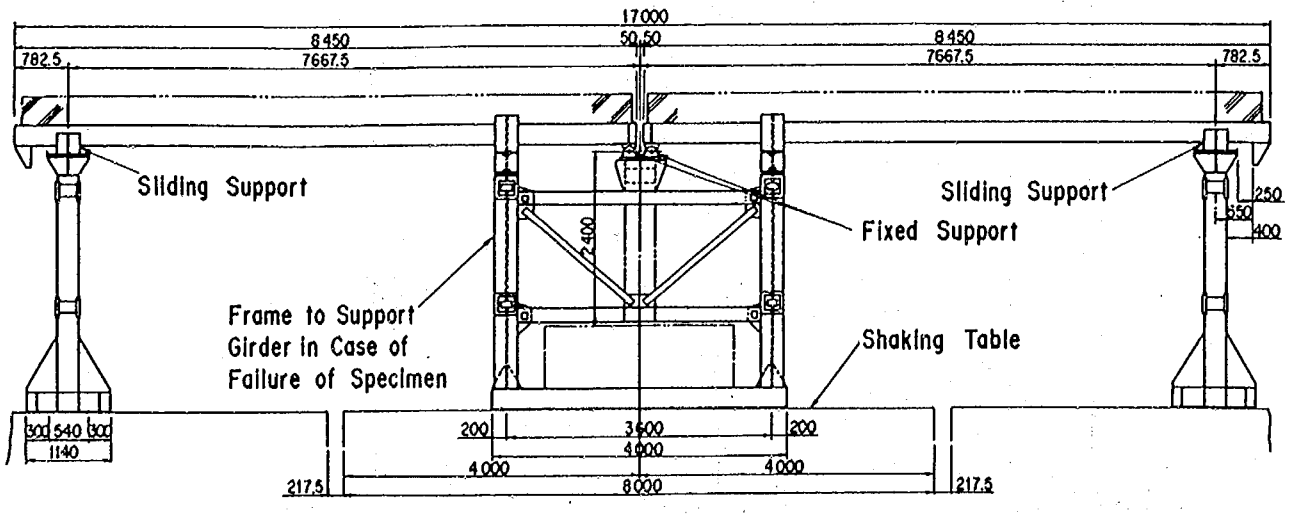
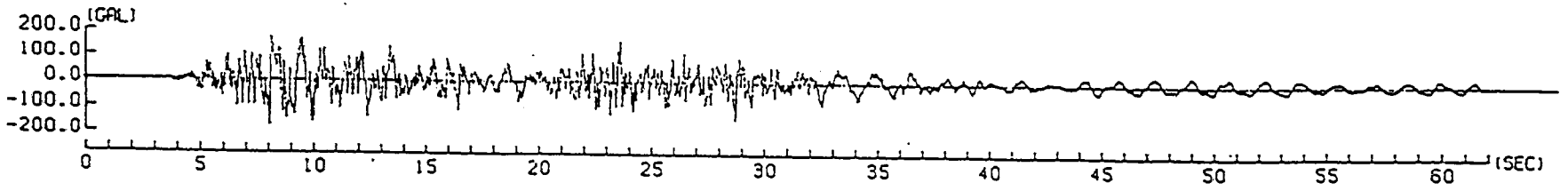
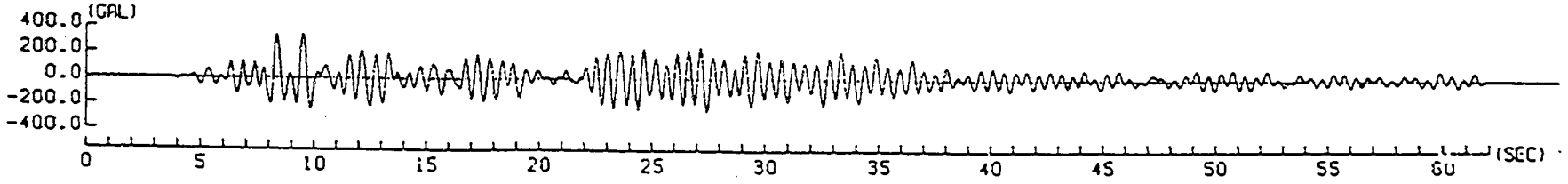


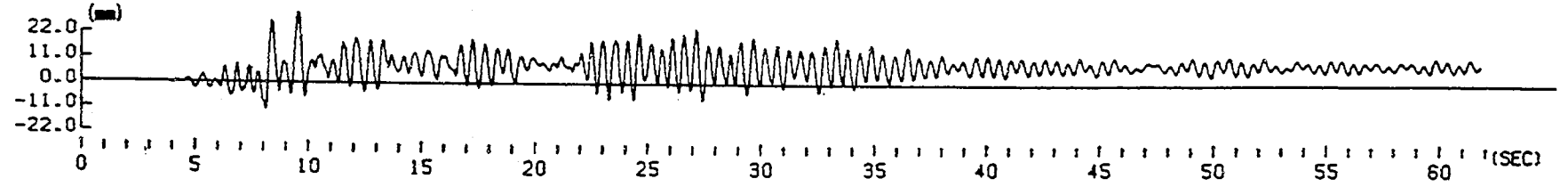
Fig. 2 Set-Up of Shaking Table Test



(a) Acceleration at Footing

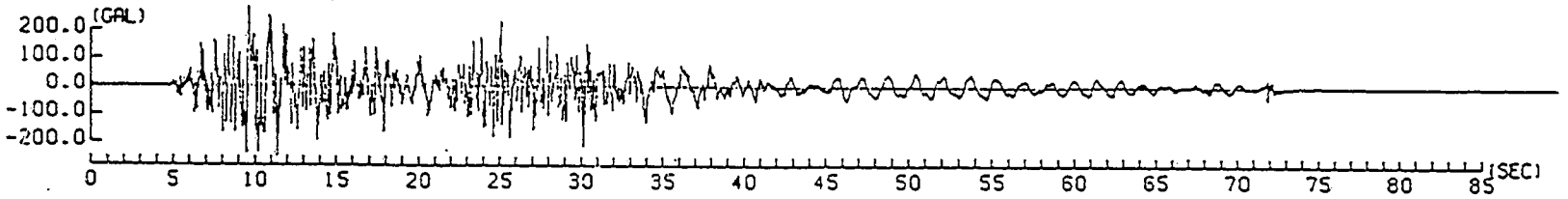


(b) Acceleration at Girder

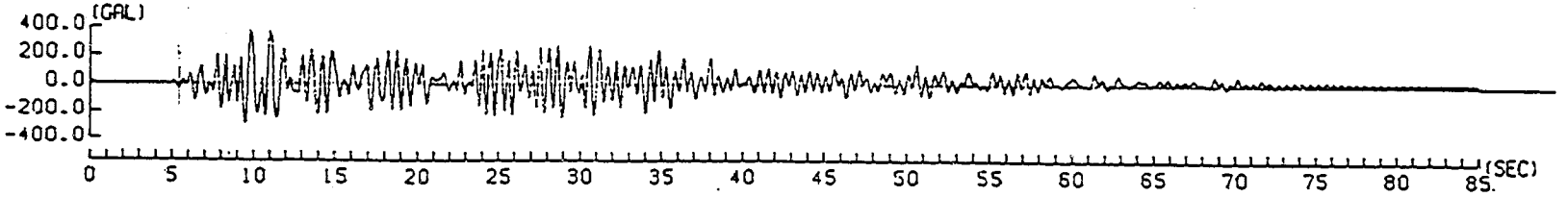


(c) Relative Response Displacement at Girder

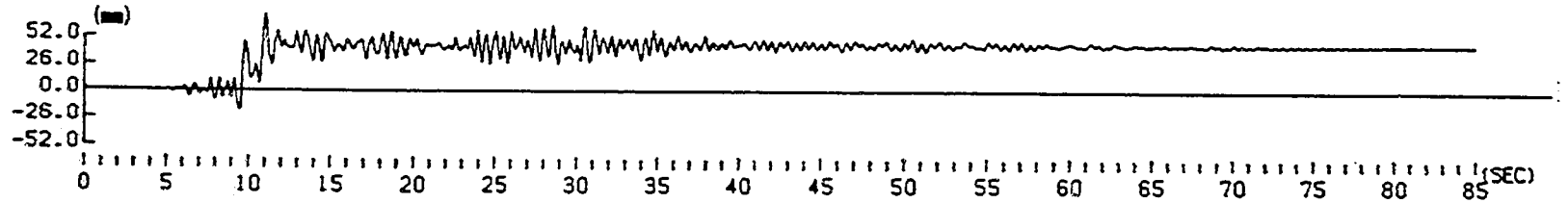
Fig. 3 Response Acceleration and Displacement in Test A



(a) Acceleration at Footing

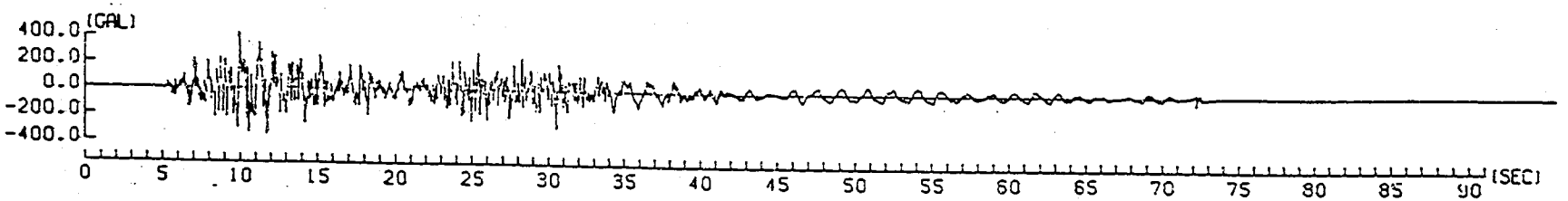


(b) Acceleration at Girder

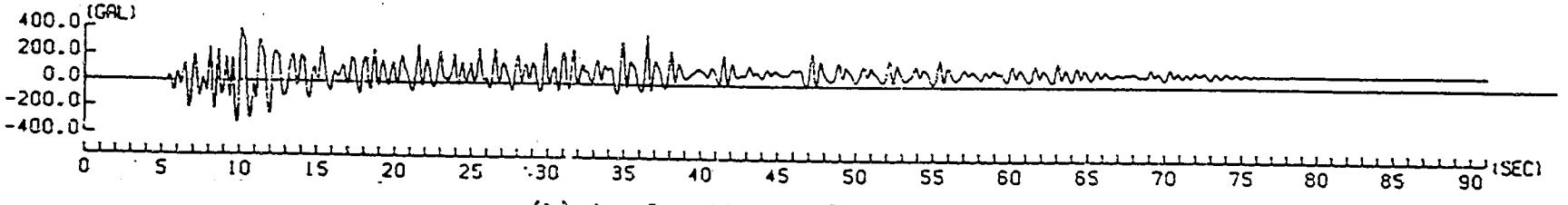


(c) Relative Response Displacement at Girder

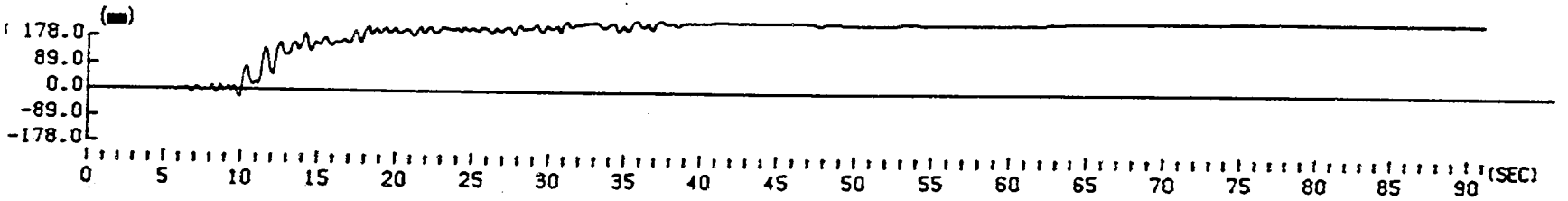
Fig. 4 Response Acceleration and Displacement in Test B



(a) Acceleration at Footing



(b) Acceleration at Girder



(c) Relative Response Displacement at Girder

Fig.5 Response Acceleration and Displacement in Test C

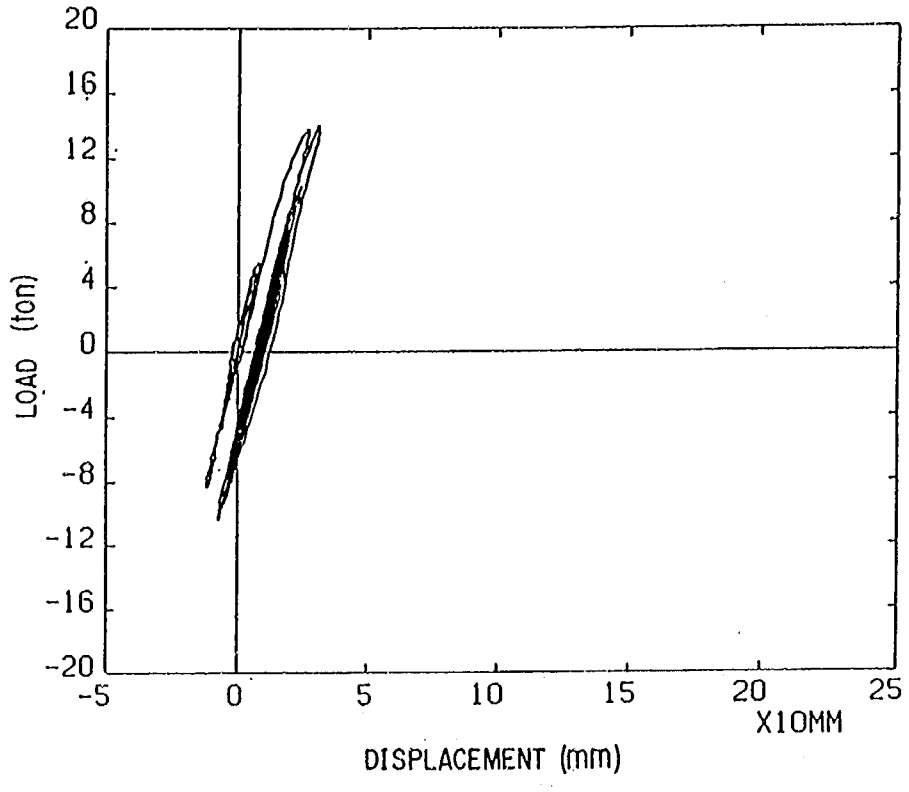


Fig. 6 Hysteresis Loop of and Displacement in Test A

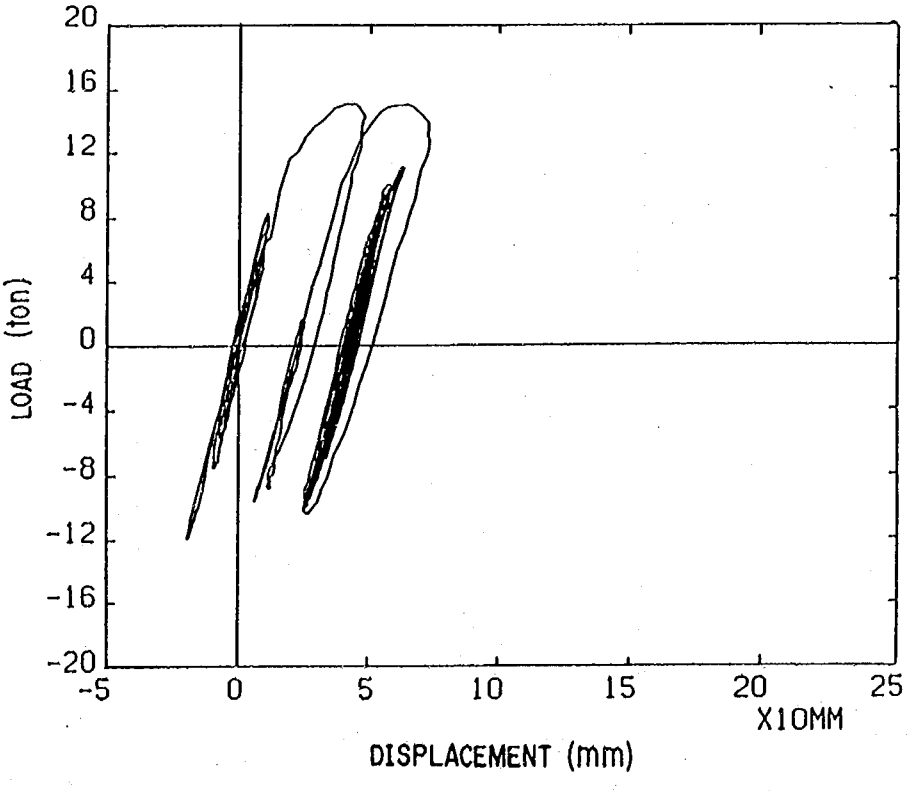


Fig. 7 Hysteresis Loop of and Displacement in Test B

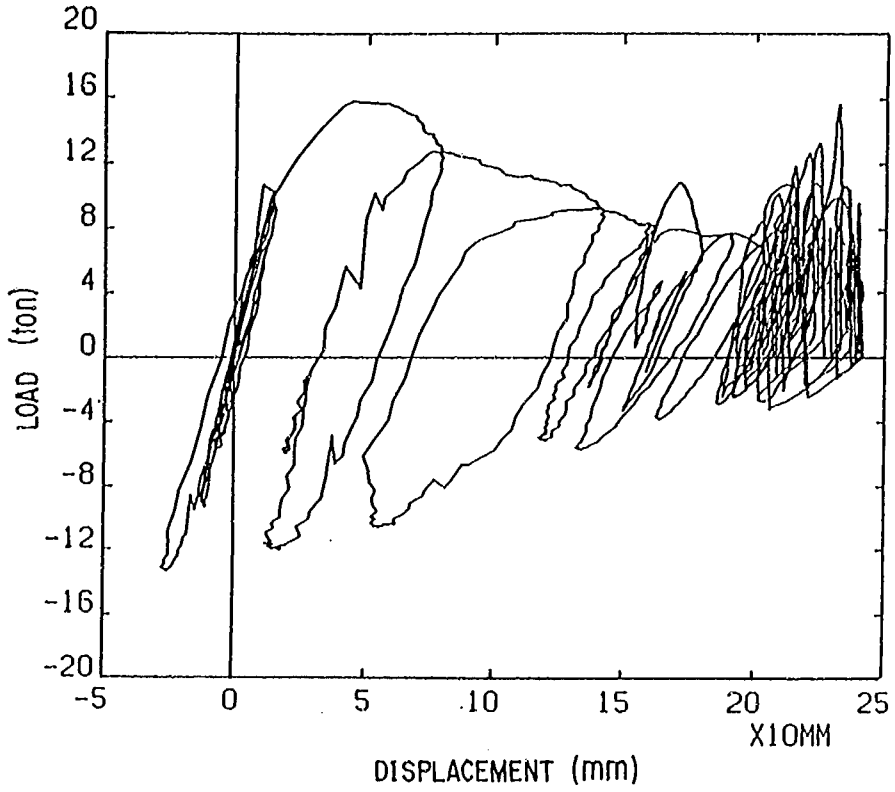


Fig. 8 Hysteresis Loop of and Displacement in Test C

Table 1 Peak Pesponse Acceleration and Displacement

	Peak Acceleration		Peak Displacement of Girder
	Footing	Girder	
Test A	0.177 G	0.350 G	31 mm
Test B	0.289 G	0.378 G	73 mm
Test C	0.440 G	0.398 G	242 mm

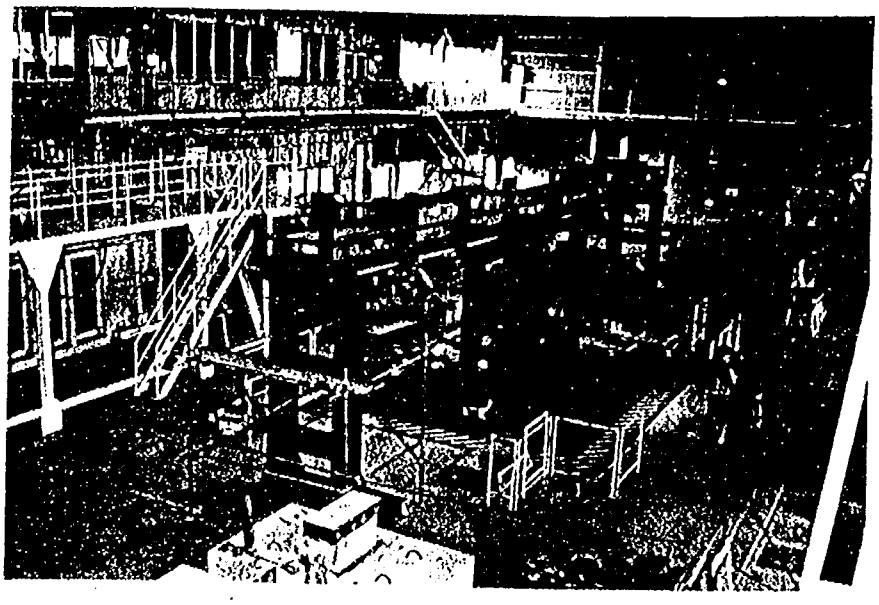


Photo 1 Set-up of Shaking Table Test

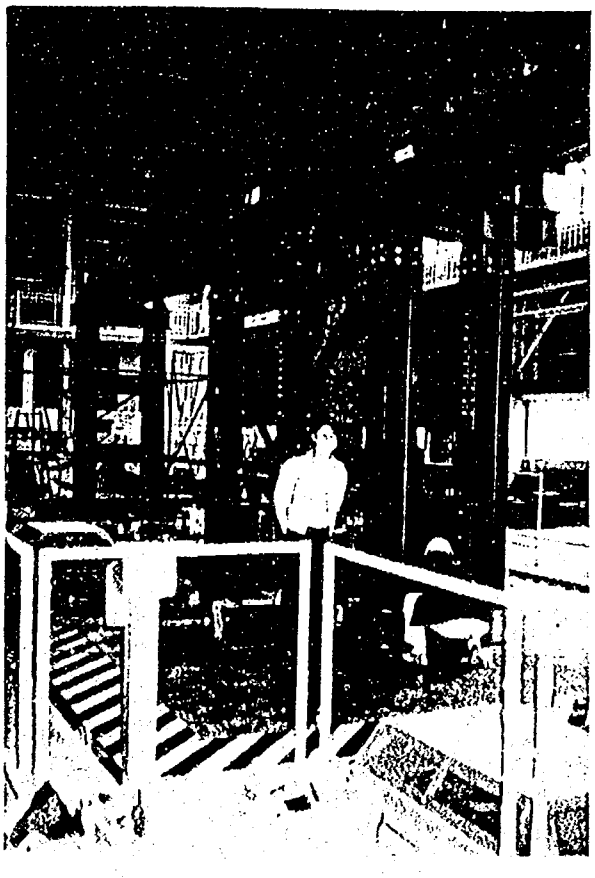


Photo 2 Specimen of Steel Bridge Pier

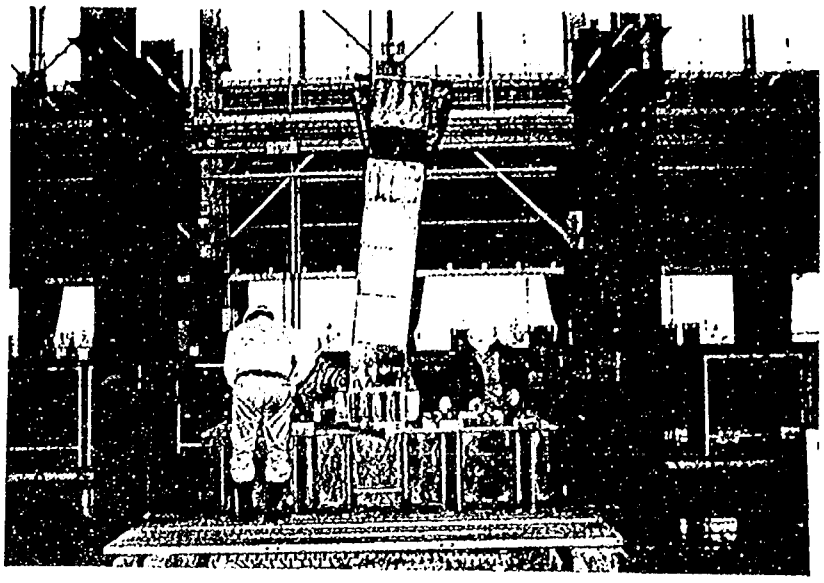


Photo 3 Inclination of Specimen after Test C

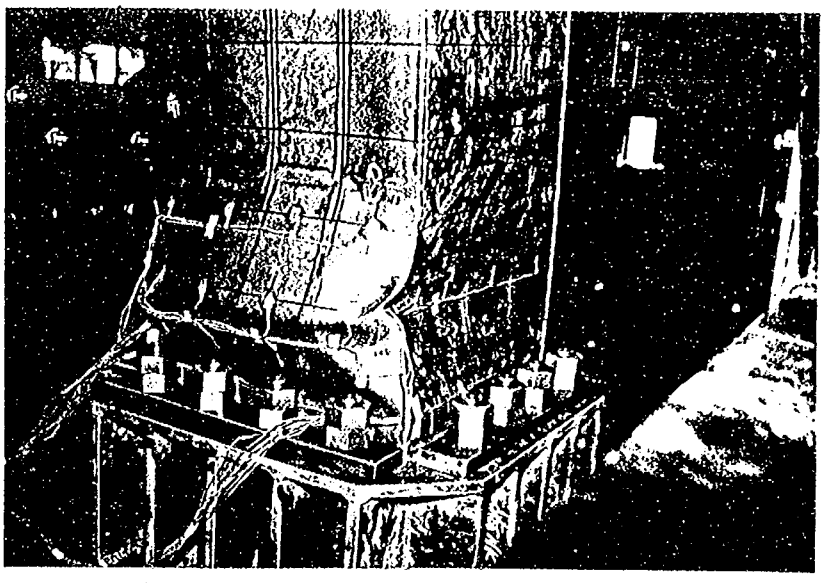


Photo 4 Buckling of Main Plate in Test C



Photo 5 Inside of Buckled Plate in Test C

Aseismatic Study of Kawasaki Manmade Island in Trans-Tokyo Bay Highway Project

Trans-Tokyo Bay Highway Corporation
Design Department
Hirosi Shinohara, General Manager
Akinori Hasegawa, Section Manager
Tsuguo Oishi, Acting Manager

Abstract

Kawasaki Manmade Island in Trans-Tokyo Bay Highway is an unique circular structure with inner diameter of 90m and height of 68.5m, which will be constructed offshore where water is 28m deep and soils beneath the bay-bottom are very soft. Structuring of steel trestle will be followed by island fill placement in the structure. A diaphragm wall is constructed in the island fill to form a cylindrical structure, then a reinforced concrete permanent wall will be constructed using "top-to-down" procedure, followed by placing of the bottom slab.

Considering these charasteristics, aseismatic strength of Kawasaki Manmade Island was studied both at construction phase and at completion phase by dynamic analysis using an axial synmetric cylindrical model which expressed both the structure and soils.

The study has revealed that extra circular reinforcement of diaphragm wall is necessary before ring compression can be expected at construction phase, and that statically determined section of permanent structure is practically seismic-proof at completion phase.

1. Introduction

As the first phase of an ambitious plan to connect Kawasaki and Chiba directly crossing Tokyo Bay over a 15km distance, the Trans-Tokyo Bay Highway project was approved by the Government to proceed with participation of the private sector. The Trans-Tokyo Bay Highway Corporation was established on Oct. 1, 1986, and is responsible for the construction.

The highway structure will consist of two-10km long tunnels under Kawasaki waters where surface traffic is heavy and the water is nearly 20m deep, a 5km long bridge over Chiba waters where surface traffic is sparse and water is shallow, and two manmade islands, of which Kawasaki Manmade Island(hereinafter dubbed KMI) is for a ventilation shaft as well as for a tunnel access shaft, and Kisarazu Manmade Island is for for a transition structure from tunnels to bridge as well as for a ventilation shaft and a tunnel access shaft as shown in Fig.1.

The size and scope of the structures are far beyond those of conventional ones. Furthermore, the structures will be constructed in very soft grounds under deep water where the likelihood of largescale earthquakes are high.

KM Island is an unique circular structure with inner diameterof 90m and height of 68.5m(pls. refer to Fig.2), which selected location is nearly 5km offshore of the Kawasaki Harbour, where water is about 28m deepand soils under the seabed are very soft for a depth of neary 30m.

Therefore, the soils are stabilized by sand compaction or similar method, followed by construction of a steel trestle structure which functions as a retaining wall, a mole structure and a working platform. "Island" fill is then placed within the structure. To form a cylindrical retaining structure, a diaphragm wall is excavated within the island fill to a specified depth. Then a reinforced concrete permanent inner wall will be constructed using the "top-down" construction procedure, followed by the placing of a bottom slab.

2. Aseismatic Study at Construction Phase

Among many stages in the construction process of the KMI, the following three stages are assumed comparatively critical during earthquake:

Case 1:At completion of diaphragm wall when dynamic water pressure and dynamic earthpressure are maximum(pls. refer to fig.3(1)).

Case 2:At concrete placing of permanent side wall at seabottom level when loading condition will be changed due to excavation depth approaching to seabottom(pls. refer to fig.3(2)).

Case 3:At concrete placing of permanent side wall at bottom slab level when earth and water pressure on the diaphragm wall are maximum constantly(pls. refer to Fig.3(3)).

Input earthquake baseground motion at this phase is reduced to one half of an earthquake "L1" which would occur once at most in the structure lifespan due to the following reasons:

(1)The reduction procedure has been conventionally and practically adopted by many authorities.

(2)Assuming 10-year construction period of the KMI, the ground motion which could be mobilized by an earthquake with non-occuring probability of 50% with 50km earthquake distance is approximately the one half of the L1 earthquake.

The structure and its surrounding soils are modelled as axial symmetric cylindrical body. The soils are assumed as solid element, diaphragm wall and side wall as shell element, and steel fabricated trestle structure as solid element with equivalent shearing rigidity as obtained from frame analysis of the trestle structure, and piles as shell element with equivalent bending rigidity.

Circular distribution of displacement and load are expressed using Fourier expansion. It is also assumed that stress and deformation could be expressed by first degree of Fourier expansion because of horizontal and one-dimensional input of base ground earthquake motion.

Maximum displacement and acceleration of the model at typical location are shown in Table 1 by the dynamic response analysis. Comparative displacements at the seabottom level are such that natural soils is displaced about 6cm, the surrounding zone of the stabilized soils 5.4-5.9cm and the strucure 2.5-3.0cm. This shows that the structure and the surrounding stabilized soils control and diminish ground displacements due to their high rigidity. Comparative maximum acceleration is 195gal in natural soils, 250-270gal in the surrounding zone of the stabilized soils, and 65-75gal and 90-100gal respectively in the structure both at the seabottom level and at the structure top level.

Dynamic earthpressure is shown in Fig.4. The dynamic earthpressure

distribution is rather uniform above seabottom, but sharply discrete at both boundary of natural soils and Deep Mixing Method(hereinafter dubbed DMM) stabilized soils(TP-54.2m), and at soils rigidity discrepant points(TP-70m and TP-90m). This shows that dynamic earthpressure depends on soils seismic behaviour due to their consistency, and the diaphragm wall flexibility to ground deformation.

Sectional forces obtained from dynamic analysis are shown in Fig.5. Vertical normal force is compressive at one half of the acceleration direction and tensile at the rest. Bending moment along vertical direction is negligible above the seabed, however large at both boundary of natural soils and DMM stabilized soils, and at soils rigidity discrepant points.

Shearing force increases from the top downwardly till showing its peak value at TP-70m, then gradually decreasing its value further down.

Circular normal force changes at TP-55m from compression to tensile. Its circular distribution is simulated by "cosine curve", and the compression in one half of the circle changes to tension state in the other half.

The safety of the structure is checked by combining sectional forces during construction phase and seismic sectional forces obtained from the dynamic analysis. Compression stress of concrete is well below the allowable level. Fig.6 shows a necessary reinforcement for both circumferential and vertical direction in the diaphragm wall. Tensile stress of vertical rebar could be controlled well below the allowable level by installing necessary reinforcement against bending moment and shearing force from both design and construction viewpoint. However, circular reinforcement of the diaphragm wall is difficult considering constructability of circular rebar assembly, because necessary reinforcement against shearing force at the completion of the diaphragm wall is large in quantity and wide in area. The reinforcement is necessary because ring compression will not be mobilized due to no difference of waterhead at both inside and outside of the structure. This implies that ring copression could be mobilized by differentiating water level through dewatering inside of the structure, whereby circular reinforcement could be reduced to a reasonable level. The issue will be further studied considering constructability of diaphragm wall and safety of partially completed diaphragm wall.

3. Aseismatic Study at Completion Phase

Structural configuration of KMI is shown in Fig.2. In the study, stabilized manmade fill in between the trestle and ventilation shaft is assumed to be removed upon completion. The diaphragm wall is assumed to be destructed at the bottom slab elevation after inside ground water level recovered, therefore only the mass of the diaphragm wall above the destruction point is counted in the study. The study is composed of the following two analysis:

(1)Dynamic analysis using axial symmetric cylinderical model

(2)Stress analysis using three dimensional FEM

The dynamic analysis is to estimate general seismic behavior of the structure and dynamic earth pressure mobilization in the surrounding soils, in which stress in the ventilation shaft can not be well evaluated due to inability to incorporate separation walls in the shaft and tunnel openings in the analysis. Therefore, reaction of the surrounding soils, inertia of the structure, and dynamic water pressure obtained from the former analysis are incorporated as working loads in the three dimensional stress analysis

to study stress level of the permanent structure.

Input earthquake base-ground motion at this phase is an earthquake "L2" which might or might not occur once in the structure lifespan.

Maximum displacement and acceleration of the model at typical location are shown in Table 2 by the dynamic analysis. Comparative displacements at t he sea-
bottom level are such that natural soils is displaced about 20cm, the surrounding zone of the stabilized soils nearly 19cm and the strucure about 12cm. This shows that the structure follows the ground movement relatively well compared with the diaphragm wall behavior at construction stage. The displacement difference at the top and the bottom slab elevation of the structure is 5cm, thus showing rocking movement of the structure.

Maximum acceleration is 345gal in natural soils and 276gal in the structure at seabottom level thus showing similarity in the seimic behavior compared with the diaphragm wall behavior at construction stage.

Among approximately 1,000 solutions in the dynamic analysis over its analytical time range of 20 seconds, a period which gives maximum displacement and maximum acceleration at the top of the structure is chosen to obtain the input working loads in the three dimensional stress analysis. Conceptual loads diagram is shown in Fig.7. The results from the stress analysis shows that statically determined section is practically seismic-proof.

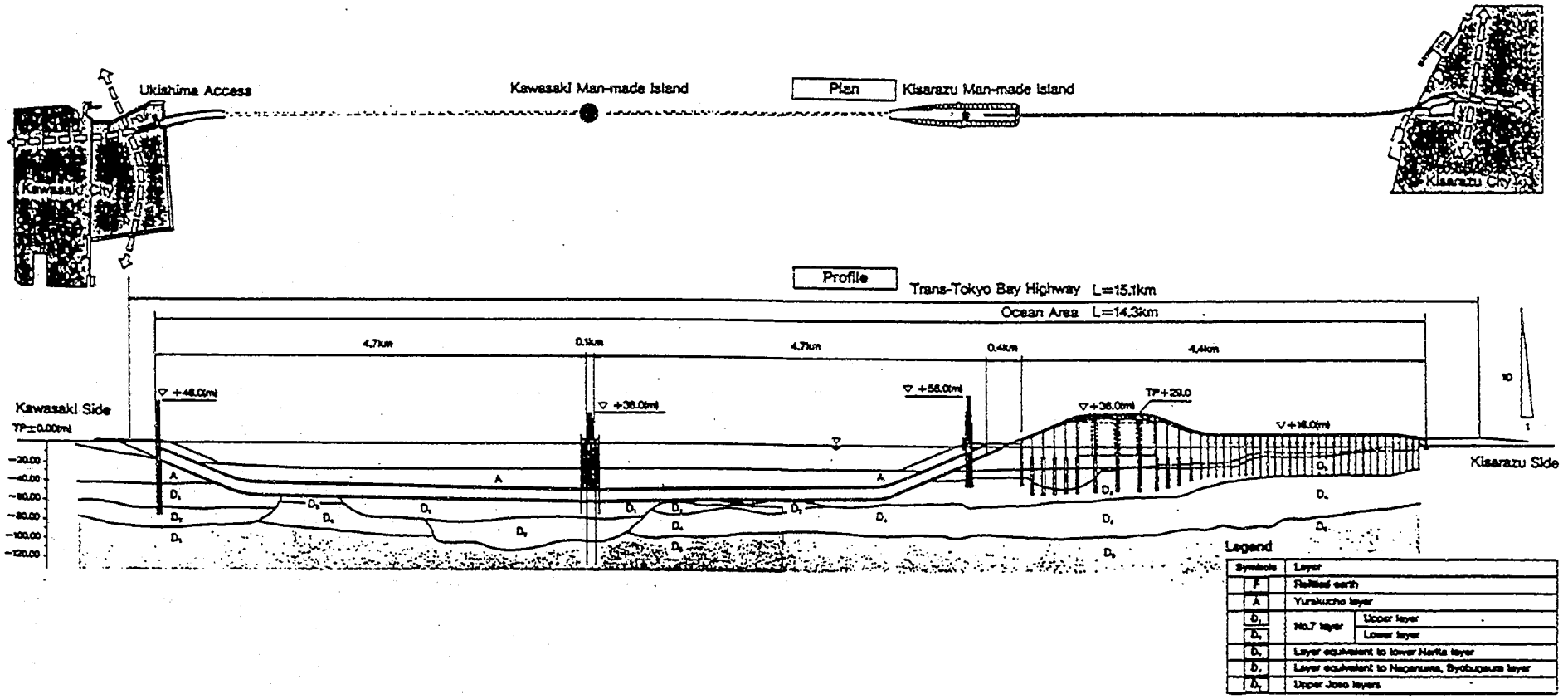


Fig.1 Plan and Profile of Trans-Tokyo Bay Highway

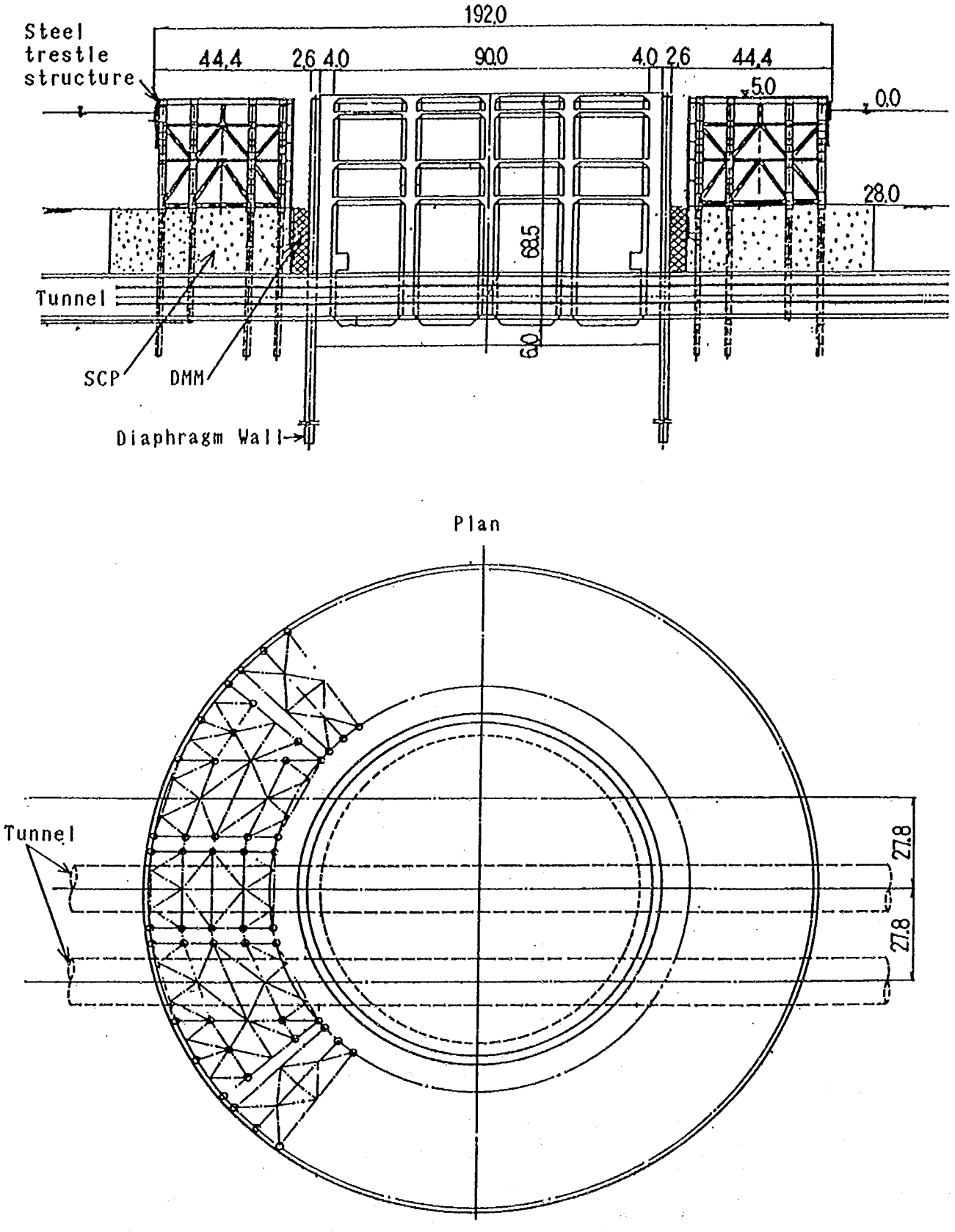
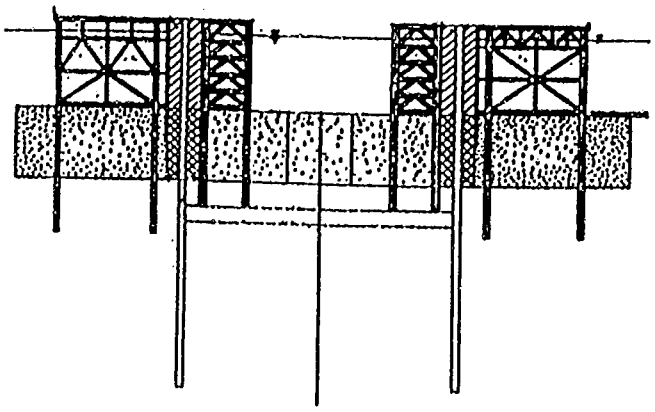
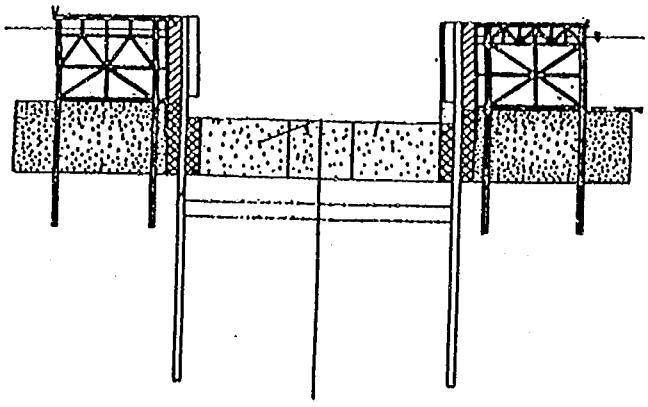


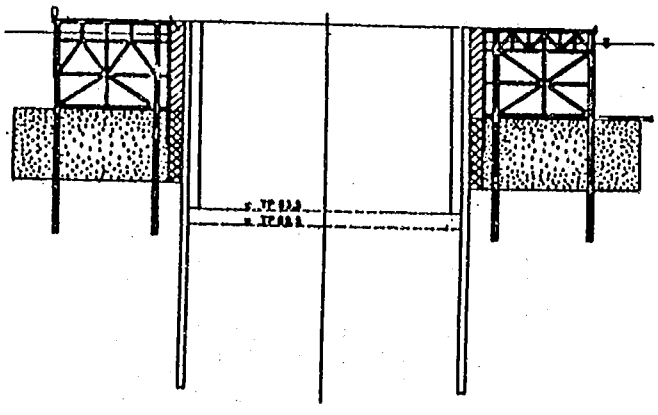
Fig.2 Plan and Profile of Kawasaki Manmade Island



(1)Case 1; Completion of diaphragm wall



(2)Case 2; Concrete placing of permanent side wall at seabottom level



(3)Case 3; Concrete placing of permanent side wall at bottom slab level

Fig.3 Construction Stage of Kawasaki Manmade Island

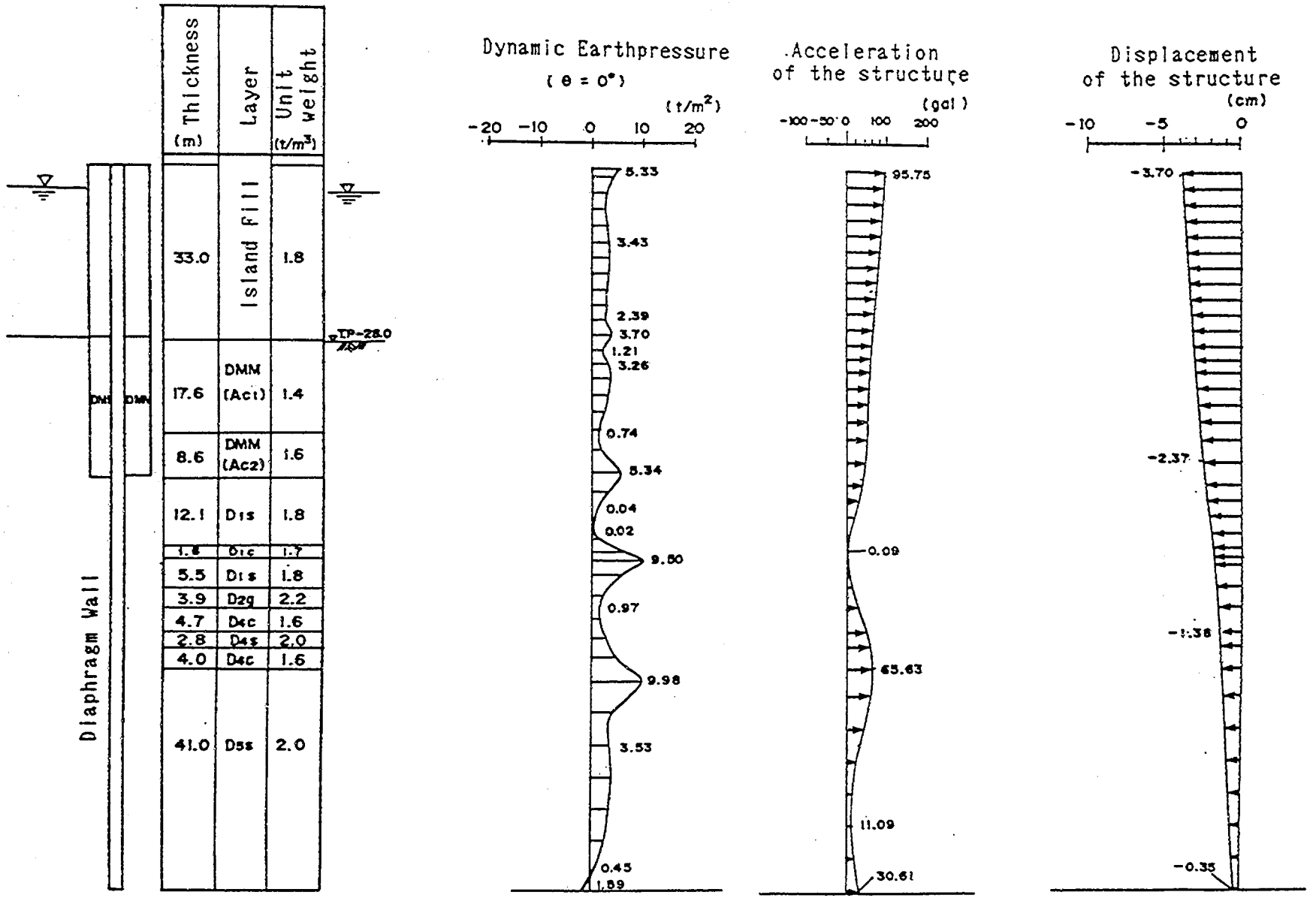


Fig.4 Dynamic Earthpressure, Acceleration and Displacement by Dynamic Analysis at Construction Phase(Case 1 t= 1.36sec)

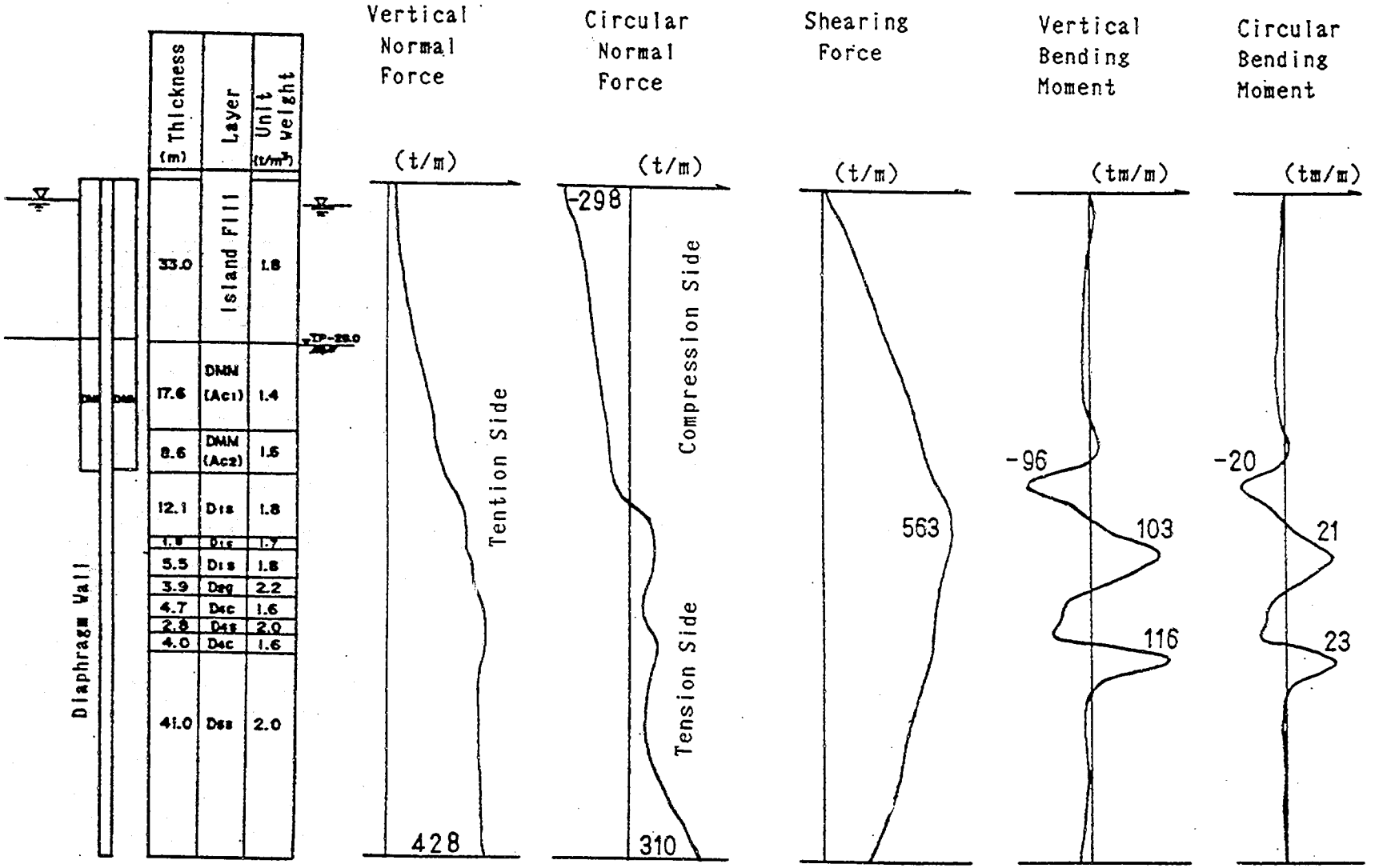


Fig.5 Sectional Forces by Dynamic Analysis at Construction Phase(Case 1 t=1.36sec)

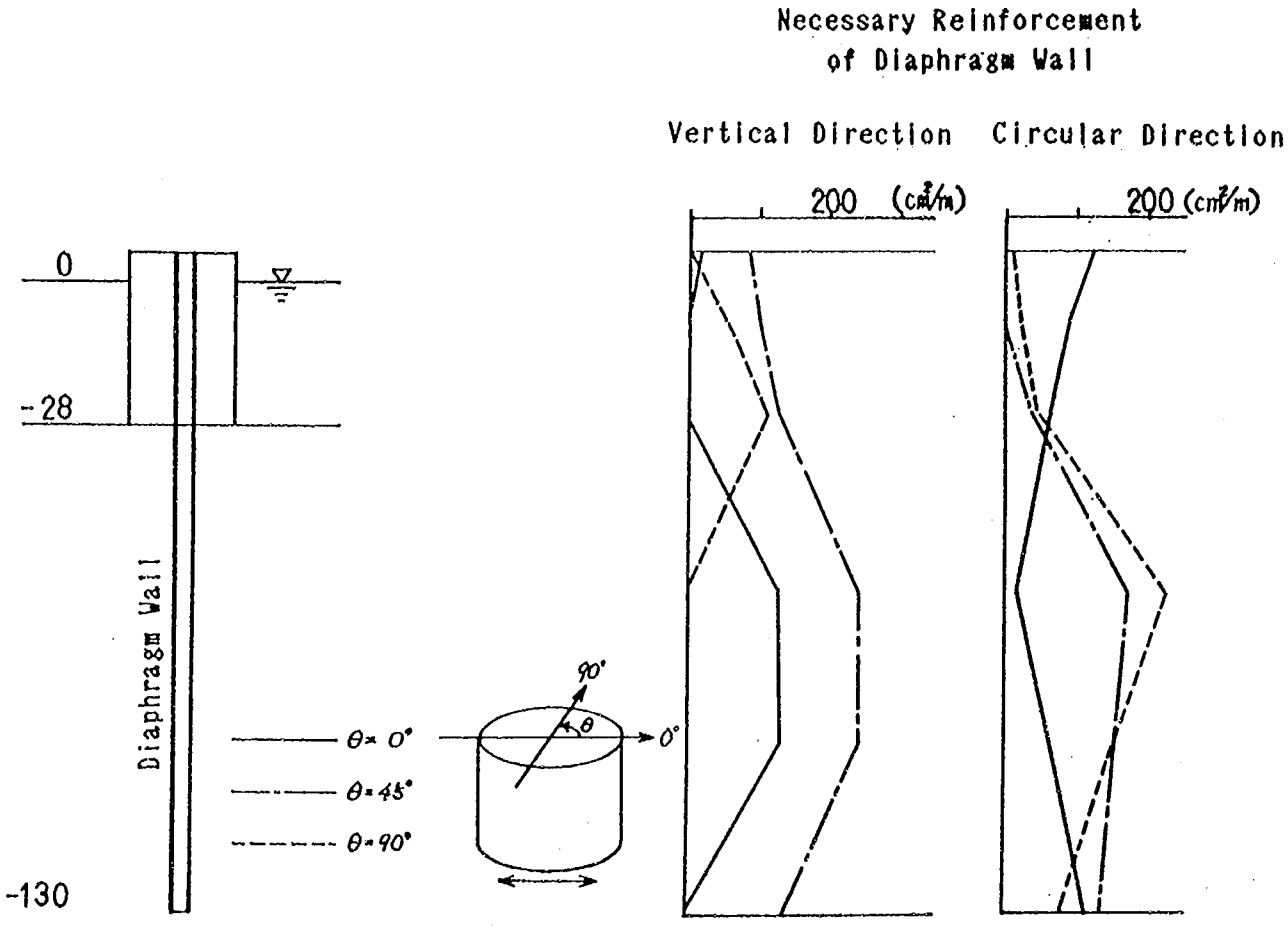


Fig.6 Necessary Reinforcement of Diaphragm Wall at Construction Phase(Case 1)

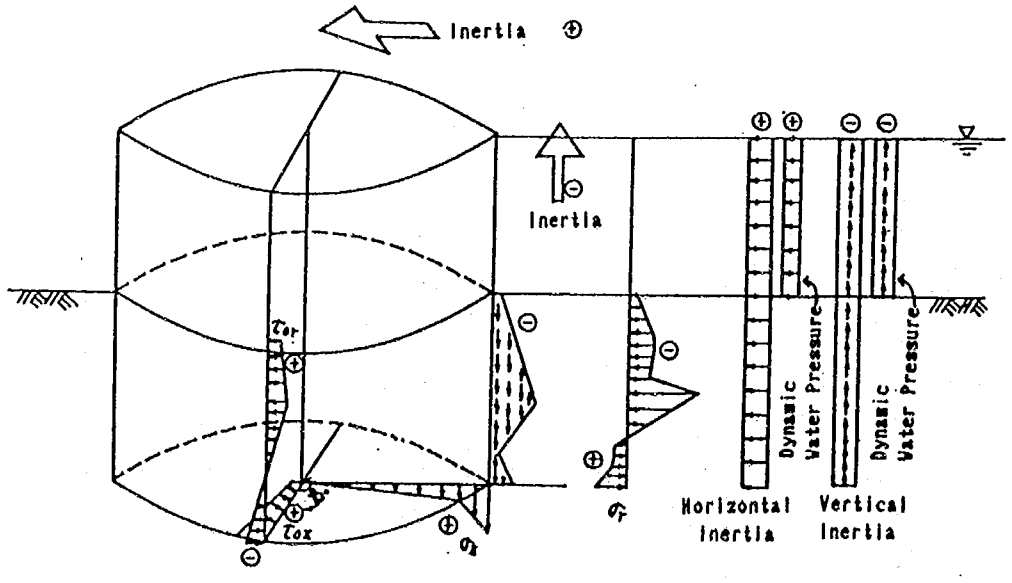


Fig.7 Conceptual Loads diagram for Dynamic Analysis at Completion Phase

Table 1 Maximum Displacement and Acceleration by Dynamic Analysis at Construction Phase

		structure top level ①	structure seabottom level ②	surroundings of stabilized soils ③	natural soils ④
Case 1	displacement in cm	3.70	2.97	5.82	6.08
	acceleration in gal	85.7	72.1	270.0	195.0
Case 2	displacement in cm	3.33	2.75	5.91	6.09
	acceleration in gal	102.0	75.2	274.7	194.0
Case 3	displacement in cm	3.02	2.53	5.38	6.13
	acceleration in gal	88.8	63.6	248.6	194.9

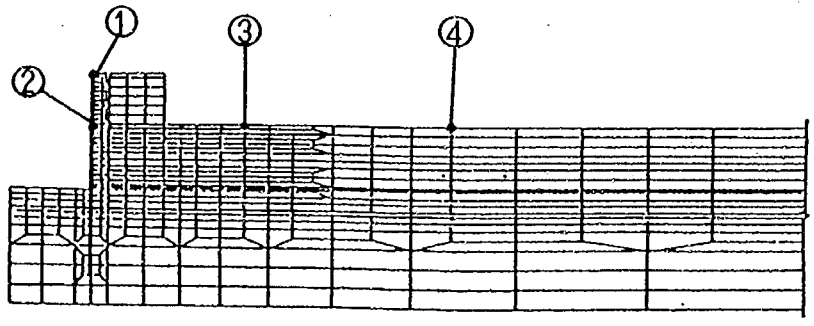
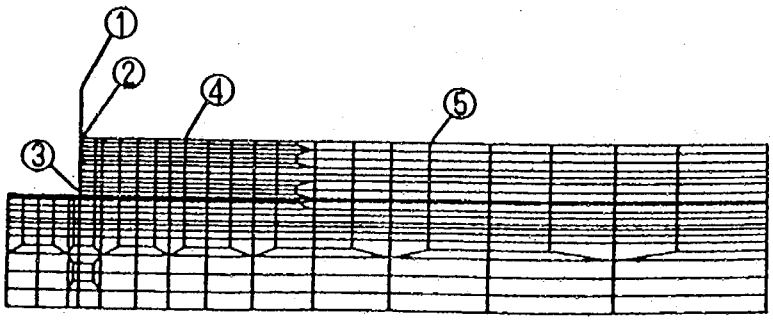


Table 2 Maximum Displacement and Acceleration by Dynamic Analysis at Completion Phase

		Structure			Soils	
		top ① TP+5.0	sea bottom ② TP-2.8	bottom slab ③ TP-88.5	surroundings of stabilized soils ④	natural soils ⑤
L1	displacement in cm	13.7	11.6	8.5	18.8	20.3
	acceleration in gal	334.8	274.5	181.1	382.5	344.6



CONSIDERATIONS FOR THE SEISMIC DESIGN OF THE CLARK CABLE-STAYED BRIDGE

by

Douglas A. Foutch[1], Thomas Havenar[2], and Shahram Pezeshk[1,2]

INTRODUCTION

The Clark Bridge is located in Alton, Illinois, which is 18 miles (28.8km) north of St. Louis, Missouri, and 242 miles (387km) southwest of Chicago, Illinois. The bridge will carry four lanes of traffic on U.S. Route 67 across the Mississippi River. When completed, the new Clark Bridge will replace the existing bridge which has been in service for more than 50 years. The bridge carries a significant amount of traffic daily between the residential areas on the Illinois side to the northern metropolitan area of St. Louis. The chief engineering firm for the design of the Clark Bridge is Hanson Engineers, Inc. (HEI), whose home office is located in Springfield, Illinois.

In the preliminary design stage, three alternates in steel and three alternates in reinforced concrete were considered. Based on cost estimates, it was decided that the main segment of the bridge for each material type should be a three-span cable-stayed bridge. The steel alternate is being designed by HEI and the reinforced concrete alternate is being designed by Figg and Muller Engineers, Inc., under a subcontract with HEI. This paper will deal only with the steel alternate.

The purpose of this paper is to discuss the considerations for the seismic design of the main segment of Clark Bridge, which is a three-span cable-stayed bridge. The bridge has several unique characteristics that will be described below. The final design of the bridge is currently underway. Thus, the final seismic analysis has not been completed to date. A description of the bridge, the recommendations for the seismic design and the preliminary results for mode shapes and frequencies are described herein.

DESCRIPTION OF CLARK BRIDGE

The Clark Bridge is 4620 ft. (1358.3m) long from abutment to abutment. Plan and elevation views of the entire bridge are shown in Fig. 1. The main segment is a three-span cable-stayed bridge which is 1360 ft. (414.5m) long with a 756 ft. (230.4m) main span and two 302 ft.

---

[1]University of Illinois at Urbana-Champaign, Urbana, IL USA

[2]Hanson Engineers, Inc., Springfield, IL USA

(92.0m) side spans. The Missouri approach unit is an eight-span continuous bridge that has a total length of 1605 ft. (489.2m). The Illinois approach unit has 11 spans and is 1655 ft. (504.4m) long with one expansion joint.

One unique feature of the Clark Bridge is the rock-fill dike that is shown in the plan view in Fig. 1. The dike is provided to guide barges as they leave a lock that is located approximately 500 feet upstream of the bridge. The dike also protects the bridge pier from scour. The top of the dike is approximately half-way between the top of the pile cap and the top of the bridge deck. Since the dike extends beyond the pylon and surrounds it, this poses a special problem for the seismic analysis of the bridge. Not only will the dike stiffen this pylon and its foundation, but additional inertial forces will be transmitted from the dike to the pylon.

Plan and elevation views of the cable-stayed bridge are shown in Fig. 2. A section of the dike is shown in the elevation view. A section view of the deck is shown in Fig. 3. The deck is 103 ft. (31.4m) wide from outside edge to outside edge. This is constructed with two longitudinal steel plate girders with transverse floor beams spaced, in general, at 17.5 ft. (5.4m) intervals. The floor beams are placed at locations where the cables are attached to the longitudinal girders and at intermediate locations half-way between these. The reinforced concrete deck is 10.5 in. (26.7cm) thick and is designed to act compositely with the longitudinal girders and the floor beams.

Single cantilever pylons are used to support the cable-stayed bridge. Elevations views are shown in Fig. 4. Individual cables pass freely over a special saddle at the top of each pylon and attach to both the center and side spans. The pylons are founded on steel H-piles driven approximately to bedrock with a 10.0 ft. (3.0m) thick reinforced concrete pile cap and a 24.0 ft. (7.3m) thick unreinforced concrete seal coat.

SEISMIC DESIGN CONSIDERATIONS

Background

This section presents the findings and recommendations of the seismicity study which was conducted by D. A. Foutch. The investigations were conducted in accordance with the guidelines and principles set forth in the Guide Specifications for Seismic Design of Highway Bridges 1983 (AASHTO, 1983), hereafter referred to as Guide Specs. In order to facilitate the application of these recommendations, they are given as direct modifications of the equations and concepts given in the Guide Specs. A more complete description of the seismicity of the area and of the techniques used to develop these recommendations is given below.

According to the Guide Specs,

> "...Guidelines are for the design and construction of new bridges to resist the effects of earthquake

motions. The provisions only apply to bridges of conventional steel and concrete girder and box girder construction with spans not exceeding 500 ft. (152.4m). Suspension bridges, cable-stayed bridges, arch type and movable bridges are not covered by the Guidelines but general considerations for designing such bridges are presented in the Commentary."

Thus, the Guide Specs were not directly applicable to the design of the cable-stayed bridge. Another complicating factor was the fact that the site is in a zone of relatively low seismicity ($A_{max} < 0.2g$). Thus, several difficult decisions concerning the level of risk to consider and the level of sophistication of analysis to use.

The seismic zones considered include the New Madrid Seismic Zone and several smaller zones that have been identified that are closer to the site. The maximum ground acceleration and velocity at bedrock at the site are estimated to be 0.15 g and 18 cm/sec, respectively. These values have about a 10% probability of exceedance in 100 years. The maximum ground displacement at the same level of risk but without consideration of surface wave effects is estimated to be about 12 cm. When surface waves are considered the maximum displacement is estimated to be 19 cm. The surface waves that would propagate from a large earthquake centered in the New Madrid Zone generate longer period motions. These longer period motions are important for the cable-stayed bridge which is expected to have significant modes of vibration in the two to five second range. These findings include the possible amplification or attenuation of the motion at the site due to the response of the soil layers to the bedrock motion. However, this effect was found to be inconsequential.

Source mechanism and wave propagation studies that are consistent with earthquakes in the Central United States indicate that the vertical motions are about the same amplitude as horizontal motions. In addition, the bedrock motions due to body waves tend to have more energy in the longer periods than do California earthquakes and more than is implied by the design response spectra given in the Guide Specs. These points are incorporated into the recommendations given below.

Equation numbers and Section numbers given in the recommendations refer to those in the Guide Specs.

Recommendations

1. The cable stayed bridge should be considered as Essential (IC=1) with a Seismic Performance Category C.

2. Analysis Procedure 2: Multimode Spectral Method should be used. However, the bridge is expected to have several modes that are three-dimensional. In addition, response of the bridge to vertical ground motions must be considered. Therefore, the combination of modal responses as outlined in Section 4.4 will not be appropriate. Further guidance on this topic will be given at the appropriate time.

3. Equation (5-2) should be used with A = 0.15 and S = 1.6.

$$C_{sm} = \frac{1.2\ AS}{T_m^{2/3}} \qquad (5\text{-}2)$$

where A is the effective peak ground acceleration, S is a dimensionless coefficient for the soil profile characteristics at the site and T_m is the period of vibration of the mth mode of vibration. The value of C_{sm} should not exceed 2.5A. Note that this is not Soil Type III even though the choice of S indicates that it might be. This value is required to give a design response spectrum at bedrock that is consistent with the ground motion parameters given above and reflects the influence of surface waves at the site.

4. Equation (5-4) may be used as appropriate if T_m exceeds 4.0 seconds:

$$C_{sm} = \frac{3\ AS}{T_m^{2/3}} \qquad (5\text{-}4)$$

5. Equation (5-2) and (5-4) should be used without reduction for computing bridge response due to vertical ground motion.

6. In addition to forces that arise from the dynamic response of the bridge, forces that arise from relative displacements that occur at the bases of the main pylons must be considered. A relative displacement of 5 cm. in the longitudinal, transverse and vertical directions should be considered. These should not be assumed to occur simultaneously. They should be considered separately and then combined with the results of the dynamic analysis in a manner that is consistent with the Multimode Spectral Method. If the ends of the cable-stayed bridge are attached to the transition piers, the motion at the bottom of a transition pier may be considered to be the same as that of the foundation of the closest pylon.

Comments

1. The design response spectrum resulting from Recommendations 3 and 4 is a little conservative for periods greater than one second. However, the Response Modification Factors used for design and the value of damping of 5% that is implicit in Equation (5-2) and (5-4) are not conservative for a cable stayed bridge. Therefore, the resulting level of safety is probably about right.

2. When Response Modification Factors greater than one are used in design, it is expected that damage will occur under the design earthquake. Note that the maximum displacements that occur in the bridge during an earthquake are about the same whether inelastic action occurs

or not. Therefore, the displacements calculated at the elastic response level (R = 1) are those that must be accommodated in the design.

Seismicity of the Area

The seismicity of the area is dominated by the New Madrid Seismic Zone. However, several smaller zones have been identified in the area, and these have been considered in the analyses that lead to the recommendations. The seismic zones considered for this study are shown in Fig. 5, along with the estimate of the body-wave magnitude for the earthquake that is expected to occur in each zone with a 10% probability in 100 years (Nuttli and Herrmann, 1981). Similar maps were used by Algermissen, et al (1982) to derive the expected acceleration contour maps that lead to the recommendations in the Guide Spec.

Estimation of Peak Ground Motions

The relationships for determining peak amplitudes from a given set of earthquake parameters that are used for engineering decisions are usually empirical equations that have been derived from observations of past seismic events. The most widely used equations for earthquakes that occur in the Central United States were proposed by Nuttli (Nuttli and Herrmann, 1981). These were used for this study and are as follows:

$$\log_{10}(a) = 0.55 + 0.5m_b - 0.83\log_{10}(r) - 0.0019r$$

and

$$\log_{10}(v) = 3.60 + 1.00m_b - 0.83\log_{1}0(r) - 0.0011r$$

where a and v are the average of the peak acceleration and velocity values, respectively, of the two horizontal components (in cm/sec^2 and cm/sec), m_b is the body wave magnitude and r is the epicentral distance in kilometers. A number of different scaling relationships are available for different parts of the world. Using these equations and assuming a hypothetical earthquake magnitude and epicenter, one may estimate the average peak ground motions for a given site.

In order to compute the probability of exceeding a given peak acceleration (or velocity) at a given site, one has to consider all of the active faults in the vicinity, the probabilities of each fault generating an earthquake of different magnitudes, and the probabilities of experiencing a peak acceleration at the site given that a specified magnitude of earthquake occurs at a known distance. Using a procedure proposed by Cornell (1968) to accomplish these calculations, Algermissen et al developed the contour maps of expected peak acceleration that lead to the map used in the Guide Spec. Nuttli and Herrmann (1981) used a similar approach to develop plots of average peak acceleration vs. annual probability of exceedance for the city of St. Louis, Missouri. These curves were used to estimate the peak acceleration and peak velocity at bedrock for the Clark Bridge site. It should be noted that due to the large scatter of data and to the scarcity of data in the Midwest, the

actual peak motions at the site for the design earthquake could be larger or smaller than the average predicted motion by a factor of two.

Effects of Surface Waves

In addition to body waves that are generated and that propagate in accordance with the principles outlined above, surface waves are also generated. These motions are particularly important for long period structures like cable-stayed bridges. Although the amplitude of motion of the surface waves near the epicenter is usually somewhat smaller than for the body waves, the rate of attenuation is much lower than for body waves. Thus, for sites that are long distances (say > 200 km) from the epicenter, the surface waves will dominate the ground motion, particularly the displacements which are most affected by the long period motions. The empirical equations for peak acceleration and peak velocity do not correctly account for the effects of surface waves for sites that are long distances from the epicenter.

A study (Jost and Herrmann, 1988) of the effects of surface waves generated by large earthquakes in the New Madrid Zone on ground motions in Chicago was used to estimate the maximum displacement at bedrock for the Clark Bridge site. Figure 7 shows the hypothetical locations of the three earthquakes considered in this study. It was estimated that, because of the surface waves, the maximum displacement at the site would be about 50% greater than what would otherwise be expected. The peak displacement would develop primarily from the fundamental mode surface wave that would have a period of about 2 seconds. This long period content of the ground motion lead to the recommendation of S = 1.6 in Recommendation 3 and the maximum relative displacement of 5 cm in Recommendation 6.

Site Effects

Another factor that can affect the motion at a site is the type of soil layers that overlay bedrock. Deep, soft clay deposits at Mexico City, for instance, greatly amplified the bedrock motion and caused the tragedy in 1985.

This factor is not considered to be important at the Clark Bridge site. The depth of soil to bedrock is only about 80 to 90 feet at the main pylon locations and the soil is a relatively stiff (blow counts in the 20 to 50 range) mixture of sand and gravel. The fundamental period of the soil at the site will be somewhat smaller than one second. Therefore, in the period range of interest, the motion at the bottom of the pylon foundations will be essentially the same as at bedrock.

SEISMIC ANALYSIS OF CLARK BRIDGE

Method of Analysis

For bridge types not covered by the Guide Specs, the Commentary suggests that (AASHTO, 1983):

The Multimode Spectral Procedure should be considered, especially if the acceleration coefficient for the bridge site is greater than 0.20. The designer should consider the pros and cons of using elastic and/or inelastic methods of the time history analysis for larger and more complex types of bridges.

Given the importance of the bridge and its dynamic complexity, it was decided that the Multimode Spectral Procedure will be used for the analysis of the bridge even though the acceleration coefficient is less than 0.20. Twelve to fifteen modes will be included in the analysis. However, elastic or inelastic time history analysis will not be used.

Mode Shapes and Frequencies

The natural frequencies and periods of vibration of the lowest thirteen modes of vibration along with the predominate type of motion in the mode are given in Table 1. Six of the mode shapes are given in Figs. 7 and 8. These are for the bridge without the dike in place. Since there is no guarantee that the dike will remain there as long as the bridge, the analysis will have to completed for both cases.

Based on these preliminary results, it appears that only three of the modes (Mode 1, Mode 6 and Mode 8) are highly coupled. The presence of the dike may change this, since one of the pylons will be stiffer than the other.

CONCLUDING REMARKS

Although sophisticated analysis of structures for seismic effects is not often done for structures located in regions of low seismicity, important structures like cable-stayed bridges require a dynamic analysis. The cost of replacement of these bridges and the effects on the economy of the region are too large to ignore the devastating consequence of a bridge collapse during an earthquake. The dynamic analysis should be based on good estimates of the characteristics of the ground motion expected at the site and on an accurate representation of the dynamic characteristics of the bridge. Both of these aspects are important if the desired level of safety is to be achieved.

BIBLIOGRAPHY

Algermissen, S. T.; D. M. Perkins; P. C. Thenhaus; S. L. Hanson; and B. L. Bender. "Probabilistic Estimates of Maximum Acceleration and Velocity in Rock in the Contiguous United States," U. S. Geological Survey Open-File Report 82-1033, 1982, 99 pp.

Cornell, C.A., "Engineering Seismic Risk Analysis," Bulletin of the Seismological Society of America, Vol. 58, 1968, 1583-1606.

Jost, M. and R.B. Herrmann, "Numerical Simulation of Ground Motions at Chicago and Atlanta for A Large New Madrid Earthquake," for URS Consultants, San Francisco, CA, 1988.

Nuttli, O. W. and I. N. Gupta. "Spatial Attenuation of Intensities for Central U. S. Earthquakes," Bulletin of the Seismological Society of America, Vol. 66, No. 3, June 1976, pp. 743-751.

Nuttli, O. W. and R. B. Herrmann, "Consequences of Earthquakes in the Mississippi Valley," ASCE Preprint 81-519, October 26-31, 1981.

Nuttli, O. W. and R. B. Herrmann, "Ground Motion of Mississippi Valley Earthquakes," Journal Technical Topics in Civil Engineering, ASCE, Vol. 110, pp. 54-69.

Somerville, P. G.; J. P. McLaren; L. V. LeFevre; R. W. Burger; and D. V. Helmberger. "Comparison of Source Scaling Relations of Eastern and Western North American Earthquakes," Bulletin of the Seismological Society of America, submitted March 1986.

TABLE 1

Mode Numbers and Periods of Vibration for the Clark Bridge

Mode (No.)	Principal Component of Motion[1]	Period (seconds)	Frequency (Hz)
1	Trans-Tors	2.361	0.424
2	Torsion	2.141	0.467
3	Vertical	1.884	0.531
4	Vertical	1.789	0.559
5	Vertical	1.360	0.462
6	Trans-Tors	1.284	0.779
7	Torsion	1.167	0.857
8	Torsion	1.129	0.886
9	Transverse	0.998	1.002
10	Torsion	0.892	1.121
11	Vertical	0.849	1.178
12	Torsion	0.844	1.185
13	Vertical	0.772	1.295

[1]Trans = Transverse; Tors = Torsion

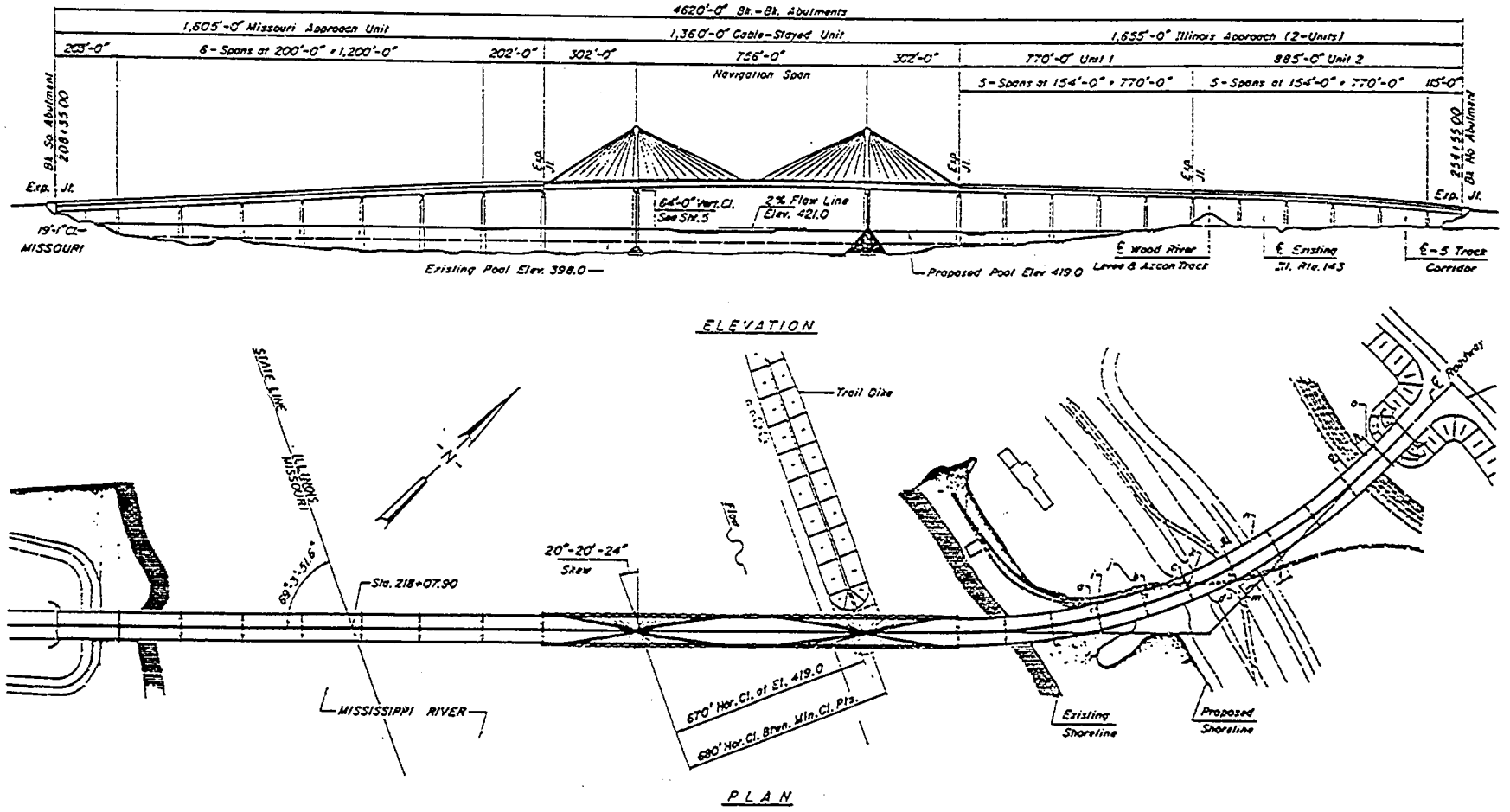


Figure 1 Plan and elevation views of the entire Clark Bridge

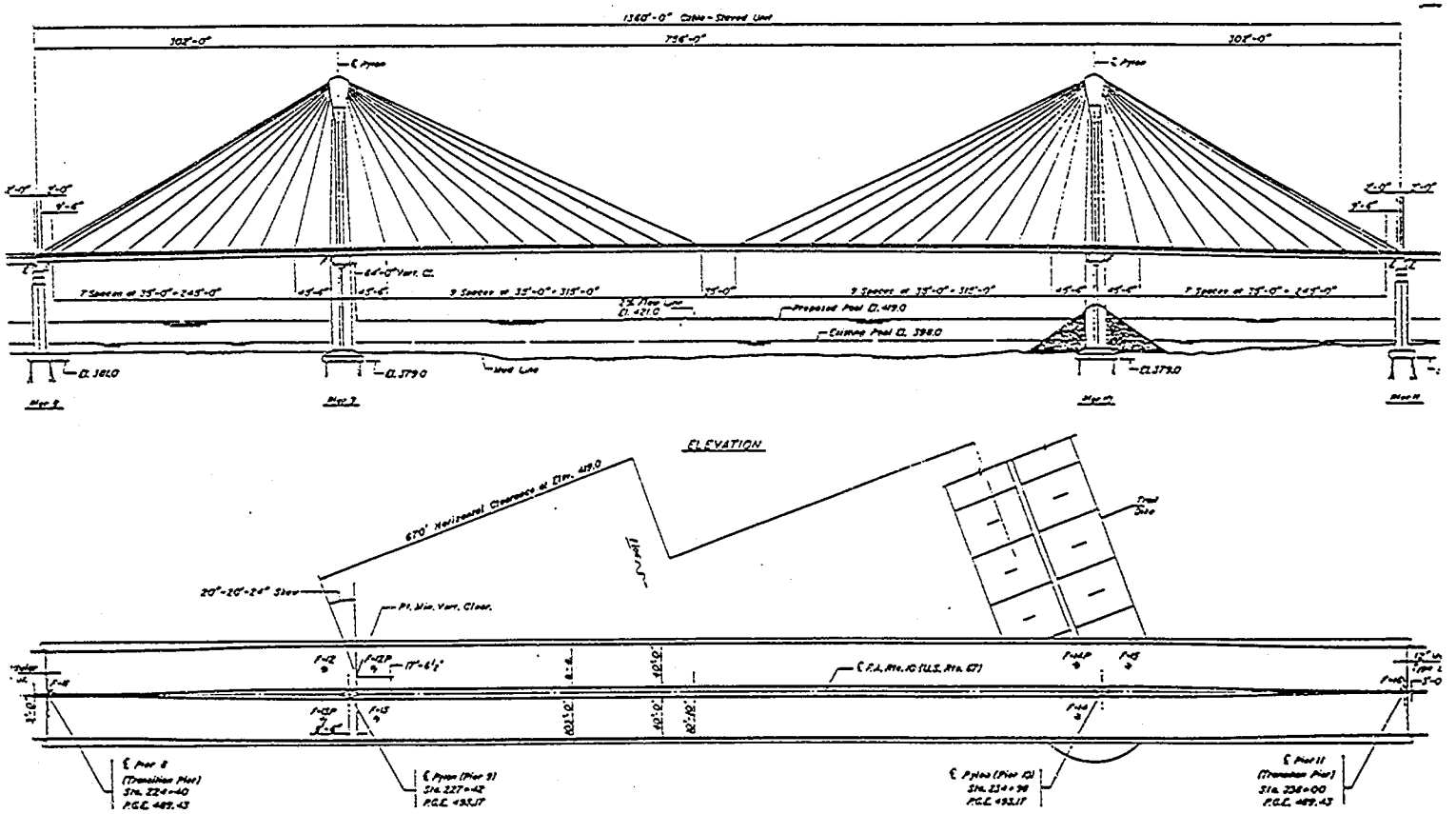


Figure 2 Plan and elevation views of cable-stayed segment of Clark Bridge

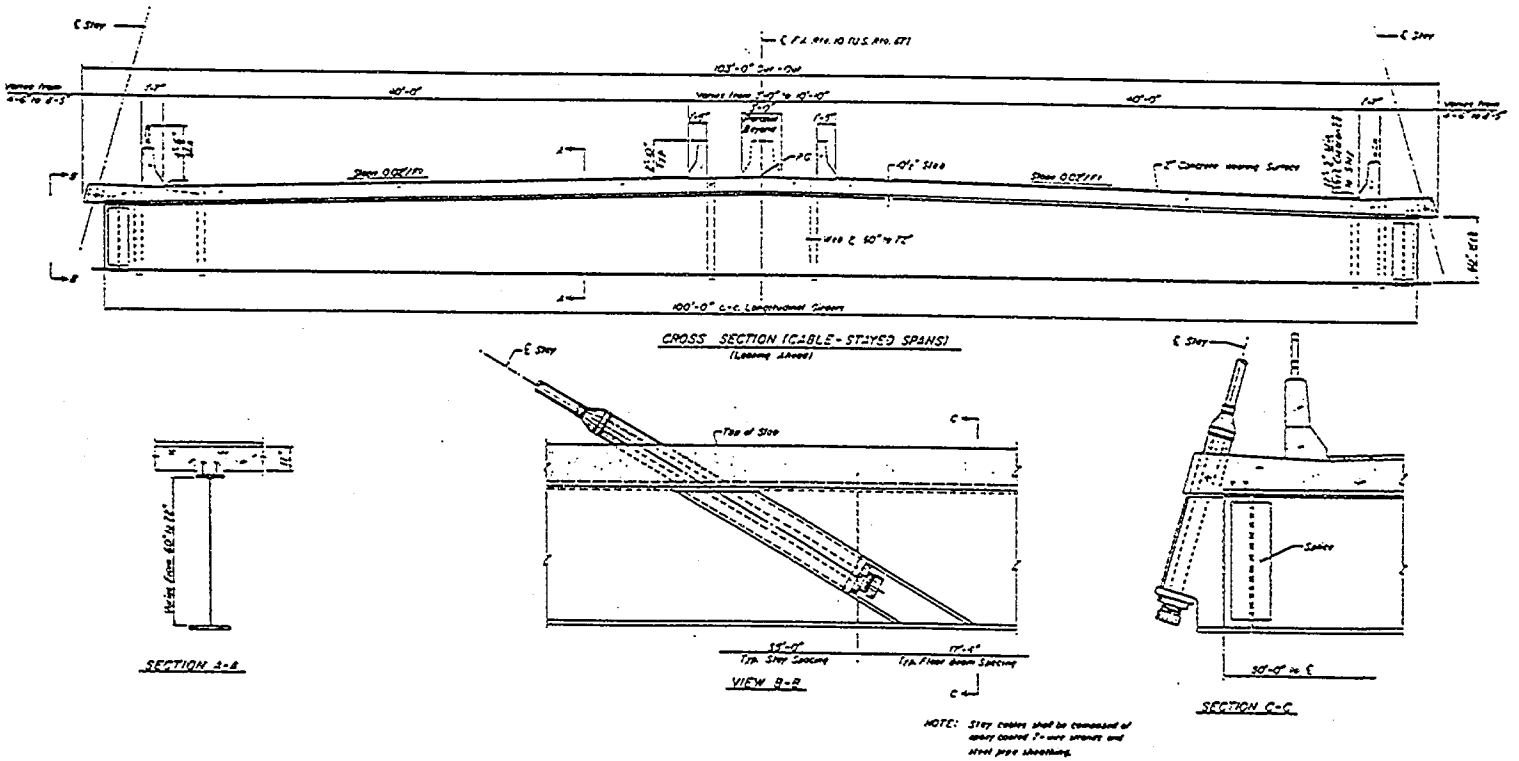


Figure 3 Section and details of deck of cable-stayed bridge

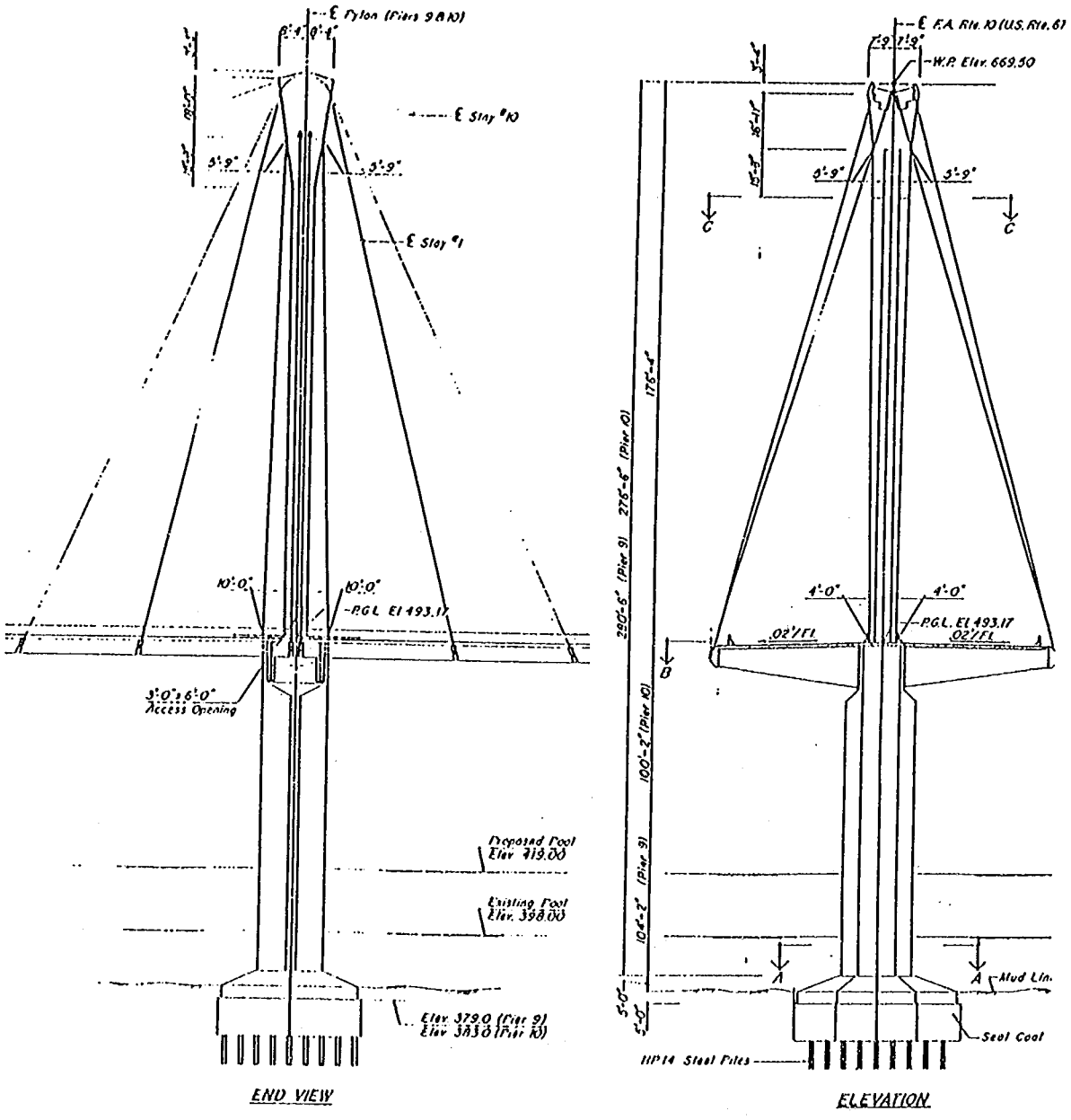


Figure 4 Pylon of cable-stayed bridge

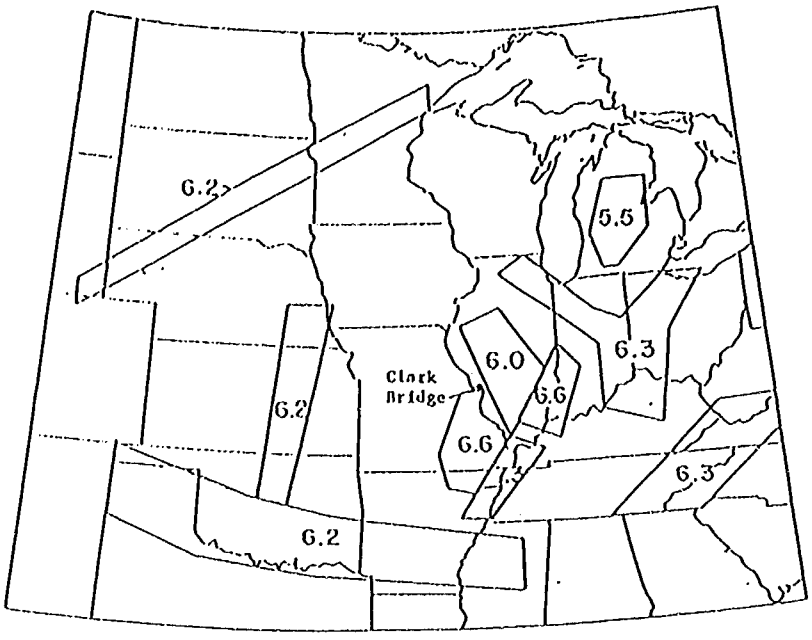


Figure 5 Earthquake source zones in the Central United States (Nuttli and Herrmann, 1981) and body-wave magnitudes of earthquakes with a probability of exceedance of approximately 10% in 100 years.

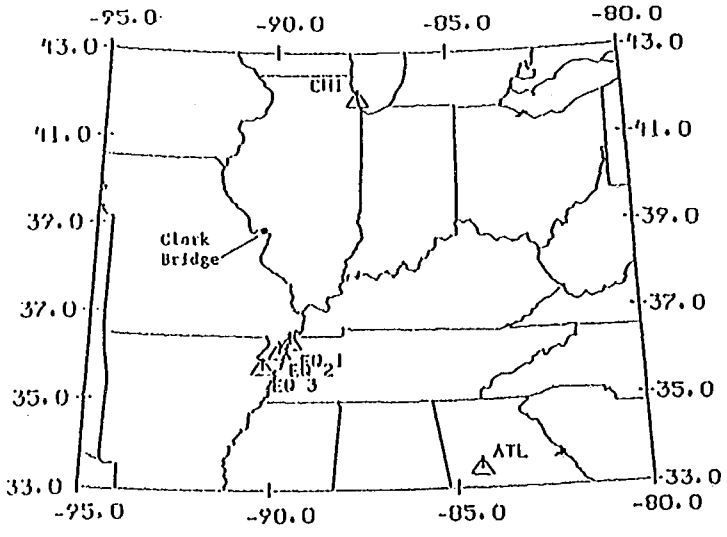
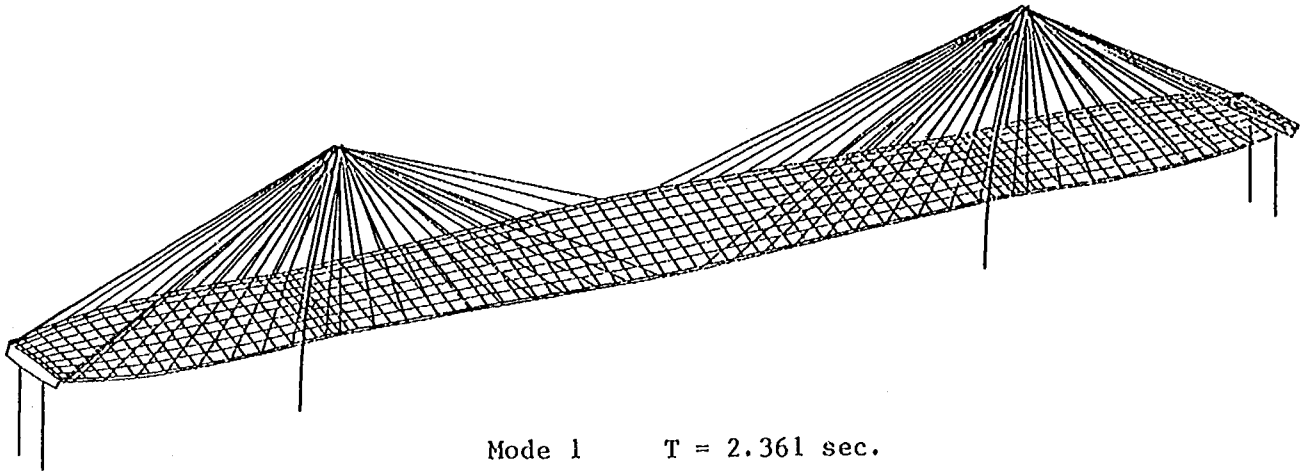
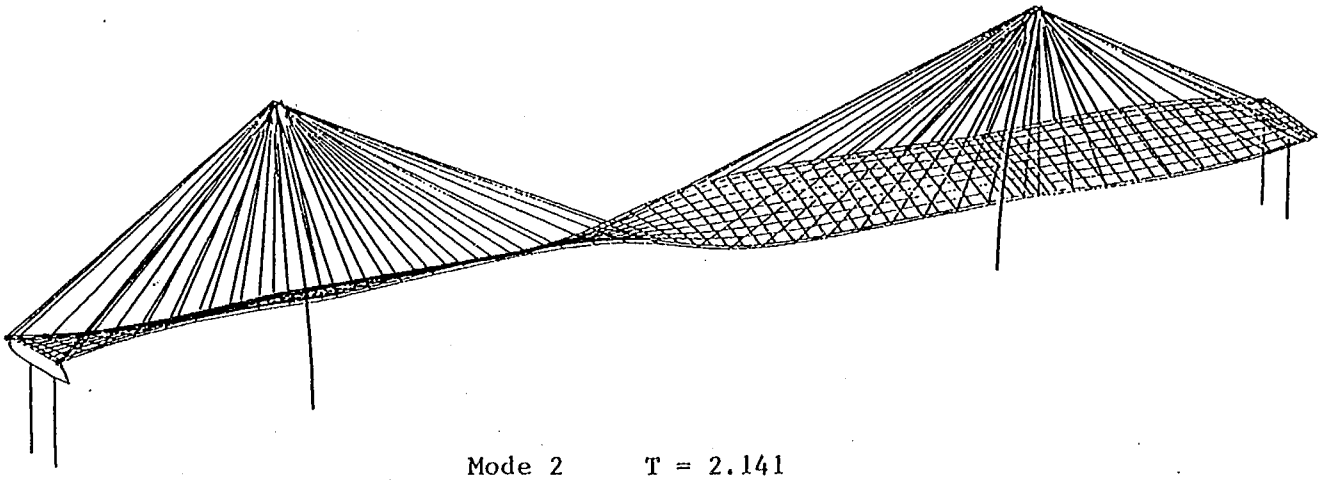


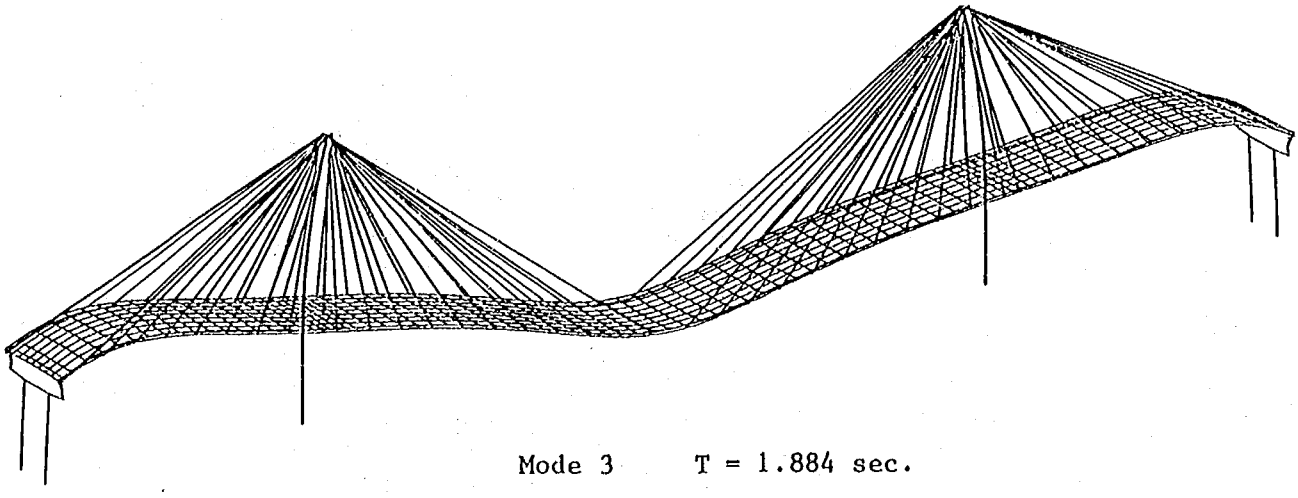
Figure 6 Locations of the three earthquakes modeled in relation to the cities of Chicago and Atlanta (Jost and Herrmann, 1988)



Mode 1 T = 2.361 sec.

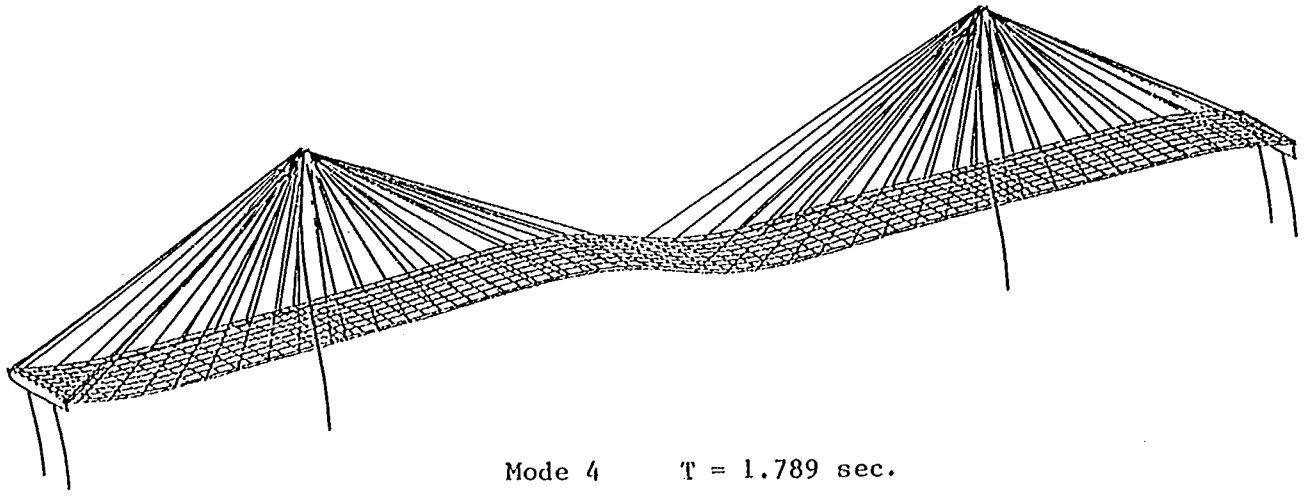


Mode 2 T = 2.141

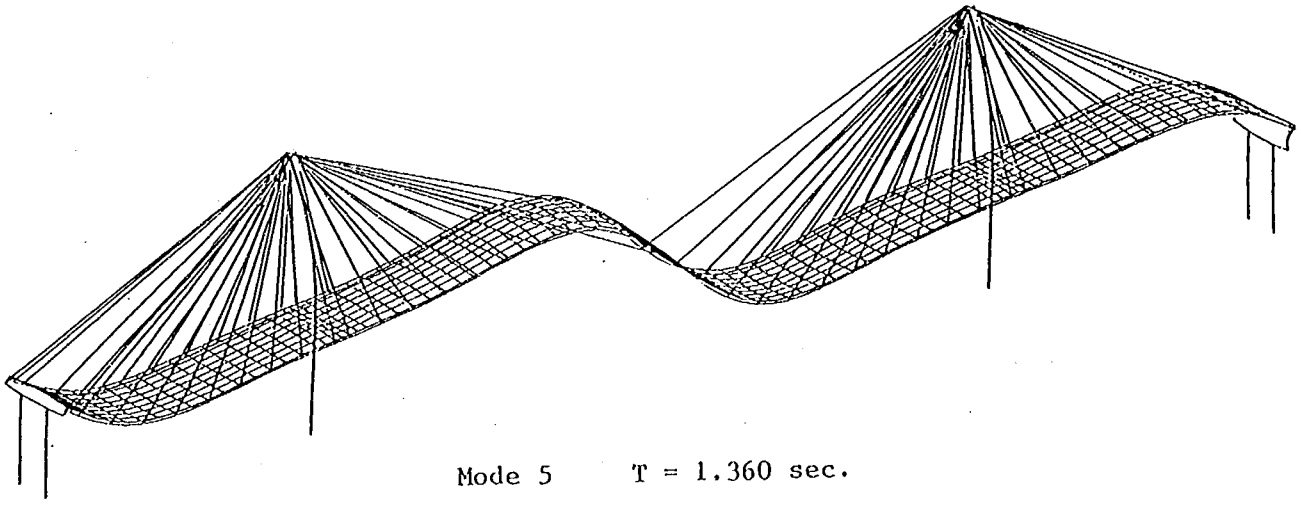


Mode 3 T = 1.884 sec.

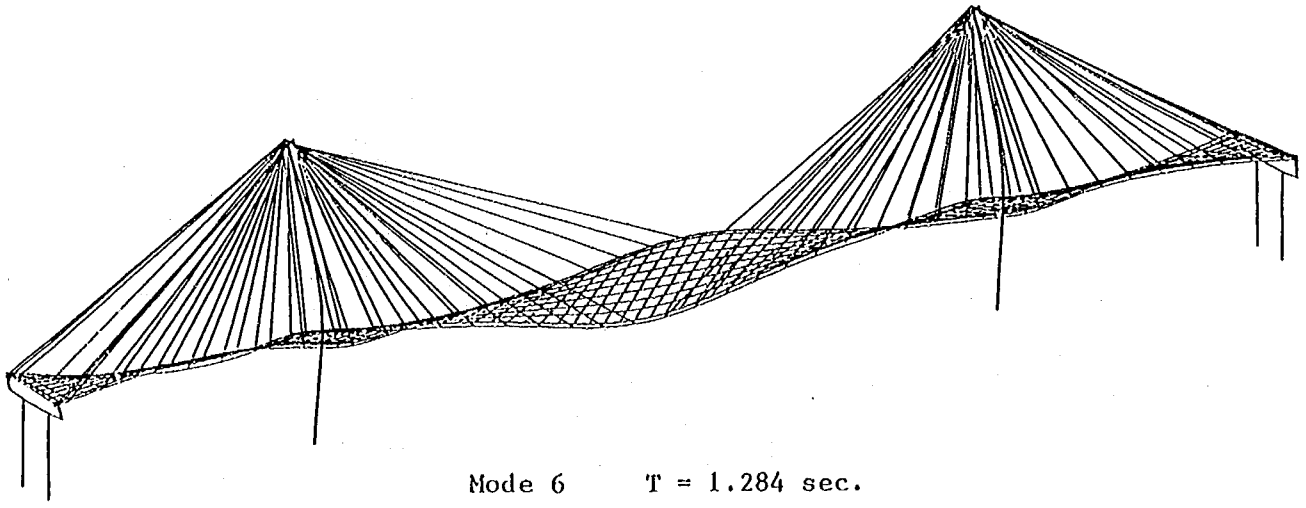
Figure 7 Mode shapes for Clark cable-stayed bridge



Mode 4 T = 1.789 sec.



Mode 5 T = 1.360 sec.



Mode 6 T = 1.284 sec.

Figure 8 Mode shapes for Clark cable-stayed bridge

(4) Session 4

SESSION 4: WIND RESISTANT DESIGN(1) 1:45pm~3:20pm
(Co-Chairman: K. Yokoyama, H.R. Bosch)

(7) K. Yokoyama※ and H. Sato: Experiment on the Effects of Turbulence on Wind-induced Vibrations of Long-span Bridges
(1:45pm~2:05pm)

(8) K, Wada, H. Takano※ and H. Makuta : Study on Suppressing Wind-induced Vibration in plane for Tower of Yokohama Bay Bridge under Construction (Design and On-site Testing of a Dynamic Damper for Cable Suspension Bridge)
(2:05pm~2:25pm)

(9) F. Ehsan and R. H. Scanlan※ : Damping Stay Cables with Ties
(2:25pm~2:45pm)

(10) T. T. Baber※ , F. W. Barton, M. Mohr, and D. Ramsey: Field Instrumentation of the I-295 Cable-Stayed Box Girder Bridge
(2:45pm~3:05pm)

DISCUSSION(4)
(3:05pm~3:20pm)



EXPERIMENT ON THE EFFECTS OF TURBULENCE ON WIND-INDUCED VIBRATIONS OF LONG-SPAN BRIDGES

Koichi Yokoyama and Hiroshi Sato

Structure Division, Structure and Bridge Department,
Public Works Research Institute, Ministry of Construction

ABSTRACT

Although a considerable amount of aerodynamic data of long-span bridges have been aquired, the data concerning the effect of turbulence are not enough at present. Therefore, the systematic wind tunnel tests were conducted using taut-strip models. Typical cross sections for cable-stayed bridges, such as rectangles, trapezoids, hexagons, two box girders and plate girders, were chosen. Wind-induced vibrations of the taut-strip models were measured in smooth flow and in three kinds of turbulent flow.

1. Introduction

Since long-span bridges have low natural frequencies and small structural damping, the effect of wind should be investigated in the stage of design. The wind resistance of most of the long-span bridges in Japan has been studied and proved according to the wind tunnel tests in smooth laminar flow using sectional models.

The present wind resistant design method in Japan may be suitable when it is applied to the bridge constructed over open sea, where the turbulence intensity of the wind is quite low. It can be anticipated, however, that the wind-induced vibrations of bridges in cities or suburbs, where turbulence intensity of wind is high, are quite different from those of bridge models in smooth laminar flow. The evaluation of the turbulence effect on wind-induced vibration seems very important in order to establish the more rational method for the wind resistant design of long-span bridges.

Although a considerable amount of aerodynamic data of long-span bridges have been aquired in Japan, the data concerning the effect of turbulence are not enough at present. Therefore, the systematic wind tunnel tests on the effect of turbulence were conducted at the Structure Division, Public Works Research Institute, Ministry of

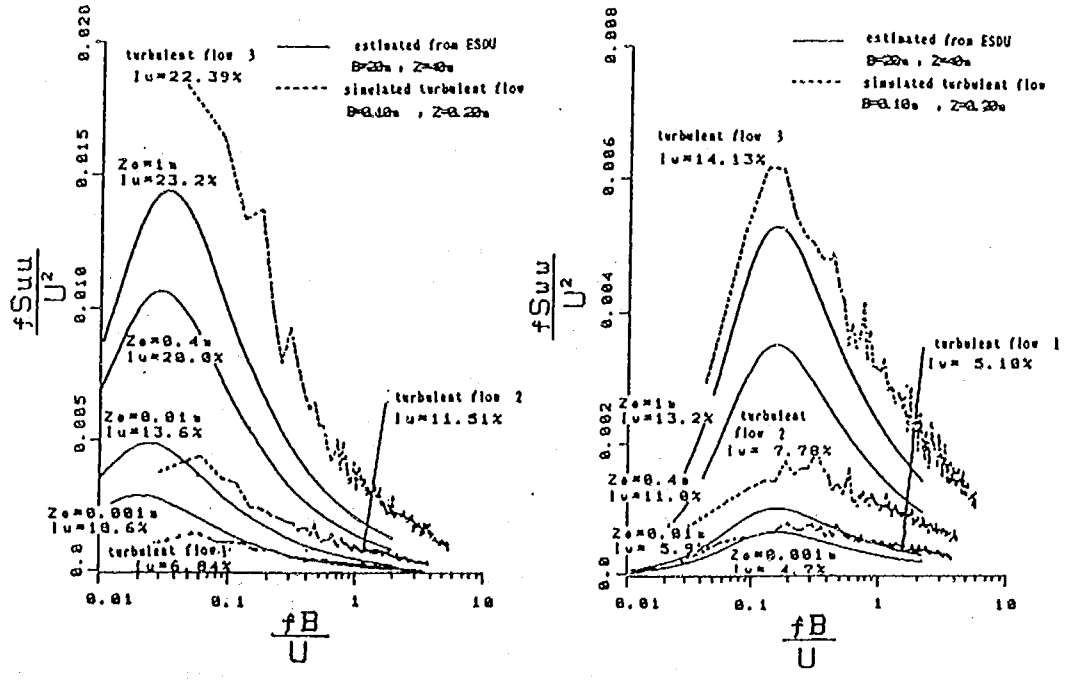
Construction.

2. Experimental condition

2.1 Flow

The experiments were conducted in Low Speed Wind Tunnel of Public Works Research Institute, whose test section is 2.5m wide, 4.0m high and 10.0m long. Smooth flow and three kinds of turbulent flow were used. The turbulent flow was generated by spires[1] and floor roughness so that its turbulence properties might become similar to those of natural wind.

Power law exponents of the turbulent flow 1, 2 and 3 were 0.12, 0.16 and 0.30, respectively. Power Spectral Density Functions (PSDF) of the wind speed at the model height (z=0.20m) are shown in Fig.1. Assuming that the scale ratio of the model was 1/200, the PSDF's of natural wind were estimated according to ESDU[2], and are shown in Fig.1. The integral scales of longitudinal wind speed of the turbulent flow were slightly smaller than 1/200 of those of natural wind, but the integral scales of vertical wind speed of the turbulent flow were about 1/200 of those of natural wind. The intensity of turbulence of the turbulent flow 1, 2 and 3 corresponded to natural wind over rough sea,



(a) longitudinal component (b) vertical component

Fig.1 Power spectral density function of turbulent flow

intermediate surface between open grassland and suburbs, and city centres, respectively.

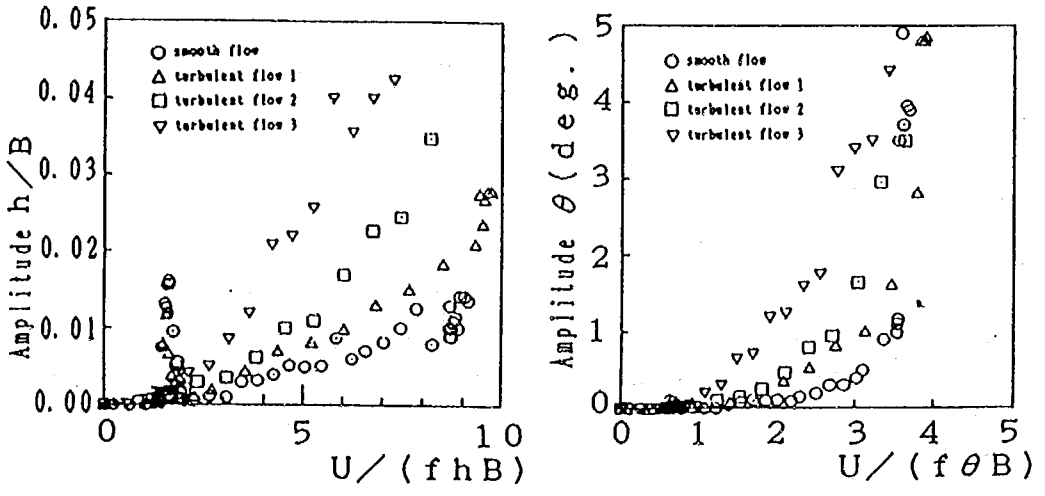
2.2 Models

Taut-strip models[3] were used in the experiment, namely, bridge deck models were attached to two parallel taut piano wires. Typical cross sections for cable-stayed bridges, such as rectangles, trapezoids, hexagons, two box girders and plate girders, were chosen. Model deck width(B) was 0.10m except for Model 11(0.20m) and 12(0.14m). The ratio of deck width to depth(D) ranged from 4 to 10. Kerbs and post-type handrails were attached to every models. Model length was about 1.2m. Mass, mass moment of inertia, natural frequency and structural damping are shown in Table 1.

3. Experimental results

Wind-induced vibrations of the taut-strip models were measured in smooth flow and three kinds of turbulent flow. As an example, the relationship between wind speed and maximum vibrational amplitude of the Model 5 is shown in Fig. 2. In the smooth flow, vortex-induced vibrations and flutter were observed. In the turbulent flow, the amplitude of vortex-induced vibrations decreased, and gust responses were observed.

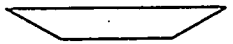
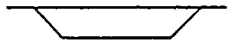
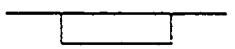
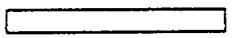
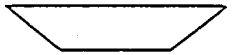
The maximum amplitude of vortex-induced vibrations of vertical bending mode and corresponding reduced wind speed are shown in Table 1. The gust responses of vertical bending mode were summarized applying the following relationship,



(a) vertical bending mode (b) torsional mode

Fig. 2 Wind speed and maximum amplitude (Model 5)

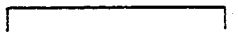
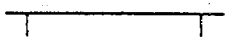
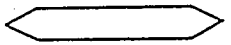
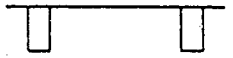
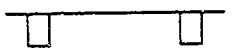
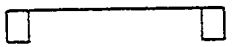
Table 1 Experimental condition and results

Model Number	Cross Section	B/D	Reduced Mass mr	Reduced Mass Moment of Inertia Ir	Natural Freq. fh (Hz)	Natural Freq. fθ (Hz)	Logarithmic Decrement δh	Logarithmic Decrement δθ	Amplitude and Wind Speed of Vortex-induced Vib. h/B	Amplitude and Wind Speed of Vortex-induced Vib. U/(fhB)	Coefficient for Gust Response $C\equiv\frac{hmr}{B\,Ur^2Iv}$	Reduced Wind Speed U/(fθB) corresponding to θ=1°	Reduced Wind Speed U/(fθB) corresponding to θ=4°
1		7.4	25.2	0.95	11.9	24.9	0.016	0.039	•	•	——	3.8	4.0
					10.3	21.1	0.011	0.037	•	•	0.18	3.0	4.4
					10.3	21.2	0.011	0.029	•	•	0.25	2.4	3.5
					10.8	21.6	0.018	0.023	•	•	0.21	2.1	3.2
2		7.4	25.2	0.82	11.6	25.8	0.027	0.034	•	•	——	3.6	3.8
					10.0	22.1	0.012	0.025	•	•	0.21	2.9	3.8
					10.2	22.8	0.013	0.015	•	•	0.20	2.5	3.8
					10.7	23.3	0.014	0.025	•	•	0.21	1.9	3.1
3		7.4	25.2	0.73	10.5	25.0	0.015	0.062	0.004	1.5	——	3.6	3.7
					10.0	22.9	0.016	0.032	•	•	0.21	2.8	3.7
					10.3	23.8	0.017	0.019	•	•	0.19	2.4	3.4
					10.7	24.7	0.017	0.019	•	•	0.22	1.8	3.0
4		10	21.1	1.30	6.9	10.1	0.014	0.030	0.010	1.0	——	4.0	4.1
					8.7	12.7	0.015	0.028	•	•	0.21	3.3	4.0
					8.1	11.7	0.014	0.027	•	•	0.20	2.7	3.9
					8.3	12.0	0.015	0.023	•	•	0.22	2.2	3.3
5		5	40.3	1.04	10.9	26.7	0.014	0.053	0.016	1.6	——	3.6	3.7
					8.3	20.4	0.012	0.026	0.012	1.6	0.26	3.2	3.9
					8.3	20.4	0.011	0.027	•	•	0.24	2.8	3.7
					8.7	20.9	0.010	0.027	•	•	0.27	1.9	3.3
6		5	40.3	0.95	9.7	25.9	0.013	0.033	0.017	1.6	——	2.7	3.1
					10.1	27.1	0.014	0.037	0.006	1.9	0.29	2.9	3.5
					8.3	22.3	0.011	0.021	•	•	0.27	2.3	3.3
					8.7	22.6	0.009	0.025	•	•	0.28	1.9	3.0
7		5	40.3	0.82	8.4	23.6	0.014	0.024	0.015	1.9	——	2.0	2.6
					8.1	22.3	0.013	0.025	0.012	1.7	0.34	2.7	3.0
					8.3	22.7	0.015	0.017	•	•	0.28	2.3	3.2
					8.6	23.5	0.015	0.015	•	•	0.26	1.9	3.0
8		5	33.8	3.02	8.4	10.3	0.008	0.037	0.023	2.1	——	4.2	4.3
					8.9	10.6	0.018	0.022	0.010	1.8	0.29	3.2	4.0
					8.8	10.4	0.007	0.013	•	•	0.33	3.0	4.0
					9.2	10.8	0.009	0.021	•	•	0.35	2.6	3.7

Lines 1,2,3 and 4 correspond to experiments in smooth flow, turbulent flow 1,2 and 3, respectively.

• No vortex-induced vibration of vertical bending mode was observed.

Table 1 Experimental condition and results (concluded)

Model Number	Cross Section	B/D	Reduced Mass mr	Reduced Mass Moment of Inertia Ir	Natural Freq. fh (Hz)	Natural Freq. fθ (Hz)	Logarithmic Decrement δh	Logarithmic Decrement δθ	Amplitude and Wind Speed of Vortex-Induced Vib. h/B	Amplitude and Wind Speed of Vortex-Induced Vib. U/(fhB)	Coefficient for Gust Response $C=\frac{hmr}{B\,Ur^2Iv}$	Reduced Wind Speed U/(fθB) corresponding to θ=1°	Reduced Wind Speed U/(fθB) corresponding to θ=4°
9		10	19.8	1.34	7.6	13.9	0.025	0.041	0.004	1.0	——	2.6	3.1
					8.8	15.7	0.022	0.030	•	•	0.22	2.7	3.0
					7.8	14.1	0.023	0.033	•	•	0.19	2.2	3.3
					7.7	14.0	0.025	0.025	•	•	0.23	2.1	3.1
10		10	19.8	1.27	9.6	18.2	0.021	0.028	0.019	1.7	——	2.7	3.2
					9.5	17.9	0.018	0.027	0.011	1.6	0.21	2.7	3.4
					7.5	14.4	0.021	0.026	•	•	0.18	2.9	3.7
					8.4	15.9	0.017	0.029	•	•	0.21	2.0	3.2
11		4	24.6	1.16	7.6	9.9	0.010	0.013	0.049	2.1	——	4.5	4.8
					7.8	10.1	0.010	0.011	0.043	2.3	0.20	2.9	4.2
					7.7	10.0	0.006	0.013	0.042	2.1	0.24	1.8	3.5
					7.7	9.9	0.007	0.014	0.036	2.0	0.25	1.7	2.7
12		7	28.5	1.89	7.4	11.1	0.008	0.015	0.026	1.3	——	5.8	6.8
					7.3	11.4	0.009	0.016	0.023	1.5	0.17	3.3	4.5
					7.4	11.4	0.009	0.016	0.020	1.4	0.21	2.7	3.2
					7.4	11.3	0.009	0.015	0.011	1.1	0.23	1.8	3.2
13		5	40.3	2.76	8.8	16.0	0.011	0.015	0.016	1.7	——	3.5	3.8
					8.7	15.7	0.009	0.018	0.014	1.8	0.31	3.5	4.1
					8.8	15.8	0.010	0.016	0.010	1.8	0.29	3.1	4.1
					8.8	15.8	0.011	0.015	•	•	0.31	2.4	3.7
14		5	40.3	4.44	9.9	12.8	0.012	0.017	0.034	1.8	——	4.7	4.8
					9.6	13.0	0.011	0.015	0.031	2.0	0.30	3.8	4.2
					9.4	13.0	0.012	0.012	0.026	2.0	0.32	3.4	4.1
					9.4	12.8	0.011	0.012	•	•	0.36	2.8	3.8
15		7.1	28.3	1.87	8.5	15.2	0.014	0.015	0.021	1.4	——	4.2	4.3
					8.5	15.3	0.013	0.012	0.018	1.7	0.21	3.4	4.4
					8.5	15.2	0.013	0.013	0.003	1.8	0.23	3.2	4.2
					8.5	15.2	0.013	0.016	•	•	0.27	2.4	3.5
16		7.1	28.3	3.07	9.3	12.6	0.016	0.016	0.016	1.9	——	3.0	3.1
					9.3	12.8	0.015	0.015	0.013	2.0	0.28	3.0	3.4
					9.2	12.6	0.014	0.016	•	•	0.27	3.0	3.7
					9.3	12.6	0.013	0.014	•	•	0.30	2.8	3.7

Lines 1,2,3 and 4 correspond to experiments in smooth flow, turbulent flow 1,2 and 3, respectively.

• No vortex-induced vibration of vertical bending mode was observed.

which seemed to be suitable as the first approximation.

$$h/B=CUr^2 Iw/mr \qquad (1)$$

where, h:maximum amplitude
C:coefficient
Ur:reduced wind speed ($\equiv U/(fhB)$, U:wind speed, fh:natural frequency of vertical bending mode)
Iw:intensity of turbulence of vertical wind speed
mr:reduced mass ($\equiv m/(\rho B^2)$, m:mass per unit length, ρ:air density)

The coefficient C is shown in Table 1. As for torsional vibrations such as flutter and gust responses, the reduced wind speeds ($U/(f\theta B)$, $f\theta$:natural frequency of torsional mode) at which maximum torsional amplitude reached 1 deg. or 4 deg. are shown in Table 1.

4. Discussions

4.1 Effects of turbulence on vortex-induced vibrations

The maximum amplitude of vortex-induced vibrations of vertical bending mode was reduced by mass-damping parameter $mr\delta h$. The relationship between the reduced amplitude $mr\delta h(h/B)$ and turbulence intensity Iw is shown in Fig. 3. The amplitude decreases with an increase in Iw. Except for hexagonal sections (Model 11 and 12) and two box girders (Model 13 and 14), no significant vortex-induced vibration was observed when Iw exceeded 0.08.

4.2 Gust responses of vertical bending mode

Significant gust responses of vertical bending mode were observed in the turbulent flow. Since only the effects of wind speed Ur, turbulence intensity Iw and mass mr are considered in equation (1), other effects such as cross sectional shape of bridge deck (aerodynamic admittance, aerodynamic damping) seem to be included in the coefficient C. As far as this experiment concerns, the C values range mostly from 0.20 to 0.30. The C value averaged for each model was plotted against B/D in Fig. 4. From the figure, it is found that C values tend to decrease slightly with an increase in B/D.

4.3 Effects of turbulence on torsional vibrations

In smooth flow, vibrational amplitude of torsional mode was very small below the critical wind speed of flutter. In the turbulent flow, gust responses of torsional mode were observed below the critical wind speed. Therefore, the reduced wind speed at which maximum torsional amplitude

reaches 1 deg. decreases with an increase in turbulence intensity (Fig. 5). The large torsional amplitude (say, 4 deg.) seems to be caused by flutter in case of low turbulence. In case of high turbulence, the large amplitude seems to be caused by flutter or approaching turbulence. As far as this experiment concerns, however, the reduced wind speed at which maximum torsional amplitude reached 4 deg. does not change much with an increase in turbulence intensity (Fig. 6).

5. Conclusion

The wind-induced vibrations of the taut-strip models with typical cross sections for cable-stayed bridges were measured in smooth flow and three kinds of turbulent flow. In the smooth flow, vortex-induced vibrations of vertical bending mode and flutter were observed. The amplitude of the vortex-induced vibrations decreased with an increase in turbulence intensity. Gust responses of vertical bending mode were observed in the turbulent flow. The maximum amplitude h/B of the gust responses was

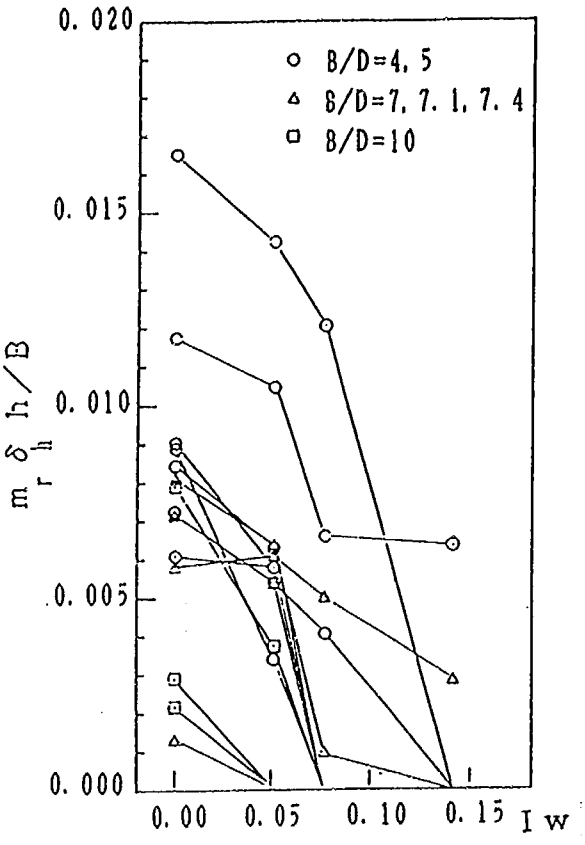


Fig. 3 Effect of turbulence on vortex-induced vibration

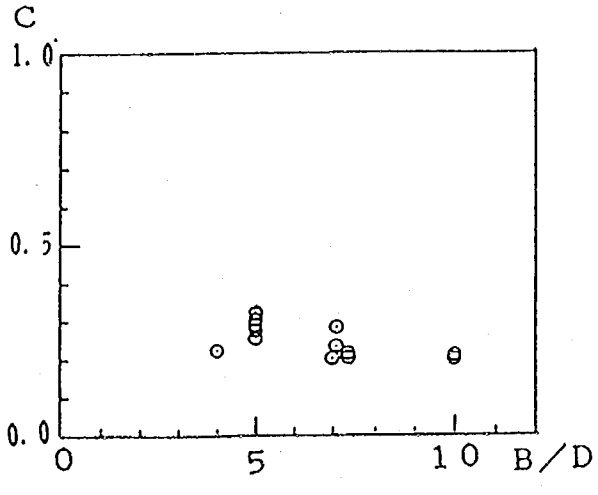


Fig. 4 Coefficient for gust response of vertical bending mode

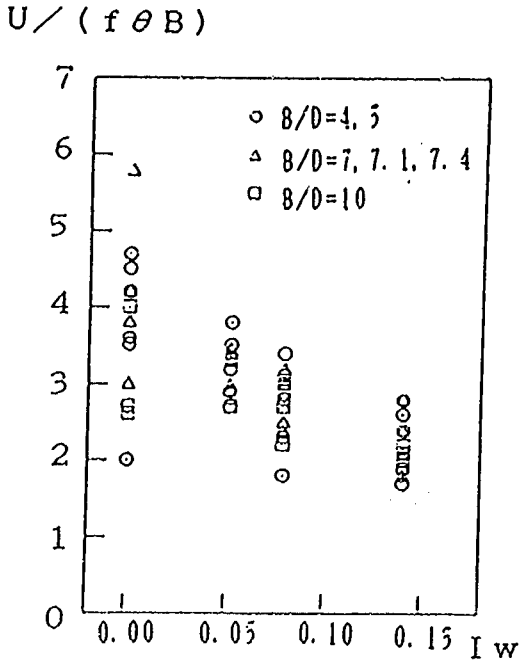


Fig. 5 Wind speed at which amplitude reaches 1 deg.

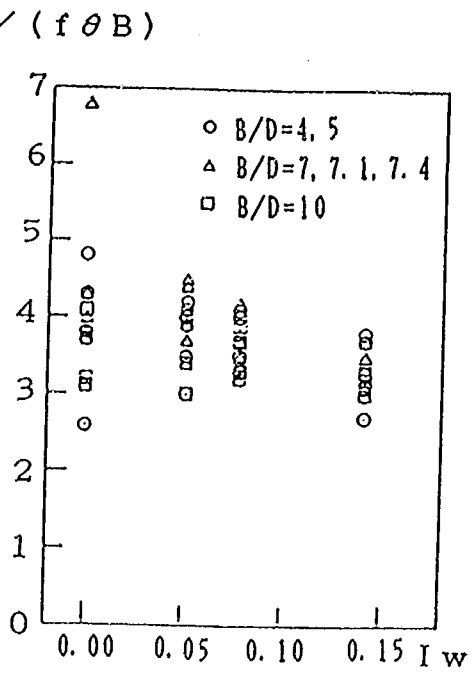


Fig. 6 Wind speed at which amplitude reaches 4 deg.

approximately proportional to $Ur^2 Iw/mr$, and the coefficient ranged mostly from 0.2 to 0.3. In the turbulent flow, gust responses of torsional mode were observed as well as flutter. The reduced wind speed at which torsional amplitude reached 1 deg. decreased with an increase in turbulence intensity, however, the reduced wind speed at which torsional amplitude reached 4 deg. did not change much.

References

[1] Irwin, H. P. A. H., The design of spires for wind simulation, J. of Wind Engineering and Industrial Aerodynamics, 7, (1981)

[2] ESDU, Engineering Science Data, Wind Engineering, Volume 1, Wind and Turbulence Data, Engineering Science Data Unit Ltd., (1982)

[3] Davenport, A. G., The use of taut strip models in the prediction of the responses of long span bridges to turbulent wind, Proc. Symp. on Flow Induced Strct. Vibrations, (1972)

STUDY ON SUPPRESSING WIND-INDUCED VIBRATION IN PLANE FOR TOWER OF YOKOHAMA BAY BRIDGE UNDER CONSTRUCTION
(Design and On-site testing of a Dynamic Damper for Cable Suspension Bridge)

- AN EXPERIMENTAL INSPECTION OF CHARACTERISTICS OF CABLE STAYED BRIDGE AND PERFORMANCE OF DAMPING DEVICE -

by

Katsuya Wada

Head of Special Structural Design Division,
Kanagawa Construction Bureau
Metropolitan Expressway Public Corporation, Japan

Haruo Takano

Deputy Head, Special Structural Design Division,
Kanagawa Construction Bureau
Metropolitan Expressway Public Corporation, Japan

Hiroshi Makuta

Assistant Chief Research Engineer,
MITSUBISHI HEAVY INDUSTRIES, LTD. TOKYO, JAPAN

ABSTRACT

This is a report on vibration experiment of bridge which was conducted as a part of evaluation of the tower of Yokohama Bay Bridge for its suppressing wind-induced vibration.
The vibration experiment on bridge was conducted in order to evaluate quantitatively such factors as the natural frequency, damping ratio of the tower and effect of cables which were used as basic data for the preliminary study, and to confirm the performance of damping device for the bridge. As the results, it was confirmed that the values were same as the established, and the appropriateness to be used as the data for reviewing aerodynamic stability in future was verified.

1. Introduction

The Yokohama Bay Bridge (YBB) is constructed between two points crossing over the bay from Honmoku pier to Daikoku pier, and it is the three span continuous cable-stayed bridges with the length of 860 m, central span of 480 m, and gross weight of 54300 tons. The construction of the bridge started in November 1981, and will be scheduled to complete in this September, and the connection of main girder at the center was completed in February this year.
As shown in Figure 1, the girder have 55 m height from the sea level at the center span, is stayed by 11 cables (max. length 221 m, min. length 74 m). The aerodynamic stability of the tower has been reviewed according to the flowchart. (Figure 2)

First, as the result of wind tunnel test using the model of 1/90 scale setted to have logarithmic decrement of tower δ=0.01, it was known that there is a possibility that galloppping may occur at higher wind velocity than 20 [m/s] when the tower stands freely, and it was concluded that a certain kind of damping device was necessary. ((I) in the Figure 2)
As for suppressing method for galloppping, two methods were studied. The one was the method to add the damping effect aerodynamically, and the other was to reduce the vibration by mechanical aspect. As the result, it was determined to adopt the tuned mass damper, and after confirming the effect by the wind tunnel test using the model (II in Figure 2) and also after investigating the structure and mechanism by the full-scale prototype model (III in Figure 2), the device was adopted formally and attached to actural structures. (IV in Figure 2)
On the other hand, as the result of wind tunnel test using the model with whole cables (that is in the state of completion) which was carried out in parallel with above experiments, the galloppping disappeared. In order to study the reason, a wind tunnel test (VI in Figure 2) using the model with acculate cable tension was conducted, and as the result, it was proven that the aerodynamic damping effect and the dynamic damper effect of cables are possible.
However, all of these studies were made on the theoretical examination based on the data obtained from the wind tunnel test, so in order to verify above investigations, this experiment by using actual bridge was planned.
From the circumstances mentioned above, this report discusses the results of the vibration experiment carried out for the purpose of verifying the availability of the base data used at preliminary investigation; that is, to grasp following characteristic under construction of tower.

(1) Vibration characteristics of tower
(2) Effect of vibration damping device
(3) Influence of cables on the vibration of tower

2. Stability against Wind-Induced Vibration Under Construction

2.1 Shape of Tower

The height of tower is 172 m, the width between both stays at the sea level is 40 m, and it has a simple shape having horizontal stiffener at the height of 45 m and 133 m from the sea level.
The cross section of tower is a rectangular box-type structure with the dimensions of 9 m x 5.8 m at the part lower than the lower horizontal stiffner and 5 m x 4 m at the part between the tower top and the lowest cable attaching point (126 m height from the sea level).
The shapes of tower at each stage under construction are shown in Figure 3.
The tower height alters according to each stage as follows.

B18 : 109.7 m　　B21 : 129.3 m　　B23 : 136.7 m
B27 : 157.4 m　　B31 : 172.0 m

At the time of tower completion, the temporary support in vertical direction on the horizontal lower stiffener that has supported the girder is removed and the girder becomes to be supported by the tower link in vertical direction. However, the girder is still supported by other temporary support in the longitudinal direction of bridge and in the horizontal direction, and these are completely removed after connecting the girder at HONMOKU side with the girder at Daikoku side.

2.2 Wind Tunnel Test

On the wind tunnel test, free standing tower model was made with the logarithmic decrement of (δ=)0.01.
Figure 4 shows the amplitude at the top of tower against the wind velocity in the free-standing state (δ= 0.01), and the state with additional damping (δ= 0.025) and further the state with dynamic damper (δ= 0.14).
Figure 5 shows the waveform of free vibration in above case. Figure 6 shows the amplitude of tower at the time just before connection of girder with all cables. As can be seen definitely from Figure 4, for the free-standing state (B31; without cable) the galloping occurs if δ= 0.01, and it has become evident that the logarithmic decrement larger than δ = 0.025 is necessary to suppressing galloping at wind velocity less than 90 [m/s].
Table 1 shows the logarithmic decrement values required for the suppression of galloping at each stage under construction which is calculated based on the date in the free-standing state, and the values obtained from the test with dynamic damper.
In conclusion, the case where the device is attached to the tower top, the logarithmic decrement for each case (B18, B31) was δ= 0.19 and δ=0.14, and it can be confirmed that the galloping does not occur in the wind velocity less than 90 [m/s] (Figure 4). On the other hand, the galloping did not occur in the case where all cables were attached. The reason is considered that the aerodynamic damping effect and the structural damping effect were increased.

2.3 Tuned-Mass Damper for Suppressing of galloping

As for the dampingdevice which were planned for suppression of wind-induced vibration, there were such method as to stretch cables in plane between tower and a certain fix point, or to attach the sliding damper equipment to the tip of its stretched cable, but from the reason that there is no suitable fixing point in the vicinity and also by judging that it may interfere the sea traffic, it was decided to adopt the tuned mass damper.
Figure 7 shows the pendulum-type damping device that was developed for this bridge. The pendulum weight of this device is changeable from 7.5 ton to 5.5 ton, and the vibration frequency can be adjusted by moving the spring mounted position and the weight position up and down, so that from 0.799 Hz (in the construction stage B19) to 0.399 Hz(at the completion stage) can be alter able. Also, the oil damper is adjustable type on damping constant so that even if the frequency changes at each construcion stage, the loga-rithmic decrement of the device is able to be constant δ= 0.70.
As shown in Figure 3, this device is attached at 110 m height of tower before the upper horizontal stiffener is constructed and moved on the upper horizontal stiffener after it is constructed, and finally when the tower is completed it is setted inside at the top of tower permanently.

3. Vibration Experiment of Actual Bridge

3.1 Purpose

The purposes of this experiment are as follows;
(1) To grasp the vibration characteristics of tower
(2) Inspection of the effectiveness of developped turned mass damper

(3) To grasp the effect of cables on the vibration of tower

3.2 Measurement of Small Oscilation

The small oscilation occured usually for the free standing tower was measured nine times for B20, B21, B23 (when the horizontal stiffener exists or not), B25, B27, B31 (with no cable, four cables, and all cables). This measurement was carried out to grasp the vibration characteristics of tower, and at the same time, to gather the data in order to adjust the damping device so as to coincide the frequency of device with that of tower at each stage of construction.
Figure 8 shows the spectrum obtained for typical stages and Table 2 shows its summary, and it was known that the tower vibrates usually with small amplitude almost at its first mode in each stage of construction, and the amplitude at the top is approximately 0.07 mm to 1.8 mm.
As for the frequency, the ratio of actually measured value/preliminary calculated value is 97% to 107%, so, it can be seen that the calculated values were considerably well coincided with actual value. It is considered that the simplicity of structure is one of the reason for this coincidence.

3.3 Excitation Test

The test was carried out four times as described below.

First time	December 1987	When B20 was constructed	
Second time	February 1988	When B31 was constructed (without cable)	in order to know the effect by cables
Third time	July 1988	When B31 was constructed (with 4 cables attached)	
Fourth time	February 1989	When B31 was constructed (with all cables attached and just after connection of girder)	

3.3.1 Exciting Method

The exciting methods at each test are shown as follows and Table 3 shows the summary.

(First time)
One of two damping devices was used as oscilator. That is, the pendulum was given the initial displacement and released. The pendulum was stopped by making the damping constant of the oil damper to be maximum.

(Second time)
Another prototype tuned mass damper setted on the upper horizontal stiffener was adopted as oscilator. According to manual excitation of its pendulum, the tower has vibrated increasingly and next, decreasingly after the movement of pendulum was stopped.

(Third and fourth times)
The special oscilator was used for the purpose of sweep excitation. This oscilator has following characteristic; stroke is 240 mm 0-P, maximum excitation force is about 7.5 tonf, and the controllable range of frequency is 0.2 to 5 Hz.

3.3.2 Measurement Method

The measuring positions of tower when B20 and B31 were being constructed are shown in Figure 9. In addition to these, the horizontal acceleration was measured at the highest attached cable of four cables on B20 stage, and at the lowest, intermediate, and topmost cables when all cables were attached (B31). Also, when the tuned mass damper worked, the displacement of the pendulum was also measured.

4. Measurement Results and Evaluation

4.1 Measurement Results

The measurement results are shown in Table 4 and 5, and in Figure 10 to 27.

4.2 Vibration Characteristics of Tower

The logarithmic decrement of free-standing tower was measured from the reduced waveform of free vibration after stopping the excitation.

(First time)

Figure 10 shows the waveform, Figure 11 shows the spectrum of vibration and Figure 12 shows the vibration mode at each frequency.

From waveform, it can be seen that the beat phenomenon with 0.1 Hz is generated. The reason is that the interaction between the vibration of first order (f=0.6 Hz, in phase mode) and of second order (0.7 Hz out of phase mode) was occured as shown in Figure 12.

The frequency is identical with the values obtained from kmeasurement of small oscilation shown in Figure 8 and Table 2, and it can be concluded that it is independent of the amplitude because, in measurement of small oscilation, the amplitude of vibration was 0.6 [mm] (shown in Table 2), and at this excit-ing test, it was about 16 [mm] (Figure 11).

Next, as for the logarithmic decrement for the tower, although to fix and stop the movement of pendulum was used so that the damping coefficient of oil damper would be maximum, the pendulum could not be fixed perfectly and it moved about 10 mm. Therefore, the measurement of pure damping value of tower was impossible, but it was calculated in the following way from the beat waveform.

Generally, the maximum values of beat waveform are plotted as shown in Figure 13, and the envelope line of maximum value Cmax. and minimum value Cmin. are drawn. Next, the values of ta, tb, Xa,b =(Cmax a,b + Cmin a, b), and Ya,b=(Cmax a,b - Cmin a,b) are calculated from the chart, and the values of two circular frequency and logarithmic decrement can be determined from the following formula.

$$\omega_1 = \frac{\pi\ (2Tb+T)}{Tb \cdot T} \qquad T = \frac{4\pi}{\omega_1+\omega_2} \qquad Tb = \frac{2\pi}{\omega_1-\omega_2}$$

ta = 12 tb = 20
ω_1 = 4.40 ω_2 = 3.77
Ya = 13.2 Yb = 10.5

$$\omega_2 = \frac{\pi\ (2Tb-T)}{Tb \cdot T} \qquad h_1 = \frac{\ell_n\ (Xa/Xb)}{\omega_1 (tb-ta)} \qquad h_2 = \frac{\ell_n\ (Ya/Yb)}{\omega_2\ (tb-ta)}$$

When applying of this method of calculation to the waveform shown in Figure 10, the logarithmic decrement of first order (0.6 Hz, in-phase) is δ=0.048. On the other hand, calculating the added damping due to the

damping device adopted as oscilator, it becomes to be 0.040 (based on another test). Therefore, it is assumed that the logarithmic decrement of tower in free-standing state is δ=0.048 - 0.040 = 0.008 or so.
The single amplitude of vibration at the top of tower (acceleration) is about 16 mm (22.7 gal),

(Second time)
The second test was composed of two cases. In one case, the test was excuted under the condition with temporary support and in the other case, with tower link. Figure 14. and 15 show the vibration waveform and the logarithmic decrement individually in former case, and Figure 16 and 17 show those in latter case.
Since these tests, the pendulum has become to be locked perfectly so the damping value of tower in free-standing state could be obtained exactly. The logarithmic decrement of free standing tower with temporary support, was about δ=0.01 in all exciting tests of five times as shown in Figure 27. As the result, it became evident that the logarithmic decrement of tower is about δ=0.01 same as assumed value at preliminary analysis regardless of the amplitude of tower. However, in the case where the girder is supported by the link, it was known that the values becomes larger with the increase of amplitude, i.e., the logarithmic decrement of tower is : δ =0.017 for the amplitude of tower of 3 mm or less, δ=0.0584 for that of 4 mm, and δ=0.0865 for that of 12mm.
The occurrence of slide at the tower link is considered to be the reason for this increase of damping.

(Third time)
Figure 18 shows the waveform of free vibration in the third test, and Figure 19 shows the logarithmic decrement.
When calculating the damping of tower, δ=0.01 for the amplitude of 3 mm orless, δ=0.0343 (4.02 mm amplitude) to δ=0.0455 (4.95 mm), and the results indicate that the damping depends on the amplitude when the girder is supported by the link and that the value increases with the increase of amplitude as indicated in the previous test.

Next, Figure 22 shows the response curve obtained from the sweep exciting test. By measuring the frequency, and logarithmic decrement from these data, they will be 0.435 Hz, and $\delta=2\pi h=\pi \Delta f/f=0.061$ (f: resonance frequency, Δf: half band width) respectively.
In these values, the frequency is same as the value obtained from waveform free vibtration test but the logarithmic decrement is indicated larger. This is because the complete resonant amplitude is not obtained due to the insufficient sweep time, and the amplitude in resonance is evaluated smaller, that is Δf is evaluated larger than actual value.
As for the frequency, all of values obtained from free vibration test, sweep exciting test, and small oscilation measurement, before-mentioned, are coincided with each other and the dependence on the amplitude was not recognized.
The effect due to attached 4 cables will be described later.

(Fourth time)
Figure 20 shows the waveform of free vibration at fourth test, and Figure 21 shows the logarithmic decrement.
By Figure 21, the logarithmic decrement is equal to 0.0083 (for amplitude of tower of 2.97 mm) and 0.010 (for 2.6 mm), that is, δ = about 0.01 for

the amplitude of 3 mm or less, and these values are same as the results obtained in previous tests.
The waveform (Figure 20) illustrates that the beat phenomena occured, and this is because the frequency of one or two cables are close to the frequency of tower as described later.
When summarizing the vibration characteristics of tower above-mentioned, it can be described as follows.

(1) In the case where the girder is supported by temporary support under construction, the logarithmic decrement of free standing tower is almost constant, i.e. $\delta=0.01$ regardless of amplitude of tower.
(2) In the case where the girder is supported by tower link, the value is almost constant as $\delta=0.01$ for the amplitude at the top of tower of 3 mm or less, but when the amplitude becomes larger than 3 mm, slide at tower link will occur and so the logarithmic decrement of tower increases with the increase of amplitude of tower.
(3) The frequency is completely independent from the amplitude and the value is almost coincided with the preliminary calculated value. The simplicity of structure is one of the reason for this coincidence.

4.3 Effect of tuned mass damper

Figure 23 and 25 show the typical waveform of free vibration in the case of working the tuned mass damper, Figure 24 and 26 show each peak values of sinusoidal reduced wave in Figure 23, 25, and Figure 27 shows the relation between the logarithmic decrement and the amplitude of tower, and Table 5 shows the comparison between the measured values and the calculated values.

(First time)

When the tuned mass damper worked, the gross logarithmic decrement is $\delta=0.066$, so that the damping increased by 0.058 (=0.066 −0.01; here is 0.01 for without damper), and this value (0.066) attains the limit of $\delta=0.025$ or more whichis required for the suppressing galloping.

(Second time)

If the tower vibrates with amplitude of 3 mm or less, the device becomes to work in dead zone of amplitude, so the gross decrement hardly increases. But the value increases to $\delta=0.0486$ and 0.0544 when the amplitude is 12 mm or more. Therefore, the damping increases due to the device by 0.0386 (=0.0486 - 0.01), or 0.044 (0.0544 - 0.01) here is, 0.01 is as same above.

(Third time)

The gross logarithmic decrement, was calculated as 0.0557. By subtracting the damping in the state supported by tower link, (shown in Figure 14, 0.0455) the net increase of damping by the tuned mass damper will be 0.0102 (0.0557 - 0.0455). The amplitude at the top of tower at this test was 6.43 mm, and calculated based on the damping constant of oil damper which depends on the amplitude, this increased value is almost same as designed value.

(Fourth time)

The gross logarithmic decrement when the tuned mass damper is worked is $\delta=0.0203$ for about 2.4 mm (amplitude of tower), and the increase by the device is 0.0103 (0.0203 - 0.01).
In this test, it was impossible to excite the tower to the extent ampli-

tude of designed value, so the increase of damping was a little. But considered the dependence of amplitude in damping constant of oil damper the increase is almost equal to calculated value.
So, in conclusion, large effect of damping by the device will be expected as the tower vibrates larger to designed value.

4.4 Effect of cable on the vibration of tower

The third and fourth test were carried out in the states where the four cables and all cables are attached respectively.
In the third test, the all four cables vibrated significantly with different frequency from excited frequency, but in the fourth test, the topmost cable and just below cable of it vibrated with excited frequency. The reason is assumed that, in the third test, the frequency of fourth cable from bottom which is most close to tower frequency (f = 0.43 Hz) compared with other cables is so high as about 1 Hz, so the cables vibrated under the influence of wind, but in the fourth test, the frequencies of the topmost cable and the tenth cable from the bottom are 0.396 Hz and 0.436 Hz respectively, and these are close to the exciting frequency of 0.413 Hz within the range of about 5%.
By numerical analysis based on exciting forces and amplitudes measured in the third test (with no added damping by cables) and the fourth test (with added damping), it is assumed that the additional damping by the cables in the fourth test is about $\delta = 0.15$.
As shown above, the amplitude of tower is suppressed due to the addition of damping by the cables, so in the fourth test, the tower did not vibrate to such a range of amplitude in which the tuned mass damper works effectively. Figure 28 and 29 shows the results of calculation which numerically simulated these phenomena.
Figure 28 shows the simulated results under the same condition as fourth test, and it can be seen that the tuned mass damper does not almost vibrate but the topmost and 10th cables are vibrating remarkably.
In the ohter hand, figure 29 shows the simulated results when the bridge is opened, that is, under the condition where the frequency of all cables are higher than 6.0 Hz, and it can be seen that the cable does not vibrate but the tuned mass damper vibrates remarkably.
From above results of simulation, it can be known that the tower does not vibrate when the frequency of cable is close to the frequency of tower due to so-called dynamic damper effect of cable, so the pendulum of the device does not vibrate because of large damping of oil damper. However, when the bridge is completed, as shown in Figure 29, the dynamic damper effect of cable is lost because the frequencies of cable are apart from the frequency of tower (0.4 Hz), so that tower becomes to vibrate larger than in Figure 28 and tuned mass damper also become to work effectively, and as the result, the damping of tower increases. (in Figure 29

5. Conclusion

In order to verify the appropriateness of wind tunnel test to review the stability of suppressing wind-induced vibration of bridge tower, the vibration test by using actual bridge was carried out, and its vibration characteristics such as frequency, logarithmic decrement, etc., can be grasped. As the results, it can be known that the frequency and damping of actual bridge are almost same as the prescribed values, and also, the quantitative evaluation of the effects by the friction of tower link and

quantitative evaluation of the effects by the friction of tower link and cables was made possible, and it is considered that the utilization of these data for backing-up the wind tunnel test can be expected in the future.

Table 1 logarithmic decrement required to suppress for galloping of free-standing tower

construction stage		B 18	B 19	B 20	B21	B23		B 25	B 27	B 31
						without h. s.	with h. s.			
calculated logarithmic decrement based on wind tunnel test		0.011	0.015	0.018	0.020	0.020	0.013	0.014	0.016	0.025
logarithmic decrement obtained by wind tunnel test with damper device	measurement	0.19	——	——	——	——	——	——	——	0.14
	assumed value	——	——	——	——	——	——	——	——	0.25

h. s. : upper horizontal stiffener —— : non calculated

Table 2 results of measurement of small oscillation occured usually

construction stage		B20	B21	B23		B25	B27	B31		
								without cable	4 cable	completion
height of tower (m)		123	129	137		147	157	172	172	172
equivalent mass (ton, S^2/m)		90.6	96.4	122.8	219.1	213.3	238.8	222.7	——	218.9
natural frequency (Hz)										
	calculation	0.575	0.529	0.401	0.560	0.547	0.509	0.457	——	0.399
	measurement	0.60	0.54	0.430	0.555	0.53	0.500	0.450	0.435	0.413
	meas./calc.	104%	102%	107%	99%	97%	98%	98%	——	104%
amp. of tower top (m)		0.6	0.5	0.7	0.07	0.1	0.08	1.8	0.3	0.2

Table 3 exciting method

test No.	exciting method
First time	damping device excitation
Second time	manually excitation
Third time	machine excitation
Fourth time	

Table 4 vibration characteristic of tower

test No.	frequency (Hz)		maximum acc. of tower (gal)	maximum amp. of top of tower (m)	logarithmic decrement of free-standing tower	note
1	0.60	1	16	11.26	0.0080	temporary support
2	0.457	1	3	3.64	0.0100	1
		2	4	4.85	0.0065	1
		3	5	6.06	0.0114	1
		4	10	12.13	0.0087	1
		5	22	26.68	0.0097	1
		6	6	7.28	0.0584	tower link
		7	10	12.13	0.0865	1
3	0.435	1	3	4.02	0.0343	1
		2	3.7	4.95	0.0455	1
		3	3.8	5.09	0.0448	1
4	0.413	1	1.75	2.60	0.0100	1
		2	2.0	2.97	0.0083	1
		3	2.3	3.42	0.0092	1

Table 5 effect of damping device

test No.	frequency (Hz)		maximum acc. of tower (gal)	maximum amp. of tower top (m)	single amp. of damping device (m)	total logarithmic decrement	logarithmic decrement of free-standing tower	increase of log. dec. (measurement)	increase of log. dec. (calculation)	calculation / measurement
1	0.60	1	16	11.26	20	0.0660	0.0080	0.058	——	—
2	0.457	1	10	12.13	50	0.0489	0.0087	0.0389	0.040	101%
		2	11	13.34	50	0.0531	0.0087	0.0431	0.040	111%
		3	11	13.34	45	0.0544	0.0087	0.0444	0.034	134%
		4	13	15.77	60	0.0486	0.0087	0.0386	0.0438	91%
3	0.435	1	4.8	6.43	11	0.0557	0.0455	0.0102	0.007	140%
4	0.413	1	1.6	2.38	unknown	0.0203	——	0.0103	——	—
		2	1.625	2.41	unknown	0.0234	——	0.0134	——	—

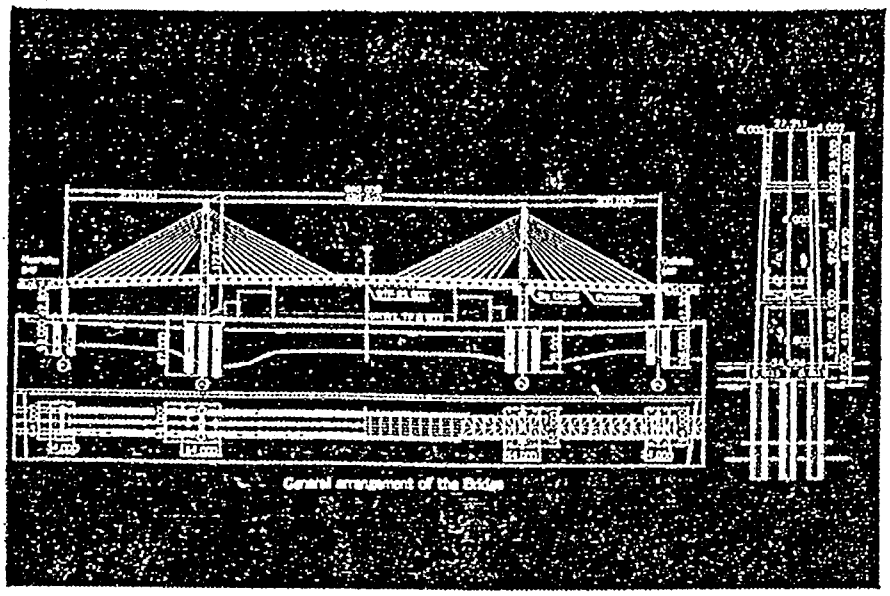


Fig. 1 General arrangement of the bridge

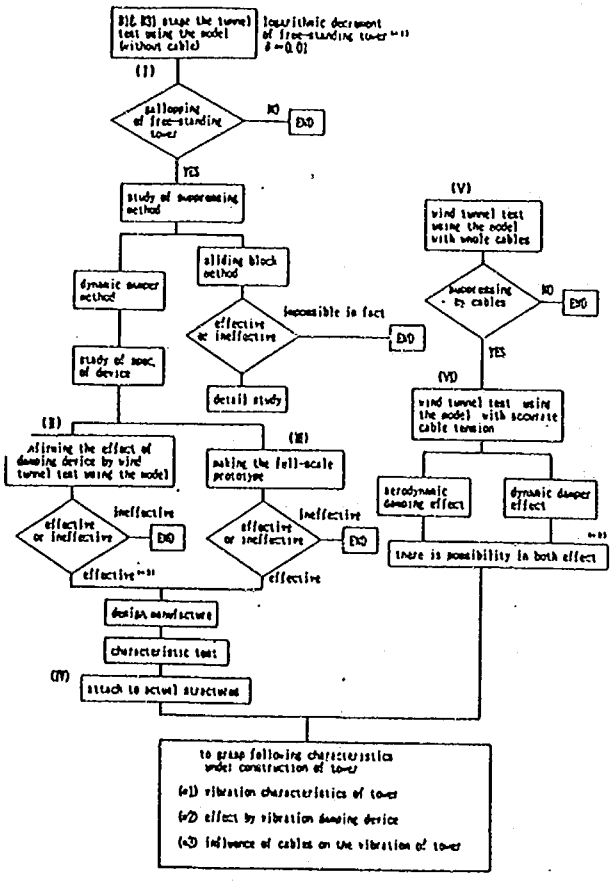


Fig. 2 Flow chart

construction stage	B 1 8	B 1 9	B 2 0	B 2 1
height of tower[m]	1 1 0	1 1 6	1 2 3	1 2 9
frequency[Hz]	0. 7 9 5	0. 7 2 2	0. 5 7 5	0. 5 2 8
equivalent mass[ton s²/m]	1 1 2. 0	1 3 3. 2	9 0. 6	9 6. 4
shape of tower		(dynamic damper) temporary Support		
B 2 3 without h.s.	B 2 3 with h.s.	B 2 7	B 2 9	B 3 1
1 3 7	1 3 7	1 4 7	1 5 7	1 7 2
0. 4 0 1	0. 5 0 0	0. 5 4 1	0. 5 0 9	0.457(0.399)
1 2 3. 8	2 1 9. 1	2 1 3. 3	2 2 0. 2	222.7(210.9)
	remount		remount	support by tower

Fig. 3 Shapes and height of tower at each constraction stage

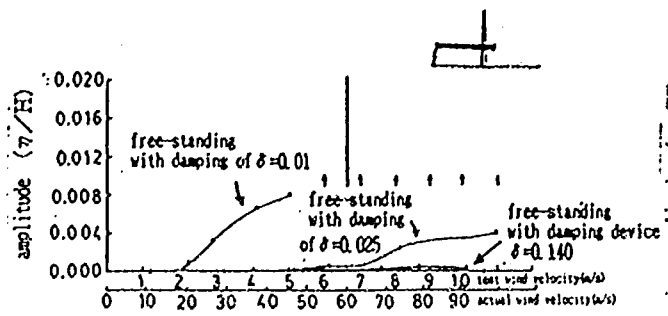


Fig. 4 Wind velocity-amplitude on wind tunnel test (B31 constraction stage in free-standing state)

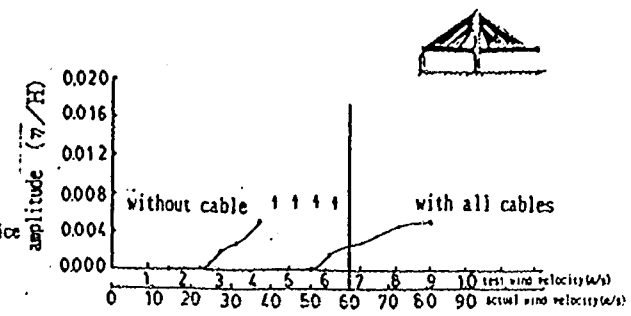


Fig. 6 Wind velocity-amplitude on wind tunnel test (when the tower is completed with all cables)

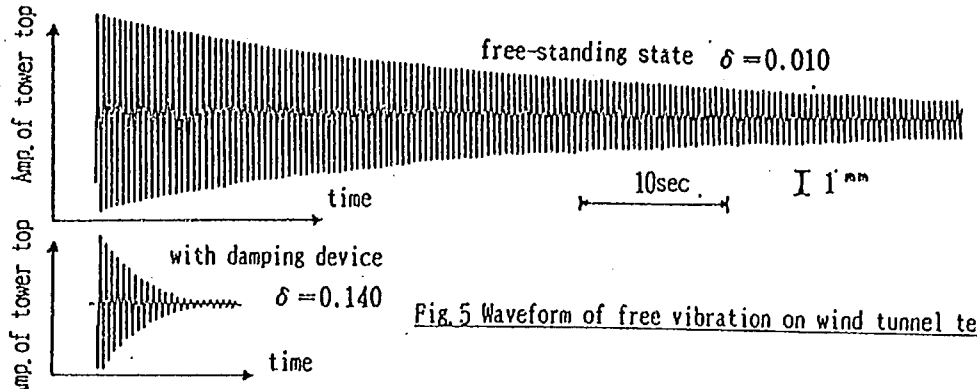
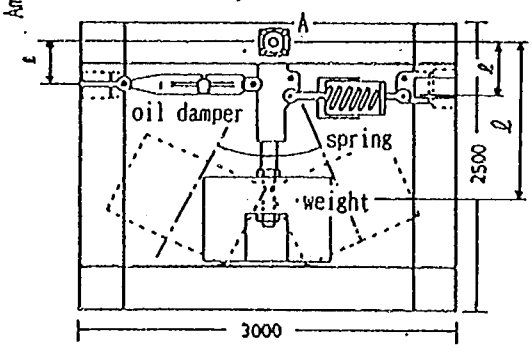
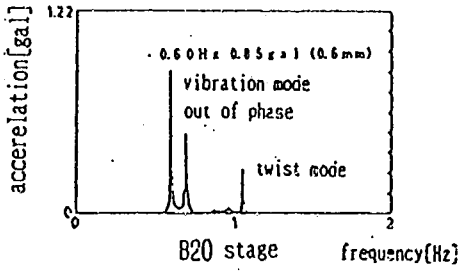


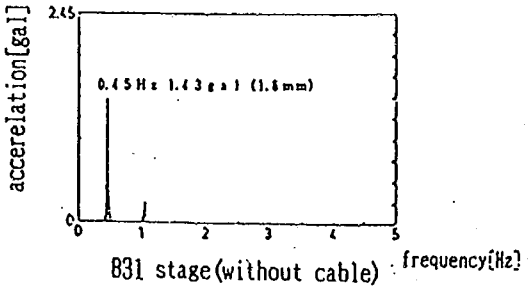
Fig. 5 Waveform of free vibration on wind tunnel test

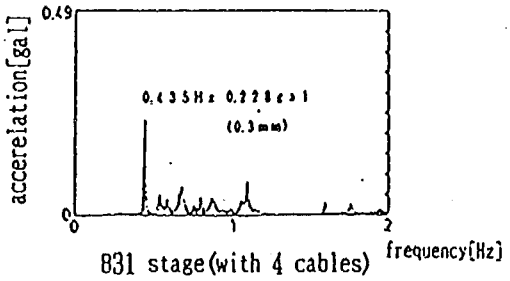


	spec.	distance from A
pendulum	W=5.5-7.5ton	180~188 (CM)
spring	K=188 (KG/CM) X2	38 (CM) or 43 (CM)
oil damper	C=20~65 (KG·S/CM) X2 changable	33 (CM)
adjustable frequency range	0.395 ~ 0.759 (Hz)	

Fig. 7 Charactristics of damping devive







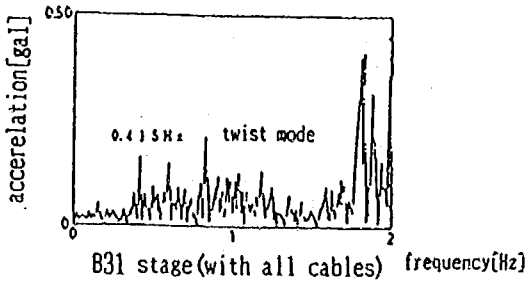


Fig. 8 Continuous measurement of small oscillation occured usually

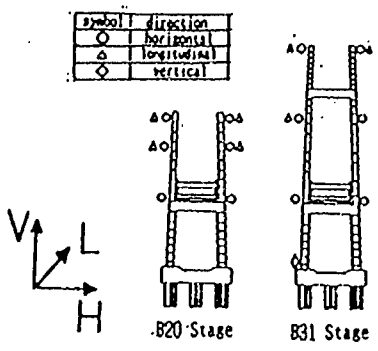


Fig. 9 Measuring position of tower accerelation

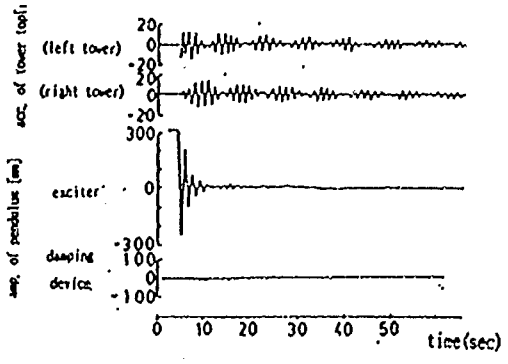


Fig. 10 Waveform of free vibration(first time)

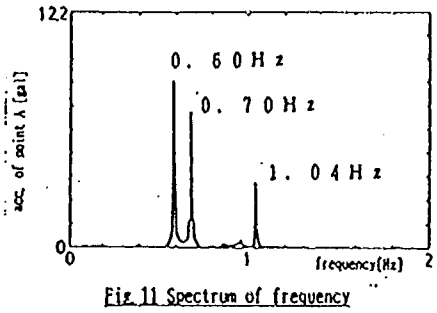


Fig. 11 Spectrum of frequency

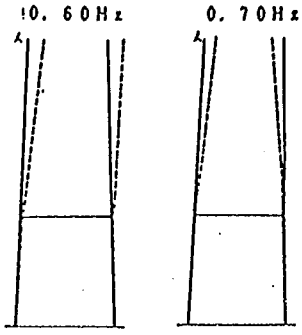


Fig. 12 Vibration mode

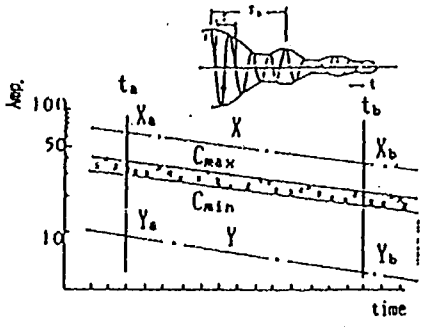
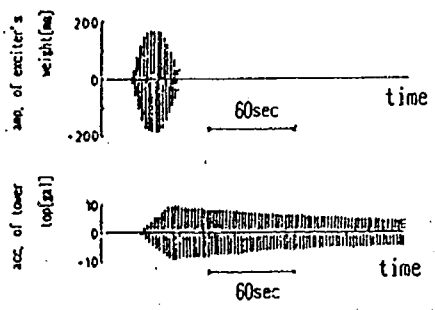
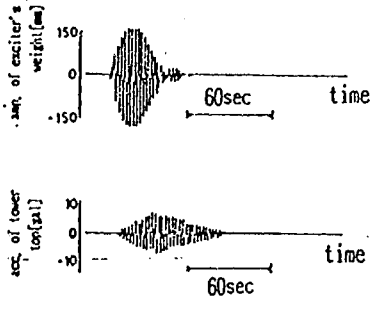


Fig. 13 Calculation method of logarithmic decrement from beat waveform





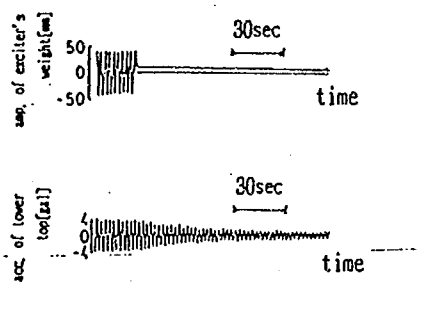


Fig. Waveform of free vibration(second time) (temporary support)

Fig. 16 Waveform of free vibration(second time) (tower link)

Fig. 18 Waveform of free vibration(third time)

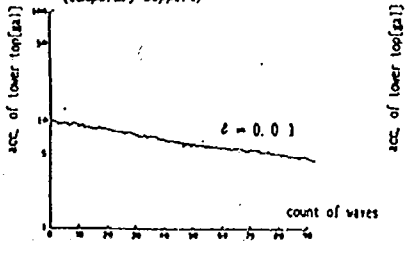


Fig. 15 Logarithmic decrement(second time) (temporary support)

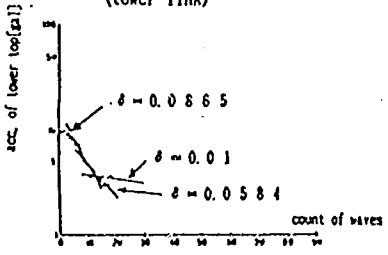


Fig. 17 Logarithmic decrement(second time) (tower link)

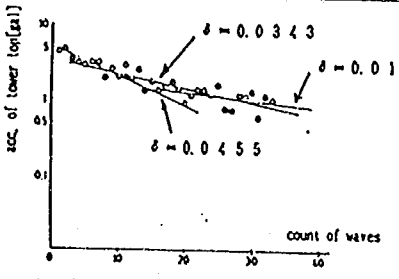


Fig. 19 Logarithmic decrement(third time)

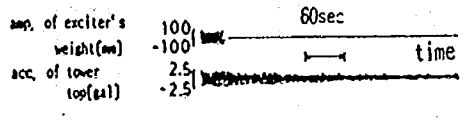


Fig. 20 Waveform of free vibration(fourth time)

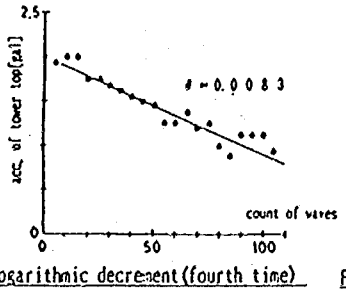


Fig. 21 Logarithmic decrement(fourth time)

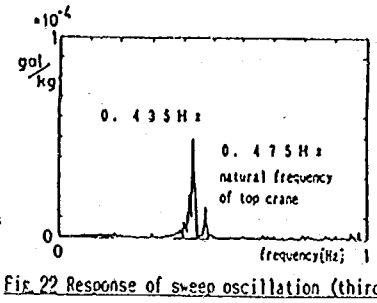


Fig. 22 Response of sweep oscillation (third time)

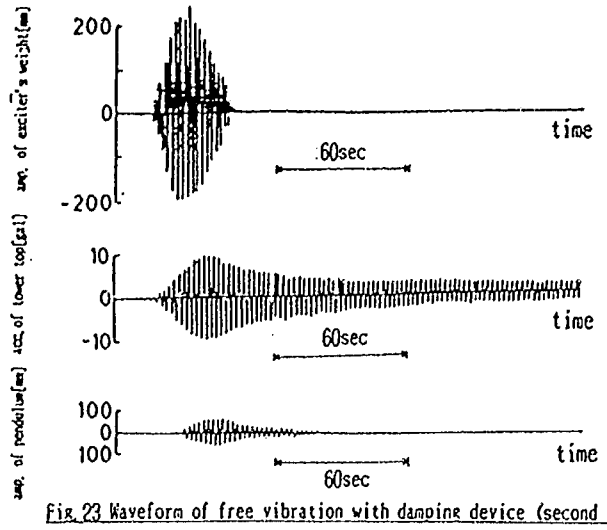


Fig. 23 Waveform of free vibration with damping device (second time)

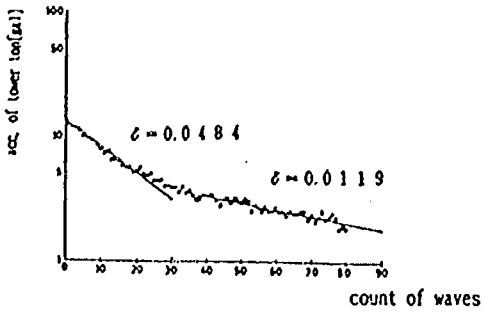


Fig. 24 Logarithmic decrement with damping device(second time)

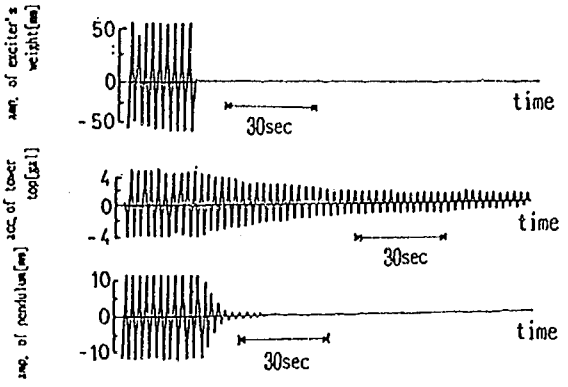


Fig. 25 Waveform of free vibration with damping device (third time)

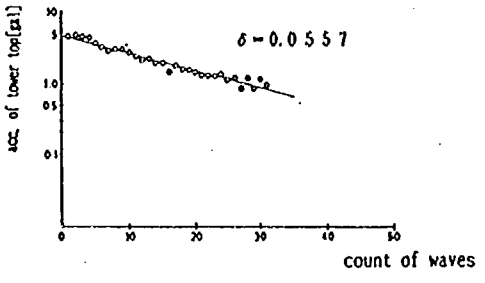


Fig. 26 Logarithmic decrement with damping device(third time)

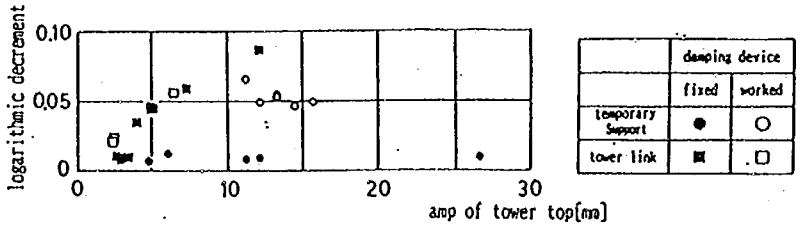


Fig. 27 Relation of logarithmic decrement to amolitude at the tower top

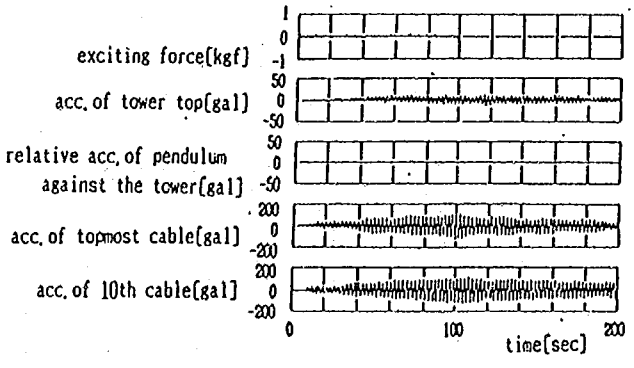


Fig. 28 The simulated waveform when the tuned mass dampers are worked on completion of the tower construction

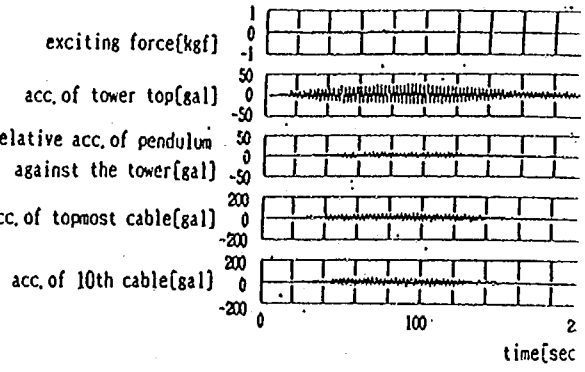


Fig. 29 The simulated results when the bridge is opened

DAMPING STAY CABLES WITH TIES

by

Fazl Ehsan[1] and Robert H. Scanlan[2]

1. Introduction

Arrays of support cables of cable-stayed bridges have, on numerous occasions, evidenced various forms of wind-induced oscillation: vortex excitation, wake and wind-rain galloping, etc. Two principal palliatives have emerged in response: mechanical dampers and cable cross ties. The present paper deals with the latter solution.

The function of either device is to drain energy away from the offending cables and/or to inhibit further aerodynamic energy capture by them. In the case of the mechanical dampers, the typical energy drain converts incipient motional cable energy directly into heat by use of hydraulic shock absorbers. In the case of cable ties, these may either provide rigid fixed points - thus greatly shortening effective cable spans and raising their frequencies - or merely tie several cables together forming a new flexible system with different mechanical and aerodynamic properties. The latter approach will be examined here in some detail, with particular attention to the redistribution of oscillatory energy that it effects.

Figure 1 illustrates a typical cable fan of a modern cable-stayed bridge. Typical cable external diameters are of the order of 200 mm. Under certain conditions of weather, many cables of the fan, or, alternatively, outer cables only, have exhibited violent wind-excited oscillation in one of their early lateral modes. In response, cross-tie cables (of the order of 6 mm diameter) have been installed in the manner shown in Figure 2. This has effectively quelled the oscillations. Analysis of the energy redistribution qualities of the cross ties, that effectively suppress the oscillation, is explored below.

2. Vibration Analysis of Cable-Tie Systems

Consider the cable-tie system pictured in Figure 3 consisting of m cables and k ties. Tie t is attached to s_t cables, where $s_t \leq m$. The "component mode synthesis" approach [1] is adopted for the vibration analysis. In this method, a large structural system is simplified by breaking it up into smaller subsystems (individual cables in this case,) which are related through the displacement and force conditions at the junction points (tie locations).

[1]Postdoctoral Research Fellow, and
[2]Professor, Department of Civil Engineering,
The Johns Hopkins University, Baltimore, MD 21218, U.S.A.

The displacement of the ith cable is assumed to take the form:

$$w_i(x_i,t) = \sum_{j=1}^{n} \phi_{ij} p_{ij} \qquad i = 1,2,...,m \tag{1}$$

where ϕ_{ij}, $j = 1,2,...,n$ are the normal modes, and p_{ij} are the associated generalized coordinates of the individual cables. The total number of coordinates assumed is thus $N = m \times n$.

Each cable tie yields $s_t - 1$ constraint equations, and the total number of such equations for this system is $M = \left(\sum_{t=1}^{k} s_t\right) - k$. Thus, the number of independant system coordinates is $r = N - M$. In general, any of the p_{ij}'s can be selected as the system generalized coordinates $q_1, q_2, ..., q_r$. The constraint equations can then be expressed in terms of the system coordinates as [2]:

$$\{p\} = [C]\{q\} \tag{2}$$

where $\{p\}$ is $N \times 1$, $[C]$ is $N \times r$ and $\{q\}$ is $r \times 1$.

2.1 System Frequencies

The matrix equation of motion of the system can be written in terms of the individual cable coordinates p_{ij} using the expresions for the kinetic and potential energy in the Lagrange equation:

$$\{\ddot{p}\} + [\Omega]\{p\} = \{0\} \tag{3}$$

where $[\Omega]$ is an $N \times N$ diagonal matrix whose terms are ω_{ij}^2, $i = 1,2,...,m$, $j = 1,2,...,n$, where ω_{ij} is the circular frequency of the ith cable oscillating in its jth natural mode. Using equations 2 and 3, and assuming $\{\ddot{q}\} = -\omega^2\{q\}$, the following eigenvalue problem can be defined:

$$\left[[R] - \omega^2[I]\right]\{q\} = \{0\} \tag{4}$$

where

$$[R] = \left[[C]^T[C]\right]^{-1}[C]^T[\Omega][C] \tag{5}$$

noting that $[C]$ is not necessarily a square matrix. The system frequencies can be obtained from (4) and (5) using individual cable frequencies. It should be mentioned here that the selection of system generalized coordinates is not entirely arbitrary. Certain choices may lead to non-invertible $[C]^T[C]$ matrices.

2.2 Distribution of Potential Energy

The distribution of potential energy among the various cables can be estimated as follows, once the system frequencies are available. Note that a total of $r = N - M$ system frequencies can be computed. Let the corresponding eigenvectors be designated $\{q\}_1, \{q\}_2, ..., \{q\}_r$. These will be refered to as the $q-$vectors. The eigenvectors in terms of the individual cable coordinates p_{ij} can be found

by substituting the $q-$vectors into (2). Let these be denoted the $p-$vectors: $\{p\}_1, \{p\}_2, \ldots, \{p\}_r$.

If ϕ_{ij} are orthogonal modes, the total potential energy, U, of the system is given by:

$$U = \frac{1}{2} \sum_{i=1}^{m} \sum_{j=1}^{n} M_{ij} \omega_{ij}^2 p_{ij}^2 \tag{6}$$

where

$$M_{ij} = \int_0^{L_i} m_i(x) \phi_{ij}^2 dx \tag{7}$$

is the generalized mass of the ith cable oscillating in its jth natural mode and $m_i(x)$ is the mass per unit length of the ith cable.

The "normalized" potential energy of the system oscillating in mode 's' is given by:

$$U_s = \frac{1}{2} \sum_{i=1}^{m} \sum_{j=1}^{n} M_{ij} \omega_{ij}^2 (p_{ij})_s^2 \tag{8}$$

where $(p_{ij})_s$ is obtained from the sth $p-$vector $\{p\}_s$. This is a normalized quantity in the sense that the maximum displacement of any single cable in the system is unity. The fraction of energy in the ith cable when the system is oscillating in mode s can then be found from:

$$U_s^i = \frac{\sum_{j=1}^{n} M_{ij} \omega_{ij}^2 (p_{ij})_s^2}{\sum_{i=1}^{m} \sum_{j=1}^{n} M_{ij} \omega_{ij}^2 (p_{ij})_s^2} \tag{9}$$

3. Application to Elementary System

Consider the elementary cable array pictured in Figure 4 consisting of three cables and two ties. An analytical study of such an array will be carried out using the approach outlined in the previous section. In order to allow hand calculations, only two modes per cable are assumed in equation 1. The modes are assumed to be sinusoidal, i.e.,

$$\phi_{ij}(x) = \sin \frac{j \pi x_i}{L_i} \tag{10}$$

The total number of individual cable coordinates p_{ij} is six, and there are four constraint equations:

$$\begin{aligned} w_1(x_1 = 3L_1/8) &= w_2(x_2 = L_2/3), \quad & w_1(x_1 = 5L_1/8) &= w_2(x_2 = 2L_2/3) \\ w_2(x_2 = L_2/3) &= w_3(x_3 = L_3/4), \quad & w_2(x_2 = 2L_2/3) &= w_3(x_3 = 3L_3/4) \end{aligned} \tag{11}$$

The number of system generalized coordinates is 2 in this case.

3.1 Frequencies of Elementary System

In this example p_{11} and p_{32} are selected to be the system coordinates, i.e., $p_{11} = q_1$ and $p_{32} = q_2$. Following the procedure outlined in the previous section,

the system frequencies are obtained in terms of the individual cable frequencies as:

$$\begin{aligned} \omega_1^2 &= 0.26\omega_{11}^2 + 0.296\omega_{21}^2 + 0.444\omega_{31}^2 \\ \omega_2^2 &= 0.46\omega_{12}^2 + 0.307\omega_{22}^2 + 0.23\omega_{32}^2 \end{aligned} \tag{12}$$

The influence of the various cable frequencies on the system frequencies becomes apparent for this simple system. The shortest cable (3) is seen to possess the potential of having the greatest impact on the first system mode while the longest cable (1) can influence the second mode more strongly. The actual contributions of individual cables will depend on their frequencies.

3.1.1 Comparison with Finite Element Solution

A finite element model of the elementary system was constructed. The finite element package *ABAQUS* [3] was used. The cables were modeled as two-noded truss elements.

The accuracy of the model was first checked by considering a single taut cable. The frequencies obtained from the finite element model were within 0.5 % of the theoretical frequencies given by:

$$f_n = \frac{n}{2L}\sqrt{\frac{T}{m}} \tag{13}$$

where L is the cable length, m is the mass per unit length, T is the cable tension and n is the mode number.

Two cases were studied for the elementary system pictured in Figure 4. The cases were:

1. Equal tension in all cables, i.e., $f_1 < f_2 < f_3$; and
2. Equal frequency for all cables, $f_1 = f_2 = f_3$.

The results are summarized in Table 1. An average of 16 elements were used to model each cable. Increasing the number of elements to 40 per cable did not affect the results upto 3 decimal points.

Table 1a. Definition of Cases Studied

Cable No.	Length (in)	Diameter (in)	Case I Tension (lbs)	Case I Freq. (Hz)	Case II Tension (lbs)	Case II Freq. (Hz)
1	400	0.5	800	2.953	800	2.953
2	300	0.5	800	3.937	450	2.953
3	200	0.5	800	5.906	200	2.953

Table 1b. Comparison of Results

Case	Frequency of System Modes		
	Theory (2 modes/cable)	Finite Element Analysis	Percent Difference
I: Equal Tension	4.727	3.711	21.5
II: Equal Freq.	2.953	2.561	13.3

It may be observed that the theoretical and finite element analysis results are not in perfect agreement. Among the main reasons for this discrepancy may be the fact that the theoretical analysis discussed above does not allow for the contribution of the higher modes (> 2) of individual cables to the system modes. Including higher modes in equation 1 results in a system of equations that is rather cumbersome to manipulate manually. In addition, a linear solution is being assumed for an inherently nonlinear problem.

Within the restrictions of the assumptions of the theoretical analysis, two factors that contribute to the discrepancy in results may be identified:

1. The first is the closeness of the actual displaced shapes of the three cables to the assumed modes (half sine waves in this case, for the first mode). This may be quantified by defining a *modal residual* for cable i oscillating in mode j:

$$(m_{res})_i = \frac{1}{L_i}\int_0^{L_i}\left(\sin\frac{j\pi x_i}{L_i} - \bar{\phi}_{ij}(x_i)\right)^2 dx_i \qquad (14)$$

   where $\bar{\phi}_{ij}(x_i)$ is the exact displaced shape (from finite element analysis) of cable i normalized with respect to the maximum ordinate. The total modal residual for the two cases were computed to be:

$$\text{Case I}: \quad \sum_i (m_{res})_i = 0.0085 \qquad \text{Case II}: \quad \sum_i (m_{res})_i = 0.0016 \qquad (15)$$

   The reduction in the modal residual value in the second case is reflected in the improved frequency estimate of the theoretical analysis.

2. The second factor is suggested in equation 12, i.e., the shortest cable has the potential of having a great effect on the computed system frequencies. In case I, the frequency of cable 3 is twice that of cable 1, while in case II the two frequencies are equal.

Both these factors are expected to contribute to the difference in the theoretical and exact frequencies. It is assumed for the remainder of this study that the theoretical results may be used to provide, at least, a qualitative picture of the energy redistribution in the elementary system.

3.2 Energy Distribution and Amplitude Reduction

The total potential energy of the elementary system oscillating in mode s, where $s = 1$ or 2, is given by:

$$U_s = \frac{1}{4}\sum_{i=1}^{3}\sum_{j=1}^{2} m_i L_i \omega_{ij}^2 (p_{ij})_s^2 \tag{16}$$

which is obtained from (6) using $M_{ij} = \frac{1}{2} m_i L_i$ for the assumed mode shapes. The eigenvectors of the system modes in terms of the individual cable coordinates are:

$$[p_{11}\ \ p_{12}\ \ p_{21}\ \ p_{22}\ \ p_{31}\ \ p_{32}]_1^T = [1\ \ 0\ \ 1.0669\ \ 0\ \ 1.3066\ \ 0]^T \tag{17}$$

$$[p_{11}\ \ p_{12}\ \ p_{21}\ \ p_{22}\ \ p_{31}\ \ p_{32}]_2^T = [0\ \ 1.4142\ \ 0\ \ 1.1548\ \ 0\ \ 1]^T \tag{18}$$

Assuming equal mass per unit length for the three cables, i.e., $m_i = m$ say, the following expressions are obtained for the maximum "normalized" potential energy of the system associated with the first two modes:

$$U_1 = \frac{1}{4} m \left[\omega_{11}^2 L_1 + 1.138\omega_{21}^2 L_2 + 1.707\omega_{31}^2 L_3\right] \tag{19}$$

$$U_2 = \frac{1}{4} m \left[2\omega_{12}^2 L_1 + 1.334\omega_{22}^2 L_2 + \omega_{32}^2 L_3\right] \tag{20}$$

The percentage of total potential energy in each cable is computed from (19) and (20) for the two cases mentioned in Section 3.1.1. The results are summarized in Table 2.

Table 2. Energy Distribution

Case	System Mode	Percent of Total Energy		
		Cable 1	Cable 2	Cable 3
I	1	16.9	25.6	57.5
	2	34.6	30.8	34.6
II	1	36.9	31.5	31.5
	2	57.1	28.6	14.3

The amount of energy in any single cable appears to depend both on the frequency of the individual cable and the system mode under consideration.

In order to calculate the reduction of amplitude of oscillation of a single cable, it is assumed that all the energy of the elementary system was originally present in that cable alone. After tying the cables together, a fraction f of the energy remains in the cable, i.e., $U_{\text{tied}} = f\ U_{\text{original}}$. Also, since the cable potential energy is proportional to the square of the oscillation amplitude, one may write: $w_{\text{tied}} = \sqrt{f}\ w_{\text{original}}$, where w is the transverse displacement. The percentage reduction in amplitude is then given by:

$$\text{Percent reduction} = (1 - \sqrt{f}) \times 100 \tag{21}$$

The percent reduction in the amplitudes of each cable is shown in Table 3.

Table 3. Amplitude Reduction

Case	System Mode	Percent Reduction of Amplitude		
		Cable 1	Cable 2	Cable 3
I	1	58.9	49.4	24.1
	2	41.2	44.5	41.2
II	1	39.2	43.8	43.8
	2	24.4	46.5	62.2

Thus a significant reduction in oscillation amplitudes is achieved by the relatively simple device of tying the cables together to form a new system.

4. Full-Scale Model

In order to examine the energy distribution characteristics in a cable-tie system of an actual cable-stayed bridge, a finite-element model of the array shown in Figure 2 was constructed. The array consists of 18 cables. Each of the 4 ties is attached to a different number of cables; in particular, the ties are attached to 4, 8, 11 and 14 cables respectively (Figure 2). The four lower cables are thus irrelevant to the dynamics of the system. In addition, it was assumed that the bridge tower and deck are perfectly rigid.

Table 4 lists the cable properties, tensions, and the number of elements used to model each cable, along with individual cable frequencies computed using the vibrating string equation (13).

Table 4. Cable Properties

Cable No.	Length (m)	No. of elements	Area (m^2)	Force (kN)	Unit Mass (kg/m)	Freq. (Hz)
1	207.87	46	0.021	3700.92	163.92	0.362
2	196.55	44	0.011	3024.79	86.37	0.476
3	184.92	42	0.011	3095.96	86.37	0.512
4	173.30	40	0.011	3247.20	86.37	0.560
5	161.98	36	0.011	3167.13	86.37	0.591
6	150.35	34	0.011	2975.86	86.37	0.617
7	138.72	32	0.011	2913.59	86.37	0.662
8	127.10	30	0.011	2708.97	86.37	0.697
9	115.77	24	0.011	2637.80	86.37	0.755
10	104.15	22	0.011	2651.14	86.37	0.841
11	92.52	20	0.011	2677.83	86.37	0.952
12	80.88	17	0.011	3020.34	86.37	1.156
13	69.57	16	0.011	2900.24	86.37	1.317
14	57.94	15	0.010	3598.61	78.46	1.848

Elastic Modulus E = 200,000 MN/m^2 (29×10^6 psi);
Density ρ = 7805.71 kg/m^3 (7.3×10^{-4} lb s^2/in^4)

In the actual bridge, "grouted bar cables" having a typical cross-sectional configuration as shown in Figure 5, were used. In order to simplify the finite element model, the truss elements used to represent the cables were assumed to be of circular section having the same cross-sectional area as the steel in the grouted bar cables. The ties were modeled as 6 mm diameter steel cables wrapped around the main cables, thus providing a total area equal to that of two 6 mm diameter cables. A total of 418 elements were used to model the cables and 33 elements were used to model the ties.

4.1 System Frequencies and Modes

The first five frequencies and modes of the cable-tie system were obtained using *ABAQUS*. The geometric nonlinearity of the problem was taken into account in the analysis. The frequencies and generalized masses of the first five modes are shown below:

Table 5. System Frequencies

Mode No.	Frequency (Hz)	Generalized Mass
1	0.631	4038.7
2	0.985	1874.0
3	1.283	893.21
4	1.322	1439.3
5	1.552	663.29

Figure 6 is a superimposed plot of the mode shapes of the 14 cables for the first system mode. Two observations can be made. The first is that the displaced shapes of individual cables may be significantly different from the normal sinusoidal modes due to the presence of the ties. This is particularly true for the outer cables of the system.

A second and perhaps more important observation is that the ties do not behave as completely rigid links, but display a significant amount of stretching. Thus, points a, b, c and d in Figure 6 would actually be a single point if the ties behaved as rigid links. If the amount of elastic stretch is known, the cable amplitudes that will cause the ties to yield may be estimated.

The maximum stretching occurs in the segment of the tie connecting nodes 296 and 320 (Figure 6). The elongation is $0.071A$ where A is the amplitude of cable 8 at node 296. The length of the tie is 3.96 m (12.98 ft) from which the strain is found to be:

$$\varepsilon = 0.0179\ A$$

where A is in metres. Taking the allowable stress in the ties to be 552 MN/m^2 (80 ksi) and using an elastic modulus value of 200,000 MN/m^2 (29×10^6 psi), the allowable amplitude of cable 8 at node 296 is 0.154 m (0.505 ft). Then using the

computed relative amplitudes at nodes 27 and 296, the allowable amplitude of the top cable at node 27 can be estimated to be 0.22 m (0.73 ft).

The axial stresses in the ties were obtained from the finite element analysis and are shown in Table 6. Note that these are the stresses that occur when the maximum amplitude of oscillation of any cable in the system is 1 ft. The tie segment discussed in the previous section is segment 8 of tie 3 (Table 6b).

Figures 7 and 8 are superimposed plots of cable vertical displacements for the system vibrating in modes 2 and 3 respectively. It may be observed that a system mode may include both symmetric and antisymmetric modes of the individual cables.

Table 6a. Axial Stresses in Ties 1 and 2

Tie 1			Tie 2		
	Stress			Stress	
Segment*	MN/m^2	ksi	Segment	MN/m^2	ksi
1	262.39	38.03	1	328.88	47.66
2	306.01	44.35	2	458.92	66.51
3	250.91	36.36	3	585.54	84.86
			4	711.99	103.19
			5	680.89	98.68
			6	587.79	85.19
			7	387.54	56.16

* see Figure 9

Table 6b. Axial Stresses in Ties 3 and 4

Tie 3			Tie 4		
	Stress			Stress	
Segment*	MN/m^2	ksi	Segment	MN/m^2	ksi
1	296.75	43.01	1	257.47	37.31
2	390.29	56.56	2	335.99	48.69
3	472.64	68.49	3	401.41	58.18
4	537.10	77.84	4	450.64	65.31
5	592.59	85.88	5	493.01	71.45
6	647.45	93.83	6	533.60	77.33
7	699.34	101.35	7	567.91	82.31
8	762.35	110.49	8	601.69	87.20
9	613.81	88.96	9	629.77	91.27
10	381.79	55.33	10	655.45	94.99
			11	687.17	99.59
			12	496.89	72.01
			13	299.46	43.40

* see Figure 9

4.2 Distribution of Energy

The distribution of strain energy among the cables was estimated directly from the deformed shapes of the cables obtained from the finite element solution. The strain energy stored in cable i is given by:

$$U_i = \frac{1}{2}(TL\epsilon)_i \tag{22}$$

where

$$\epsilon = \frac{S_i - L_i}{L_i} \tag{23}$$

and S_i is the deformed length of the cable. The portion of the total energy in each cable can thus be estimated if the system mode shapes are known. The deformed length is computed from the *ABAQUS* output as:

$$S = \sum_{\text{all elements}} \Delta S \tag{24}$$

where

$$\Delta S \approx \sqrt{(y_{j+1} - y_j)^2 + (x_{j+1} - x_j)^2} \tag{25}$$

where y_j is the transverse displacement at the node located at x_j. The computed strain energies are listed in Table 7. It may be observed that the portion of energy in each cable depends on the vibration mode. In the first mode, the energy is distributed quite evenly over all the cables while in higher modes, the energy appears to become concentrated in the longest cable.

Table 7. Energy Distribution

Cable No.	Mode 1	Mode 2	Mode 3
1	11.69	28.12	52.29
2	8.690	14.69	9.310
3	9.630	14.78	7.100
4	11.04	16.85	6.270
5	8.030	4.600	2.680
6	8.690	4.450	3.410
7	8.370	3.510	2.550
8	9.850	3.210	3.600
9	5.180	1.590	2.790
10	5.960	1.930	3.600
11	7.180	2.000	4.120
12	1.880	1.440	0.820
13	1.530	1.140	0.530
14	2.280	1.680	0.920

The energy distribution is shown graphically in Figure 10. The amplitude reduction of the top cable (1) can be computed as described in Section 3.2. In the

first mode, the amplitude of the top cable oscillating alone with the same amount of energy would be reduced by 66 %. The reduction is 47 % and 28% in the second and third modes respectively.

5. Comments and Conclusions

Some observations that may be made in conclusion are summarized below:

1. Cable cross ties are very effective in redistributing the energy that may be present in a single (untied) cable over the whole array, particularly in lower modes. In the higher modes, the energy becomes more concentrated in the longer cables.

2. Design of cable ties should include a dynamic analysis of the system. As demonstrated in Section 4.1, the ties may be subjected to very large stresses. However, their very presence may prevent oscillations from being initiated.

3. Reasons for the discrepancy between the theoretical results, obtained using the component mode synthesis approach, and those obtained from the finite element analysis should be investigated.

As regards future research, the aeroelastic behavior of a cable-tie system, particularly its vortex-induced and galloping response, should be investigated and compared to the behavior of a single cable. The conditions under which cable vibrations may excite the bridge deck may also be investigated.

References

Hurty, W. C. "Vibrations of Structural Systems by Component Synthesis", *J. Engr. Mech. Div., Proc. of ASCE* (August 1960), pp. 51-69.

Thomson, W. T. *Theory of Vibration with Applications,* 2nd ed., Prentice-Hall, Inc., Englewood Cliffs, N.J., pp. 355-360.

Hibbitt, D., Karlsson, J., and Sorensen, E. P. *ABAQUS Version 4.6*, HKS Inc., Providence, RI (1987).

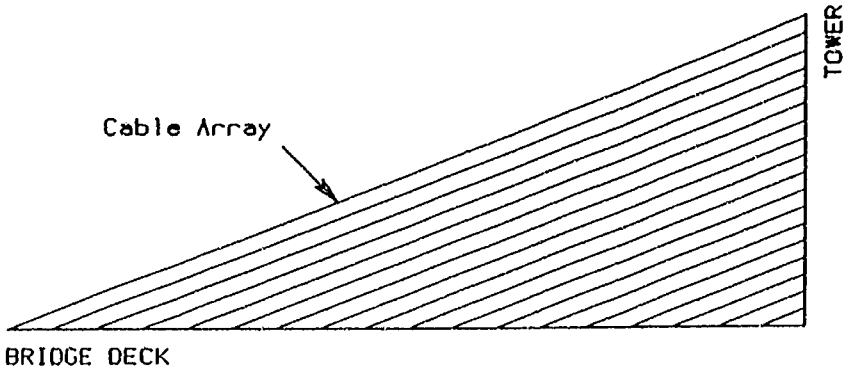


Figure 1. Typical Cable Fan

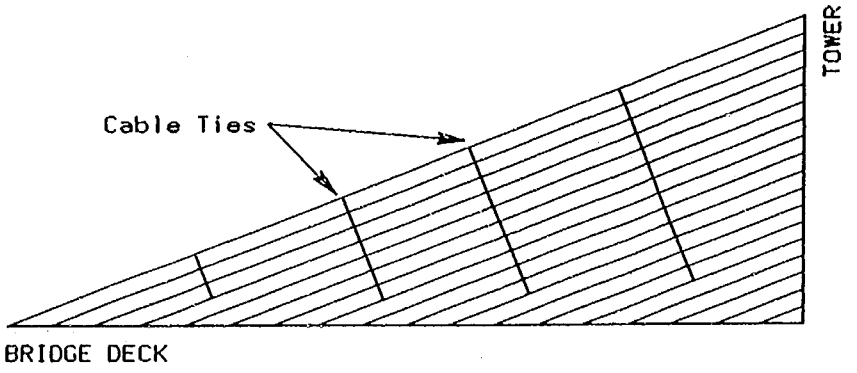


Figure 2. Cross-Tie Cables

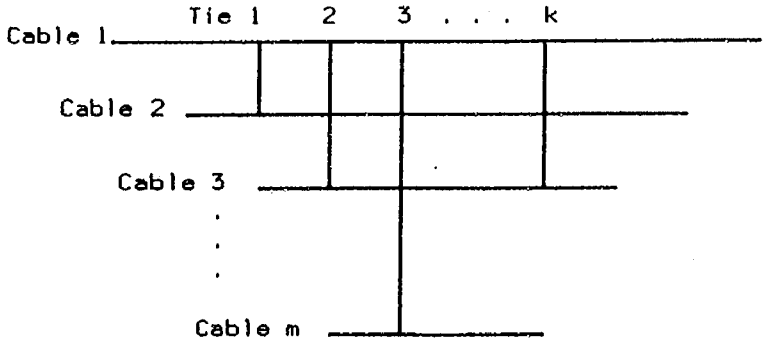


Figure 3. Cable-Tie System for Analysis

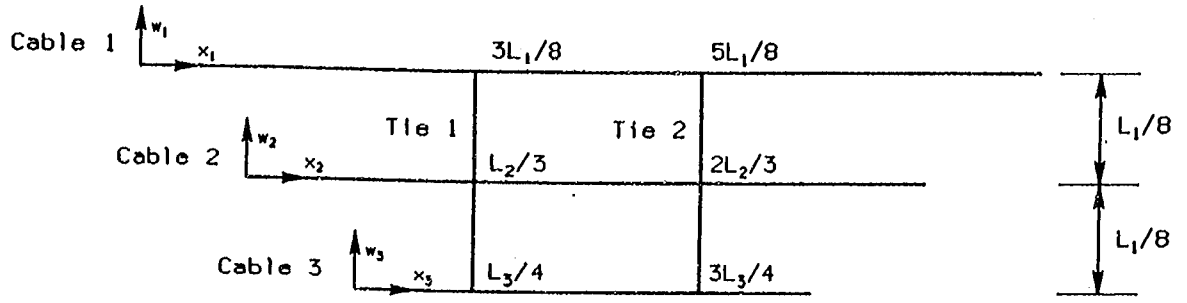


Figure 4. Elementary Cable-Tie System
$L_1:L_2:L_3 = 4:3:2$

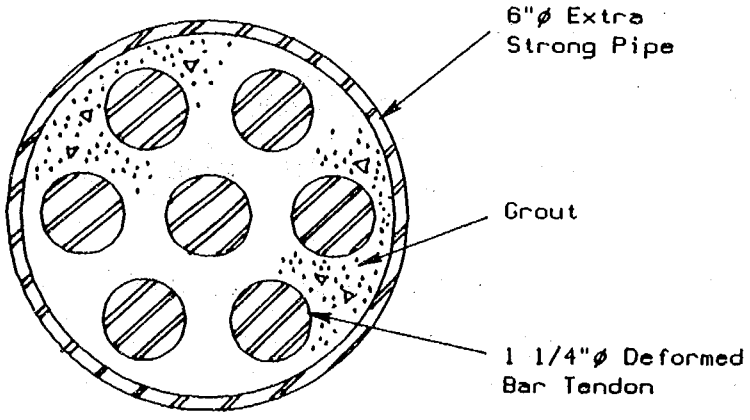


Figure 5. Cross-section of Typical Cable

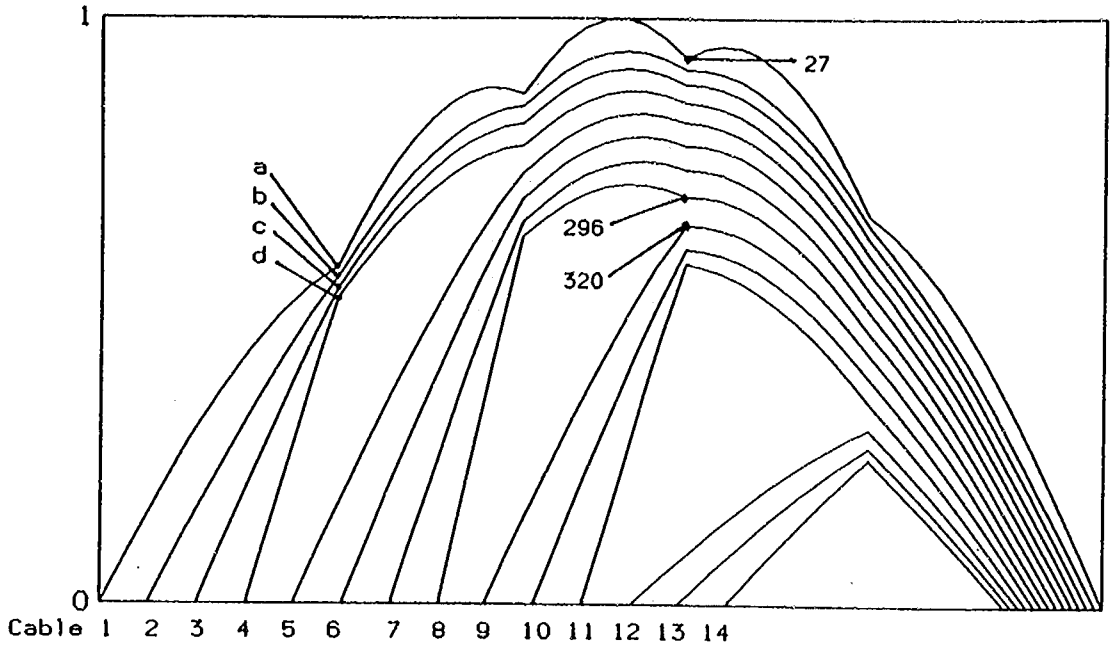


Figure 6. Superimposed plot of cables showing relative amplitudes: Mode 1.

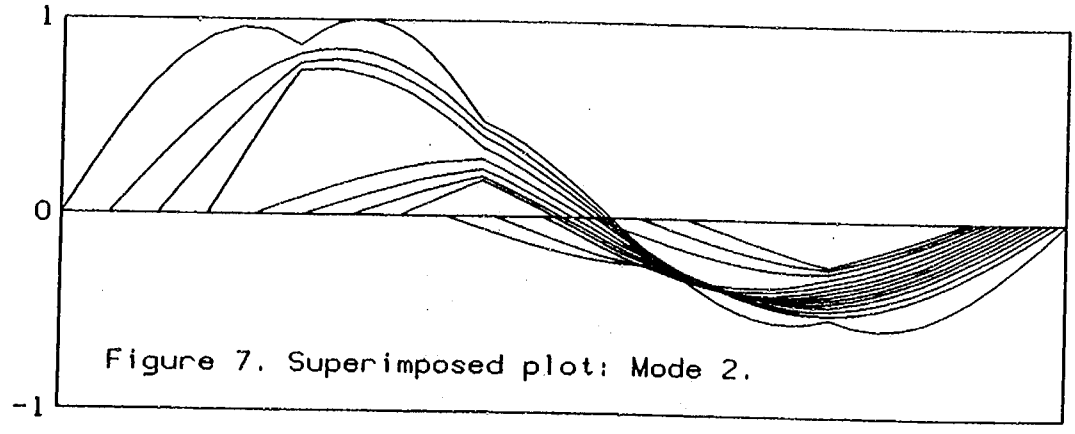


Figure 7. Superimposed plot: Mode 2.

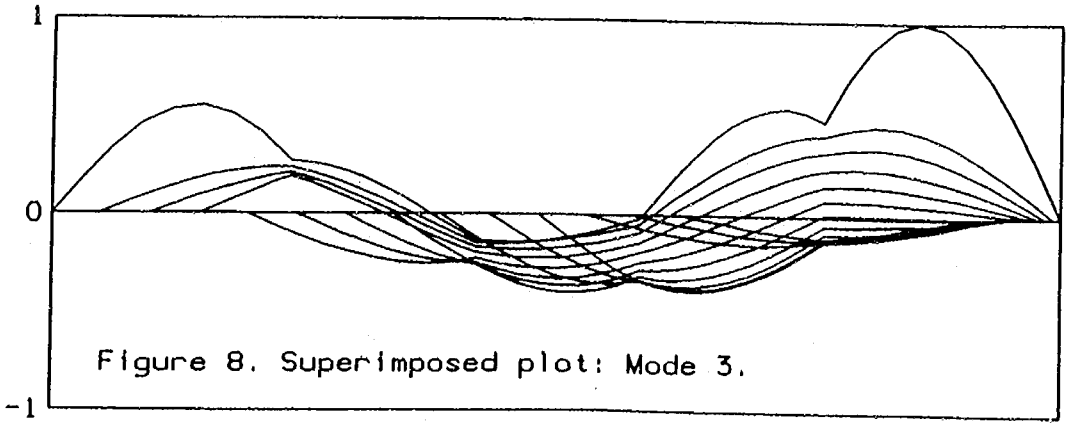


Figure 8. Superimposed plot: Mode 3.

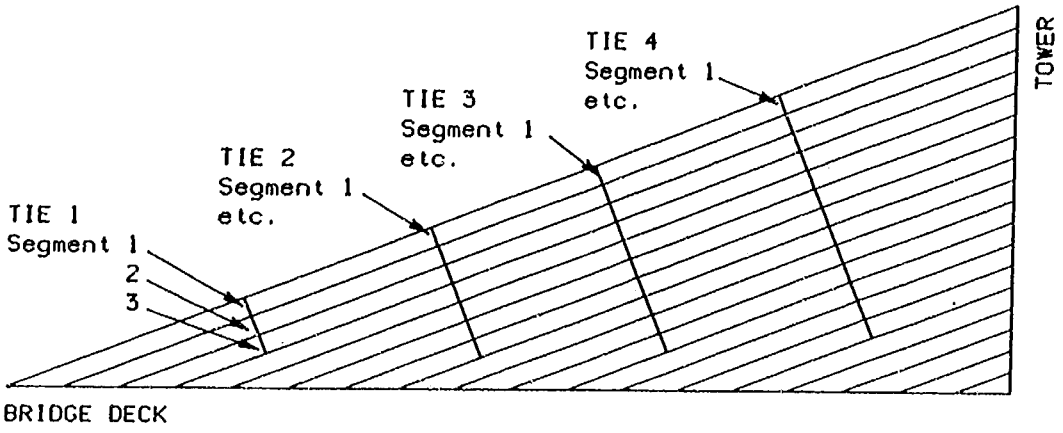


Figure 9. Tie segments

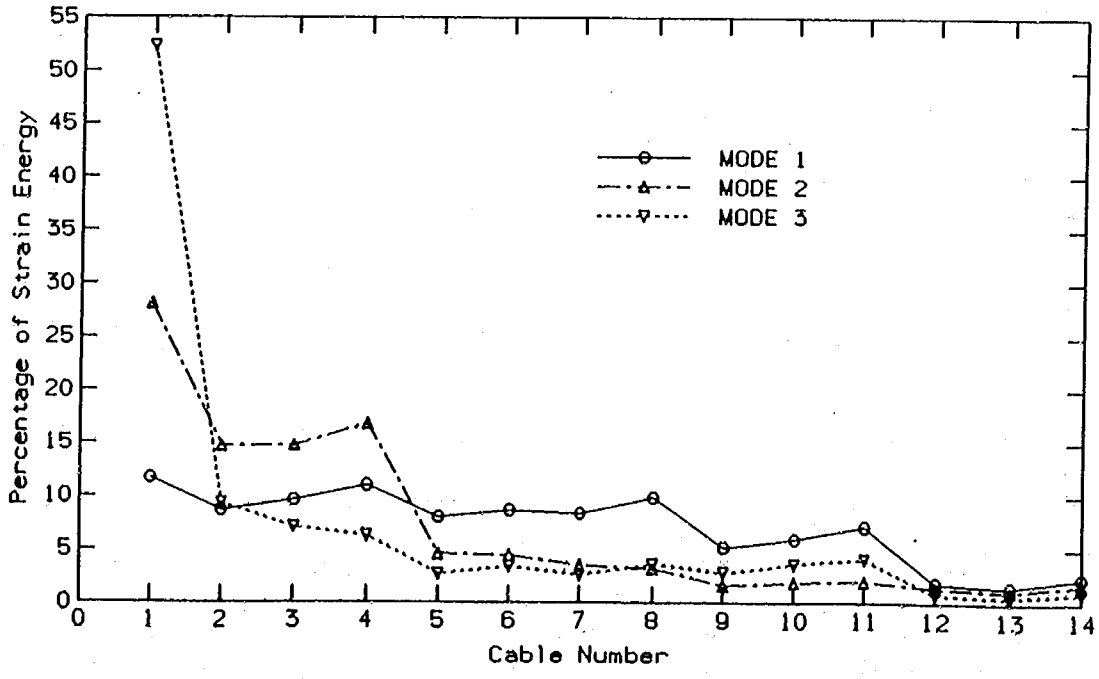


Figure 10. Distribution of Strain Energy

FIELD INSTRUMENTATION OF THE I-295 CABLE STAYED BOX GIRDER BRIDGE

T. T. Baber, F. W. Barton, M. Mohr, and D. Ramsey
The University of Virginia, Charlottesville, VA

SYNOPSIS

The cable stayed I-295 Bridge over the James River near Richmond Virginia is described. The Virginia Transportation Research Council and the University of Virginia have developed and implemented an instrumentation plan to measure static strains in the bridge components and the stay cables during construction and subsequently during service. The University of Virginia, under separate funding, is engaged in the dynamic instrumentation of the bridge during construction. Progress to date, and some preliminary results are reported from these studies.

I. INTRODUCTION AND OVERVIEW

Considerable effort has been expended in developing suitable techniques for the analysis of segmentally prestressed and cable stayed bridges [1]. Field studies have been conducted on several segmentally erected prestressed bridges but none of the studies completed to date in the U. S. have involved cable stayed segmental bridges. Thus, additional evaluation of field behavior is desirable, especially when new design features frames are being used.

Long span bridges, such as cable stayed bridges, are subjected to a variety of dynamic excitations. The most critical dynamic responses are likely to be caused by natural hazards, specifically wind and earthquake loadings. It is essential that the dynamic characteristics of such bridges be determined. Toward this end, full scale dynamic testing is needed for evaluation of actual in-service performance to serve as a benchmark for existing computer models used in design and to provide valuable comparisons with small scale model studies.

A number of earlier studies have addressed the need for reliable data on the dynamic characteristics of long span bridges and several models have been developed to assist in predicting such behavior. Abdel-Ghaffar and coworkers obtained response data for the San Pedro-Terminal Island bridge and more recently conducted ambient vibration studies of the Golden Gate Bridge [2,3]. Accelerometers were used to obtain all dynamic response measurements and subsequent Fourier analysis allowed estimation of natural frequencies and mode shapes. Bampton and others reported on wind and motion data on the Pasco-Kennewick Bridge where anemometers identified potentially dangerous wind speeds and then accelerometers provided response data along the span

[4]. Similar data was obtained on the Sitka bridge in Alaska. A sophisticated instrumentation and analysis package has been installed on the Luling Bridge in Louisiana and has been reported by Bourgeois [5]. All of the previous studies of dynamic response measurements were conducted on bridges where construction was complete.

This paper discusses static, thermal, and dynamic studies currently underway on the I-295 James River Bridge. This work comprises two separate studies, funded by the Federal Highway Administration (FHWA) and the National Science Foundation (NSF). The initial study, funded by FHWA, was undertaken by a joint team of researchers from the University of Virginia (UVa) and the Virginia Transportation Research Council (VTRC). At the request of the FHWA, additional studies were subsequently undertaken with the objective of more closely monitoring the construction process. The FHWA sponsored studies are discussed in section 3. Under NSF funding, the UVa researchers have undertaken dynamic studies of the bridge, to be carried out both before and after the cantilever phase of construction is completed. This study is discussed in section 4 of the paper. The current status of the ongoing investigations is discussed in section 5.

2. DESCRIPTION OF THE BRIDGE

The I-295 bridge over the James River between Chesterfield County and Henrico County, Virginia, shown in Figure 1, is a highly complex structure. The river crossing is the 630 ft. middle span of a seven-span continuous structure consisting of twin precast, segmentally posttensioned concrete box girders. On either end of this structure are a number of approach spans of similar construction, separated by periodic expansion joints.

The middle five spans of the bridge are supported by multiple cable stays arranged in a single plane harp configuration from pylons located at either end of the main span. Cable stay forces will be transferred to the twin box girders through precast delta frame assemblies. A typical cross section of the bridge, illustrating the twin box girders and the delta frame, is shown in Figure 2. The three approach spans on either end of the main span were constructed of 20 ft. segments using the span by span technique. The middle span is being constructed of 10 ft. segments as twin cantilevers. Posttensioning consists of two parts. Temporary bars are placed for tensioning during construction. Permanent strand posttensioning, located inside the boxes is installed subsequently. Closure of the main span cantilever is anticipated sometime in May, 1989. Subsequent to main span closure, continuity posttensioning will be added.

The substructure consists of 8 ft. x 18 ft. precast, segmentally erected posttensioned hollow box piers. The pylons are cast in place up to the deck level, and precast, segmentally

erected above the deck level. Both the piers and the pylons are founded on concrete piles.

3. LONG TERM, CONSTRUCTION, AND THERMAL INSTRUMENTATION

3.1. Objectives

Specific objectives of the combined FHWA study are to evaluate the following aspects of the bridge behavior:

- to determine the live load induced stress range and spectrum in the cable stays
- to evaluate stresses and stress resultants in typical deck segments as a means of predicting load carrying mechanisms
- to evaluate the performance of the delta frame assemblies in distributing cable stay forces to the supported box segments
- to obtain thermal gradient data for the box girder segments, the pylons and the cable stays;
- to collect sufficient strain data during the construction phase to permit an evaluation of such factors as shear lag in the deck segments during and after stay tensioning, and to monitor overall force distributions in the critical elements of the bridge during construction.

3.2. Instrumentation Plan

Instrumentation proposed for this study consists of an extensive array of electrical resistance strain gages and thermocouples to be installed in the main span (span 16) on both the north and south bound lanes. These strain gages have been installed in three deck segments of the main span on the south half of the bridge, in two segments of the south pylon, and on three stay cables associeted with each pylon. In addition to the electrical resistance strain gages, mechanical strain gage locations are being installed on twenty deck segments, four pier segments and both pylons on both the north and south sides of the bridge.

3.3. Stay Cable Instrumentation

A major concern in the long term performance of a cable stayed bridge is the satisfactory fatigue performance of the stay cables. As designed, the stay cable system in the I-295 bridge utilizes between 72 and 90 high-strength steel seven-wire strends per stay. The tendons will be encased in polyethylene pipe and grouted with a portland cement mortar to provide corrosion protection. Since the strains in the stay cables are the quantity of interest, direct instrumentation of the stays

appeared to be the most desirable approach.

It was decided to mount foil resistance strain gages directly on the wires in the strand. Stays S2, S7, and S13 on each side of the bridge were originally selected for instrumentation. To provide for a reliable determination of average strains in the cable, and to show distribution of strains throughout the cable cross section, eight gages were to be placed on each stay cable. All gages were wired independently, in the event that some gages are lost during subsequent tensioning and grouting operations. The original instrumentation plan called for two strain gages to be installed on each of four strands [6]. After the loss of multiple gages as a result of twisting of the strands during tensioning of several stays, it was decided to modify this approach and to use six individual gages with independent dummy gages on six different strands. Lead wires from all of the gages exit through the expansion joint in the polyethylene pipe and from there either to a data acquisition system on the south side, or to switch and balance units and strain indicators to be read manually on the north side. It was subsequently found to be advantageous to install additional strain gages on stays 1 and 5

3.4. Deck Segment Instrumentation

Primary deformation response of the main span and approach span girders of the bridge is expected to include bending within the vertical plane of the bridge and torsional twist of the sections. An additional response of interest is the transfer of stay cable forces through the delta frames to the main deck segments. Electrical resistance strain gages have been installed in three deck segments of the main span on the south cantilever.

Based upon a review of previous work, contact with a number of researchers, and laboratory experiments to verify and evaluate proposed methods, it was decided to mount the foil strain gages on four ft. lengths of reinforcing bar, and to imbed these bars in the instrumented deck segments prior to casting. Up to 35 strain gages have been placed throughout the cross section of the sections to be instrumented. A sketch of these locations is shown in Figure 3. Three bar "rosettes" are placed in the locations indicated by "R".

Using a similar scheme, two of the pylon segments on the south side were instrumented with electrical resistance strain gages. One location was the cast-in-place segment at deck level and the second was a precast segment just below stay approximately 65 feet above deck level.

The strain gaged reinforcing bars in both the deck segments and the pylon segments were placed in the reinforcing cages during the time between cage construction and placement in the

precasting forms. The gaged bars were carefully wired into place against the reinforcing cage and lead wires run along the reinforcing to a block out in the wall of the box which is near the data acquisition system scanners.

Ten deck sections of each cantilever were instrumented with mechanical gages, with two segments at each section. Of these ten sections, six sections were located in the main span cantilever, three sections were located in the first adjacent approach span, and one section was located in the next adjacent approach span. At each segment, five gage points were installed transversely across the deck and three across the lower flange of each box as shown in Figure *. The gage points consisted of a pair of brass plugs, each with a small hole drilled to accept the points of the mechanical gage. The gage points were imbedded in the concrete after casting using nonshrink grout. The gage length on all of the gages was approximately 250 mm, but a Whittemore gage with English units was used on the north side segments, while a Demec gage was used on the south side.

Similar mechanical gage installations were placed on eight pier segments, one each on four piers closest to the main span on either side of the river. These were located at the lowest accessible segment for ease in recording. Two segments in each of the two pylons have also been instrumented with the same mechanical gages, one segment just above the footing and one just above deck level.

3.5. Thermocouple Instrumentation

Thermal data is being obtained from type T thermocouples located in both boxes of a single deck section, from thermocouples in a pylon segment, from thermocouples on a stay cable, and from surface temperature measurements taken when strain readings from the mechanical gages are recorded. The deck segments with the thermocouples are located on the south side and this data will also be automatically recorded using the data acquisition system.

3.6. Data Acquisition and Analysis

The data acquisition system (DAS) was selected to be a unit that would be serviceable in the field, one that would fit the needs of the instrumentation layout and that had good software for data transfer and recording. After considering a number of alternatives, a system manufactured by the John Fluke Company was selected. The system uses a Helios main controller to communicate with a number of individual remote scanning "extender chasses", which can be located near the instrumented sections. The data is transmitted digitally by RS-422 data lines to the main unit. Permanent data storage is accomplished by connecting the control unit to a personal computer. Communication between

the PC and the DAS is accomplished using software supplied by Fluke, and Quick BASIC programs constructed at the VTRC. For environmental control and ease of access, the computer, a Compaq portable, will be located in the offices of the Virginia Department of Transportation in Richmond and will communicate with the DAS by telephone. The computer has been programmed to automatically dial up the DAS and download the data to a diskettee which will be regularly retrieved by VDOT personnel.

The electrical resistance strain gages and the thermocouples on the south side will be automatically recorded using the data acquisition system. All of the mechanical strain data must be recorded manually. This requires an almost continuous presence of research staff on the bridge, especially when significant changes, such as cable tensioning or segment erection, are taking place. The manually recorded data is then placed on a computer spreadsheet file for reduction, analysis and plotting.

One major objective during this investigation has been the appropriate analysis and interpretation of the large amount of data that is being compiled. All data will require some analysis, but proper interpretation of the measured strain responses in the box girder and pylon sections and long term strain variations measured in the stay cables will require especially careful reduction and evaluation.

The longitudinal strains measured by the strain gages in the box sections will allow a reasonably complete estimate of the strain field at these sections. In particular axial compression and bending moments acting in the double box may be estimated from the strain data. The strains recorded from both the electrical resistance and mechanical strain gages should allow the shear lag present in the box sections to be identified. The rosettes located in the webs and flanges of the box sections will provide information regarding the magnitude of shear stresses in the walls of the segments which will allow estimates of torsion in the box to be obtained. Design calculations for the bridge have been made available to the investigators and this information will be used for comparison with the measured field response to verify design assumptions and to provide additional insight and understanding into the behavior of cable stayed bridges.

3.7. Preliminary Results

At this time, much of the construction period data has been obtained from the manually read mechanical gages and the electrical resistance strain gages on stay cables on the north side of the bridge. Analysis is underway, and promises to continue for some time. Some preliminary results of interest are discussed.

As a result of some early difficulties with the instrumentation, the researchers decided to apply strain gages to stay number 5 on the north side of the bridge. The switch and balance unit channels to which these gages were attached were initially zeroed with the stay in the slack state. Four of the gages functioned well during and subsequent to the tensioning operation. Figures 4(a)-(d) illustrate the strain response of the four instrumented strands over a period of roughly three and a half months. Figure 4(a) shows the response during initial tensioning. Two gages responded relatively uniformly, straining to roughly 3000 $\mu\epsilon$ during tensioning. One gage responded very slowly, straining to only slightly more than 1600 $\mu\epsilon$. One gage displayed an unexpected shift, to nearly 2000 $\mu\epsilon$, followed by an initial straining up to over 5000 $\mu\epsilon$. At this point the strain suddenly dropped to around 3600 $\mu\epsilon$. Shortly after tensioning a further drop in tension to around 3000 $\mu\epsilon$ occurred. During this period, the technician recording the data reported hearing considerable noise from the stay cable strands shifting position. Following tensioning, three of the instrumented strands had strains in the range near 3000 $\mu\epsilon$, while the fourth strand had a tensile strain only about half as large.

Initially, this data was viewed with considerable skepticism. It was suspected that some malfunction of the strain gages might have occurred. Subsequent readings suggest that this was not the case, however. Following the initial, very irregular readings, the remainder of the readings obtained from the four gages displayed quite uniform behavior. Figures 4(b)-(d) illustrate this response. In general, a small, sudden increase in the strain occurred when a new segment was hung on the end of the cantilever. A decrease in the strain occurred when a subsequent stay was tensioned. The highly uniform strain changes which were measured during the subsequent three months suggested that the gages are all functioning properly, and led the researchers to re-evaluate the initial data. The initial tensioning operation had been carried out from a fully slack condition using a multi-strand jack pulling all strands at the same time. This fact, together with the prior observance of considerable shifting of strands during tensioning by the researchers suggested that the single pass, multi-strand tensioning procedure may lead to considerable non-uniformity of strain in the individual strands. It is suspected that the strand that displayed the initial high strain may have been pinched and unable to strain uniformly along its length, until at some point during the tensioning, it slipped free. At this point the strain probably dropped to a more representative value. The strand whose strain was low may have been in a bent slack state, and it appears likely that considerable straining of the other strands may have occurred before that strand started to carry its share of the strain. These observations suggest that a simple multi-strand tensioning operation for stay cables may result in considerable nonuniformity of strain in the strands. Since the

fatigue resistance may be adversely influenced by a higher than anticipated strain in individual strands, the potential implications could be significant.

Additional preliminary results are available from the mechanical strain gage measurements recorded on the north cantilever of the bridge. Longitudinal strains were measured before and after major construction and erection activities such as stay tensioning and post-tensioning of the segments and spans. Incremental strains and their pattern of distribution were determined. Symmetry of load distribution was evaluated by comparison of strain data in corresponding segments of the north and south bound lanes. Using an assumed modulus, approximate stress magnitudes were compared with the loading applied to the segments.

Extensive analysis of the data has been undertaken and is reported in further detail elsewhere [7]. Complete interpretation of the plots requires more details of the across the deck posttensioning than can be included here. For comparison, the strain changes recorded in segments N1 and S1 of span 16 during tensioning of stay 9 are shown in Fig. 5(a). Although the magnitudes of the strain increments are larger in S1, the pattern of strain distribution is very similar for both segments. Figure 5(b) depicts strain increments in segments N5 and S5 during tensioning of the same stay. In this case also, the strain increments in the south-bound lane segment are slightly larger but there is still a fairly even distribution and the magnitudes, even though different, are still close to the same level.

4. DYNAMIC STUDIES

4.1 Basic Instrumentation Plan

All dynamic response data is being collected using accelerometers as the transducer and collecting and processing the data through the use of a dynamic data acquisition system. Data analysis will be accomplished through the use of specifically designed software on a main frame computer and a signal analyzer for use both in the field and later in the lab.

The data acquisition system is a Megadac System 2210C which is a portable, high speed data acquisition, signal conditioning and data recording system. The system captures and records dynamic analog data at any continuous rate up to 20,000 samples per second with 16-bit resolution. The 2210C accepts up to 128 channels of differential inputs from a wide variety of transducers which are scanned in any order. For the present study, only 16 channels of accelerometer input will be used. An additional 16 channels of digital input is reserved for ambient wind data, which is being collected from U-V-W anemometers

located on the bridge. The incoming data is filtered, digitized, and stored as digital records on magnetic tape cartridges. The Megadac system provides signal conditioning and filtering, eliminating the need for separate equipment for this purpose. In this study the system will interface directly with an AT-type personal computer although interface through the cartridge reader is also possible. Software provided as part of the overall system can be used to carry out preliminary spectral analysis on the personal computer or a communications interface can be utilized to analyze the data on the University of Virginia CDC Cyber 855 mainframe computer which supports a full complement of signal processing software.

An alternative means of data analysis used in this study is a model CF-350 Ono Sokki signal analyzer with two channel capability. Such analyzers not only have the ability to perform the analyses needed for interpretation of the spectral data, but are also capable of providing filtered, digitized data for additional digital analysis.

The accelerometers used are Model SA-102 servo accelerometers manufactured by Terra Technology. The accelerometers have a frequency response of 0 Hz to 100 Hz. The accelerometers are field rangeable with outputs from 5 VDC/.05 g to 5 VDC/1 g. In preliminary experiments, the most sensitive range has been found to be difficult to use, since a minor tilt of the axis relative to the horizontal (or vertical, depending upon the configuration of the gage) causes the reading to go out of range. In order to facilitate further adjustments of the scale, the accelerometers have been modified by adding a variable resistance pot resistor. This will permit field adjustment of range, as necessary.

U-V-W vane anemometers will be used to provide wind data during the ambient vibration studies. These anemometers will be mounted near the bridge deck to provide a measure of the near wind field.

Mode shapes will be determined by comparison of transducer response with a reference transducer placed at a location of maximum response. Preliminary analytical studies on a finite element model of the bridge and its components will be used to identify the location of node locations in the first several modes to insure that the reference measurements avoid these locations. This data will be sufficient to provide basic information on frequencies and mode shapes. Along the deck, accelerometers will also be placed at locations along the span to provide similar data for modal analysis. In the case of the deck instrumentation, particular care will be given to locating the reference station and at other locations accelerometers will be placed at transverse locations to identify torsional response.

Prior to closure of the main cantilever span, instrumentation will be placed along the cantilever portion to clearly identify the response characteristics of this part of the structure. Results from the analytical studies indicate that the natural frequencies for this unsupported part of the structure will be somewhat lower than those for the span after closure as would be expected.

4.2. Methods of Excitation

Most of the dynamic data will be obtained using ambient excitation of wind or, after bridge completion, vehicular traffic. This form of excitation should be sufficient to provide information on modes and frequencies as well as som indication of damping. More specific dynamic characteristics, however, can be measured from excitations that are either harmonic or from an impulsive type load, and these types of excitations are more difficult to apply, especially when funding is limited.

A number of schemes for providing forced input to the bridge are being considered. One of the most obvious techniques would be to use a counter-rotating mass shaker to provide harmonic forcing to various bridge components. However attractive this would appear, however, the size and weight of these types of shakers make their use impractical since they would have to be placed in locations where cranes would have to be used for lifting and where attachment would, in any case, be extremely difficult. These limitations are primarily of concern in the dynamic analysis of components where access is difficult at best. After completion of the bridge, it is fully expected that some form of harmonic exciter will be used for subsequent data collection.

Several other schemes are also under consideration for forcing the bridge. Preliminary studies have been executed using impulse loadings generated by the instrumentation van driving over one or a sequence of 4"x4" timbers. Alternately, the bridge has been excited by simply driving the van onto the bridge, with no attempt to generate additional impact loading. Braking the van repeatedly during driving passes has also been attempted. All of these methods appear to excite the bridge, however, the dominant frequencies excited are not the ones of greatest interest. The transient dieout period after such an excitation pass does appear to have the most important frequencies dominant. Alternatively, the researchers are presently investigating the feasibility of obtaining a heavy duty electrohydraulic shaker with electronic control. Such shakers are capable of developing harmonic forcing functions on the order of several thousand pounds at the relatively low frequencies of interest.

4.3. Data Analysis

Data collected during this investigation will include the simultaneous measurement of vertical, lateral and longitudinal response of the cable-supported deck as well as the lateral and longitudinal motions of the pylon. In addition, simultaneous wind data will also be measured and recorded from the anemometers.

The initial analysis of data will consist purely of extracting natural frequencies and mode shapes. The frequency information will be automatically provided through the spectrum analysis performed by either the personal computer or by the signal analyzer. Additional frequency response analyses are being contemplated using the CDC or IBM main frames, and customized FFT analysis packages available on those systems. Mode shapes will require somewhat more care in determining. Amplitudes provided in the frequency plot, which are a measure of the strength of a particular mode, will be compared with data measured at a fixed reference station and these relative amplitudes will define the mode shape at that frequency. Care must be taken in the location of transducers, and especially the location of the reference transducers, to ensure that good modal identification is achieved.

Since this investigation has available only sixteen transducers, it is necessary to take successive readings at the different locations on the bridge, leaving only the reference station transducers in a fixed location. Also, the anemometer data requires three channels for each station and this will reduce the simultaneous accelerometer channels accordingly.

The transducer excitation is provided by the data acquisition system and the response measured and recorded on the tape cartridge unit which has a capacity of 64 Mb of memory. This data will, in turn, be read in to the hard disk unit of the PC where preliminary analysis functions will be performed using the OPUS software provided by Optim, the manufacturers of the Megadac unit. Alternatively, the data from the hard disk, in digitized form, may be reconverted to an analog signal and fed directly into the signal analyzer for direct processing. Output from either the software analysis or from the signal analyzer can be easily presented in either printed format or used as input to a plotter for easier representation.

4.4. Preliminary results

Figure 6 illustrates some preliminary time and frequency data obtained using a single driveby of the instrumentation van. It is clearly seen from the spectral analysis that the dominant frequency is around 15 Hz, well above the anticipated natural frequencies of the structure. These natural frequencies appear

to be higher order modes, related perhaps to the oscillation of the deck between the cable stays. The low level ambient vibration recorded to the left of the time pulse appears to be dominated by a much lower frequency motion, although the amplitude on the plot does not allow for a very accurate analysis. Wind conditions on the day that the data was gathered were unusually calm on the bridge, so it is likely that more representative ambient vibration data will be obtained.

5. STATUS OF THE INVESTIGATION

At the time this paper is written, all of the electronic strain gages, all of the thermocouples, and all of the mechanical strain gage points have been installed on the bridge. The distributed data acquisition system has been installed, and is providing data. All strain gages except those in the final two box segments have been connected to the system. The thermocouples are presently being added. Manual data collection is complete for the pre-closure stage on the north cantilever, and well underway on the south cantilever. Procedures have been established for the recording and reduction of the manually obtained data. Much of the north cantilever data has been recorded.

The data acquisition system, accelerometers, and anemometers have been acquired and tested for the dynamic studies. Some data has been obtained. The accelerometers have been modified by addition of adjustable resistor pots to permit convenient field ranging. The data reduction software has been installed and tested on the PC. An analog communication channel has been established from the Megadac 2210c to the Ono Sokki FFT analyzer. Available software on the UVa mainframes has been surveyed, and suitable software for auxilliary analysis have been identified. Modal analysis hardware/software on an existing Hewlett Packard Structural Dynamics Analyzer has been evaluated.

ACKNOWLEDGEMENTS

The long term studies reported herein are sponsored by the Federal Highway Administration under HPR Study 2468. The ambient and forced vibration studies reported are sponsored by the National Science Foundation under grant no. CES-8715463. All support for this work is gratefully acknowledged. The views expressed in this paper are those of the authors and do not necessarily reflect the views of the National Science Foundation or the Federal Highway Administration.

REFERENCES

1. Marshall, V. and Gamble, W. L., "Time Dependent Deformations in Segmental Prestressed Concrete Bridges," SRS 495 University of Illinois, Urbana, IL, October, 1981.

2. Abdel-Ghaffar, A. M., "Dynamic Analyses of Suspension Bridge Structures," Rept. No. EERL 76-01, Earthquake Engineering Research Laboratory, California Institute of Technology, Pasadena, CA, 1976.

3. Abdel-Ghaffar, A. M., and Scanlan, R. H., "Ambient Vibration Studies of the Golden Gate Bridge," Journal of Engineering Mechanics, ASCE, Vol. 111, No. 4, pp. 463-482, April, 1985.

4. Bampton, M. C. C., et. al., "Pasco Kennewick Cable Stayed Bridge Wind and Motion Data," FHWA Rept. Battelle Pacific Northwest Labs, Richland WA., 1983.

5. Bourgeois, B. S., et. al., "Wind Instrumentation of the Luling Bridge," Project Report No. 79-1ST, Tulane University, New Orleans, LA., 1982.

6. Baber, T. T., Hilton, M. H., McKeel, W. T., and Barton, F. W., "Field Monitoring on the I-295 Bridge over the James River, Instrumentation Installation and Construction Period Studies," Interim Report, VTRC, April, 1988.

7. Barton, F. W., Baber, T. T., Ramsey, R. D. and McKeel, W. T. Jr., "Field Measurements of Strains in the Deck Segments of a Cable Stayed Box Girder Bridge During Construction," Proceedings, 1989 Annual Conference of the Canadian Society of Civil Engineers (CSCE), St Johns, Newfoundland, June, 1989.

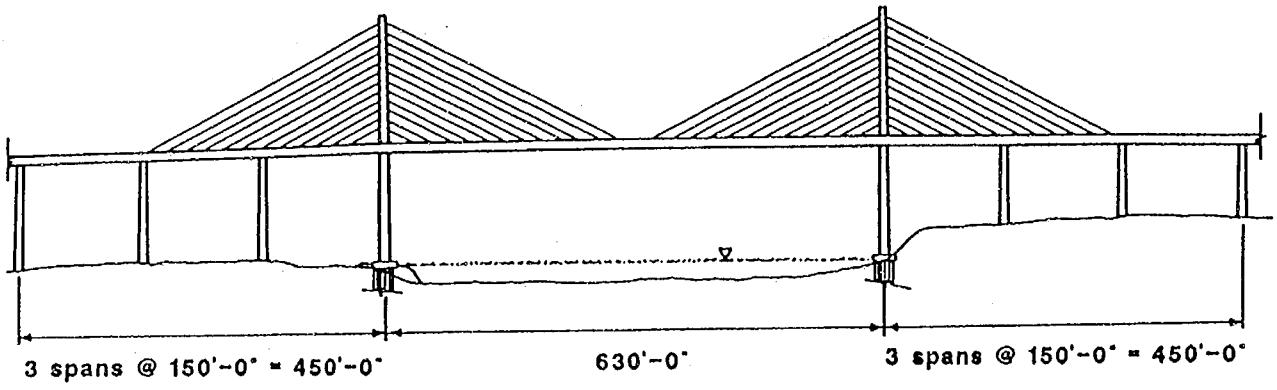


Figure 1. The I-295 James River Bridge

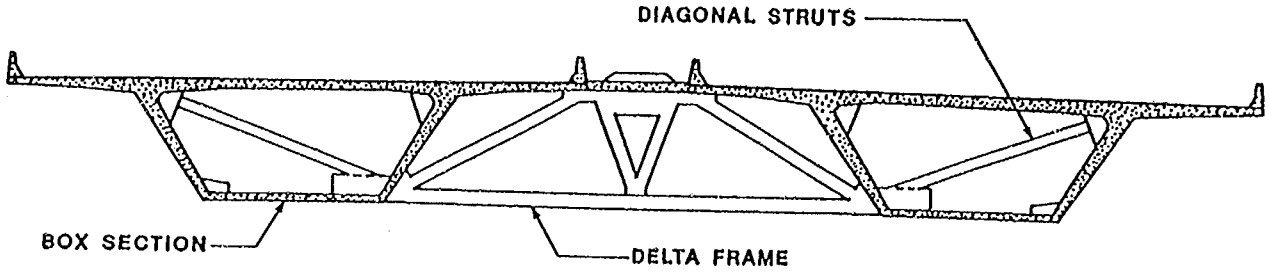
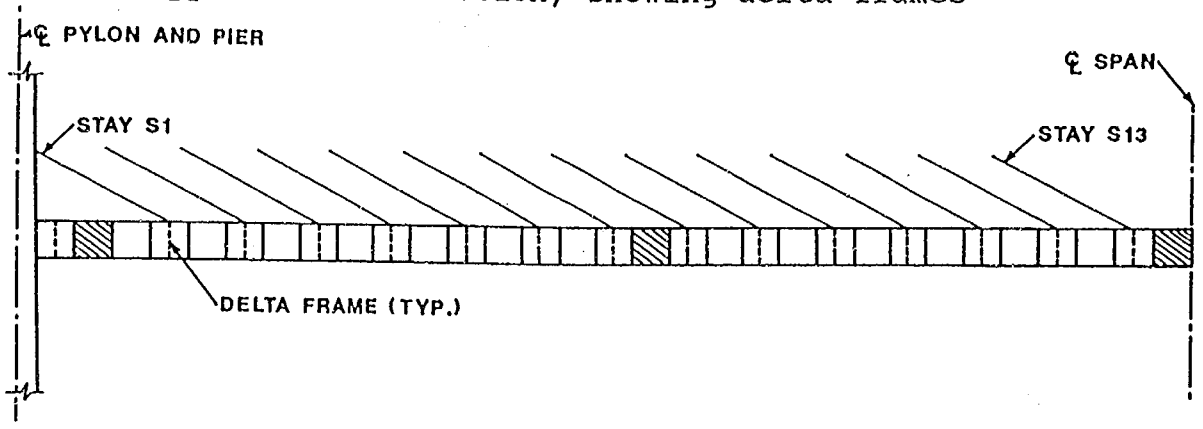
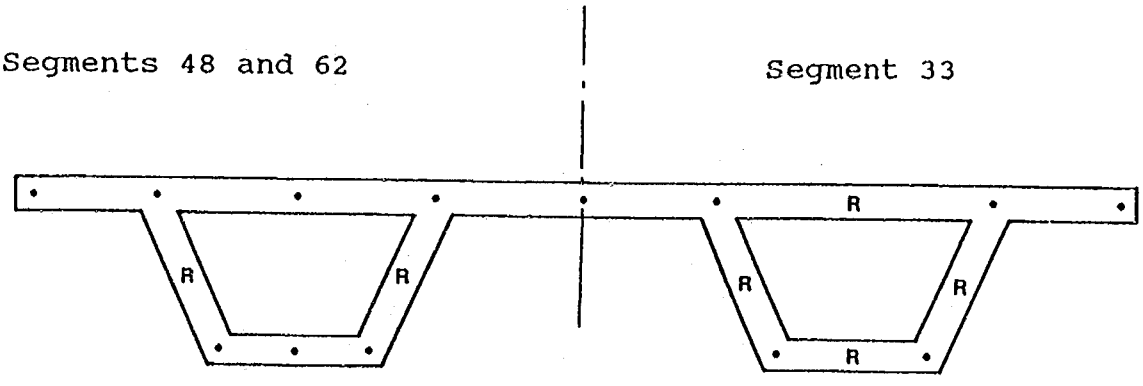


Figure 2. Typical Cross section, showing delta frames

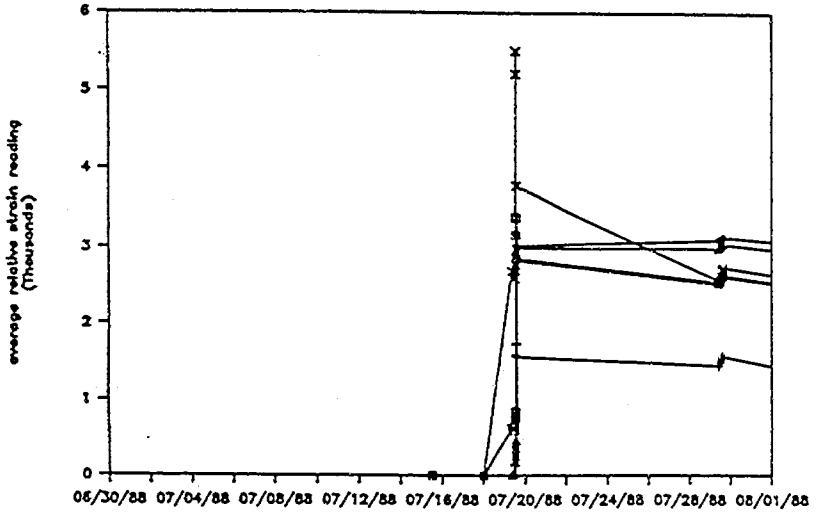


(a) Locations of instrumented box sections

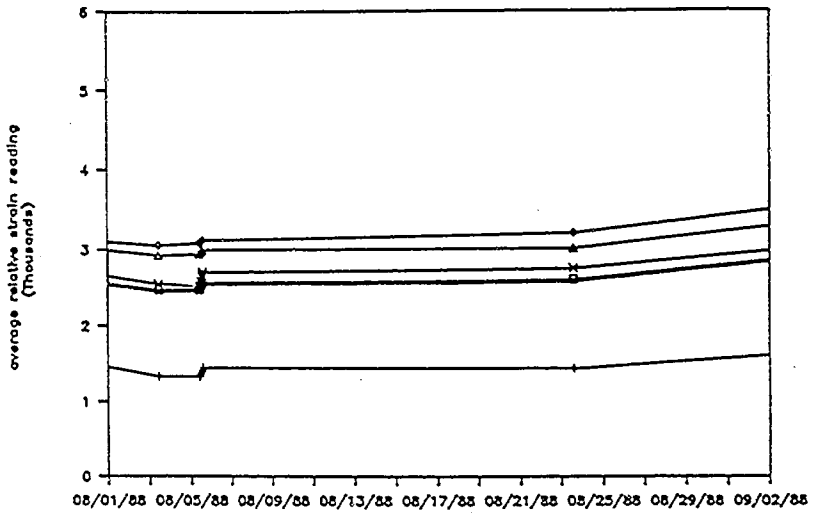


(b) Locations of gages in box sections

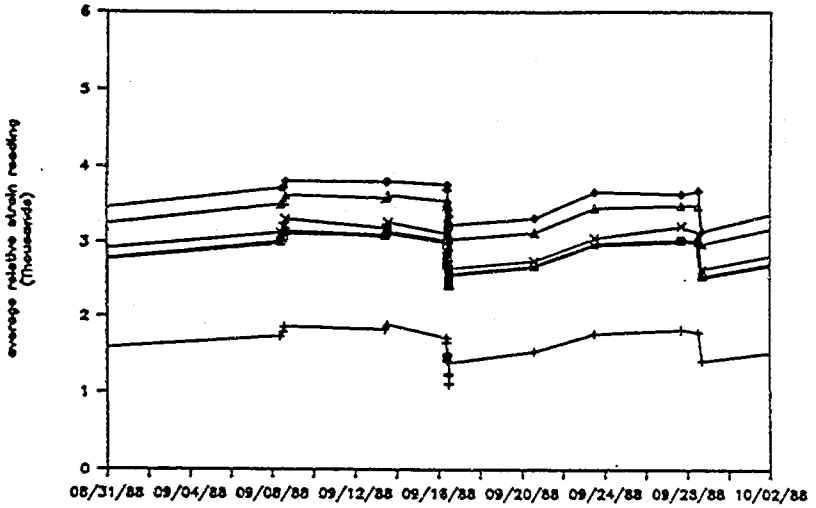
Figure 3. Locations of Strain Gaged Reinforcement in Box Sections



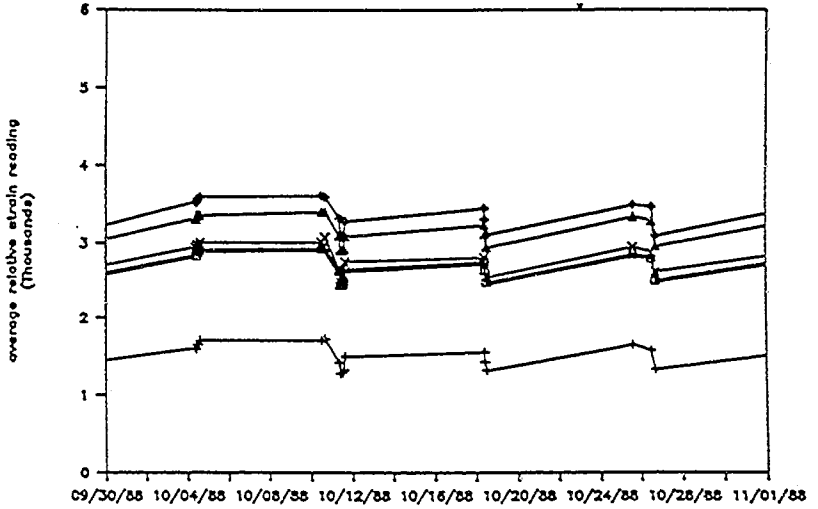
(a) July, 1988



(b) August, 1988



(c) September, 1988



(d) October, 1988

Figure 4. Strain data from Stay Cable 5

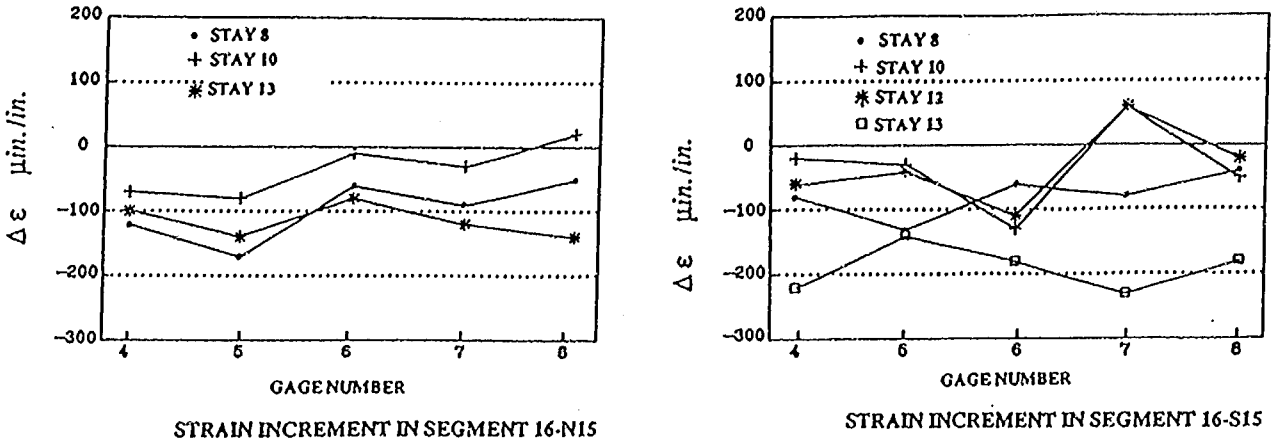


Figure 5. Representative Incremental Strain Data During Construction

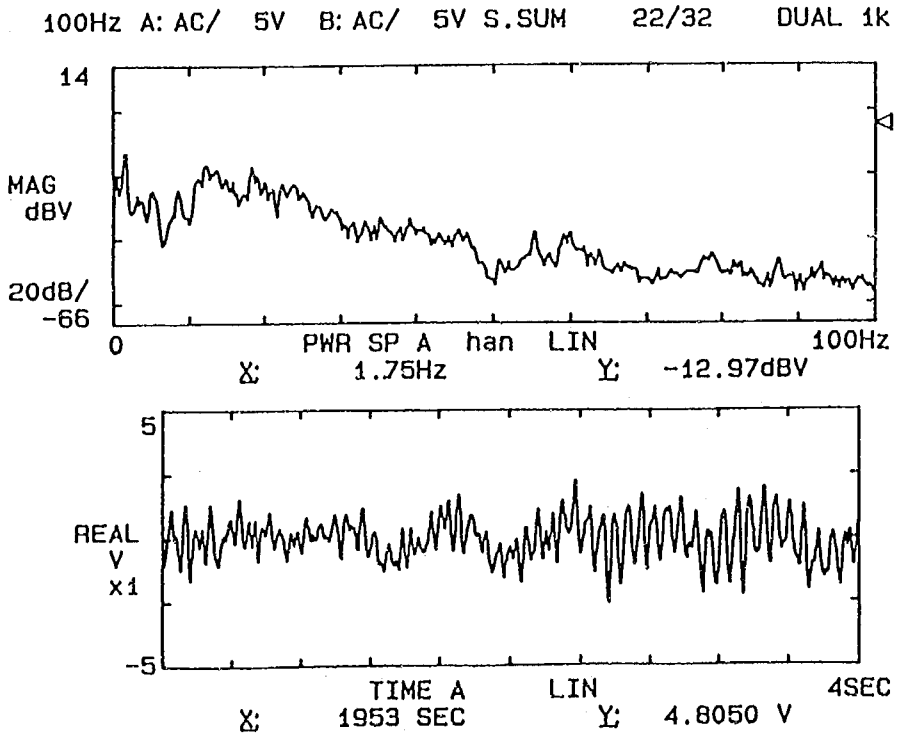


Figure 6. Some Preliminary Dynamic Data with Higher Mode Dominance

(5) Session 5

SESSION 5: WIND RESISTANT DESIGN(2) 3:35pm~5:10pm

(Co-Chairman: K. Yokoyama, R. H. Scanlan)

(11) M. Tatsumi, K. Hata※ and M. Takeuchi: Wind Resistant Design of Akashi Kaikyo Bridge
(3:35pm~3:55pm)

(12) H. Bosch※ : Structural Modification for Enhanced Aerodynamic Behavior of of a Suspension Bridge
(3:55pm~4:15pm)

(13) H. Kosaka※ , H. Hanno and Y. Fujino: Wind Tunnel Test on Tokyo Port Bridge
(4:15pm~4:35pm)

(14) S. Motoyama, M. Hoshino, N. Takahashi※ and T. Maruyama: Aerodynamic Stability of Three Parallely Located Box-Girder Bridges
(4:35pm~4:55pm)

DISCUSSION(5)
(4:55pm~5:10pm)



WIND RESISTANT DESIGN FOR THE AKASHI KAIKYO BRIDGE

by

Masaaki TATSUMI,[1] Kensaku HATA[1] and Masahiko TAKEUCHI [1]

ABSTRACT

The Akashi Kaikyo Bridge, whose main span is about 2km, has extremery flexible features, and the wind resistant design for this bridge becomes much more important than for the existing long bridges. The main part of the superstructure of this bridge is determined to cope with the strong wind. For these reasons, great amount of research was carried out on wind ploblems of this bridge for many years.

Recently, these studies were summed up and the draft of "Wind Resistant Design Code for the Akashi Kaikyo Bridge was established. Here, the general idea of the code is reported.

INTRODUCTION

The Akashi Kaikyo Bridge is a suspension bridge with a center span of 1990m and total length of 3910m.

Because this bridge has a extremely long span, it is low in rigidity and easy to deform, and main part of the superstructure of this bridge is determined to cope the storong wind. So, the wind resistant design for this bridge becomes much more important than for other existing bridges. Furthermore, there are many problems due to the extremely long span of this bridge.

For these reasons, great amount of research was carried out on wind problems of this bridge for many years.

For the wind resistant design for the Honshu-Shikoku Bridges, "Wind Resistant Design Criteria(1976)"[1] was established in 1976.

But, for the Akashi Kaikyo Bridge, because of the importance of wind resistant design, the studies for the wind resistant design were summed up and "Wind Resistant Design Code for the Akashi Kaikyo Bridge"[2] was established recently.

This paper describes the outline of this design code.

---

[1] First Design Division, Design Department, Honshu-Shikoku Bridge Authority
5-1-5 Toranomon, Minato-ku, Tokyo 105 JAPAN

1. PROCEDURE OF WIND RESISTANT DESIGN

The "Wind Resistant Design Criteria for the Honshu-Shikoku Bridges" classify the critical conditions of the bridge due to wind actions as shown in Fig-2 in consideration of the convenience of the design.

The procedure of wind resistant design for the Akashi Kaikyo Bridge is almost same as that for the other Honshu-Shikoku Bridges. In the first stage, the drag component of aerodynamic force that affects the determination of the sectional dimension of structural members is replaced with static load, taking into account the gust response in the direction of the drag (horizontal and perpendicular to the bridge axis in the case of stiffening girder). This static load is assumed as the design wind load, and the stress calculations are performed against this design load to decide the section of members (hereinafter referred to as "static design"). Subsequently, in the second stage, the buckling of the structure and the harmful vibrations are checked for the obtained structure by the use of dynamic analysis, wind tunnel test and so on (hereinafter referred to as "checking").

For the Akashi Kaikyo Bridge, the followings are different from the "Wind Resistant Design Criteria".

1) Not only horizontal deflection components, but also vertical and torsion components of gust responce were taken into account, thereby enabling a more strict wind resistant design.

2) For the wind tunnel test, not only smooth wind but turbulent wind can be used. Also, the full-scale aerodynamic model can be used if necessary.

3) The wind characteristics were determined according to the mesurement at bridge site.

The procedure of wind resistant design is shown in Fig-3.

2. WIND CHARACTERISTICS

2.1 Basic Wind Speed

The basic wind speed (mean wind speed during 10 minutes at 10m above the surface of the sea) is the basic of wind resistant design. This was determined from the measurement record of wind speed at observation tower near the bridge site considering the life span of the bridge.

The measurement of wind speed has been conducted for more than 20 years at the observation tower. Using these records, which have been recorded at 80m above the ground, the wind recurrent expectation over 150 years at 80m above the ground was estimated. Then, considering the correction for elevation, and the difference between the wind at bridge site and at the observation tower, the basic wind speed was determined as 46m/s. To estimate the difference between bridge site and observation point, a topographic model test in wind tunnel was conducted.

To determine the basic wind speed, some previous researches for the wind at bridge site such as typhoon simulation were also considered.

2.2 Design Wind Speed

Because the basic wind speed is the mean wind speed during 10 minutes at 10m above the surface of the sea, corrections considering the elevation and wind turbulence should be made.

For the Akashi Kaikyo Bridge, the design wind speed was determined by making a correction to the basic wind speed taking into account the elevation of the structure.

Correction for the elevation of the structure is made based on the idea that distribution of wind speed in the direction of elevation follows the rule of power, and the power index is 1/8.

The power index was determined from the record of wind near the bridge site. Also, the power index provided in the wind resistant design code in other countries are considered.

The design wind speed is given by the following equation.

$$U_z = \mu_1 U_{10} \quad \cdots\cdots\cdots\cdots\cdots\cdots\cdots\cdots\cdots\cdots\cdots\cdots\cdots\cdots (1)$$

where; U_z :Design wind speed,
U_{10} :Basic wind speed,
μ_1 :Correction factor for elevation $\mu_1 = (\frac{z}{10})^{1/8}$
and z :Elevation of the structure.

2.3 Wind Turbulence Characteristics

For the wind resistant design for the Akashi Kaikyo Bridge, the checking for the gust response should be made, and turbulent flow can be used for the wind tunnel tests. So, the wind turbulence characteristics were determined.

The power spectrum S(n) of wind speed was determined considering the shape and peak value of the measured record of wind.

The equation (2) and (3) are the equation of the power spectrum for horizontal and vertical wind speed respectively.

$$\frac{nSu(n)}{\overline{u}^2} = 0.475 \frac{n}{n'} \left\{ 1 + \left(\frac{n}{n'} \right)^2 \right\}^{-5/6} \quad \cdots\cdots\cdots\cdots\cdots (2)$$

$$\frac{nSw(n)}{\overline{w}^2} = \frac{2.11 \times f}{1 + 11.2 \times f^{5/3}} \quad \cdots\cdots\cdots\cdots\cdots\cdots (3)$$

where; u :horizontal component of wind turbulence,
v :vertical component of wind turbulence,
n :frequency,
n' :$= 0.632 \times Z^{-0.75}$
and f :$=nz/U_z$

The intensity of the wind turbulence was determined as 10% for the horizontal component at the elevation of stiffening girder, and the intensity for the vertical component is determined as half of that for horizontal component considering the records of wind and previous researches.

2.4 Angle of attack

Self-excited vibration and Vortex-induced vibration of the structure are affected by the angle of attack of the wind, and it should be determined considering the turburance characteristics of natural wind and responce of the structure. But it

is difficult to consider the responce of the structure. For the design of the Akashi Kaikyo Bridge, the angle of attack of -3° to 3° is determined to be considered according to the previous research.

3. STATIC DESIGN

3.1 Design wind load

In the calculation of the design wind load, dynamic responce of the bridge due to the turbulence of wind, known as the gust response, should be taken into account.

The gust responce varies according to the scale and dynamic behavior of the bridge.

In the "Wind Resistant Design Criteria(1976)", to consider the gust responce, the scale of the bridge was considered as the correction factor for the design wind speed, and the dynamic behavior was considered as that for the design wind load. But, this procedure sometimes causes confusion and the scale and dynamic behavior are to be considered as one correction factor.

So, for the design for the Akashi Kaikyo Bridge, the scale and dynamic behavior of the bridge is considered using one correction factor for the wind load. The design wind load is calculated using the following equations.

Wind load acting on cables and stiffening girder:

$$P_D = \mu_2 \frac{\rho U_z^2}{2} C_D A_n \quad \cdots\cdots\cdots\cdots\cdots\cdots\cdots\cdots (4)$$

Wind load acting on tower:

$$P_D = \mu_3 \frac{\rho U_z^2}{2} C_D A_n$$

where; μ_2 μ_3 :Correction facter
ρ :Air density(=0.12),
U_z :Design wind speed,
C_D :Drag coefficient,
and A_n :projection area of the structure,

The correction factor is shown in Table-1. This factor is obtained by the gust response analysis considering the turbulence of natural wind and the scale and dynamic behavior of the structure. For example, the result of the gust response analysis for the truss type stiffening girder is shown in Fig-4. Using the gust responce factor where maximum member force acts, the correction facter for the stiffening truss(1.55) is determined. The correction factor for the box type stiffening girder and for the tower is determined using the same procedure.

The design wind speed is determined according to 2.1

The drag coefficients are shown in Table-2. The coefficient for the stiffening truss should be determined by the result of wind tunnel test, because the coefficient differes considerably depending upon the dimensions of the bridge members. For the design of the tower, the drag coefficient is same as that is provided in "Wind Resistant Design Criteria(1976)", but it is recommended to check using the wind tunnel test. The drag coefficient for the cable is same as that provided in "Wind Resistant Design Criteria(1976)".

3.2 Loading of the wind load

Once the design wind load is determined, it is loaded as a uniform load to the structure, and the sectional member force and resulting deformation can be obtained from general structural analysis.

For the design of the members such as expansion joint, the displacement of the structure controls the design, and not only the longitudinal component but transverse component of the wind should be considered.

3.3 Combination with other load

As the combination with the other load, only the combination with dead load and the effect of temperature should be considered. For the design of other Honshu-Shikoku Bridges, only this combination decided the members when considering the wind load, so only this combination should be considered.

4. CHECKING

4.1 Checking for unstable phenomena

The unstable phenomena of the structure such as lateral buckling caused by the wind load should be checked. The minimum wind speed which causes lateral buckling should be greater than 1.7 times as the design wind speed.

4.2 Damping of the structure

The damping of the structure is determined as the structural decrement. The structural decrement (the logarithmic decrement of vibration when the wind speed is zero) is shown in Table-3. These values are determined considering the result of actual bridge vibration test conducted on the four completed Honshu-Shikoku Bridges. Also the provision of "Wind Resistant Design Criteria(1976)" is considered.

4.3 Checking for the gust response

The suspension bridge is deformed not only horizontally but vertically and torsionally when the wind acts on it. Also, the vertical and torsional gust response due to lift and moment will occur. But, the stress caused by vertical and torsional gust response is generally small compared with that by horizontal force.

So, only horizontal component of wind load including gust response is considered for the static design for the suspension bridge according to this idea.

For the Akashi Kaikyo Bridge, the static design can be conducted according to this procedure, but the stress caused by vertical and torsional gust response cannot be neglected, especially for the box type stiffening girder.

So, after decided the dimension of the sections by the static design, the influence of horizontal, vertical, and torsional gust response should be checked by gust response analysis.

The stresses caused by these three components should superimposed, and if that stress exceeds 5% more than allowable stress the section should be redesigned.

4.4 Checking for Self-excited Vibration.

Because there is no possibility that galloping will occur at the stiffening girder of the Akashi Kaikyo Bridge, only the possibility of torsional flutter and bending-torsional flutter should be checked when considering self-excited vibration due to the negative damping effect of aerodynamic force.

Self-excite vibration threatens the bridge with a collapse in a short time, certainly a serious matter requiring attention.

The phenomena is difficult to grasp theoretically in the case of bridge girders, particularly those with a complicated sectional feature such as truss type stiffening girders. For this reason, it is provided that self-excied vibration should be checked using wind tunnel tests.

The self-excited vibration should not occur by the wind whose speed is less than the checking wind speed U_F. This checking wind speed is given by the following equation.

$$U_F \geqq 1.2 \times \mu_F \times U_z$$

where; U_F :Checking wind speed,
U_z :Design wind speed,
and μ_F :correction factor for wind turbulence

In this equation, 1.2 is a safety factor for the error of the wind tunnel test and importance of the structure and so on.

4.5 Checking for Forced Vibrations

The forced vibration is the vibration with a limited amplitude or that cause by the wind with limited range of velocity. For the design of the bridge, Vortex-induced vibration and gust response caused by the wind whose speed is less than the design wind speed should be considered.

The vortex-induced vibration is estimated using the wind tunnel test, and gust response is estimated by the gust response analysis.

The fatigue strength of the member and the serviceability of the structure should be checked against the forced vibration caused by the wind.

CONCLUSION

The outline of wind resistant design for the Akashi Kaikyo Bridge is described briefly.

To establish the "Wind Resistant Design Code for the Akashi Kaikyo Bridge", the investigations and studies were carried out under the guidance of the Wind Resistant Research Subcommitee of Japan Society of Civil Engineers.

The authors much appriciate the members of this subcommitee.

References

1) Wind Resistant Design Criteria for Honshu-Shikoku Bridges (in Japanese), Honshu-Shikoku Bridge Authority, Mar.1976.
The outline of this criteria was reported in "Civil Engineering in JAPAN, 1988", Japan Society of Civil Engineering, Dec.1988.

2) Report for the Wind Resistant Research Subcommitee (in Japanese), Japan Society of Civil Engineers, Mar.1988.

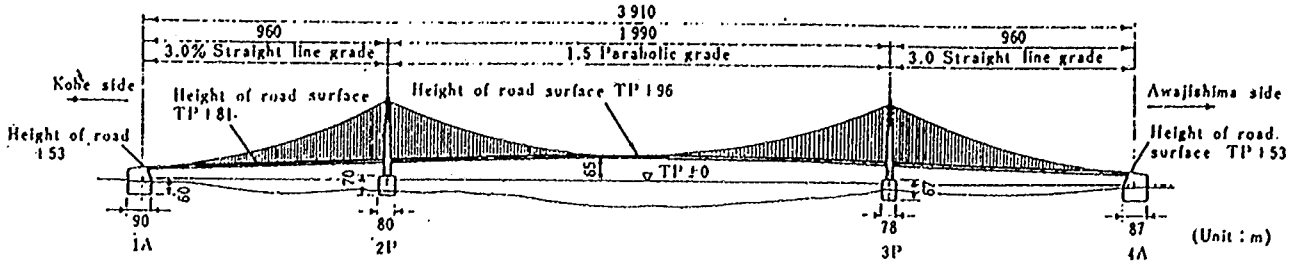


Fig-1 General Plan of Akashi Kaikyo Bridge.

Static behaviors { Deformation and stress due to static wind face
Unstable Phenomena { Lateral buckling
Divergence

Dynamic behaviors { Forced vibration { Irregular vibration due to wind turbulence (gust response)
Vortex-induced vibration
Self-excited vibration due to negative damping effect of aerodynamic force
(Torsional flutter, bending-torsional flutter, galloping)

Fig-2 Response of Bridge Members Against Wind.

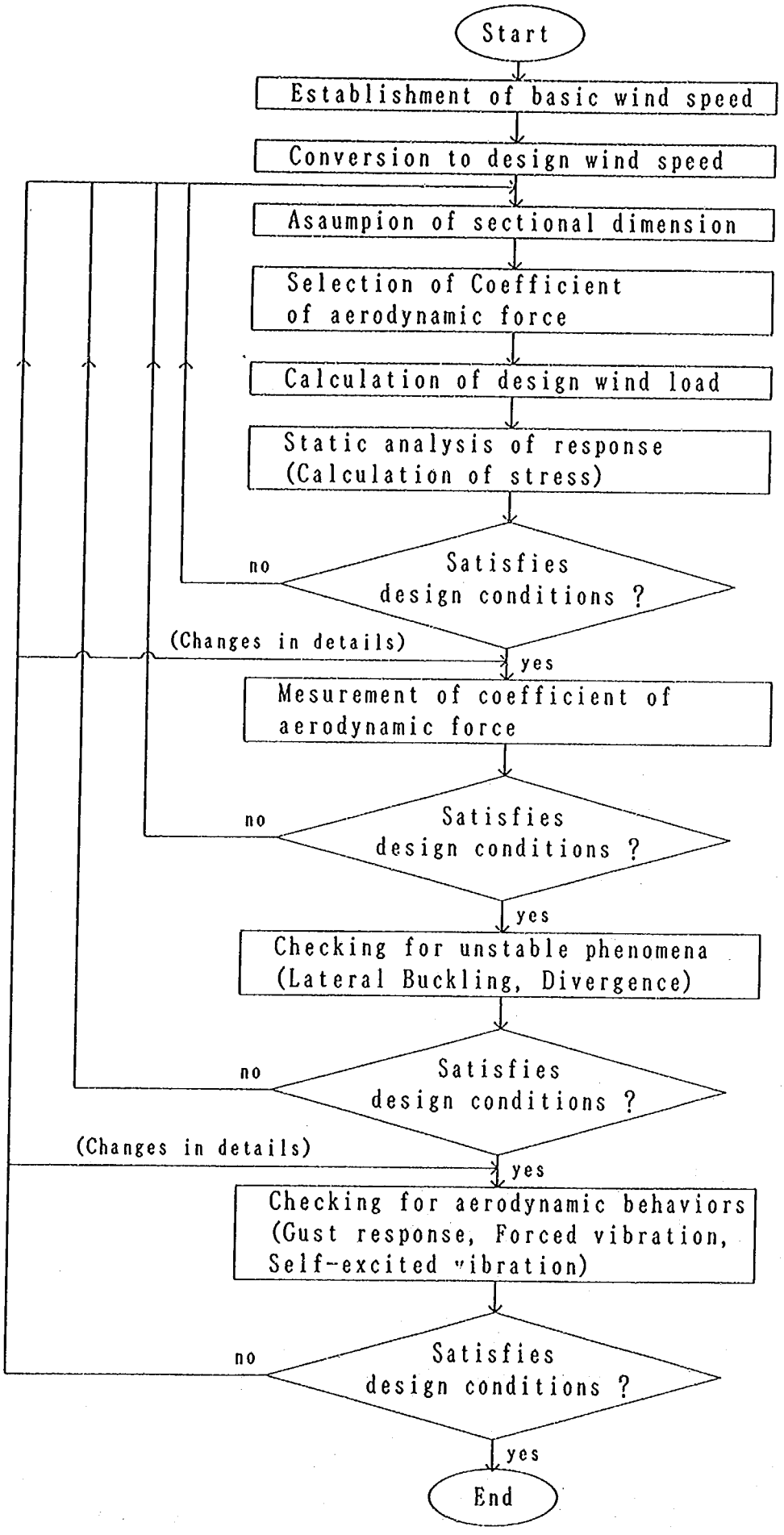


Fig-3 Flow Chart of Wind Resistant Design.

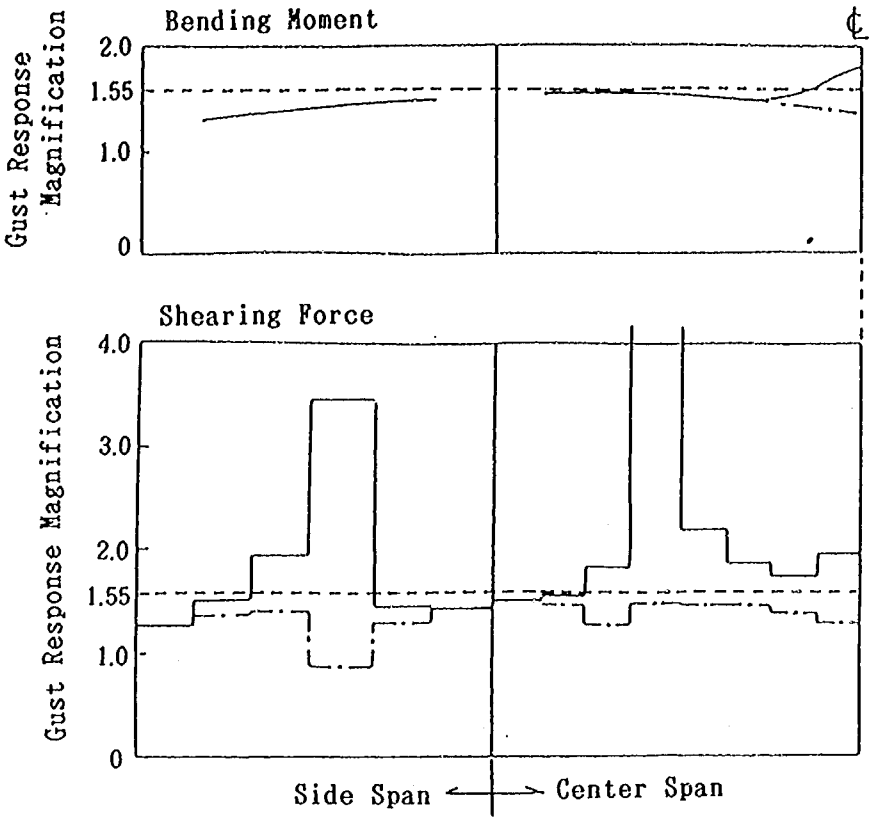


Fig-4 Gust response for truss type stiffening girder.

Design Object / Direction of Force / Structural member	Correction Factor	Stiffening Girder			Tower		
		Transverse		Longitudinal	Transverse		Longitudinal
		Truss type Stiffening Girder	Box type Stiffening Girder		Truss type Stiffening Girder	Box type Stiffening Girder	
Cable	μ_2	1.55	1.70	—	1.35	1.40	—
Hanger Rope	μ_2	1.55	1.70	1.25	1.35	1.40	1.25
Stiffening Girder	μ_2	1.55	1.70	1.25	1.35	1.40	1.25
Tower	μ_3	———		—	1.55		After complition of Bridge 1.50
							During Construction 1.75

Table-1 Correction Factor μ_2, μ_3

Structural Member		Transeverse Direction	Longitudinal Direction
Stiffening Girder	Truss type	Use the result of wind tunnel test	60% of the drag coefficient for transeverse direction
	Boy type	Same as above	30%
Tower		1.8	1.8
Cable	Single	0.7	Not Considered
	Double	1.0	
Hanger Rope		0.7	$0.7 / \sqrt{2}$

Table-2 Drag coefficient

	Bending vibration	Torsional vibration
Truss type Stiffening Girder	0.03	0.02
Box type Stiffening Girder	0.02	0.02
Tower after Completion of Bridge	0.02	
Tower during Construction	0.01	

Table-3 Dumping of Structure (Logarithmic Decrement)

STRUCTURAL MODIFICATIONS FOR ENHANCED AERODYNAMIC BEHAVIOR OF A SUSPENSION BRIDGE

Harold R. Bosch[1]

ABSTRACT

Flexible bridges and other structures can be sensitive to the turbulent forces of wind. To provide adequate resistance to these forces, it is often necessary to increase the stiffness of the main structural elements or to refine the structural shape into a more effective aerodynamic form. This paper will describe some of the techniques which have been employed to enhance the aerodynamic behavior of suspension bridges. The application of these methods to a specific suspension bridge will be presented.

KEYWORDS: Bridge; shape; stability; stiffness; suspension; wind.

1. INTRODUCTION

History has shown that the greatest danger to long-span bridges lies in their vulnerability to aerodynamic forces. Since the Tacoma Bridge disaster in 1940, designers of suspension bridges have been keenly aware of the need for considering the aerodynamic stability of their structures. The principal approaches for securing or improving aerodynamic stability have been to increase the rigidity of the structure, to increase the damping in the structure, or to modify the shape of the structure.

Almost any method of increasing rigidity is also generally effective in augmenting the structural damping. Increases in rigidity and damping to resist vertical and torsional instabilities can be accomplished through use of deeper stiffening girders or trusses, longitudinal cable stay systems (Figure 1), continuous construction, or unloaded back stays. Resistance to torsional instability can be further enhanced by using transverse diagonal stay systems (Figure 2), installing top and bottom lateral bracing systems, increasing the torsional stiffness of support towers, raising the location of suspender connections relative to the center of gravity of the section, or lowering the center of gravity of the section.

The aerodynamic stability or instability of a bridge design is largely a function of the form, proportions, and details of the cross section. Bridge sections can be devised or modified to produce the desired stability. The designer must choose between shallow and wide or deep and narrow profiles, truss or girder (either plate or box) stiffening systems, open grid or solid deck sections, slotted or solid curbs and

---

[1]Research Structural Engineer, Federal Highway Administration, 6300 Georgetown Pike, McLean, VA 22101-2296, U.S.A.

walkways, and open or closed barriers and railings. In addition, he may also consider the use of special aerodynamic details such as fairings, flaps, and edge plates.

To demonstrate how these methods can and have been applied, the remaining sections of this paper will focus on a specific example bridge where both stiffening and shape modification have been considered. The structure selected for this purpose is an existing, girder-stiffened suspension bridge which has been stiffened in several stages through addition of stay cables and cable ties. At its Aerodynamics Laboratory located in McLean, Virginia, the Federal Highway Administration (FHWA) has recently identified an improved aerodynamic shape which is currently being considered for implementation on this structure.

2. DETAILS OF THE BRIDGE

The Deer Isle-Sedgwick Bridge is a girder-stiffened suspension bridge similar in cross section to the original Tacoma Narrows Bridge. As illustrated in Figure 3, the structure consists of a main span of 1080 ft (329.2m) in length, side spans of 484 ft (147.5m) each, and approach spans of 130 ft (39.6m) each, resulting in a total structure length of 2308 ft (703.5m). The stiffening girders are 6.5 ft (2.0m) deep and spaced 23.5 ft (7.2m) apart. The 2-lane roadway consists of a 4.5 in (11.4cm) reinforced concrete slab having a width of 20 ft (6.1m). The spacing of the suspender cables is 28 ft (8.5m).

3. STRENGTHENING OF THE BRIDGE SPAN

3.1 Original Design

Built as a special Public Works Administration (P.W.A.) project, the Deer Isle-Sedgwick Bridge, spanning Eggemoggin Reach on the Coast of Maine, was completed in June of 1939. The "lean design" of this structure was the direct result of the extremely unsettled economic conditions existing at the time. Construction costs increased more than 50% between the time of the original estimates in 1933, at the bottom of the Depression, and the time of final authorization to proceed in 1938. Difficult foundation conditions at the site forced designers to increase the main span from 800 to 1080 ft (244 to 329m) and the War Department required that navigation clearance be increased from 50 to 85 ft (15 to 26m). Considerable ingenuity and resourcefulness was needed in order to design and construct a suitable structure within the limited funds available. The task was accomplished by sacrificing stiffness, while providing adequate strength for the normal loads expected. The flexible span which resulted had a coefficient of rigidity (K) of 69, second only to that of the original Tacoma Narrows Bridge (see Table 1, from Reference 1).

3.2 Light Stay System

After finishing the original design and before completing construction of the bridge, its designers partially anticipated the potential sensitivity to the forces of wind and incorporated certain inexpensive features into the design. These details included center ties (stays) near the middle of the main span (Figure 4) and cable-stays at the tower ends of the

stiffening girders (Figure 5). According to calculations by the designer, D.B. Steinman, this light stiffening system more than doubled the coefficient of rigidity and the damping increased from 0.013 to 0.053. It is generally felt that this modest stay system enabled the Deer Isle Bridge to survive a number of major storm events including a notable one on December 2, 1942. On this date, the structure was subjected to transverse gale force winds estimated at 60 to 80 mph (92 to 129km/h) and underwent vertical, single-segment undulations in the main span of 10 to 12.5 ft (3.0 to 3.8m) single amplitude. These vibrations lead to uplift and displacement of the cable bents, slippage of the suspension cable at the tower and cable bents, slippage of the cable bands at the center ties, failure of 25% of the stay supports, and damage to the expansion joints.

3.3 Comprehensive Stay System

In light of the damage to the Deer Isle Bridge in 1942 as well as the dramatic collapse of the similar Tacoma Narrows Bridge just two years prior, attention was quickly focused on investigating possible remedial measures for the bridge. A number of methods for enhancing the structural behavior were considered including: cutting holes in the web of the stiffening girder; replacing the solid deck with an open grid or vented deck; replacing or supplementing the stiffening girders with an open stiffening truss; adding a more extensive longitudinal stay system; and adding a transverse diagonal stay system. Following careful evaluation, it was determined that the addition of both longitudinal and transverse stays offered the most effective means for stiffening the structure and improving its overall aerodynamic stability. According to calculations by the designer, a comprehensive stay system would increase the stiffness coefficient from its original value of 69 to 1571, resulting in a structure 23 times as rigid. This, in turn, would significantly increase critical wind velocities while reducing amplitudes at higher wind speeds. The cost of this retrofit was extimated at $79K and would add less than 70 lb/ft (104kg/m) to the dead load of the structure. In 1944, a comprehensive system of longitudinal diagonal stays (Figure 6), complemented by transverse stays and rigid struts at 10 panel points (Figure 7), was implemented on the bridge. All intersections between the stays were clamped. In addition to the stay system, the fixed-pin support for the stiffening girder at the cable bent was replaced by a movable rocker support (Figure 8). This measure was intended to eliminate cable bent displacements and saddle slippage.

3.4 Rigid Cable Ties

Although the stays installed in 1944 did significantly improve the vertical and torsional behavior of the bridge, they did not adequately restrict the longitudinal motions of the suspended spans, especially the side spans. On several occasions since their installation, high winds and/or heavy truck loadings have resulted in contact being made between the ends of the stiffening girders and the adjacent cable bents, causing local buckling in the flanges, warping of the webs, and overstressing in nearby stays. The most dramatic incident of this type occurred on February 3, 1972 during a severe gale. As a result of damage to the girders sustained during this storm, additional modifications were made

to the bridge in the summer and fall of the same year. The first of these involved the addition of six rigid cable ties at the center of the main span and near the ends of the side spans (Figures 8 and 9) to provide strong connections between the suspension cables and the stiffening girders and thus control longitudinal motions. The second improvement was the addition of floor beam brackets to support the top flanges of the girders midway between the suspenders. This detail reduced the unsupported length by half and considerably increased the load carrying capacity of the girders. The third modification to the structure was the addition of cover plates to the flanges of the girders in the four end panels adjacent to the cable bents. This measure was intended to reinforce the stiffening girders specifically in those areas where, over the years, higher stresses have likely occurred thus providing a greater factor of safety against fatigue.

4. MODIFICATION OF THE BRIDGE SHAPE

4.1 Wind Tunnel Testing

Wind tunnel tests were conducted on the 1:25 scale section model representing a segment of the existing bridge span [2]. Since the structure under investigation has a shape similar to that of the original Tacoma Narrows Bridge and has exhibited significant wind induced response throughout its many years of service, several modifications to the basic bridge section were also evaluated (Figure 10). Section model studies were performed in both smooth (laminar) flow and simulated (large-scale) turbulent flow conditions, with wind speeds ranging from 0 to 40 fps (0 to 12.2m/s). The details of this simulation technique are described elsewhere [3]. Static lift, drag, and pitching moment forces were obtained for the basic section model and the "best" alternate at several different wind speeds with wind angles ranging from -10 to +10 degrees. Root-mean-square (RMS) response amplitudes were measured for the vertical and torsional degrees-of-freedom to identify the regions of aerodynamic sensitivity. Flutter coefficients were computed using damping and frequency measurements obtained from free oscillation tests on the section model. All flutter tests were conducted at a fixed wind angle of zero degrees.

4.2 Existing Bridge Cross Section

4.2.1 Static Forces

Dimensionless force coefficients for the Existing Section and Alternate A are presented in Figure 11. For the existing cross section, mean wind forces were measured at several wind speeds ranging from 10.8 to 18.6 fps (3.3 to 5.7m/s). The force coefficients exhibited only slight variation with wind speed. The drag coefficients vary from 0.36 to 0.48 over a 20 degree range of wind angle. For a horizontal wind with a mean velocity of 100 mph (161km/h), the drag force is calculated to be 240.4 lb/ft (357.8kg/m), with a corresponding pressure of 37.0 psf (1772pa). In comparison, the United States bridge design specifications recommends that a pressure of 50 psf (2394pa) be used for design [4]. The minimum and maximum coefficients yield pressures of 33.3 and 44.4 psf (1594 and 2126pa), respectively.

The lift curve for this cross section develops a negative slope in the middle region, -5 to +5 degrees, and flattening of the slope near the ends. These are undesirable aerodynamic characteristics indicating a tendency for galloping in the vertical mode. As Figure 12 clearly demonstrates, this trend is quite similar to that observed during testing of the original Tacoma Narrows Bridge.

4.2.2 Dynamic Response

A series of dynamic tests were conducted in laminar flow and at low damping to evaluate the overall behavior of the section model. Results of the tests on the Existing Section and Alternate A are presented in Figures 13 and 14 for the torsional and vertical modes, respectively. The Existing Section exhibited the largest RMS rotation response, 1.42 degrees, and the widest "active" range. In the vertical degree-of-freedom, the Existing Section clearly displays two distinct regions of activity centered at 3.8 and 11.2 fps (1.2 and 3.4m/s), respectively, with the beginnings of a third evident at 17 fps (5.2m/s). Note that this test had to be terminated at 18 fps (5.5m/s) due to rapidly growing vertical motion.

A second series of tests were conducted with structural damping increased to 0.90% and 1.25% of critical for torsion and bending respectively. With this increased damping, the response of the sections changed dramatically. This change is illustrated in Figures 15 and 16 for the Existing Section. For the condition of high damping, rotational response did not increase suddenly at 11 fps (3.4m/s); however, there were signs of increased activity at 15 fps (4.6m/s) and the test still had to be terminated prematurely. Vertical motion of the section within the first region was reduced to 1/10th its original level. At a velocity of 6 fps (1.8m/s), however, vertical response builds rapidly and does not "peak" as it did with low damping. This is due primarily to the absence of torsional motion.

4.2.3 Flutter Stability

The flutter stability of the Existing Section was evaluated in neutral (smooth) and strongly turbulent (20% intensity) air flows. All tests were conducted at a wind angle of zero degrees. A plot of the A_2^* coefficient, which indicates the aerodynamic damping in the torsional mode, is presented in Figure 17. The coefficient exhibits a trend toward instability at a relatively small "reduced velocity" (V/NB) of 2.25. The introduction of turbulence has a slight modifying effect on the aerodynamic damping; however, it does not alleviate the overall trend toward instability.

4.3 Modified Bridge Cross Section

4.3.1 Existing Curb and Sidewalk Vents

Originally, the sidewalk portion of the curb-sidewalk detail was decked with timber planking. In 1957, the planking was replaced by open grating. To evaluate the significance of the curb and sidewalk vents at each edge of the roadway, tests were repeated with the vents sealed off.

Test results for the Existing shape are presented in Figures 18 and 19. The results indicate that the vents perform a very useful function--they weaken the potential vortex-induced response of the section. Closing the curb vents results in more frequent response, greater bridge motion amplitudes, and activity at lower wind speeds.

4.3.2 Proposed Deck Vents

Since the bridge deck was scheduled for replacement, venting of the new deck was considered. Tests were performed with a deck vented in the center of each traffic lane and results are shown in Figures 20 and 21. Although venting of the deck does reduce vortex-induced motion, it does not eliminate it entirely. On the other hand, torsional motion amplitudes were increased by a factor of two. Divergent vertical response was not noticeably affected by deck venting and reappeared at about 17 fps (5.2m/s). Based upon these results, venting of the new deck does not seem warranted.

4.3.3 Proposed Fairings

Of the various arrangements of fairings and steering plates considered during the testing, Configuration Alternate A provided the greatest enhancement to overall performance. As Figure 13 clearly demonstrates, the addition of asymmetric fairings results in a significant reduction in the torsional vibration amplitudes. Perhaps the more important result is that the tests on Alternate A revealed negligible vertical response (Figure 14) over the full velocity range to 40 fps (12.2m/s).

For Alternate A, force coefficients were obtained over a range of wind velocities from 5.6 to 25.8 fps (1.7 to 7.9m/s). In this case, drag coefficients vary between 0.20 and 0.48, with a value of 0.27 at zero degrees (Figure 11). This results in a calculated pressure of 25.0 psf (1195pa), which is less than half the AASHTO value for 100 mph (161km/h). The slope of the lift curve for this alternate is positive over the full range of wind angles indicating improved aerodynamic stability.

Alternate A was tested in neutral and modestly turbulent (2-4% intensity) air flows to determine its resistance to flutter instability. Figure 22 presents the A_2^* coefficients for this sequence of tests. It is readily apparent from this plot that the torsional stability has been greatly improved. Although the coefficient briefly enters the positive region, indicating potential for instability, it quickly returns to the negative (stable) side. In fact, if 0.5% structural damping is assumed, this configuration should remain stable over the range of test.

5. CONCLUSIONS

History has shown that flexible structures can be sensitive to the turbulent forces of wind. This paper has highlighted the techniques which have been employed on suspension bridges to enhance their aerodynamic behavior. One approach, stiffening the structure, places emphasis on resistance to a dangerous inherent aerodynamic characteristic. The other, aerodynamic design of the shape, aims to

avoid or remove the undesirable characteristic. For the Deer Isle-Sedgwick Bridge, stability has been partially secured through addition of a comprehensive system of stays and cable ties. A modification to the bridge shape is presently being evaluated and may soon be implemented.

6. REFERENCES

1. Steinman, D.B., "Rigidity and Aerodynamic Stability of Suspension Bridges," Transactions, American Society of Civil Engineers, Volume 110, 1945.

2. Bosch, H.R., "A Wind Tunnel Investigation of the Deer Isle-Sedgwick Bridge (Phase I)," Federal Highway Administration, Report FHWA/RD-87/027, Washington, D.C., August 1987.

3. Huston, D.R.; Bosch, H.R.; Tanaka,H., "The Effects of Large-Scale Upstream Gusting on the Aeroelastic Behavior of Section Models," Proceedings of 18th UJNR Panel Conference: Wind and Seismic Effects, Washington, D.C., May 1986.

4. AASHTO, "Standard Specifications for Highway Bridges," American Association of State Highway and Transportation Officials, pp. 24-25, 1983.

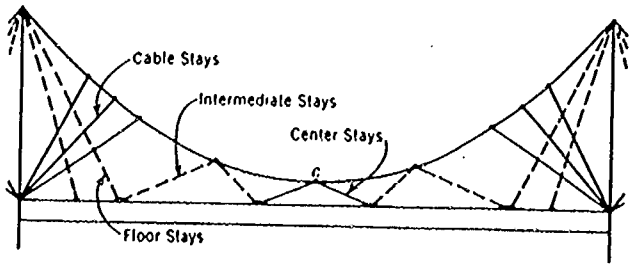


Figure 1. Various Types of Longitudinal Stays.

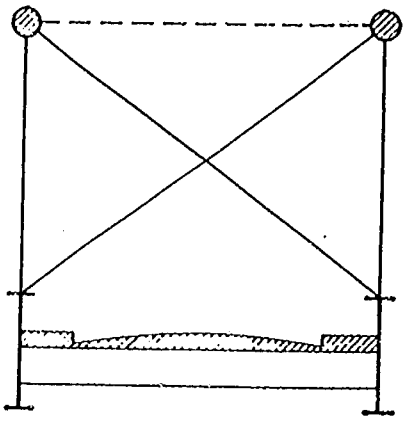


Figure 2. Transverse Stays.

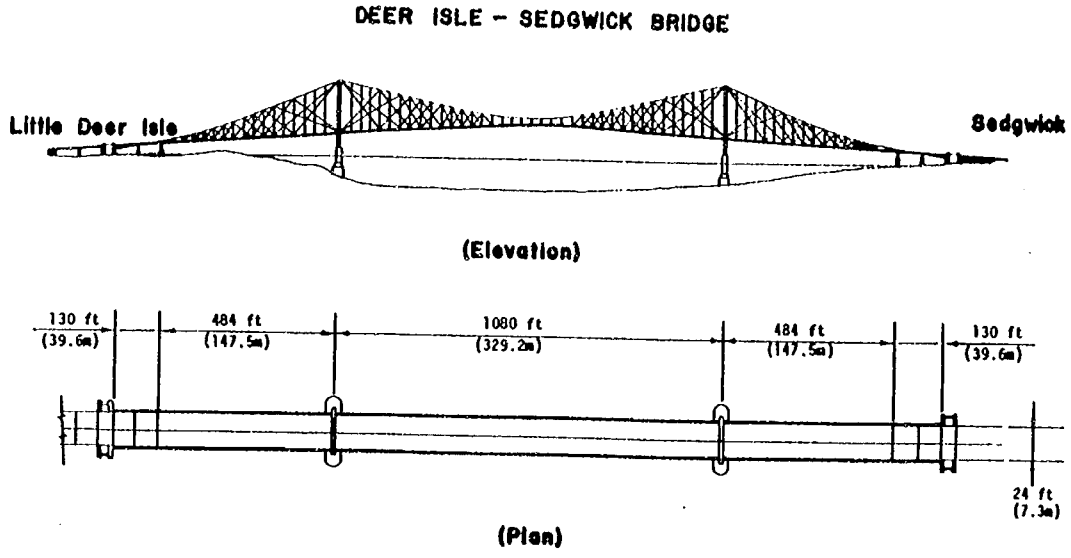


Figure 3. Suspension Bridge Configuration.

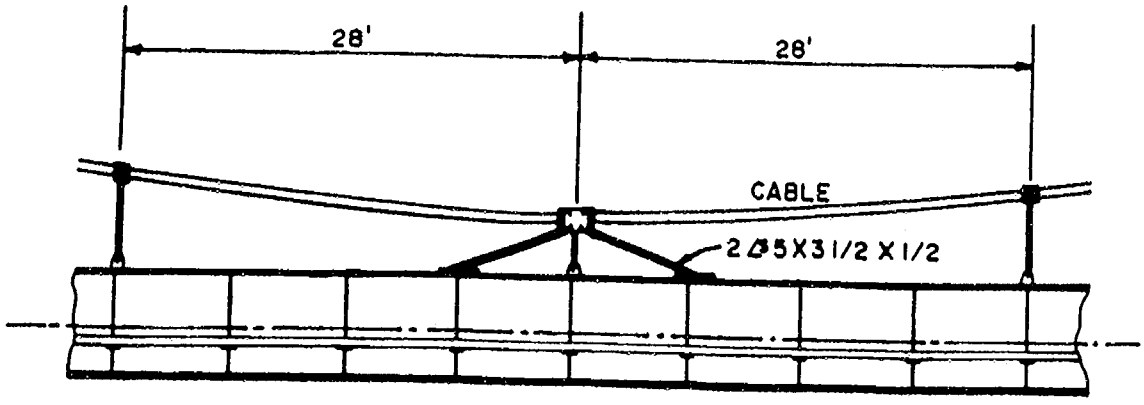


Figure 4. Center Cable Stays - Deer Isle.

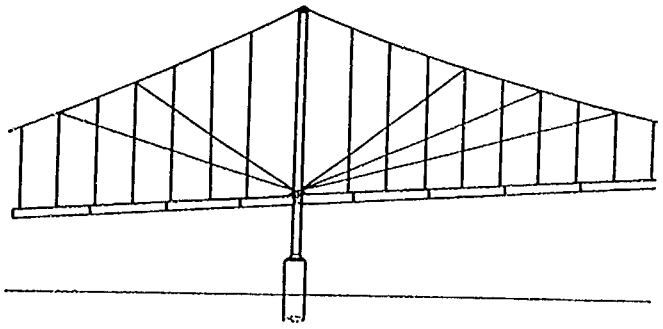


Figure 5. End Cable Stays - Deer Isle.

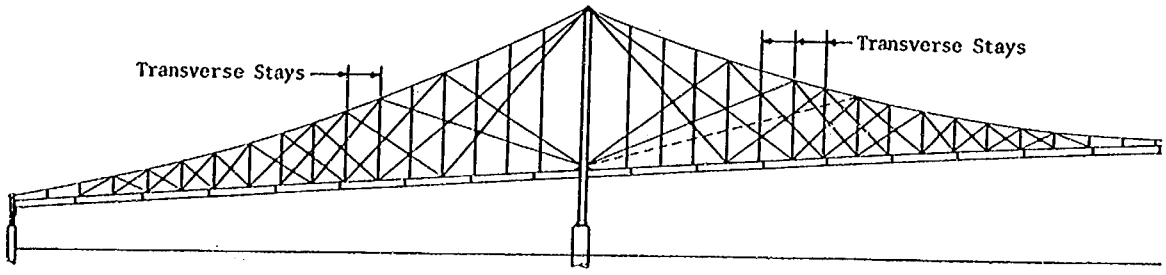


Figure 6. Longitudinal Stays - Deer Isle.

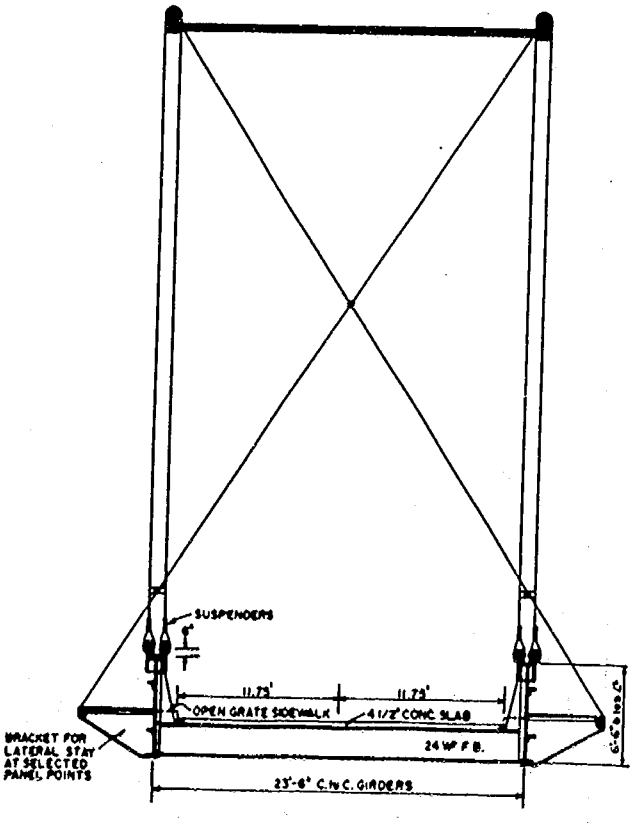


Figure 7. Transverse Stays - Deer Isle.

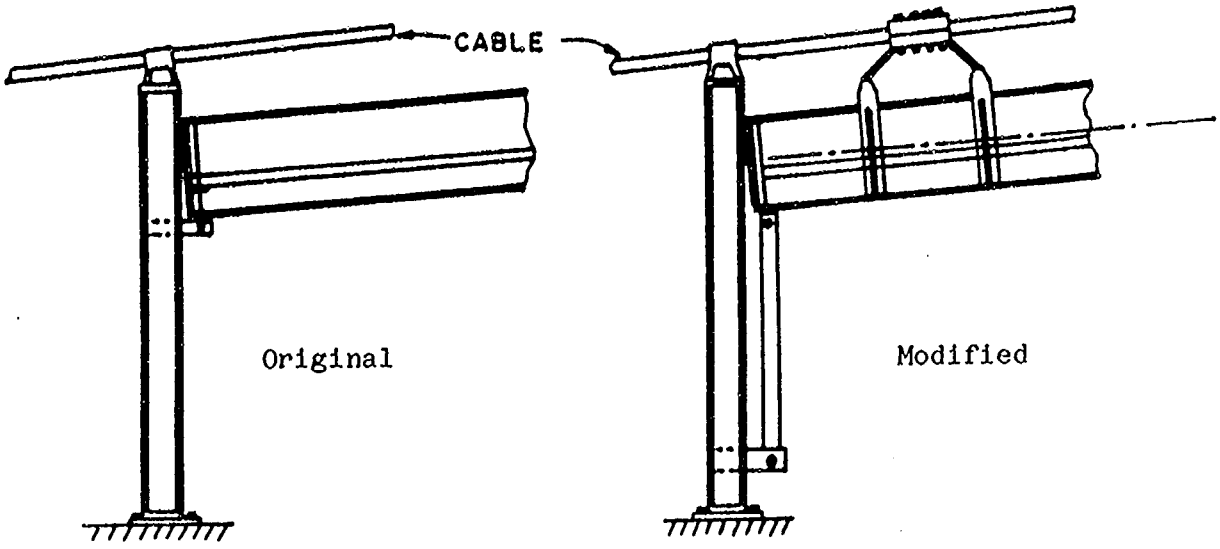


Figure 8. Rocker Support and Cable Tie - End Span.

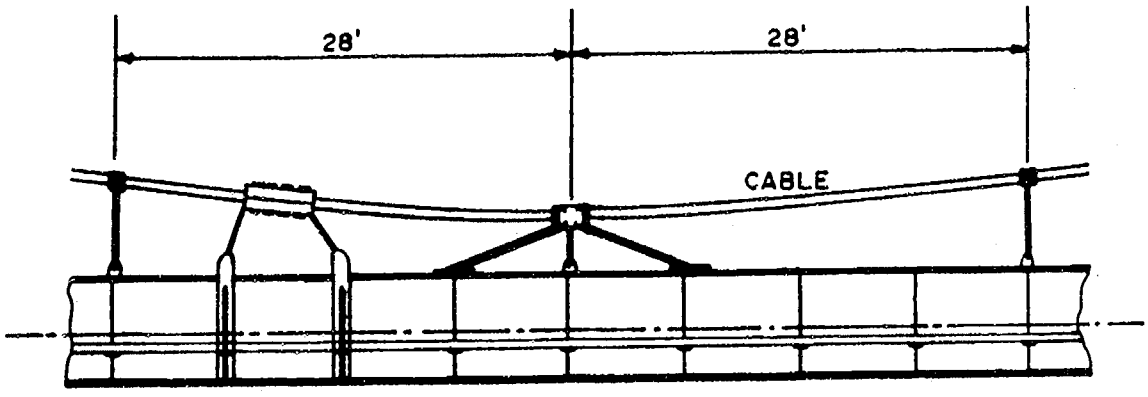


Figure 9. Rigid Cable Tie - Center Span.

(A)

(B)

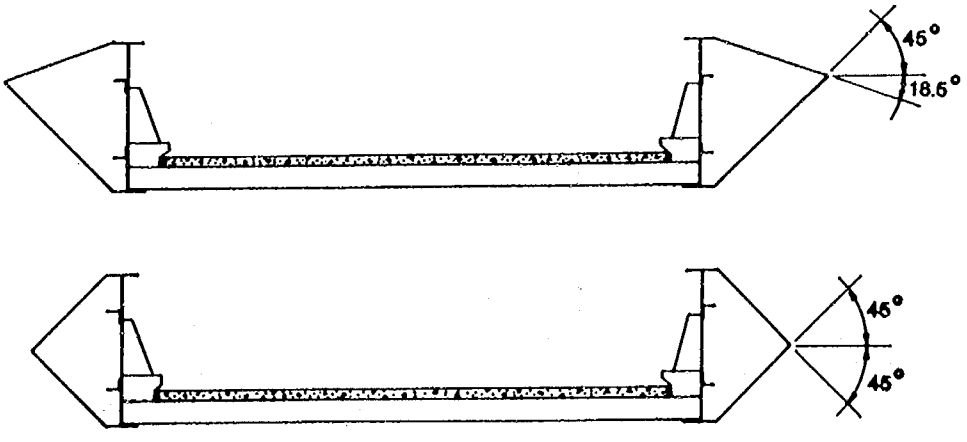
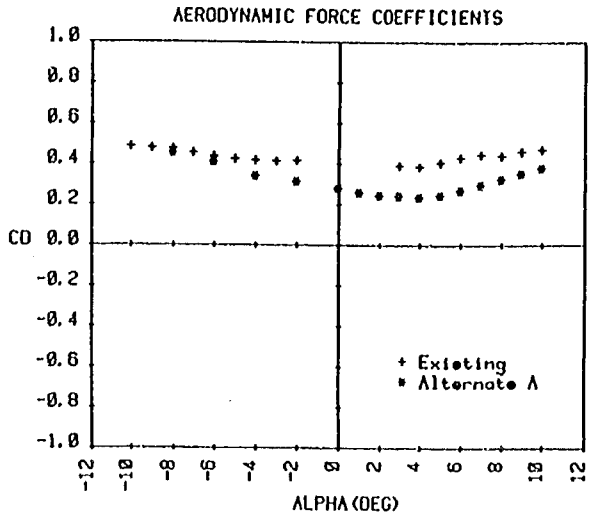
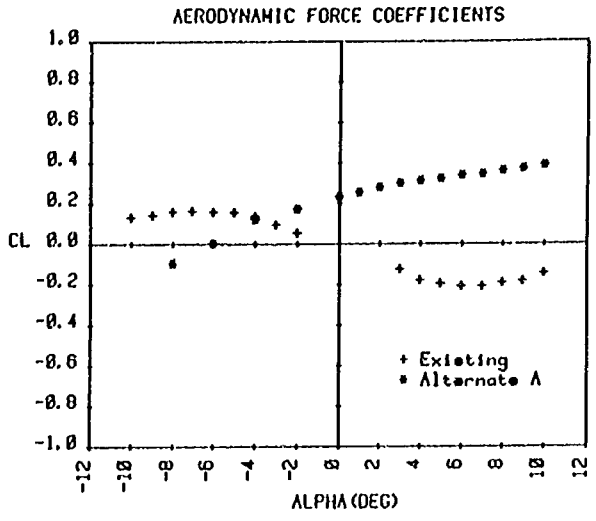


Figure 10. Alternate Cross Sections - Deer Isle.





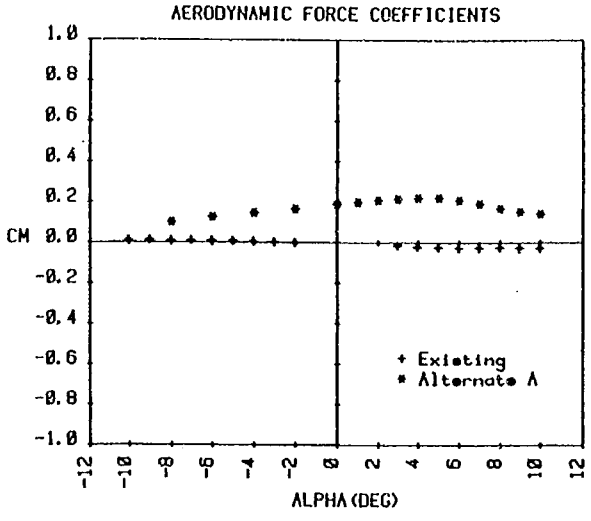


Figure 11. Wind Force Coefficients.

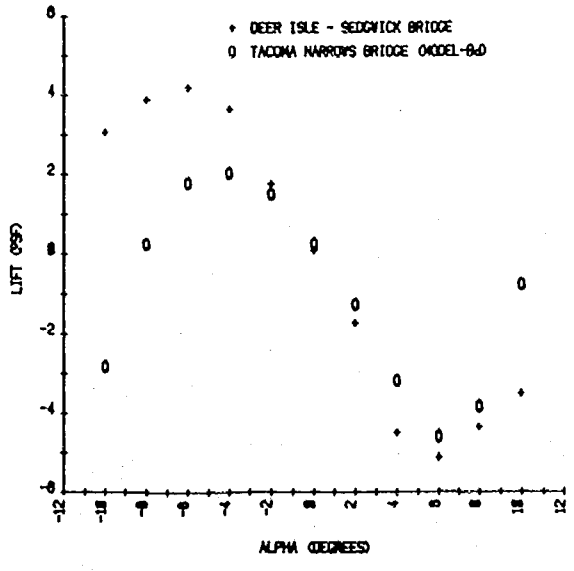


Figure 12. Comparison of Lift Force.

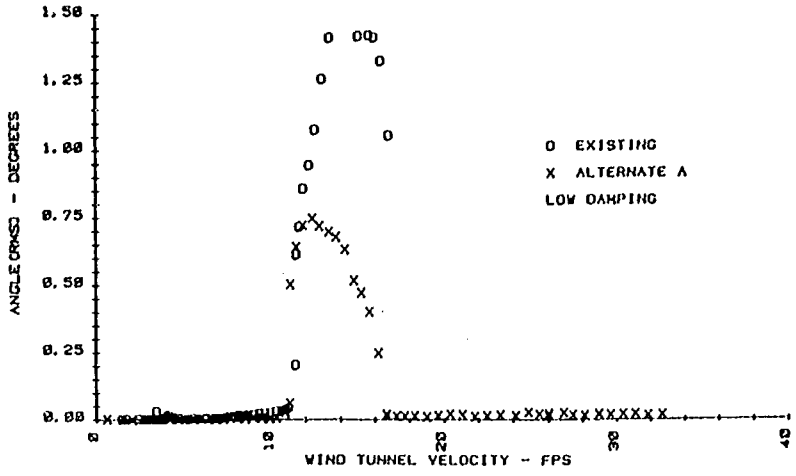


Figure 13. Torsional Response - Low Damping.

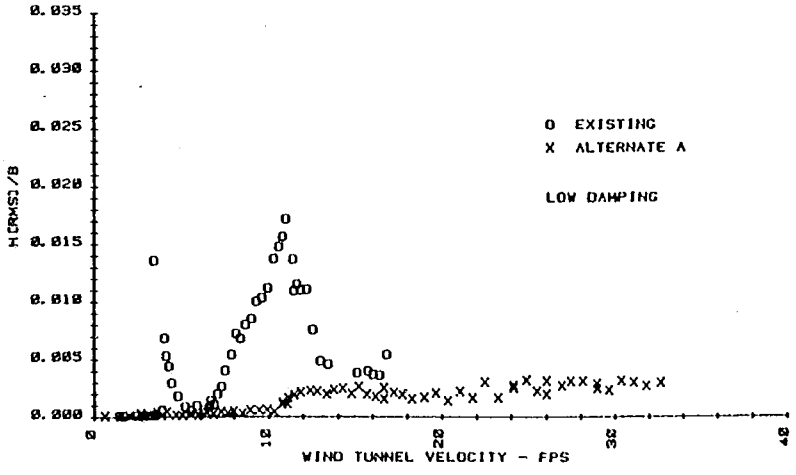


Figure 14. Vertical Response - Low Damping.

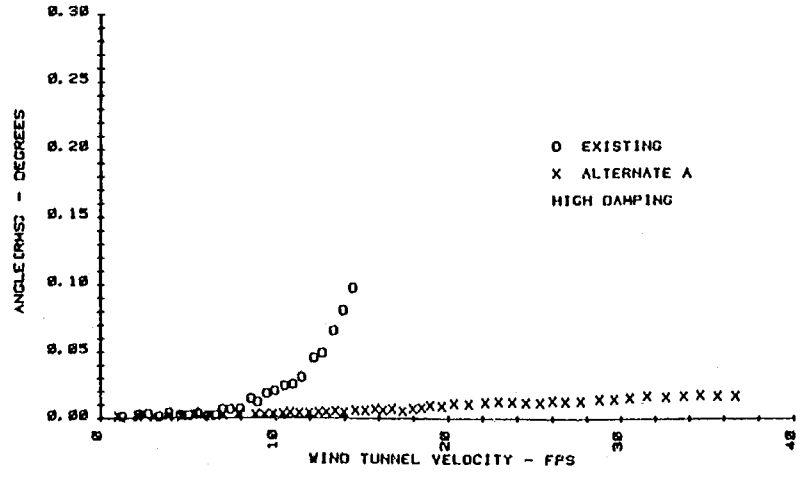


Figure 15. Torsional Response - High Damping.

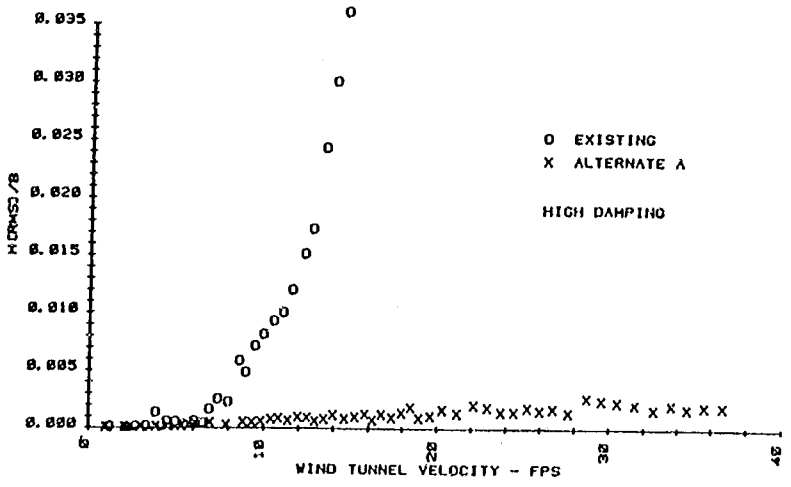


Figure 16. Vertical Response - High Damping.

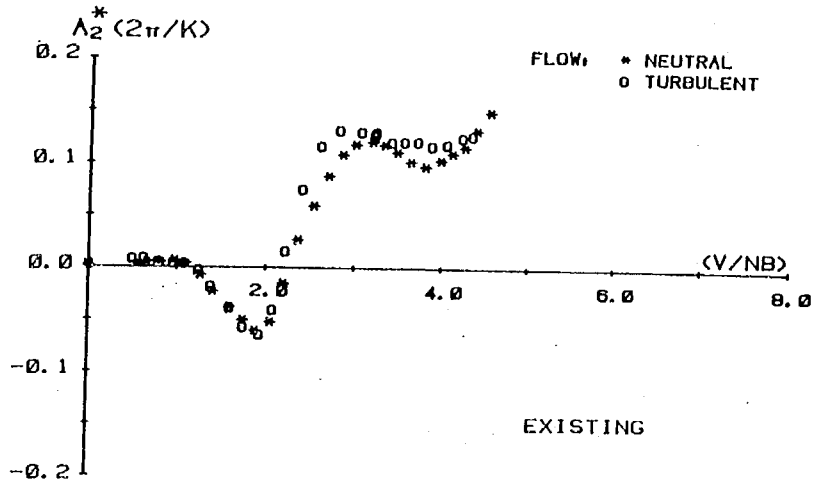


Figure 17. A_2^* Flutter Coefficient - Existing Shape.

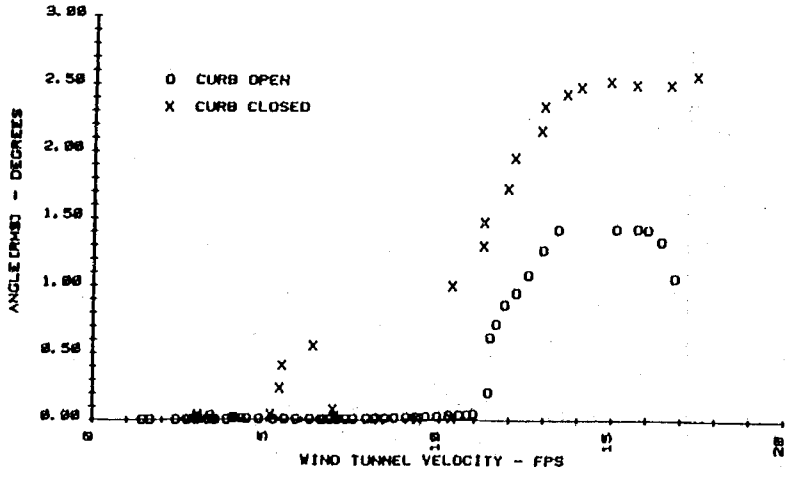


Figure 18. Torsional Response - Curb Open/Closed.

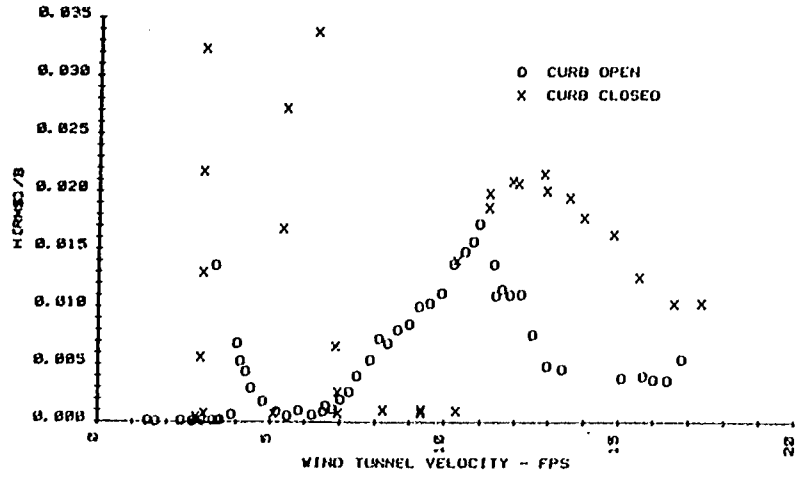


Figure 19. Vertical Response - Curb Open/Closed.

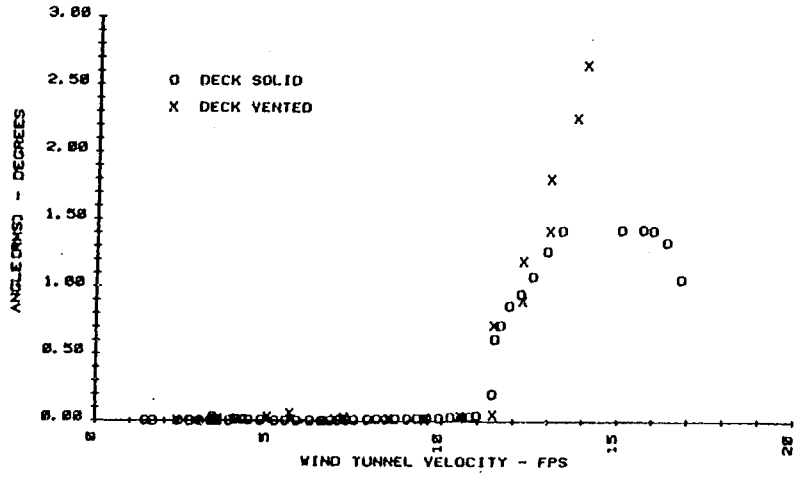


Figure 20. Torsional Response - Deck Solid/Vented.

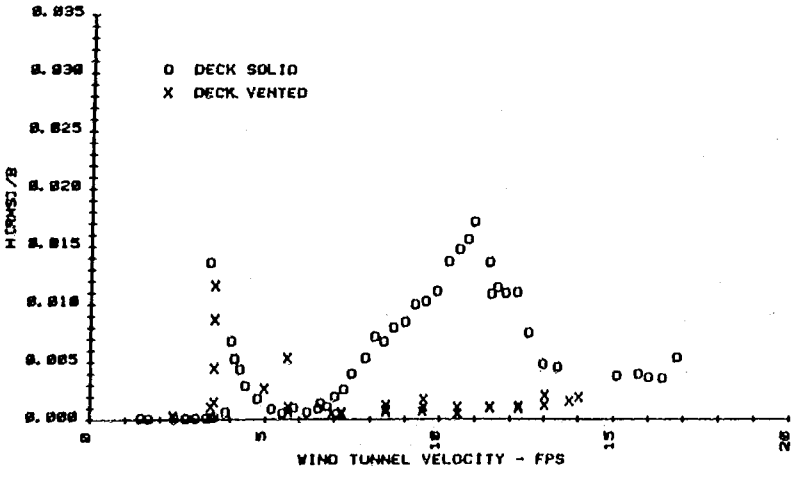


Figure 21. Vertical Response - Deck Solid/Vented.

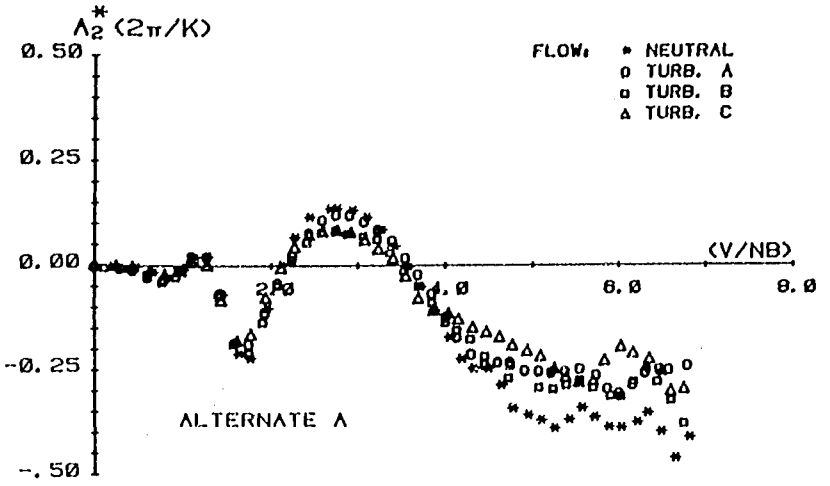


Figure 22. A_2^* Flutter Coefficient - Alternate A.

Table 1. Values of K for Various Suspension Bridges. (from Reference 1)

Date	Bridge	K per cable	K per foot	PERCENTAGE DUE TO:	
				Cable	Girder (R)
1903	Williamsburg	1,082	32.40	22	78
1939	Wabash River*	327	26.20	0	100
1931	Manumee River*	648	22.00	51	49
1926	Philadelphia	735	16.52	44	56
1931	Waldo-Hancock	212	15.14	56	44
1929	Grand Mére	188	14.48	34	66
1909	Manhattan	618	12.88	31	69
1930	Mid-Hudson	262	12.50	56	44
1929	Mount Hope	201	11.82	54	46
1936	Triborough	547	11.18	66	34
1936	Transbay	324	9.81	62	38
1931	St. Johns	252	9.70	65	35
1938	Thousand Islands*	141	9.25	74	26
1938	Thousand Islands*	127	8.30	78	22
1929	Detroit	212	7.13	71	29
1939	Deer Isle*	69	5.85	80	20
1938	Vancouver	112	5.62	67	33
1931	George Washington	244	4.60	100	0
1939	Bronx-Whitestone*	141	3.81	97	3
1940	Tacoma*	62	3.16	98.5	1.5
1937	Golden Gate	116	2.56	95	5

*Denotes construction with solid-web stiffening girders.

INVESTIGATION OF AERODYNAMIC PERFORMANCE OF TOKYO PORT BRIDGE

Hiromi Kosaka[1], Hisamitsu Hanno[2], and Yozo Fujino[3]

1. Assistant Section Leader, Tokyo Metropolitan Highway Authority, Construction Department 3, Design Section.
2. Engineer, Tokyo Metropolitan Highway Authority, Construction Department, Design Section.
3. PhD., Associate Professor, Engineering Research Institute, Faculty of Engineering, University of Tokyo.

Summary

This paper reports on the results of various experiments carried out to determine the performance under wind loading of the Tokyo Port Bridge.

The bridge is planned as a three span suspension bridge with a trussed stiffening girder. Whilst the bridge is not of exceptional scale, it is of a two deck type with various features which distinguish it from conventional suspension bridges. The upper deck is to carry a four lane highway, and the lower a four lane bay-side road, pedestrian route, and a rail track as part of a new transport system. In addition the attachment of protective enclosures is being investigated. From research into the observed wind conditions at the bridge site, and extensive wind tunnel testing, the stability of the bridge under wind load was confirmed.

1. Introduction

The Tokyo Bay waterfront is an important industrial base, and the increasing demand for land has lead to active land reclamation work. In particular plans for a secondary peripheral center for Tokyo on reclamation zone 13, and ideas for the development of Toyosu Wharf area have been gaining attention in recent years. The Tokyo Port Bridge will connect these reclaimed areas directly to the city centre. Whilst from the viewpoint of the development of the area it is hoped that the bridge can be completed in a short period, the solution must preserve smooth traffic conditions over a wide area (fig. 1-1).

The bridge is to cross the extension to the major shipping route in Tokyo Bay, with a central suspended span of 570m, and an overall length of 798m. The center span dimensions were determined by considerations of shipping clearances and turning arcs, whilst the side span layout was controlled by the horizontal alignment of the highway (minimum bend radius). In addition the tower height was restricted to about 130m by the flight paths of aircraft departing and arriving at Tokyo International Airport (fig. 1-2).

Although much research has already been done in many areas related to suspension bridge design, the weak foundation conditions for this bridge, together with various restrictions imposed on form and appearance as a

result of its location in the city centre, meant that adequate fresh research was necessary. There were also several areas in the design where it was required to develop new techniques for analysis.

An advisory research committee was established in 1982 to oversee the design of the Tokyo Port Bridge (chairman: Mr S. Saeki, Ministry of Construction, Civil Engineering Research, Bridge Structures Director). The committee has commissioned investigations and research to address technical problems relating to the construction of the bridge. Research work is extending over a wide field, from engineering problems, to investigations into aesthetics.

The following is the committee's report on the results of the investigation into the aerodynamic stability of the bridge.

2. Research into Observed Wind Conditions

2.1 Outline of Study.

In order to understand the characteristics of the wind around the proposed site, the following investigations were made.

1)Wind speed records for Tokyo Bay, reclamation zone 13.
Observation period 20/9/1981-31/10/1984.
Main observations: 10m height - direction, average speed, gust speed
25m height - wind speed x,y,z components, temperature
(direction obtained from velocity components).

2)Collection and cataloging of past wind data held at the area meteorological agency.
The Central Tokyo Meteorological Observatory and the Yokohama Area Meteorological Observatory were selected for this site.

3)Analysis.
Based on recommendations given in "Honshu Shikoku Link Bridges - Standard for Aerodynamic Design" (referred to hereafter as "the code"), the wind design for the bridge was carried out under the following headings:
a)Investigation of the wind characteristics at Tokyo Bay reclamation zone 13
b)Establishment of the basic site wind speed
c)Establishment of the design wind speed.

2.2 Wind Characteristics

The wind frequency chart and wind direction with speed relevant to the site at 10m height are shown in figure 2-1. On an annual basis the most frequent wind direction is north, occurring over 15% of the time. This is followed by N.N.W, N.N.E, and south. The wind observations for the site show that the highest speeds are distributed mainly in the north and south directions, which is the least favourable for the bridge structure.

For estimates of the wind speed distribution from ground level up to 150m height, the well established empirical power law relationship was employed, namely

$$V_Z = V(10)*(Z/10)^{\alpha}$$

where V(10) is the 10m height site wind speed,
V_Z is the speed at height Z,
α is the power law coefficient.

Based on the site wind speed observations, power law coefficients were established for various wind directions as shown in table 2-1. Additionally, from the data for average wind speeds greater than 10m/s, the power law coefficient α, and the wind speed - direction relationship are shown in table 2-1 and figure 2-2. It can be seen that α is approximately inversely proportional to the wind speed. Taking into consideration the basic 100 year return wind speed of over 40m/s, and giving sufficient weight to the occurrence of south winds, a value of $\alpha = 1/8$ was adopted from the above results.

Average values for the gust factor obtained from the site observations for various directions are given in table 2-3.

Site observations of wind incidence angle (using an ultra-sonic anemometer at 25m height) for the ten minute average wind speed, and associated wind direction, are shown in table 2-4. For high winds occurring during the observation period (average wind speed greater than 15 m/s), a contrast is given between the observed incidence angle, and the guidelines from the code, in figure 2-3. These observations all show an angle of incidence for the site of less than three degrees.

2.3 Estimation of Wind Speed Return Period

The site observations were taken over a period of only three years. For use in the estimation of a reliable wind speed return period, data from such a short period is completely inadequate. For this reason data taken from two nearby meteorological stations over a long period (1929-1984) was applied in this case. The two stations were the Central Tokyo Meteorological Observatory (referred to hereafter as "Tokyo"), and Yokohama District Meteorological Agency ("Yokohama"). By estimating the wind speed return period from these two sources, and then determining the correlation between this data and the site observations, an estimate was made of the wind speed return period at the bridge site. This relationship is shown in table 2-5. Based on the results from Tokyo and Yokohama, which show reasonably good correlation, the results were extrapolated to arrive at an estimated value of 43.5 m/s for a 100 year return period.

2.4 Analysis of Wind Speed Fluctuations

Since the 100 year return period wind speed is greater than 40 m/s, data for the analysis of speed fluctuation was only taken from strong wind observations with speeds greater than 15 m/s (height 25m).

The relationships between average wind speed $\bar{U}$, and the standard deviation of speed fluctuations for the horizontal component σ_u, and vertical

component σ_w, were investigated for the area (reclamation zone 13). Values for the intensity of turbulence were obtained as follows:

$$I_u = \sigma_u/\bar{U} = 0.17$$
$$I_w = \sigma_w/\bar{U} = 0.08$$

The value of the vertical intensity is about half of the horizontal intensity, which agrees with generally observed trends.

Figure 2-4 shows the normalized power spectrum for the average horizontal component of the analysed data. The full line shows the average value, and the broken line the average plus or minus one standard deviation. The HINO type spectrum calculated with $\sigma = 0.17\ \bar{U}$ and $\alpha = 0.19$ is shown by the dotted line on the same figure. It can be seen from the figure that within the range $n \times Z/\bar{U} \lesssim 0.25$, where n is the normalized frequency, the peak frequencies for the average spectrum can be separated from the lower frequencies, to give comparatively good agreement with the HINO spectrum.

3. Investigation of the Main Tower Aerodynamics

3.1 Outline of Experiments.

A traditional problem arising during the construction of suspension bridges is vibration of the main towers when free-standing due to excitation from wind perpendicular to the axis of the bridge. For the current study this aspect was investigated by wind tunnel tests to check for aerodynamic instability during both construction and complete stages.

The forms of tower tested are shown in figure 3-1. These shapes were proposed after considerations of economy, aesthetics, and other factors. The results of the wind tunnel tests were to be used to assist in the final choice of the tower form.

Models which simulated stiffness in three dimensions (scale 1/140) were tested in the wind tunnel to investigate their dynamic response. Tests were principally made in smooth flow, but several tests in turbulent flow were made for limiting cases.

Traditionally, wind tunnel tests on suspension bridge towers almost always investigate aerodynamic stability for flow perpendicular to the bridge axis. Over recent years research has started into the behaviour of cable-stayed bridge towers in winds along the bridge axis. The possibility of self-excited oscillation (galloping) has been noted on several bridges, in particular the S - Cable-stayed Bridge (2), Yokohama Bay Bridge (3), East Kobe Waterway Bridge (4), and possibly Aratsu Ohashi Bridge (5). It is thought that there is latent potential for aerodynamic instability of suspension bridge towers in flow along the bridge axis, and for this reason both the perpendicular and along axis cases were investigated. Based on the code, the logarithmic decrement for the towers can be assumed to be $\delta = 0.01$. However, to be sure that an effective margin against oscillation was present during construction, tests were made for various values of logarithmic decrement.

For investigation of the assumed completed form, the effect of the mass of cables and deck on the dynamic behaviour of the towers was modelled by

substituting equivalent masses at the tower head. The presence of cables and deck was found to improve aerodynamic stability.

3.2 Aerodynamic Stability of Towers During Construction

Taking the test results for tower type B as an example, the aerodynamic stability during construction is shown on a V - A diagram in figure 3-2. The design wind speed for the towers is 69.4 m/s. In compliance with the code, this gives a reference wind speed for catastrophic self-excited oscillation of 69.4 × 1.2 = 83 m/s. The design wind speed and flutter reference speed for the construction stage have not yet been decided. However, according to the code recommendations, these should be taken as 50 m/s and 58 m/s respectively.

(1) Response Characteristics in Flow Perpendicular to Bridge Axis.

Tower type A, with the lowest structural damping value (δ = 0.007), was found to suffer single-axis vortex excited vibration (maximum amplitude approximately 3m) at a wind speed equivalent to 10 m/s for the actual bridge. If the structural damping is increased to δ = 0.015 (roughly doubled), then the amplitude can be reduced to 20-30 cm (actual bridge scale). Similar results were obtained for tower types B and C ; a single-axis , vortex-forced oscillation (maximum amplitude approximately 3m). However, if the structural damping is increased to δ = 0.02, then no significant vibration occurs.

Vortex excited twisting oscillations about one axis occurred at 40 m/s, just below the design wind speed for the construction phase. For types A and B large oscillations occurred over a rather wide range of incidence angle. For structural damping δ = 0.01, the maximum amplitude at the tower head was about 3.5 m at each edge (0.35 radians). Increasing the structural damping to δ = 0.02 did not lead to a great reduction in amplitude, the value being about 2 m at each edge (type B). Type C, with a truss structural form, did not display any marked vortex vibration. This is thought to be due to the large amount of structural damping inherent in this form. Conversely, where the damping is light, as for types A and B, vortex excitation can be expected.

The single axis twisting oscillations occurred at significant amplitudes, but only at equivalent wind speeds of greater than 50 m/s, and so are not thought to present a problem during the construction period.

For tower type B a test was performed in turbulent flow at 3 degree incidence (I_u = 11.4 % , scale = 3-4 cm). The results are compared with the smooth flow case in figure 3-3. Limited bending oscillations about one and two axes caused by the turbulent flow, displayed peaks which overlapped. For twisting oscillation, the results were found to be almost identical to the smooth flow case.

(2) Response Characteristics in Flow along the Bridge Axis.

Tower types A and B exhibited galloping for δ = 0.015 at real bridge wind speeds of approximately 20 m/s. However, if the damping is increased to

0.02, the onset wind speed exceeds the construction stage design speed (>50 m/s), and for δ = 0.03, galloping is almost eliminated.

For type C, the structural damping inherent in the form prevented the occurence of galloping at speeds less than 100 m/s (real bridge equivalent).

3.3 Aerodynamic Characteristics of Towers at Bridge Completion

Unlike the towers of cable-stayed bridges, the in-plane deflection of suspension bridge towers exhibit coupling of the tower, cable and deck deflections in the completed state. In terms of dynamics this means that the lowest mode for the tower is composed not only of the tower contribution, but also those of the cable and deck. This means that the modal mass is larger than that for the free-standing tower. For wind flow along the axis of the bridge, it was thought that the strength of excitation of the towers in-plane would be the same for both free-standing and completed stages. Since the addition of the cable and deck mass makes the tower relatively more heavy, the tendency for oscillation should be reduced in the completed stage. However, since the frequency of tower oscillation in the completed stage will be lower than for the free-standing case (due to the deck and cable mass, and torsional stiffness effects), the aerodynamic characteristics cannot be argued simply on the basis of mass. Caution is needed on this point.

Tower type B was used for this testing. A simplified investigation into the possibility of in-plane oscillations (galloping) was made by adding mass to the tower head and using the results from an analysis of the complete system oscillation in the modal shape where the tower in-plane deflection was greatest.

The results of these tests are shown in figure 3-4. It can be seen that there is a trend of increasing oscillation onset speed with increasing mass. In addition, figure 3-1 shows the results for generalized mass and mass damping parameter for the principal in-plane mode of the towers, as derived from the dynamic analysis of the bridge. Figure 3-5 shows the relationship between speed for onset of oscillation (taken as when tower head deflection exceeds 1/500), and the mass damping parameter. It can be seen that as the mass damping parameter is increased, so the onset speed rises, improving stability. On the same figure are shown the design wind speed, and the mass damping parameter for different values of the tower structural damping.

The possibility of galloping is present below the design wind speed for values of the single axis in-plane tower oscillation structural damping of $\delta \leq 0.02$. However, in reality, it is thought that the value of structural damping at the complete stage is likely to be about δ = 0.03 due to aerodynamic damping and other effects from the cable and deck. Also there is only a slow increase in the magnitude of galloping oscillations with wind speed when the tower mass has been increased. For these reasons, it is not felt that the aerodynamic stability of the towers is threatened.

4. Aerodynamic Testing of Stiffening Girder

4.1 Outline of Experiment.

Truss type stiffening girders are often employed on two-deck suspension bridges for road and rail, but only in the configuration of road on the upper level and rail on the lower. Many examples of aerodynamic stability in bridges of this form can be cited (for instance Seto Ohashi Bridge (6)). However, as stated at the beginning of this report, the present bridge was conceived as a two-deck form without following previous examples too closely; for example there are studies in progress on the attachment of new items to the bridge. The current experiments aimed to determine the influence on aerodynamic stability that these attachments may have, and also to test measures aimed at improving the flutter characteristics of the girder.

The tests used a model which represented as faithfully as possible the footpath, new transport routes, protective screens, and other features. The model provided a two dimensional replica of the structural characteristics of the bridge (table 4-1). Particular attention was paid to the accuracy of the protective screens, gratings, and other attachments. Self-weight and ultimate bending moment are scaled for the basic cross-section (table 4-2, case 1). For other cases fine adjustments were made depending on the Scruton Number. The target value for the structural damping was set at $\delta = 0.03$. However, for case 6 the logarithmic decrement was varied in order to test the influence of using a turbulator grille. In table 4-2, cases 1 to 6 show the influence of attachments, and cases 7 to 14, the effect of openings in the upper and lower decks.

4.2 Tests on the Attachment of Various Items to the Basic Cross-section.

The design wind speed for the stiffening girder is 67.4 m/s (table 4-1). Code requirements for this bridge dictate that within a range of incidence angles from -3 to +3 degrees, catastrophic flutter must not occur at speeds less than 1.2 times the design windspeed i.e. 80.8 m/s (limiting wind speed). For all cases 1 to 6 flutter was found to occur within the limiting flutter wind speed. By way of a full example, the results for case 1 are shown in figure 4-1. The flutter is coupled in bending and torsion, but the torsional component predominates. Following the methods given in "Honshu-Shikoku Link Bridges - Details of Wind Tunnel Testing" (7), the measurements of limiting flutter wind speed are plotted against incidence angle (corrected average value) in figure 4-2.

The conclusions from these results are as follows:
1) For two level deck construction, with wide floors, no gratings, and screening of only the pedestrian route (case 1), the resistance to flutter is not great.
2) The attachment of decorative panels to the upper and lower levels reduces the aerodynamic stability (cases 2,3).
3) Wind protection of the pedestrian route (complete coverage), results in a marked decrease in aerodynamic stability (cases 4,6).

4) The presence of protective nets on the new transport route section (case 5) reduces the aerodynamic stability. The effect is particularly pronounced in the range of incidence angles 0 to +3 degrees.
5) With both the wind protection of the pedestrian route, and the new transport section net in place, the aerodynamic stability falls over the whole range of incidence angles -3 to +3 degrees. The limiting wind speed is reduced well below the required speed for the site.
6) Increase of the structural damping to values of δ = 0.04 and 0.05 does produce an increase in the wind speed for onset of flutter, but the increase is at most 10%.
7) Forced bending oscillations were apparent when wind protection was attached to the pedestrian route, but only for large incidence angles (α = -5, -7 degrees), and at small amplitudes. This is not thought to be a problem (cases 4, 6).
8) No significant differences were noted with the occurence of flutter in turbulent flow (I_u = 11.4%, scale 3-4 cm) from that in smooth flow. However, depending on the degree of turbulence, vertical buffeting was observed.

It is clear from the above test results that the addition of attachments to the bridge deck reduces the aerodynamic stability. As far as is possible, attachments should be minimized, and the solidity ratio decreased in order to improve the aerodynamic performance. However, even for the basic section (case 1) there are few attachments, and it is difficult to achieve further real reductions. Another improvement method was required.

4.3 Tests on Improved Cross-sectional Shape.

As a result of both decks of the bridge being closed, the aerodynamic stability was found to be insufficient. For this reason, schemes were employed to improve the flow characteristics of the section. Openings were formed in the surface of the upper deck road shoulders, and the midline and zone within the new transport system rail tracks on the lower deck. It was anticipated that the topical spilling-air effect would ease the aerodynamic forces. Tests were performed on the cross-section to check this (table 4-2, cases 7-14).

As shown in diagram 4-2d, the experimental results reveal a general improvement in the performance of the section. The conclusions from the tests are given below:
1) Initial improvement in the flutter performance was obtained by providing wide gratings in the roadway shoulders of the upper deck (cases 7, 8).
2) The provision of gratings alone on both the upper and lower decks does not provide sufficient improvement in aerodynamic stability (cases 10, 11).
3) Flutter characteristics are improved by separating the upper deck roadways, and providing an opening between them. If employed together with gratings on the line of the new transport railway on the lower deck, the grating opening width should be about 2 m (case 14).

The current situation is that since the presence of at least some attachments cannot be avoided, the basic stiffening girder (case 1) has been

changed by separating the upper deck flows to introduce a central opening, and providing a grating on the lower deck outside the line of the new transport system railway (case 14).

5. Testing of Full Bridge Model

5.1 Outline of Tests.

From the results of the previous tests it was clear that there is almost no problem with the main towers in the completed bridge stage. With the stiffening girder also there were thought to be no real difficulties. However, a two-dimensional stiffness model has the limitations that the vibration mode, the effects of structural variations along the axis of the bridge, and the influence of spatial variations in the wind flow, cannot be adequately considered. If a more detailed investigation into these areas is desired, then a full three-dimensional model is needed. It was decided to perform tests using a full model of the bridge at 1/70 scale to verify the aerodynamic stability of the stiffening girder.

In normal testing practice, such full bridge models use wood to represent the geometric form, and a single steel bar positioned near the shear centre of the section to model structural stiffness. However, since this girder is of the truss type, the presence of the stiffening bar directly in the air flow would have a great effect on the results. Additional complications are caused by the importance in this case of the attachments to the girder, which influence the aerodynamics. For these reasons the stiffness was provided in this case by four bars, giving the physical arrangement shown in diagram 5-1. These were positioned within the upper and lower decks so that they lay within the horizontal projection of the timber stringers. Tests were performed in smooth flow (incidence angles 0, +3, -3 degrees), and turbulent flow (incidence angle 0 degrees). Details of the model are given in table 5-1.

5.2 Experimental Results.

For smooth flow, the tests showed that no significant oscillations occurred within the design wind speed ($V = 67.4 \times 1.2 = 80.8$ m/s). The results are shown in diagram 5-1, and confirm the aerodynamic stability of the stiffening girder cross-section. The relationship between wind speed and logarithmic decrement for the experiments are shown in diagram 5-2.

The tests in turbulent flow revealed a marked response to vertical gusts. The standard deviation of response to vertical gusts is shown in diagram 5-3. Subject to the design wind speed, the response standard deviations from the reference datum of the stiffening girder at quarter and half-span positions after conversion to full scale are 32 cm and 22 cm respectively. The ten minute peak amplitude can be approximated by taking three times these values, i.e 1.0 m and 70 cm. Whilst these values represent rather large displacement, on comparison of the power spectrum of vertical fluctuations of the wind tunnel air flow with that expected in reality (using the Bush and Panofsky method), it was concluded that the

tests overestimate the response (by a factor of two). For the calculation of the anticipated power spectrum of the actual bridge, a representative value for turbulence intensity of $I_w = 0.05$ (8) was used. The results from meteorological observatories near the site suggest a larger value with $I_w = 0.08$, however, it is felt that this value includes influences from flow over land.

From the above considerations it is anticipated that the peak response to vertical gusts will be 50 cm (quarter span) and 35 cm (half span).

Since a pedestrian route is planned for the bridge, it is necessary to give attention to the influence of the gust response of the bridge on pedestrians.

There has been little research carried out into human response to low frequency vibration. However, recent work by Matsumoto et al (9) suggests that for a frequency of 0.2 Hz (the order of the single axis bending mode frequency here), at an amplitude of 10 cm (corresponding to the peak response amplitude for this bridge in an average wind speed of 20 m/s) 10% of humans will perceive the vibration. At an amplitude of 30 cm there will be few people who do not find the motion unpleasant. It follows from this that no serious problems with regard to human response will arise. When the average wind speed is 20 m/s, the gusts may reach 25-30 m/s, but it is unlikely that pedestrians would be using the bridge in such conditions. In conclusion, the gust response has hardly any influence on pedestrian useage.

6. Conclusions

In order to investigate the aerodynamic stability of Tokyo Port Bridge, the wind observations at the site were researched, and various wind tunnel tests carried out. The conclusions of the study are given below.

The occurrence of single axis bending and torsional vortex excited oscillations of the main towers when free-standing was apparent at low wind speeds. In addition it was established that, as for cable-stayed bridges, in plane galloping oscillations occur below the construction stage design wind speed. Although unstable, forced in and out of plane oscillations arose at significant amplitudes below the design wind speed for the towers in the completed stage, this was not thought to threaten safety.

Regarding the stiffening girder, it is clear that the presence of various attachments to the double deck (wind protection, protective screens etc.) reduces the aerodynamic stability. In order to redress this tendency it is necessary to provide as many openings as possible in both decks. From the full bridge experiments in turbulent flow, the gust response is not judged to be a problem.

The remaining difficulties relate to the provision of measures against instability of the towers in the construction stage. It has been decided to carry out further wind tunnel testing into this matter once the final detailed cross-section of the towers has been fixed. The need for further measures against vibration can then be assessed. Similar doubts remain

measures against vibration can then be assessed. Similar doubts remain about the self-excited oscillations of the towers (galloping) in the completed stage under wind flows along the axis of the bridge. Again, further testing is planned for the final cross-section. However, it is thought unnecessary to perform further tests on a full bridge model, and simplified approaches similar to those used here will be sufficient for this work.

References

1) Honshu-Shikoku Link Bridge Authority : "Standard for Aerodynamic Design" (1976), with Explanatory Notes, March 1976.
2) Ohno, S., Sano, S., Morimoto, C., "Study of Aerodynamic Stability of Cable-stayed Curved Bridge and Its Countermeasures against Wind-induced Vibration", International Colloquium on Bluff Body Aerodynamics and Its Applications, Kyoto, 1988, J. W. Eng. in Japan, vol.37.
3) Saito, T., Ito, M., Yamauchi, H., Eya, S., "Yokohama Bay Bridge - Use of a Dynamic Damper for Aerodynamic Stability of its Support Tower", 4th Joint U.S. - Japan Workshop on Bridge Engineering, San Diego, 11,12 May 1988.
4) Ogawa, K., Matumoto, M., Kitazawa, M., Yamasaki, T.,"Aerodynamic Stability of the Tower of a Long-spanned Cable-stayed Bridge (Higashi-Kobe Bridge)", International Colloquium on Bluff Body Aerodynamics and Its Applications, Kyoto 1988, J. W. Eng. in Japan, vol. 37.
5) Nagino, T. et al. "Aerodynamic Stability of Aratsu Ohashi Bridge Tower", J. Structures and Materials in Civil Engineering, vol. 1 1986, pp 21-35, (in Japanese).
6) Tatumi, M., Akiyama, H., Kiyota, R., "Behaviour of Long Span Suspension Bridges under Strong Wind", Proceedings of 10th National Symposium on Wind Engineering, Tokyo, Dec. 1988, (in Japanese).
7) Honshu-Shikoku Link Bridge Authority : "Honshu-Shikoku Link Bridges - Details of Wind Tunnel Testing" (1980), with Explanatory Notes, June 1980, (in Japanese).
8) Japan Institute of Civil Engineers : "Details of the Aerodynamic Design of Akashi Straights Bridge", with Explanatory Notes (draft), March 1988.
9) Matsumoto, M., Shiraishi, H., and Fukui, Y., "Human Response against Bridge Vibration", Second East Asia - Pacific Conference on Structural Engineering & Construction, Chang Mai, 11-13 January 1989, (in Japanese).

Table 2.1 Direction-dependent Mean Profile Parameter α (wind speed v≧5m/s)

Wind Direction	NW-NNE	NE-ESE	SE-S	SW-WNW	WNW-E	ESE-W	All
No. of Data	4 628	1 352	2 685	1 363	5 658	4 405	10 063
α	0.234	0.186	0.106	0.230	0.227	0.149	0.193

Table 2.2 Mean Profile Parameter α (wind speed v≧10m/s)

Wind Speed	10	11	12	13	14	15	16	17	18	19	20	21	22
NW-NNE	0.272 (66)	0.272 (66)	0.260 (47)	0.255 (25)	0.223 (9)	0.176 (2)							
NE-ESE	0.218 (8)	0.218 (8)	0.218 (8)	0.218 (8)	0.218 (8)	0.217 (6)	0.193 (1)						
SE-S	0.133 (34)	0.133 (34)	0.133 (34)	0.133 (34)	0.133 (34)	0.130 (33)	0.126 (31)	0.129 (27)	0.122 (21)	0.121 (16)	0.124 (9)	0.123 (5)	0.110 (3)
SSW-WNW	0.235 (62)	0.232 (61)	0.231 (59)	0.226 (46)	0.223 (39)	0.191 (22)	0.179 (17)	0.162 (12)	0.168 (5)	0.175 (4)	0.171 (2)		
All	0.228 (170)	0.227 (169)	0.217 (148)	0.204 (113)	0.188 (90)	0.161 (63)	0.146 (49)	0.139 (39)	0.131 (26)	0.132 (20)	0.133 (11)	0.123 (5)	0.111 (3)

( ) : Number of Data

Table 2.3 Mean Gust Factor

		NW-NNE	NE-ESE	SE-S	SW-WNW	WNW-E	ESE-W	All
H= 10 m	No. of Data	11 148	5 674	5 536	2 825	15 891	9 401	25 292
	Gust Factor	1.53	1.49	1.36	1.54	1.52	1.42	1.48
H= 25 m	No. of Data	10 766	6 578	5 059	3 287	16 268	9 426	25 694
	Gust Factor	1.45	1.38	1.29	1.41	1.43	1.33	1.40

Table 2.4 Mean Angle of Wind Inclinatio (wind speed v≧5m/s)

Wind Direction	NW-NNE	NE-ESE	SE-S	SW-WNW	WNW-E	ESE-W	All
No.of Data	6 530	2 607	2 913	1 927	8 603	5 375	13 978
Inc. Angle (c)	0.55	1.78	2.00	1.48	0.87	1.76	1.21

Table 2.5 Recurrence of Wind Speed at Hight of 10m on Tokyo Port Reclaimed Land No.13 (m/s)

Return Period (year)		5	10	20	50	100	200
Point of Explanatory Valiable	Tokyo	27.8	31.4	38.4	39.1	42.3	45.6
	Yokohama	23.4	26.2	29.0	32.5	35.1	37.7
	Tokyo & Yokohama	28.4	32.1	35.6	40.1	43.5	46.8

Table 3.1 Generalized Mass in First Mode of Tower (Completed Stage)

Mode		Tower (ton)	Cable (ton)	Girder (ton)	Total (ton)	δ	$\frac{m \cdot \delta}{m_0}$
First	In-phase	1 445	3 021	661	5 128	0.020	43.64
	Out-phase	1 529	3 433	434	5 399		44.44
Second	In-phase	1 237	1 297	1 546	4 097		40.17
	Out-phase	1 354	1 780	3 928	7 073		71.81

δ :Logarithmic Decrement

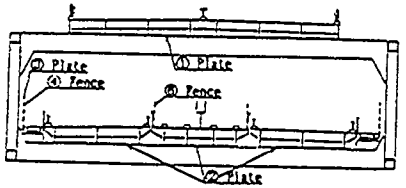
Table 4.1 Dimensions of Model

	Prototype Value	Required Value
Reduced Scale	1	1/66.7
Weight	41.539 t/m	9.346 kg/m
Polar Inertia	4882.3 tm²/m	24.72 kgcm²/cm
Bending Freq.	0.240 Hz	1.96 Hz
Torsional Freq.	0.421 Hz	3.44 Hz
Rate of Freq.	1.75 Hz	1.75 Hz
Design Wind Speed	67.36 m/s	8.25 m/s

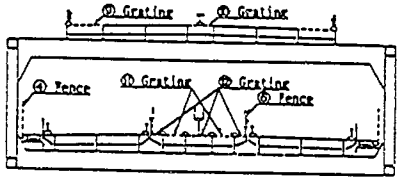
Table 4.2 Cases of Experiment with Various Attachments and by Improved Sections

Case	Plate under Deck		Side Walk			Loewr Deck Fence for Trains	Upper Deck		Gratings			
			Wind Fence Plate	Pence Hett.	Roof		Div. or Undiv.	Center Hett-ing	Upper Deck		Traffic Track	
	Upper	Lower							edge	center	in	out
	①	②	③	④	⑤	⑥	⑦	⑧	⑨	⑩	⑪	⑫
1	–	–	–	○	–	–	Undiv.	–	–	–	–	–
2	○	○	–	○	–	–	〃	–	–	–	–	–
3	○	–	–	○	–	–	〃	–	–	–	–	–
4	–	–	○	–	–	–	〃	–	–	–	–	–
5	–	–	–	○	–	○	〃	–	–	–	–	–
6	–	–	○	–	–	○	〃	–	–	–	–	–
7	–	–	–	○	–	○	〃	–	○	○	○	○
8	–	–	–	○	–	○	〃	–	○	○	–	○
9	–	–	–	○	–	○	〃	–	–	○	–	○
10	–	–	–	○	–	○	〃	–	○	○	–	–
11	–	–	–	○	–	○	〃	–	–	–	○	○
12	–	–	–	○	–	○	Div.	–	–	–	–	○
13	–	–	–	○	–	○	〃	○	–	–	–	○
14	–	–	–	○	○	○	〃	○	–	–	–	○

Case 1~6



Case 7~11



Case 12~14

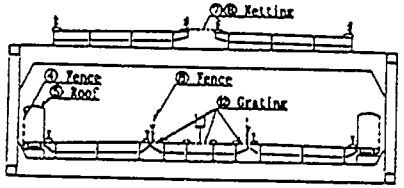


Table 5.1 Dimensions of Full Bridge Model

		Prototype Value	Required Value
Reduced Scale		1	1/70
Bridge Length		798.0 m	1140.0 cm
Tower Hight		119.0 m	170.0 cm
Truss Width		29.0 m	41.43 cm
Truss Hight		8.9 m	12.71 cm
Bending Freqency	1st mode (Asym.)	0.168 Hz	1.41 Hz
	2nd mode (Sym.)	0.239 Hz	2.00 Hz
Torsional Freqency	1st mode (Sym.)	0.419 Hz	3.51 Hz
	2nd mode (Asym.)	0.637 Hz	5.33 Hz
Logarithmic Decrement		0.03	0.03

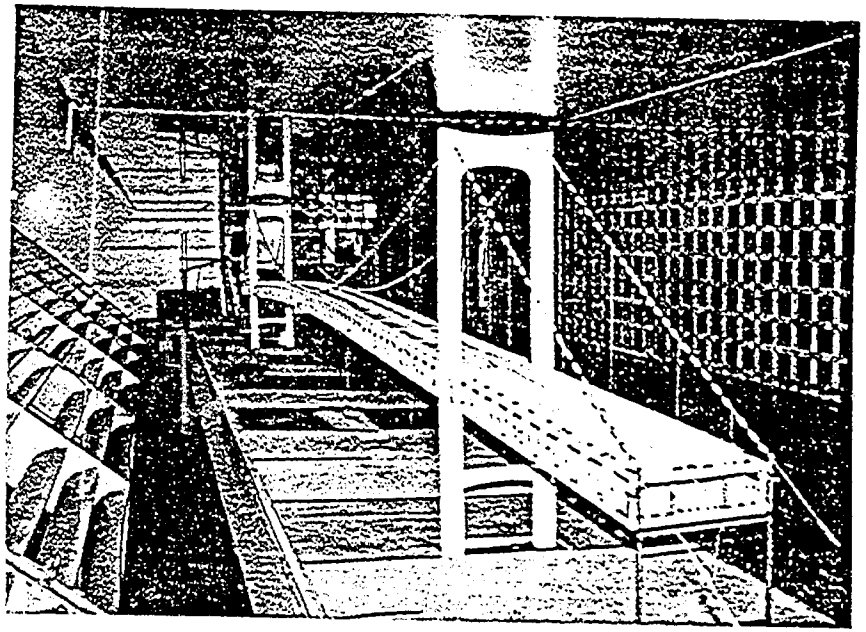
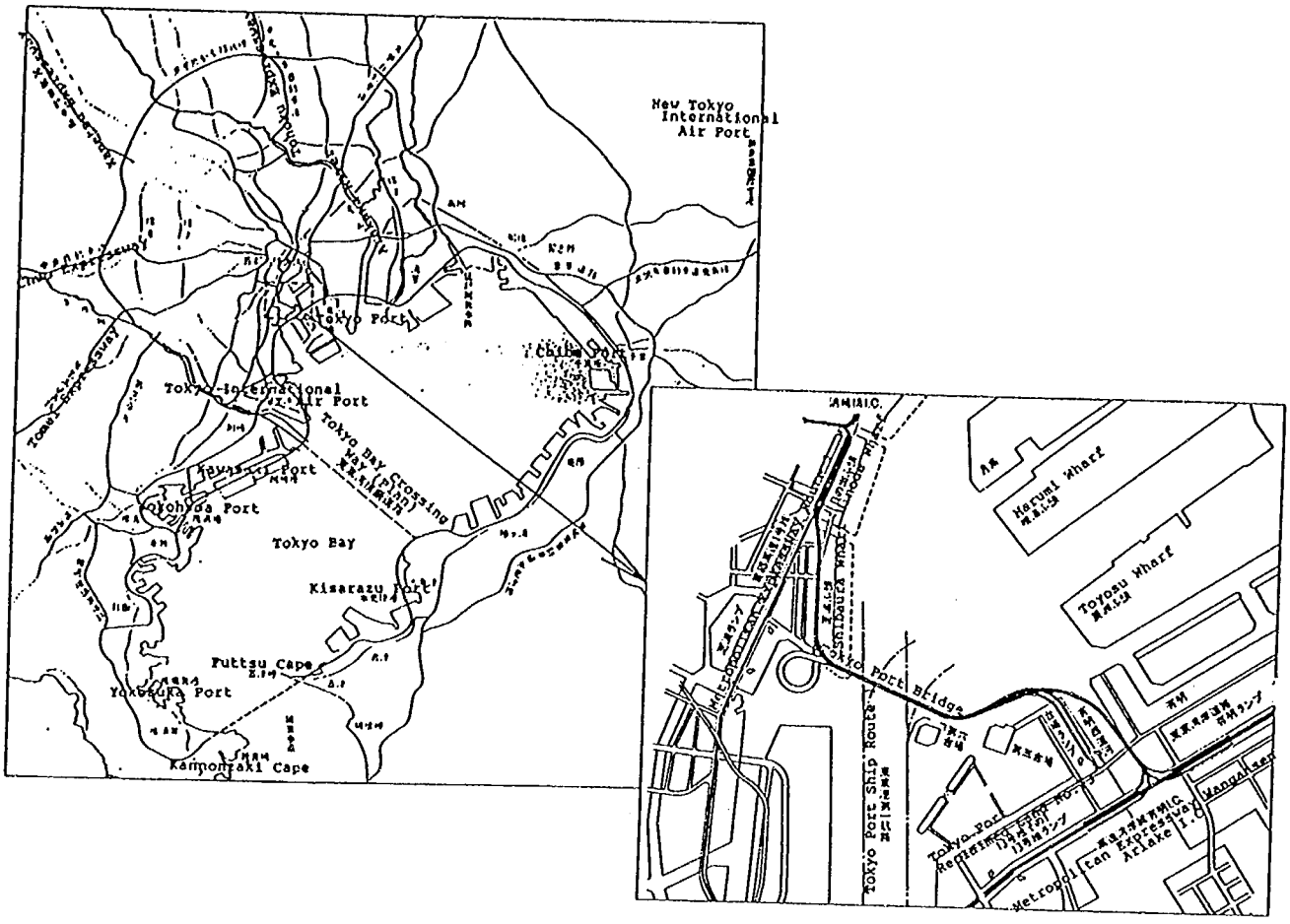
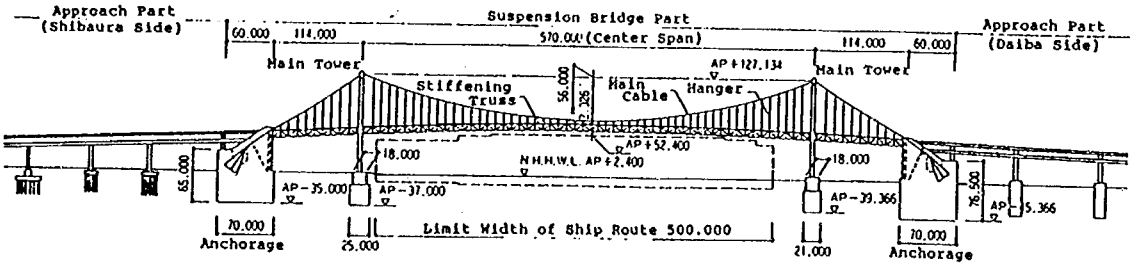
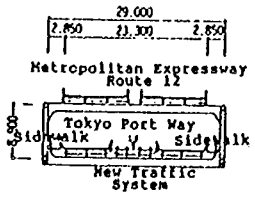


Photo 1 Full Bridge Model in Wind Tunnel

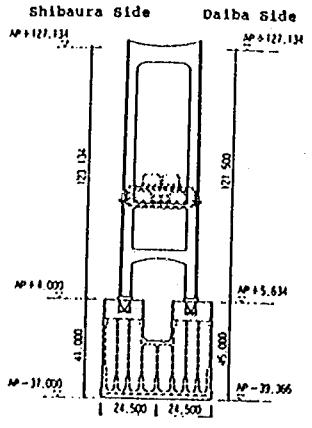




Elevation



Cross Section of Stiffening Truss



Cross Section of Main Tower

Fig. 1.1 General View of Tokyo Port Bridge

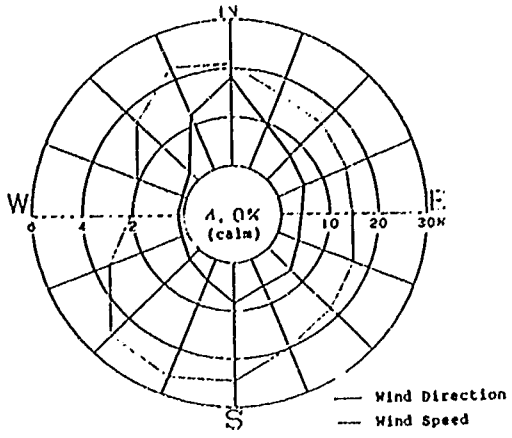


Fig. 2.1 Windrose at a Hight of 10 meters

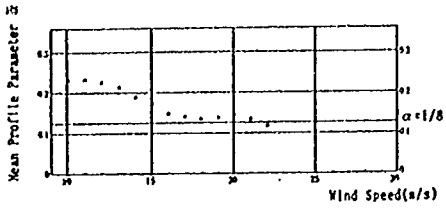


Fig. 2.2 Mean Profile Parameter α vs Wind Speed ($v \geqq 10$m/s)

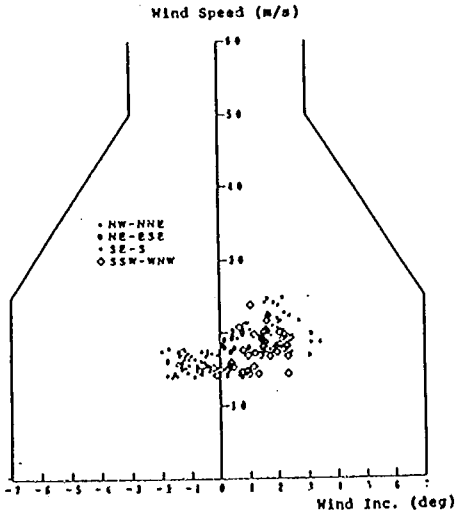


Fig. 2.3 Wind Inclination vs Wind Speed

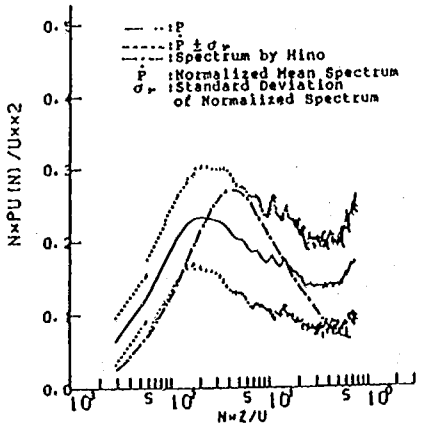


Fig. 2.4 Mean Power Spectra of Horinzontal Wind

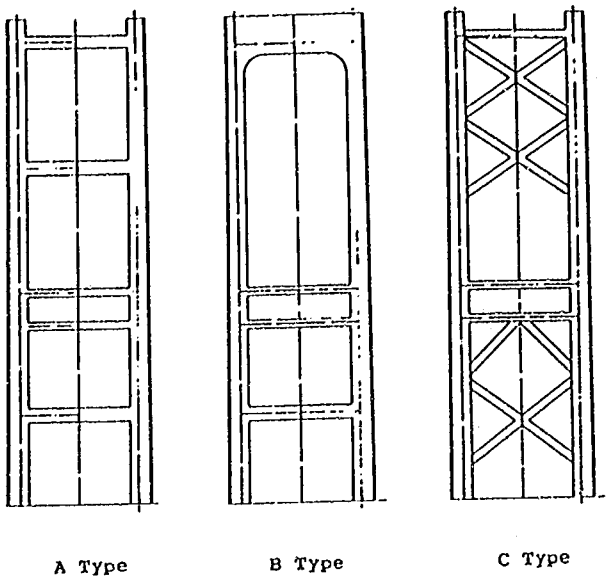


Fig. 3.1 Models of Tower

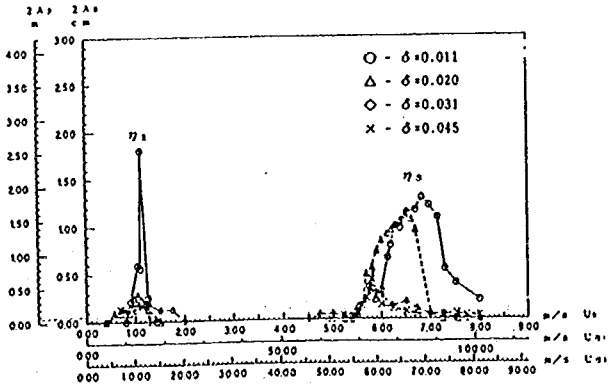


Fig. 3.2a Effect of Structural Damping on Out-Plane Bending Oscillation

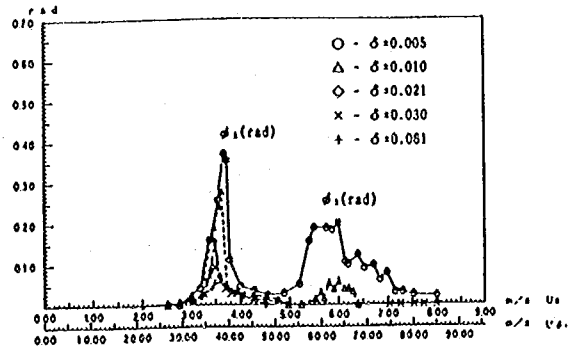


Fig. 3.2b Effect of Structural Damping on Out-Plane Torsional Oscilation

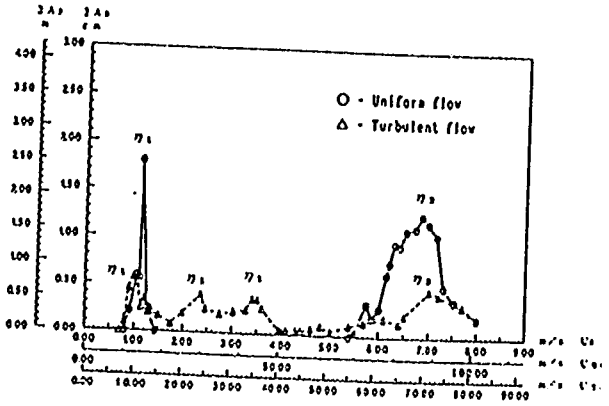


Fig. 3.3a Effect of Turbulence on Out-Plane Bending Oscillation

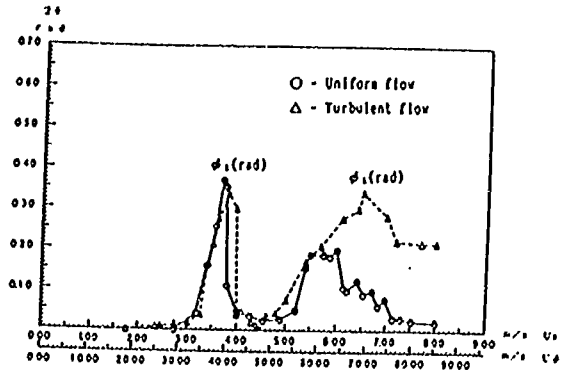


Fig. 3.3b Effect of Turbulence on Out-Plane Torsional Oscillation

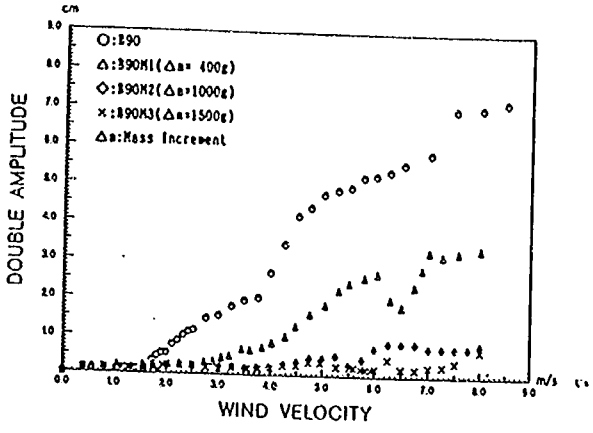


Fig. 3.4 Effect of Mass Damping on the Galloping of Tower

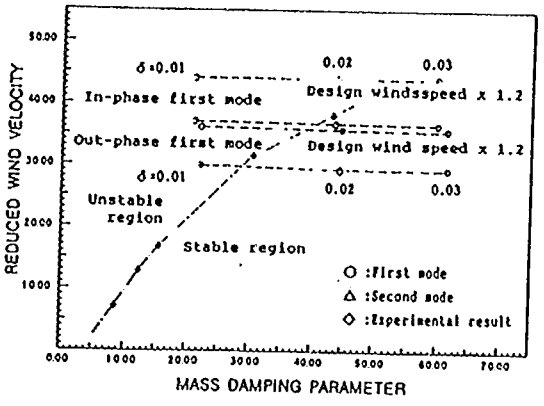


Fig. 3.5 Mass Damping Parameter vs Onset Wind Speed of the Galloping of Tower

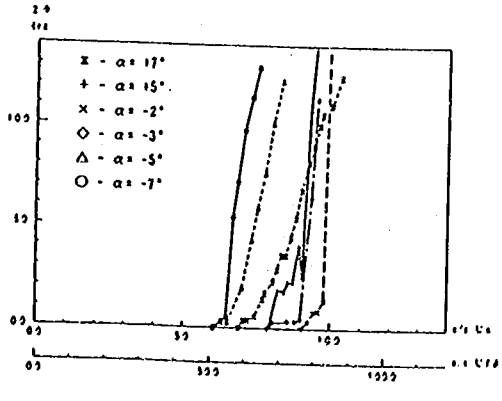


Fig. 4.1a Torsional Oscillation (case 1)

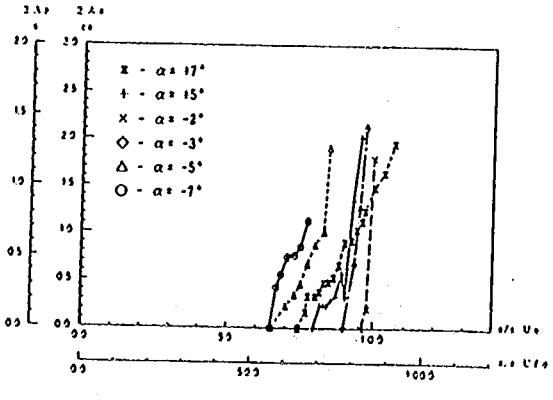


Fig. 4.1b Bending Oscillation (case 1)

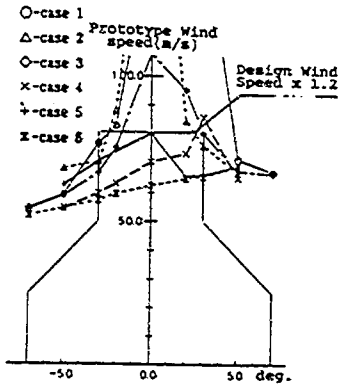


Fig. 4.2a Onset Wind Speed for Various Angles of Attack

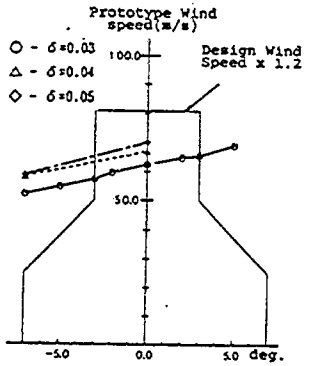


Fig. 4.2b Onset Wind Speed for Various Angles of Attack (case 6)

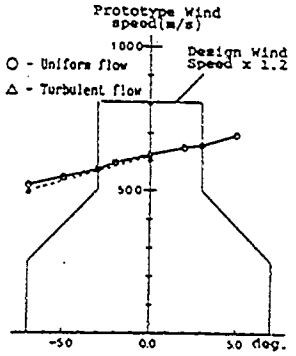


Fig. 4.2c Onset Wind Speed for Various Angles of Attack (case 6)

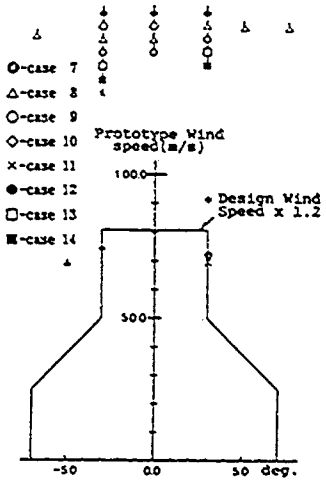


Fig. 4.2d Onset Wind Speed for Various Angles of Attack

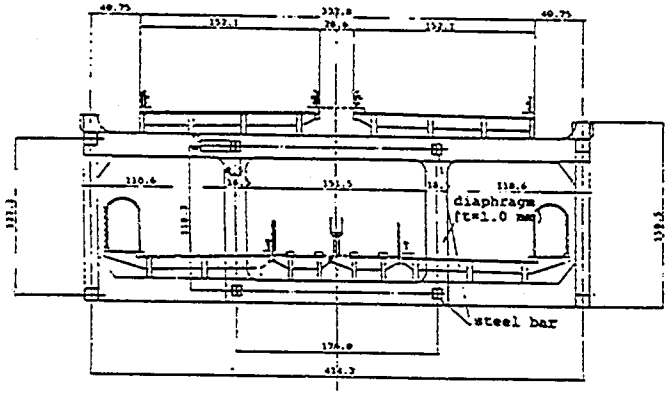


Fig. 5.1 Section of Full Bridge Model with 4 Steel Stiffening Bars

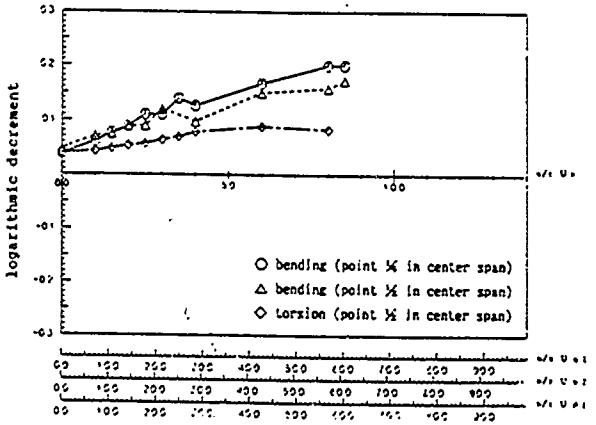


Fig. 5.2 Logarithmic Decrement vs Wind Speed

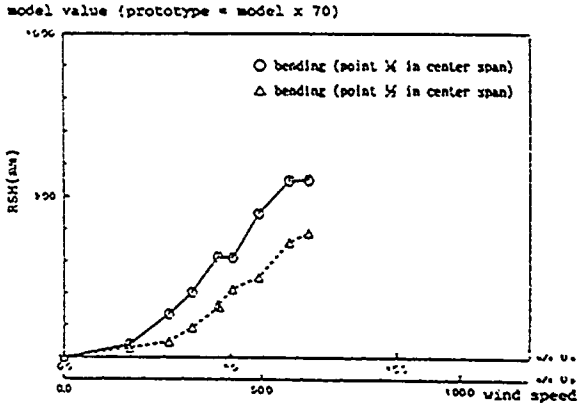


Fig. 5.3 Standard Deviation of Vertical Gust Response

AERODYNAMIC STABILITY OF THREE PARALLELLY LOCATED BOX-GIRDER BRIDGES

by

Shigeru Motoyama* , Mitsuru Hoshino **, Noboru Takahashi***
and Tadaaki Maruyama ****

ABSTRACT

The paper describes the aerodynamic stability and the corrective means of steel decked box-girder bridges forming part of the Kansai International Airport Access Bridge.

The bridge, having a span length of about 100 m, will be constructed by varying spatial locations of the three bridges in order to approach to the airport island. Consequently, it was thought that the mutual aerodynamic interference would make the response characteristics resulting from the dynamic aerial force become complicated. Then, by using two-dimensional models and a three dimensional model, a series of wind tunnel tests were conducted.

The test results and design contents of the dynamic vibration absorbers employed as the corrective means will be reported.

§ 1 INTRODUCTION

Kansai International Airport is an airport under construction about 5 Km offshore Sensyu, Osaka Prefecture. The only fixed-link connecting the airport with the main land is the Airport Access Bridge of 3750 m overall.

Box-girder bridge extending about 700 m in length from the airport island to constitute nearly one-fifth of the Access Bridge is being designed as a combination of two roadway bridges and one railway bridge.

Supported at about 100 m intervals, two roadway bridges run in parallel each other with the railway bridge in between, thus making up triple runs of bridges together. The railway bridge changes its relative elevation to the flanking roadway bridges along the way.

When designing the box-girder bridges, a series of wind tunnel tests was conducted using bridge models to evaluate the aerodynamic stability of the bridges, considering the fact that the box-girder bridges, though relatively short in its span, would essentially consist of the three bridges running side by side [1) , 2)] .

In this paper, the results of wind tunnel tests by use of two-dimensional models are demonstrated in § 2 and the test results by using a three-dimensional model with the three-span portions are demonstrated in § 3 to explain the effective antivibration device.

Furthermore, in § 4, an explanation is made to dynamic vibration absorber which is an antivibration device in a practical application.

---

* Managing Directer & Vice President, Kansai International Airport Company, Ltd. Japan
** General Manager, 2nd Engineering Department, ditto
*** Special Assistant to General Manager, ditto
**** Staff Engineer, ditto

§ 2 TWO DIMENSIONAL ELASTIC MODEL TEST

LIST OF SYMBOLS: B: breadth of girder, η : oscillating amplitude
α : attack angle (deree)
δ : logarithmic decrement of damping
V: wind speed
Ⓐ, Ⓑ, Ⓒ, Ⓓ: cross section of bridge (See Fig.1)

1. OUTLINE OF WIND TUNNEL TEST

Box-girder cross section models, 1/20 in scale, were each externally supported by springs, and their response to the air blown at them in the wind tunnel were measured. The models were tested singly or in combination of the three arranged side by side in four different relative positions (See Fig.1 Ⓐ, Ⓑ, Ⓒ, Ⓓ).

The test was carried out as per the flow chart of Fig.2.

In step-Ⅰ, models of original design was investingated to estimate aerodynamic stability both singly and in combination. Tested cross section were Ⓐ, Ⓑ, Ⓒ and Ⓓ, especially Ⓑ and Ⓓ, being unsymmetric in cant of deck, were tested in both wind direction.

In step-Ⅱ, aerodynamic stabilizer (plates on side surface of main girder) which can eliminate galloping oscillation was investigated. Tested cross section were Ⓒ and Ⓓ which was found to be the most unstable in this oscillation.

In step-Ⅲ, aerodynamic stabilizer (flaps and skirts on parapet) which can depress vortex-induced oscillation was investigated. Tested cross section was Ⓒ which was found to be the most unstable.

2. STABILITY OF ORIGINAL DESIGN (STEP-Ⅰ)

Before wind tunnel test, weight and vertical frequency were estimated for each bridge (See Table 1).

2.1 ISOLATED MODEL TEST

Each bridge, tested singly was unstable because of vortex-induced oscillation or galloping oscillation (See Fig. 3~Fig 5).

The roadway bridge oscillated slightly when wind speed was between 20 and 25 m/s. At higher wind speed, catastrophic oscillation occured (galloping oscillation).

The railway bridge experienced the same galloping oscillation at the lower wind speed (45 m/s).

2.2 COMBINED MODEL TEST

When the bridges were arranged side by side, the response characteristics changed (See Table 2).

Compared with Fig. 3~Fig. 5, it was assumed that the aerodynamic interference would vary according to the relative position of each bridge.

Section Ⓐ remained stable on both vortex-induced oscillation and galloping oscillation. Only the railway bridge (ⅱ) slightly oscillated at wind speed of 30 m/s.

Section Ⓑ remained nearly almost stable at the wind speed under 70 m/s, except that east-ward roadway bridge (ⅲ) oscillated in the wind speeds of 40 m/s ~50 m/s.

Section Ⓒ remained stable only on galloping oscillation, and its vortex-induced oscillation increased about three times than that in the isolated state.

it was when tested singly. The aerodynamic interference was found to vary according to the relative position of each bridge.

(3) As for the cross section in the original design, there is a possibility of vortex-induced oscillation at the lower wind speed, and galloping oscillation at higher wind speed.

(4) It was found that galloping oscillation of the three bridge cross sections arranged side by side could be controlled by providing appropriate damping plates on the sides of the main girder.

(5) It was found that vortex-induced oscillation of the three bridge cross sections arranged side by side could be controlled by installing the flaps and skirts.

On the basis of the preceding results, tests by using the three-dimensional elastic model were conducted as to the three-span portion.

§ 3 THREE-DIMENSIONAL ELASTIC MODEL TEST

1. OUTLINE OF WIND TUNNEL TEST

Before the commencement of the wind tunnel test, Table 6 indicates the results of vibration analysis of the three span portion, including the piers, in order to grasp the characteristics of vibration of the actual bridge. As their features, the outstanding vibration frequencies of both the roadway bridges are situated adjacent extremely to generate the coupled vibration.

A wind tunnel model (scale = 1/55) is shown in Photograph 1. The piers are modeled in a configuration with rigid rods inserted, following a vibration analysing model.

Furthermore, the aerodynamic stability was investigated with regard to the cross sections having damping plates for stabilizing galloping oscilattion, and also with regard to the cross sections provided additionally with flaps and skirts for stabilizing vortex-induced oscillation.

2. CHARACTERISTICS OF CROSS SECTION WITH DAMPING PLATES

Table 7 indicates the response characteristics against the horizontal wind flow in case of the structural damping, δ, of the model being adjusted to 0.03, 0.06, and 0.10. Catastrophic galloping oscillation at the higher wind speed was restricted, but, at the wind speed over 20m/s, vortex-induced oscillation of the respective vibration mode occurred almost continuously. Vortex-induced oscillation has a tendency to be stabilized by an increase in the structural damping and the turbulence of wind flow.

Shown in Fig. 9 is the relation between the structural damping in a uniform flow and the maximum response amplitude of vortex-induced oscillation of the respective mode.

In the response obtained by actuating the turbulent flow prepared by the use of the cascade damper method in the wind tunnel, [4] the amplitude of vortex-induced oscillation decreases, but buffeting oscillation resulting from the turbulence of wind flow has a tendency of increment at the higher wind speed.

Consequently, in order to asess aerodynamic stability of this section, it is necessary to evaluate vortex-induced oscillation depending markedly upon the structural damping and buffeting response at the high wind speed.

Section Ⓓ was unstable in both vortex-induced oscillation and galloping oscillation. The amplitude of vortex-induced oscillation increased three times than that in the isolated state and hard-type galloping oscillation occurred at higher wind speed.

In general, aerodynamic stability became gradually spoiled as the railway bridge (ii) went down from the level of roadway bridge at both side.

From this result, aerodynamic improvement should be given especially for cross section Ⓒ and Ⓓ.

In order to investigate mechanism of amplification of vortex-induced oscillation, additional test was carried out. Namely, with one or two models held fixed, the response of the rest of the models was measured.

The maximum amplitude measured of each bridge is indicated in Table 3. From this table, it is clear that oscillation of the upward-located roadway bridge (i) exerts the major effect of amplifying vortex-induced oscillation of the downward-located bridges (ii), (iii). And the vortex-induced oscillation of the upward-located roadway bridge (i) was amplified even when the downward-located bridge (ii), (iii) did not oscillate.

3. IMPROVEMENT OF STABILITY AGAINST GALLOPING OSCILLATION (STEP-II)

The original design, section Ⓓ, was unstable against the catastrophic, galloping oscillation. Therefore, further investigations were made to find out how to improve the stability.

3.1 ISOLATED MODEL TEST

In order to stabilize galloping oscillation, the authors investigated the use of damping plates on side surfaces of the girder [3]. Its size and location were parametricaly changed until galloping oscillation was eliminated (See Fig.6~Fig.8).

However, vortex-induced oscillation was amplified to about twice compared with the original design (c.f.Fig.3~Fig.5).

3.2 COMBINED MODEL TEST

Stability in combined state was investigated (See Table 4).

It was found that galloping oscillation was stabilized also in the combined state and the amplitude of vortex-induced oscillation was not amplified so much compared with the original design in combination (cf. Table 2).

4. IMPROVEMENT OF STABILITY AGAINST VORTEX-INDUCED OSCILLATION (STEP- III)

Vortex-induced oscillation changed according to the location of the bridges each other. Therefore, this test was carried out only with the three bridges in combination (See Table 5).

The relative location simulated the section Ⓒ, and a stabilizing device of flaps was added to the top of the bridge. And for the roadway bridge, with the solid parapet, the effect of an additional device of skirts was investigated.

5. TEST RESULTS

(1) Vortex-induced oscillation and galloping oscillation took place when tested singly.
(2) When tested in combination, with the three bridge cross sections side by side, however, aerodynamic interference was produced in each instance and the aerodynamic stability was found to differ from what

3. CHARACTERISTICS OF CROSS SECTION WITH DAMPING PLATES, FLAPS, AND SKIRTS

Table 8 indicates the same test results as those in 2. In case of the structural damping of 0.03, some amount of vortex-induced oscillation occurs at the low wind speed, but in case of the structural damping of 0.06, the oscillation is stabilized markedly. In case of the sturctural damping of 0.03, however, the action of the turbulent flow eliminates most of vortex-induced oscillation, and buffeting oscillation occurs only at the high wind speed.

So aerodynamic stability of this section is considered to be improved with them.

4. TEST RESULTS

From the preceding test results, the three-span portion of the present bridge is considered to require the stabilization by damping plates and the addition of structural damping, or by the aerodynamic stabilizer such as the installation of damping plates, flaps, and skirts.

§ 4 DESIGNING DYNAMIC VIBRATION ABSORBER

As the result of various kinds of investigation based on the preceding wind tunnel test results, it is determined that, as the antivibration device for aerodynamic stability, the present bridge is to be provided with dynamic vibration absorbers (also called tuned mass dampers) for adding the structural damping, and with damping plates. The reason why the method of flaps and skirts was not employed is that vibration absorbers are excellent in the aspects of the economical property and appearance.

Vibration absorbers employed will be described next.

1. CHRACTERISTICS OF DYNAMIC VIBRATION ABSORBERS [5]

For the purpose of simplification, noting the particular vibration mode to be suppressed, the bridge structure is expressed as an equivalent single-degree-of-freedom system each other. The equation of motion of the bridge with the vibration absorber can then be expressed as:

$$[M]\{\ddot{x}\} + [C]\{\dot{x}\} + [K]\{x\} = \{f\} \qquad ①$$

where

$$[M] = \begin{bmatrix} M_D & 0 \\ 0 & M_S \end{bmatrix} \quad [C] = \begin{bmatrix} C_D & -C_D \\ -C_D & C_D + C_S \end{bmatrix}$$

$$[K] = \begin{bmatrix} K_D & -K_D \\ -K_D & K_D + K_S \end{bmatrix} \quad \{x\} = \begin{Bmatrix} x_D \\ x_S \end{Bmatrix} \quad \{f\} = \begin{Bmatrix} f_D \\ f_S \end{Bmatrix}$$

M_D : absorber mass
M_S : generalised mass of bridge
C_D : damping of vibration absorber
C_S : equivalent damping of bridge
K_D : stiffness of vibration absorber
K_S : equivalent stiffness of bridge
X_D : displacement of absorber mass
X_S : displacement of bridge
f_D : external force on vibration absorber

f_S : equivalent external force on bridge

Eliminating the external force term in Eq.①, and substituting the following assumption

$$\{x\} = \{\phi\} e^{\lambda t} \qquad ②$$

where

$$\{\phi\} = \begin{Bmatrix} \phi_D \\ \phi_S \end{Bmatrix}, \quad \lambda = \mu + i\omega$$

into Eq.①, the eigen value λ and the vibration mode $\{\phi\}$,i.e. the characteristics of the vibration absorber can be obtained. Fig.10～12 show the results of the eigen value calculation, Where $h_D = C_D/2\sqrt{M_D K_D}$, $\omega_D = \sqrt{K_D/M_D}$, $\omega_S = \sqrt{K_S/M_S}$. The damping ratio h is obtained from the eigen value λ, as

$$h = \frac{-\mu}{\sqrt{\mu^2+\omega^2}} \qquad ③$$

In the figures, the smaller damping ratio h and the corresponding relative displacement mode $|\phi_D - \phi_S| / |\phi_S|$ are shown out of the two damping ratios and modes obtained from Eq.①. Fig.10, 11 shows that, as h_D is increased, $|\phi_D - \phi_S| / |\phi_S|$ will be kept nearly constant within the range of smaller h_D, while h will be increased almost proportionally. When h_D is further increased, $|\phi_D - \phi_S| / |\phi_S|$ will begin to decrease, and h will decrease inversely to the further increase of h_D, after reaching its maximum. Fig.12 shows the relation between h and ω_D / ω_S, incases where h_D takes the optimum value h_{DA} in Fig.10, 11 on condition of $M_D/M_S = 0.02$ and where h_D takes the excessively greater value h_{DB} in Fig.10, 11 on condition of $M_D/M_S = 0.05$. Assuming that the desired value h, for example, is more than 0.05 in Fig.12 (taking into consideration errors and variations in h_D, ω_D and ω_S in practical application) the latter's vibration absorber provides an allowable range of ω_D / ω_S about 3 times as large as that of the former's and restrains the amplitude of the absorber mass to about twice than that of the bridge corresponding to a decrease to about one fourth of the former's amplitude.

The vibration absorber reported herein belongs to the latter's type. Its characteristics are summarised, as follows:

(1) The absorber mass is capable of restricting its amplitude to nearly that of the bridge.
(2) There is little deterioration in the antivibration effect with changes in frequency of the vibration absorber or the bridge. This provides wider allowable error ranges of frequency to make for easier tuning and maintenance as well as greater structural safety.
(3) There is also little variation in the antivibration effect with changes in the damping ratio h_D of the vibration absorber. In addition, if h_D becomes smaller due to the deterioration of the absorber elements, etc., the amplitude of the absorber mass will become greater to increase the damping ratio h of the bridge inversely. This characteristic of the absorber also provides greater structural safety.

2. DESIGN OF VIBRATION ABSORBERS

On the basis of the wind tunnel test results, vibration absorbers were designed so that the logarithmic decrement of damping, δ, might be more than 0.10. On this occasion, the following requirements had to be met :-

(1) As the vibration absorbers are installed in the extremely narrow spaces in the box-girder bridges, due consideration should be taken that weights of vibration absorbers not hitting against the bridge

member in case of the vibration absober vibrating.

(2) In the B1 and B2 modes, the vibration frequencies are nealy equal each other. Compared with the installation of vibration absorbers corresponding to the respective mode, the vibration absorbers which actuate effectively to both B1 and B2 mode are more economical.

With regard to (1), the characteristics capable of accepting a small degree of the amplitude in the preceding 1.(1), are utilized. With regard to (2) also, the characteristics of the scope of vibrations in the preceding 1.(2) being obtained widely are utilized effectively.

As the investigation results, the installation places and types of vibration absorbers have become as shown in fig.13.

In addition, Table 9 indicates the particulars of vibration absorbers of various types. Furthermore, the appearances of the vibration absorber are indicated in Fig.14. The vibration absorber consists of one weight, two coil springs, and two oil dampers. This device is installed on the lateral rib in the box-girder bridge, and it vibrates in the vertical direction, in case of the bridge vibrating. The adjustment of the vibration frequencies is executed with the weight shifted on either side.

§ 5 CONCLUSION

As described above, the wind tunnel tests by use of two-dimensional and three-dimensional models were executed to investigate the aerodynamic stability of box-girder bridges intended for the triple runs of bridges in parallel in the Kansai International Access Bridge. On the basis of these test results, the installation of damping plates and dynamic vibration absorbers was determined as an antivibration device. Of them, the design outline of the dynamic vibration absorbers was introduced.

The present bridge and dynamic vibration absorbers are under fabrication now and they are scheduled to be erected in the next spring. After erection, vibration experiments will be executed for the confirmation of characteristic performances of the dynamic vibration absorbers. The results thereof will be reported on another occasion.

Finally, the authors would like to thank MITUSBISHI HEAVY INDUSTRIES,LTD. who has taken the design and fabrication of the wind tunnel test and dynamic vibration absorbers.

REFERENCES

1) Johns, D.J.1982, "Wind Tunnel Tests of a Twin-Deck Bridge Model" Int. Conf. on Flow Induced Vibrations In Fluid Engineering.
2) Shiraishi,N., Matsumoto,M., Shirato,H. 1986, "On Aerodynamic Instability of Tandem Structure" J.of Wind Eng. and Ind. Aerodynamics, vol.23.
3) Egusa,T., Saito,T., Abiru,H., Sasaki,N. 1988, "Stability of Bridge Against Wind (2) " Mitsubishi Heavy Industries, Ltd. Technical Review, vol.25 No.1.
4) Sakata,H., Watanabe,T., Saito,T., Honda,A. 1987, "Stability of Bridges Against Wind (1) " Mitsubishi Heavy Industries, Ltd. Technical Review, vol.24 No.4.
5) Abiru,H., Matsumoto,T. 1988, "Prevention of Induced Vibration of Steel Chimney by Heavily Damped Vibration Absorbers" Pre-print of 6-th International Chimney Conference, Brighton-England.

Table 1 Weight and virtical frequency of each bridge

Bridge \ Section	Ⓐ	Ⓑ	Ⓒ	Ⓓ
Road way bridge	9.60 (ton/m) / 1.232 (Hz)	10.0 (ton/m) / 0.754 (Hz)	10.0 (ton/m) / 0.890 (Hz)	←
Rail way bridge	17.64 (ton/m) / 1.226 (Hz)	18.33 (ton/m) / 0.833 (Hz)	18.13 (ton/m) / 0.907 (Hz)	←
span length	90 m	2 @ 109 m	3 @ 109 m	

Table 2 Response of each bridge tested in combination

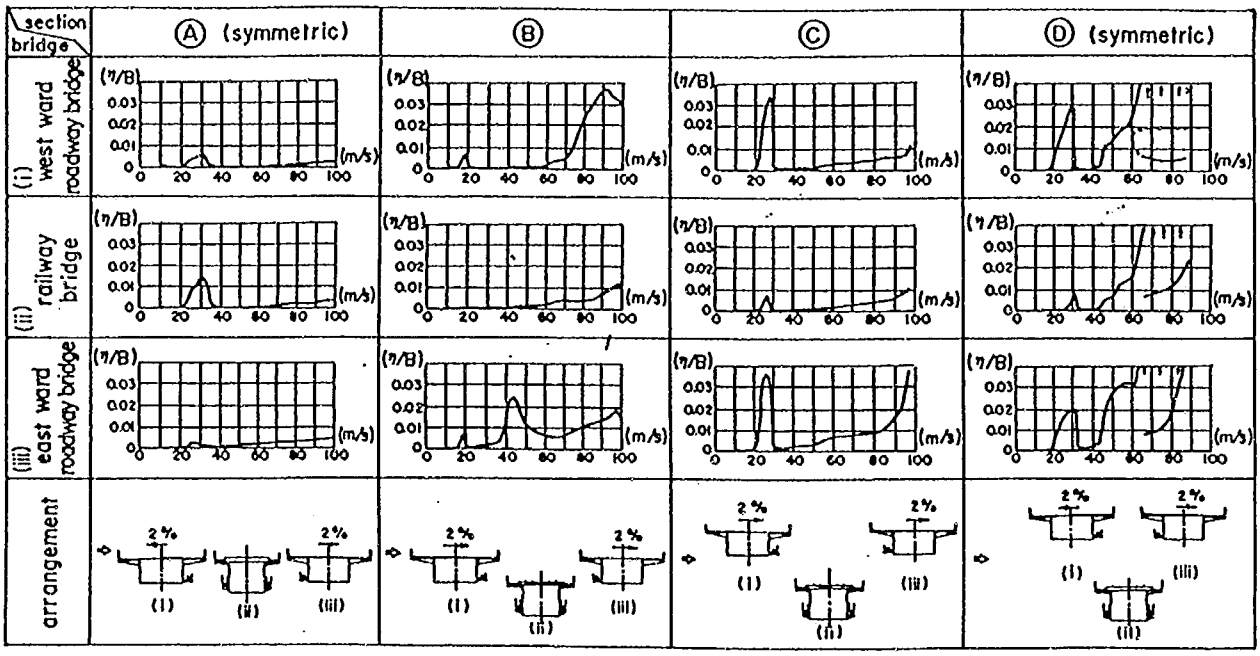


Table 3 Maximum amplitude and wind speed of vortex-induced oscillation (section Ⓒ, $\alpha = 0°$, $\delta = 0.03$)

MEASURED BRIDGE \ FIXED BRIDGE	NO (FREE)	(i)	(ii)	(iii)	(i) + (ii)	(ii) + (iii)	(i) + (iii)
(i)	500 mm (27 m/s)		509 mm (28 m/s)	533 mm (29 m/s)		534 mm (28 m/s)	
(ii)	81 mm (27 m/s)	36 mm (23 m/s)		92 mm (28 m/s)			41 mm (23 m/s)
(iii)	532 mm (26 m/s)	198 mm (24 m/s)	521 mm (26 m/s)		116 mm (23 m/s)		

Table 4 Response of improved bridges tested in combination ($\alpha = 0°$, $\delta = 0.03$)

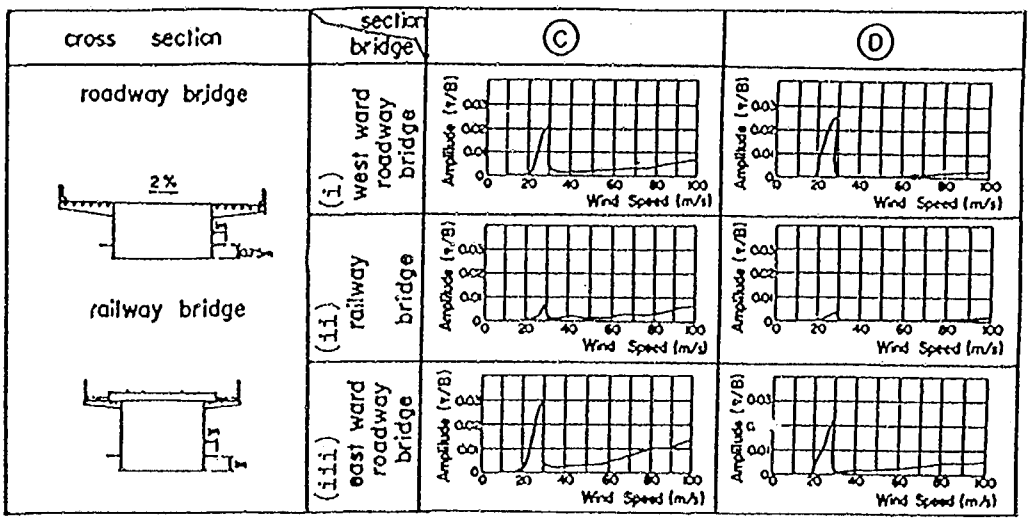


Table 5 Response of improved bridges tested in combination ($\alpha = 0°$, $\delta = 0.03$)

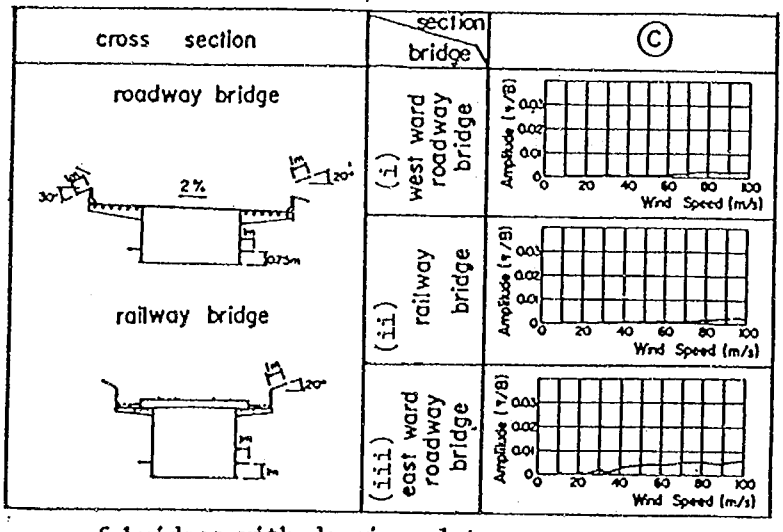


Table 7 Response of bridges with damping plates ($\delta = 0.03, 0.06, 0.10$)

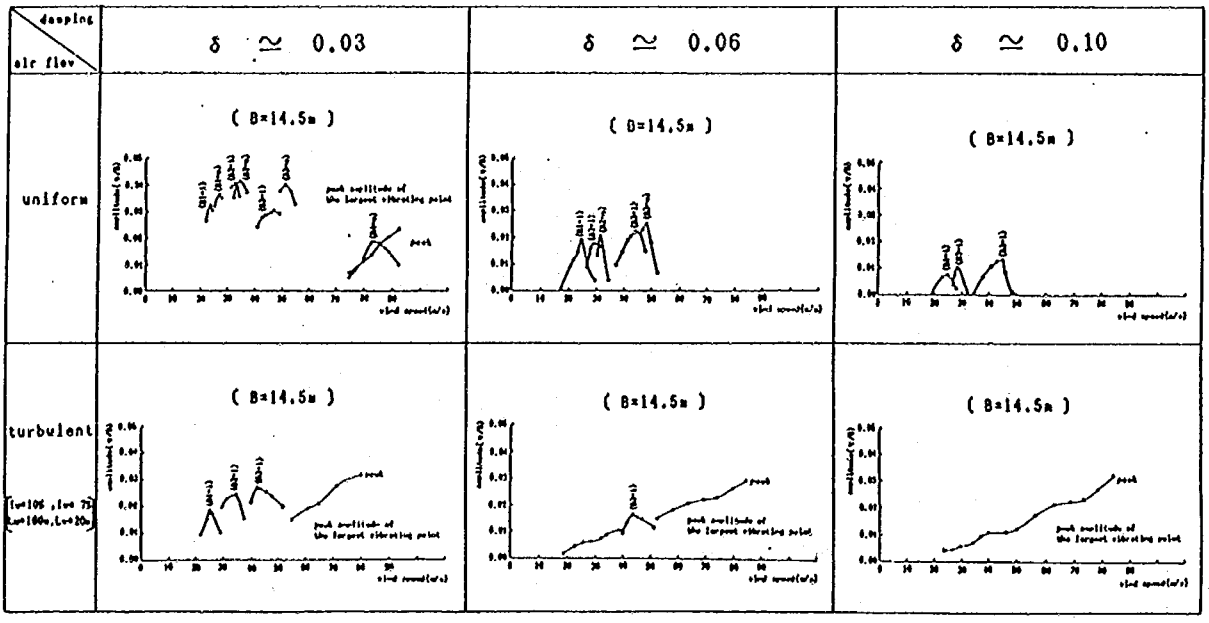
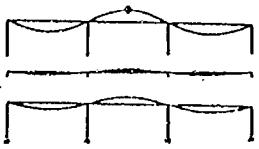
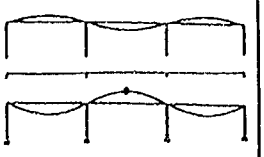
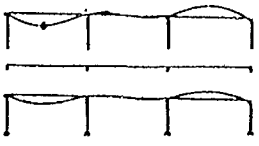
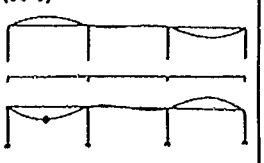
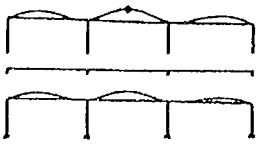
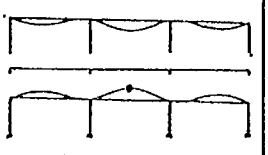
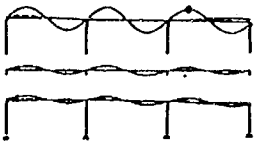
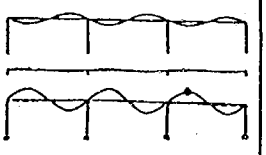


Table 6 Results of vibration analysis of three span portion

mode \ phase of both roadway bridge	in-phase	out of phase
B 1	(B1-i)  Fp=0.774Hz Fn=4.870Hz	(B1-o)  Fp=0.780Hz Fn=4.987Hz
B 2	(B2-i)  Fp=0.999Hz Fn=6.340Hz	(B2-o)  Fp=1.014Hz Fn=6.420Hz
B 3	(B3-i)  Fp=1.439Hz Fn=8.434Hz	(B3-o)  Fp=1.468Hz Fn=8.690Hz
B 4	(B4-i)  Fp=2.978Hz Fn=16.90Hz	(B4-o)  Fp=2.984Hz Fn=17.76Hz

note1) upper bridge : west word roadway bridge
middle " : railway bridge
lover " : east word roadway bridge

note2) ● : measuring point of vibration
Fp : frequency of prototype bridge
Fn : frequency of model

Table 8 Response of bridges with damping plates, flaps, and skirts ($\delta = 0.03,\ 0.06$)

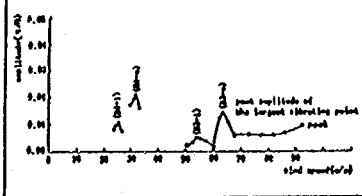
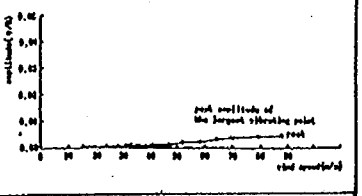
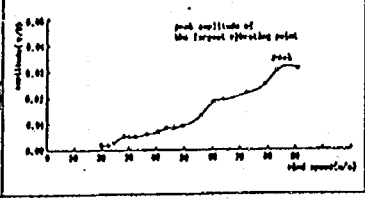
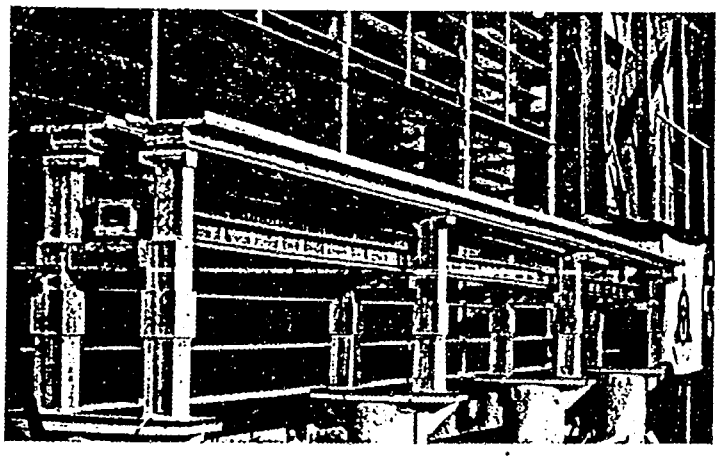
air flow \ damping	$\delta \simeq 0.03$	$\delta \simeq 0.06$
uniform	(B=14.5m) 	(B=14.5m) 
turbulent [Iu=10% ,Iv=7% Iw=16% ,L=20m]	(B=14.5m) 	

Table 9 Paticulars of dynamic vibration absorbers

	TYPE A	TYPE B	TYPE C	TYPE D
WEIGHT (TON)	7.5	8.0	10.4	8.0
Lk (mm)	1167	1902	1400	2012
Lc (mm)	514	595	567	641
FREQUENCY (HZ)	0.76	1.20	0.83	1.38
VIBRATION MODE	B1,B2 MODE	B3 MODE	B1,B2 MODE	B3 MODE
KIND OF BRIDGE	ROAD-WAY BRIDGE		RAIL-WAY BRIDGE	

Photograph 1 Three dimensional elastic model



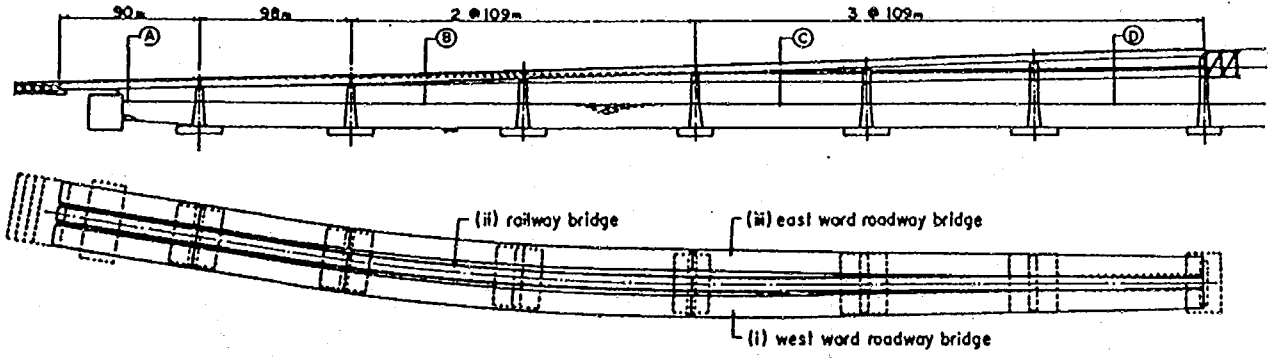


Fig. 1 Side-view & plane-view of box-girder bridges

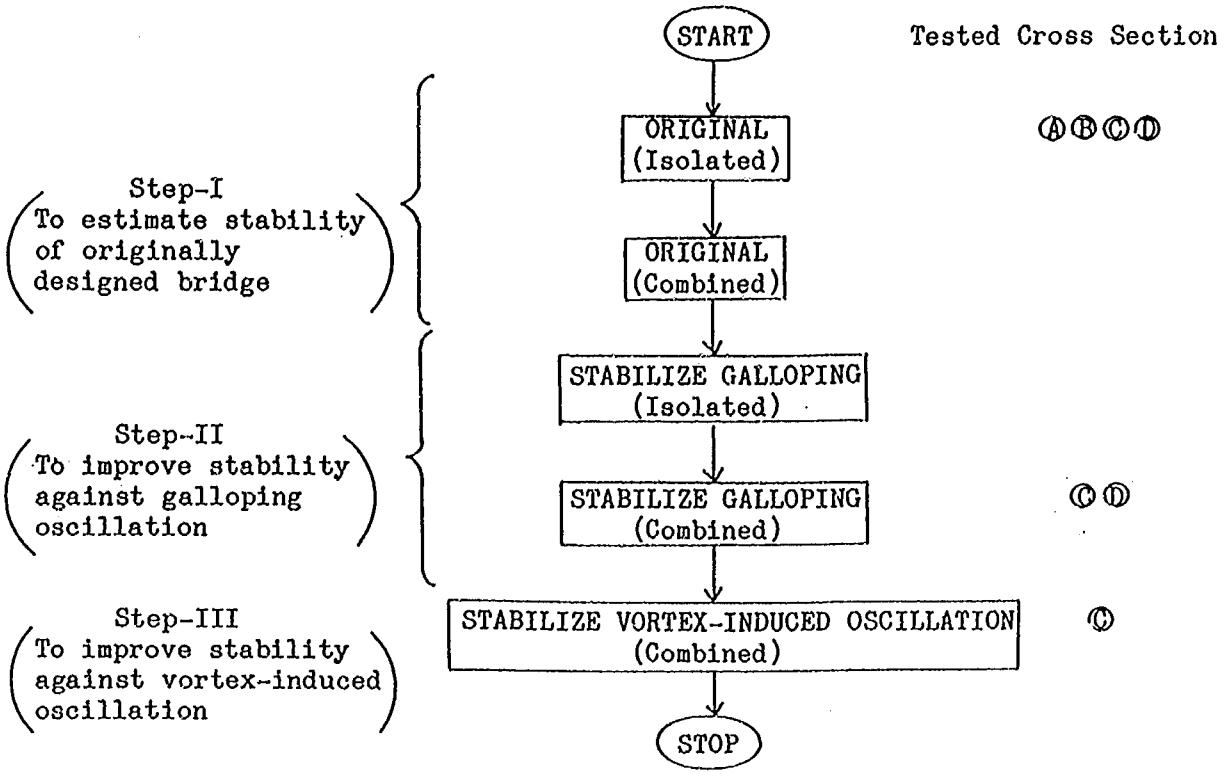


Fig. 2 Flow diagram of wind tunnel test

ORIGINAL

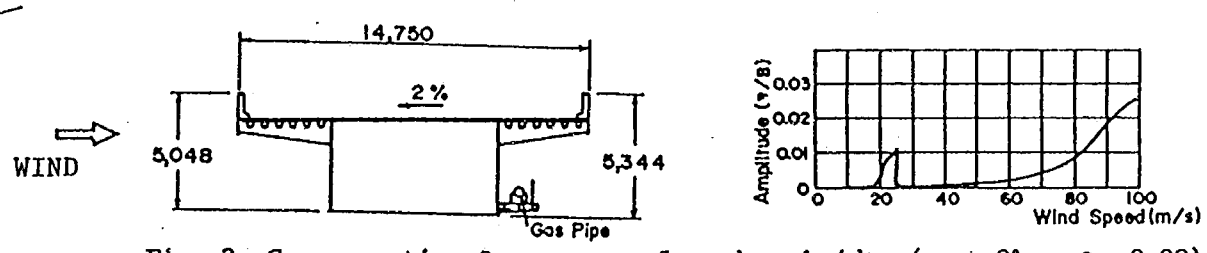


Fig. 3 Cross section & response of roadway bridge ($\alpha = 0°$, $\delta = 0.03$)

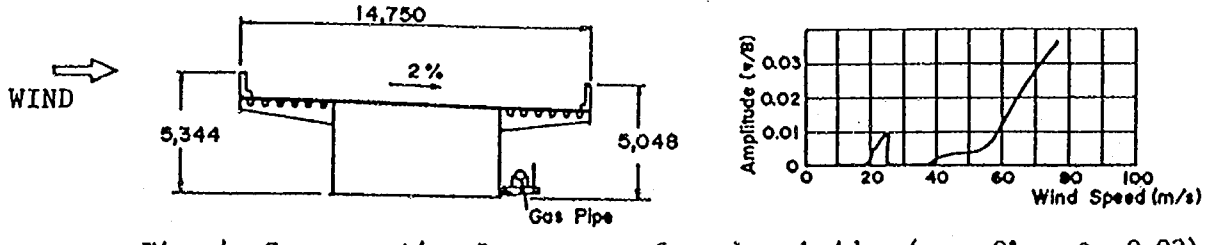


Fig. 4 Cross section & response of roadway bridge ($\alpha = 0°$, $\delta = 0.03$)

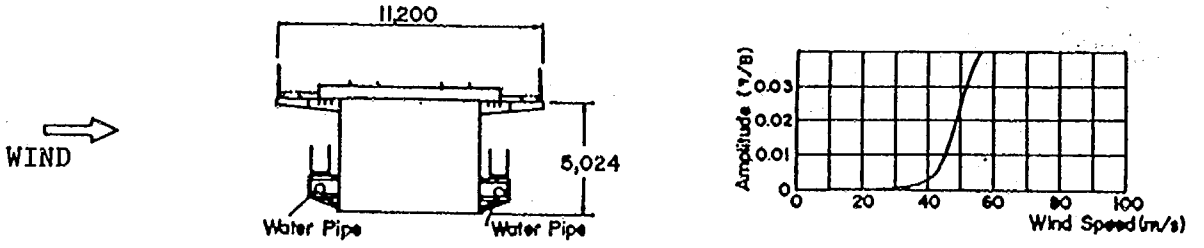


Fig. 5 Cross section & response of railway bridge ($\alpha = 0°$, $\delta = 0.03$)

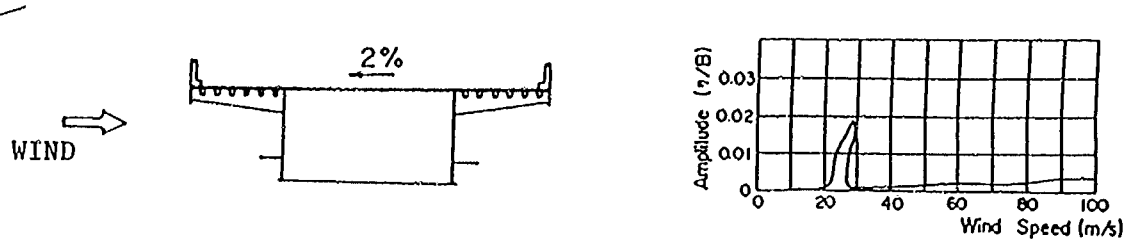


Fig. 6 Improved cross section & response of roadway bridge
($\alpha = 0°$, $\delta = 0.03$)

IMPROVED

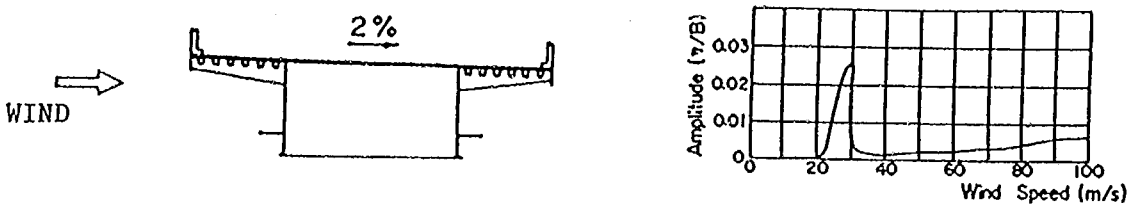


Fig. 7 Improved cross section & response of roadway bridge
($\alpha = 0°$, $\delta = 0.03$)

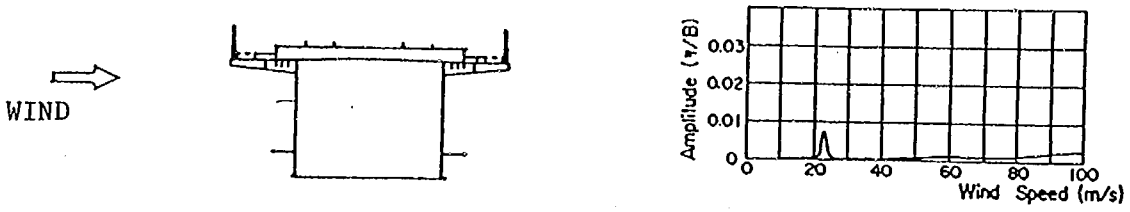


Fig. 8 Improved cross section & response of railway bridge
($\alpha = 0°$, $\delta = 0.03$)

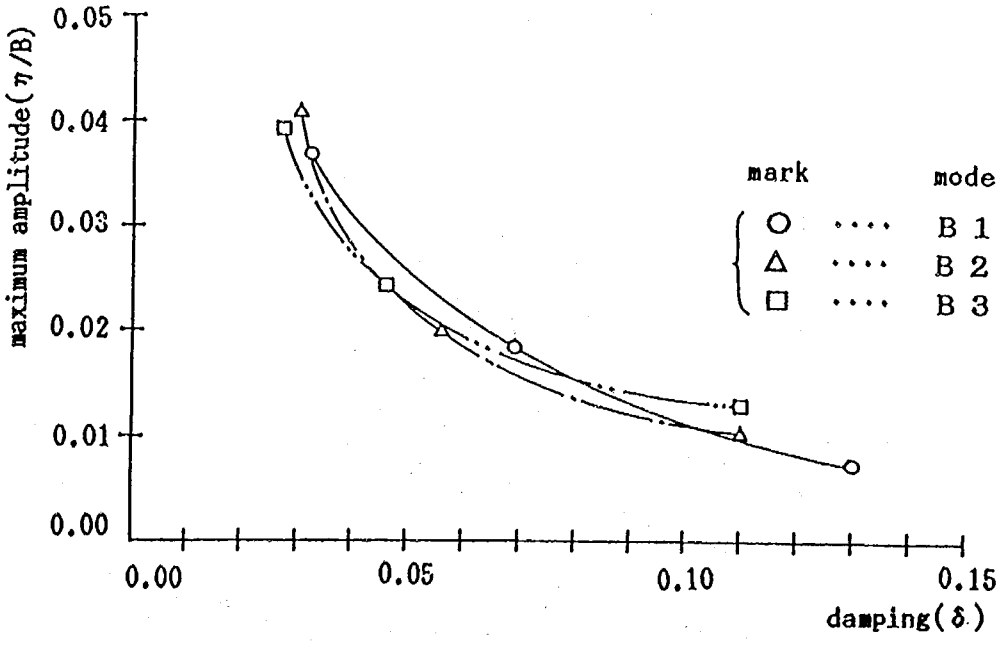


Fig. 9 Relation between structural damping & response amplitude

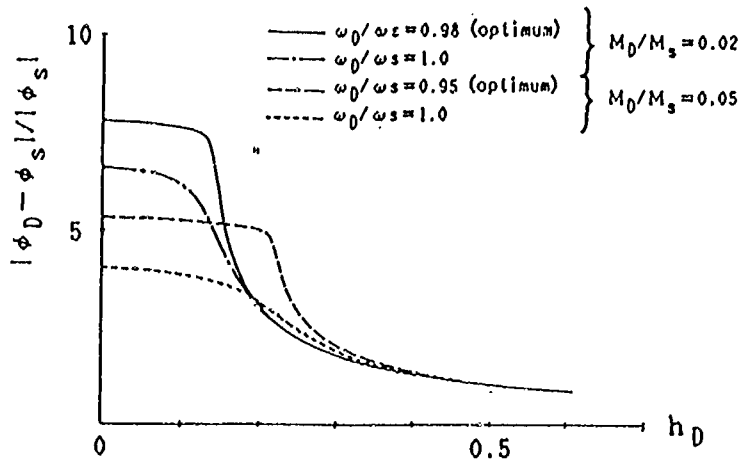


Fig. 10 Relation between $|\phi_D - \phi_S| / |\phi_S|$ & h_D

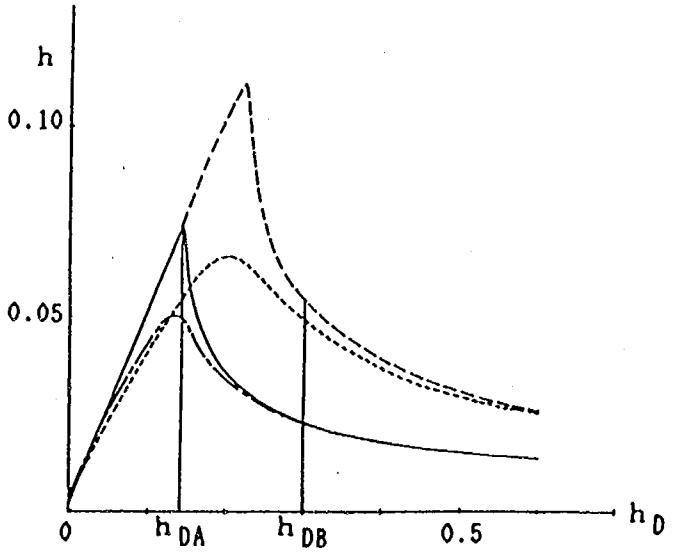


Fig. 11 Relation between h & h_D

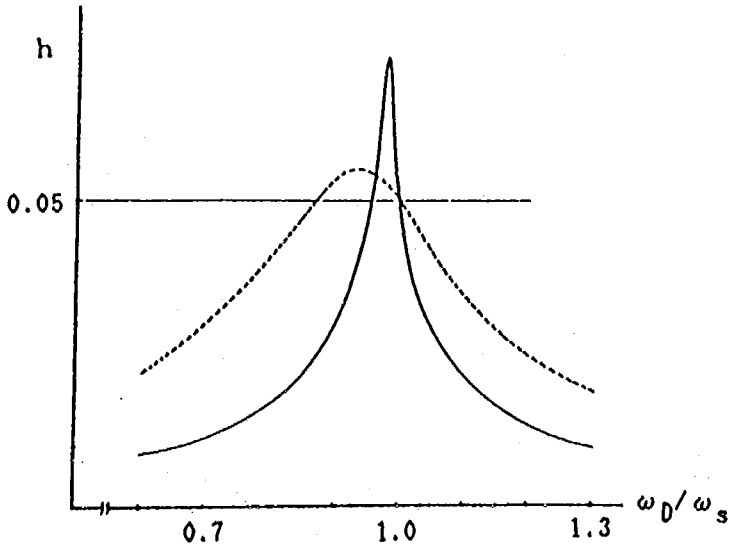


Fig. 12 Relation between h & ω_D / ω_S

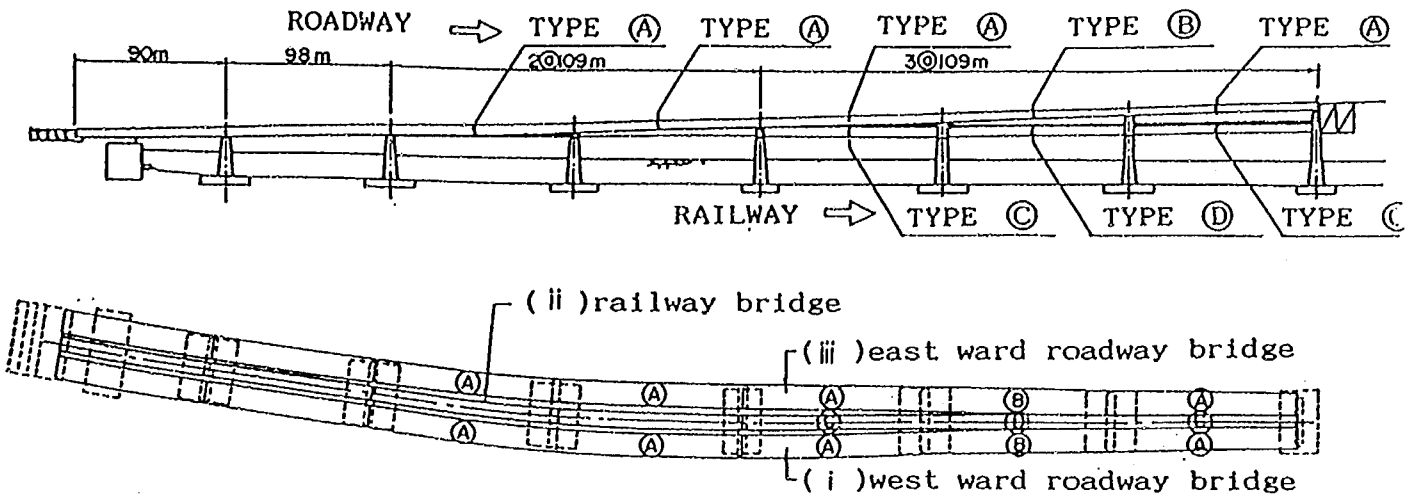


Fig. 13 Installation places & types of dynamic vibration absorber

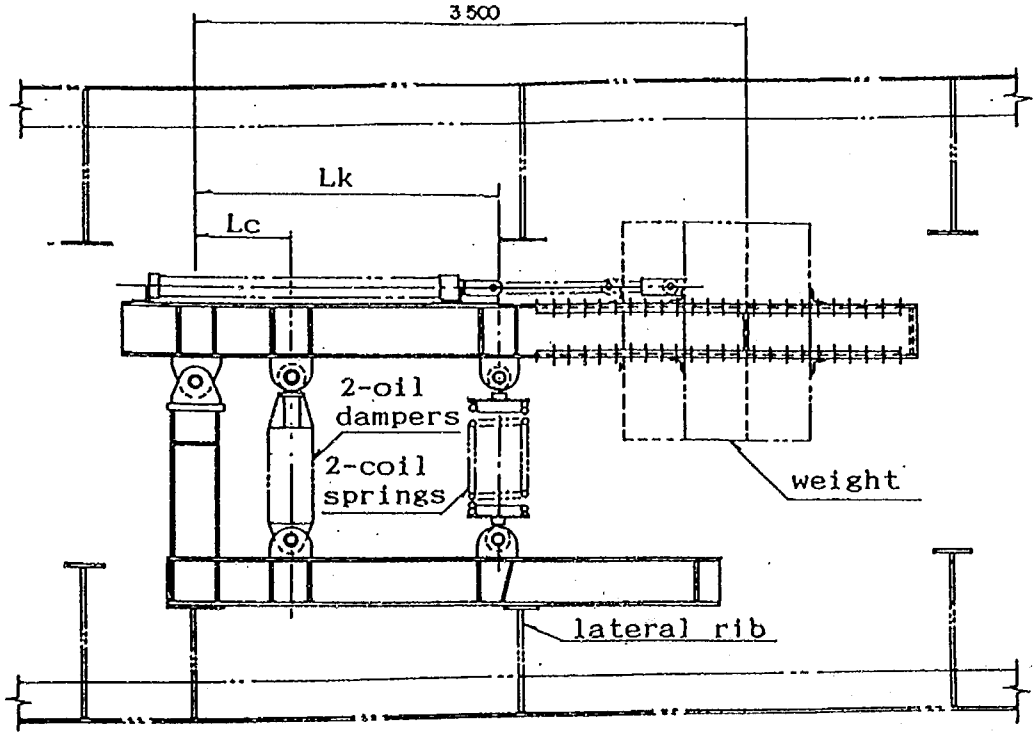


Fig. 14 Outview of dynamic vibration absorber

(6) Session 6

Wednesday, May 10, 1989 Place: International Conference Room (8F) PWRI

SESSION 6: BRIDGE CONSTRUCTION(1) 9:00am~10:15am
(Co-Chairman: M. Okahara, H. Seible)

(15) H. J. Farran※ : Current Research on Cable-Stayed Bridges at Caltrans
(9:00am~9:20am)

(16) N. Yoshikawa, I. Sugiyama and F. Hakamada※ : A Study on Design Method of Nielsen-Lohse Bridge
(9:20am~9:40am)

(17) H. E. Waldner and J. M. Kulicki: Quality Control Testing for Construction of Cable-Stayed Bridge at Quency, Illinois
(9:40am~10:00am)

DISCUSSION(6)
(10:00am~10:15am)



CURRENT RESEARCH ON CABLE-STAYED BRIDGES AT CALTRANS

By

Dr. H.J. Farran

California State Polytechnic University

Pomona, California 91768-4064

U.S.A.

Introduction

The purpose of this report is to present a comprehensive document on cable-stayed bridges that incorporates prestressed concrete segmental construction. This report presents the basic fundamental theory required to understand the complex procedures involved in the analysis and design of cable-stayed bridges as well as segmental construction. As part of the implementation of the research done at various Universities across the United States, in particular the research done at the University of Pittsburgh, and the University of California at Berkeley, this report contains a study of various structures that were studied in an attempt to arrive at a defense of the most logical geometrical configuration for a certain bridge. The support material presented also provides the engineer with a ready reference source that eliminates the exhaustive search for textbooks and concentrates on the application of various concepts of structural analysis to cable-stayed bridges as well as segmental structures.

It is imperative to note that the concepts of cable-stayed bridges as well as segmental structures represent the state of the art in the Civil Engineering profession today. In Europe, Germany and France have occupied the positions of leadership in cable-stayed bridge technology as well as precast prestressed segmental construction. A significant number of bridges of various geometrical configurations have been built and are currently in the design stage in many countries around the world. In the United States, there are many bridges proposed by various highway departments and consultants calling for cable-stayed as well as segmental construction. This new technology emphasizes material optimization but might present the contractor with complex and unconventional techniques. It is hoped that in the future we shall witness a compromise that advocates the concepts of economy, mass production as well as construction feasibility.

Cable-Stayed Bridges

There are basically 2 types of cable-supported structures: The suspension type and the cable-stayed type. Suspension bridges are utilized for very long spans and the support system consists of a major cable and a set of vertical suspenders that transmit the load from the roadway or deck to the parabolic profile cable. The main cable is a relatively flexible structure whose shape is dependent on the load as well as the position of the load. If the cable is loaded by a uniformly distributed load that essentially consists of the self weight of the strands, the cable acquires a characteristic shape as known as the catenary. The catenary is similar to the parabolic profile but it does not coincide exactly with the parabolic profile. The United States has impressive long span suspension bridges that have earned a world-wide reputation for elegance and beauty everywhere. The Golden Gate Bridge as well as the Oakland Bay Bridge are notable examples of such structures in the State of California. For long span bridges, dead loads constitute a significant portion of the design loads, thus a relatively light material is advocated like steel. The vertical suspenders in a suspension bridge are located at short equal intervals along the main cable profile.

The concept of cable-stayed bridges is not a new one. Engineers have indeed designed such structures back in the 18th and 19th centuries. The failure of a few cable-stayed structures in Europe as well as the United States resulted in a delay in the implementation of the concept until the 20th century. Early engineers utilized chains and high strength bars for the stays. The failure of 2 bridges, one in the United Kingdom and another in Germany caused a lot of engineers to go back to the concept of designing with suspension type systems. The truth of the matter is that methods of structural analysis as well as material behavior are not very well understood. Roebling used cable-stayed design as well as suspension designs for the Niagara Falls Bridge as well as the Brooklyn Bridge and the Old St. Clair bridge in Pittsburgh. Suspension systems and cable-stayed systems are not a very efficient combination. Some engineers advocate the use of cable-stays as a backup system in case of failure.

The modern concept of cable-stayed bridges started in Germany in the early fifties. Germany, after the second World War, found itself in need of many bridges as part of a plan to rebuild the destroyed transportation system. Materials were in short supply, and the German engineers had to use elaborate mathematical analysis and models to save on material costs. This was the time when the concepts of the orthotropic bridge deck systems came about. Cable-stayed bridges utilize taut and relatively inflexible cable supports at several points along the span length of the deck. The cables are inclined to the horizontal position. On many bridge design alternatives in the United States engineers decided to select a cable-stayed system to reduce the amount of steel needed to erect cantilever truss

systems as well as to minimize the costs of maintenance, inspection, and rehabilitation. One of the advantages of a cable-stayed system is the significant reduction in design moments compared to conventional orthotropic type designs. It is to be noted that most of the failures of earlier designs were attributed to the use of timber, round bars, as well as chains for the cable-stays. The performance of such elements as structural members under tensile loads is indeed very poor. The German engineers introduced the modern concept of cable-stayed bridges to improvise economy, ease of fabrication, erection, as well as aesthetics.

The cable-stayed design concept is not new to the United States. Many bridges were built in the State of Washington, few of which had problems. In 1972 many bridges were proposed for various locations across the country. The selection of a bridge type for a certain site is an art as well as a science. The Pasco-Kennewick inter-city bridge in the State of Washington was designed by Arvid Grant and Associates of Olympia, Washington. Another bridge designed by the same firm appears in Huntington, West Virginia over the Ohio River. In the State of Florida the Sunshine Skyway Bridge near Tampa has been designed by Figg & Muller Engineers, Inc. The Neches River Bridge in the State of Texas is also designed by Figg & Muller, Engineers, Inc. Many other bridges are proposed for locations in Virginia, Florida, Texas, South Carolina and Georgia. It is very possible that such bridges are very competitive when compared to other alternatives in the 600 to 1200 feet span range. Cable-stayed bridge designs are currently contemplated for the Houston Ship Channel in Texas, the Talmadge Memorial Bridge in Georgia, and the Weirton-Steubenville bridge over the Ohio River and the Cooper River Bridge in South Carolina. Some of the consulting firms involved are: Howard Needles Tammen & Bergendoff, Modjeski & Masters, Figg & Muller, Engineers, Inc., Michael Baker Jr., Inc., and Greiner Engineering Sciences, Inc.

Cable-Stayed Bridge Configuration

Cable Stayed bridges are ideal for spanning wide rivers and deep valleys. They are also viable solutions in spanning wide interstate highways for vehicles as well as pedestrians. Many span arrangements are possible. Three basic configurations exist: the 2-span symmetrical and asymmetrical, the 3-span, and the multiple spans. It has been noticed that among many European bridges that the longer span in a 2-span asymmetrical structure ranges from 60 to 70% of the total length of the bridge. For a 3-span bridge, the length of the central span is 55% of the length of the entire bridge.

Description of the Structural Models - Single Phase Plane Cable-Stayed Bridge Model 18

The computer program CSB-3D developed at the University of Pittsburgh, by John Fleming, was utilized to study the behavior of a single plane cable-stayed bridge. Six models were considered, 18A, 18B, 18C, 18D, 18E, and 18F.

All models utilize the same basic configuration where 2 pylons constitute the compression elements of the structure, and a set of 8 cables on either side of each one of the towers. There are 32 total cables in this bridge. The finite element model of the bridge consisted of 62 joints and a total number of members equal to 93 elements. The elements are made up of the cables, the pylons and the deck elements.

The structure can be drawn on a sheet of plain paper, with all the nodes having a Z-coordinate equal to zero. The structure has a 6 total supports located at the pylon and the flanking segments on the deck girder. The global X-axis was selected as a line that passes through the longitudinal axis of the bridge.

The Y-axis was selected as a line that is parallel to the tower. Both axes had their origin at node number 1, which is located on the left hand side of the longitudinal axis of the bridge. The total length of the first model bridge, that is 18A, was 1075 feet. It basically consisted of 43 equal segments, each of which are 25 feet in length. The length of the central span of the structure was equal to 575 feet. Each of the flanking side spans was 250 feet. Thus the cable-stayed bridge model selected was a symmetrical structure. The height of the pylon for model 18A was chosen as 300 feet above the roadway deck, and it extended a distance of 100 feet underneath the deck where the rigid foundation is located. The above constitutes the overall bridge geometry.

The cable-stays consisted of 200 7-wire strands, whose total equivalent area was equal to 0.2125 square feet per cable. It was assumed that each cable was coated with zinc for protection against corrosion and that a polyethylene type exterior pipe was provided.

The weight of each cable was computed as 0.104 kips per foot of length along the longitudinal axis of the cable. The deck of the system was assumed to consist of prestressed post-tensioned concrete segmental construction. Each segment was assumed to be 25 feet long and as wide as the bridge itself.

The typical segment geometry consisted of a trapezoidal cross-section with cantilevered slabs. The width of the top flange of the segment was assumed equal to 60 feet. The width of the bottom slab was set equal to 30 feet. Overall segment depth was assumed to equal 7 feet. No provisions for a haunched girder was assumed. The thickness of the top slab was set equal to 24

inches, the bottom slab 12 inches, and the webs were assumed to have a thickness of 16 inches. Assuming that structural concrete of a density equal to 150 pounds per cubic foot, the weight of a typical segment was determined to be equal to 24.536 kips per foot.

The input file for the models consisted of a set of lines with a prespecified format utilized by the computer program CABLESTAY.

It was assumed that the segmental deck had longitudinal as well as transverse prestressing, but neither of these facts mattered as far as the input was concerned. This was so because the gross geometric properties of the concrete were used for the deck.

The initial tension in the cable can be estimated by the use of the following equation:

$$Ti = \frac{w\ell}{\sin\alpha}$$ where;

w = the uniformly distributed load on the deck
ℓ = length along the deck between attachment points
α = angle of inclination of the cable with respect to the horizontal

The angle of inclination of the cable is measured with respect to the horizontal X-axis of the structure.

The difference between the various models is the fact that each has a different distance between cable attachment points on the deck. Model 18A assumes 25 feet as the distance between 2 consecutive attachment points. The distance between attachment points is models 18B, 18C, 18D, 18E, and 18F is 50, 100, 200, 75, and 125 feet, respectively. This was done in order for us to evaluate the effects of different cable arrangements and span lengths. All models utilize the following material and geometric data:

Effective elasticity modulus of the cable = 3,600,000 k/ft^2
Cross-sectional area of the deck segment = 163.56 ft^2

I_x for the deck = 41,104 ft^4

I_y for the deck = 41,104 ft^4

I_z for the deck = 870.7 ft^4

Elasticity modulus for the concrete deck = 635,971.7 k/ft^2

Modulus of rigidity for the deck = 264,913.2 k/ft^2

Cross-sectional area of the tower = 680.0 ft^2

Tower inertia values $I_x = I_y = I_z = 38{,}081\ ft^4$

Weight of all cables = 0.104 k/ft

Weight of all deck segments = 24.536 k/ft

Weight of all pylon elements = 101.4 k/ft

The preliminary computer run is not based on optimal design configurations. Also it was assumed that the initial tension in all cables was the same, this is not exactly right. The value of the tension in the cable increases as the angle of inclination with respect to the horizontal axis decreases. Thus the longer cables have more tension in them.

The single plane cable-stayed bridge models displayed were part of an initial check on program capability. After the computer prints out an echo of the input data, it displays a computation of the initial cable equivalent modulus. This is followed by the joint displacements, the final cable tension and equivalent modulus, as well as the final member stress resultant. At the end of the output file, the external reactions at the supports are displayed in the 3-dimensional configuration expected.

It is very important to note that even though the single plane cable-stayed bridge models considered were 2-dimensional, the output displays a 3-dimensional response. The end of the output file has a message reminding the user that the program algorithm did consider the nonlinear effects of the cable stiffness, but it ignores the change in geometry due to the loads. If no other data is encountered, the program will quit execution.

Description of Model 20J Double Plane System

Model 20J is a double plane cable-stayed bridge structure that is indeed 3-dimensional.

The structure has 2 pylons and a total number of 120 cables in 2 planes. There are 15 cables on either side of the pylon leg.

The pylon has 2 legs consisting of a frame configuration for the tower. There is a total number of 329 elements in structure including the cables. There are 142 joints or nodes used to generate the finite element model of the cable-stayed bridge. There are 8 supports, 4 under the pylons, and 4 in the flanking spans. The same segmental deck configuration was utilized here as in model 18A.

The segment dimensions are exactly the same. The properties of the steel cables as well as the prestressed concrete did not change. The bookkeeping task here is a little more complicated than the single plane cable-stayed bridge of model 18A. The iteration number of cycles for convergence is also different. The acceptable error tolerance here should be specified in such a way that unrealistic precision should be avoided. The computer may quite execution if the value of the value of the unbalanced load specified is too small. For purposes of fitting the structural stiffness matrix in the core, the sizes of few arrays in the program had to be modified. This is a time consuming task because mainframe computers may require that the user specify a storage allocation which is very close to the one really required.

It is to be noted that the process of preparing an input data file for the computer program utilized, STRUDL AND CABLESTAY, sectional dimensions comparable to existing bridges were utilized. In future research applications, the Pasoc-Kennewick cable-stayed bridge in the State of Washington, as well as the East Huntington bridge in the State of West Virginia will be studied. Static as well as dynamic analysis of both bridges are contemplated as models for studies in the future. The tower configurations in these 2 bridges are different.

All models have been analyzed by 2 computer programs: STRUDL AND CABLESTAY. Both computer programs display a static analysis of these bridges, but only STRUDL was utilized to plot the modal shapes and generate the frequencies based on an assumed location of structure and input earthquake. In determining the intensity of the earthquake utilized, the Caltrans Specifications pertaining to recommended acceleration response spectrum were used. The Benecia-Martinez crossing was selected as a representative site to locate the cable-stayed bridge.

Notes on Practical Design

Based on the computer output of models 18A through 18F, we note that the distance between cable attachment points as the deck should be around 25 to 30 feet. Larger attachment point distances will lead to very large member forces at the end of the structural analysis.

In the double plane cable-stayed bridge, the attachment points were selected at 25 feet, and large answers were obtained for cable stresses and other member forces. The computer can provide the engineer with ample assistance when it comes to selecting a feasible geometric configuration for the bridge. In the following sections, we shall comment more on our observations of the behavior of the bridge structures studied.

Notes on Cablestay

The computer program CABLESTAY developed at the University of Pittsburgh by John Fleming, was used to perform a static analysis of models 18A through 18F, which are basically single plane cable-stayed bridges with varying distances between attachment points along the deck.

The first set of runs consists of static analysis of symmetrical cable-stayed bridges, with distance between attachment points varying from 25 feet to 200 feet. This was done to substantiate that when the distance between attachment points along the deck becomes large, huge forces and bending moments are generated in the structure. The use of more cable-stays in the structure leads to a more economical design. The stress distribution in the structure is also more uniform. From a practical standpoint, the use of smaller diameter cable-stays minimizes special anchorage details and other construction problems during erection.

The symmetry in the models was with respect to the supports as well as the number of cables on either side of both pylons. The cable-stayed bridges studied consisted of structures that had flanking spans on either side of the towers. Four unsymmetrical models were also studied. These consisted of models 18A through 18D, where the roller supports on the flanking spans were not positioned symmetrical with respect to the center of the bridge. This was done to get a feel for the bridge performance and to verify static checks for the problem.

Notes on Strudl

The computer program STRUDL was utilized to run static as well as dynamic analysis of the structure. Only model 18A, where the distance between attachment points along the deck is 25 feet was studied. Static analysis for the bridge was compared to STRUDL.

The first 25 modal frequencies were computed and 16 of them are plotted to check for vertical vibration as well as lateral and torsional vibration of the structure. For the double cable-stayed bridge model J20, a detailed analysis was performed and the first 25 modal shapes were plotted and few of them are shown in the report. The first 25 modes were plotted by STRUDL and are available on file at the California Department of Transportation, Division of Structures, in Sacramento. These were plotted on the full scale plotter and they display the importance of the higher modes of vibration as far as tower performance is concerned. The output files for all models 18A through 18F are in Volume II in extensive detail for comparison and further research in the future.

Notes on Nonlinear Analysis

It is to be noted that the program CABLESTAY ignores the change in geometry associated with the structure. Fabian, in a thesis on cable-stayed bridge performance, also at the University of Pittsburgh, mentions that the use of STRUDL to analyze a cable-stayed bridge structure is adequate. He mentions the fact that the initial tension in the cable is a concept that is not very well defined and may not be needed at all to solve the structure. He conducts a comparison between linear and nonlinear analysis and arrives at the conclusion that the real difference is less than 1 percent. This is very important because if there is indeed no difference, substantial savings in computer run time can be achieved. This will be checked in further studies in the future.

The output for model J20 appears in Volume III of the report. Static as well as dynamic analysis are displayed and few of the vibration modes of the structure.

Two structures were considered in detail: A 3-span symmetrical bridge and a 9-span symmetrical bridge. The detailed description of both bridges appears in text form at the start of the input file. Since both bridges were symmetrical, only half of the structure was modelled by introducing an artificial vertical restraint (roller) at the center of the span. This boundary condition allows for vertical displacement at the center of the bridge. The computer program S-frame was utilized to solve for the time dependent response of both segmental structures. The computer program S-Frame models the structure along lines similar to its actual construction sequence. All detailed output appears in Volume IV.

Figure 1 displays the profile of the single plane bridge. Figure 2 is the profile of the double cable-stayed bridge. Figure 3 and 4 are sketches of the tower deck attachment for cable-stayed bridges. Figure 5 is a sketch of the cable cross-section used for the stays. Figure 6 displays the segmental deck utilized for both model bridges, the single plane and the double plane. Figure 7 displays the actual cable-stayed bridge prototype and its simulated mathematical equivalent continuous beam on elastic supports. Deflection curves are also displayed under dead and live loads.

Future Research Needs

More research is needed in various areas pertaining to segmental construction as well as cable-stayed bridge design. Studies are proposed for the evaluation of various configurations of cable arrangements as well as tower and deck layouts. What constitutes a safe design as well as an optimal design? The answer to the above question may be simple when it comes to safety issues, but the optimum design of a cable-stayed bridge structure is a very complex problem indeed. Any change in the

cable arrangements leads to a new structural system. Research is proposed by Farran to study various cable system configurations and the effect on the deck performance as well as the tower. Numerous models of cable-stayed bridges to be considered include the structural analysis of a model bridge where the span is maintained a constant at first, and the number of cables as well as the configuration of the cable geometry are changed to see the variation in the deck and tower moments and axial forces. The task of data generation for such a study is time consuming and also the graphical display of the results of the analysis is complex. Such studies serve the purpose of providing the design engineer with information pertaining to the efficient systems in cable-stayed bridge design. All possible configurations including radiating, harp, fan, and star are to be considered as well as the bundled radiating cable configuration, or bundled harp, bundled fan, or bundled star configurations. The development of preliminary design procedures in the area of segmental construction and cable-stayed bridge structures is anticipated. The practical use of sophisticated time-step analysis including non-linear behavior for design purposes is envisioned. Significant research has been done in the area of dynamic analysis and response to earthquake excitations. The practical implementation of such complex research efforts is a must for production engineers.

The state of the art in sophisticated involves the development of a computer program for the analysis and design of cable-stayed bridge structures with post-tensioned prestressed concrete segmental box-girder decks. The computer program should incorporate the construction sequence of the bridge in the analysis for time-dependent behavior and moment redistribution in the structure. Creep, shrinkage, as well as tendon relaxation cause the time-dependent behavior in segmental structures. The development of a mathematical model for creep and shrinkage should be investigated for proper correlation with experimental tests performed on the concrete mix. Strain gage instrumentation used in experimental setups should be checked for proper correlation with suggested relaxation expressions used in mathematical models. The results obtained from structural analysis by STRUDL OR CABLESTAY should be contrasted and deflection studies should be performed.

In the area of dynamic analysis and the use of sophisticated programs to compute the frequencies and the modal shapes, it is recommended that such results be correlated with wind tunnel tests and experimental determination with the vibration frequencies. This is very important in studying the effects of turbulence and vortex shedding. Instrumentation of various cable-stayed bridges should be done and a data acquisition system should be utilized to post-process the vibration data gathered.

Research on Corrosion

The corrosion of the cable-stays will be the most important research topic in the future. On all federally funded cable-stayed bridge projects, a cable replacement program is required as part of the project documents. As evidenced by field inspection and investigation of many bridges around the world, we are convinced that corrosion is a very serious problem for these flexible structures. A cable-stayed bridge is different from a suspension bridge. If one of the vertical hangers on a suspension bridge were to fail, the consequences to the integrity of the rest of the bridge may be minimal. But the failure of a stay or 2 on a cable-stayed bridge may be catastrophic, since these inclined cable-stays are primary load carrying systems. Research is proposed by Farran to study the performance of a cable-stayed bridge when 1 or more cable-stays fail. This is very important for State agencies and design consultants in order for us to determine a realistic factor of safety for the overall system design. The redistribution of stresses due to failure of sub-components in a structural system is very important. The flexibility of cable-stayed bridge system warrants careful examination of system reliability under severe wind and earthquake loading.

Research on cable technology continues in different countries around the world. The Germans are studying the use of fiber optics for cable-stays. Coating techniques as well as the use of proper grouting materials is currently under investigation. Corrosion of metals and research in various areas of expertise in metallurgy can enhance the quality of material to be used for future tendons and stays.

For the time, the actual response of cable-stayed bridges under severe wind and earthquake loading is still to be seen. Inspection for corrosion and replacement programs are crucial for the prevention of structural failure on existing cable-stayed bridges.

Conclusion

This report has basically presented the fundamental concepts needed to understand segmental technology and cable-stayed bridge design. In the various chapters of Volume I, the essential concepts of matrix structural analysis, computer methods of structural analysis, finite element methods, prestressed concrete design materials, segmental post-tensioned construction, cable-stayed bridges, non-linear behavior, as well as dynamic analysis have been presented. Volume II displays the analysis of model cable-stayed bridges performed using the computer program CABLESTAY developed at the University of Pittsburgh by John Fleming, as well as the analysis of a double plane cable-stayed bridge by STRUDL. The implementation of STRUDL for the analysis of a cable-stayed bridge is a little more difficult than CABLESTAY. The stiffness matrix of the cable-element has to be

input as a special element to account for the non-linear behavior caused by sag, interaction of axial and bending forces in the deck and the tower, as well as the effects of large displacements on the structure. Most research done on the topic of segmental structures as well as cable-stayed bridges advocates the development of software to model the construction sequence of the bridge. This seems to be a realistic requirement since the effects of creep, shrinkage, as well as tendon relaxation, are all time-dependent and will affect the performance of the bridge. A temperature analysis is also warranted but that is feasible even on a program like STRUDL. Ongoing research is essential to understanding the performance of these flexible bridges.

References

1. "Construction and Design of Cable-Stayed Bridges", by Walter Podolny, Jr. and John B. Scalzi, published by the John Wiley Interscience Company.

2. "Construction and Design of Prestressed Concrete Segmental Bridges", by Walter Podolny Jr. and Jean M. Muller, published by the John Wiley Interscience Company.

3. "Construction of Prestressed Concrete Structures", by Ben C. Gerwick, Jr., published by the John Wiley Interscience Company.

4. "Construction Glossary: An Encyclopedic Reference and Manual", by J. Stewart Stein, published by the John Wiley Interscience Company.

5. "Dynamic and Seismic Analysis Considerations for the Design of Long-Span Cable-Stayed Bridges", by Ahmed Abdel Ghaffar and Ali Nazmy, Published in the proceedings of the 1987 Public Works Research Institute, Ministry of Construction, of Japan. The paper appeared in the 3rd U.S.-Japan Workshop on Bridge Engineering.

6. "Damping Characteristics of Cable-Stayed Bridges", by K. Kawashima and S. Unjoh, published in the proceedings of the 3rd U.S.-Japan Bridge Workshop.

7. "An Evaluation of Seismic Design and Retrofit Methods in California and the U.S.", by James Gates, published in the 3rd U.S.-Japan Bridge Workshop conference proceedings, 1987.

8. "Comparative Wind Tunnel Testing of Bridge Road Decks", by Wardlaw, Tanaka, Zan, Savage, and Yamada, published by the Ministry of Construction, Public Works Research Institute of Japan, 1987 proceedings.

9. "On Interpreting Model and Prototype Responses of Suspended-Span Bridges to Wind", by R.L. Scanlan, paper published in the 3rd U.S.-Japan Workshop on Bridges in 1987.

10. "Aerodynamic Stability of the Cables of a Cable-Stayed Bridge Subject to Rain", by Ohshima and Nanjo, paper published by the 3rd U.S.-Japan Bridge Workshop in 1987.

11. "Vibrational Characteristics and Earthquake Resistant Design for Cable-Stayed Prestressed Concrete Bridge-Inagawa II Bridge", by Sugiyama, published by the 3rd U.S.-Japan Bridge Workshop in 1987.

12. "Vibrational Test of the Completed S-Curved Cable-Stayed Bridge", by Ohno, Yamazaki, and Kikkawa, paper published in the 3rd U.S.-Japan Bridge Workshop in 1987.

13. "A Report on the Analysis and Design of Three U.S. Cable-Stayed Bridges", by S.L. Stroh, published by the 3rd U.S.-Japan Bridge Workshop in 1987.

14. "Static and Dynamic Analysis of Cable-Stayed Bridges", by John Fleming, Joseph Zenk, and Benjapon Wethyavivorn, published by the Civil Engineering Department of the University of Pittsburgh, in Pittsburgh, Pennsylvania, 1987.

15. "Historical Development of Cable-Stayed Bridges", by Walter Podolny and John Fleming, proceedings of the American Society of Civil Engineers, Volume 98, No ST9, September 1972.

16. "Dynamic Behavior of Cable-Stayed Bridges", by John Fleming and E.A. Egeseli, International Journal of Earthquake Engineering and Structural Dynamics, Volume 8, No. 1, 1980.

17. "Skytrain Crosses the River", by Lawrence Bush and M.S. Kahlil, article published in the American Society of Civil Engineers magazine, March 1988.

18. "Japan Spans the Inland", by Dennis Normile, an article published in the American Society of Civil Engineers Magazine, April 1988.

19. "Cables in Trouble", by S.C. Watson and D. Stafford, an article published by the American Society of Civil Engineers in the Civil Engineering Magazine, April 1988.

20. "Seismic Design and Retrofit Manual for Highway Bridges", a report published by the U.S. Department of Transportation of the Federal Highway Administration, May 1987.

21. "Seismic Design of Highway Bridges Workshop Manual", published by the Federal Highway Administration, January 1981.

22. "Long Span Prestressed Concrete Bridges of Segmental Construction, State of the Art, by Lacey and Breen.

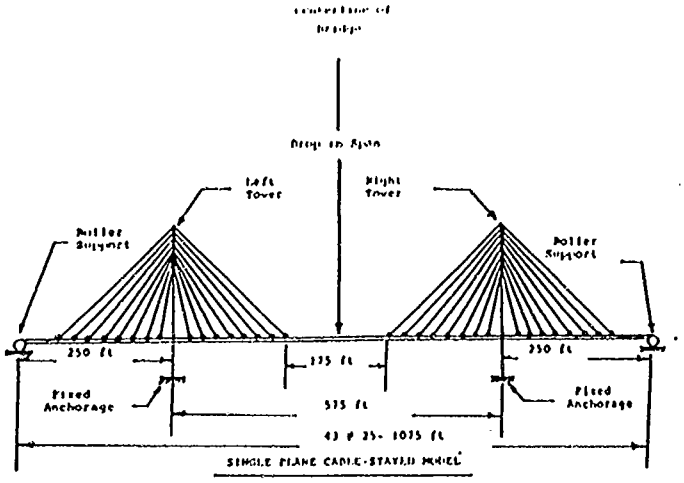


Figure 1

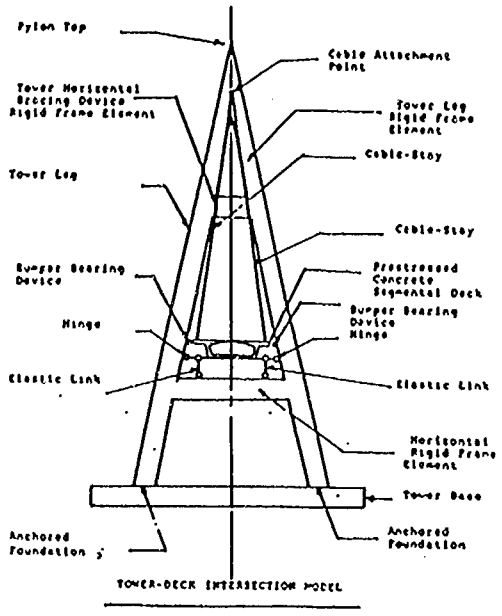
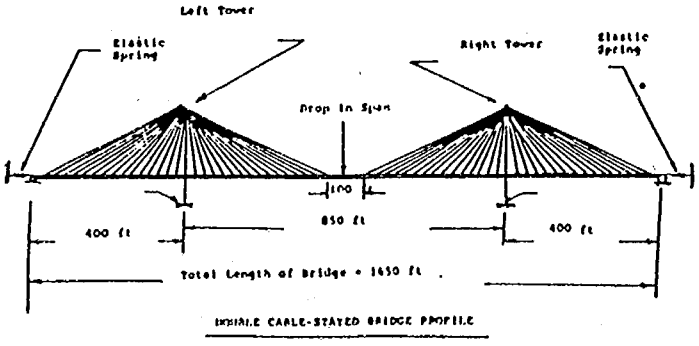
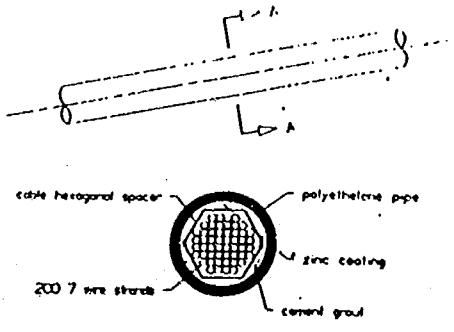


Figure 4





Cable Cross-section A-A

Figure 5

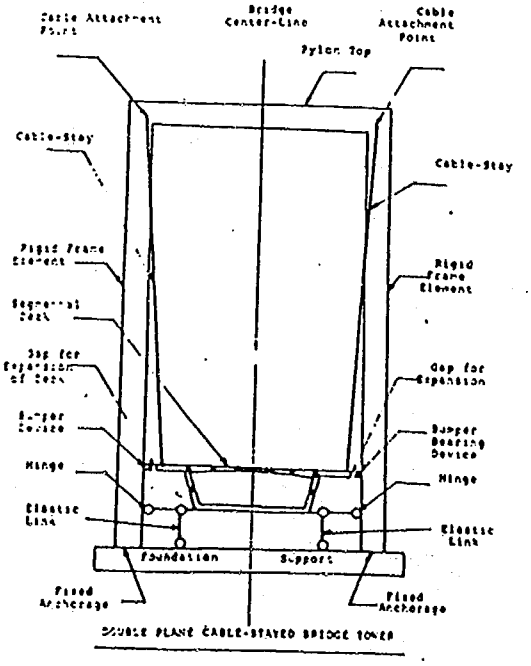
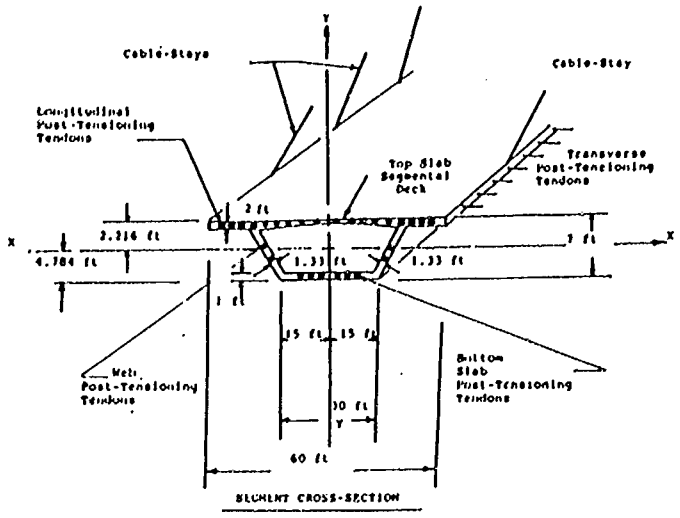


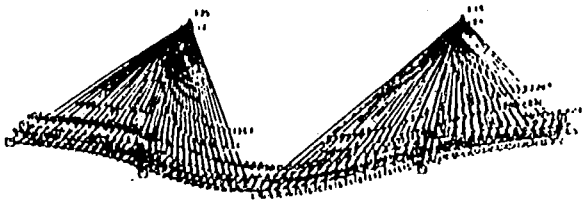
Figure 3



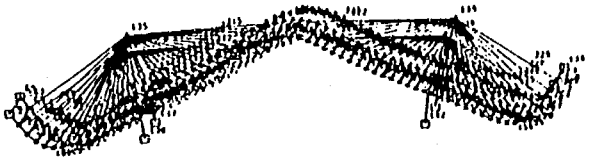
SEGMENT CROSS-SECTION



DOUBLE CABLE STAY



MODE 6



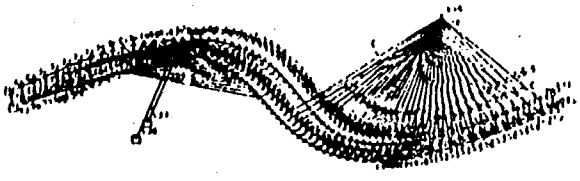
MODE 1



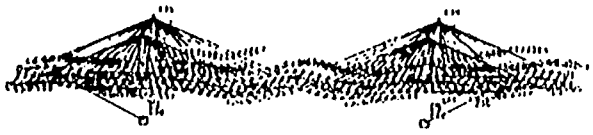
MODE 7



MODE 5



MODE 9



MODE 11



MODE 13



MODE 12



MODE 24

DESIGN AND EXPERIMENTS ON SHIN-HAMADERA OOHASHI BRIDGE

by

Osamu Yoshikawa 1), Isao Sugiyama 2)
Fumio Hakamada 3) and Shun-ichi Kaneko 4)

ABSTRACT

Shin-Hamadera Oohashi bridge now under construction on the way of harbor highway along Osaka Bay route is a unique bridge with inclined arch ribs, and Nielsen type hanger cable. The span length of 254m is one of the largest of this type. Several structural analyses were performed for the detail design consideration. For the sake of deciding effective length of the arch rib member in the longitudinal direction as well as in the transverse direction, detailed structural analyses were performed. One to thirty scale model test was also performed to see the failure mode of this type of bridge. The article shows other design considerations.

1. INTRODUCTION

Hanshin Expressway is an elevated type highway system which is now grown to be a trunk of traffic network in the urban area of West Japan. It has 10 routes, one of which is called Osaka Bay route.

Osaka Bay route is 80 km long highway along the rim of Osaka Bay, connecting Kansai International Airport in the south and Akashi Oohashi bridge in the west, both of which are under construction. Among the 80km highway, 19km length is completed and in operation.

Shin-Hamadera Oohashi bridge is a Nielsen system tied arch bridge, spanning over water canal between artificial islands of industrial use. The center span of 254m is the maximum size of this type of bridge.

Before starting detail design, several investigations are made to be applied in this project. Included are structural analyses concerning effective length of arch rib and ultimate strength, stress distribution at intersection, and vibration characteristics. Then several experiments are executed in relation to cable relaxation, bending of beam with oval cross section, and ultimate strength of arch structure.

The results of these investigation were great help for detail design of the bridge. Several notes for the design are also revealed thereafter.

2. DESIGN REQUIREMENTS

The design criteria are shown in Tab. 1. Tab. 2 shows examples of large span arch bridges.

Fig. 1 shows artistic view of the bridge. Fig. 2 shows general view of the bridge.

The structural features are counted as follows.

1) To secure vehicle room above road surface, the spacing of the arch ribs was selected to be 25.5 m at road surface and 3.5 m at the top. The total height of the bridge should be less than 60 m in view of aesthetic

---

1 Chief Engineer, Maintenance Division, Hanshin Expressway Public Corporation, 4-1-3 Kyuutarou-Chou, Chuuou-Ku, Osaka 541 JAPAN.

2 Chief Engineer, Osaka First Construction Division, Hanshin Expressway Public Corporation, 2-11-8 Kitakagaya Suminoe Osaka, 559 JAPAN.

3 Kobe Construction Division, Hanshin Expressway Public Corporation, 16-1 Shinkou-chou Chuuou Koube, 650 JAPAN.

4 Yokogawa Bridge Works, 2 Chikukou-Shinmachi Sakai Osaka, 592 JAPAN.

consideration and aviation regulation.

2) In the consequence, an arch rise of 36m, arch rise ratio of 1/7 was selected. The inclination in the front view is 17 degree.

3) The geometry of the arch rib and the strut follows parabolic.

4) The floor system consists of steel deck plate and floor beam system. The steel deck is composited with strut. The deck is stiffened by U-shaped rib. The floor beam comprises of longitudinal girder at center and floor beam placed every 12 meters. Transverse ribs are distributed every 3 meters.

5) The hangers are inclined with 60 degree, 12 m apart. The end hangers are placed vertical not to cause compression by live load.

6) Nine horizontal struts are placed. From an aesthetic consideration oval or circular cross section was selected.

7) A traveling scaffold is to be installed below the deck. The purpose is periodical inspection of lower deck and assistance of falsework assembly in case of repainting. The installation is yet to be decided, but the load must be taken into consideration for detail design. The rail is installed for the time being.

8) Construction method is placement by making use of a deck barge in order to minimize the construction period and to minimize the construction facility at site. So due investigation must be made to be compatible with this construction method.

3. STRUCTURAL ANALYSIS

3.1 ELASTIC BUCKLING ANALYSIS

In order to evaluate the strength elastically, elastic analyses were executed. The results of the three dimensinal elastic buckling analysis shown in Fig.3 are as follows,

1) The buckling stress given by two dimensional model : The collapse load coefficient of α is 17.37, which shows in-plane elastic buckling would never happen. α is defined as a load factor to design load D+L, where D is a dead load and L is a live load.

2) The buckling stress given by three dimensional model : The collapse load coefficient α is 6.49, which is also significantly large. In this case collapse mode is out-of-plane. It is unavailable that in-plane bucking can be seen in lower modes.

3) The first mode of the three dimensional model was three half wave mode with peaks at first strut and arch crown.

3.2 INELASTIC BUCKLING ANALYSIS

Inelastic analysis was performed by using a program EPACS [1]. This is a program that can include material inelasticity, geometrical inelasticity, initial imperfection, and residual stress. When some of the element is expected to remain elastic, the program can assume the element to be elastic to save cpu time. In this case members other than arch ribs and struts are assumed to be elastic. The results are shown in Fig.4 and can be concluded as follows.

1) The load coefficients for several load combinations are also shown in Fig.4. where D is a design dead load, L is a design live load, and W is a design wind load. Different types of live load are considered. The load factors are shown below.

JSHB : $P_u = \alpha (D+L)$

AASHTO : $P_u = 1.3D + \alpha L$

Compared with design load coefficients, the results obtained by the

analysis show that the bridge sustains good durability against buckling.

2) The yielding starts at the arch crown, and gradually pervades downwards.

3) The failure mode is caused by buckling of the lowest part of arch rib connecting end floor beam and first strut, by making nodes at both ends.

4) The program can incorporate residual stresses and initial imperfections. The analysis shows no significant effect can be seen for the ultimate strength with these terms.

3.3 INTERSECTION OF ARCH RIB AND STRUT WITH OVAL CROSS SECTION

An intersection between strut and arch rib makes a complicated structure. Because the arch rib has a curvature in the arch rib plane and is inclined inside, and the strut has a round cross section, structural analysis by Finite Element Method was performed to evaluate the stress distribution.

Firstly, diaphragm at the intersection was set as shown Fig.5. In this way, stresses of arch rib web plate and arch rib stiffeners become moderate. The detail of the intersection is a little complicated, but not too much to be unable for inspection and repainting.

Then analysis was performed for the model shown in Fig.6. At the boundary, internal forces were applied to arch rib and to the strut. As for the arch rib element, stiffeners and diaphragms were also modeled. The stress distribution at the arch web is not symmetric, because the strut intersects obliquely.

The strut plate is connected to the web by full penetrated welding. Considering that the web is a thick plate, stresses perpendicular to the plate were calculated. The results are shown in Tab.3. From this table, structural steel prepared against lamellar tearing was adopted for the arch web plate at the intersections of first through third strut.

3.4 VIBRATION MODES

Compared with vertical hanger system, Nielsen system tied arch bridges are very stiff structure in the plane of arch rib. Therefore significant structural improvement can be obtained in its vertical stiffness, structural stability, and vibration mode. In Fig.8 are listed vibration modes for the first five modes with each individual eigen period.

From observation one can see the following,

The first mode is half wave transverse sway. The second mode is half wave vertical displacement. The third mode is two half wave sway of arch ribs. The fourth mode is two half wave vertical displacement. Note that the vertical displacement is not the lowest mode and the modal shape is not "complete" half mode. This is due to the crossed hanger disposition inherent in Nielsen system tied arch bridges. No torsional mode can be detected in lower order modes.

4. EXPERIMENTS

4.1 STRESS RELAXATION OF CABLE

Because of the interior high indeterminate structure, when large creep or relaxation occurs to Nielsen system tied arch bridges, the induced stress might not be neglected. Therefore, creep and relaxation test concerning cables was performed.

There are two types of cables, PWS(parallel wire strand) and LCR(locked coil rope), and two types of anchorage, HiAM and zinc casting. Cable and anchorage of New PWS and NS socket was also tested. The last one is a cable developed for good manipulation in transportation and

installation.

Each cable is placed in a rigid frame, then one third of ultimate load is applied continuously for one to two years. Measured are load induced in cable, strains at rigid frame, "elongation" at anchorage.

The experiment showed that HiAM and PWS case has only 3.4% stress relaxation and 1.1% creep elongation. These are parameters compatible with theory modeled with dash-pot and spring. A combination of New PWS and NS socket shows similar favorable results. Fig.8 shows one of the results.

4.2 ULTIMATE STRENGTH OF BEAM WITH OVAL CROSS SECTION

There are no experiments relating to round shape cross section made of thin plate. In order to evaluate the ultimate capacity of such a beam and to establish a stiffening plate configuration, a series of experiment were executed.

Specimens are shown in Fig.9. The models were designed so that the ratio be/b mentioned in Fig.9 is identical with prototype, where b is width and be is an effective width given by the following formula.[2]

$$be/b = \begin{cases} 1.0 & R \le 0.3 \\ 0.702R^3 - 1.64R^2 + 0.654R + 0.926 & 0.3 \le R \le 1.3. \end{cases}$$

where,

$$R = \frac{b}{t}\sqrt{\frac{\sigma_y}{E}}\sqrt{12(1-\nu^2)/\pi^2 k}\ , \quad k = 4.$$

Three kinds of specimen were prepared for three load conditions. Therefore 9 specimens were prepared. Three different specimens are,

a) specimen with no stiffening plate,

b) specimen with identical stiffening plate,

c) specimen with five times "stiffer" stiffening plate than that of b.

Each specimen was loaded axially to cause compression failure. Others were loaded laterally to cause bending moments around major axis as well as minor axis respectively.

Examples of experiment results are shown in Fig. 10.

The results are summarized as follows,

1) Each specimen behaves almost identical to axial load, and reaches its maximum capacity. The final strength is decided by local buckling at the end.

2) Bending around minor axis shows that stiffeners are required to reach its plastic moments Mp. The stiffness of the stiffener is not a control parameter.

3) Bending around major axis shows that beam exhibits almost identical load history irrelevant to the existence of stiffeners.

4) Additional stiffeners can increase the capacity and the ductility significantly as shown in Fig.11, which was embodied in the detail design of the strut.

4.3 GLOBAL MODEL TEST

Arch rib of Nielsen system tied arch bridge is exposed to dominant axial force, and bending moments around major and minor axes. For practical design of such members under axial forces, an idea of effective length is essential. But the effective length for design application is not a priori in this case, therefore there have been several ways of design method. Inelastic structural analysis shown above revealed that conventional method is apt to be too conservative. In order to evaluate the failure mechanism experimentally, and to get a rational idea concerning the effective length of arch rib member, global model test was executed. The numerical results shown in chapter 3 can be compared with the

experimental results.

The following parameters were considered and listed in Tab.4. The notations are,

1) In-plane slenderness ratio of arch rib λ_{yu},

where,

$$\lambda_{yu} = \frac{1}{\pi}\sqrt{\sigma_y/E}\ L/r_{yu}.$$

2) Out-of-plane slenderness ratio of arch rib λ_{zu}.

where,

$$\lambda_{zu} = \frac{1}{\pi}\sqrt{\sigma_y/E}\ l_{zu}/r_{zu}$$

3) Cross sectional area ratio between rib and strut A_u/A_ℓ

4) Cross sectional area ratio between arch section and hanger section EA_a/E_hA_h

5) Ratio of out-of-plane moments of inertia of arch rib to strut I_{ea}/I_s

Other notations are,

L : total span length, E : Young's Modules, lza (=.7*l) ,

l : strut spacing, r_{yu}. r_{zu}: out-of-plane radius of gyration

Model was designed so that items 1 through 3 are chosen to be identical. Material test was performed to obtain Young's Modules, yield strength, Poisson's ratio by the material used for the model.

A partial box model was made to know the residual stress caused by welding. The result was introduced into the analysis, where inelastic analysis was executed for the model to be compared with experimental results. The coherency would ensure the applicability of the analysis method.

For measurement of strains, four gauges were placed at four corners of the arch rib, to compensate temperature, axial strain, or bending moments. By combination of these data, one can get axial strain, bending strains in two directions respectively.

Two one to thirty scale models were fabricated and tested to examine the analysis and to secure ultimate capacity of the bridge. Restrictions of test field, available steel plates, transportation, fabrication decide 1/30 scale model. One for vertical load, and the other for transverse load test.

The load cases considerbd are as follows,

1) $P = \alpha(D+L)$: vertical load test,

2) $P = 1.3D + \alpha W$: transverse load test.

Picture is shown in Fig.12 for vertical load test. Load and displacement relation, load strain relations are shown in Fig.13.

The results are summarized as follows,

1) Strain distribution agrees well with numerical results in an elastic region.

2) Ultimate strength of the two models are shown in Tab.5. The vertical load model agrees well with analysis. While transverse model given by experiment shows greater strength than analysis.

3) The following design method was confirmed to be appropriate,

Effective length of out-of-plane buckling : 0.7*strut spacing,

Effective length of in-plane buckling : hanger spacing.

4) Failure mode occurs when four hinges were formed at four corners of the lowest trapezoidal frame.

5. DETAIL DESIGN OF STRUCTURAL ELEMENT

5.1 STRUCTURAL MODEL

As for the structural design, the structure was evaluated in-plane model and out-of-plane model individually. The vertical load was applied to three dimensional model, then the results were compared with that of two dimensional model and concluded that they are similar. As for the

evaluation of transverse load, such as earthquake load or wind load, three dimensional model was used to evaluate internal forces of the strut.

The evaluation of the wind load is important for such structures as arch bridges against transverse force. Shin-Hamadera Oohashi Bridge has 36m of arch rise whose height varies from 21m to 57 m, therefore the design wind should be evaluated in the accordance. This causes complications in the design process, so the equivalent wind speed of 57 m/s was selected so that it causes the identical internal force at the root of the arch rib. This method follows the design of tower against transverse wind specified by Honshu Shikoku Bridge Authority, where wind speed follows to the power of 1/7 of the height. There is no interaction of turbulence between the two adjacent arch ribs.

5.2 ARCH RIB

The arch rib is a member under compression as well as bending moments around two axes. In accordance with JSHB(Steel Bridges) it is specified as follows,[3]

1)completed structure under compression and two axial bending moments,

$$\frac{\sigma_c}{\sigma_{cal}}+\frac{\sigma_{bcy}}{\sigma_{bay}\left(1-\frac{\sigma_c}{\sigma_{cay}}\right)}+\frac{\sigma_{bcz}}{\sigma_{baz}\left(1-\frac{\sigma_c}{\sigma_{caz}}\right)}\leqq 1$$

$$\sigma_c+\frac{\sigma_{bcy}}{\left(1-\frac{\sigma_c}{\sigma_{cay}}\right)}+\frac{\sigma_{bcz}}{\left(1-\frac{\sigma_c}{\sigma_{caz}}\right)}\leqq\sigma_{cal}$$

2)On a deck barge under tensile force and two axial bending moments,

$$\sigma_t+\sigma_{bty}+\sigma_{btz}\leqq\sigma_{ta}$$

$$-\frac{\sigma_t}{\sigma_{ta}}+\frac{\sigma_{bcy}}{\sigma_{bay}}+\frac{\sigma_{bcz}}{\sigma_{baz}}\leqq 1$$

$$-\sigma_t+\sigma_{bcy}+\sigma_{bcz}\leqq\sigma_{cal}$$

where,

σ_t,σ_c : normal stress due to axial forces.

$\sigma_{bty},\sigma_{btz}$ $\sigma_{bcy},\sigma_{bcz}$: Flexible tensile and compressive stress due to bending moments.

σ_{ta} : Allowable tensile stress.

σ_{caz} : Allowable axial compressive stress around minor axis.

σ_{bay} : Allowable flexural compressive stress around major axis without local buckling.

σ_{baz} : Upper limit of allowable flexural compressive stress.

σ_{cal} : Allowable stress for local buckling.

$\sigma_{cay},\sigma_{caz}$: Allowable Euler buckling stress.

σ_{caz} $\sigma_{cay},\bar{\sigma}_{caz}$ are functions of effective length l.

Notation y or z shows bending around major or minor axis, respectively.

Generally speaking, arch members are designed as members under axial force and bending moments with an aid of effective column length. Generally speaking, an effective column length of twice of the hanger spacing is selected against in-plane buckling, and an effective column length of strut spacing against out-of-plane buckling. But these are merely conventional ideas, therefore they do not have a theoretical foundation. Inelastic as well as elastic buckling analysis revealed that fairly small value is

enough, which was also confirmed by model test. Consequently, the two effective lengths are specified as follows,

1) in-plane buckling : Effective buckling length be one hanger spacing. when $L/r_y<600$.

where L : span length.
r_y : in-plane radius of gyration.

2) Out-of-plane buckling : Effective column buckling length be 70% of strut spacing when $l/r < 80$.

where l : strut spacing.
r_z : out-of-plane radius of gyration.
inclination of arch rib = 17 degrees.

By introducing this idea, one can get more rational design of arch member.

Most of the arch rib section is critical when full live load is applied except those area as around third strut. The arch rib is temporally supported there. Consequently, fairy large negative moment is applied during navigation, and the maximum thickness reaches 70 mm by SM58. Transverse forces cause bending moments in the strut, then out of plane stresses are induced at arch web.

For fear of lamellar tearing of thick steel plates, lamellar tear resistant steel plates are chosen at first through third struts, where out-of-plate stress fluctuation may reach a significant value.

5.3 STRUT

Strut defines the effective length of out or in-plane arch rib buckling. When transverse forces such as wind force or earthquake force is applied it works as a beam element. Because some of the struts have circular cross section, finite element analysis were performed to obtain stresses at the intersection between arch rib and strut as shown in Chap.3.

Model test were also executed for partial circular section as shown in Chap.4 to evaluate the ultimate strength, failure modes, and thereafter to design stiffeners.

5.4 TIE BEAM

Longitudinal component of axial force of arch rib is applied to tie beam. By introducing composite structure between the girder and steel deck, part of the traction force is provided by the steel deck.

In order to evaluate the stress distribution at the deck corner, Finite Element Analysis was performed. The stress distribution varies little to the bending stuffiness of end floor beam, which is placed between two arch ribs under steel deck.

Effective width of the deck is decided by,

$$\lambda = \int \sigma dy / \sigma_0$$

where, λ : effective width,
σ : longitudinal stress,
σ_0 : traction of tie beam

Fig.14 shows effective width given by the analysis and used for design. Effective width is selected so that it increases gradually with an angle of 27 degrees.

Bending moment of tie beam caused by hanger tension, live load and and moment must also be taken into consideration.

At the connection of the tie beam, arch rib, end floor beam and steel deck, Finite Element Analysis was performed to evaluate the stresses.

5.5 HANGER

Parallel Wire strand cable(PWS) was selected. The allowable stress is 5300 kgf/cm2(519.4 MPa). Compared with hangers of suspension bridge, hangers of Nielsen system tied arch bridge is exposed to high cyclic live load fluctuation. Hanshin Expressway Public Corporation has investigated status quo of truck live truck load on the highway.[4] By introducing the probabilistic parameters deduced from this investigation, close investigation was made in view of fatigue problem. It was revealed that tendency of large stress fluctuation can be seen, yet to be harmful.

Because of the inevitable variance of stress adjustment of hangers at field assembly and final adjustment, 10 % of dead load is taken into consideration for the design of hanger. Long term effect expected from the test are evaluated within this redundancy. For the selection of hanger type, synthetic consideration including cost, fatigue and maintenance was made.

6. ERECTION

It is planned to construct the whole bridge by a deck barge. Firstly, whole assembly is made at nearby flat assembly field, then shipped by a deck barge to the site. By making use of the tidal difference, The whole bridge is set to the specified point. Due to the manuability, pedestal frame type bearing support is adopted, where a thick steel plate is placed on top of substructure, then after the placement of superstructure, the bearings attached to superstructure are welded to the plate at site. Structural analysis was also executed for a model during navigation, which is a crucial load condition around the arch rib of temporary support.

7. ACKNOWLEDGMENT

The model experiment and inelastic analysis were executed under the supervision of Professor H. Nakai of Osaka City University, and Associate Professor T. Kitada of Osaka City University. The program EPACS belongs to Osaka City University. The experiment concerning cable relaxation was performed by Professor E. Watanabe of Kyoto University. The detail design considerations were executed by Sogo Consultant and Yokogawa Bridge Works and Matuo Bridge Company. They are all greatly appreciated. The bridge is due to complete in 1990.

REFERENCES

[1] Nakai, H., Kitada,T.,Ohminami,R., and Nishimura,T. : Elasto-Plastic and Finite Displacement Analysis of Cable-Stayed Bridges, Memoirs of the Faculty of engineering, Osaka city University, Vol.26, pp.251~271, Dec.1985.

[2] Komatsu,S.,Kitada,T. : Ultimate compressive strength of steel plate with initial imperfections, JSCE report, Vol.270, pp.1~14, Feb.1978.

[3] Japan Road Association : Japanese Specification of Highway Bridges, Part 2, Steel Bridges, Feb.1980.

[4] Hanshin Expressway Public Corporation : Final Report on Site Investigation and its Statistical Analysis of Live Load on Highway, Mar.1986.

Tab.1 Outline of the Shin-Hamadera Oohashi Bridge

type of bridge	Nielsen system tied arch with inclined arch rib
design speed	80 km/hr
design live load	TL-20, TT-43
span length	254.0 m
roadway width	20.25 m (four lanes)
clearance above sea level	20 m
arch rise	36 m (arch rise ratio 1/7)
steel weight	3921 tons
total weight	6000 tons
hanger	parallel wire strand with d = 7 mm
construction method	yard assembly then placement by deck barge
foundation	cast-in-place concrete pile with d = 2 m

Tab.2 Nielsen System Tied Arch Bridges of Large Span Length

Order	Bridge name	Span length (m)	Location	Completion year	Inclination of arch ribs
1	Kizugawa	305.0	Osaka (Japan)	under construction	inclined
2	Van Brienenoord	287.1	Holland	1965	parallel
3	Shin-Hanadera	254.0	Osaka (Japan)	under construction	inclined
4	Fehmarnsund	248.4	West Germany	1962	inclined
5	Utsumi	220.0	Hiroshima (Japan)	under construction	inclined
6	Lower Merwede	202.8	Holland	1967	parallel

Tab.3 Stresses Perpendicular to Web Plate of Arch Rib

strut number	Grade of steel	Web plate thickness (mm)	Maximum tensile stress (kgf/cm^2)	Ratio to allowable stress	Ratio to yield stress	Load case
1	SM58	36	2023	0.78	0.55	Wind
2	SM50Y	32	1892	0.90	0.63	Wind
3	SM58	42	1734	0.67	0.49	Dead+Wind
4	SM50Y	19	928	0.41	0.32	Dead+Wind
5 (at crown)	SM50Y	19	196	0.09	0.05	Dead+Wind

Tab.4 Non-Dimensional Parameters

Non-dimensional parameter	Proto-type	Specimen	
		Designed	Measured
λ_{V_s}	3.71	3.71	4.01
λ_{Z_s}	0.53	0.53	0.57
A_s/A_q	1.44	1.44	1.37
EA_s/E_hA_h *	95.1	24.7	25.6
I_{Z_s}/I_Z	1.13	2.17	2.17

* Note : $EA_s/((E_hA_h)/2)$ for specimen

Tab.5 Ultimate Strength Given by Test Result and Numerical Analysis

Specimen	Collapse Load by Test (tf)			Collapse Load by Analysis (tf)			Test/Analysis
	Vertical P_U'	Horizontal P_H'	Resultant R'	Vertical P_U	Horizontal P_H	Resultant R	R'/R
No.1	36.8	——	36.8	36.1	——	36.1	1.03
No.2	18.0	5.39	18.8	18.0	2.75	18.2	1.03

Note : $R'=\sqrt{P_U'+P_H'}$, $R=\sqrt{P_U+P_H}$

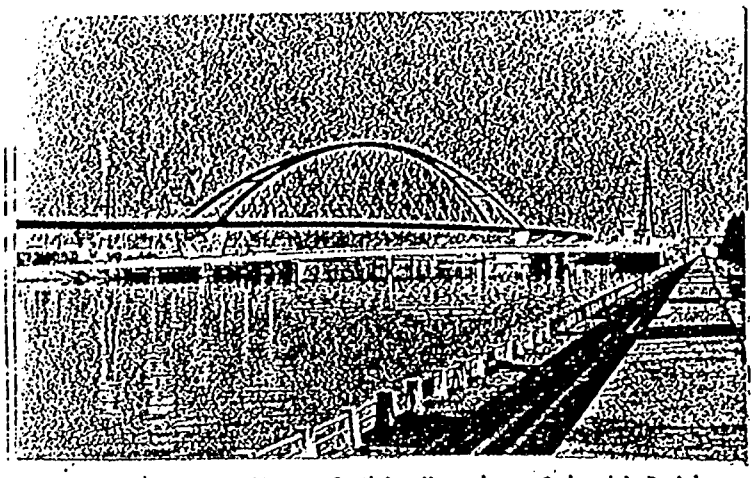
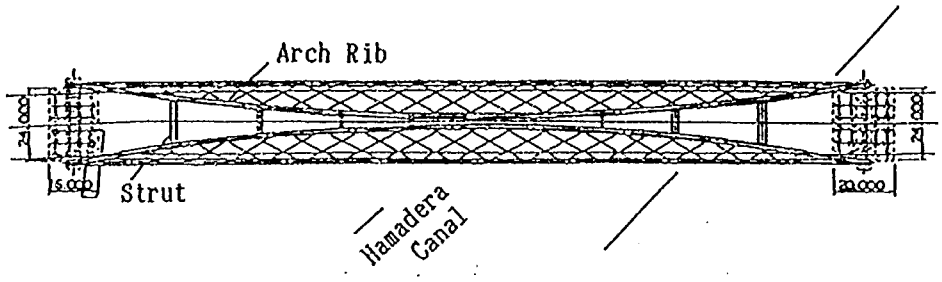
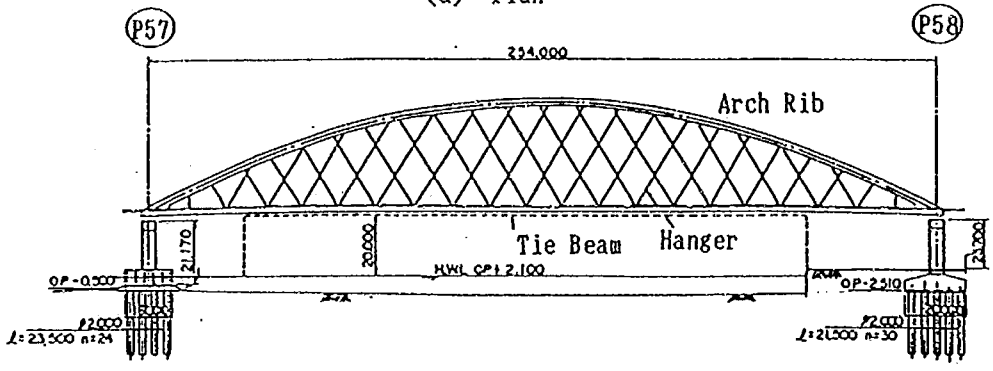


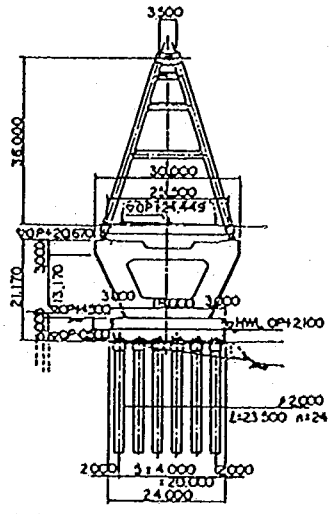
Fig.1 Artistic View of Shin Hamadera Oohashi Bridge



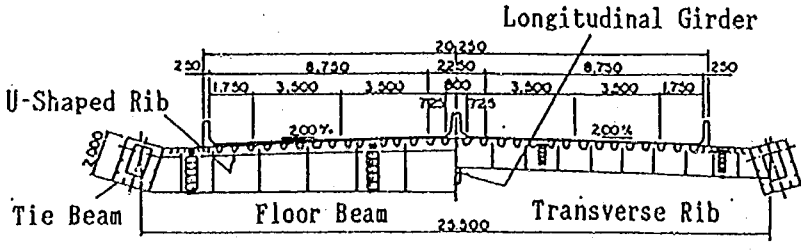
(a) Plan



(b) Elevation

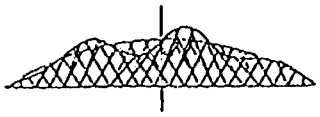
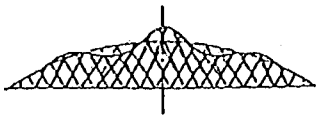
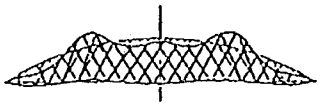
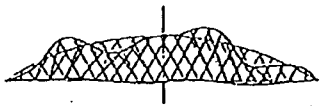


(c) Front View at P57

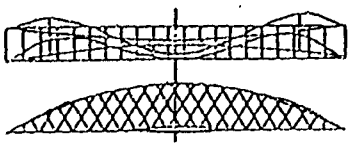
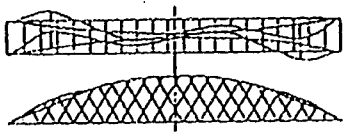
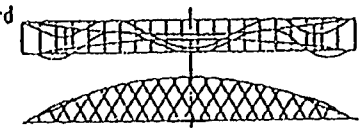
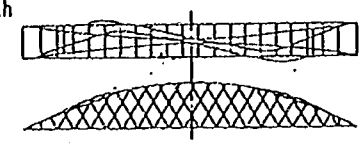


(d) Typical Cross Section of Deck

Fig.2 General View of The Bridge

Load Factor	Buckling Mode
α = 17.37	1st 
α = 17.96	2nd 
α = 20.31	3rd 
α = 21.34	4th 

(a) Two Dimensional Analysis

Load Factor	Buckling Mode	Upper Fig. : Plan Lower Fig. : Elevation
α = 6.49	1st 	
α = 6.98	2nd 	
α = 7.83	3rd 	
α = 8.57	4th 	

(b) Three Dimensional Analysis

Fig.3 Results of Elastic Buckling Analysis

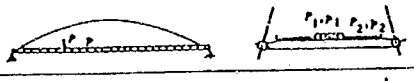
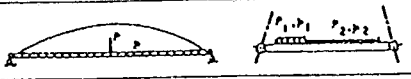
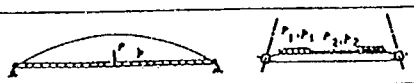
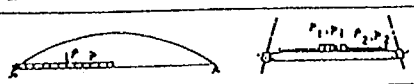
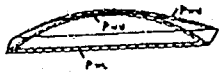
Item / Loading Cases	Applied Live or Wind Loads	JSHB α	JSHB α_{req}	JSHB $\frac{\alpha}{\alpha_{req}}$	AASHTO α	AASHTO α_{req}	AASHTO $\frac{\alpha}{\alpha_{req}}$
① - a		2.38	1.70	1.40	7.60	2.17	3.56
① - b Residual Stress		2.40		1.41	8.00		3.69
① - c Residual Stress, Initial Deflection		2.40		1.41	7.90		3.64
②		2.42		1.42	8.50		3.92
③		2.40		1.41	7.60		3.50
④		2.38		1.40	7.70		3.55
⑤		2.53		1.49	11.6		5.35
⑥ - a		2.23	1.36	1.64	3.64	1.30	2.80
⑥ - b Consider Strut as Elast-Plastic Element		2.00		1.47	3.47		2.67

Fig.4 Results of Inelastic Buckling Analysis

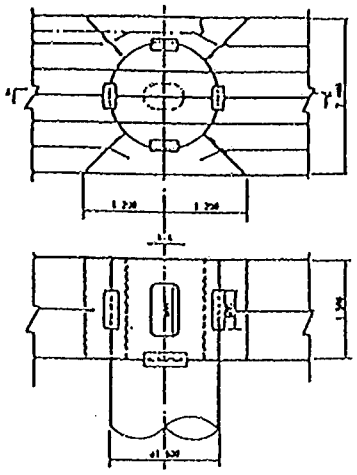


Fig.5 Intersection of Arch Rib and Strut

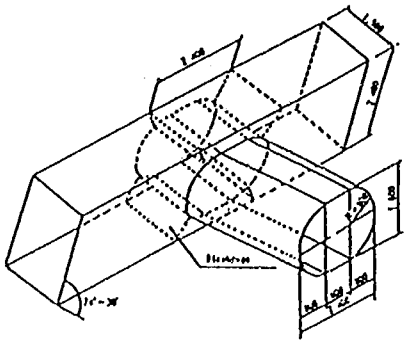
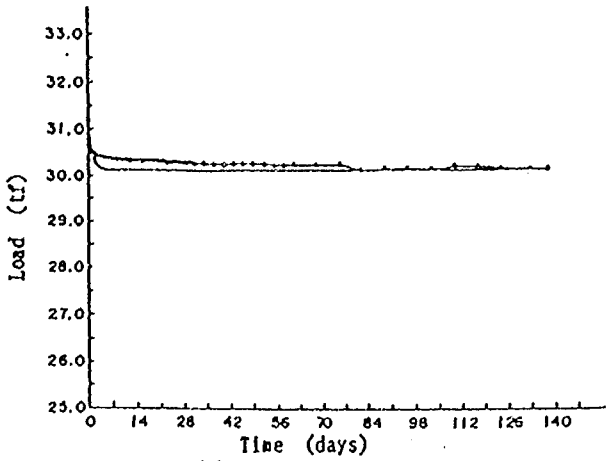


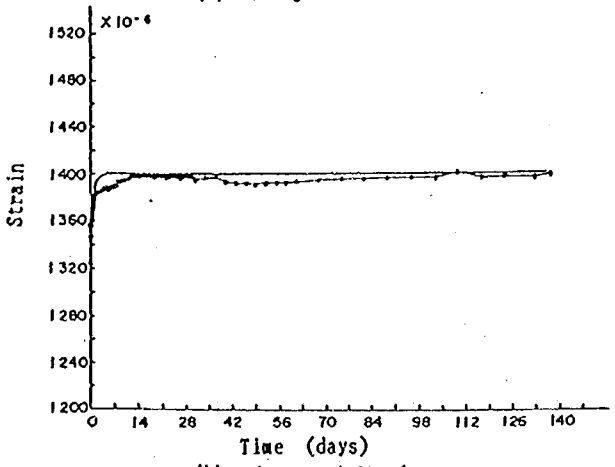
Fig.6 Analytical Model of Intersection

Mode Number	f:Frequency (Hz) T:Period (sec)	Mode Shape
1	f = 0.514 T = 1.946	
2	f = 0.787 T = 1.271	
3	f = 0.811 T = 1.233	
4	f = 0.921 T = 1.085	
5	f = 0.968 T = 1.033	

Fig.7 Vibration Mode

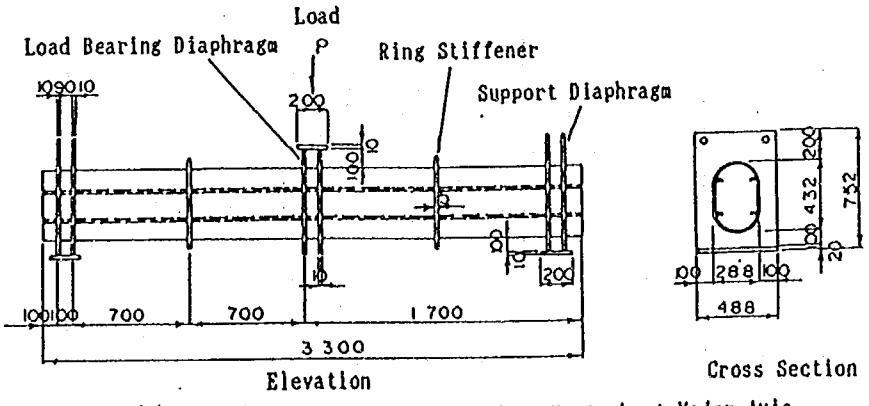


(a) Change of Load

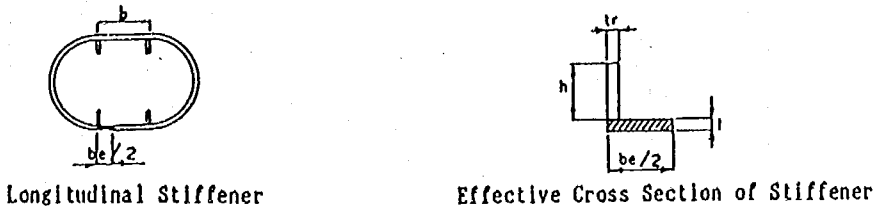


(b) Change of Strain

Fig.8 Creep and Relaxation Test Results (HiAm Anchor,PWS Cable)



(a) Specimen for Laterally Loading Test about Major Axis



Longitudinal Stiffener

Effective Cross Section of Stiffener

(b) Longitudinal Stiffeners and Effective Section

Fig.9 Test of Strut with Oval Cross Section

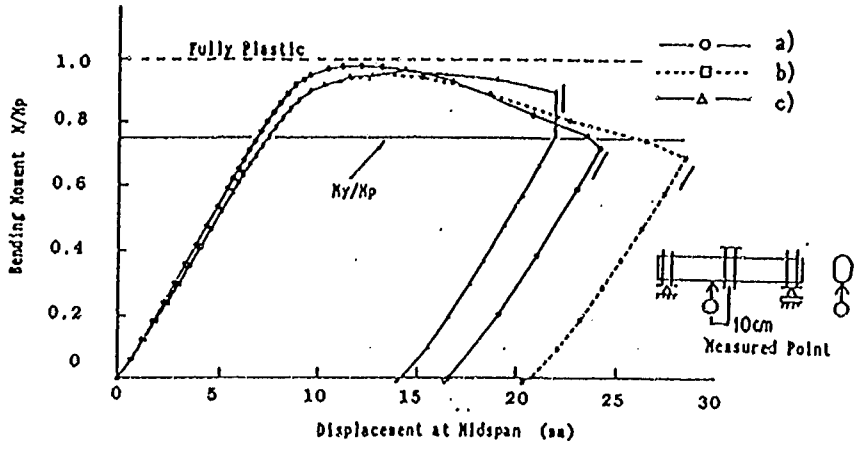


Fig.10 Results of Laterally Loading Test about Major Axis

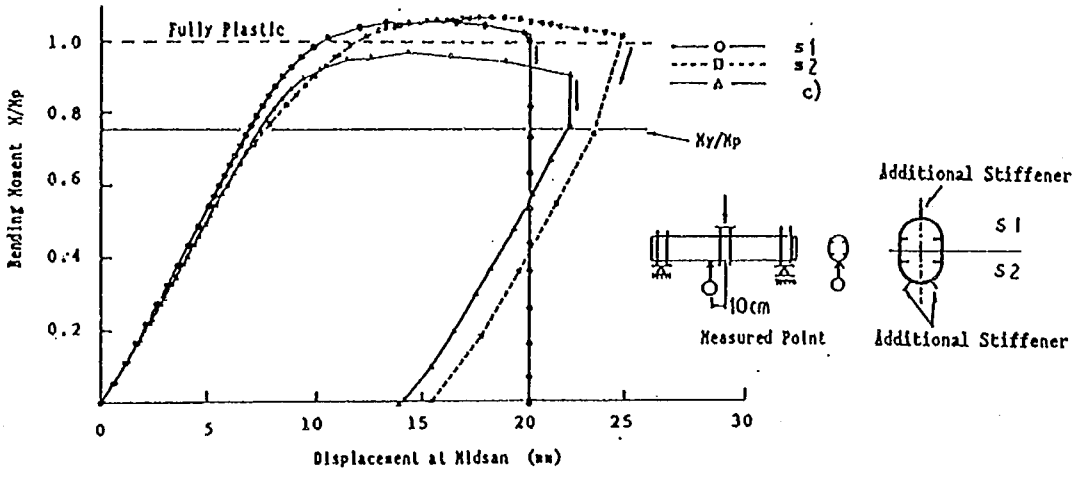


Fig.11 Test Result with Additional Stiffeners

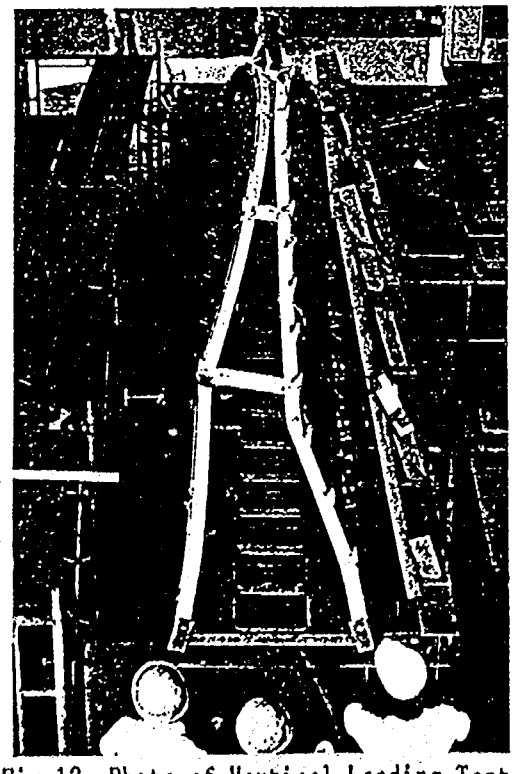


Fig.12 Photo of Vertical Loading Test

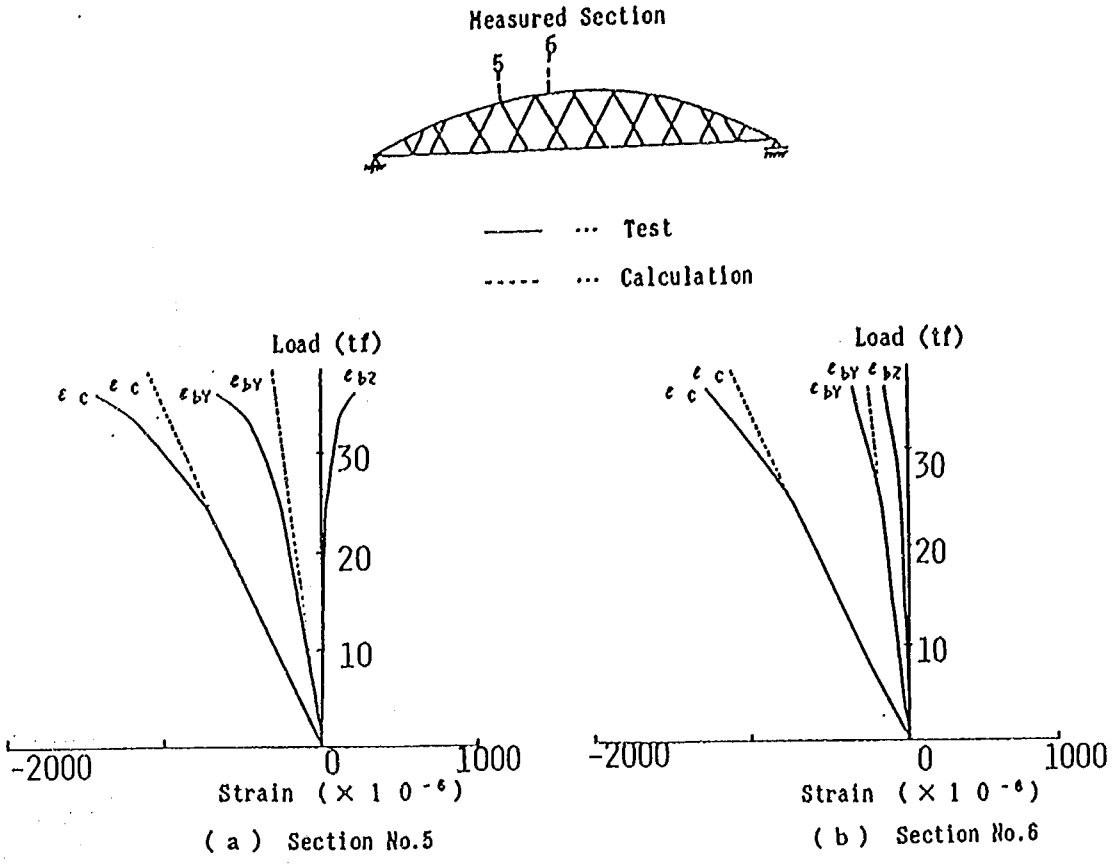


Fig.13 Relationship between Load and Strain

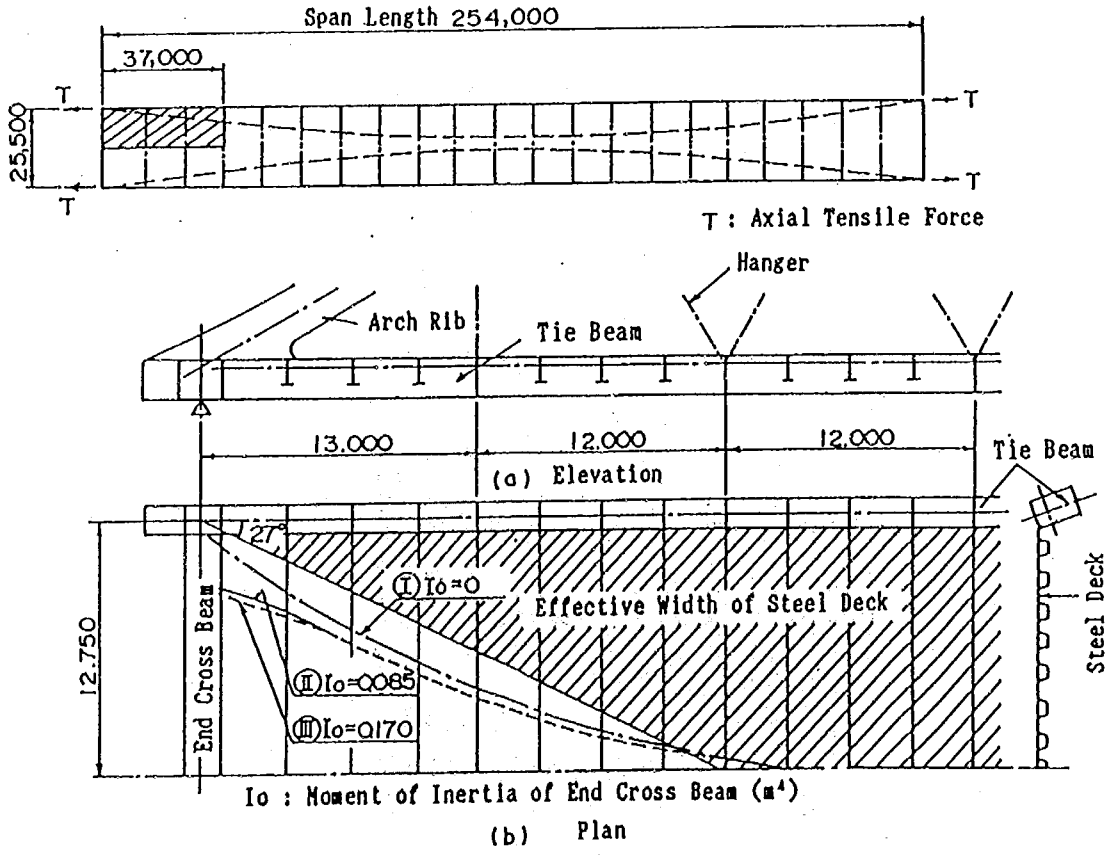


Fig.14 Effective Width of Steel Deck

MODJESKI AND MASTERS

5TH U. S. - JAPAN WORKSHOP ON BRIDGE ENGINEERING

MAY 1989

QUALITY CONTROL TESTING FOR CONSTRUCTION OF CABLE-STAYED BRIDGE AT QUINCY, ILLINOIS

BY

H. EUGENE WALDNER, P. E.

AND

JOHN M. KULICKI, Ph.D., P. E.

MODJESKI AND MASTERS
CONSULTING ENGINEERS
HARRISBURG, PENNSYLVANIA, USA

ABSTRACT

The cable-stayed bridge carrying westbound traffic across the Mississippi River at Quincy, Illinois, was completed in 1987. The structure includes composite steel girders with a concrete slab deck, and twin concrete towers. The cable system utilizes epoxy-coated seven-wire strand grouted in polyethelene pipe. Several special requirements for testing and quality control were included in the construction contract to assure that the final structure provided the features intended by the designers. This paper describes the design and construction of the bridge, and discusses the requirements and results of the special quality control provisions that were specified for the construction phase of the project.

The cable-stayed bridge crossing the Mississippi River at Quincy, Illinois, was completed in 1987. A photograph of the bridge is shown in Figure No. 1. The structure, known as the Quincy Bayview Bridge, is owned by the Illinois Department of Transportation and carries two lanes of westbound traffic on Route U. S. 24. The original Route U. S. 24 truss spans were recently rehabilitated and continue in service to carry the eastbound traffic.

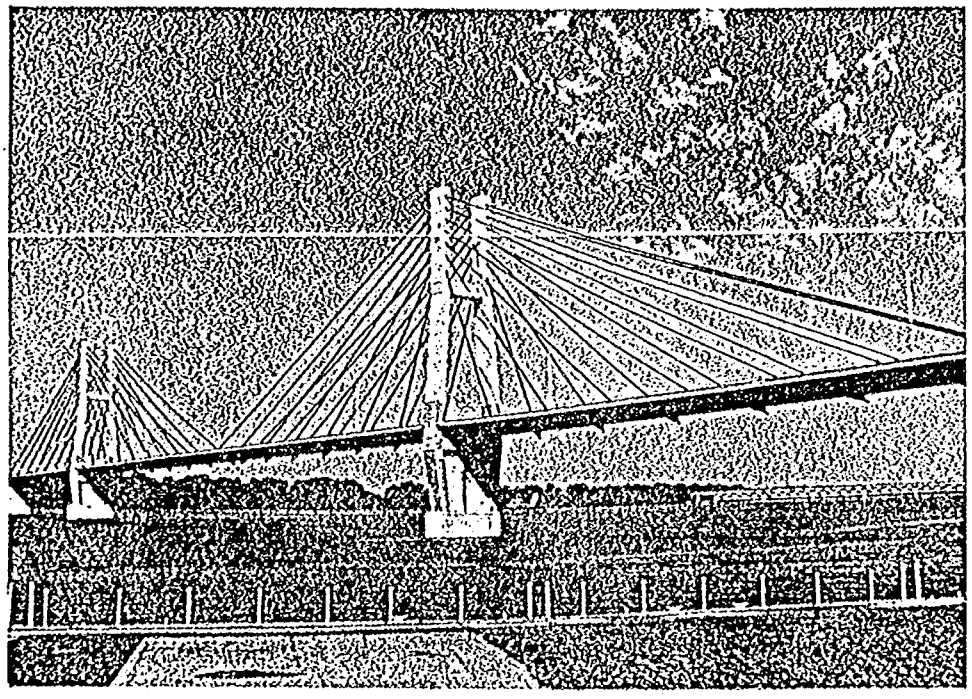
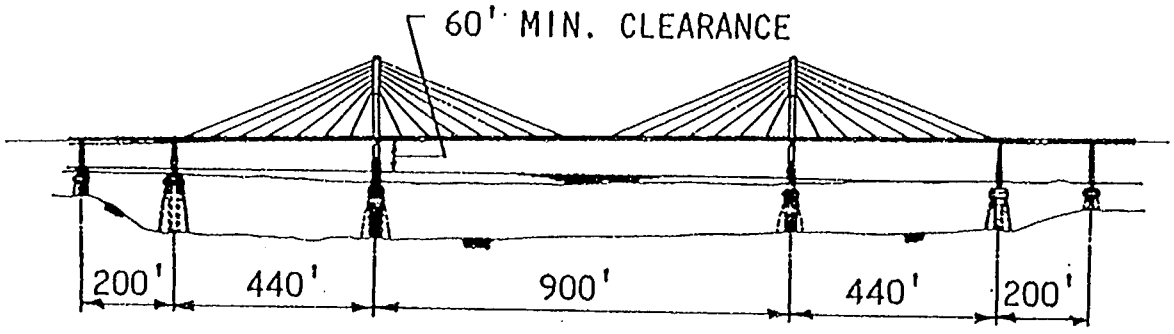


Figure No. 1 - Quincy Bayview Bridge

The bridge location and general type was selected as part of a preliminary study by the Illinois Department of Transportation. The main bridge piers were then designed and constructed under a contract that included the bridge approach structures. The span arrangement was decided during the preliminary study, and during final design a decision was made to keep the same spans for both the steel and concrete alternatives.

The main bridge superstructure was built under a separate contract in order to get substructure construction under way as soon as possible. The hybrid steel and concrete structure was successfully bid in competition with a precast segmental concrete alternative structure, which incorporated similar concrete towers and was similar in overall configuration to the hybrid alternative, but with an increased number of more closely spaced stay cables. Both alternatives were designed by Modjeski and Masters, acting as a Subconsultant to Booker Associates, Inc.

The superstructure contract included construction of the five spans shown in Figure No. 2 and included the two reinforced concrete towers, and completion of the upper shafts of the two reinforced concrete anchor piers. The General Contractor was McCarthy Bros. Construction Company of St. Louis, Missouri, with major Subcontractors DSI-USA, and Stupp Brothers, who furnished the stay cables and fabricated structural steel, respectively.



STEEL ALTERNATIVE

Figure No. 2 - Elevation View

The main bridge consists of a three-span cable-stayed structure, with span lengths of 440 ft, 900 ft and 440 ft. The structure provides vertical clearance over the navigation channel of 60 ft. The cable-stayed structure consists of two cast-in-place towers of reinforced and prestressed concrete, which provide anchorage for the steel stay cables. The roadway deck section is composed of precast concrete deck slabs which are supported by, and are composite with, structural steel framing, including welded longitudinal girders, transverse rolled-section floorbeams and longitudinal roadway stringers. The girders are supported by the stay cables, which are spaced at approximately 60 ft intervals in the longitudinal direction. A total of 56 stay cables are arranged in two vertical planes.

Total length of the structure between abutments is 4,508 ft. The approaches to the cable-stayed spans consist of conventional welded steel girders with cast-in-place concrete deck slabs.

Figure No. 3 shows a typical roadway and deck cross-section. The relatively narrow roadway width of 32 ft permitted the concrete deck slabs to be designed for casting of full-width, full-depth sections up to 11 ft in length. Maximum weight of the individual precast pieces is approximately 30 tons. The slabs were required to provide a minimum compressive strength of 6,000 psi and were stored for a minimum of 180 days prior to erection, to allow for shrinkage and creep control. Steel stringers spaced at 7 ft 3 in. support the slab panels, and the stringers are supported by floorbeams spaced at approximately 20 ft.

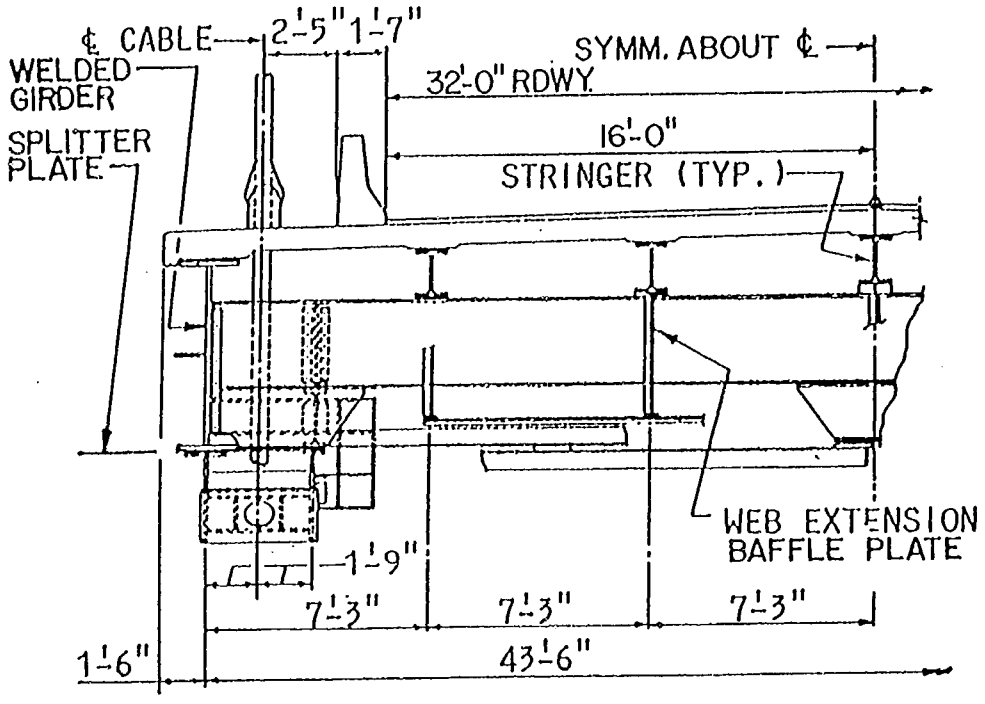
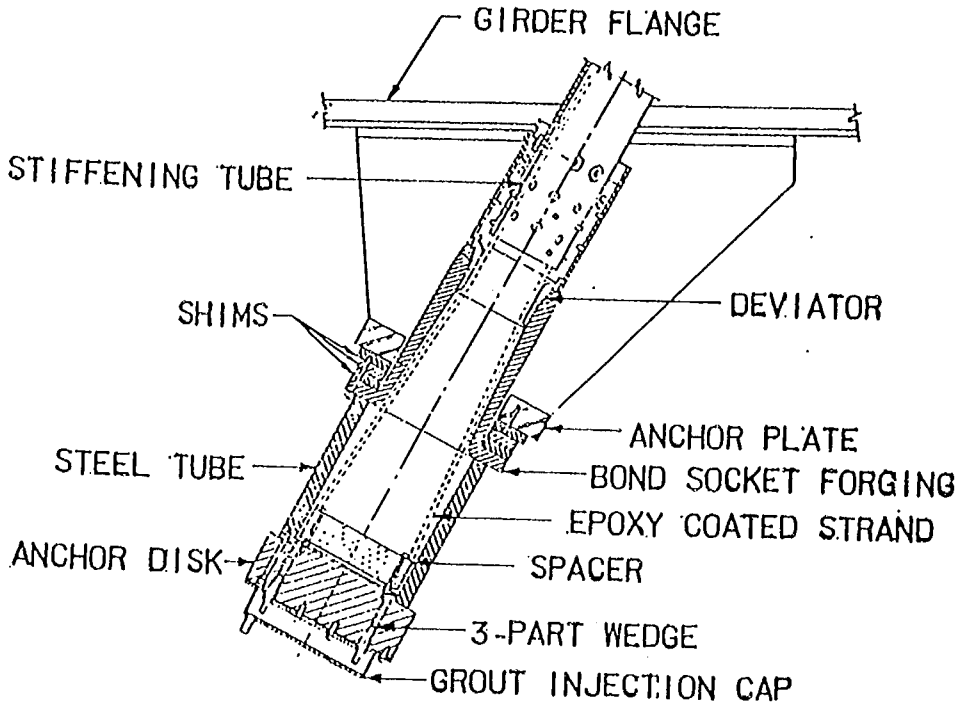


Figure No. 3 - Typical Cross-Section

The stay cables are composed of 0.6-in. diameter Grade 270, seven-wire low relaxation epoxy-coated prestressing strands, arranged in a parallel configuration in each cable. The use of parallel seven-wire strands for this type of cable was one of the first such applications in the United States, and the use of epoxy-coated strands is believed to have been the first such use for stay cables in the world. The cables are composed of 18 to 61 individual strands, depending on design load. Each cable is contained within a full-length polyethylene pipe, and the pipe is completely filled with cement concrete grout. A summary of the cable specification requirements and typical details of the sockets are shown in Figure No. 4.

A change which was implemented after the award of the contract resulted in the cables being furnished with epoxy-coated strands. The cable sockets are weldments which include a bond socket forging with a section of steel tube forming the anchorage end of the socket. The strands are splayed and retained in an anchor disk by wedges which were specially designed to function with the epoxy-coated strands. The sockets are filled with Portland cement grout.



Strands	- ASTM A416, Grade 270, 0.6-in. diameter seven-wire, low relaxation strand
Protection System	- Polyethylene pipe and cement mortar grout
Properties	- Same product of area and modulus of elasticity as originally designed cables, and approximately same weight per unit length.
Testing Required	- Full scale cable tests - Individual strand fatigue acceptance testing

Figure No. 4 - Cable Socket Details and Summary of Specification Requirements for Alternative Cables

The height of the two reinforced concrete towers is approximately 260 ft above normal river level. The tower design incorporates inclined legs which slope inward above and below the roadway deck level, as shown in Figure No. 5. This feature permitted the stay cables to be placed in vertical planes, and allowed smaller pier foundations, resulting in more economical total costs for the towers. The transverse struts at the pylons and below the roadway level are post-tensioned.

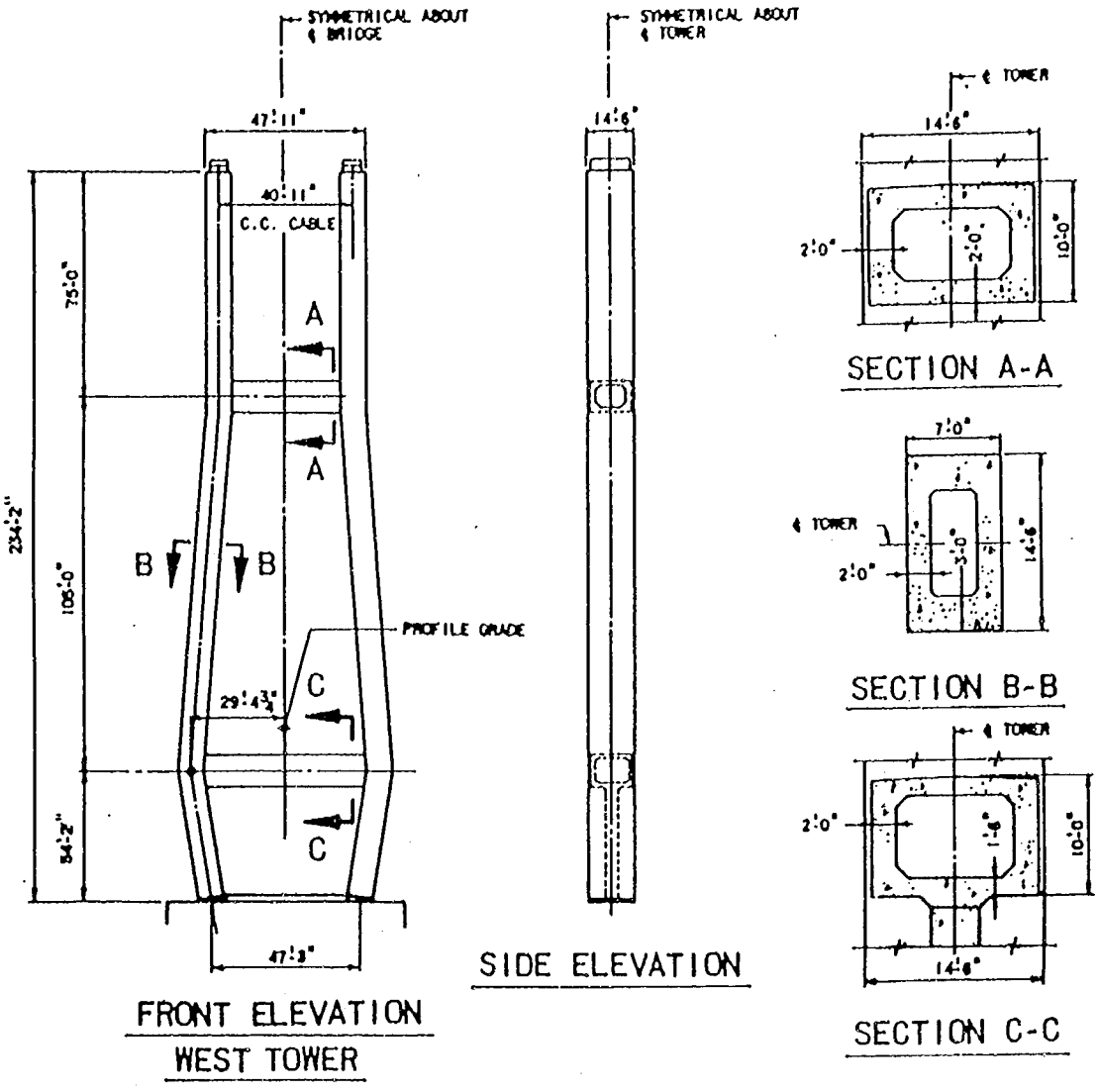


Figure No. 5 - Concrete Tower: Elevations and Sections

The upper vertical tower pylons are post-tensioned in three directions to provide for transfer of the cable loads into the tower. The pylons include short, 7 ft long post-tensioning thread bars, which required extra precautions to assure that adequate final post-tensioning forces were maintained.

An extensive series of wind tunnel tests was conducted during final design by the Low Speed Aerodynamics Laboratory of the National Research Council in Ottawa, Canada, to determine the response of the structure under wind loading (1). As a result of the testing program, modifications were made to the 900 ft main span, which included adding vertical baffle plates beneath the roadway stringers and the addition of intermittent horizontal "splitter" plates in the plane of the girder bottom flanges, as shown in Figure No. 3. These relatively modest modifications were added as precautionary devices to prevent undesirable structure movement under certain low-speed wind conditions, and were considered acceptable when compared to

the increased costs of utilizing an alternative deck section, which may have been more aerodynamically desirable, but would be less economical in performing its basic structural functions.

The construction contract required that three stay cable samples be tested in fatigue for approval prior to actual construction. The samples, each consisting of two sockets, a total length of cable of approximately 17 ft, strand wedges, grout and other components proposed for use on the actual bridge. Three samples, containing 61 strands, 44 strands and 37 strands, were assembled at the Technical University at Munich, West Germany, stressed between two concrete bulkheads and subjected to a fluctuating load superimposed on the initial tensioning load. The choice of number of strands in each test specimen was based on the supplier's intention to utilize two socket sizes; one socket for cables having from 18 to 37 strands and one socket for cables having between 38 and 61 strands. Thus, two of the tested samples involved fully-populated sockets, and one sample involved a relatively open strand pattern. All of the test samples were originally proposed to use uncoated seven-wire strand. As interest built in converting to the epoxy coating strand system, two of the test specimens were eventually made utilizing this product.

Test No. 1 (4) involved 61 uncoated strands stressed for 2,000,000 cycles of 21.6 ksi stress range. Following the application of the 2,000,000 cycles of fatigue loading, the sample was subjected to a tensile test and failed at a load equivalent to 105% of the Guaranteed Ultimate Tensile Strength (GUTS). Dissection of the cable sample indicated that all failures occurred in the free length of the cable; no wires failed at the wedges.

Test No. 2 (5) involved 37 of the epoxy-coated strands and was originally planned to have 2,000,000 cycles at 21.6 ksi. After the specimen had successfully passed this test, it was decided to do some exploratory testing by increasing the stress range in increments, with the understanding that this exploratory testing might result in a lowered tensile test result following fatigue cycling. In addition to the originally programmed 2,000,000 cycles, 250,000 cycles at a stress range of 24.4 ksi were added, followed by 250,000 cycles at 29.7 ksi, followed by 100,000 cycles at 35.1 ksi stress range. During the cycling at the 35.1 ksi stress range, acoustic emission detection equipment indicated that some of the wires in the strands were beginning to fail. Fatigue testing was stopped after 100,000 cycles of this higher stress range (total of 2,600,000 cycles), after which the sample was tested in tension and achieved 83% of the GUTS. Dissection of this sample indicated that some wire corrosion was present, and most of the fatigue damage found in dissection following the tensile test had apparently occurred due to fretting of the corroded areas. There was some speculation that the corrosion was pre-existing due to the presence of pitting which was hard to reconcile with the relatively short test period and some speculation that during vacuum-assisted pressure grouting, water from the grout had intruded under the epoxy coating, presumably by infiltration around the center wire of the seven-wire strand. This experience led to a modification of the field assembly process, requiring that epoxy paint be applied to the ends of the strand anytime a strand was cut. Construction inspectors were rigorous in enforcing this requirement. As a final step in reducing water intrusion, the ends of the

strands were fitted with plastic caps secured with epoxy sealing material. Additionally, periodic random samples of strand have been uncoated and disassembled to inspect for corrosion and, in very isolated cases, parent reels of strand have been rejected.

The third cable sample (6) involved a 44-strand unit and was originally programmed to have 700,000 cycles at a stress range of 29.7 ksi. The test was actually performed on coated samples, and 800,000 cycles of the 29.7 ksi stress range was applied, followed by an additional 627,000 cycles at a stress range of 35.1 ksi. This was followed by a tensile test indicating 109% of GUTS. In this case, tensile testing of companion strand samples was also undertaken, which indicated that the failure load was also equal to 99% of the true strength of the strand.

Testing of 24 individual strand samples was also performed in an exploratory evaluation program. The results of this test series are shown in Figure No. 6. Eight of the samples were tested in Munich and all of the testing was arbitrarily stopped at relatively high numbers of cycles. Half of the samples were then tensile tested, and no broken wires were observed during the tensile testing. As best as could be determined from visual inspection of the remaining five samples, no wire damage was noted. Fourteen samples were tested at Lehigh University's Fritz Engineering Laboratory (7). Some of these tests were carried to extraordinarily large numbers of cycles, as indicated in Figure No. 6.

All of the strand sample testing was done with the modified wedge designed for the use of epoxy coating, and in addition, the 14 specimens tested at Lehigh University had the wedges forceably driven home to simulate a pre-blocking procedure, which was employed in the field to increase the uniformity of the bite of the wedges through the epoxy into the wires of the seven-wire strand.

All of the results of the fatigue testing program are shown on Figure No. 7, along with the recommended strand testing and cable testing, and fatigue design criteria presented in the Post-Tensioning Institute's "Recommendations for Stay Cable Design and Testing" (8). Those test samples which were not actually tested to destruction are shown distinguished from those samples which failed during the testing program. Consideration of this information will show that the results of the fatigue testing program were quite satisfactory.

The upper vertical pylons of the towers utilize 7 ft long post-tensioning bars which required very careful monitoring of the final bar stresses to assure that adequate tension remained in the bars after release of the jacking pressure. The specifications required that the bars be tensioned a second time after a 30-day interval had elapsed subsequent to the initial jacking. The Contractor was also required to apply strain gages to approximately 5 percent of the short bars in order to verify the actual bar stresses, thus providing verification of the prestressing forces required by the pylon design.

DSI Single Strand Tests Epoxy-Coated Strands

No. of Cycles	Stress Range (ksi)	Note
2,150,000	24.3	
1,000,000	29.7	
700,000	35.1	No broken wires observed before tension test
600,000	40.5	
1,510,000	24.3	
1,590,000	29.7	No fatigue failures - All tests arbitrarily stopped
1,300,000	35.1	
700,000	40.5	

Lehigh University Single Strand Tests Epoxy-Coated Strands

No. of Cycles	Stress Range (ksi)	Note
4,130,000	35.0	No failure
510,000	47.5	Failure in grips
315,300	47.5	Failure in grips
295,000	47.5	Failure in strand
3,016,000	40.6	No failure
3,303,400	40.6	No failure
343,400	47.5	Failure in strand
592,000	55.0	Failure in grips
1,627,300	55.0	Failure in grips
1,625,000	55.0	Failure in grips
7,082,000	50.6	Failure in grips
1,568,200	55.0	Failure in grips
855,500	55.0	Failure in grips
266,900	55.0	Failure in strand

Figure No. 6 - Results of Tests of Individual Strand Samples

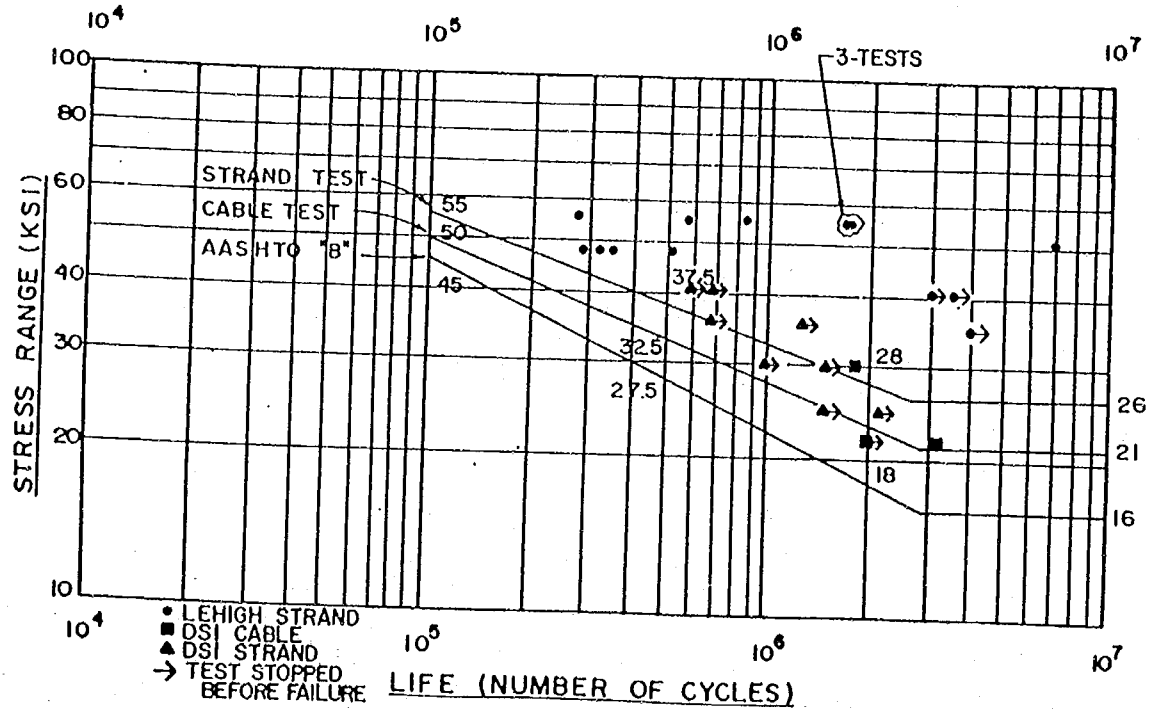


Figure No. 7 - Results of the Fatigue Tests

The results of stressing of the 7 ft post-tensioning bars in the pylons were investigated statistically to determine whether the design requirements were being achieved. Elongations were measured for each bar, as were strain readings for bars equipped with strain gages. The results for the Pier 9 pylons are shown in Figure No. 8 as a histogram of elongation and the following statistical data:

- The total number of bars, average elongation, standard deviation of elongation, and percent of target elongation indicated by the average elongation
- The information above for the bars equipped with bell anchors, rather than plate anchors
- The information above for the instrumented bars
- Comparable information for the stress in the instrumented bars

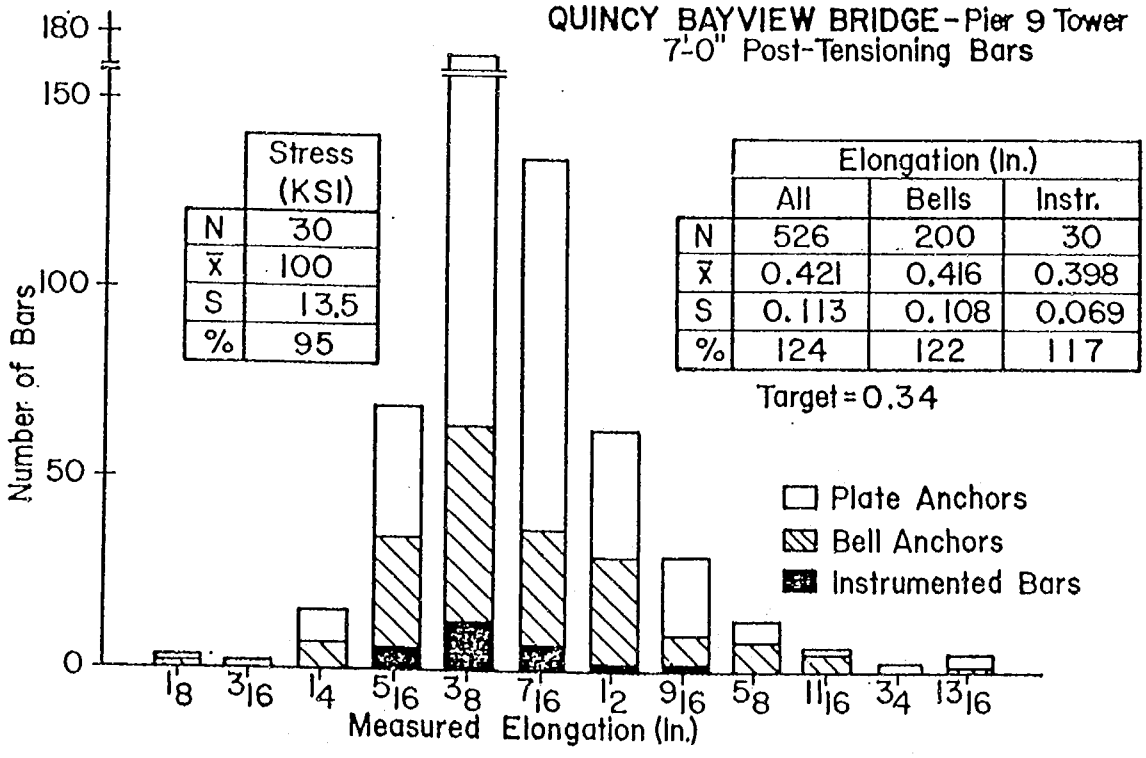


Figure No. 8 - Pier 9 Tower, 7 ft Post-Tensioning Bar Summary

It was concluded that the statistics, in terms of elongation are similar for all bars, bars with bells, and instrumental bars, although the standard deviation of elongation for the instrumented bars is noticeably smaller. Also, the desired stress was reasonably attained in the instrumented bars. Comparison of the elongation of bars with and without strain gage instrumentation implies that the design stress was reasonably well attained in the full population of bars.

It should be noted that the bell anchors were reinforced with a circular steel base plate 1-1/4 in. thick. This improved the behavior of the bell anchors in conjunction with such short bars.

Additional testing conducted during the construction phase included a test to assess the effectiveness of the grouting procedures used to obtain composite action between the precast slabs and the steel girders. A mock-up model was constructed which consisted of steel girder and stringer elements, and a section of concrete slab. The model was then grouted using the same procedures that were to be used for the actual operations. The model was later cut into sections, which further confirmed that the results were acceptable.

A full-scale test also was conducted to verify the methods and materials to be used to grout the cables and cable sockets. The test included grouting of a 40 ft section of cable with sockets on both ends, as shown in the photograph in Figure No. 9. The grouting was accomplished under actual field conditions, using the same equipment to be used on the bridge. The test section was later cut apart at several locations to verify the anticipated results, as shown in the photograph in Figure No. 10. The proper functioning of the socket is dependent upon the integrity of the grout. The test, and later examination of the results, aided in determining that the intended conditions were attained.

The installation of permanent strain gages in the roadway deck elements of the structure was included as a requirement in the construction contract, so that the gages would be available for use in monitoring stresses during construction, and they also would then be available to provide for the continuation of monitoring of stresses after the bridge was placed in normal service. Temperature gages were also installed in the tower sections, mainly for use in monitoring concrete temperatures during the concrete curing period.

Strain gages were embedded in the concrete deck slabs, and attached to the main girder webs, for purposes of recording stresses in the deck cross-section. All gages were oriented to measure primary strains in the longitudinal direction of the structure. The gages used for embedment in the concrete slabs were Carlson strain meters. Weldable strain gages were used on the steel girder webs, since it was determined that long-term bonding of strain gages to ASTM A588 steel has been unreliable. Gages were located near the top and bottom of the web at each selected location, in order to provide for determination of the total stresses caused by the combined bending and axial forces in the girders. A total of seven gages were placed at each of six selected cross-sections located along the length of the west half of the structure. Combined strain and temperature gages were placed at four of the six cross-section locations.

The actual use of the gage readings was minimal during the construction phase. It would have been somewhat cumbersome, and unnecessary, to routinely process and interpret the readings in time to provide for adjustment or modification of the construction sequence or procedure at any given construction stage. The intended construction sequence was established to be independent of the information provided by the gage readings. However, the information was available, in the event that it would have been needed at any stage.

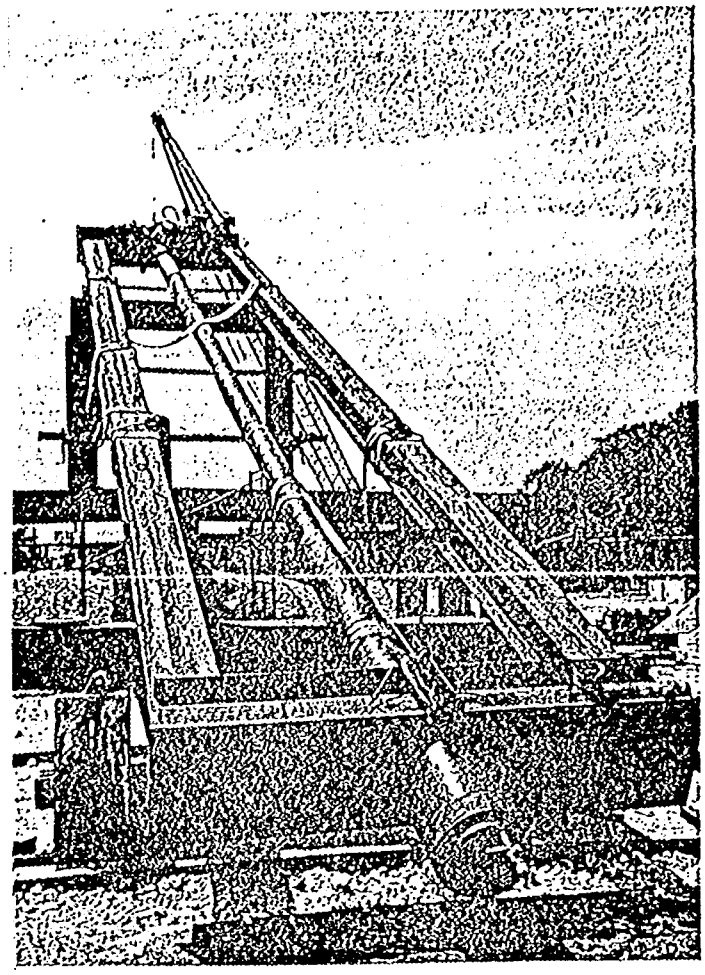


Figure No. 9 - Cable Grouting Test Setup

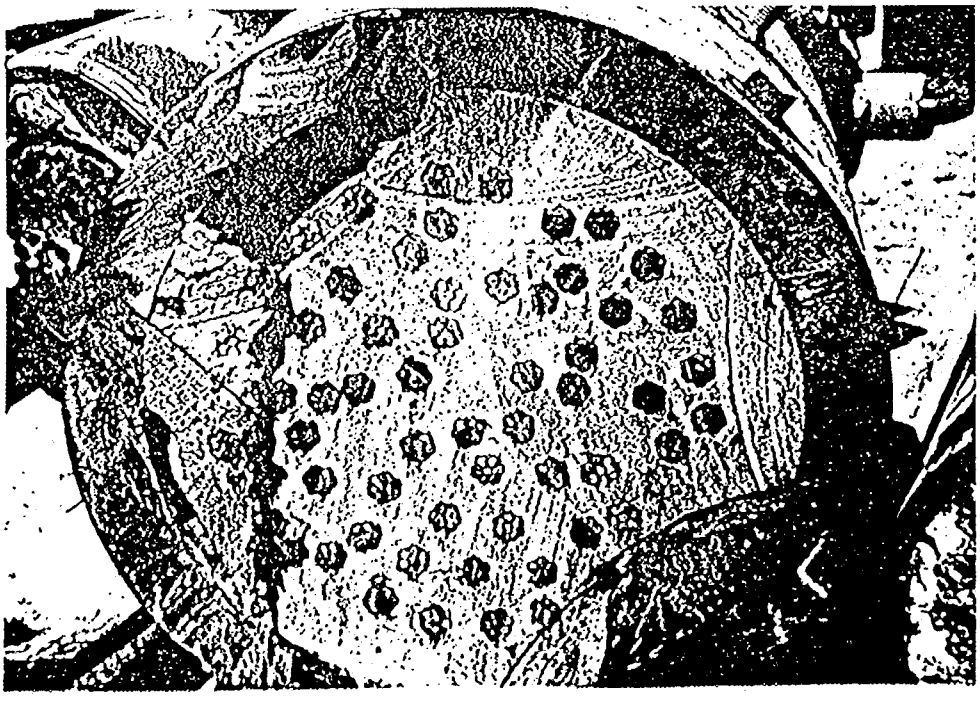


Figure 10 - Section Through Grouting Test Socket

It was found that, in most instances, the observed strain readings for the girder webs were in general agreement with the computed theoretical strains, but correlation with the concrete slab gage readings was much less consistent, perhaps attributable to differences between actual and assumed behavior of the composite section. Records of strain gage readings are continuing to be recorded at periodic intervals by Illinois Department of Transportation personnel, for purposes of long-term monitoring of the structure.

The stay cables were assembled on site, as opposed to the possible alternative use of prefabricated stays. The full-length polyethylene cable pipe was erected first and was supported by several strands which functioned initially as erection strands. The remaining epoxy-coated strands were then placed by pushing them down through the pipe individually, using a strand-pushing device. The strands were temporarily supported at the tower socket to assure that all strands remained parallel and in the proper orientation in the anchor socket. Figure No. 11 shows a photograph of a typical lower socket with the strands in place. After all strands in a cable were placed, the entire cable was loaded by using a multi-strand jack placed at the lower end of the cable. The load was then transferred from the jack and the strands were permanently secured by wedge-type anchors positioned in a steel anchor disk placed on the end of the cable socket assembly. The wedges were especially designed to be compatible with the epoxy-coated strand to assure that the wedge teeth cut through the epoxy and cleanly into the wires of the strand.

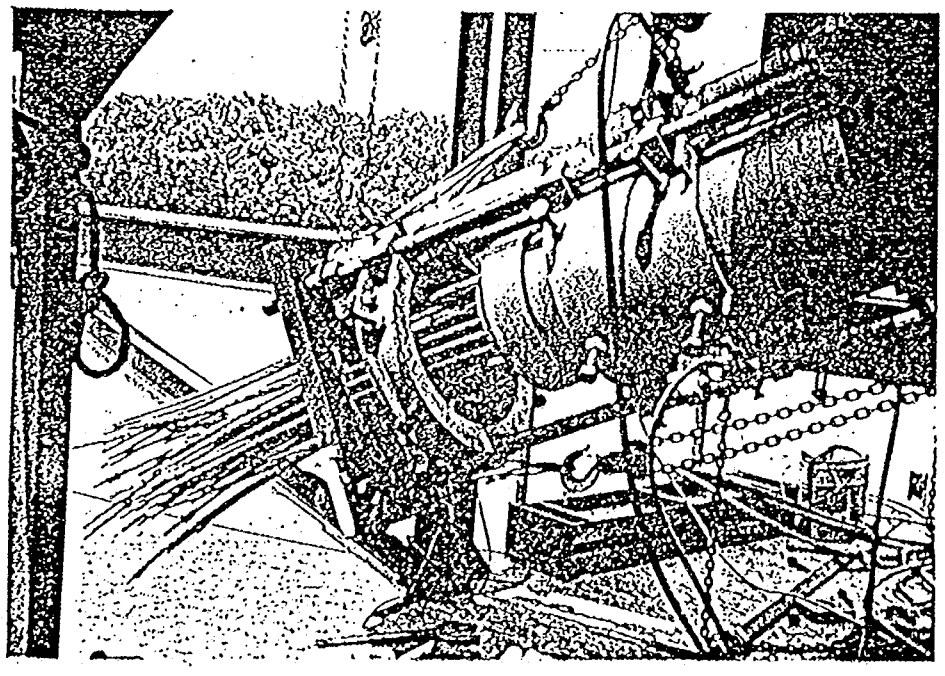


Figure No. 11 - Cable Anchor Socket Assembly

Two means of adjustment of the cable length were available: pulling strands relative to the socket and resetting the wedges, or adding shims between the socket and the bearing plate. The adjustment of length by pulling strand relative to the socket was soon abandoned in favor of shim

adjustments, because it became apparent that when attempts were made to reset the wedges, they were not separating cleanly from the epoxy on the strands. There was a tendency for epoxy to build up in the teeth and pull off of the strand. The change to exclusive use of shim thickness adjustments eliminated this problem.

The erection of the deck followed a specific sequence in order to accomplish the required final design conditions, which included post-tensioning of the deck slab in the longitudinal direction, and the slab being made composite with the supporting structural steel members, after post-tensioning. Each deck section is approximately 60 ft in length, which is the distance between cables. Referring to Figure No. 12, the construction of a typical section of the deck followed the numerical sequence shown.

Precise control of loads and geometry was required during erection of the deck sections. Elevations were monitored frequently, and were compared with previously-computed theoretical values, in order to assure that the cables were being adjusted properly to obtain the correct position for closure of the spans, and that the final stresses would be in accordance with the design requirements.

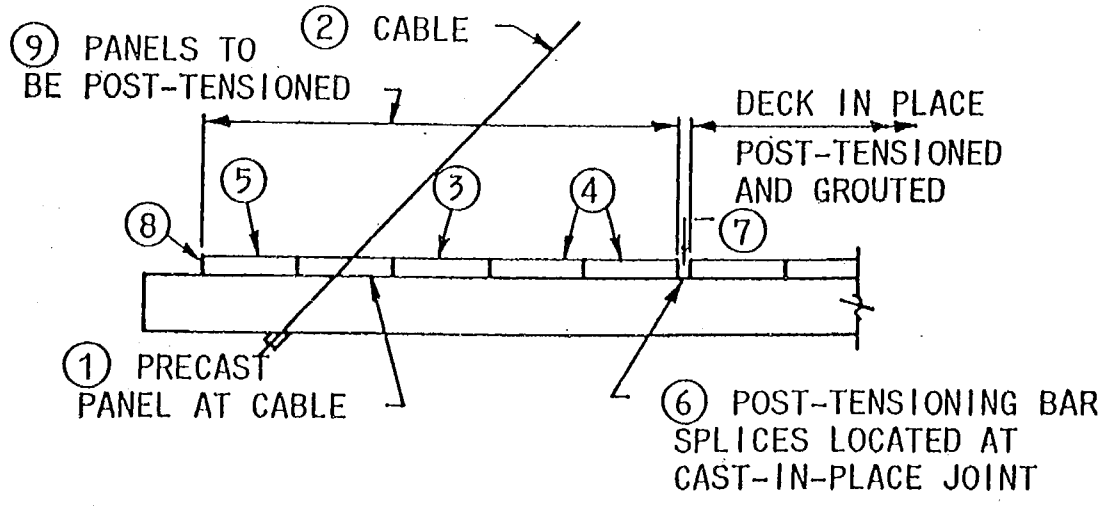


Figure No. 12 - Deck Panel Erection Sequence

A prefabricated cable system would have provided an accurate means of monitoring and controlling the installed cable lengths. However, since the cables were actually assembled in place, a method was developed to determine the length while a cable was being installed. During the erection of a cable, one strand was measured initially, with the strand in place before stressing, and a reference mark was provided on the strand near the lower socket. The reference mark could then be used to determine the final installed length. Since all strands in a cable were jacked

simultaneously by the same amount with the multi-strand jack, it was necessary to measure and mark only one strand in each cable. The necessary cable length adjustments required to complete a cable installation were then made based on observed girder elevations with the cable partially stressed, which were compared with previously calculated required girder positions. The cable length was then established by jacking to a calculated length correction; while comparing the actual and estimated jacking loads, to assure that the cable was not being overstressed. The originally computed cable length was used as a means of verifying the results, but was not used as the actual controlling factor to set the final cable length.

The original design concept assumed balanced erection of the structural steel girders, deck framing, and the precast slabs using floating equipment. The Contractor's erection procedure, however, incorporated the use of two deck-mounted derricks, one on each side of the tower, as part of the balanced cantilever erection process. The derricks were used to erect the precast deck slab units, while a barge-mounted crane erected the structural steel. This method caused construction loadings that exceeded the design service loads, resulting in a proof loading of the cables and their girder and tower connections, of most girder segments, and of the moment capacity of the tower pylons. The erection method used required some minor changes in the dimensions of the precast slabs, but they were constructed essentially as originally designed. The balanced cantilever erection of the deck structure began at each tower and extended alternately in each direction, one section at a time.

After erection of all deck sections was completed on the west half of the bridge, the deck section was anchored at the west approach anchor pier. Balanced erection of the east half of the structure then continued until closure at the center of the main span was accomplished by joining the structural steel members and then casting a closure section of deck slab at mid-span. The final closure was made on the east end anchor pier. Placement of precast parapets and a 1-3/4-in. asphalt wearing surface were then required to complete the bridge roadway.

The final operation in the construction process was the grouting of the cables, which consist of pumping a concrete grout mixture into the void between the group of steel strands making up the cable and the polyethylene pipe sheathing.

ACKNOWLEDGEMENTS

The Authors wish to express their appreciation for the cooperation, assistance and guidance provided by the Illinois Department of Transportation's personnel during the design and construction of the Quincy Bayview Bridge. We especially recognize James T. Rayburn, Engineer of Bridges and Structures, and his predecessor Carl E. Thunman, Jr., and District Engineer, District 6, James C. Slifer and his predecessor, William E. Burns, and their staffs.

REFERENCES

1. Waldner, H. E. and Kulicki, J. M., "Construction of the Cable-Stayed Mississippi River Bridge at Quincy, Illinois, 4th Annual International Bridge Conference, Pittsburgh, Pennsylvania (June 1987)

2. Waldner, H. E. and Kulicki, J. M., "Quincy Bayview Bridge - Construction Control", Cable-Stayed Bridges, Proceedings of the Structural Division of the American Society of Civil Engineers, May 1988

3. Wardlaw, R. L., Tanaka, H., and Savage, M. G., "Wind Tunnel Investigation of the Mississippi River Bridge Steel Alternative, Quincy, Illinois", National Research Council. Canada, National Aeronautical Establishment (February 1984)

4. Dywidag Systems International USA, Inc., "C61 Dywidag Strand Cable Fatigue Acceptance Test" (March 1985)

5. McCarthy Brothers Construction Company and Dywidag Systems International USA-Lemont, "Fatigue Acceptance Tests-C37 Dywidag Strand Cable" (April 1985)

6. Dyckerhoff and Widmann AG, "Report on the Dynamic Test with Subsequent Tensile Test on a Cable with End Anchorages 44 Strands 0.6-inch Diameter; Nominal Ultimate Load 11.47MN" (May 1985)

7. Slutter, R. G., Letter Report Entitled "Quincy Bridge, Monostrand Fatigue Tests" (Private Communication) (November 1985)

8. Post-Tensioning Institute, "Recommendations for Stay Cable Design and Testing" (January 1986)

(7) Session 7

SESSION 7: BRIDGE CONSTRUCTION(2) 10:30am~11:45am
(Co-Chairman: M. Fujiwara, H. E. Waldner)

(18) M. Okahara※ , S. Takagi, H. Obata and H. Mori : Large-scale Plane Strain Bearing Capacity Test of Shallow Foundation on Sand
(10:30am~10:50am)

(19) F. Seible※ : Evaluation of Tendon Coupling Joints in Continuous Post-Tensioned Concrete Bridges
(10:50am~11:10am)

(20) M. Fujiwara, K Minosaku※ , M. Adachi and T. Yamashita: Application of Carbon Fiber Reinforced Plastics to Prestressed Concrete Bridges
(11:10am~11:30am)

DISCUSSION(7)
(11:30am~11:45am)



LARGE-SCALE PLANE STRAIN BEARING CAPACITY TEST OF SHALLOW FOUNDATION ON SAND

by
Michio OKAHARA[1], Shouji TAKAGI[2], Hiroshi OBATA[3], and Hiroki MORI[4]

ABSTRACT

In recent years, after conducting several model tests and element tests concerning the bearing capacity of the shallow foundation, the necessity for reconsideration of the conventional design formulas, derived from the theory of rigid plasticity, has become a theme of discussion.

However the above discussion has only been based on test results by small-scale models in a plane-strain condition with maximum footing width of 10cm and by centrifugal models.

Besides, although centrifugal model tests are generally used to simulate the stress condition in large-scale model tests at the gravitational field, the bearing mechanism, such as the effect of particle size of sand, has not yet been cleared, and therefore the simulation by centrifugal model tests does not always express the actual phenomenon.

Considering the above questions, we have conducted the largest scale two-dimentional model test(width of foundation = 50cm) by using Toyoura sand, standardized soil, as the basis material.

This paper reports the characteristics of bearing capacity and the progress of failure in sandy ground basing on the above test results.

INTRODUCTION

The main problem in studying characteristics of the bearing capacity of shallow foundations is the difficulty in conducting the full-scale loading test in situ, which is normally carried out for a pile foundation. The bearing capacity of shallow foundations has been approximately estimated from formulas based on the theory of rigid plasticity and the results of small-scale model tests. Methods on the theory of rigid plasticity have been commonly adopted in various design standards, and the following expression (1.1) has been used to estimate the bearing capacity (Q) of shallow foundations on sandy ground.

$$Q = 1/2 \cdot \gamma \cdot B \cdot N\gamma \cdot A \quad \cdots\cdots (1.1)$$

1 Head, Foundation Engineering Division,
Structure & Bridge Department, Public Works Research Institute, Ministry of Construction, Japan
2,3 Research Engineer, Foundation Engineering Division,
Structure & Bridge Department, Public Works Research Institute, Ministry of Construction, Japan
4 Foundation Engineering Division,
Structure & Bridge Department, Public Works Research Institute, Ministry of Construction, Japan

γ : unit weight of sand
$N\gamma$: bearing capacity factor
B : width of foundation
A : area of foundation

However, the following problems have been revealed with the progress of study on the bearing capacity of sandy ground through model and element tests.

1) Sand is neither an isotropic nor homogenous material but an anisotropic and compressive material, and the characteristics of its strength and deformation vary depending on constraining pressure.
2) There is a wide gap between the bearing capacity obtained from a strictly controlled small model test and that from the conventional formula to put in soil properties obtained from an element test.
3) The failure observed in a model test is the progressive failure.
4) The phenomenon, scale effect, that the bearing capacity factor NY, decreases with the increase of foundation width has been observed experimentally.

Since the centrifugal model test has the advantage of simulating actual stress conditions, many tests concerning bearing capacities have recently been conducted by this method. Some centrifugal tests have been reported, saying there exists the scale effect of NY. Fig. 1 shows the result of the centrifugal model test conducted by the Foundation Engineering Division, Public Works Research Institute, in 1987-1988. On dense ground, scale effects are observed up to the range of fairly wide foundations (B = 400cm), but on loose ground the convergence of scale effects seems to have appeared within the range of the wide foundation.

However, the effect of particle size on the obtained bearing capacity, or of particle size ratio to width of foundation, which cannot be taken into account of in centrifugal model tests, has recently been pointed out. In fact, there is a report showing that the experimentally obtained value of $N\gamma$ and the tendency of scale effects from centrifugal model tests do not coincide with those from model tests at the gravitational field in a range of small foundation widths ($B \leq 10$cm).

Considering the above problems, large-scale two-dimensional model tests have been conducted to study the bearing capacity and the form of failure. Also, a comparison has been made with past small-scale model test and centrifugal model test.

1. Test Method

The large two-dimensional test pit (2m wide, 7m long, 4m deep) illustrated in Fig. 2 is used. An observation window of acryl board (2m longitudinally, 3m horizontally, 5cm thick) is set in the central part of the diaphram to permit observation of the progress of failures. The front of the acryl board is reinforced with H-steels to be prevented from bulging. Consequently, the maximum deflection of acryl board at the time of loading is only about 0.8mm, thus the condition of plane-strain is satisfied.

1.1 Preparation of Test Ground

The model ground is formed by Toyoura sand dropping from a self-propelled hopper. The thickness of the ground layer is about 2m. The hopper is designed to give the prescribed density by adjusting the hole size and the dropping height, and prior to commencement of the model test, advanced examinations were carried out.

The results are obtained as follows:

	Hole diameter	Dropping height	Moving speed	Unit weight of sand
1	6mm	2m	7m/min	1.59 tf/m^3
2	7mm	2m	7m/min	1.56 tf/m^3

A thin coat of silicon grease is applied on the side wall,and a latex membrane (thickness: 0.2mm) is overlapped on it in order to reduce the friction between the acryl board/sidewall and the model ground.

1.2 Footing and Two-directional Load Cell

In order to measure the distribution of load acting on the footing (50cm x 200cm), the footing is divided longitudinally into three sections (Fig. 3). In addition, the central section is divided latitudinally into 11 parts and each of end sections into three parts. Then, independent load cells are equiped with at all these parts. The base plates of load cells are arranged so as to have intervals of 0.3mm and not to interfere with each other. Silicon rubber is injected into the gaps between base plates to prevent the intrusion of sand. Also, sandpapers are attached to base plates to maintain a coarse surface condition.

As indicated in Fig. 4, the portal type load cell is used to measure vertical and shearing force. Vertical stress and shearing stress are obtained by measuring the strain from the Wheatstone bridge circuit of the four-guages which are attached to the thin part in each of two directions. The performance of each load cell was confirmed by a verification test.

1.3 Items of Measurement and Method of Loading

As indicated in Fig. 2, the settlement of footings is measured by the contact type displacement guage. Displacement at the ground surface at each loading stage is measured by the method of setting guage marks at certain intervals and reading the distance from the fixed point by photographing. Non-contact displacement gauges (accuracy: 0.01mm) are also adopted for this purpose.

Loading is applied at a speed of about 2mm/min using the loading apparatus in the laboratory, and displacement and load are measured after the settlement of each 2mm (load holding period of 4min.). At the first stage, the applied load is reduced to the dead weight of the footing (1.1 tf) after the settlement at the center of the footing reached 10mm. At the second stage, the applied load is continued to increase up to the maximum load.

2. Test Results

2.1 Maximum Load and Settlement

Table 1 shows $N\gamma$, ultimate unit bearing capacity and settlement at central 1/3 part of footing. The values of $N\gamma$ obtained from this test are 85 and 73 in Cases 1 and 2 (void ratio e = 0.69) and 110 in Case 3 (e = 0.66). These values are smaller than those obtained from small-scale model tests and centrifugal model tests.

2.2 Load Settlement Curves

Figs. 5 ∿ 7 show load-settlement curves for Cases 1∿3. A solid line represents the value measured by the load cells at the central 1/3 part of the footing and a dotted line represents the value obtained from the total load. According to these figures, the curves are rather linear up to about 1/2 of the maximum load (settlement: about 10mm), but beyond this point the curves become non-linear. In Cases 1 and 2 where the ground is rather loose, no increase of load is observed after the settlement of about 20mm, however, in Case 3 where the ground is dense, the gradient of the load-settlement curve is rather constant until it reaches the maximum load. In all these cases, settlement at the time of maximum load is about 26-28mm. And beyond this point, the load gradually decreases to the point of the settlement of 30-40mm and then increases again.

2.3 Form of Failure and Failure Line

Photos 1∿4 show the progress of failure lines. The initial failure line occurs from the edge of the footing at the load level of 1/2 Pmax (settlement: 10mm). The failure line gradually spreads with the increase of load, and at the point of maximum load it reaches to 1/2 depth of the final wedge. After that, with the increase of settlement, several failure lines follow to occur, and finally the wedge zone is formed by lines occurring inside of the initial line. The width of the initial failure line is 3-4mm, and with the increase of load, the 2nd, 3rd lines and so forth follow to occur in a manner in which they overlap the previous lines. Thus, finally a failure line with a width of 15-20mm is formed.

From the above observations, it is clear that the form of failure is progressive.

2.4 Comparison with Small-scale Model Test

Fig. 8 compares $N\gamma$ obtained from this test with that from the previous model tests (small-scale). In the figure, Δ represent results of small-scale model tests and ▲ represent results from this test (same range of e = 0.65 0.66). The value of $N\gamma$ does not converge even at the foundation width of 50cm, however the degree of decrease of $N\gamma$ for wide foundations (width ≧ 10cm) is much smaller than that for narrow foundations (width < 10cm). Fig. 9 compares load settlement curves obtained from small-scale model tests (width = 10cm) and large-scale model tests (width = 50cm). The two cases show rather similar tendencies.

2.5 Comparison with Centrifugal Model Test

Fig. 10 shows load-settlement curves obtained from this test and the centrifugal model test (footing width: 2cm, with acceleration of 25g) in the case of a void ratio of 0.69 (unit weight: 1.56 tf/m^3). From this figure it is seen that at the initial stage of loading the result of the centrifugal model test coincides with that of the large-scale model test. However, as for the maximum load and settelment, the centrifugal model test produces a larger value. Fig. 11 compares sf/B_0 values (sf: settlement at the maximum load, B_0 : footing width), and Fig. 12 shows $N\gamma$ of both tests. In these figures, Δ represent the results of the small-scale model test, o represent the the results of the centrifugal model test, and ▲ represent the results of this test. All of these tests were conducted within the range of e=0.65 ∿ 0.66. The values of $N\gamma$ of centrifugal model tests are larger than those of small-scale and large-scale model tests. Although both results show scale effects, $N\gamma$ of centrifugal model tests decrease almost with the logarithmic proportion, whereas large-scale model tests (width ≧ 10cm) give a smaller degree of decrease of $N\gamma$. As for sf/B_0, the values from centrifugal model tests increase with the increase of the width of the foundation, however, the values from the gravitational field tests remain at the same amount, or rather tends to decrease with the increase of the width of the foundation.

Fig 13 shows the relationship between s/q value (footing settlement/footing average pressure) and foundation width B (in centrifugal model tests, nB_0) at the load level of 1/2 the maximum load. Herein, s/q represents the reciprocal of the load-settlement curve at the initial stage of loading. In this figure, ● represent the results of the small-scale model test, o and □ represent the results of the centrifugal model test, and ▲ represent the results of our test. Both the results from centrifugal model tests and model tests at the gravitational field tend to show similar properties of deformation, and the difference of particle size (against the width of the foundation) seems to have no effect on the characteristics of deformation at the initial stage of loading.

From the above mentioned, at the initial stage of loading, at which properties of sand elements can be considered as a continuous material, the results of centrifugal model tests coincide with those of model tests (at gravitational field). But it is considered that the phenomena in both tests changes with the development of the failure line, and it seems that this difference is originated from the difference of particle size.

Conclusion

The followings have been concluded from our test results for shallow foundations:

(1) The value of bearing capacity factor $N\gamma$ obtained from this test are smaller than those from small-scale model tests (width of foundation < 10cm) because of scale effects, however, the degree of decrease of N for wide foundations (width ≧ 10cm) is smaller than that for narrow foundations (width < 10cm).

(2) The initial failure line develops from the edge of the footing at the load level of 1/2 Pmax. The failure line goes on with the increase of applied load, however it does not form the wedge zone even at the time of maximum load. At later stages, the 2nd, 3rd lines and so forth occur with the increase of settelment, and finally the wedge zone is formed by

lines developing inside of the initial line. The occurrence and progress of failure lines prove progressive failure of ground.

(3) The following have been confirmed by comparisons with the results of a centrifugal model test:

1) The centrifugal model test gives a larger value for $N\gamma$. Also, the degree of decrease of $N\gamma$ in centrifugal model tests is different at foundation widths of 10cm or over, thus the result does not coincide with that of model tests at the gravitational field.
2) The value of sf/B_0 in the centrifugal model test tends to increase with the increase of the width of the foundation, whereas the value in the model test at the gravitational field tends to be constant. When the foundations are of the same width, sf/B_0 of the model test at the gravitational field is smaller than that of the centrifugal model test, and therefore the tendencies in both tests are completely different.
3) At the initial stage of loading, both tests coincide each other in the inclination of load-settlement curve. Therefore, only at this stage, the centrifugal model test is useful to simulate the stress condition in the model test at the gravitational field.

REFERENCES

1) H.Ymaguchi,T.Kimura,N.Fujii:Experimental Studies on The Bearing Capacity of Shallow Foundation by The Used of a Centrifugal,Proceeding of JSCE NO.233,Jan.1975

2) T.Kimura,N.Fujii,K.Saitoh,O.Kusakabe:An Investigation on The Bearing Capacity of Shallow Footing on Sand,Proceeding of JSCE NO.319,Mar.1982

3) T.Kimura,N.Fujii,K.Saitoh,O.Kusakabe,A.Shidai:On The Effect of Anisotropy on Bearing Capacity and Deformation of Sand,Proceeding of JSCE NO.319,Mar.1982

4) M.Okahara,S.Takaki,H.Obata,H.Mori,M.Tatsuta:Centrifugal Model Bearing Capacity Test of Shallow Foundation on Sand,Proceeding of The 43rd Annual Conference of JSCE ,Oct.1988

5) K.Tani,F.Tatsuoka,T.Maeda:Experimental Study on Bearing Capacity of Strip Footing on Sand Ground (1,2),Japan National Conference on Soil Mechanics and Foundation Engineering,1985~1986

6) K.Tani,F.Tatsuoka,H.Mori:Effect of Pressure Level and Model Size on Bearing Capacity of Model Strip Footing on Sand The 22th Japan National Conference on Soil Mechanics and Foundation Engineering,Jun.1987

7) K.Tani:Mechanisum of Bearing Capacity of Shallow Foundation on Sand,Geotechnical Engineering Report,University of Tokyo,1986

8) K.Yosida:Bearing Capacity of Characteristics of Shallow Foundation on Sand,University of Tokyo,1988

9) De Beer,E.E:Bearing Capacity and settlement of Shallow Foundations on Sand,Symp. Bearing Capacity and Settlement of Foundations,Duke Univ.,Durham,1965

10) De Beer,E.E:The Scale Effect on The Phenomena of Progressive Rupture in Cohesionless Soils,Proc.6th ICSMFE,Vol.2,1965

11) Muhs,E.:Discussion,Session 4,.Proc.6th ICSMFE,Vol.3,1965

12) Steenfelt,J.S.:Scale Effect on Bearing Capacity Factor Nγ.Proc.9th ICSMFE,1977

13) Vesic,A.S.:Analysis of Ultimate Loads of Shallow Foundations,Proc.ASCE Vol.99,SM1,1973

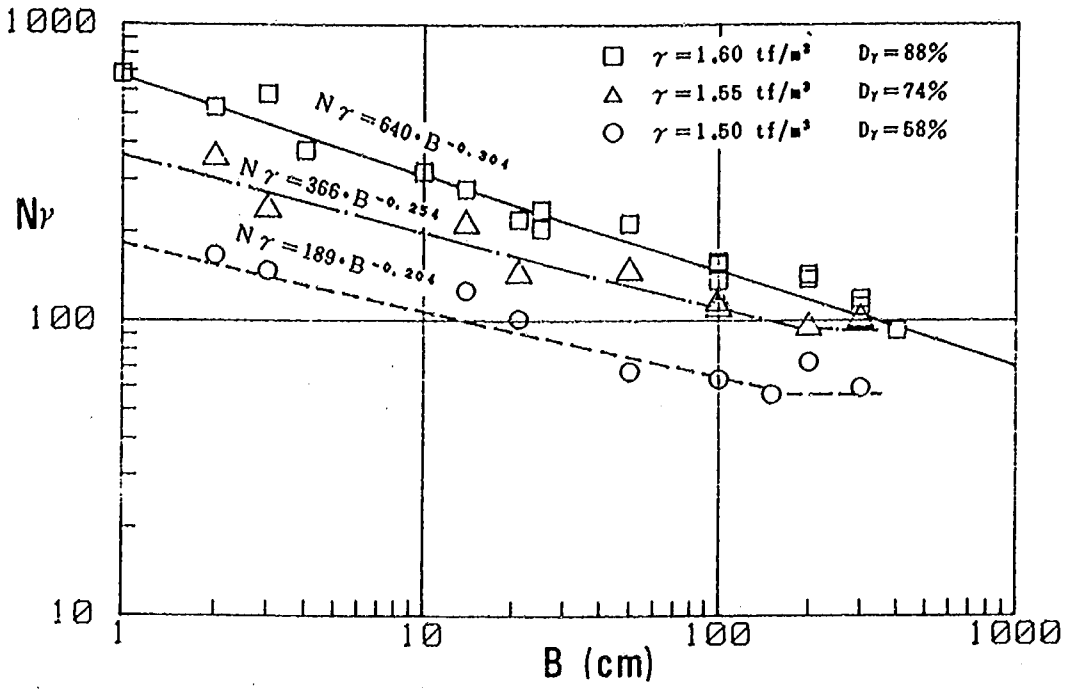


Fig. 1 Scale Effect of Nγ by Centrifugal Model Test (Toyoura sand)

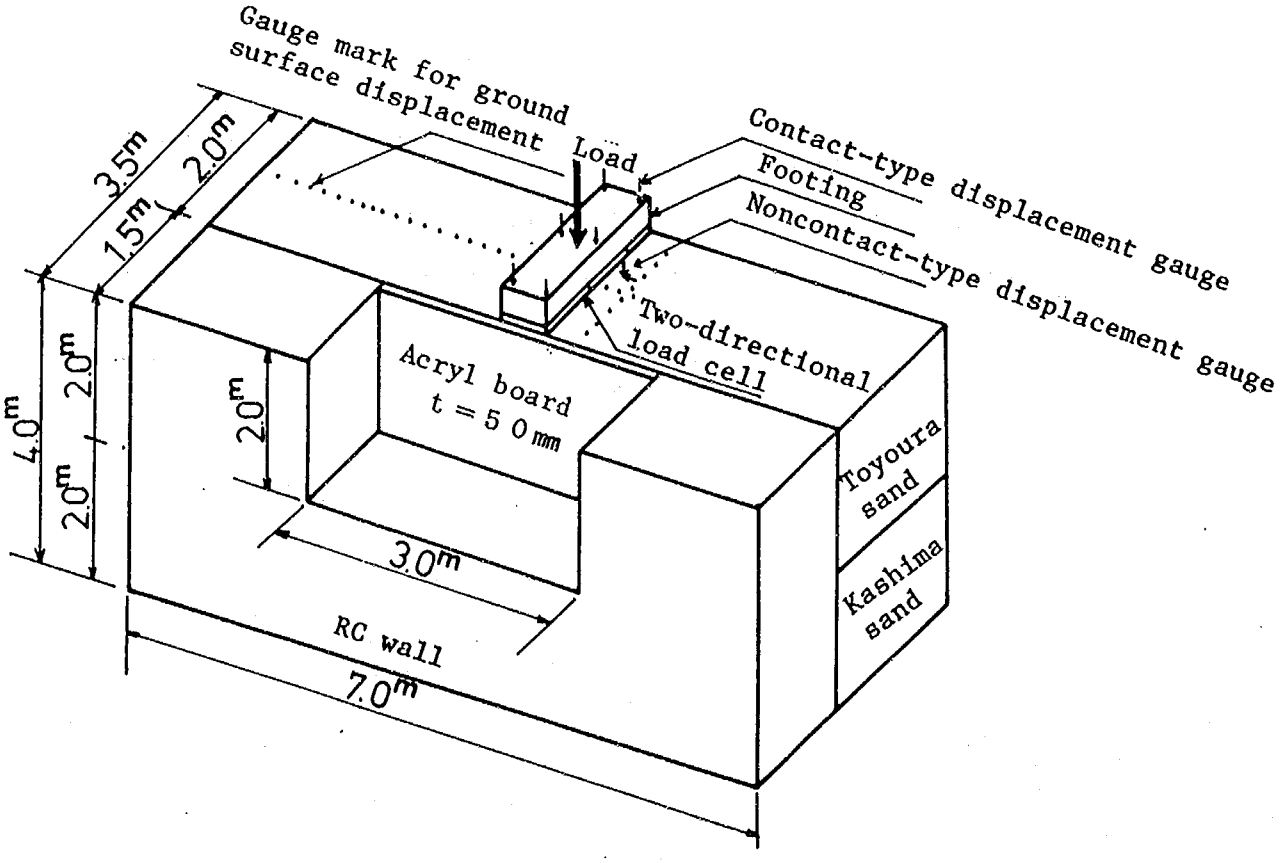
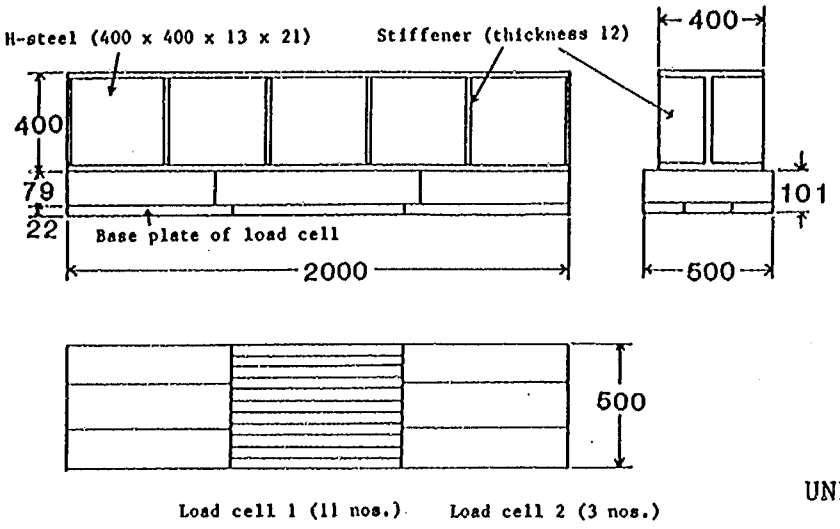


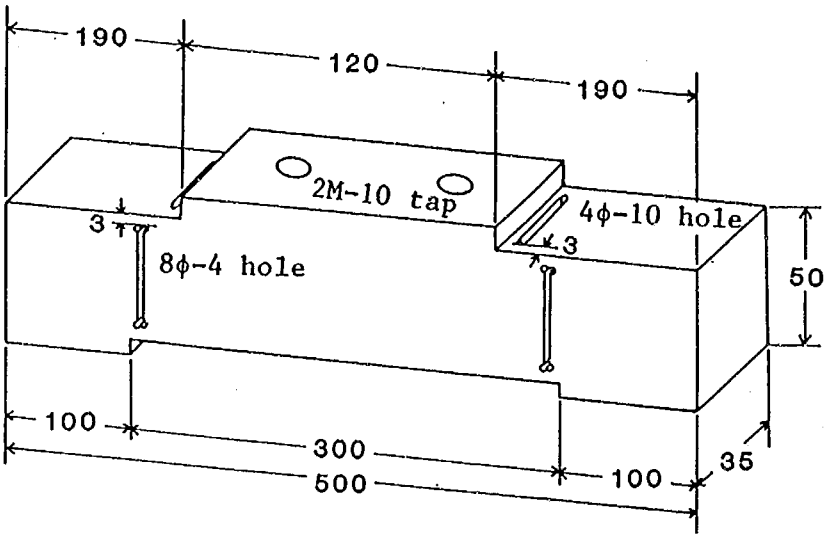
Fig. 2 Large Two-dimensional Test Pit



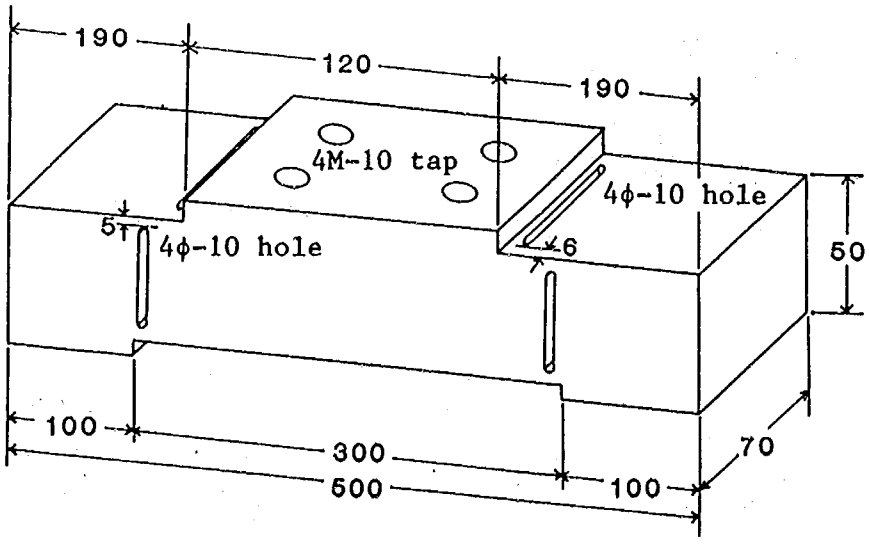
UNIT: mm

Fig. 3 Footing

Load Cell 1



Load Cell 2



UNIT: mm

Fig. 4 Load Cell

Table 1 Test Results

Case No.	Unit weight (tf/m^3)	Ultimate unit bearing capacity (tf/m^2)	Bearing capacity factor Nγ	Settlement at time of maximum load (mm)
CASE 1	1.56	33	85	28
CASE 2	1.56	28	73	26
CASE 3	1.59	44	110	27

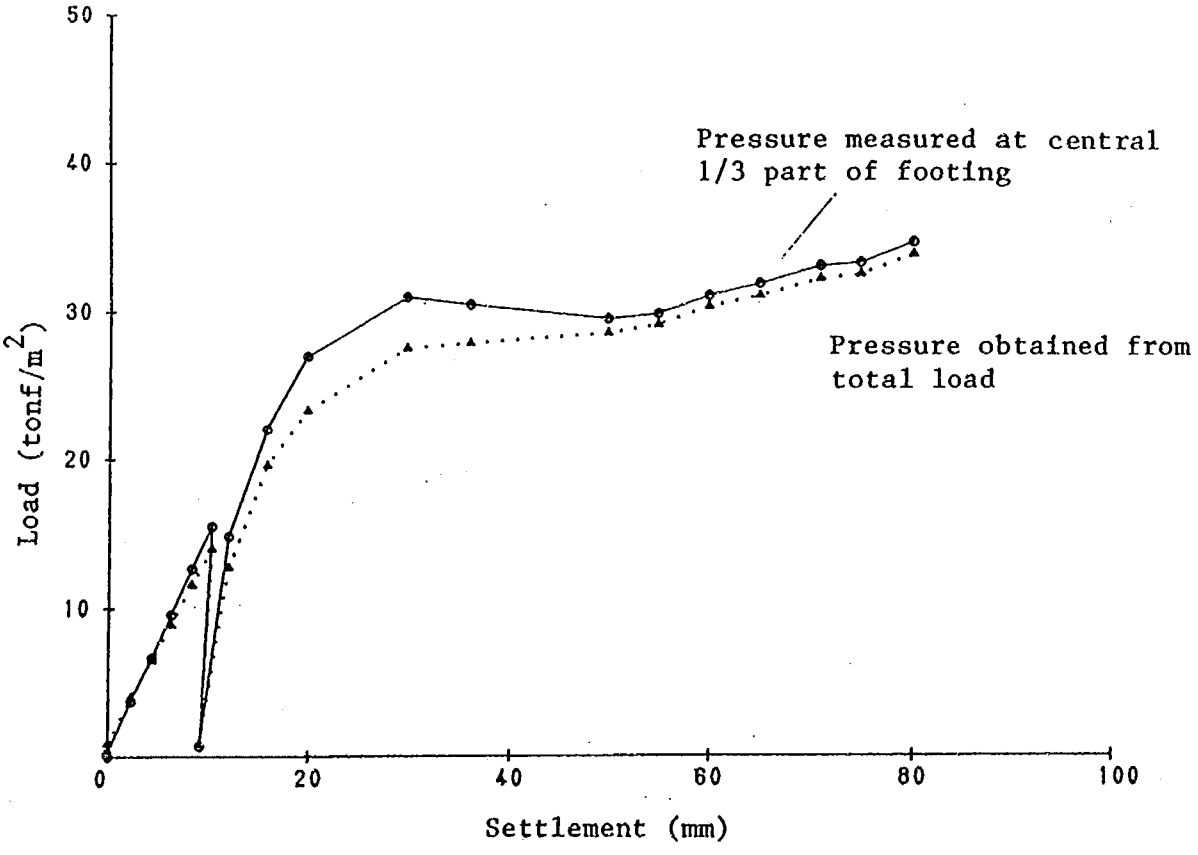


Fig. 5 Load-Settlement Curves (CASE 1)

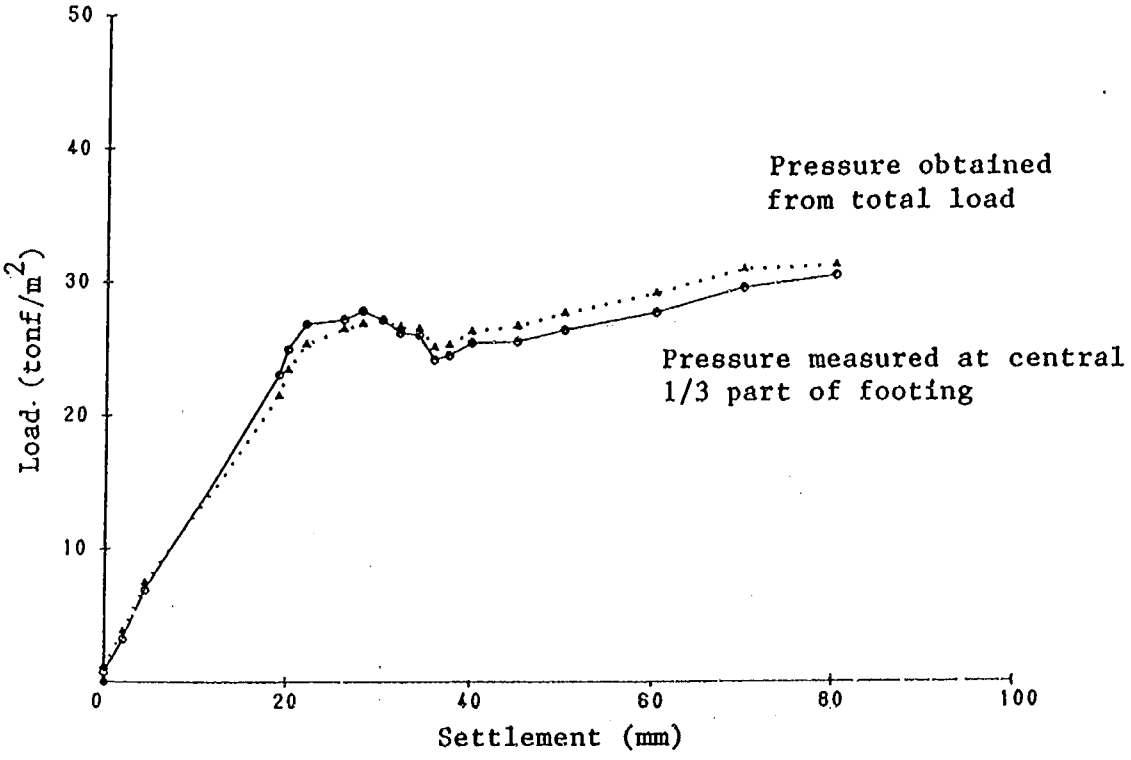


Fig. 6 Load-Settlement Curves (CASE 2)

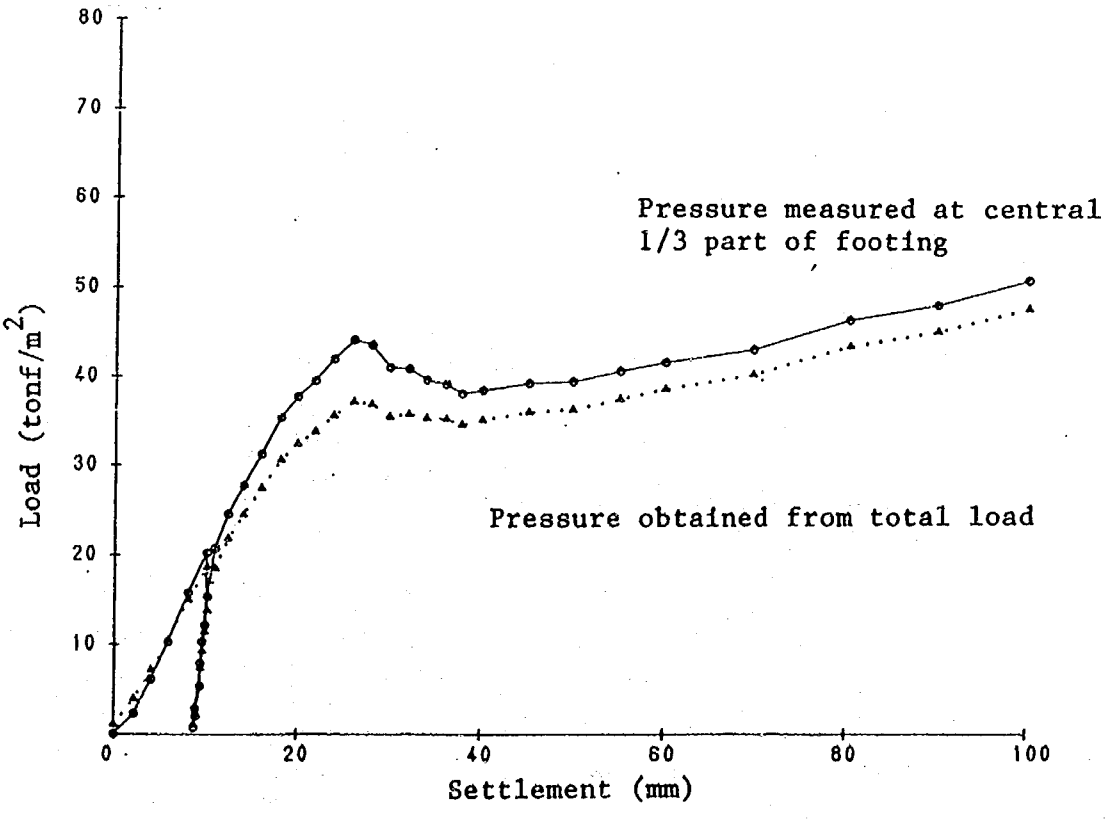


Fig. 7 Load-Settlement Curves (CASE 3)

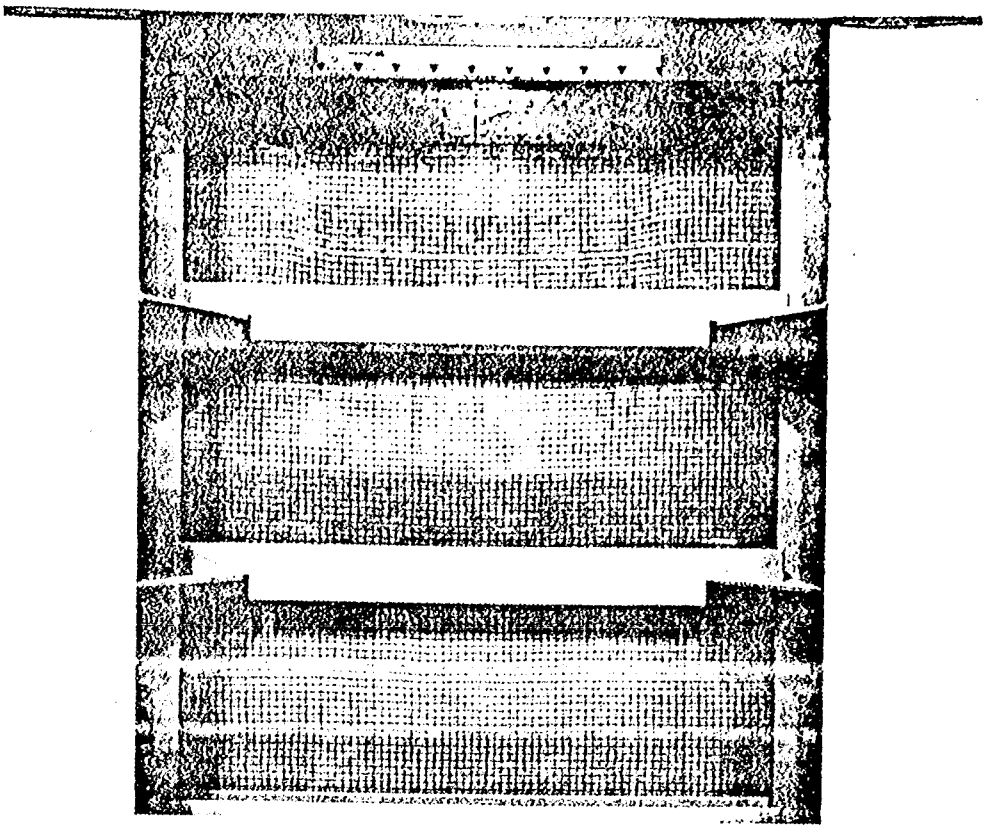


Photo 1 State of Occurrence of Failure Lines: CASE 3
(load 21 tf, settlement 18 mm)

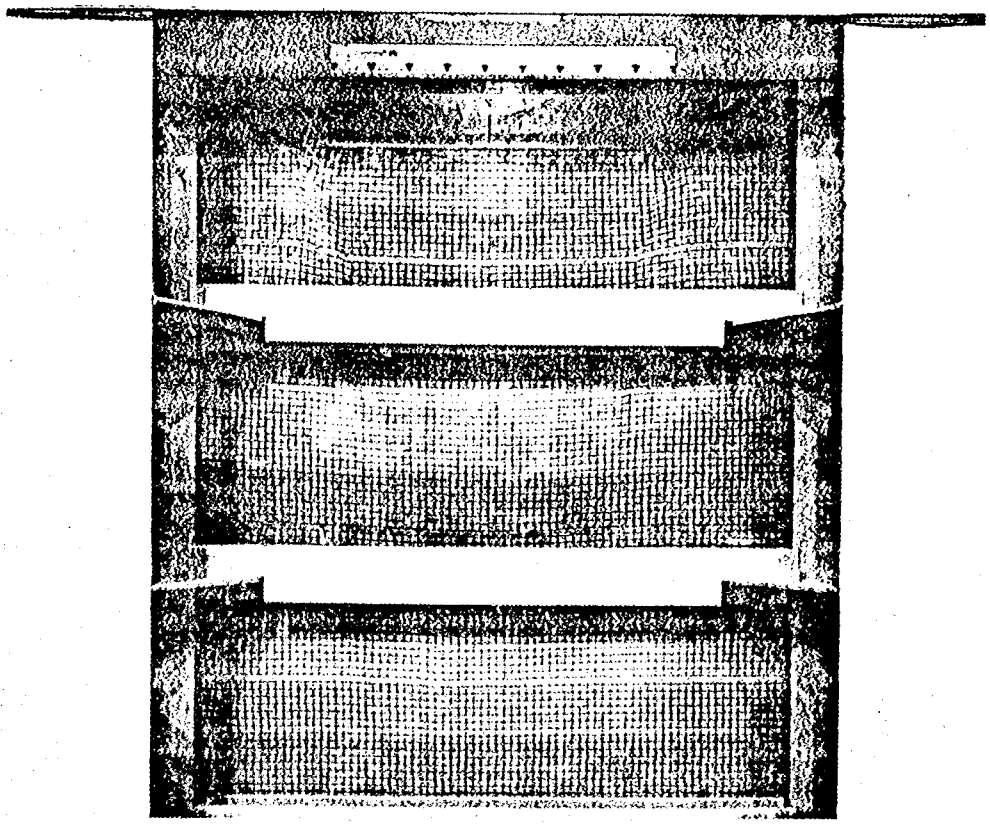


Photo 2 State of Occurrence of Failure Lines: CASE 3
(Vicinity of maximum load, settlement 28 mm)

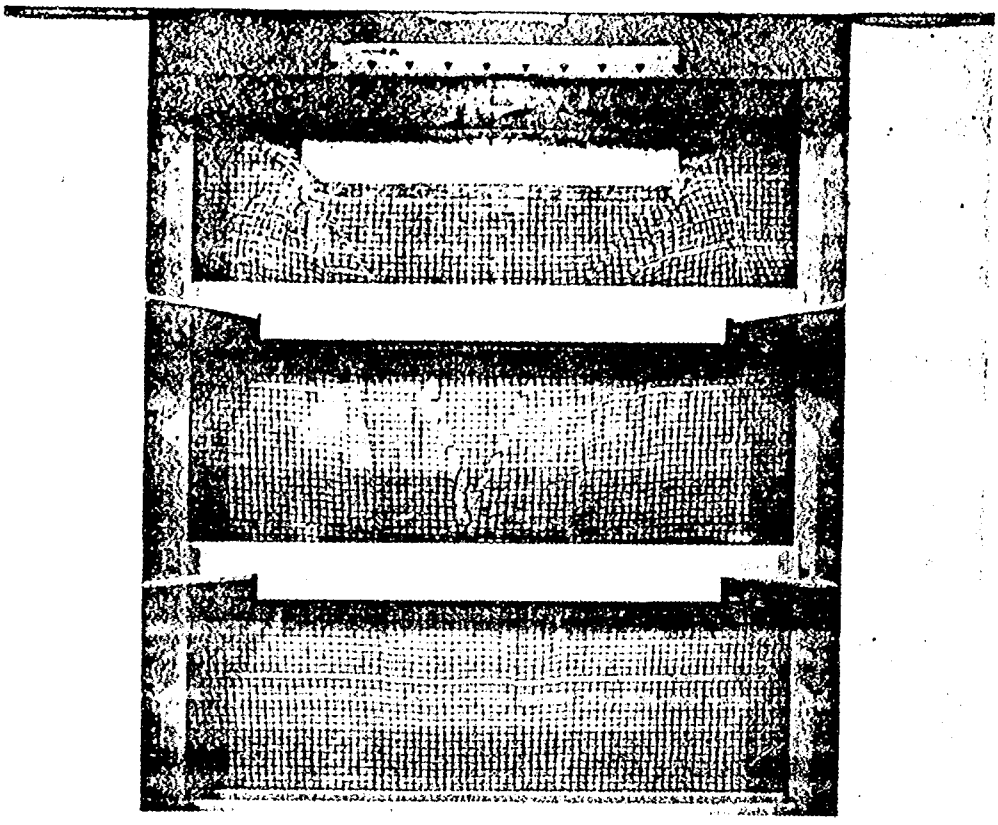


Photo 3 State of Occurrence of Failure Lines: CASE 3 (final-shape, settlement 80 mm)

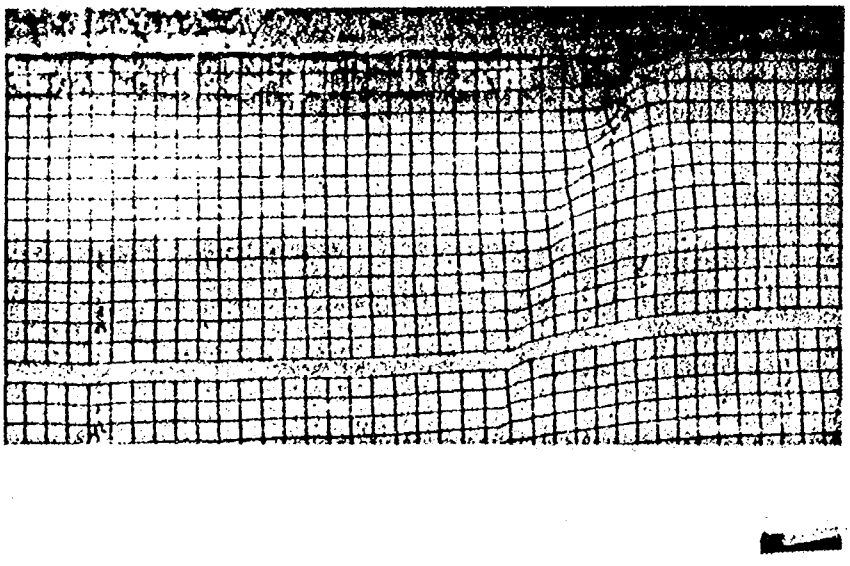


Photo 4 Failure Lines (CASE 3 settlement 28 mm) (mesh intervals 10 mm)

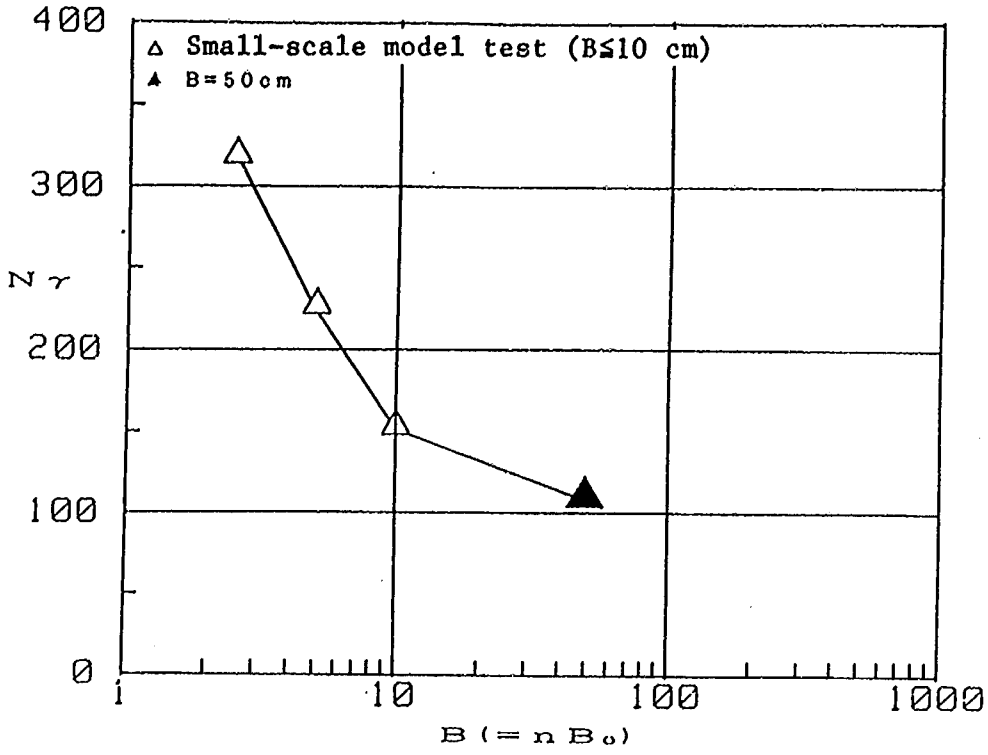


Fig. 8 Scale Effect of Nγ in Gravitational Field Test

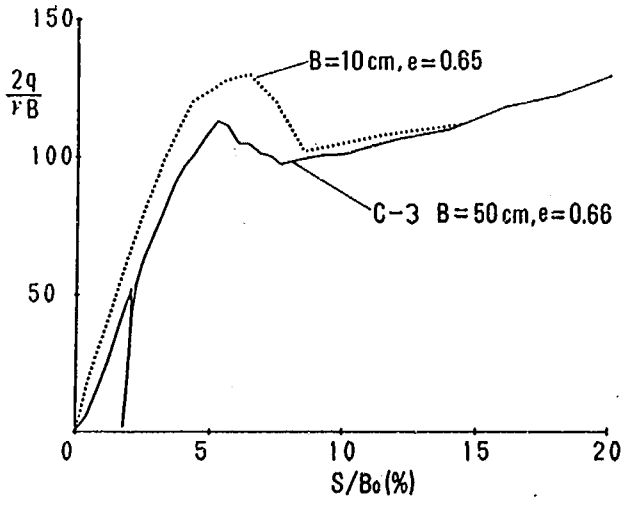


Fig. 9 Comparison with Small-scale Gravitational Field Test of Foundation Width of 10 cm (load-settlement curves)

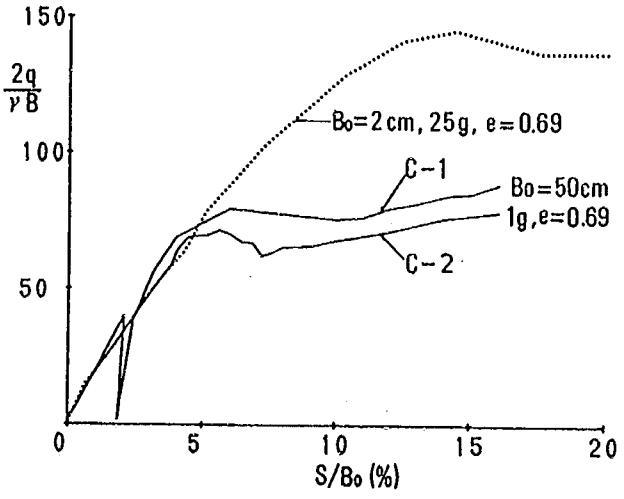


Fig. 10 Comparison with Centrifugal Model Test (load-settlement curves)

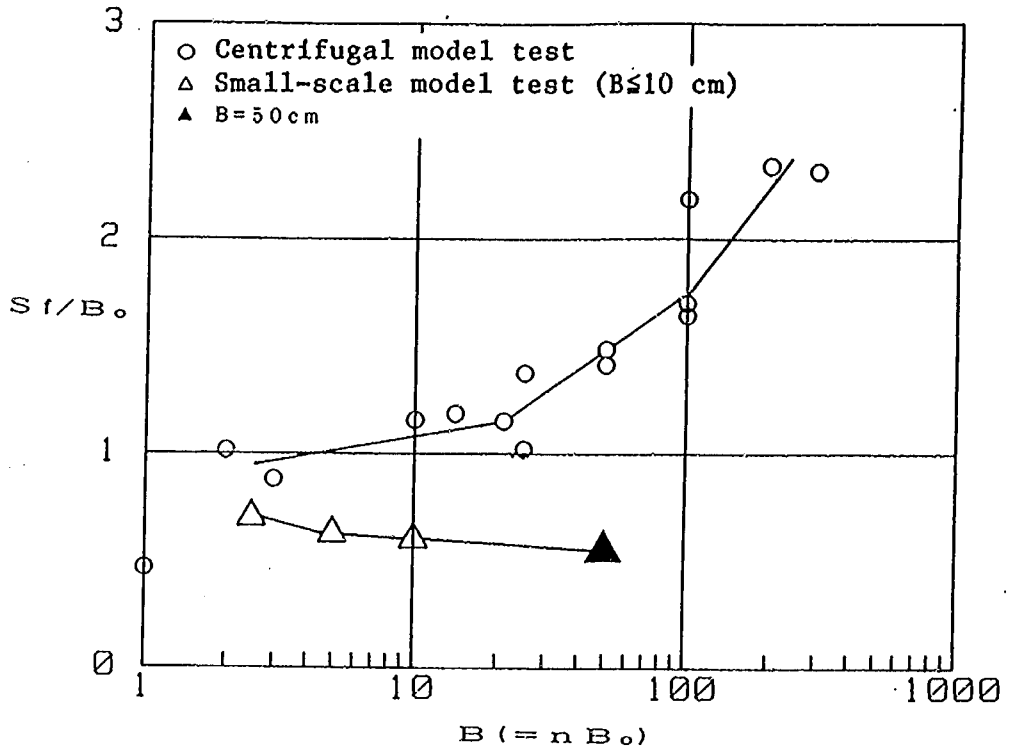


Fig. 11 Comparison with Centrifugal Model Test ($B\text{-}S_f/B_o$)

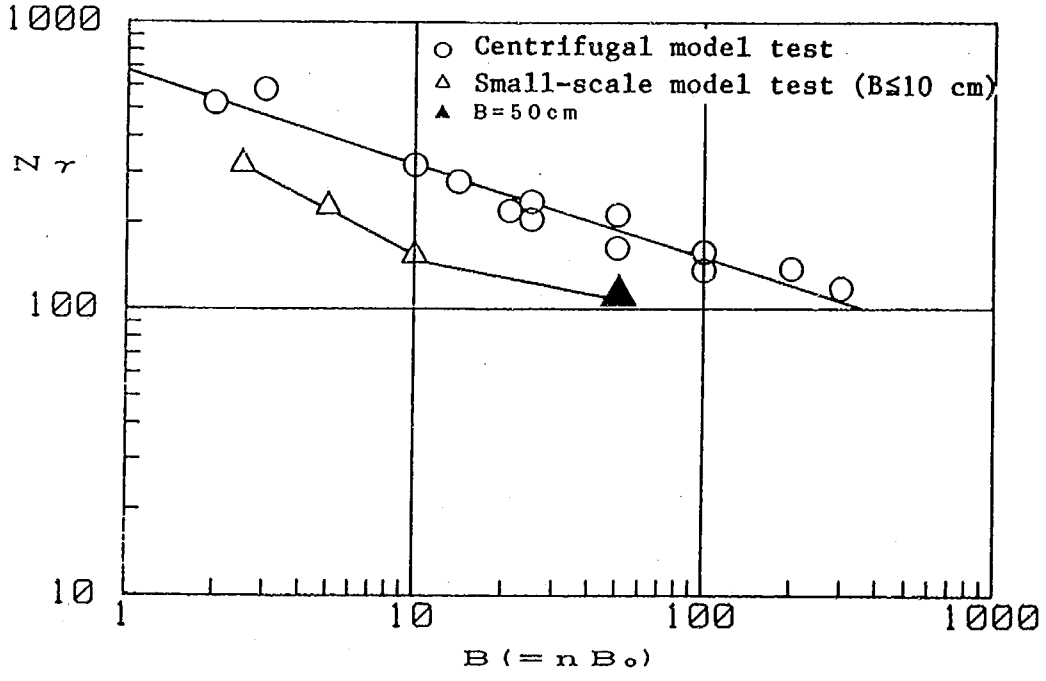


Fig. 12 Comparison with Centrifugal Model Test (scale effect of Nγ)

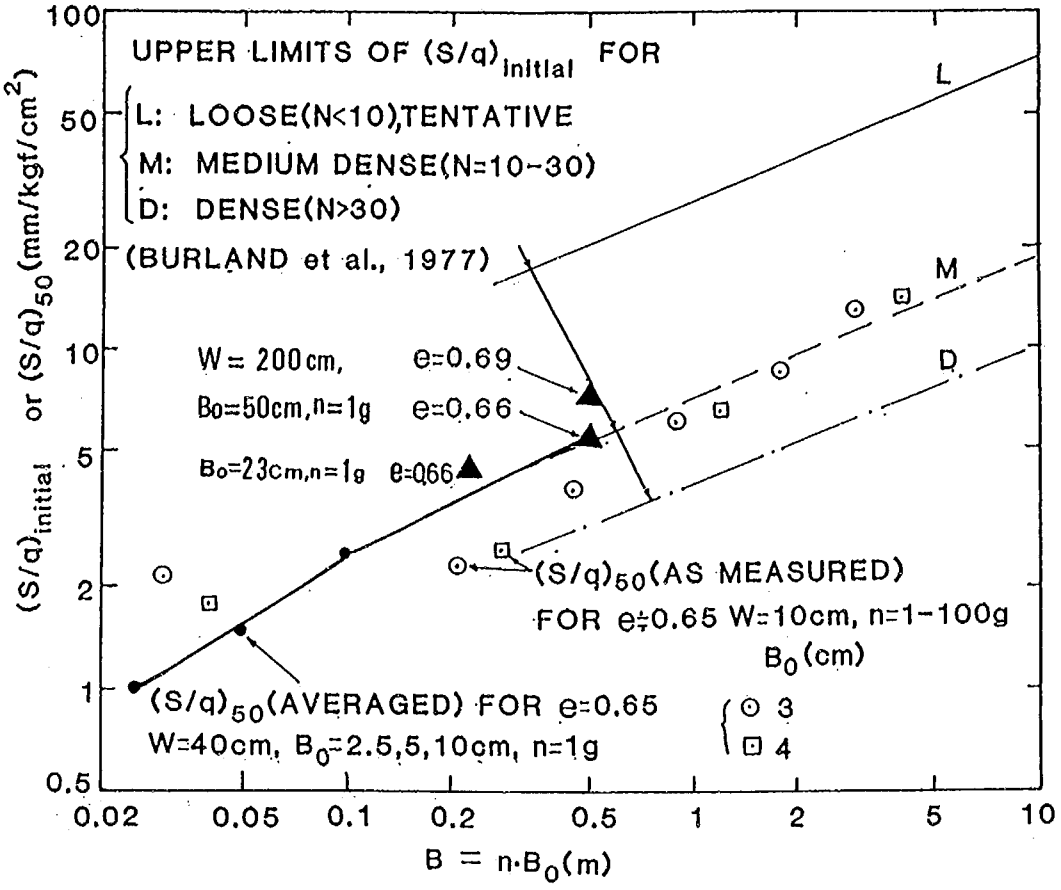


Fig. 13 Comparison of Inclination of Load-Settlement Curves at Beginning of Loading

5TH U.S.-JAPAN WORKSHOP ON BRIDGE ENGINEERING
STRUCTURAL MONITORY, SAFETY AND NONDESTRUCTIVE EVALUATION
MAY 9 & 10, 1989, TSUKUBA, JAPAN

EVALUATION OF TENDON COUPLING JOINTS IN CONTINUOUS POST-TENSIONED CONCRETE BRIDGES

by

Frieder Seible

Associate Professor of Structural Engineering
Department of Applied Mechanics and Engineering Sciences, R-011
University of California, San Diego
La Jolla, CA 92093

Tel. (619) 534-4640
Fax (619) 534-6373

ABSTRACT

Wide cracks and in some cases ruptured tendons encountered in the coupling joint vicinity of post-tensioned continuous concrete bridges have led to an extensive inspection program of existing prestressed concrete bridges which were constructed utilizing mechanical tendon couplers in the construction joints. Numerous analytical investigations have provided behavioral models and possible explanations. Full-scale tests under controlled laboratory conditions have now confirmed some of these models while others could not be verified experimentally. A complete description of a comprehensive research program into the behavior of coupling joints in continuous post-tensioned concrete bridges is presented.

1. INTRODUCTION

Short and medium span reinforced concrete bridge structures with a large number of repetitive spans can be very economically built using segmental construction procedures. For cast-in-place structures, span-by-span erection with traveling self-supporting falsework and for precast structures the casting and erection of segments or complete spans are proven construction methods in all situations where falsework or scaffolding for conventional in-situ construction is eliminated due to economical, usage/operational, clearance or height restrictions. Benefits of the two procedures discussed above are combined in the incremental launching method where all sections of the bridge superstructure are cast to close tolerances at one end of the bridge site under almost factory like conditions prior to being pushed in the bridge direction over the pre-erected bridge piers, temporarily spanning the final bridge spans by means of a launching nose, see Fig. 1. Subsequent segments are match-cast in the same construction pit and coupled to the previous segment prior to being launched with the already completed bridge superstructure.

All of the above methods have in common that no traffic restrictive scaffolding is required and that individual sections or segments have to be connected or coupled to previous segments in a construction or coupling joint. These methods have been primarily developed and used in Europe where, similar to Japan, bridge construction is typically required in already densely populated areas. However, also in the U.S., more and more bridge work is needed in urban areas to accommodate increased traffic volume while not interrupting steady state traffic flow which makes these self-supporting erection schemes economical alternatives to more conventional construction techniques.

With most medium span concrete bridge superstructures being prestressed (post-tensioned), construction and coupling joints require the continuity of the prestressing element or tendon through the construction joint. European practice typically calls for mechanical tendon coupling devices or couplers, while U.S. practice generally overlaps tendons in the construction joint. Overlapping tendons, however, require more cross-section, e.g., in the web of a thin walled box section, more tendon length to develop the full strength in the joint, as well as complicated construction joint details with tendons for the next segment penetrating the joint area.

The simplified construction detail provided by a mechanical tendon coupler in the construction joint warrants serious consideration from an economical point of view, provided that no technical problems are introduced. Large cracks, and in one case even ruptured tendons found during routine bridge inspections in the Federal Republic of Germany, in the direct vicinity of coupling joints of continuous post-tensioned concrete bridges showed potential problems with these mechanical coupling joints. It is the subject of this research project to investigate and identify possible problem sources associated with mechanical tendon couplers and ultimately, based on analytical and full-scale experimental behavior studies, recommend design guidelines [1] which will allow the safe and economical application of tendon couplers in an effort to advance bridge construction technology in the United States and Japan.

PROBLEM STATEMENT

Routine bridge inspections are often limited to a visual survey of the concrete surface for cracks to determine the state of the structure. While small and repetitive cracks are commonly accepted as the material behavior of reinforced concrete, larger isolated cracks with crack width of more than or 0.01 in. (0.25 mm) could point to a potential structural deficiency. Especially in prestressed concrete structures, the formation of large isolated cracks and their penetration to the prestressing reinforcement is of particular importance due to the increased susceptibility of high strength steel to corrosion, and due to the concentrated cyclic mechanical action in the isolated crack leading to fatigue failure.

Large cracks encountered in the direct vicinity of coupling joints of continuous post-tensioned concrete bridges were the cause for an intensified bridge inspection program of prestressed concrete bridge superstructures in West Germany. A total of 2,431 prestressed concrete bridge superstructures with 11,458 spans were inspected. In this bridge inspection survey bridge structures were classified by bridge type, construction technique and encountered crack width. Two kinds of bridge cross-sections are typically used for bridge construction methods with coupling joint; namely box girder and T-beams with varying numbers of webs and bottom soffit arrangements. The wide cracks encountered in the coupling joint vicinity strongly suggested a distinction between structures with and without coupling joints. The most important aspects of this comprehensive bridge inspection report are summarized in Table 1 [1,2], where the number of cracked bridge structures, the encountered crack width and the cracked region for both T-beam and box girder type bridges with and without coupling joints are depicted. Table 1A shows that only 34% of all the bridge superstructures with coupling joints were virtually crack free compared to 80% for bridges without coupling joints. The severity of the encountered cracks is also emphasized by the fact that 39% of the cracks in structures with coupling joints exceeded 0.01 in. (0.25 mm) in width while only 10% of the "uncoupled" bridge structures featured cracks of this magnitude.

Additional information on crack distribution over the cross-section was available for a subset of 329 of the total of 583 bridge structures with coupling joints. This subset consisted to 90% of T-beam or box girder type cross-section, and detailed results for these two bridge types are presented in Table 1B. It should be noted that more than one crack pattern can be encountered in a bridge superstructure at different coupling joints which results in a slight numerical distortion in Table 1B. However, two clear tendencies can be established, namely that box girder type cross-sections are more susceptible to cracks and there particularly large cracks in the coupling joint region and that the majority of cracks occurred in the bottom flange and webs of the cross-section. A typically encountered crack pattern in one span of a "coupled" two cell box girder section is given in Table 1C to illustrate the findings of Tables 1A and 1B. The cracks encountered in the webs or bottom soffit were generally parallel to the construction joint and limited to its direct vicinity.

To properly understand possible reasons for the presence of these encountered cracks in the coupling joint vicinity some design considerations relevant at the time of the design and construction of these bridge structures have to be reviewed. The majority of coupled bridge structures which showed cracks in the coupling joint vicinity were erected in span by span construction with traveling self-supporting falsework, see Fig. 2.

TABLE 1: SUMMARY OF BRIDGE INSPECTION

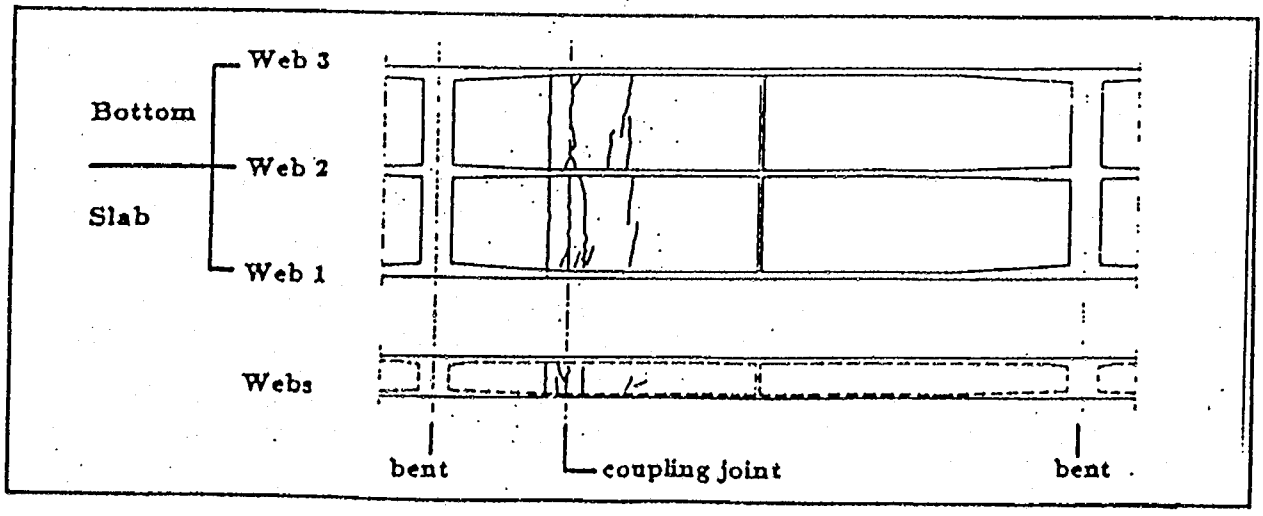
A. CRACKS ENCOUNTERED IN PRESTRESSED CONCRETE BRIDGES

Prestressed Concrete Bridge Structures	total	without coupling joints	with coupling joints
	2431 (100%)	1848 (100%)	583 (100%)
no cracks	1673 (69%)	1477 (80%)	196 (34%)
cracks $\leq$ 0.2mm	347 (14%)	187 (10%)	160 (27%)
cracks > 0.2mm	411 (17%)	184 (10%)	227 (39%)

B. CRACK DEVELOPMENT IN COUPLING JOINT VICINITY

Cross Section	total	without cracks	with cracked region ▬ width [mm]	A	B	C	D	E	F
T-Beam	114 (100%)	51 (45%)	cracked region						
			$\leq$ 0.2	5	34	2	3	1	0
			> 0.2	2	17	2	2	2	0
Box Girder	184 (100%)	54 (30%)	cracked region						
			$\leq$ 0.2	5	29	32	5	37	6
			> 0.2	1	4	31	3	54	4

C. TYPICAL CRACK PATTERN IN A TWO CELL BOX GIRDER SPAN



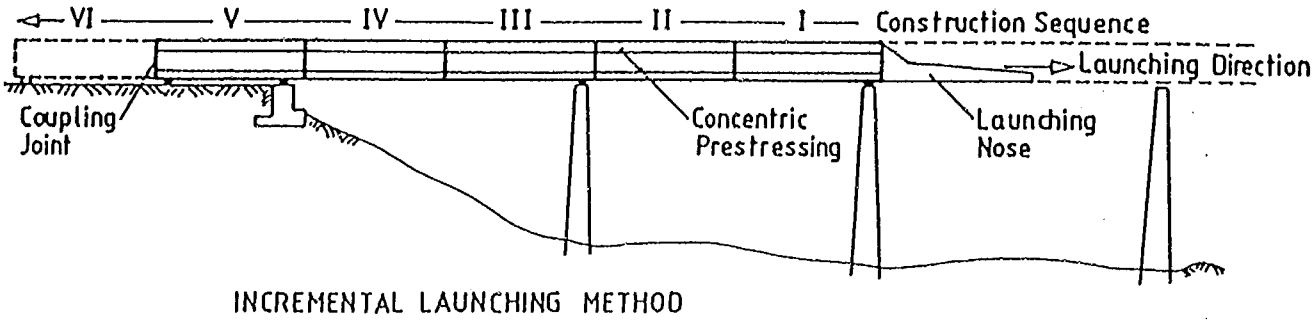
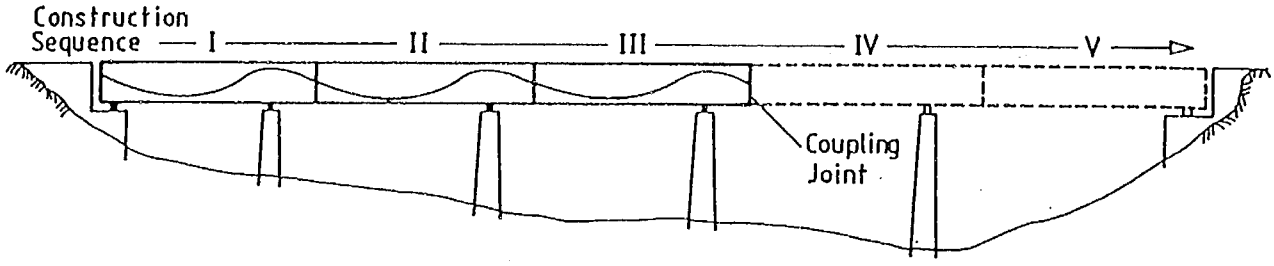


FIG. 1 SEGMENTAL BRIDGE CONSTRUCTION INCREMENTAL LAUNCHING



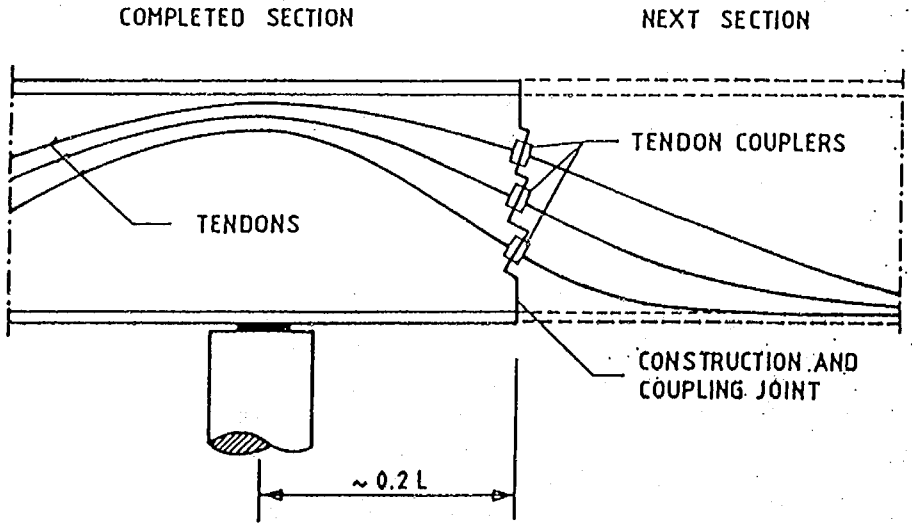


FIG. 2 SPAN-BY-SPAN CONSTRUCTION WITH INFLECTION POINT COUPLERS

Where possible, construction joints were placed at the point of inflection for sustained loads, in order to minimize the amount of reinforcement required at that section. Generally, only minimum reinforcement or a minimum amount of prestress was provided in the design.

However, the location of the point of inflection can change due to variations in the sustained loads, e.g., variations from design values in dead load and prestressing forces, thus introducing moments at the design point of inflection. If these moments are superimposed with possible variations in the determination of secondary temperature effects, support settlements and overestimated moment redistributions in the structure due to the span-by-span erection process and creep and shrinkage, the design moment at this location can change significantly, not only in magnitude but also in sign. Small moment changes in areas of large design moments are generally sufficiently provided for by the applied load and safety factors, whereas areas of small design moments, such as inflection point vicinities, do not have this built-in safety, see Fig. 3b.

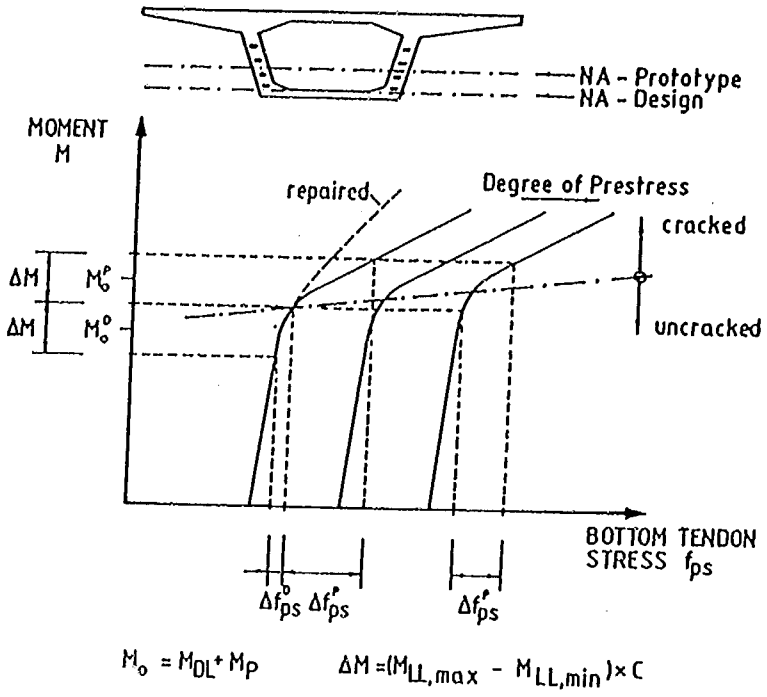
Shifts in the inflection point location and superimposed cyclic moment changes can subsequently lead to the formation of cracks in the coupling joint vicinity and with it to significantly increased cyclic stress levels in the post-tensioning tendons, see Fig. 3a. These observations, combined with reduced fatigue limits of tendon anchorage and coupling joint assemblies [3], are cause for special design considerations for coupling joints of post-tensioned concrete bridges.

BEHAVIOR MODELS

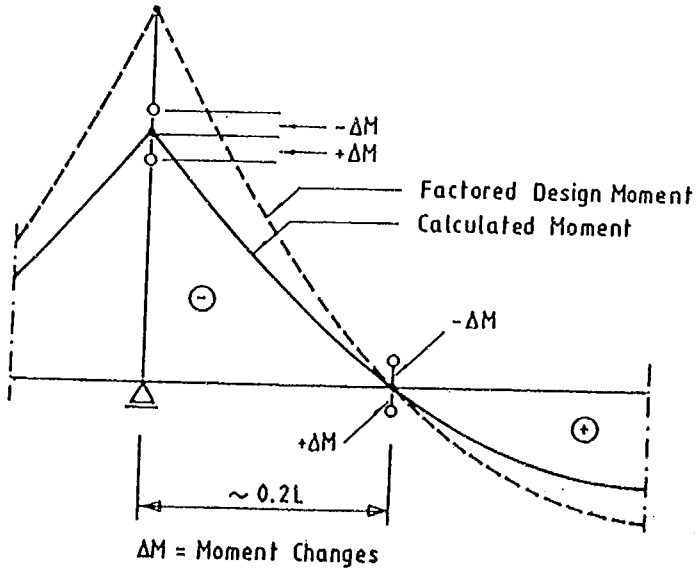
Comprehensive studies into the coupling joint behavior attribute the cause and effect of the encountered cracks to a variety of sources. A detailed summary of models and analytical investigations into the coupling joint behavior was presented in [4] identifying the highly nonlinear stress state due to the construction and prestressing sequences, unaccounted differences in the actual and predicted moment state as well as increased prestress losses in the tendon coupler as contributing effects.

An analytical model of a thin walled concrete member concentrically post-tensioned with a single tendon coupled at the construction joint was used to demonstrate the effects of the above identified sources on the actual stress state in the segmentally erected specimen.

Contrary to the commonly made assumption of a uniform state of prestress after the segmental construction of a concentrically post-tensioned concrete member, a highly non-uniform state of precompression is encountered in the direct vicinity of the coupling and construction joint as shown in Fig. 4. The amount of this deviation from the assumed uniform state of precompression can be directly obtained from a superposition of the stress states obtained for the post-tensioning of the individual segments, since the concrete section can be assumed uncracked and in the linear elastic range under the applied prestress. The combined stress state in the longitudinal direction for the segmental construction clearly depicts a reduced state of prestress along most of the construction joint of only 0.5 f_{po} or 1/2 of the assumed uniform prestress f_{po} and a region of 0.3 f_{po} or 1/3 of the assumed uniform prestress at a distance of 0.2 times the height (construction joint length) along the edge of the member. While, as assumed, the state of prestress is uniform outside the St. Venant



a) Influence of Shift in N.A.



b) Design Assumptions

FIG. 3 EFFECT OF MOMENT CHANGES

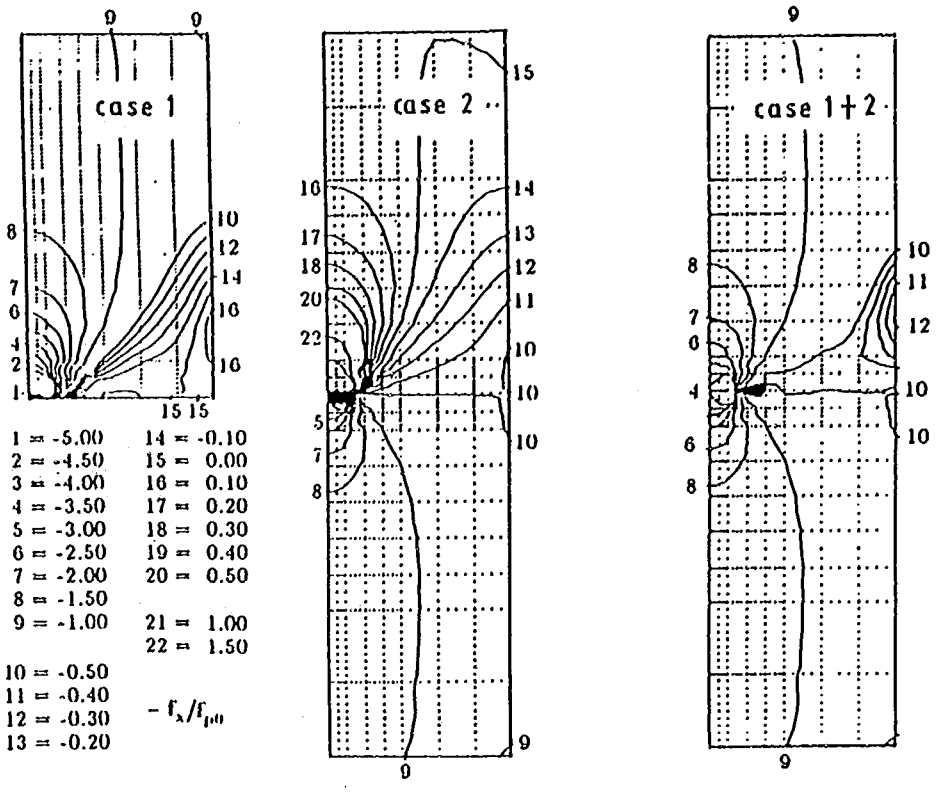


FIG. 4 LONGITUDINAL COMPRESSIVE CONSTRUCTION STRESS STATE

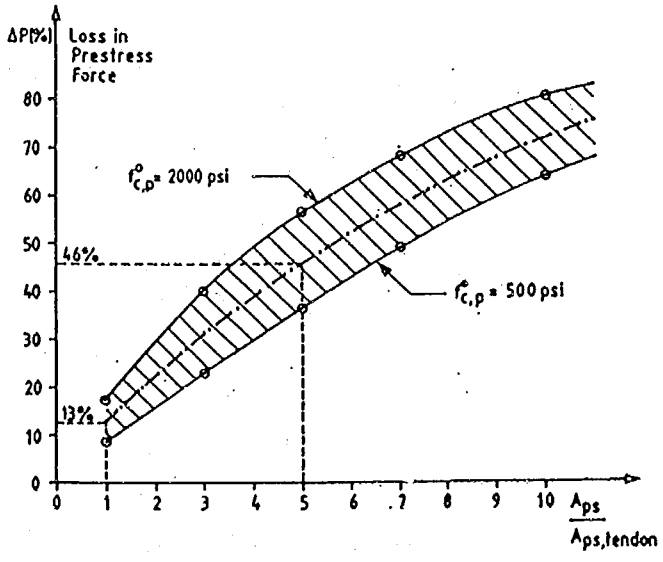


FIG. 5 MODEL FOR COUPLER PRESTRESS LOSS

region, a drastic reduction of compressive stress reserves in the direct coupling joint vicinity has been predicted by the analytical model.

An additional phenomenon was stipulated to contribute to the complex stress state in the coupling joint vicinity [4], namely the prestress loss in the tendon coupler. The simple assumption of a uniform time-dependent shortening of the entire member due to creep and shrinkage would result in a uniform strain increment Δ_{c+s} over the entire member length. With Young's modulus E_p assumed to be the same for both prestressing tendon and coupler, theory of elasticity shows direct proportionality between the loss of the prestress Δ_p and the cross-sectional area of the tendon. However, this area can be substantially larger in the coupler than in the strand or bar portion of the tendon due to the use of lower strength steel. This increase in area at the coupler directly translates to an increase in prestress loss in the coupling element which, as a function of compatibility between concrete and tendon, results in a prying force on the concrete at the coupler as schematically depicted in Fig. 5. A theoretical estimate of the magnitude of this potential force or prestress loss in the coupler can be obtained based on the CEB/FIP [5] interaction for creep and shrinkage as

$$\Delta_{fp,c+s} = \frac{\varepsilon_s E_p + n\phi\left(f^o_{c,DL} + f^o_{c,p}\right)}{1 - n\left(\frac{f^o_{c,p}}{f^o_p}\right)\left(1 + \frac{\phi}{2}\right)} \qquad (1)$$

where A_p, E_p represent the area and modulus of the prestressing tendon, $n = (E_p/E_c)$ the ratio of steel and concrete moduli, f_p, f_c the stress state of the tendon and concrete and ε_s, ϕ the shrinkage and creep coefficients. Superscript ^{o} denotes the time of prestressing and subscript p, c the prestressing steel or concrete state, respectively, due to c + s, creep + shrinkage or DL and p, dead load and prestressing, respectively. With creep and shrinkage coefficients for general outside conditions, and $f_{c,DL}$ assumed to be negligible at the point of inflection, Eqn. (1) predicts the loss of prestress in the coupler with coupler area expressed in multiples of the tendon areas as depicted in Fig. 5.

It can be seen that very quickly theoretical prestress losses of unacceptable magnitude can occur as a result of this analytical model which needs experimental verification.

A superposition of stress states for the two cases discussed above with the combined construction load case stresses showed for an assumed tensile stress limit equal in magnitude to the average prestress level f_{po}, the same crack pattern developments parallel to and in the vicinity of the construction joint as encountered in actual bridge structures, see Table 1C. The crack origination started in the construction joint and in the area of the reduced state of precompression, for the construction plus prying force and the construction plus additional moment case, respectively. The element stiffness deterioration and crack orientation were determined by a weighted averaging procedure of principal stress states over all element integration points. The direction of the sequential crack propagation was found based on an error accumulation method.

All of the above model studies are described in detail in [1] and represent the current state of research. While all of the presented models are plausible to contribute to the actual stress state and crack development of the coupling joint

region, a quantification of the individual effects without full-scale experimental verification is virtually impossible.

EXPERIMENTAL VERIFICATION

The principal objective of the full-scale experimental research was the determination of the stress/strain state in the coupling joint vicinity introduced by the segmental construction and post-tensioning sequence. Primary focus is given in the following to the strain state along the edge of the concentrically post-tensioned specimens where analytical predictions identified a significant reduction in the compressive stress state, the transverse splitting stresses along the specimen centerline and the time-dependent development of the longitudinal strain state.

Four test specimens with different tendon and coupling hardware as shown in Fig. 6 were segmentally constructed post-tensioned and the strain state was monitored for a time period of at least 180 days. Test specimen 1 was post-tensioned with two 1 3/8" ϕ (35 mm) DYWIDAG bars (Grade 150), coupled in the construction joint with threadbar coupling sleeves. Specimens 2 and 3 were post-tensioned with nine 0.6" ϕ (15 mm) 7 wire strands (Grade 270) coupled with a coupling disk and individual staggered strand couplers, respectively. Finally, specimen 4 was post-tensioned with twelve 0.6" ϕ (15 mm) 7 wire strands (Grade 270) coupled in the construction joint with a coupling disk. Lock-in force levels for the post-tensioning of each segment ranged from 340 to 408 kips (154 to 185 tons). The ducts were grouted with portland cement grout immediately following each segmental post-tensioning operation.

Longitudinal Compressive Strain State

The measured longitudinal compressive strain state in the test specimens after the segmental construction and post-tensioning procedure is depicted in Fig. 7 for longitudinal strains along the top, center and bottom of the test specimens (measured by DEMEC readings). All four specimens show top strains slightly higher than bottom strains which can be attributed to the constraining effect of the formwork during the post-tensioning operation, while the centerline strains nicely fall between the top and bottom readings at the midsection of each segment. This validates St. Venant's principle of a uniformly distributed influence of a concentrated load at distance h away from the point of load application. Clearly, towards the segment ends, the longitudinal strain state increases at the centerline with a clearly defined maximum next to the construction joint in segment 1.

All experimental measurements show a definitive drop of longitudinal compressive strains in the coupling joint vicinity along the member edge. While the concrete compressive strain state at the center of each segment is between 150 to 200 $\mu\varepsilon$, strain levels encountered close to the construction joint can drop to strain levels of 60 $\mu\varepsilon$ which corresponds with the theoretical prediction of a reduction of the compressive strain state up to 1/3 of its nominal uniform value. It is of interest to note that experimental strain data shows a decrease in compressive edge strains to both sides of the construction joint, while analytical predictions put the low point in segment 1 at a distance of 0.2 d.

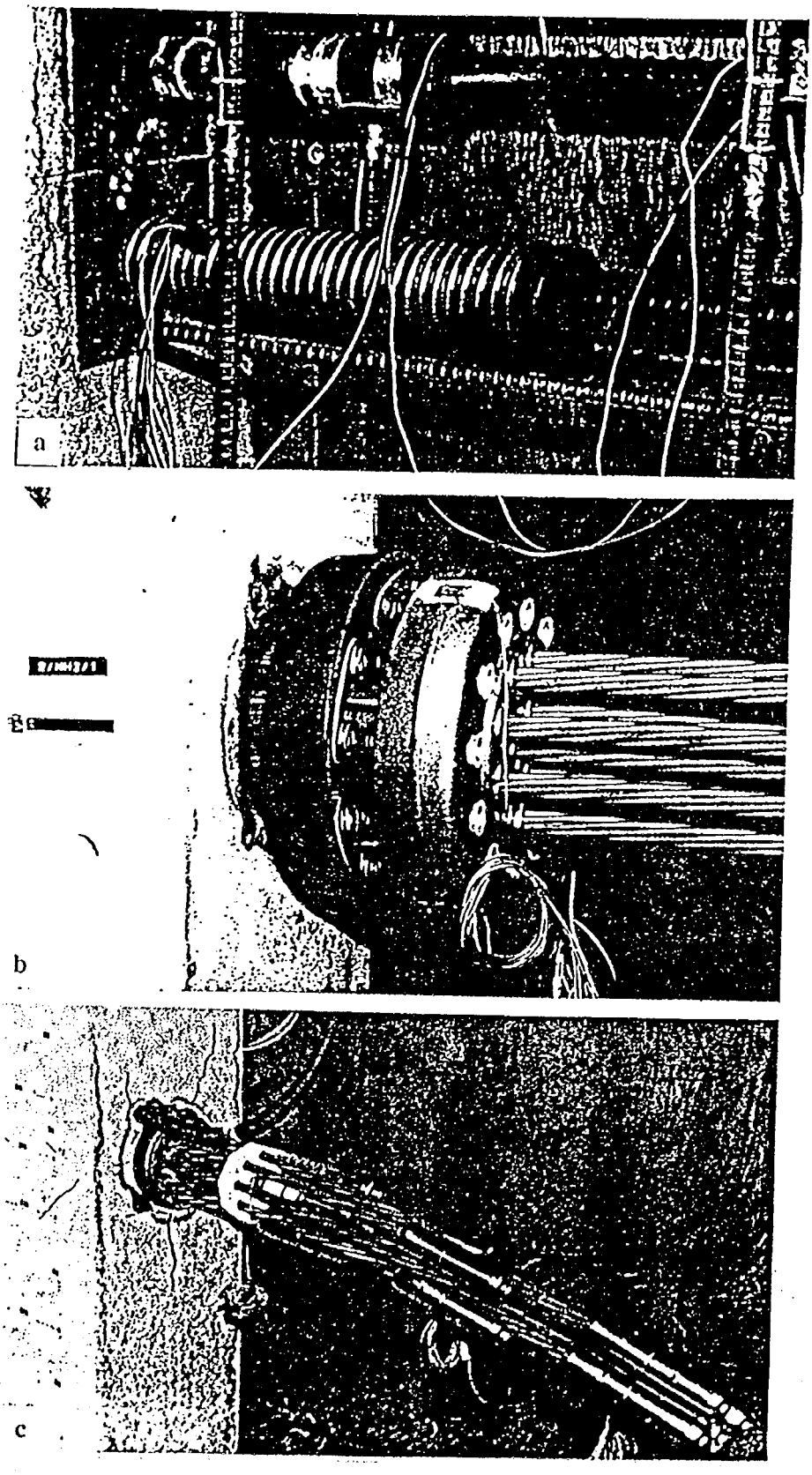


FIG. 6 TENDON COUPLING JOINTS, SPECIMENS 1 TO 3

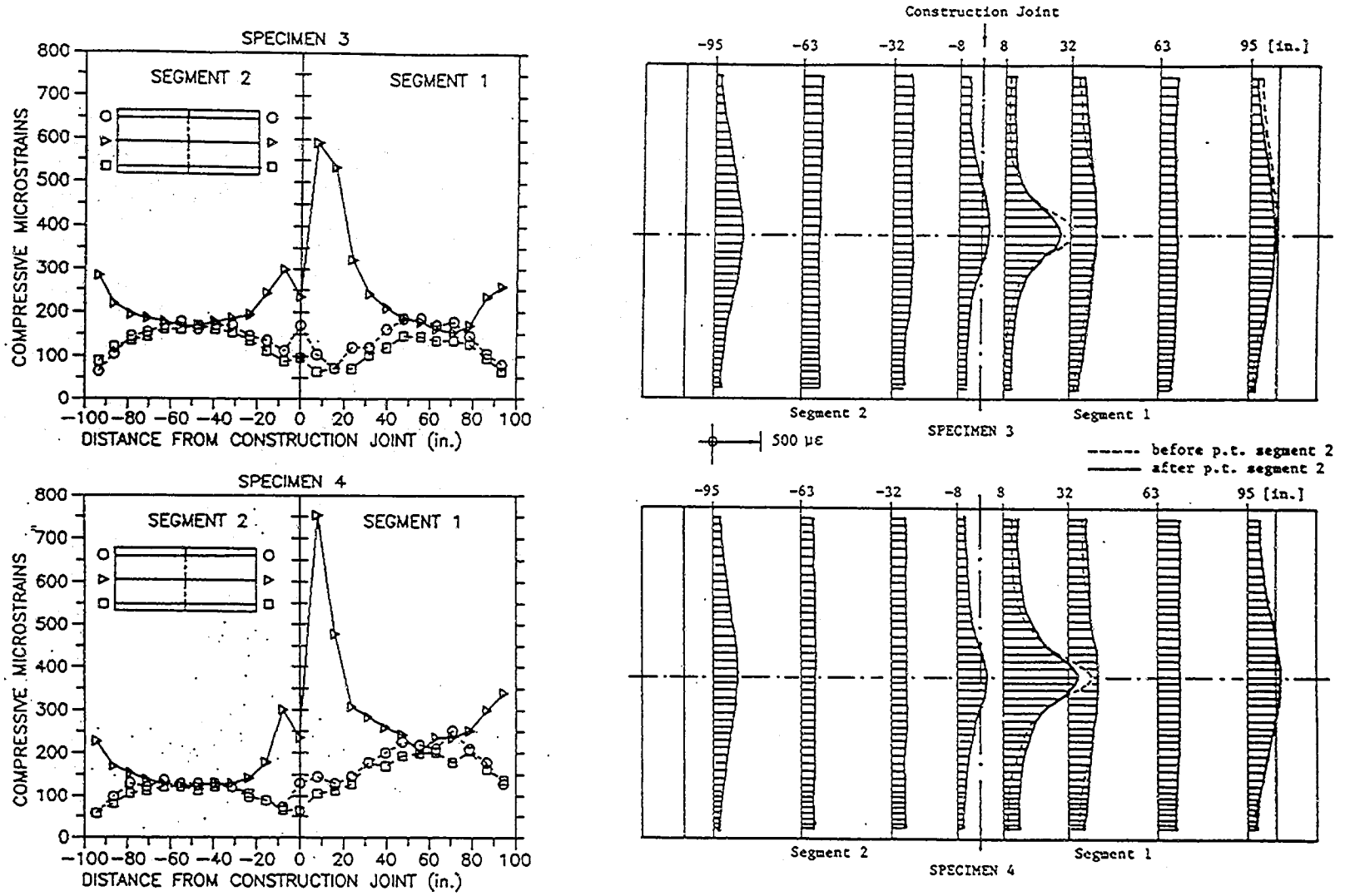


FIG. 7 TRANSVERSE DISTRIBUTION OF LONGITUDINAL STRAIN STATE

Transverse Strain State

The transverse strain state along the centerline of the test specimens is of particular importance, since splitting tensile strains can dominate the design of transverse reinforcement. While most analytical models evaluate the splitting stress problem as a 2-D plane stress case, experimental investigations have shown that particularly large tendon anchorages cause micro-cracking in the local anchorage zone which causes stress and strain states completely different to plane stress predictions. Similar findings were obtained from the present studies, where fairly high concentrated forces (~400 kips) were anchored off at each post-tensioning step. While all theoretical plane stress predictions show large concentrated transverse compressive stress states immediately behind the anchor plate, experimental transverse strain measurements indicate high tensile strain values (or longitudinal cracks) in the local anchorage region both, at the coupling/construction joint and the flanged ends, see Fig. 8. The magnitude of tensile strain in the construction joint vicinity of the initial segment is reduced by the coupling and post-tensioning of the subsequent segment, but also penetrates into the second segment where typically no local anchorage zone reinforcement is provided. A clear difference was noted in the transverse splitting strains in the two bar specimen 1, with substantially lower tensile strain values in the coupling joint, which can be attributed to the multiple or two tendon anchorage compared to the single tendon anchorage of specimens 2 to 4.

Time-Dependent Strain Development

A recurring question is the time-dependent redistribution of internal self-equilibrating stress components which are superimposed on a uniform stress field. Particularly the encountered drop in longitudinal stresses along the edge of the concentrically post-tensioned segmentally erected specimen is of interest since a force redistribution with time inside the test specimen could lead to the restoration of the uniform compressive stress field. Time-dependent development of DEMEC readings along the top edge of test specimen 2 are presented in Fig. 9 as an example and show, with remarkable consistency, that the basic strain distribution profile does not change with time. An overall shortening of the test specimens by 400 to 500 $\mu\varepsilon$ over the investigated 30 to 40 week time period can be established, with clear indications that the time-dependent changes are significantly slowing down after the considered time interval.

A 500 $\mu\varepsilon$ overall shortening of the test specimens translates approximately to a 500 $\mu\varepsilon \times E_p = 500 \times 29 \times 10^3 = 14{,}500$ psi (100 N/mm^2) loss in prestress in the fully grouted tendons or a loss in nominal prestress force of 12.4, 9.6, 11.0 and 8.2% of the measured lock-in forces for specimens 1 to 4, respectively.

Time-Dependent Strain Development in the Direct Coupling Region

The second objective behind the full-scale experiments was an attempt to observe and validate the increased prestress losses in the coupling elements as predicted by the analytical model described above, see Fig. 5. Concrete strain data in support of the theoretical model should clearly show an increase in concrete surface strains measured with time across the construction joint at the center or tendon location over and above strains measured across the construction joint at the edges of the specimens. This phenomenon should be

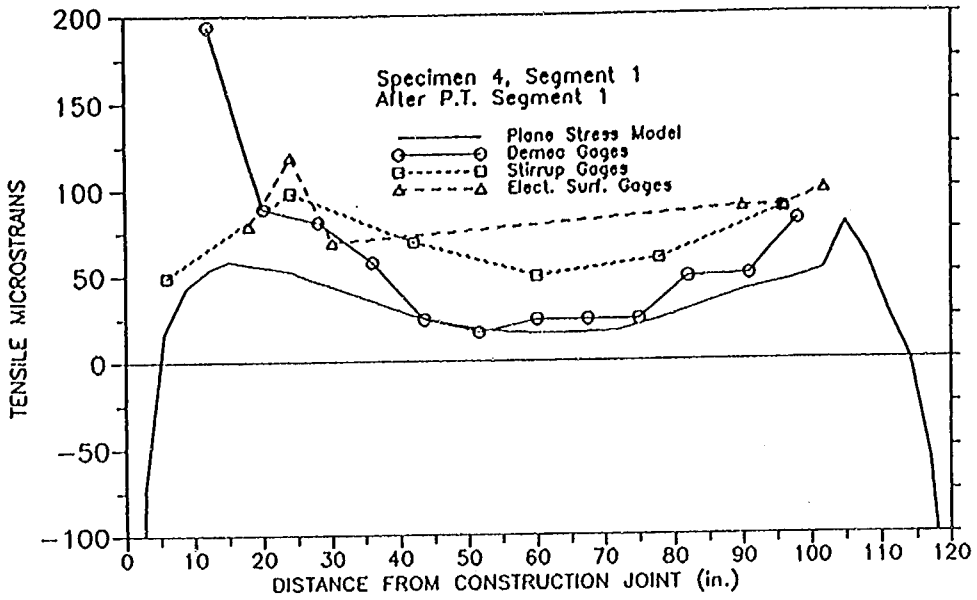


FIG. 8 SPLITTING STRESS DISTRIBUTION

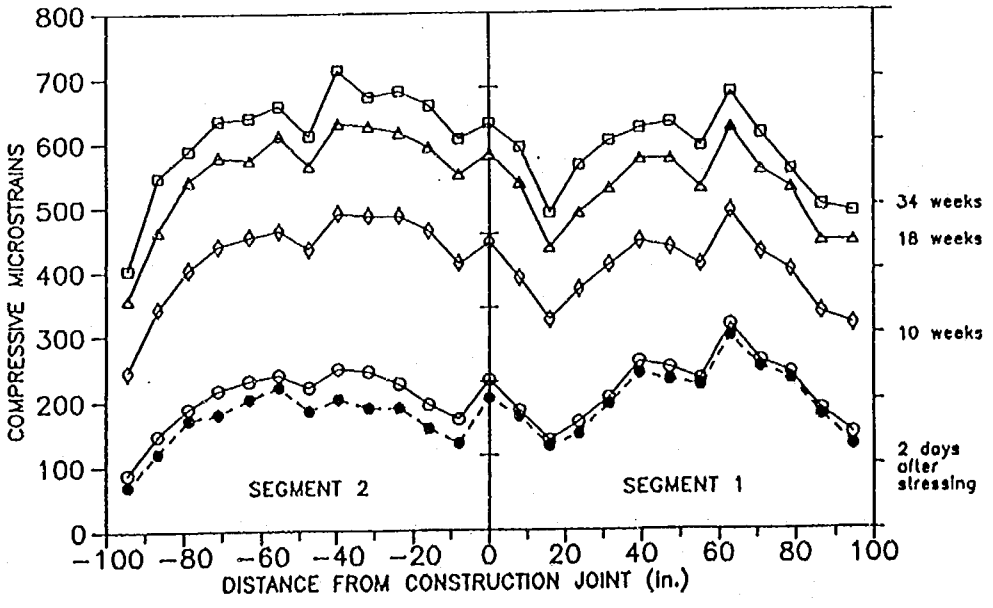


FIG. 9 TIME-DEPENDENT LONGITUDINAL STRAIN DEVELOPMENT, TOP OF SPECIMEN 2

particularly pronounced for specimens 2 and 4 where large coupling disks were employed.

However, a comparison of measured concrete surface strains across the construction joint by DEMEC readings showed virtually no difference in time-dependent concrete strains at the center and the top and bottom of the specimens. Thus, it is difficult to validate the theoretical model by the performed measurements and indications are that rather than only the size of the coupling disk, the sizes of the anchor plates have some effect.

These few measurements cannot be considered conclusive to derive quantitative coupler prestress loss data and do not at this time substantiate the analytical model discussed above. Only specimen 1 showed some of the expected effects which suggests strongly that not only the coupler dimensions but also the anchorage dimensions in the construction joint have to be considered.

CONCLUSIONS

The four full-scale laboratory experiments on segmentally erected post-tensioned concrete girders with coupled tendons have clearly demonstrated some of the key behavioral aspects to be considered during the design phase. Of particular importance are the following experimental results:

- The state of precompression in the concentrically post-tensioned segmentally erected girders is far from uniform. While a distance h (h = height of girders) away from the member ends and the coupling joint a uniform state of prestress is achieved (St. Venant's principle) longitudinal compressive stress state reductions in the direct construction joint vicinity of one half of the nominal uniform prestress level have been consistently encountered, measured with all three instrument types (DEMEC gage, rebar strain gage, and concrete surface strain gage).

- Low points of the state of precompression of less than one half the nominal uniform prestress level were encountered on both sides of the construction joint along the edge of the test specimens.

- Transverse splitting stains show that large tendon units cause high tensile surface strains in the local anchorage zone which ultimately lead to splitting cracks. Comparable cracks were not encountered in the two bar specimen 1.

- Time-dependent strain profiles of the longitudinal compressive strain state along the edge of the test specimen preserved the original shape, indicating that no significant strain redistribution occurred in the test specimens with time.

- Measured strain states in the couplers and across the construction joint were not conclusive to validate theoretical models of increased prestress losses.

The above experimental findings can be directly used to verify analytical and behavioral models developed in order to predict the coupling/construction joint behavior. In particular, the development and distribution of the non-uniform longitudinal stress/strain state in the construction joint vicinity was shown to be accurately predicted by analytical plane stress models. However, behavioral models for the local anchorage or coupling zone of large tendon units clearly

can no longer be based on linear elastic homogeneous material models and require special design considerations. Behavioral models for drastically increased prestress losses in the coupling element could not be verified with the current experimental work.

ACKNOWLEDGEMENTS

The presented research project was jointly sponsored by the National Science Foundation under Grant No. CES 85-52672 and DYWIDAG Systems International, USA, Inc., under the Presidential Young Investigators Award Program.

REFERENCES

[1] Seible, F., Latham, C. and Krishnan, K., "Structural Concrete Overlays in Bridge Deck Rehabilitation - Summary of Experimental Results, Analytical Studies and Design Recommendations," University of California, San Diego, Structural Systems Research Project, Report No. SSRP-88/04, June 1988, 81 pp.

[2] Seible, F., "Problems with Coupling Joints of Prestressing Tendons in Continuous Post-tensioned Concrete Bridges," Proceedings of the Second International Conference on Short and Medium Span Bridges, Vol. 2, Ottawa, Canada, August 1986, pp. 93-106.

[3] Naaman, A., "Prestressed Concrete Analysis and Design Fundamentals," McGraw-Hill Book Company, New York, 1982, 670 pp.

[4] König, G. and Zichner, T., "Berücksichtigung der Temperaturdifferenz ΔT, der Steuung des Eigengewichts und der erhöhten Spannkraffverluste an Spanngliedkopplungen bei der Bemessung Massiver Brücken." Proceedings of the 8th International FIP Conference, London, England, 1978.

[5] CEB-FIP, "Model Code for Concrete Structures International Recommendations," 3rd edition, Federation Internationale de la Precontrainte, T. Telford, London, England, 1978, 347 pp.

[6] Rüsch, H., Jungwirth, D. and Hilsdorf, H., "Creep and Shrinkage, Their Effect on the Behavior of Concrete Structures," Springer Verlag, New York, 1983, 284 pp.

APPLICATION OF CARBON FIBER REINFORCED PLASTICS TO PRESTRESSED CONCRETE BRIDGES

by

Minoru Fujiwara: Head, Bridge Division, Structure and Bridge Department, Public Works Research Institute, Ministry of Construction

Koichi Minosaku: Research Engineer, Ditto

Minoru Adachi: Head, Road Construction Division, Public Works Department, Ishikawa Prefecture

and

Takeaki Yamashita: Section Chief, Bridge Section of Road Construction Division, Ditto

ABSTRACT

In recent years, some concrete bridges mainly in coastal areas where the effects of splash and sea breeze are strong, have exhibited cracking and delamination of concrete and corrosion of steel materials at early stages after the construction due to chloride ions penetrating into the concrete. To cope with this condition, Public Works Research Institute and Ishikawa Prefecture have been carrying out a study on the application of Carbon Fiber Reinforced Plastics(hereinafter, "CFRP") to a tendon of a prestressed concrete member. Based on the result of this study, Ishikawa Prefecture constructed the Shinmiya Bridge in 1988, which is first PC slab bridge using CFRP as a tendon in Japan. This paper presents an outline of a study on the application of CFRP to a tendon of a prestressed concrete member as well as an outline of construction of the Shinmiya Bridge.

1. INTRODUCTION

Because deterioration of concrete bridges due to chloride ions has emerged in the coastal areas of Hokkaido, Tohoku and Hokuriku Regions facing the Sea of Japan and in Okinawa Prefecture since around 1981 as shown in Figure 1, the Ministry of Construction carried out the comprehensive technological development project "Development of Technology for Improving the Durability of Concrete" for three years since 1985. As s result of this research project, "Guidelines for Design and Construction of Concrete Structures in Coastal Areas

(Draft)", "Guidelines for Repair of Concrete Structures Damaged by Chloride Ions (Draft)" and etc. were prepared.

In general, the deterioration of concrete structures in coastal areas is found in forms of cracking and delamination of concrete as well as rust stain of steel. These are mainly caused by the permeation of chloride ions into the concrete followed by the corrosion of steel. In order to prevent the deterioration of concrete structures due to chloride ions, it is required that chloride ions reaching the steel are decreased, that the steel is changed to a corrosion-resisting one, or that a corrosion-resisting material in place of the steel is used.

Currently, measures to cope with deterioration of concrete structures due to chloride ions include the increase of the cover of steel, the improvement of quality of concrete, the use of coated reinforcing bars, and the coating of concrete surface. These measures are intended to control the amount of chloride ions reaching the steel.

On the other hand, the technology for application of cables composed of new fiber materials to a tendon of PC members, which are manufactured by compounding fibers such as a glass fiber and a carbon fiber with resins, has been developed. These new fiber materials have been already applied to the fields of space and aerial industries as well as an automobile industry. In the area of civil engineering, fiber-reinforced concrete expecting to prevent cracking has been already put in practice. Cables made from these new materials are free from corrosion, and have the strength equivalent to or higher than cables made from conventional steel materials.

Public Works Research Institute and Ishikawa Prefecture have been carrying out a study on the application of CFRP to a tendon of a prestressed concrete member. Based on the result of this study, Ishikawa Prefecture constructed the Shinmiya Bridge in 1988, which is first PC slab bridge using CFRP as a tendon in Japan. This paper presents an outline of a study on the application of CFRP to a tendon of a prestressed concrete member as well as an outline of construction of the Shinmiya Bridge.

2. AN OUTLINE OF THE SHINMIYA BRIDGE

The Shinmiya Bridge was constructed at the location on the national road 249 in Tomiki Town of Ishikawa Prefecture facing the Sea of Japan, where the north-west seasonal wind is strong during winter. The old RC slab bridge was replaced because of the occurrence of corrosion of reinforcing bars as well as the cracking and delamination of concrete. In constructing this bridge, a proper measure to prevent deterioration due to chloride ions was essential.

Based on detailed examination on quality characteristics of a CFRP cable and etc., a CFRP cable was employed as a tendon of the Shinmiya Bridge.

Figure 2 and Figure 3 show dimensions and Shape of the Shinmiya Bridge, and cross sections of a girder of the Shinmiya Bridge, respectively. This bridge is a pre-tensioned PC slab bridge with the span of 5.76m and the width of 7.0m. 24 pieces of I-shaped girders were used for the construction of this bridge. 6 pieces of CFRP tendons in the lower flange and 2 pieces of CFRP tendons in the upper flange, which have the diameter of 12.55mm, were embedded for each girder. The concrete was placed into the space between two girders. The epoxy-coated reinforcing bars with the diameter of 6mm were used as a stirrup.

3. AN USED CFRP CABLE

Currently available CFRP cables include a pan type one made from an acrylic-nitrogeous polymer fiber and a pitch type one made from a pitch of petroleum and coal. Of them, a pan typed CFRP cable was adopted as a tendon of the Shinmiya Bridge because a pan typed CFRP cable is advantageous in terms of strength and durability. In addition, regarding the kind of shape of a CFRP cable, a linear shaped CFRP cable were selected, which has a higher bonding strength to the concrete compared with a rod shaped CFRP cable. The used CFRP cable with the diameter of 12.5mm was made by inter-twisting 7 pieces of carbon filaments which was manufactured by gathering unhardened one-directional carbon fiber with epoxy resin as shown Figure 4.

4. QUALITY CHARACTERISTICS OF A CFRP CABLE AND LOAD-DEFLEXION CHARACTERISTICS OF PC GIRDERS USING A CFRP CABLE

4.1 Quality Characteristics of a CFRP Cable

(1) Tensile Strength, Elastic Modulus, and Extensibility in Breaking

A tensile strength test was performed in accordance with JIS Z 2241 for metal materials by fixing a cable at both ends with resin-filled sockets. The average of 20 samples was 210kg/mm^2 with the standard deviation of 8.4kg/mm^2.

Figure 5 gives typical stress-strain relationships of a CFRP cable and a steel cable. A steel cable shows a yielding phenomenon, while the CFRP cable keeps linearlity up to the breaking point. The elastic modulus and the extensibility measured were 1.32~1.47$\times 10^5$kg/cm^2 and 1.36~1.72% which are about 2/3 and 1/3 of those of a steel cable, respectively.

(2) Fatigue Strength

A fatigue strength test was carried out by fixing a cable with the length

of 1.6m at both ends in the same way of the tensile strength test. In this test, the number of repetition until breaking was counted to evaluate the fatigue strength charactristics of a CFRP cable by changing the minimum load and the maximum load.

Table 1 summarizes results of the test. When the minimum load and the maximum load were fixed to 1,000kg (stress of a cable P=13.2kg/mm^2) and to 4,000~8,000kg (P=52.6~105.2kg/mm^2), respectively, any cable did not break within the range of 2 million repetiton. However, when the minimum load and the maximum load were 5,000kg (P=65.7kg/mm^2) and 10,000kg (P=131.5kg/mm^2), two samples broke after 620,000 repetition and 45,000 repetiton, respectively. Thus, the fatigue strength of a CFRP cable tends to be influenced by the maximum load more than the stress region compared with a steel cable.

(3) Relaxation

A relaxation test was performed to understand effects of temperature and tensile load on the relaxation characteristics of a CFRP cable. Two temperature conditions were set so that the temperature is constant at 20℃ for 10 testing hours for one case, and that the temperature is constant at 60℃ for the first 16 hours of the total 50 hours testing period and at 20℃ for the remaining testing period for the other case. As to the tensile load condition, 11,000kg (P=144.7kg/mm^2) and 8,000kg(P=105.2kg/mm^2) were set. For comparison, PC steel wires with the diameter of 12.4mm were tested in the same condition.

Figure 6 gives results of the test. In any conditon, the value of relaxation of a CFRP cable is smaller than that of the PC steel wire. In particular, in the condition of the larger tensile load, this characteristics becomes remarkable. For instance, in the same temperature condition of 60℃ for the first 16 hours and then 20℃ for the remaining 14 hours, the values of relaxation of the PC steel wire for two different tensile load conditions of 8,000kg and 11,000kg are approximately 5% and 2.5%, respectively, while the value of relaxation of a CFRP cable is approximately 2.0% in each condition.

On the other hand, the relaxation value of a CFRP cable tends to become larger similar to a PC steel wire when it is subjected to high temperature. For example, in the same tensile strength condition of 8,000kg, the relaxation values of a CFRP tendon after 10 hours from the start of the test in two different temperature conditions of 20℃ and 60℃ are approximately 0.5% and 2.0%, respectively.

(4) Alkali Resistance

A PC tendon inside the concrete is required to have sufficient alkali

resistance. 3 pieces of CFRP cable with the diameter of 10.6mm were immersed in an alkaline solution (ph≒13, temperature≒60℃) applying the tensile load of 6,000kg for 9 months.

As a result, the approximately 2.0% change in weight due to exfoliation of a residual material on the surface was observed, but no change was recognized in apperance, elastic modulus and tensile strength. This means that a CFRP cable has sufficient alkali resistance.

(5) Linear Expansion Coefficient

Table 2 summarizes results of the linear expansion coefficients measured for CFRP cables with the diameter of 4.2mm at the temperature elevation rate of 2℃/min. The expansion coefficient tends to become larger with rising the temperature as being 0.01×10^{-6}/℃ at 50℃, 0.35×10^{-6}/℃ at 100℃, and 0.58×10^{-6}/℃ at 200℃. The expansion coefficient of a CFRP cable is, however, much smaller than that of concrete or the PC steel wire.

4.2 Characteristics of PC Girders Using a CFRP Cable

(1) Bonding Strength to Concrete

In order to know the bonding strength of a CFRP cable to the concrete, a transfer length test was performed. In this test, the change in strains of both cables and the concrete were measured when cables with the diameter of 10.5mm being pulled at the 70% of the tensile strength. For comparison, the same test was performed for the PC steel wire with the diameter of 10.4mm.

Figure 7 illustrates the results of the test. The length from the tensioned edge to the position, where the strains of cables and the concrete are constant, is approximately 70 cm for a CFRP cable. This value is nearly same as that of the PC steel wire.

(2) Load-Deflexion Characteristics

Figure 8 illustrates relationships between load and deflexion of the PC girders using a CFRP cable and a PC steel wire obtained from static bending tests. Two specimens of girder using same CFRP cable with the diameter of 12.5mm as that of the Shinmiya Bridge(hereinafter, "CFRP girder") and one specimen of girder using the PC steel wire with the diameter of 12.4mm (hereinafter, "S girder") were tested. Each of them is a I-shaped pre-tensioned girder with the height of 0.325m and the length of 6.06m which are same as the shape and the dimensions as those of the Shinmiya Bridge.

In the static bending test, the specimen was simply supported in the same span as that of the Shinmiya Bridge. The concentrated load was applied

statically at two points of 0.5m away from the center of span. Regarding the load-deflexion relationships for CFRP girders, the increase rate in deflexion is proportional to the the increase rate of load until the occurrence of bending cracking, while it becomes larger after the occurrence of bending cracking as almost same as that for the S girder.

Table 3 shows the cracking load and the failure load for each specimen. The theoretical value of cracking load was calculated on the assumption that cracking occurs when the tensile stress at the lower edge of the girders reaches the sum of the bending tensile strength of concrete and the effective prestress. The theoretical value of the failure load was obtained on the assumption that the cables and the concrete resist as one body to the load in accordance with the method shown in "Speicifications for Highway Bridges III, Concrete Bridges".

The measured value of cracking load for the S girder is larger by 40% than the theoretical value of cracking load, while as to the cracking load for the CFRP girder and the failure loads for the S girder and the CFRP girders, the measured values are nearly same as theoretical values.

Thus, the CFRP girder has the load-deflexion relationship similar to that of an ordinary PC girder. In addition, it was found that the ordinary methods for a PC girder can be used to calculate the cracking load and the failure load.

5. Design Parameters for a CFRP Cable used in the Construction of the Shinmiya Bridge

Table 4 summarizes allowable tensile stress and physical constants for a CFRP cable used in the construction of the Shinmiya Bridge. These constants were decided with a large margin for safety considering the results of the above-mentioned tests and their testing conditions, and that the Shinmiya Bridge is first PC bridge using CFRP as a tendon in Japan.

6. CONCLUSION REMARKS

This paper presents an outline of a study on the application of CFRP to a tendon of a prestressed concrete member as well as an outline of construction of the Shinmiya Bridge. The followings are conclusions of this paper.

(1) A CFRP cable used in the construction of the Shinmiya Bridge keeps linearlity up to the breaking point. Its elastic modulus and extensibility were $1.32\sim1.47\times10^5$ kg/cm^2 and 1.36~1.72% which are about 2/3 and 1/3 of those of a steel cable, respectively.

(2) The fatigue strength of a CFRP cable used in the construction of the Shinmiya Bridge tends to be influenced by the maximum load more than the stress region compared with a steel cable.

(3) The value of relaxation of a CFRP cable used in the construction of the Shinmiya Bridge is smaller than that of the PC steel wire, and tends to become larger similar to a PC steel wire when it is subjected to high temperature.

(4) A CFRP cable used in the construction of the Shinmiya Bridge has sufficient alkali resistance.

(5) The expansion coefficient of a CFRP cable used in the construction of the Shinmiya Bridge tends to become larger with rising the temperature, and is much smaller than that of concrete or the PC steel wire.

(6) The bonding strength to the concrete of a CFRP cable used in the construction of the Shinmiya Bridge is nearly same as that of the PC steel wire.

(7) The CFRP girder used in the construction of the Shinmiya Bridge has the load-deflexion relationship similar to that of an ordinary PC girder. In addition, it was found that the method applied to ordinary PC girders can be used to calculate the cracking load and the failure load.

In constructing the Shinmiya Bridge, after the superstructure was completed, two exposed girders was placed near both outside girders in order to study the durability of the PC girder using a CFRP cable. The results of this exposed test will be reported in future U.S-Japan Bridge Workshop.

Table 1 Results of Fatigue Test

NO.	Test Condition				Test Results	
	Maximum Load(kg)	Minimum Load(kg)	Stess Region (kg/mm^2)	Frequecy (Hz)	Repetion Number ($\times 10^4$)	Results
1	4,000	1,000	61.9	1.0	200	unbroken
2	5,000	1,000	82.5	1.0	200	unbroken
3	5,000	1,000	82.5	2.0	200	unbroken
4	6,000	1,000	103.1	1.0	200	unbroken
5	7,000	1,000	123.7	1.0	200	unbroken
6	8,000	1,000	144.3	1.0	200	unbroken
7	9,000	6,000	61.9	1.0	200	unbroken
8	9,000	6,000	61.9	2.0	200	unbroken
9	10,000	5,000	103.1	1.0	62	broken
10	10,000	5,000	103.1	1.0	4.5	broken

Table 2 Results of Linear Expansion Coefficient

Temperature (℃)	50	100	150	200
Linear Expansion Coefficient($\times 10^{-6}$/℃)	0.01	0.35	0.40	0.58

Table 3 Results of Bending Test of Girders
(Cracking Load and Failure Load)

		CFRP Girder	S(PC Steel)Girder
Cracking Load	Mesured Value Pm(kg)	7,200	9,100
	Theoretical Value Pt(kg)	6,970	6,480
	Pm / Pt	1.03	1.40
Failure Load	Mesured Value Pm(kg)	13,500	16,400
	Theoretical Value Pt(kg)	13,390	16,350
	Pm / Pt	1.01	1.00

Table 4 Allowable Stress and Physical Constant of a CFRP Cable used in the Construction of the Shinmiya Bridge

Item		Unit	CFRP Cable	PC Steel Wire
Allowable Tensile Stress	During Tensioning	kg/mm^2	110(0.6 σ pu)	135(0.8 σ pu)
	After Tensioning		101(0.55 σ pu)	127(0.7 σ pu)
	Under Service load		83(0.45 σ pu)	105(0.6 σ pu)
Elastic Modulus		kg/mm^2	1.4×10^6	2.0×10^6
Poisson's Ratio		—	—	0.3
Linear Expansion Coefficient		/℃	0.0×10^{-6}	10.0×10^{-6}
Nominal Relaxation Ratio		%	5.0	5.0

Note: σ pu means the breaking strength of cables

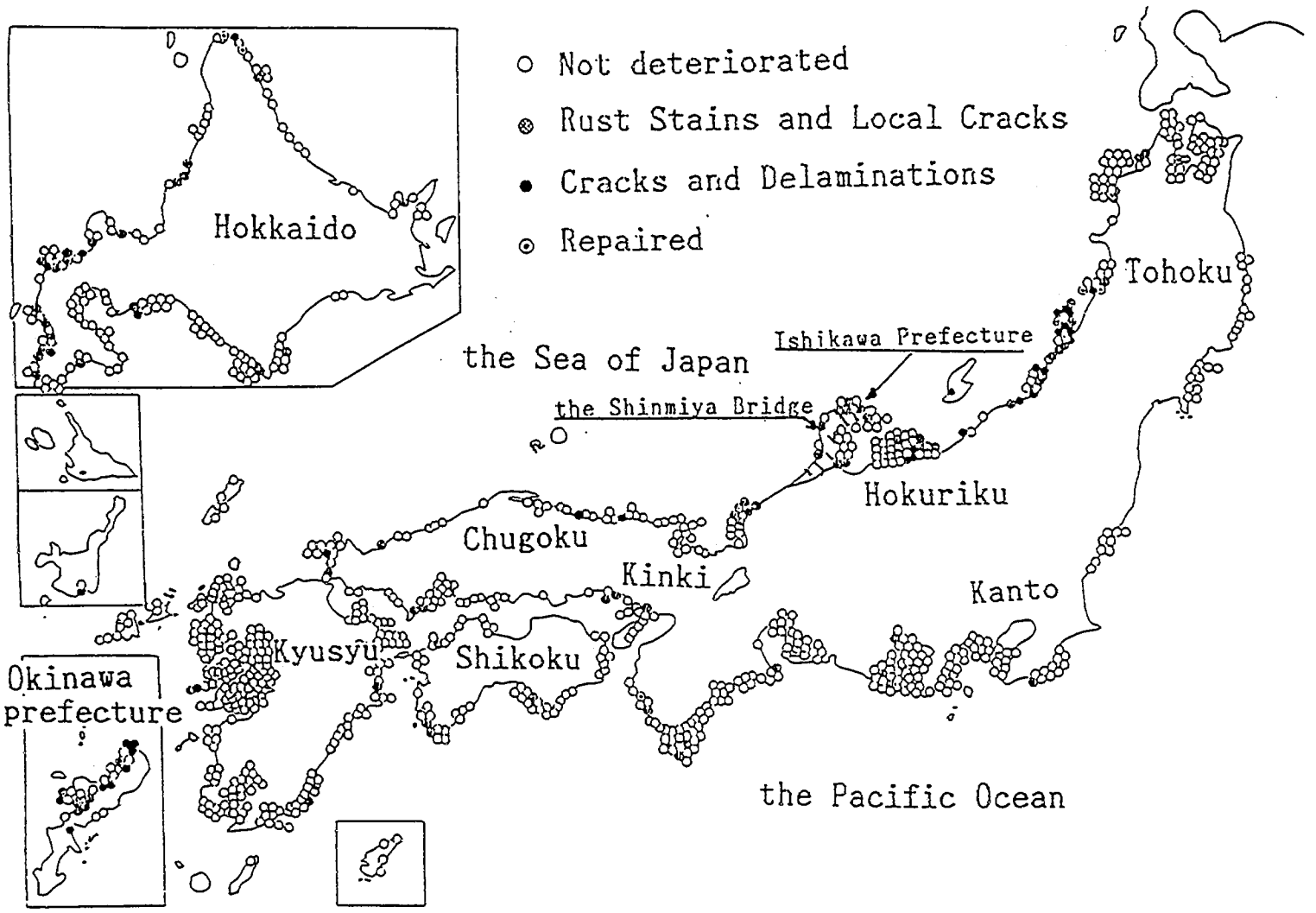


Figure 1 Actural Condition of Concrete Bridges in Coastal Areas
(Result of a macroscopic survey in 1982 for 920 concrete bridges
located in areas within approximately 500m from the shoreline)

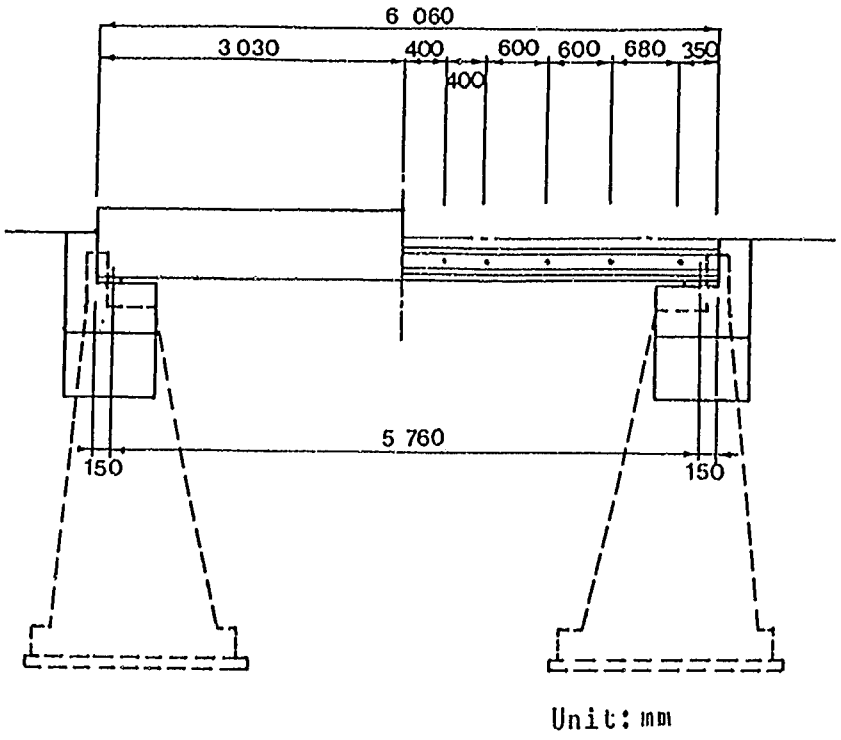


Figure 2 Dimensions and Shape of Shinmiya Bridge

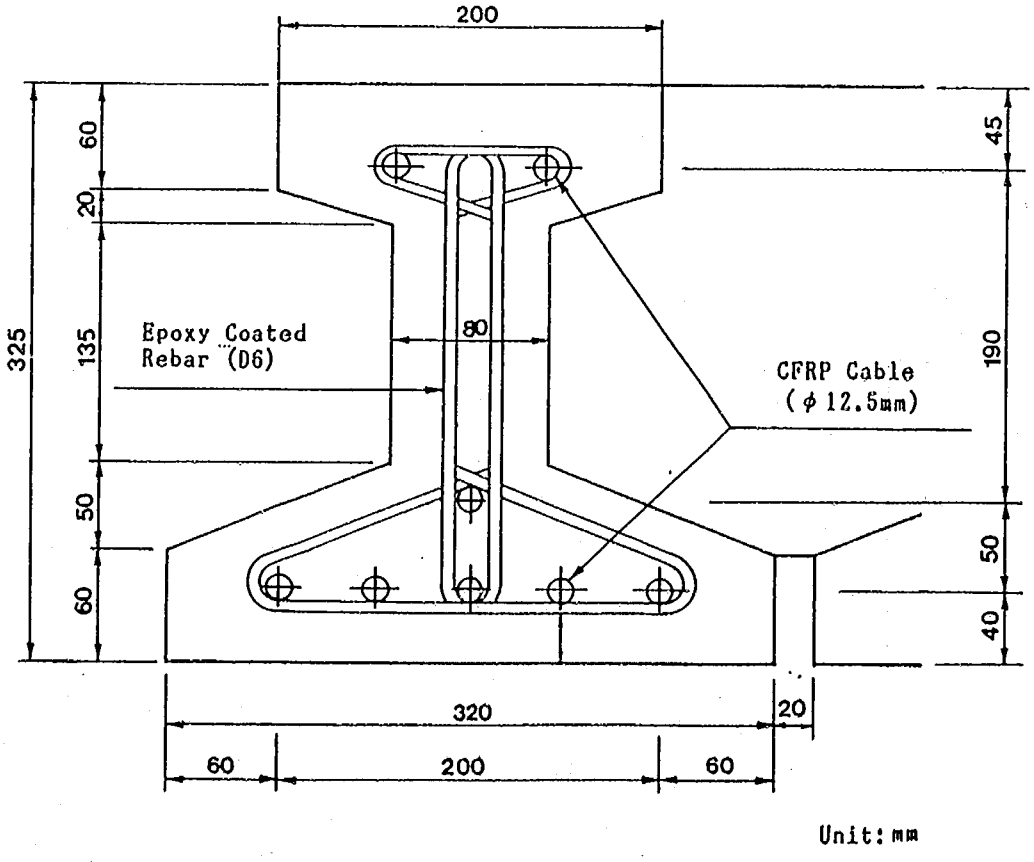


Figure 3 Cross Section of a Girder of Shinmiya Bridge

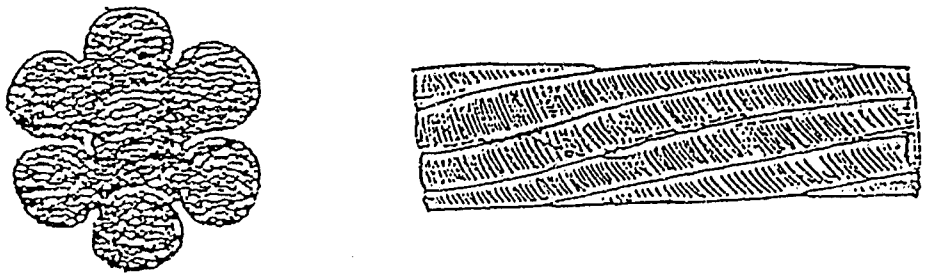


Figure 4 Appearance of
a Used CFPR Cable
(ϕ 12.5mm)

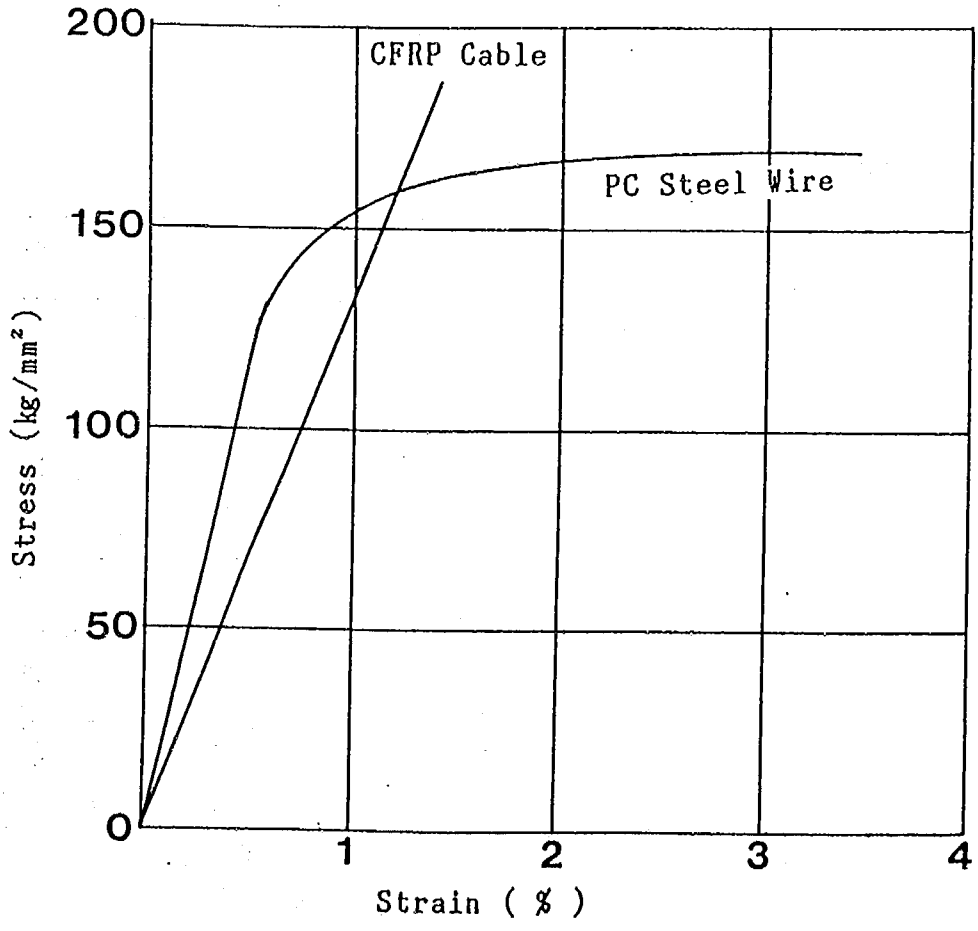
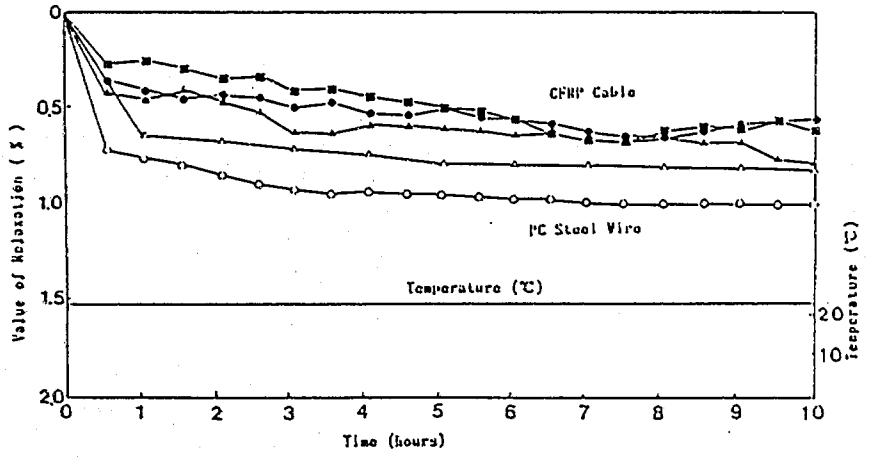
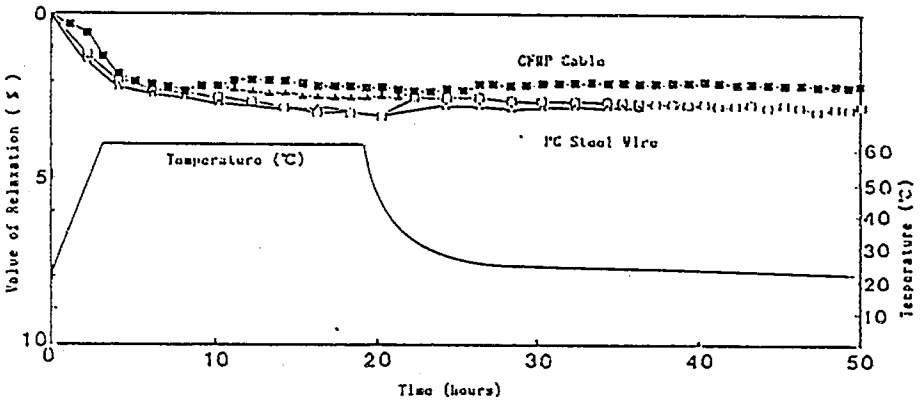


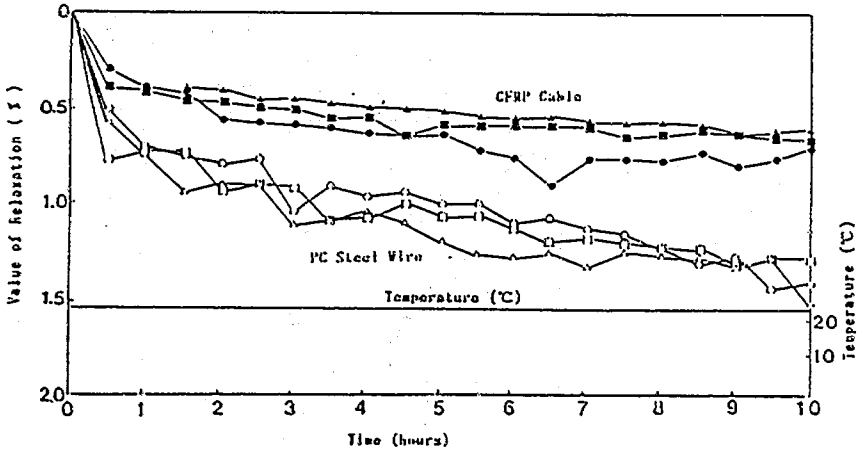
Figure 5 Typical Stress-Strain Relation
of a CFRP Cable and a PC Steel Wire



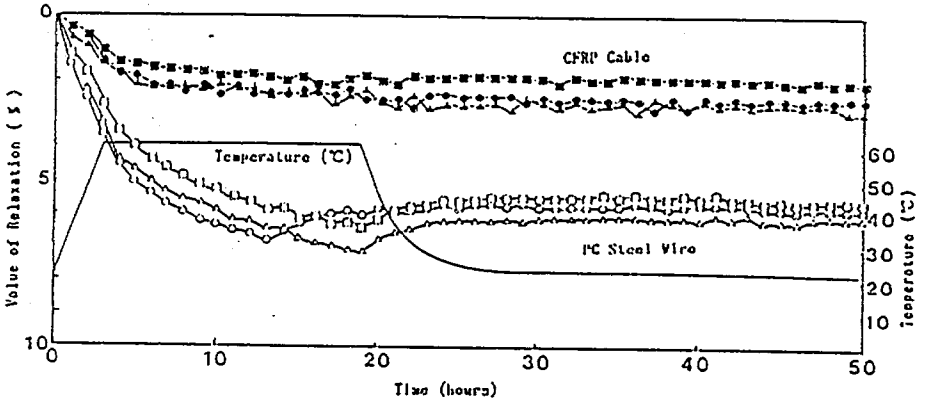
(a) Temperature: 20℃
Tensile Load: 8,000kg



(c) Temperature: 20℃⇒60℃
Tensile Load: 8,000kg



(b) Temperature: 20℃
Tensile Load: 11,000kg



(d) Temperature: 20℃⇒60℃
Tensile Load: 11,000kg

Figure 6 Results of Relaxation Test

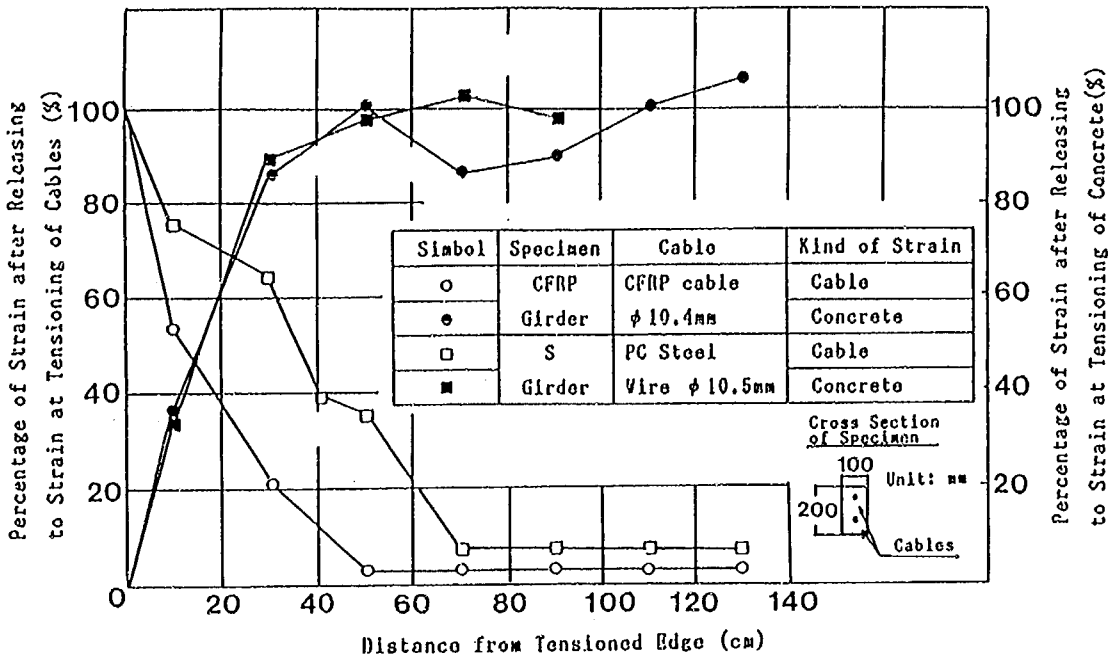


Figure 7 Results of Transfer Length Test

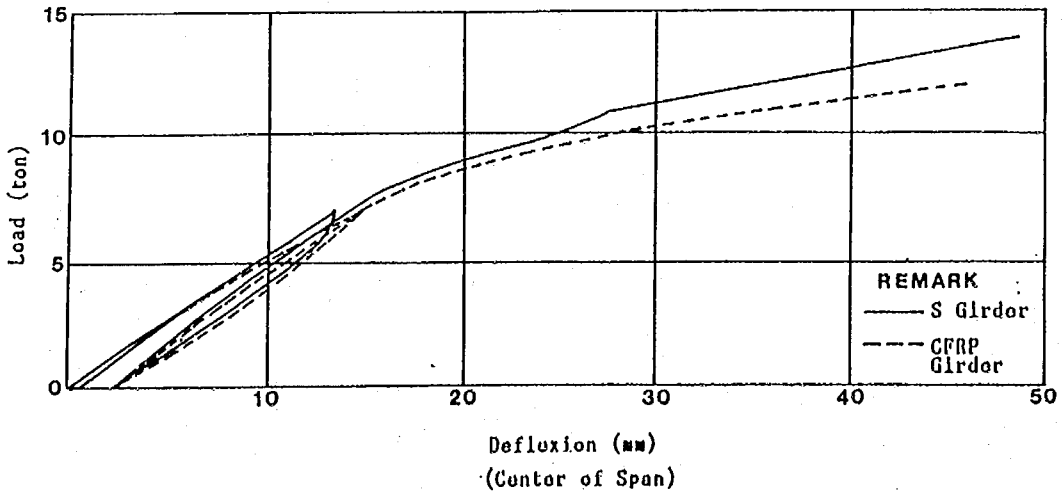


Figure 8 Load-Deflexion Relationships

(8) Session 8

SESSION 8: BRIDGE MAINTENANCE 0:45pm~2:00pm
(Co-Chairman: M. Fujiwara, A. M. Abdel-Ghaffar)

(21) M. S. Agbabian and S. F. Masri※ , M.I Traina and O. Waqfi: Detection of Structural Changes in a Bridge Model
(0:45pm~1:05pm)

(22) S. Kato, S. Uto, M. Ishizuka and S. Motomura※ : A Program and Evaluation of Inspection System for Road Structures on Hanshin Expressway
(1:05pm~1:25pm)

(23) Y. Ito and Y. Oka※ : An Experimental Study on Deterioration of Bridge Deck Slabs and Their Repair
(1:25pm~1:45pm)

DISCUSSION(8)
(1:45pm~2:00pm)



DETECTION OF STRUCTURAL CHANGES IN A BRIDGE MODEL

by

M.S. Agbabian S.F. Masri M.-I. Traina O. Waqfi
Department of Civil Engineering
University of Southern California
Los Angeles, California 90089-0242

SUMMARY

This paper presents some preliminary results from an exploratory study of a highly idealized physical bridge model to gauge the potential of system-identification procedures to detect structural changes on the basis of response measurements.

1 INTRODUCTION

1.1 Motivation

Nondestructive evaluation (NDE) methods for the detection of damage in structural systems have been receiving increasing attention in the recent past. Among the promising NDE methods are those based on the analysis of structural dynamic response measurements to identify a suitable mathematical model corresponding to the (changing) state of the physical structure.

The use of system identification (SI) approaches for NDE problems has expanded in recent years due to (1) development of practical analytical methods for the solution of inverse problems related to the identification of mathematical models on the basis of experimental response measures, and (2) advances in data processing and signal analysis capabilities brought on by developments in sensor technology and the continually increasing computational power and economy of microprocessors.

1.2 Background

The potential of using SI approaches for damage detection in structures has been recognized by many researchers. Similar approaches have been used extensively in other fields, including (among others) nonintrusive medical diagnostics using tomology and geophysical prospecting using seismology. Noteworthy recent efforts to apply formal SI concepts to the problem of damage detection in structures include the works of Yao (1985), Stephens (1985) and Natke (1986). A workshop exclusively devoted to structural safety evaluation based on system identification approaches was recently held in Germany, (Natke and Yao, 1988).

In February 1988, an NSF-sponsored international workshop titled "Nondestructive Evaluation for Performance of Civil Structures" (Agbabian and Masri, 1988) was organized by the authors in order to (1) review the state-of-the-art of all NDE techniques, present, emerging, and future ones that offer the promise of being an effective tool for use in conjunction with *civil* structures, (2) identify the instrumentation requirements of the field, and (3) prioritize the research needs of the Workshop subject. Even though this Workshop encompassed all NDE methods (e.g., acoustic

emission, imaging techniques, ultrasonics, x-ray, etc.), not just system identification approaches, nevertheless the priority list of research needs gave a prominent ranking to the use of system identification techniques as a tool for global structural performance evaluation.

Several technical challenges play a major role in SI applications to structural damage detection. For example, uniqueness and observability problems are inherent in many structural systems due to the presence of redundant structural members and limited sensor locations. In addition, the available physical measurements from the sensors always contain small amounts of noise superimposed on the desired signal. The presence of such noise can lead to serious problems with the accuracy and reliability of various SI algorithms. Finally, the available response measures of some structural systems are inherently insensitive to changes in structural parameters of interest, making it difficult to devise an adequate test arrangement.

1.3 Scope of Paper

This paper explores the potential of an identification procedure to detect structural changes on the basis of response measurements. Section 2 of this paper presents the formulation for the identification procedure under discussion. The usefulness of this approach for damage detection is demonstrated in Section 3 where a preliminary study is presented in which a highly idealized model bridge is used to conduct experiments to generate data sets that are subsequently analyzed to assess the capability of the procedures under discussion for damage and deterioration monitoring.

2 IDENTIFICATION PROCEDURE

Consider a discrete MDOF linear system that is subjected to dynamic excitations. The frequency response functions (FRF) of the structure relate the response (output) of the structure to the set of excitations (input). The relationship between the response at point i and excitation at point j can be expressed in the frequency domain as:

$$Y_i(\omega) = H_{ij}(\omega)X_j(\omega), \tag{1}$$

where

$Y_i(\omega)$ = response at point i for frequency ω,
$H_{ij}(\omega)$ = frequency response function of response i with respect to excitation j for frequency ω,
$X_j(\omega)$ = excitation at point j for frequency ω.

The least-squares solution of Eq. (1) for the frequency response function H is given by (Ewins, 1984) :

$$H = \frac{\sum_{k=1}^{p} G_{yx}}{\sum_{k=1}^{p} G_{xx}}, \tag{2}$$

where

G_{xx} = excitation auto spectrum,
G_{yx} = response cross spectrum,
p = number of samples of spectra.

3 EXPERIMENTAL STUDY

3.1 Bridge Model Characteristics

To illustrate the method of approach under discussion, consider the model bridge shown in Fig. 1. The beam consisted of a grid of aluminum rectangular beams spaced at 5 inches center-to-center that resulted in a structure with an overall length of 45 inches and width of 10 inches.

The model design allowed the convenient excitation and response monitoring at 24 discrete locations corresponding to the physical grid points. A load cell was used to measure the applied dynamic load, and servo accelerometers were used to measure the response.

The boundary conditions for the beam assembly had an adjustable stiffness constraint. Lumped masses were placed at various locations in order to conveniently control the mass distribution and thereby modify the dominant frequencies and corresponding mode shapes as well as reducing the effects of the instrumentation on the model response. Selected locations allowed the introduction of adjustable levels of "defects" in the bridge model.

A finite element analysis of the bridge model yielded the frequencies and mode shapes shown in Fig. 2. The fundamental frequency was equal to $f_1 = 7.8$ Hz and it was associated with the first vertical bending mode.

3.2 Test Procedure

The method under consideration imposes no restrictions on the nature of the excitation source to be used as a probing signal. In the present test, a location near the center of the model was subjected to a multi-sine signal covering the frequency band 6 - 45 Hz. with variable amplitude.

In this preliminary phase of the study, three accelerometers were used to monitor the motion of the locations indicated in Fig. 1. The excitation time history was measured by means of a force gauge connected through a "stinger" to an electrodynamic exciter.

Sample time histories of the excitation and acceleration records obtained during a typical test are shown in Fig. 3.

3.3 Identification of Frequency Response Functions

The analog measurements obtained as discussed above, were subsequently filtered and analyzed using conventional digital signal processing techniques to obtain some pertinent structural dynamics response measures. Among the key items obtained from this data processing phase were the model's frequency response functions that relate the structure's (output) acceleration and the applied (input) load.

Figure 4 shows sample FRF plots indicating the influence of the load application position and the monitoring station location on the dynamic characteristics of the model bridge before and after the introduction of an intentional "defect."

Table 1
Influence of Structural Changes on Dynamic Characteristics
Excitation at Node L_1

Case #	Damage Location	Response Location	f_1 (Hz)	f_2 (Hz)	f_3 (Hz)	$\delta f_1/f_1$ (%)	$\delta f_2/f_2$ (%)	$\delta f_3/f_3$ (%)
1	*none*	n_{15}	7.81	20.60	39.74	0.0	0.0	0.0
2	*none*	n_{21}	7.81	20.70	39.74	0.0	0.0	0.0
3	*none*	n_3	7.81	20.60	39.74	0.0	0.0	0.0
4	d_1	n_{15}	7.81	19.53	38.38	0.0	−5.2	−3.4
5	d_1	n_{21}	7.81	19.53	38.38	0.0	−5.2	−3.4
6	d_1	n_3	7.81	19.53	38.38	0.0	−5.2	−3.4
7	d_2	n_{15}	7.52	19.92	37.11	−3.7	−3.3	−6.6
8	d_2	n_{21}	7.52	19.92	37.11	−3.7	−3.3	−6.6
9	d_2	n_3	7.52	19.92	37.11	−3.7	−3.3	−6.6
10	d_3	n_{15}	7.71	19.53	36.62	−1.3	−5.2	−7.8
11	d_3	n_{21}	7.71	19.53	36.62	−1.3	−5.2	−7.8
12	d_3	n_3	7.71	19.53	36.62	−1.3	−5.2	−7.8

4 DISCUSSION

The variation of the identified model bridge dominant frequencies with and without "damage" is summarized in Table 1 under a variety of monitoring stations and defect positions. Subject to the limitations of the test under discussion, analysis of the results shown in this table indicates the following:

1. the structure's dominant frequencies can be adequately, and consistently determined using any reasonable monitoring location
2. the percentage change (due to "damage") in a given frequency is not sensitive to the location of the monitoring location
3. the FRFs are sensitive to even a relatively small change in the structural characteristics of the monitored system
4. the percentage change in a specific frequency depends on the the "damage" location
5. higher frequencies tend to be more sensitive to structural changes
6. the nature of the transmission path between monitoring locations can give some idea about the location of damage
7. the presence of "damage" or deterioration influences the shape (amplitude,width) of the FRF in a noticeable way; by monitoring several frequencies, it is easier to detect even relatively small changes/deterioration in the structure
8. the frequency spectrum of the excitation may have a significant influence on the relative contribution of various modes

5 SUMMARY AND CONCLUSIONS

As was stated earlier, this study was not meant to be a comprehensive treatment of the title subject, but rather an exploratory investigation of the usefulness of various structural parameter estimates, that can be conveniently extracted during an experimental test, to quantify changes in the characteristics of physical systems. On this basis it appears that system identification techniques may offer some useful and reliable tools for detecting the extent of changes in monitored structures.

6 ACKNOWLEDGEMENTS

This study was supported by grants from the US National Science Foundation.

7 REFERENCES

Agbabian. M.S. and Masri, S.F., (Editors), (1988), Proceedings of the *International Workshop on Nondestructive Evaluation For Performance of Civil Structures,* Dept. of Civil Engineering, University of Southern California, Los Angeles, CA 90089-0242.

Agbabian. M.S., Masri, S.F., Miller, R.K., and Caughey, T.K., (1988), "A System Identification Approach to the Detection of Changes in Structural Parameters," *Structural Safety Evaluation Based on System Identification Approaches*, Edited by H.G. Natke and J.T.P. Yao, Friedr. Vieweg & Sohn, Braunschweig/Wiesbaden.

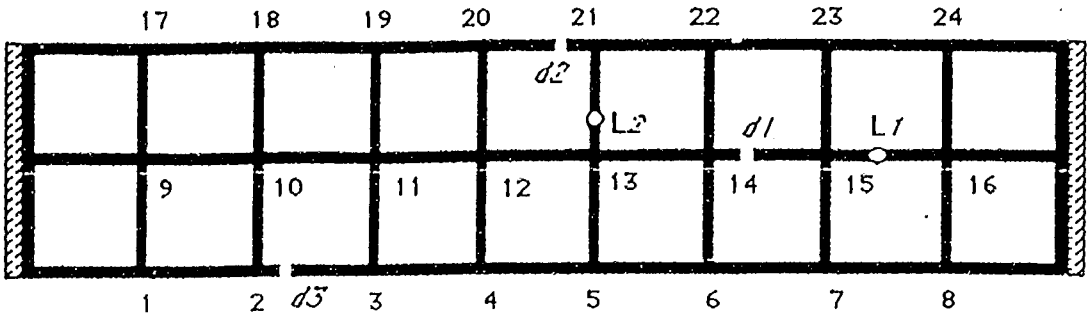
Ewins, D.J., (1984), *Modal Testing: Theory and Practice*, John Wiley & Sons Inc.

Natke, H.G., and Yao, J.T.P., (1986), "Research Topics in Structural Identification", Proc. Third Conference on Dynamic Response of Structures, EM Div./ASCE, UCLA, 31 March - 2 April.

Natke, H.G., and Yao, J.T.P., (1988), "Structural Safety Evaluation Based on System Identification Approaches," *Proceedings of the Workshop at Lambrecht/Pfalz*, Friedr. Vieweg & Sohn, Braunschweig/Wiesbaden.

Stephens, J.E., (1985), "Structural Damage Assessment Using Response Measurements", Ph.D. Thesis, School of Civil Engineering, Purdue University, West Lafayette, IN.

Yao, J.T.P., (1985), *Safety and Reliability of Existing Structures*, Pitman Advanced Publishing Program, Boston.



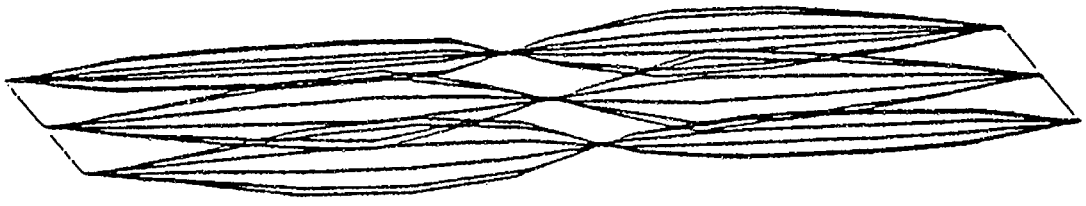
L : LOAD LOCATION

d : DAMAGE LOCATION

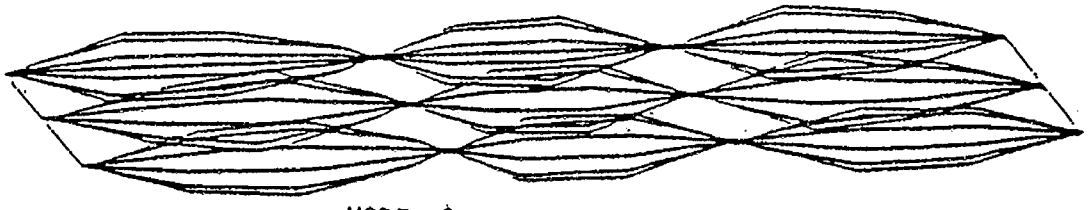
FIGURE 1



MODE 1 frequency = 7.79 HZ



MODE 2 frequency = 20.49 HZ



MODE 3 frequency = 39.42 HZ

FIGURE 2

TIME HISTORY PLOTS
PLOTS OF LOAD INPUT AND ACCELERATION
OUTPUTS AT THREE LOCATIONS FOR UNDAMAGED CASE

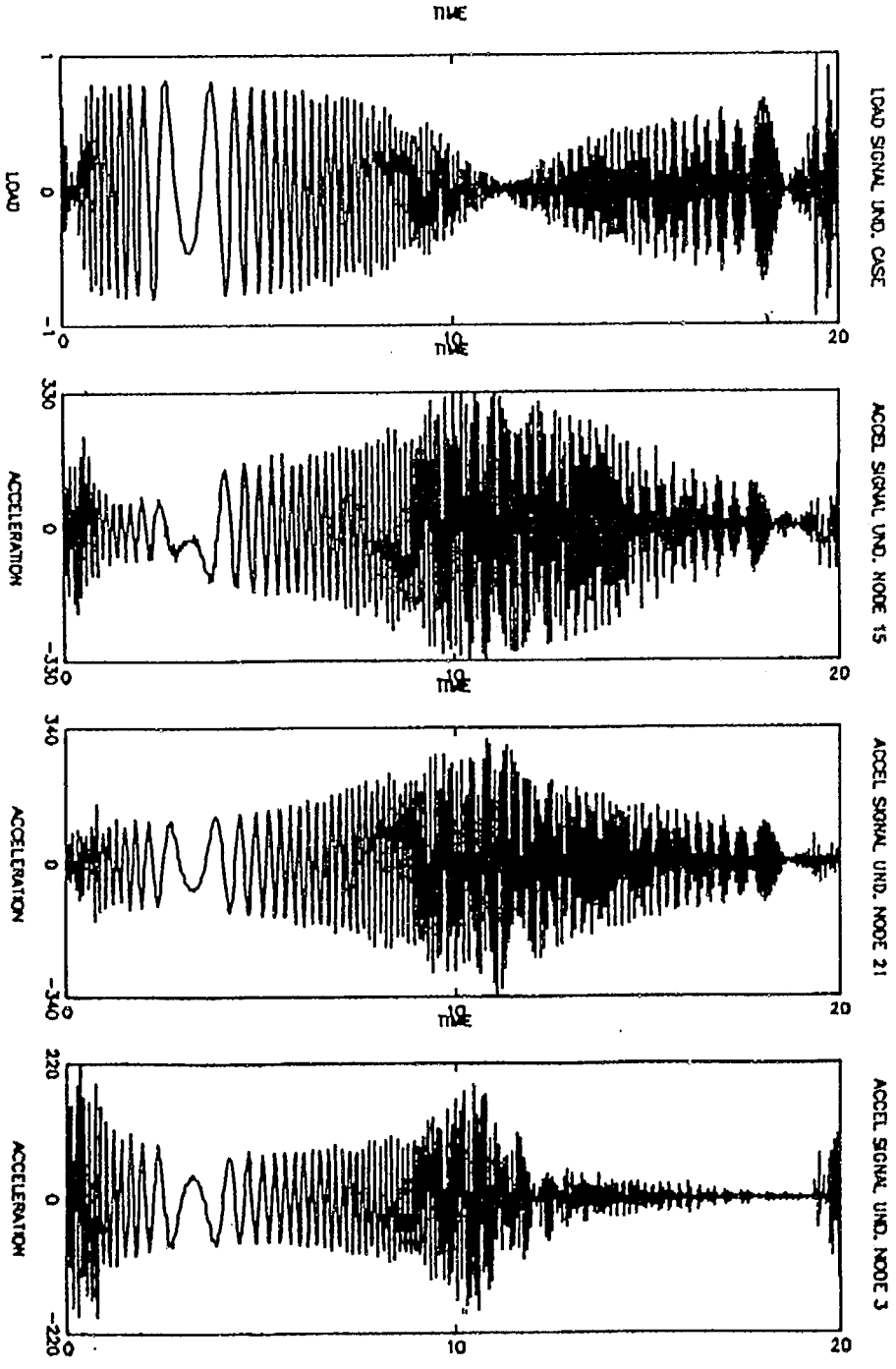


FIGURE 3

FREQUENCY RESPONSE FUNCTION
EXCITATION AT L1 AND DAMAGE AT D1
SOLID LINE FOR UNDAMAGED
NODES 15,21 & 3 RESP.

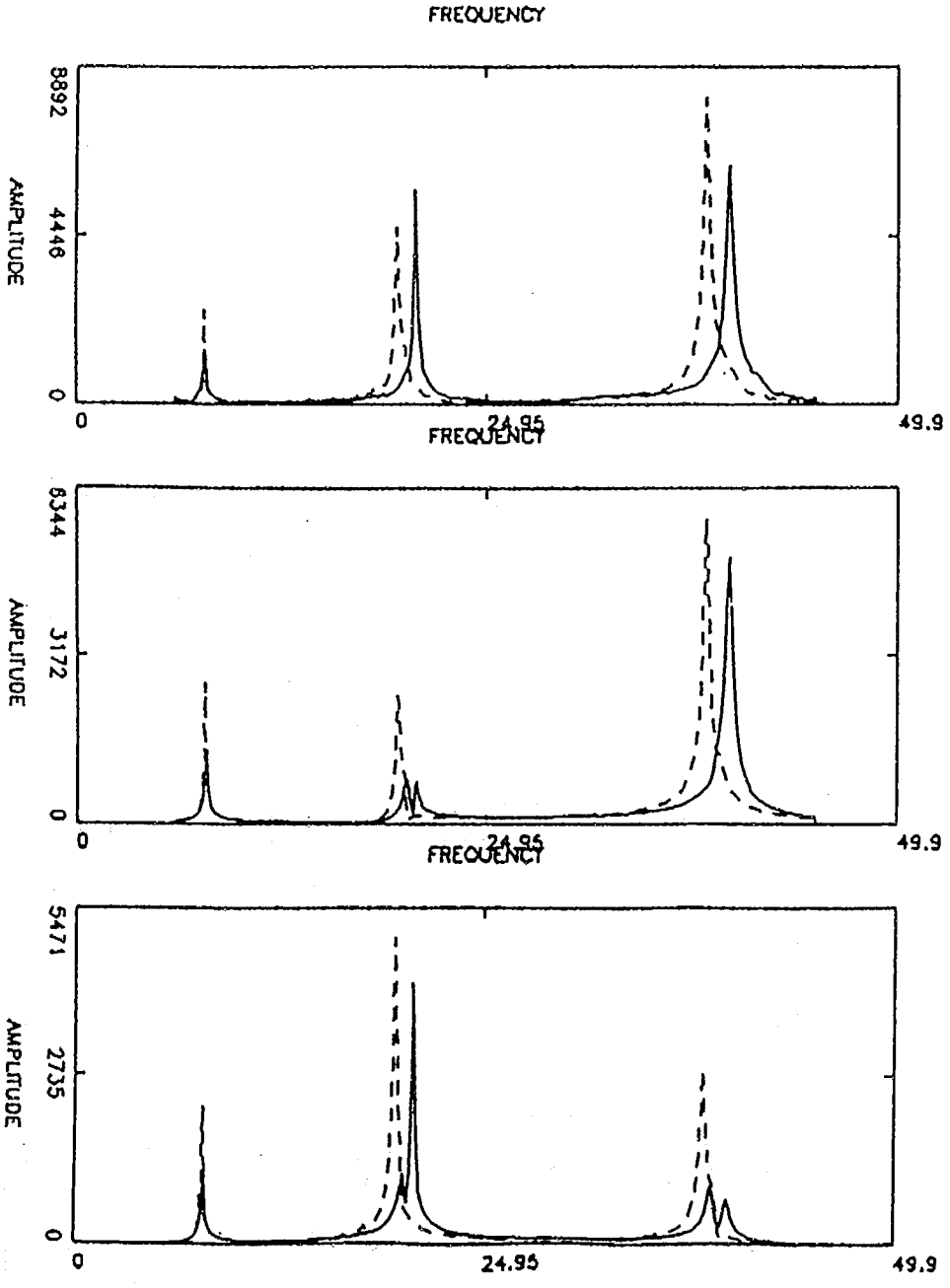


FIGURE 4

A PROGRAM AND EVALUATION OF INSPECTION SYSTEM FOR ROAD STRUCTURES ON HANSHIN EXPRESSWAY

Shugo Katoh
Deputy Director, Third Osaka Construction Division,
Hanshin Expressway Public Corporation
Shigeru Utoh
Deputy Director, Osaka Management Division,
Hanshin Expressway Public Corporation
Shunnichi Motomura
Manager of Research and Development
Hanshin Expressway Administration and Technology Center
Mikitake Ishizuka
Counselor,
International Engineering Research Institute

Summary

Hanshin Expressway, the 143.5 km 13-route toll expressway network in the Hanshin Metropolitan area, has been in service with its first section opened to traffic in June 1964.

Its 96.4 % of the total length are elevated structures, namely, 5,798 spans of bridges with huge number of members.

The basic duties of administrators are to keep a smooth traffic to road users, to maintain the expressway's structures in optimum condition, to prevent the occurrence of an incident and to quickly remove the abnormalities when an incident occurs on the structures. From that viewpoint, we discuss in this paper about the actual state of inspection and repair of the Hanshin Expressway, and also, introduce the ideal way for maintenance work of the expressway in the Metroporitan area.

1. OUTLINE

Since the 2.3 km of Osaka-Ikeda route was opened to traffic in June 1964, the total length of the Hanshin Expressway was extended to 143.5 km (103.6 km in Osaka area and 39.9 km in Hyogo area) for 13 routes, as shown in Fig. 1, which is travelled by 770,000 vehicles per day. The Hanshin Expressway is an essential to economic activities of the Hanshin area as a main artery.

Since the 38.6 km long (27% of the total service length) of the expressway in the OSAKA city was opened to trffic more than 22 years ago and 83.3 km (58%) has been opened for over the past 15 years, its quality essentially depends on the method of management and organization to keep it in good condition for a long time as an important urban facility in social against the progressing deterioration due to heavy volume and load of traffic.

The 138.3 km (96.4%) long Hanshin Expressway, except for the 4.2 km of Kita-Kobe route which runs through a mountainous area, is consisted of elevated structures in the both cities OSAKA and KOBE, while 1 km long is made up of earthwork (see Fig. 2). Characteristically, the expressway is different from ordinary roads and streets completelly, requiring so many varieties of facilities such as toll booths, traffic surveillance and control system, which need as an enormous support for maintenance systems.

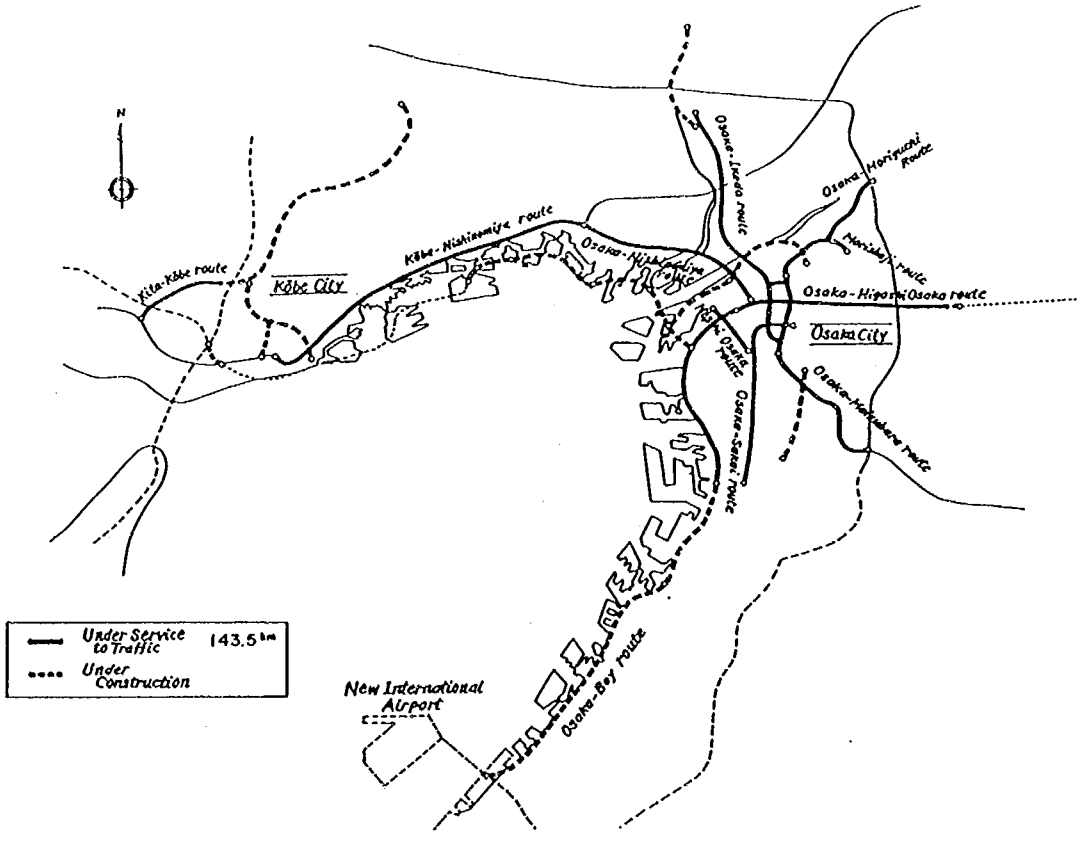


Fig. 1 Hanshin Expressway Network

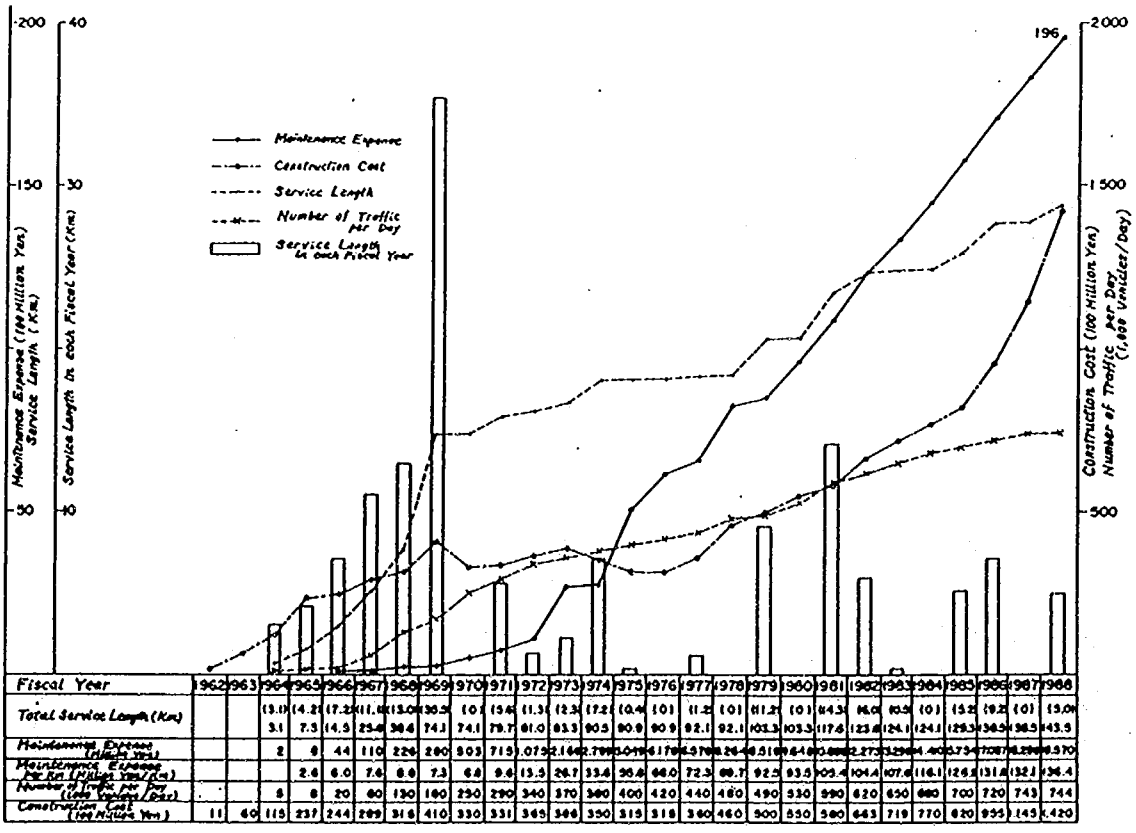
Bridge 138.3 km (96.4%)		Earthwork 4.6 km (3.2%)
Steel Girder 110.8 km (77.2%)	Concrete Girder 27.5 km (19.2%)	Tunnel 0.6 km (0.6%)

Fig. 2 Structures of Hanshin Expressway

2. PURPOSE OF MAINTENANCE

In the latest past decade, the Hanshin Expressway has expanded 1.6 times of the service length, the traffic increased 1.6 times of the volume, and the Corporation put out 2.4 times expenditure in amount of money for the maintenance works including repairs of structures.

The purpose of maintenance is to preserve the expressway in optimum condition, keeping smooth traffic flow in safe to users. The Corporation has been invested large amount of money for the works, year by year, adjusting the ever-increasing traffic volume and passing larger and heavier vehicles, environmental protection measures such as a noise barrier in response to social demands, and repair of various road accessories and facilities for improvement of urban expressway function, as shown in Fig. 3. They have continualy carried out an ordinary work such as repaint, repavement of surface and replacement of expansion joits and also, they have completely conducted major scale repair and future reinforcement of structures, even for having a serious unknown damage which was not predicted since the construction stage. Major Corporation properties are shown in Table 1.



Fiscal Year	1962	1963	1964	1965	1966	1967	1968	1969	1970	1971	1972	1973	1974	1975	1976	1977	1978	1979	1980	1981	1982	1983	1984	1985	1986	1987	1988
Total Service Length (Km)			(3.0) 3.1	(4.2) 7.3	(7.2) 14.5	(11.8) 25.8	(13.0) 38.8	(35.2) 74.1	(0.1) 74.1	(5.6) 79.7	(1.3) 81.0	(2.3) 83.3	(7.2) 90.5	(0.4) 90.9	(0.1) 90.9	(1.2) 92.1	(0.1) 92.1	(11.2) 103.3	(0.1) 103.3	(14.3) 117.6	(6.0) 123.6	(0.5) 124.1	(0.1) 124.1	(5.2) 129.3	(9.2) 138.5	(0.1) 138.5	(5.0) 143.5
Maintenance Expense (100 Million Yen)			2	6	44	110	226	290	503	719	1,075	2,166	2,799	3,019	3,178	3,708	3,784	4,051	4,184	4,400	2,273	3,254	4,400	3,754	4,707	4,234	4,570
Maintenance Expense per Km (2 Ways 1 Line) (Km)				2.6	6.0	7.6	8.8	7.3	6.8	9.6	13.3	26.1	33.4	36.6	46.0	72.3	80.7	92.5	93.5	105.4	104.4	107.6	116.1	126.5	131.8	132.1	136.4
Number of Traffic per Day (1,000 Vehicles/Day)			8	8	20	60	130	190	250	290	340	370	380	400	420	440	480	490	530	590	620	650	680	700	720	743	744
Construction Cost (100 Million Yen)	11	60	115	237	244	289	316	410	330	331	369	346	350	315	318	360	460	900	550	580	643	719	770	820	995	1,145	1,420

Fig. 3 Change of Expenditure for Maintenance Works

In the present, the corporation practices several special works such as a big expansion for parking area, an additional provision of exits and improvement of traffic control system, aiming alleviation of traffic jam and betterment of service to road users. Moreover, the corporation has a policy to design new expressways from a view or improve in service so as to bring them into harmony with urban areas.

An inspection is the most important work in the expressway maintenance. The first step of structure management is to grasp the up-to-date condition of structures. In other words, for instance, it is like maintaining a clinical chart of the structures with historical data, which record the time when it caught a cold or had an operation and what treatment it received at that time, etc. The corporation further endeavours to prevent the structure deterioration by making daily, periodical and provisional inspection, reminding the old saying "10 years for construction, 100 years for maintenance".

Table 1 List of Facilities

Kind	Unit	OSAKA	HYOGO	Total
Length in Service	km	103.6	39.9	143.5
Entrances	No.	68	25	93
Exits	-do-	64	25	89
Piers	-do-	4462	1266	5728
Girders	Span	4456	1342	5798
Painted Area	1000m²	5324	1781	7105
Paved Area	-do-	1904	828	2732
Emergency Parking	No.	125	18	143
Parking Zone	-do-	1	2	3
Emergency Exits	-do-	50	29	79
Traffic Sign Board	-do-	3037	1231	4628
Lighting Pole	-do-	8543	2700	11243
Road Information Board	-do-	217	64	281
TVs for Traffic Control	-do-	77	31	108
Emergency Telephones	-do-	384	171	555
Radios for Information	-do-	18	5	23
Tollbooths	-do-	57	23	80

3. CONCEPT OF INSPECTION

A three-category inspection service on the expressway structure ; daily, periodical and provisional (special) inspection is defined in the "Inspection Standard for Structures" as follows ;

(1) Daily inspection shall be performed of the expressway structures in the road and from the ground. When damages detected in their early stages, the necessary action and countermeasure shall be taken to secure safe and smooth traffic flow and to preserve the structures themselves. This daily inspection shall be executed by contractors. Of all routes of expressways, three parties shall patrol once a day on the road (6 times/day) and two parties shall patrol once a month from the ground (12 times/year).

The inspection results shall be reported to the staff of corporation on the next day. When and where the parties judge, however, that damages and circumstances require prompt attention, they shall immediately report to the staff of corporation over phone, etc. to take an urgent action.

(2) Structures of the expressway shall be fully inspected through periodical inspection to be quickly detected and to be evaluated with their functional deterioration. This inspection shall be performed through tapping by hammer or touching by hand gaining access to the point to be inspected by such available means as scaffoldings or special vehicles.

Periodical inspection shall be performed by qualified engineers under the corporation's instruction. Every year, area and items to be inspected shall be selected according to an annual plan based on the long-term plan. Detail method for major structures such as Slab, Pier, Girder, Pier Settlement and Pavement is standardized in the Inspection Standard.

(3) Provisional inspection shall performed to prevent damages from spreading, when actually confronted by abnormal conditions or serious damages, or when foreseeing such threatening. This inspection shall slso be performed according to such aims as evaluation or checking of the results from other inspections, as finding possible causes, as surveying or examining repair methods, etc.

Provisional inspection, it is called a special inspection, nowadays, has to be carried out of the various structures for the reasons of ;

① Fiercely increasing traffic volume demanded to be catered for,

② Vehicles themselves getting heavier,

③ Variety of changes on the expressway's structures in its aging.

The followings are the mains of the special inspection carried out recently as ;

① Inspection of cracks in the welding of steel girders,

② Inspection for High-Strengh Bolt to reseach of basic characters about static fatigue phenomenon,

③ Inspection on concrete structures damaged by Alkali-Aggregate Reaction to get statistical data, basic characters and to design the proper repair method on them.

The inspection system on the Hanshin Expressway can be summarized as follows ;

(1) Daily Inspection ; for quick discovering any abnormalities or damages, ensuring smooth and safe traffic flow, protecting injurious conditions to the third persons.

1) In the Expressway ; for the following structures,
   a) pavement ; 5 times/week (for main line), 1 time/week (for sub-line)
   b) expansion Joint ; -do- -do-
   c) railling, Accessories, earthwork and tunnel ; 1 time/week
2) From the Ground ; for maijor concrete and steel structures, concrete slab, railling and main accessories ;
   1 time/week (on the ground), 1 time/year (in the water)
3) For earthwork ; for earthwork and tunnel ; 1 time/2 weeks

(2) Periodical Inspection ; for grasping soundness of structures, quick treatment against damages to lower their function, keeping the structures in good.

1) For superstructure ; slab, concrete girder, steel girder, railling and various structures on the pier ; 1 time/5～7 years
2) For substructures ; slab, various structures on the pier, concrete and steel pier ; 1 time/5～7 years
3) For Earthwork ; for the following structures,
   a) slope and drainage facilities ; 1～2 times/year
   b) tunnel and culvert ; 1 time/5～7 years
4) For special structures ;
   a) pavement ; 1 time/1～2 years
   b) substructure settlement ; 1 time/5～7 years

(3) Provisional or Special Inspection ; for quick discovering of external abnormalities and serious damages to make the structure's function lower, protecting an expansion of damsges, investigating or reseaching considerable causes and condition of damage in progress, making dicision for the repair works to be necessary or not, reseaching and designing the repair methods to remove a functional decrease caused by damages. This shall be applied on all kinds of structures when it needs.

4. EVALUATION OF THE INSPECTION SYSTEM

With a combination of the inspection system when it needs as well as daily and periodical inspection, the most suitable inspection work can be applied on the structures as required by a qualified officer. All results from the inspections have been efficientry utilizing to reach the goal of the expressway management as an essential information, as shown in Fig. 4.

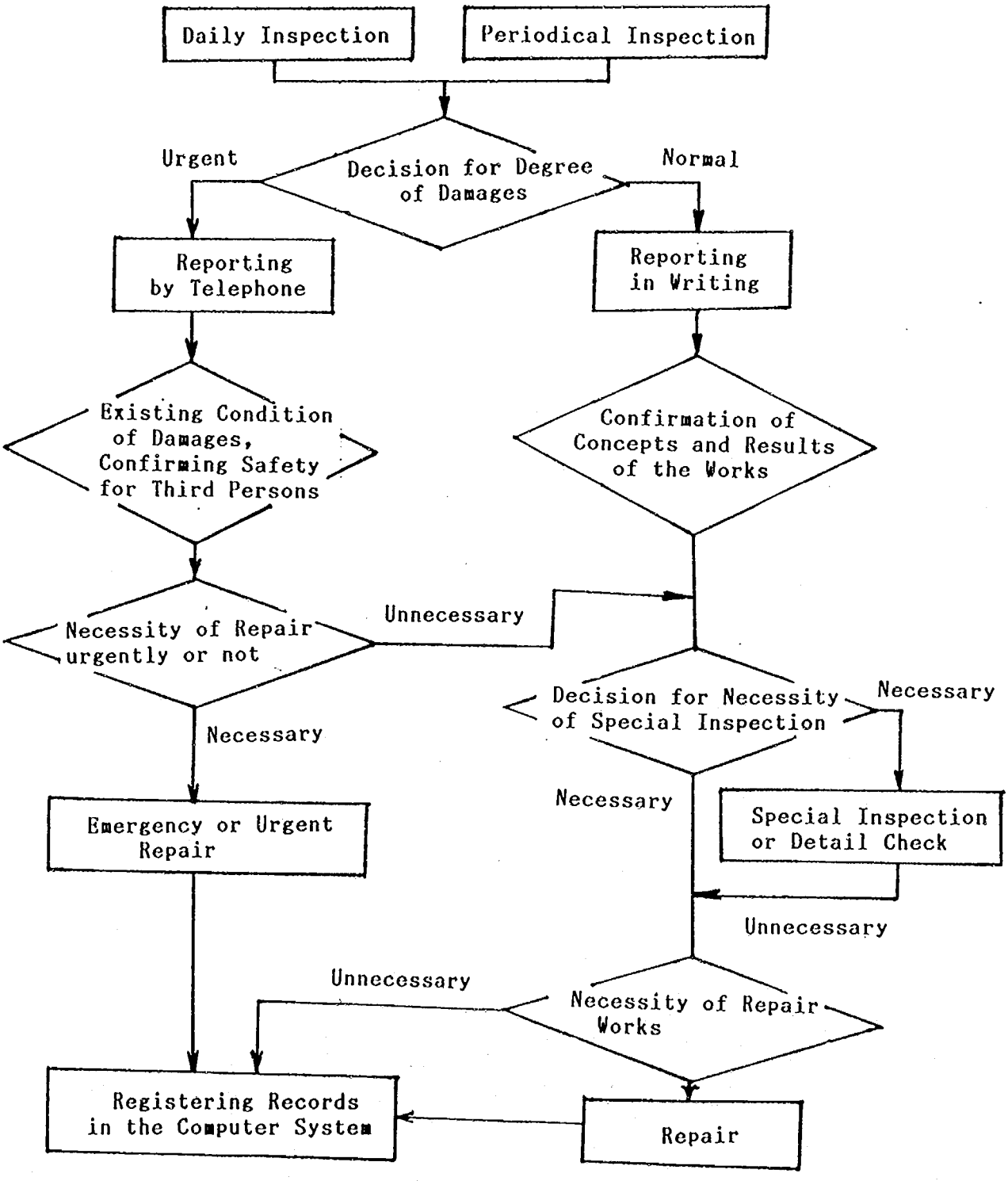


Fig. 4 Flow from Inspection to Repair

5. REPAIR WORK AND APPLICATION OF INSPECTION

Nowadays, so many difficulties come up, especially for maintenance works of the structures in the urban expressway, as described in Fig. 5.

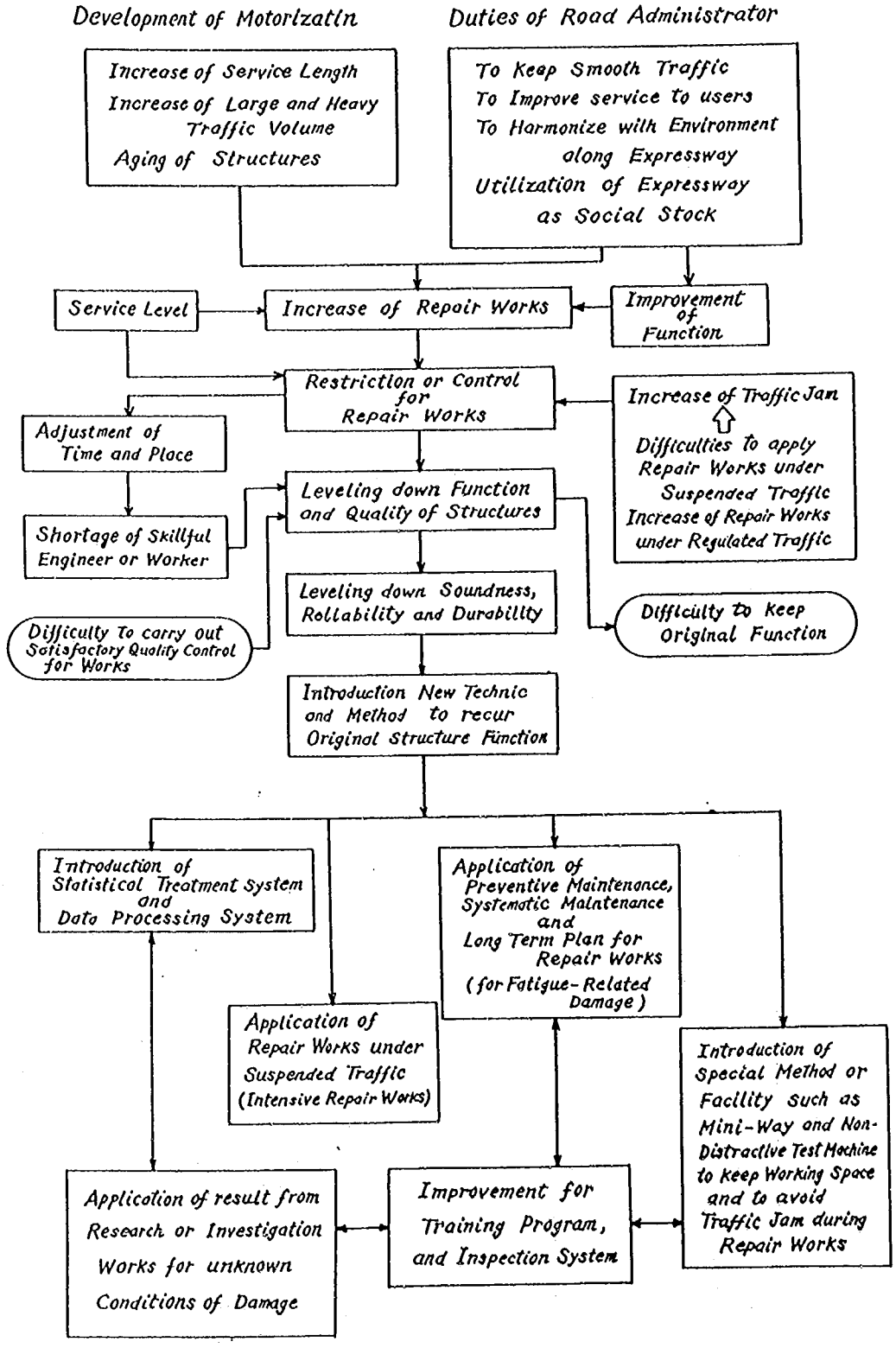


Fig. 5 Difficulties to conduct Repair Works in Hanshin Expressway

The most serious condition is how to keep the quality of the repair work regulating traffic service. To recure an original quality or function of the structures is very much difficult in the repair works, even suficient quality control and supervision did, because the work shall be performed under so severe restrictions.

Repair works on the expressway such as repavement and replacement of expansion joints inevitably accompany with traffic control, and they cause severe traffic jam during the daytime except on some special routes.There are only a few business areas along the Hanshin Expressway.

It roadside areas are crowded with residential houses and the residents' consciousness is high enough to react sharply against the noise of nighttime repair works. Therefore, from the early stage, repair works accompanying noise has been basically done during the daytime on holidays.

With the increase of both traffic volume and repair works, traffic jam caused by repair works on holidays is becoming a social problem, with requiring urgent measures. To cope with this problem, the followings are mainly undertaken or under study :

(1) Repair work under suspended traffic
Work is done intensively, closng one direction of a route entirely or a part of it for several days.

(2) Repair work under large scale regulated traffic
Work is done intesively regulating one lane of a route for 5～13 km during daytime of holidays.

(3) Adjustment of repair work among expressway routes
Work is adjusted in terms of time and location of the route in order to make a driver meet one work per trip.

(4) Shift to nighttime repair works
Work is shifted to nighttime according to work item, work method and surrounding conditions.

(5) Development of provisional surface suport vehicles
Development of vehicles which have provisional surface over the regulated section.

It is becoming a regular cycle to repair one radial route a year by rotation, carrying out the repair work under suspended traffic which aims at efficiently performing various and large volume of works in a short period of time. Drivers prefer this method to the repair work with a large scale regulated traffic method because the later causes severe traffic jam. However, effects of that on the trunk route in the urban areas are countless and it needs most careful preparation with all agencies concerned.

Results from inspection works are efficiently utilized to determine type, location, volume and period of time for the repair works.

6. RELATIONSHIP BETWEEN COST AND SERVICE LENGTH

How long we can maintain an urban expressway or its structures in good condition. It is very difficult to say an exact period, because lots of factors shall be considered. Relationship between an accumulated cost and a service length can be theoretically said that total investment to keep a certain degree of level of serviceability on the expressway route or a single structure for a certain period will make an individual pattern, getting the longest service length of the route or structure as shown in Fig. 6.

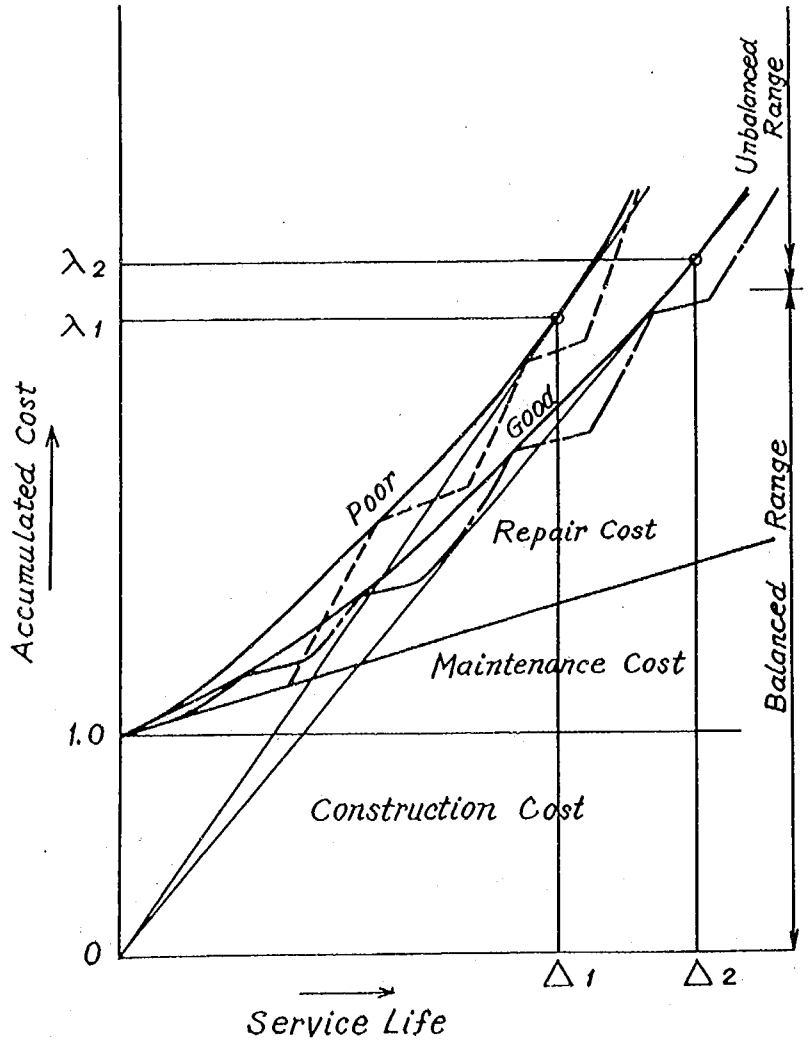


Fig. 6 Considerable Relationship between Total Cost and Service Life

Each structure has, characteristically, each basic pattern, depending upon an original life in design, a policy of road management in degree of the service, a social value in use, traffic conditions in future and a feasible limitation of budget to be invested for a total period in use.

We hope that a reasonable level inspection will results an optimum length in service with a minimum cost, lengthening the original life of the road to protect and to forecast any fatigue troubles from statistical inspection results.

7. CONCLUSION

Nowadays, an expressway management is getting more difficult because of a stronger impact in social, aging life of structures and balanced condition in economic, especially for a toll expressway management. We are making an effort utilizing inspection results, effectively, to minimize a total cost to be invested. We think we have to improve an inspection work, further more, by introducing new ideas and technics.

8. REFERENCE

1) Supervision and maintenance of expressways by Hanshin Expressway Public Corporation ; S. Katoh, M. Shimizu
2) Deterioration and repair of bridge structure in Hanshin Expressway ; published by Hanshin Expressway Administration and Technology Center
3) Inspection Standard for Structures ; published by Hanshin Expressway Administration and Technology Center
4) Profile of Hanshin Expressway ; published by Hanshin Expressway Public Corporation

AN EXPERIMENTAL STUDY ON DETERIORATION OF BRIDGE DECK SLABS AND THEIR REPAIR METHODS

Yoshinori Ito
Manager, Structural Engineering Division,
Engineering Department
Japan Highway Public Corporation (JHPC)

Yoneo Oka
Engineer, Concrete Engineering Division
Laboratory of Japan Highway Public Corporation (LJHPC)

1. INTRODUCTION

Nihon Doro Kodan (Japan Highway Public Corporation) constructs, operates, and maintains all exressways in Japan. 4400km of expressways including 5000 bridges have been constructed and have been in operation since 1957.

The deterioration of bridge deck slabs, particularly of steel bridges, is a serious problem in Japan. Deteriorated bridge decks are often found where deicing chemicals are seldom used. These decks exhibit partial depression and fall-off, not scaling nor spalling. Because air-entrained concrete is used for all bridge deck slabs in Japan, deterioration due to freezing and thawing is seldom seen.

Bridge deck slabs designed before 1970 exhibit a great deal of deterioration and damage. The span between main girders of these bridges is about 4 m and the depth of the slab is 16 to 18 cm. Concrete cover over both top and bottom reinforcement is 3 cm. Most of these bridges have been repaired by partial reconstruction of the bridge deck, reinforcement with an additional stringer between main girders, steel-plate bonding, and slab thickness increment.

After 1970 the specification for Highway Bridge, which is the guideline for bridge design in Japan, had been revised to require that the span between main girders be shorter and slab depth be more deep (shown in Figure 1) while the specification of a concrete cover over top reinforcement did not change. To study the cause of deterioration, investigate methods of repair and reinforcement, and establish a method of evaluating bridge decks, many fatigue tests of brige deck slabs have been carried out in the laboratory of Nihon Doro Kodan since 1976. In this paper the deterioration mechanism of steel bridge deck slabs is discussed based on experimental tests. Also their repair methods for the deterioration of slabs which are taken most generally in expressways are discussed.

2. PREVIOUS WORKS

The following results have been obtained from full-size model tests. According to the fatigue trests on full-size model bridge decks, fatigue strength to static strength is about 0.5. Model bridge decks are that of 18cm in depth designed based on the old standards with a static strength of 490kN and 22cm in depth designed based on the new standards with static strength of 930kN. Their fatigue strength were 250kN and 440kN respectively (1). (2).

On the other hand observations of deteroirated bridge decks indicated that (3).

- Deterioration is found only in limited parts of bridge decks.
- Deterioration on one-lane roadways is heavier than that of two-lane roadways.
- Most deteriorated parts exhibit a gridlike pattern of cracks that progress because of water infiltration and leakage. Free lime, concrete powder, and rusty liquid from reinforcements are found on the bottom surface of bridge decks.

On the basis of these observations it was hypothesized that water leakage through cracks that run the entire depth of the deck was one of the most important factors in deck deterioration. To test this hypothesis a model bridge deck that exhibited the characteristics that had been observed in the field was reconstructed in the laboratory. Model slabs with severe, artificially induced penetrating cracks were constructed and repeated loading tests (fatigue test) were carried out in the presence of water leakage. The results were a great quantity of abraded concrete Progrepowder and many broken pieces that flowed out with water leakage. Progressive deterioration was clearly observed and as a result fatigue strength dropped considerably. Details are given in the following section.

3 FATIGUE TESTS ON AN ARTIFICIALLY CRACKED MODEL SLAB

3.1 Preperation of a model slab

A model bridge deck slab was fabricated on model steel girders under unfavorable construction conditions. The properties of the cement of this slab were

Compressive strength —— 21.9 MPa
Water to cement ratio —— 0.70
Slump —— 21.3 cm
Entrained air —— 3.6 %
Temprature —— 30 °C

The slab was dried by the artificial wind of an electric fan. There was no moisture curing. Details of this specimen are shown in Figure 2. The result was that many cracks, mainly above the positions of reinforcements, were generated in about 30 minutes after the concrete was cast. By the beginning of the fatigue test, about 3 months after construction, these cracks had grown wider because of shrinkage of the concrete and restriction of the steel girders as shown in Figure 3 (a). Some of the transverse cracks are more than 1 to 2 mm in width. Figure 3 (b) shows that wider transverse carcks reached the bottom surface of the slab, and during rainfall some free lime with water leakage could be observed.

3.2 Loading Method and Repetition Patterns

Figure 2 shows the loading apparatus, the positions of the moving load, and the water that was ponded on top of the slab during fatigue loading of the top surface of the slab. As a preliminary loading, approximately 20000 −78.4 kN repeated loading were applied to points 1 to 23 to produce a gridlike pattern of cracks over the entire bottom surface.

The fatigue loading pattern were as follows. The loading point was

changed to the next point after every cycle (0.3 million repetitions).

- Case 1. Fatigue load level was 78.4 to 24.5 kN one cycle on points 3, 5, 13, 19, and 21, respectively; three cycles on points 4, 11, 12, and 20, respectively; 5.1 million repetitions total.
- Case 2. Fatigue load level was 103 to 24.5 kN one cycle on points 11, 12, 20, 101, and 102, respectively; 1.5 million repetitions total.
- Case 3. The upper load level was decreased to 88.3 kN; three rounds of one-cycle loadings on the same points as in case 2 ; 4.5 million repetitions total.
- Case 4. The loading point was moved to point 103, which was between points 101 and 102 where serious damage had been observed. Fatigue load level was 88.3 to 24.5 kN; and after 0.65 million repetitions at this point fatigue failure occurred.

Various kinds of measurement were carried out by the static loading of points 9 through 15 after one cycle loading had been applied to all points. Water that leaked was collected in a container under the specimen slab at every cycle on each point and its volume was measured. The water was then allowed to evaporate and any remains were measured as abrasion weight.

3.3 Fatigue Test Results

Figure 4 shows how the deterioration of the specimen progressed under repeated loading from case 1 through case 4. Figure 4 (a) shows the loading process (one unit of the abscissa indicates one cycle or 0.3 million repetitions of load). In case 1 tensile strain of the bottom reinforcement was 400 ~500 x 10^{-6} and the change in crack width was about 0.1 mm. Water leakage was slight and little deterioration occurred except for the flowage of some white, soft, free lime. In case 2 the upper limit of tensile strain of the reinforcements was arranged to be about 900 x 10^{-6} so that fatigue failure of the reinforcements would not occur, and the upper load level was increased to 103 kN. The result was that the volume of water leakage from cracks suddenly increased to 1000 to 2000 cm^3 per hour and abrasion weigh during one cycle of loading reached 5 to 10 gm. The change of crack width due to loading was more than twice as large; clearly, deterioration was remarkably rapid [see Figrue 4(b), (c), (d) and (e)].

Because the tensile strain on the bottom reinforcement increased as deterioration progressed, the upper load was decreased to 88.3kN and repeated loading was continued. As shown in Figue 4, deterioration progressed even as the load level was dropped to 88.3 kN.

Figure 5 shows that abrasion volume increased in proportion to the increase in total water leakage volume. Apparently water infiltration of cracks and abrading action occurred.

After loading in case 3, the loading point was moved to point 103 in case 4. When point 103 was loaded, water leakage volume increased considerably to 4000 to 5000 cm^3 per hour, and at 0.65 million repetations of load it increased significantly. Therefore the loading machine was stopped and the specimen was examined in details. Observation showed that fatigue punching shear occured at 103. Figure 6 shows a cross section connecting loading point thruogh 103. Fatigue punching shear cracks, including vertical bending cracks generated at the position of reinforcements, were observed. Figure 7 shows crack caused by loading the inside width of the crack expanded to about 0.5 mm and its edge was round. A similar pattern

of deterioration can often be seen on deteriorated in-service slabs after removal of the asphalt overlay.

After fatigue tests were completed static loading tests were carried out on points A and B shown in Figure 1. Static strength was 282 kN at point A and 273 kN at point B. If the average of these values is taken as the static strength of this slab, the ratio of fatigue upper loads of 88.3 kN and 103 kN to static strength is 0.32 and 0.37 respectively. These values are remarkably low compared with the value usually obtained without water infiltration.

4. DETERIORATION OF BRIDGE DECK SLABS

As it is discussed in previous sections the deterioration mechanism of bridge deck slabs will be summarized as follows :

(1.) Break-out of penetrating cracks that would be caused by drying shrinkage and faulty construction.
(2.) Infiltration rainwater into a slab and leakage of rainwater from cracks.
(3.) Wheel loads great enough to cause abrasion.

To confirm these findings, in 1983 the condition of cracks on the 24 bridge decks on the Tomei Exprssway (Tokyo to Nagoya) was investigated. Asphalt overely section 1 m x 2 m were torn off and cracks on the top surface of bridge decks was studied. Cracks, serious or not, occurred in all parts of the top surface of decks. In most of examined parts it can be seen that cracks on the top surface of a deck are similar to those on the bottom surface and that rainwater is infiltrating penetrating cracks. (Only cracks on the bottom surface from which free lime flowed were observed) Consequently, it would be concluded that the mechanism described above is essential to the deterioration of bridge deck slabs.

5. REPAIR METHODS

In this section repair methods which have been employed in steel bridge decks to strengthen slabs of expressways are discussed. Most of those slabs to be repaired were designed based on the old specification. The methods are summarized in Table 1 and are also shown in Figure 8. The features of the methods are described in related to the deterioration mechanism.

(1.) Slab thickness increment method

As is mentioned in previous section the thickness of a slab is one of fundamental factors which control the static and fatigue punching shear strength. Therefore this method is essential for strengthening slab as far as bond strengh bewteen existing slab and incremented slab part is guaranteed. Several types of this method including cement concrete with reinforcment and/or steel fiber have been examined in fatigue tests and have been confirmed the effectiveness of this method.

(2.) Addtional stringer method

The idea of this method is to reduce the span btween main girders so that bending moment due to wheel loads be smaller. This is because that in the new specification wheel load had taken larger than that of old one by 20 % Actually the deflection movement occured in midspan of the slab strenghed with the stringer is decreased considerably. In this point of view this method is effective for reducing abrasive action However according to the experimental result bending moment does not decrease so much and shear stress is still the same at the position of 1/4 (midspan of main girder and additional stringer). Therefore if wheel load acts on this point it is hard to expect the strengthening effect.

(3) Steel plate bonding

This method has been employed very often in expressways. Steel plates strengthen reinforcements which are to be increased in the new specification According to the experimental results punching shear capacity is increased by 20 % to 30 % Thouth, there are shortcomings in this method One is that water infiltrated into the slab would remain inside slab and steel plate. Hence there is no guarantee of durability both in concrete material and in the mechanical performance of the slab The other one is maintenance difficulty. Once steel plates are installed in the bottom of the slab examinations of their soundness are almost impossible. Conesequently, this method is not popular now

(4) Partial reconstruction

It is often found that only the part of a slab is badly damaged The reasons for this would be traffic condition and initial fault of construction In this case this method is effective for temporary repair work because it is economical and short time to work out. But it may not be a permanet solution

In addition to above methods waterproofing membranes are also considered to be effective. Because preventing water infiltration into slabs, as alluded in the previous section, keeps slabs in good condition So this method is combined with other methods such as partial reconstruction in order that rehabilitation be more effective. Besides this, as to a basic countermeasure to the deterioration of slabs, expansive concrete is tried to use. Fundamental experiments of expansive concrete show that it is effective in preventing crack break out. Several experimental constructions have been executed and confirmed to be effective to reduce drying shrinkage craks. Follow up surveys are carried out. It is believed that this method may be one of the most effective methods to prevent the deterioration of bridge deck slabs.

6 CONCLUDING REMARKS

Deterioration mechanisms of steel bridge deck slabs and their repair methods are discussed in this paper based on the model slab tests and field surveys of bridges in service. The results may be summarized as follows :

Fatigue failure, due to punching shear, is observed in a model slab test which is prepaired to have construction induced cracks. The fatigue

strength of this specemen was about one third its static strength and was remarkably low compared with the usual fatigue strength of RC members. From the test results the deterioration mechanism of bridge deck slabs was estimated to be the combination of three conditions : break out of penetrating cracks caused by drying shrinkage or fault construction, infiltration and leakage of rainwater, and wheel loads that generate abrasive action.

Several repair methods for the deteriorated steel bridge deck slabs have been employed in repair works. The slab thickness increment method becomes popular because an execution method has been developed so that traffic regulation be minimum and one-lane traffic be possible. Another reason is that the slab thickness can be increased so as to have enough punching shear capacity. However it is very difficult to decide that which stage of the deterioration and what method are appropriate in the course of rehabilitation work (repair work) . Follow up surveys keep going in experimental constructions of slabs. The data of the surveys will be utilized for the management system for the mentenance of bridge deck slabs which will be needed.

7. REFERENCES

1. Y. Iioka, T. Higai, and H Muraki. :Experimental Research on Fatigue Strength of Reinforced Concrete Slabs. Report of The Laboratory of Nihon Doro Kodan. Tokyo Japan, Dec. 1977, pp. 132-142

2. Y. Iioka, T. Higai, and N Fujita. :A Fatigue Test of Reinforced Concrete Slab Decks. Report of The Laboratory of Nihon Doro Kodan. Tokyo Japan, Dec. 1978, pp. 198-209

3. S. Fujita and Y. Kimura. : Investigation of the Evaluation of Bridge Deck Slabs. Report of The Laboratory of Nihon Doro Kodan. Tokyo Japan, Dec. 1980, pp. 134-146

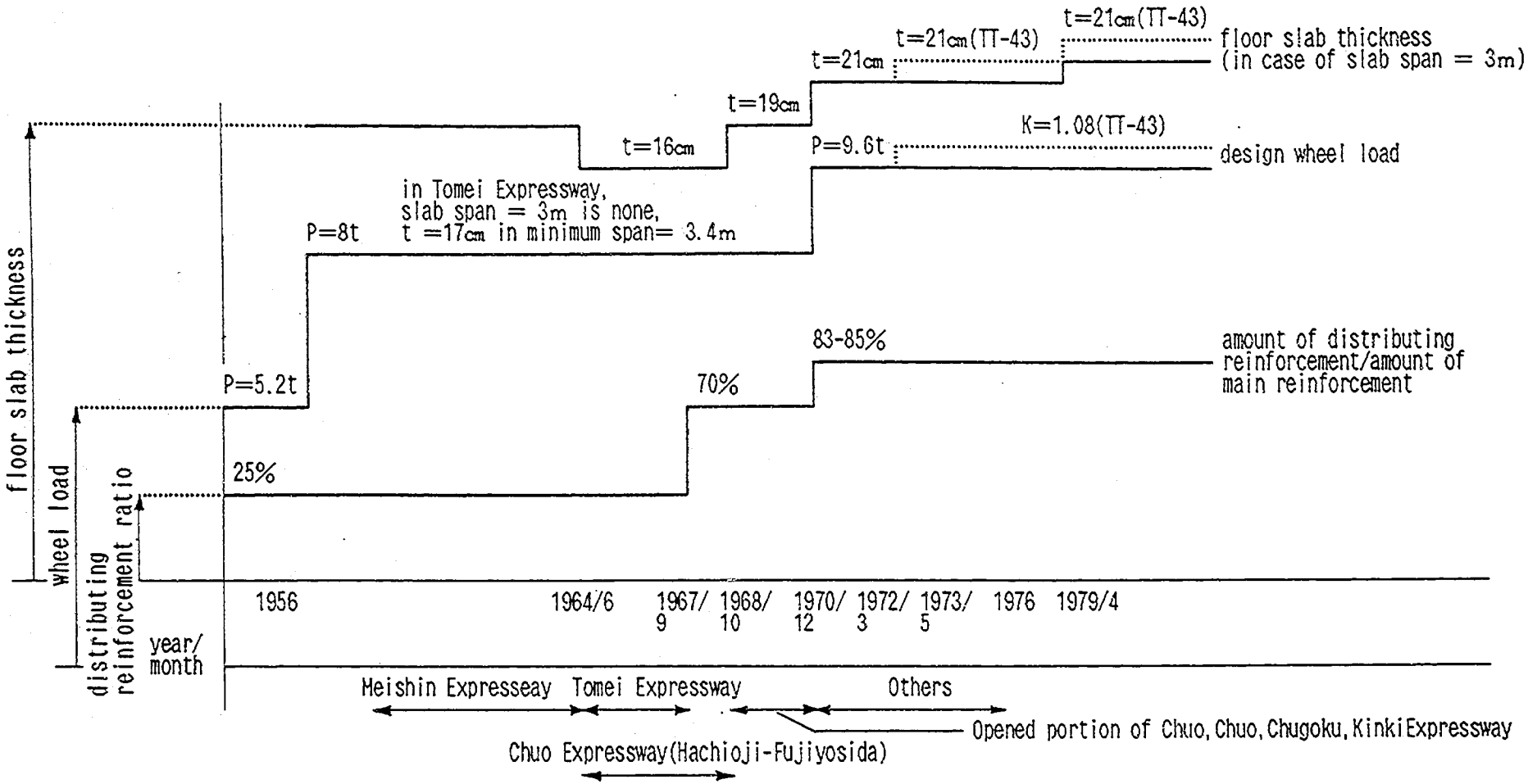


Figure 1. Transition of Steel Bridge Floor Slab Design

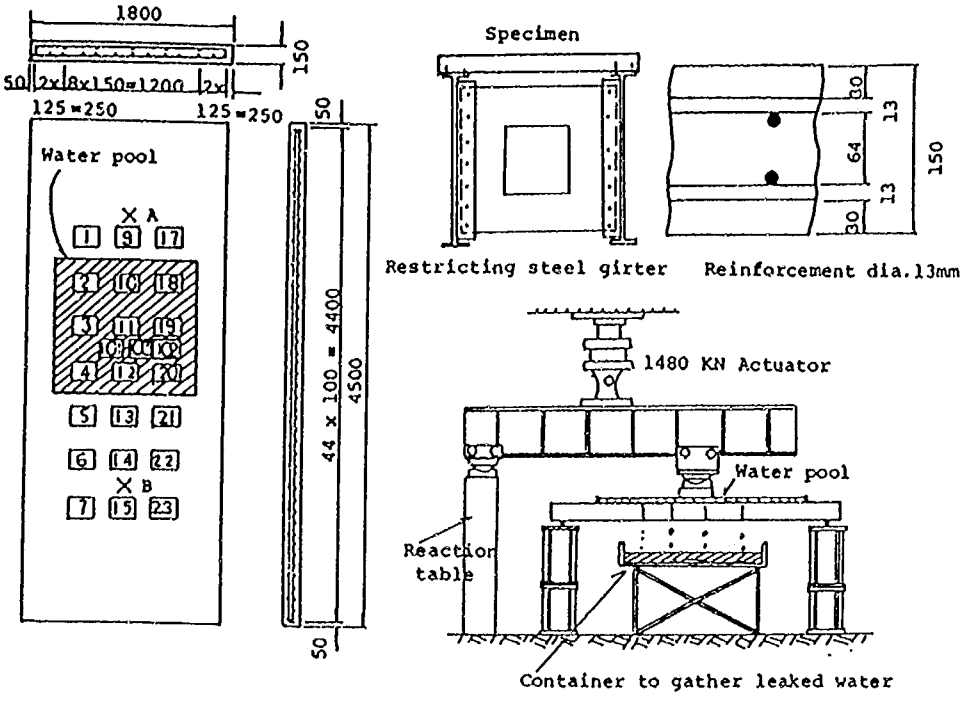


Figure 2 Shape of Specimen, Loading and Loading Apparatus

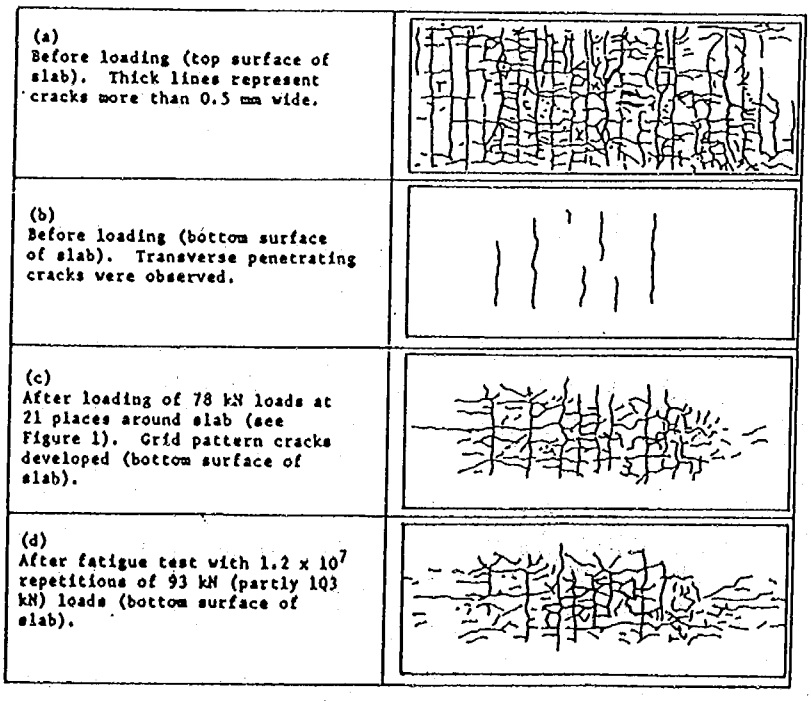


Figure 3 Change in Cracks of Slab Soecimen

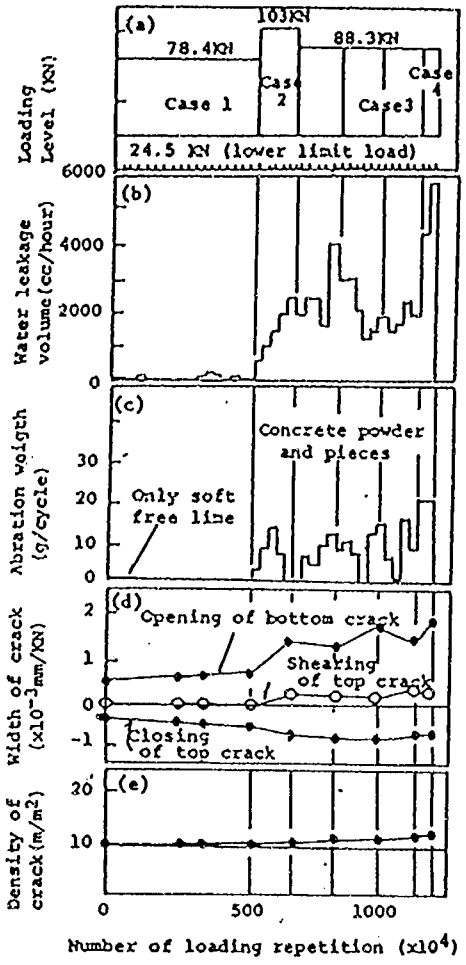


Figure 4 Progress of Deterioration Caused by Loading Repetition

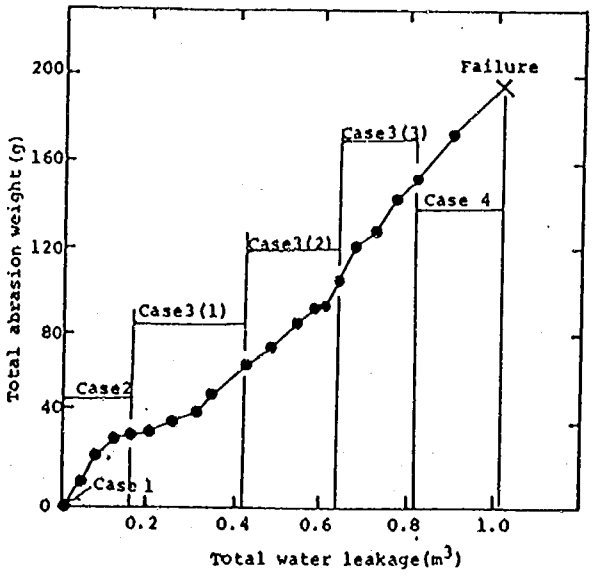


Figure 5 Relation beteen Total Water Leakage and Total abrasion Weight

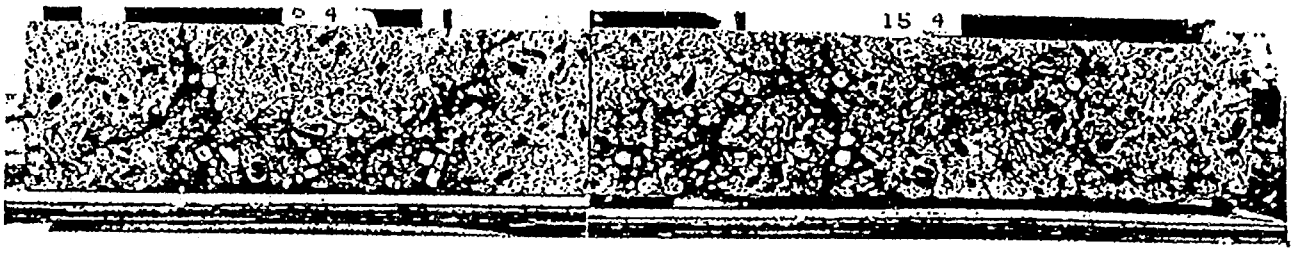


Figure 6. Cross Section where Punching Shear Failure took place.

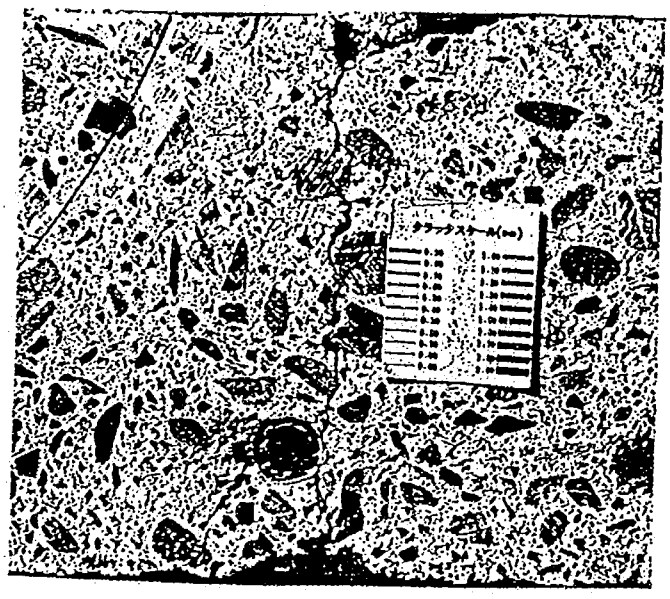
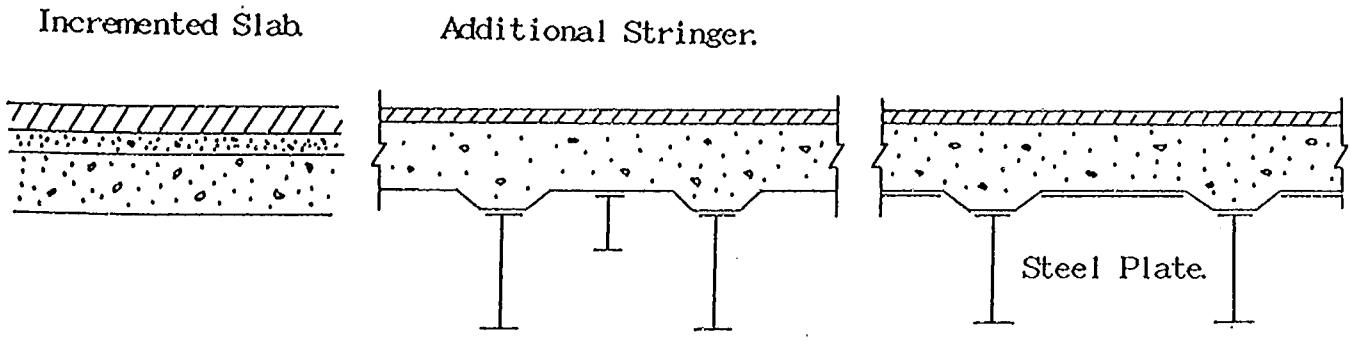


Figure 7. Crack Penetrating Slab

Table 1 Repair Methods

			Slab Thickness Incremation	Additional Stringer	Steel-Plate Bonding	Partial Reconstruction
Effectiveness	Bearing Capacity	Moment	Very good	Good	Good	· Damaged parts can be recover · No strengthening
		Shear	Very good	Poor	Fairly good	Ditto
	Water Proofing		Fairly good	No	No	No
	Abrasive Action		Very good	Fairly good	Fairly good	Good
Execution			· Traffic regulation · Very difficult	No traffic regulation	No traffic regulation	· Traffic regulation · Difficult
Problem			· The formation should be controlled · Sometimes expansion joint to be replaced	· Poor for punching shear · Negative moment above stringer	· Water remains inside slab · Can not be examined	· Bond strength in construction joint



(1) Slab Thickness Increment Method

(2) Additional Stringer.

(3) Steel Plate Bonding

Figure 8 Repair Methods.

(9) Session 9

SESSION 9: CLOSING SESSION 2:00pm~2:25pm

(Co-Chairman: M. Fujiwara, A. M. Abdel-Ghaffar)

Remarks: Harold R. Bosch (U.S. Representative, T/C(J))

Remarks: Shoichi Saeki (Japanese Chairman, T/C(J))





(10) 討　　議　　録

Q. Kawashima

なぜ試験終了後に変位が0にならないのか。

A. Douglas

永久変位（offset）のためである。

Q. Kawashima

試験終了後にジャッキは桁から完全に離れているか。

A. Douglas

そうだ。

Q. Narita

減衰（対数減衰）が自由振動の場合より大きくないか。

A. Douglas

地盤の減衰が寄与しているものと考えられる。

Q. Foutch

減衰はどれくらいか。

A. Douglas

3～4％である。

Q. Seible

解析には震央距離が種々異なるアレー記録を用いたか。

A. Tamura

気象庁のネットワークから得られた記録を用いた。

Q. Seible

震央距離の平均はどれくらいか。

A. Tamura

300 km程度である。

Q. Scanlan

解析に用いた記録は地盤上で得られた記録か。

A. Tamura

そうである。

Q. Scanlan

明石海峡大橋の基礎は水面下にある。解析に用いたデータに関連して水面下の情報と上部構造の情報をどう区分しているか。

A. Tamura

本解析で対象としているような長周期地震動は水面下の下部構造および表層地盤により増幅されることは少ないものと考えられる。したがって，本解析で提案した地震動が直接上部構造に作用するものと考えられる。

Q. Iwasaki

基礎の下の地盤の剛性をどう評価したのか。

A. Maragakis

鉛直と回転のばねとして評価した。

Q. Iwasaki

回転ばねは線形と仮定したのか。

A. Maragakis

そうだ。

C. Iwasaki

非線形領域における研究を希望する。

Q. Kawashima

橋台の裏込め土の剛性をどう見込んでいるか。

A. Maragakis

裏込め土の影響もばね定数（式(2)）に含めている。

Q. Kawashima

裏込め土に引張力が作用する場合はどう考えるのか。

A. Maragakis

裏込め土は初期状態では圧縮されており，引張力が作用して圧縮力が開放されてもなお圧縮状態である。

Q. Okahara

降伏変位はどのようにして決めるか。

A. Maragakis

降伏点の算出方法については論文の9～10ページを参照されたい。

Session 3 Seismic Design (Ⅱ)

Q. Scanlan

人工島の設計ではベッセル・インパクトが考慮されているか。

A. Oishi

ベッセル・インパクトについては解析が行われている。30万トンタンカーの衝突に対して換気塔は，3次元解析が行われており，許容応力度以下であることを確かめている。

Q. Yokoyama

耐風設計は行われているか。また，風洞実験は行われたか。

A. Foutch

設計はまだ完了しておらず，最終段階である。ウェスタンオンタリオ大学で二次元モデルの風洞実験が行われていた。さらに，詳細な実験及び解析が同大学で行なわれ，耐風性能についての評価が行われるであろう。

Q. Baber

ＦＥＭモデルにおいて，逸散減衰を表すような特別な境界条件は考慮していないのか。

A. Oishi

サイドの境界条件は，水平方向には自由，鉛直方向には固定である。また，基盤は剛体でモデル化しており，これに剛結としている。また，構造物の応力度レベルを調査したかったので，構造物の直径の５倍の幅で地盤をモデル化しており，境界条件は自由である。

C. Kawashima

大石氏が答えたように，境界条件で特別な配慮は行われていない。これは，構造物に比べて十分な大きさの領域でＦＥＭのモデル化を行っており，固有周期特性を表すのにこれで十分であるためである。

Q. Tokita

各基礎のおける入力地震動の位相差は考慮しているか。

A. Foutch

応答スペクトル法で解析を行っており，位相差は考慮していない。

Q. Douglas

模型の縮尺はいくらか。さらに振動台実験を行う予定か。

A. Hasegawa

模型の原型はないが，約1/4～1/6程度と考えている。実験はさらに行う予定である。

Q. Foutch

薄板の局部座屈においては，初期不整が大きな影響を与えるが，初期不整を正確に測定したか。また，その点で適切な模型であると考えるか。

A. Hasegawa

概略の測定は行っている。しかし，この実験では降伏後の座屈が生じており，初期不整は大きな影響を与えないと考えている。

Session 4 Wind Resistant Design (I)

C. Scanlan

乱れの影響の考慮にあたっては，乱れが予期したほど生じないことがかなりあり，危険になる場合

があることに十分に配慮したほうが良い。

A. Yokoyama

ありがとうございます。

Q. Seible

連結ワイヤーの本数を図－9のように決定した理由を教えてほしい。

A. Scanlan

景観や，本数と剛性の関連などについて，実際の橋梁での状況を踏まえ考慮した。しかし，ここで紹介したのは，連結ワイヤーを用いる方法の一例と受け取ってもらいたい。

Q. Yokoyama

ステイケーブルの振動の実橋での例で5 m/sの風速での振動の起振源は何と考えるか教えてほしい。

A. Baber

施工中の特殊な段階で発現したことや，振動周期を考慮して，桁の鉛直振動から励起される2次的な振動と判断した。

Session 5 Wind Resistant Design (Ⅱ)

Q. Scanlan

セクションモデルに働く変動空気力について教えてください。

A. Hata

変動空気力は計測されたと思いますが，すぐに出せるデータではありません。

C. Yokoyama

最初のステップとして解析のために静的空気力係数を使ったのです。

Q. Farran

あなたの解析結果に基づいて，ローブリングの原点の設計に関する意見を述べてほしい。

A. Bosch

耐風性を向上させるために剛性を上げるという方法に戻ることは，問題を回避する方法であっても最高の方法とは考えない。問題の解決のためには，単純に補強して対抗する方法と，熟考することから始めるという全く異なったアプローチがあると考える。

Q. Ishizaki

ブルックリン橋が，あなたが包括的システムと呼んだものと同様のシステムを持っていたと思うが，このようなシステムを持つ橋の例はいくつ程あるのか。

A. Bosch

5つか6つ程度だと思う。

C. Scanlan

これらはきわめて古いタイプの橋梁である。ローブリングがブルックリン橋に先立つ彼の橋梁につい

て書いたレポートには¼点に軸方向のスティを取りつけることが述べられており，風への危険も述べられている。これは，初期の優れたものであるが，不静定次数が高く，劣化による交換が頻繁なためコストは高くなってしまった。

Q. Yokoyama

こちらではしばしば付加的なケーブルを用いるか。

A. Bosch

Deer Isle 橋の場合は剛性を高めたり，軸方向の変位を抑えるなどするためにいくつかの時期に渡りケーブルを追加していった。

Q. Ghaffer

東京ボートのスパンと土質の条件から考えると，アンカレッジにかなりの重量を要求するようだが，代替案として斜張橋は考えたか。

A. Kosaka

空航路の高度制限からタワーが低くなり，斜張橋は経済的にならなかった。

C. Scanlan

プレートを使って耐風性を向上させるのは最も好ましい方法の一つと考える。

Session 6 Bridge Construction (I)

Q. Yokoyama

Dr. Farran に 2 つの質問がある。形状に関する検討は行ったか。つまり，主塔において，H型とA型の比較を行ったか。A型はねじりや振動に対して有効だと思う。また，ケーブルの配置についても検討したか。

A. Farran

全ケーブルが主塔の上から出ているタイプが最も経済的な配置であることがわかっている。このタイプの構造が応力的にも有利である。

Q. Yokoyama

2 番目の質問ですが，設計荷重はどんな荷重を考えたか。

A. Farran

設計荷重としては，基本的に AASHTO の荷重を考えている。支間が長くなると死荷重が卓越してくるようである。様々な組合せの活荷重で応力を検討したが，このタイプの構造では，活荷重による応力は，死荷重によるものに比べて非常に小さい。

Q. Yokoyama

地震荷重と風荷重についてはどうですか。

A. Farran

スペクトル解析により，構造の動的解析を行った。そのために，カリフォルニア道路局の地震・地

質図に基づいて，地震をシミュレートした。

Q. Fujiwara

Dr. Waldner の発表，特にケーブル自身の疲労試験に関心をもった。ケーブルの疲労試験は，ケーブル軸方向のみで行われていたようである。ソケット部における，ケーブルの曲げに関する疲労試験について，何か考え，あるいはコメントはありませんか。

A. Waldner

写真にもあったように，この橋では，ケーブルのソケット端からスラブの上に達する管を設けている。ケーブルは，この管の中を通っており，ケーブルと管との間に，緩衝材としてワッシャーを入れている。これにより，ケーブルの横方向の動きをかなり減少できるので，ソケット部におけるケーブルの曲げ疲労については，あまり考える必要がなかった。

Q. Scanlan

ケーブル内のグラウト圧が，ポリエチレン管に与える影響について，何か問題はなかったか。

A. Waldner

この橋では，グラウト圧を測定して，ポリエチレン管の圧力を制御した。ポリエチレン管に圧力がかかりすぎるのを防ぐために，グラウトはいくつかの段階が必要である。我々のこの試験では，2段階のグラウトを行い，グラウト圧が管に与える影響を評価した。

Session 7 Bridge Construction (Ⅱ)

Q. Mr. Hoshino

Mr. Okahara に質問したい。ここで得られた大型基礎模型実験の結果に対して，現在各種基準で用いられている基礎の支持力算定式についてどのように考えているか。

A. Mr. Okahara

ここで実施した実験は大変先進的なものであり，ここで得られた結果はすぐに基準にとりこめるものではない。しかしながら，今後良い結果が得られれば，それを新しい基準に反映させていくことは可能であると考えている。

Q. Prof. Scanlan

遠心模型試験と重力場での載荷試験では，なぜ結果に違いが生じるのか。

A. Mr. Okahara

遠心模型試験では，模型のサイズが土の粒径と比較して相対的に小さくなっており，この粒径の影響が無視できなくなるためであると推測している。

Q. Prof. Baber

Mr. Minosaku に質問したい。CFRP ケーブルを用いた桁とＰＣ鋼棒を用いた桁では，破壊形態に違いはあるのか。

A. Mr. Minosaka

桁の破壊は，圧縮側のコンクリート破壊によるものである。その点に関してはCFRPケーブルを用いた桁とPC鋼棒を用いた桁では違いはないと考えている。両者の違いをより詳しく知るには，さらに試験が必要であると考えている。

Q. Prof. Baber

CFRPケーブルはダクティリィーが乏しいが，その点に関しては問題にならないか。

A. Mr. Minosaka

実験においてCFRPケーブルを用いた桁とPC鋼棒を用いた桁では，荷重と変位の関係に違いが見られないことからダクティリィーは十分であると考えている。しかし，CFRPケーブルによる補強の割合がここで用いた試験体よりも大きくなれば，桁の破壊形態は変わると考えられ，その点に関しては検討しなければならないと考えている。

Q. Prof. Douglas

CFRPケーブルを用いた桁のコストはどれくらいか。

A. Mr. Minosaka

正確なコストはわからない。製造メーカーの話によれば，ケーブルのみについて比較すると，PC鋼棒の100倍ぐらいであり，桁で比較すると2倍程度であるとのことである。

Q. Mr. Fujiwara

Prof. Seible に質問したい。我国では，特に海岸部において海塩粒子によるコンクリート桁の劣化損傷が問題となっているが，これに対して良い対策はあれば教えて頂きたい。

A. Prof. Seible

私自身は，塩分によるコンクリート桁の劣化損傷について研究していない。しかし塩分による劣化損傷に対しては，十分な防水工を施すのが最良の方法ではないかと考えている。

Session 8 Bridge Maintenance

Q. Prof. Scanlan

Dr. Masri に質問したい。問題は様々な損傷の感知にこの方法が適用できるかどうかであるが，その点に関してコメントいただきたい。

A. Dr. Masri

ここでは非常に理想化されたモデルに対して，まず基本的な問題において損傷の感知の可能性を検討している。したがって実用化するには今後，解決すべき重要な問題が多くあると考えている。

Q. Prof. Douglas

Mr. Ishizuka に質問したい。応急橋を作るのにどのくらいの時間がかかるのか。

A. Mr. Ishizuka

30分以内で作ることができる。

Q. Prof. Seible

応急橋上ではどのくらいの速度が出せるのか。

A. Mr. Ishizuka

40～60 km/hr 程度と考えている。

Q. Prof. Baber

応急橋には，全ての車両を走行させるのか，それとも大型車は他のレーンを走行させるのか。

A. Mr. Ishizuka

大型車両は，橋上を走行させずに他のレーンを走行させるようにしている。

Q. Prof. Scanlan

Mr. Oka に質問したい。補修に用いるコンクリートに特殊なものを使っているが説明していただきたい。

A. Mr. Oka

損傷が限られた箇所で部分的な打ち換えの場合には，エポキシコンクリートを用いて補修している。また，床版の増厚の場合には，超速硬コンクリートを用いて補修している。

5. 視 察 旅 行 記

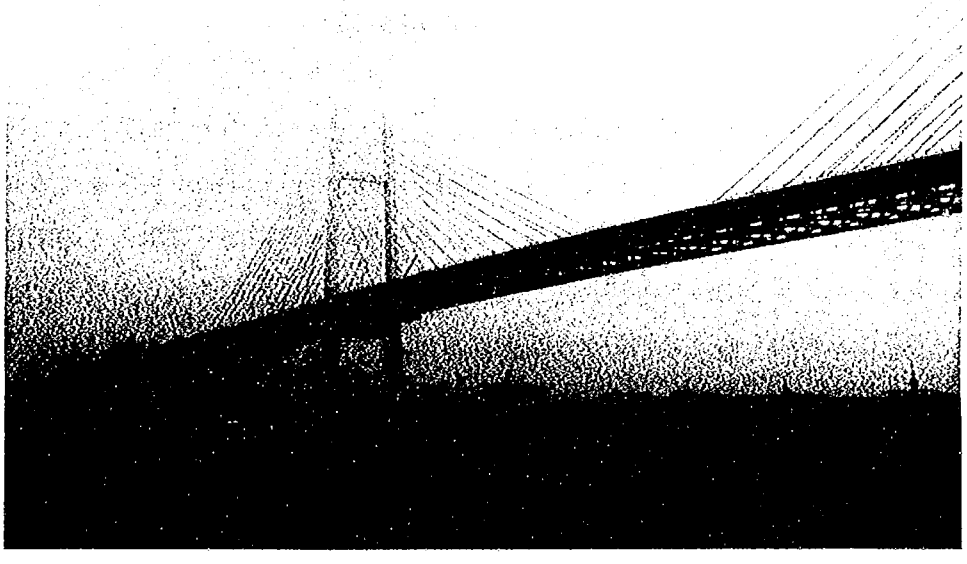
視　察　旅　行　記

5月10日から13日まで，日米橋梁ワークショップの視察旅行が行われた。旅行では2日目に首都高速道路公団の横浜ベイブリッジ，3日目に阪神高速道路公団の安治川橋梁および北港ジャンクションと関西国際空港の建設現場及び本州四国連絡橋公団の明石大橋のケーソン，4日目に本州四国連絡橋公団の児島～坂出ルートと日本を代表する高速道路橋梁や大型プロジェクトの現場を訪問した。

初日5月10日，水曜日。午前中は，土木研究所で3つのセッションと閉会式を行い，午後，土研のマイクロバスで東京のホテルに向かった。到着後は，フリータイムとなりショッピングや観光で過ごしたようである。

2日目5月11日，木曜日。朝からあいにくの雨のなか，9時にホテルを首都高速道路公団のバスで最初の視察地である横浜に向かった。途中，首都高速道路の説明をして頂いた。

現場は高速湾岸線に架かる横浜港横断橋で，横浜港の山下埠頭と大井埠頭を横断する全長860mの長大斜張橋（図－1）である。最初に事務所で説明を受けたのち，ほぼ完成している橋に上がった。橋の上では，高さ172mの塔の上まで登り，雨にけむる横浜の景色を楽しんだ。その後，首都高速道路公団が用意して下さった船に乗り横浜港から横浜ベイブリッジの全景を視察した（写真－1）。天気が悪いためか船は木の葉のように揺れたが気分が悪くなった人はいなかった。最後に，一人一人に横浜ベイブリッジを渡った証明書を頂いた。見学後，首都高速道路公団の招きで和やかに昼食会が横浜市内で行われた。



写真－1　横浜港横断橋

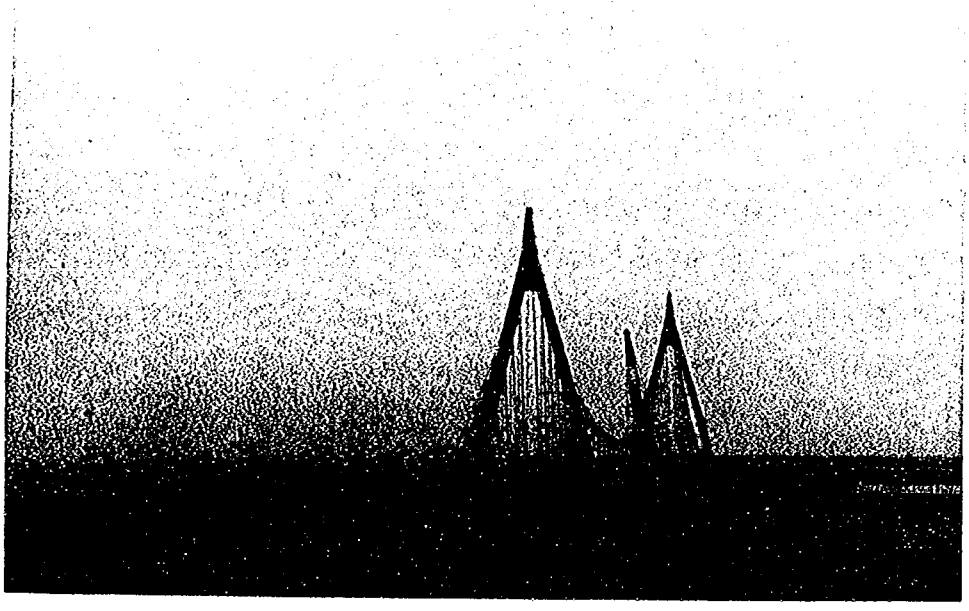
午後は，新幹線で次の視察地である大阪に移動した。新幹線は新型車両だったため，体の大きい Dr. Douglas 氏でもゆっくりと座ることができた。

大阪のホテルに到着後，阪神高速道路公団と関西国際空港㈱の招きで歓迎レセプションが行われた。レ

セプションは盛大に行われ，参加者は東京からの移動の疲れも見せず，大変和やかに行われた。

3日目5月12日，金曜日。9時に元基礎研究室長であった阪神高速道路公団工務部の大志万和也氏らの案内で最初の視察地である北港ジャンクションに向かった。北港ジャンクションは，大阪港の北側に位置する安治川の河口付近にある5層の立体ラーメン脚で構成されている建設中のジャンクションである。説明を受けたのち工事用のエレベータで5層の最上階まで上がり，現在供用中の港大橋や建設途中の安治川橋梁を視察した(写真－2)。

次の視察地の安治川橋梁は，安治川を跨ぐ橋長640 m，中央径間350 mの3径間連続鋼斜張橋である。橋は現在ほぼ完成しており，歩いて渡ることができた。



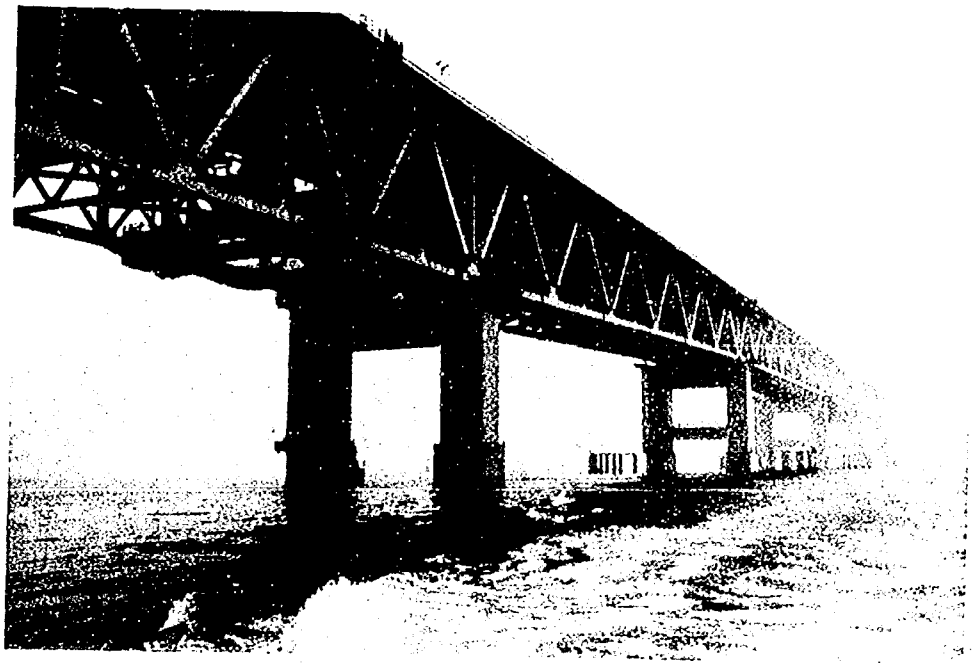
写真－2　北港ジャンクション付近

次に訪れた関西国際空港は，大阪湾南東の泉州沖約5 kmの海上に建設中の空港である。連絡橋は，空港島と南大阪湾岸整備事業埋立地を結ぶ延長3.75 kmの道路・鉄道併用橋（図－2）で，海上中央部は上段に道路，下段に鉄道を配した鋼トラス構造併用橋，空港島と陸岸側は道路・鉄道各々の鋼箱桁分離形式の橋梁として建設中である。関西国際空港㈱に用意して頂いた船で泉佐野市の港を出発し，途中連絡橋の現場を視察のち空港島建設現場を海上基地の上から視察した。連絡橋は海上部の橋脚設置が進められ，上部工架設工事も進められている（写真－3）。空港島は，平均水深18 mの海底の軟弱な粘土層の上に約511ヘクタールにおよぶ大規模な埋立によって建設される。現在は，護岸築造工事が終わり，埋立工事が進められている（写真－4）。

最後に，本州四国連絡橋公団の明石海峡大橋のケーソンの現場を見学した。昨日に続き天候がすぐれなかったが船が大きかったせいかあまり揺れず，室内から出て盛んに橋梁の写真を取っていた。

岡山のホテルに到着後，本州四国連絡橋公団の招きで夕食会が行われた。旅の疲れも見せず，大変和やかに行われた。

4日目5月13日，土曜日。土曜日にもかかわらず，本州四国連絡橋公団には，マイクロバスの用意から



写真－3　関西国際空港連絡橋

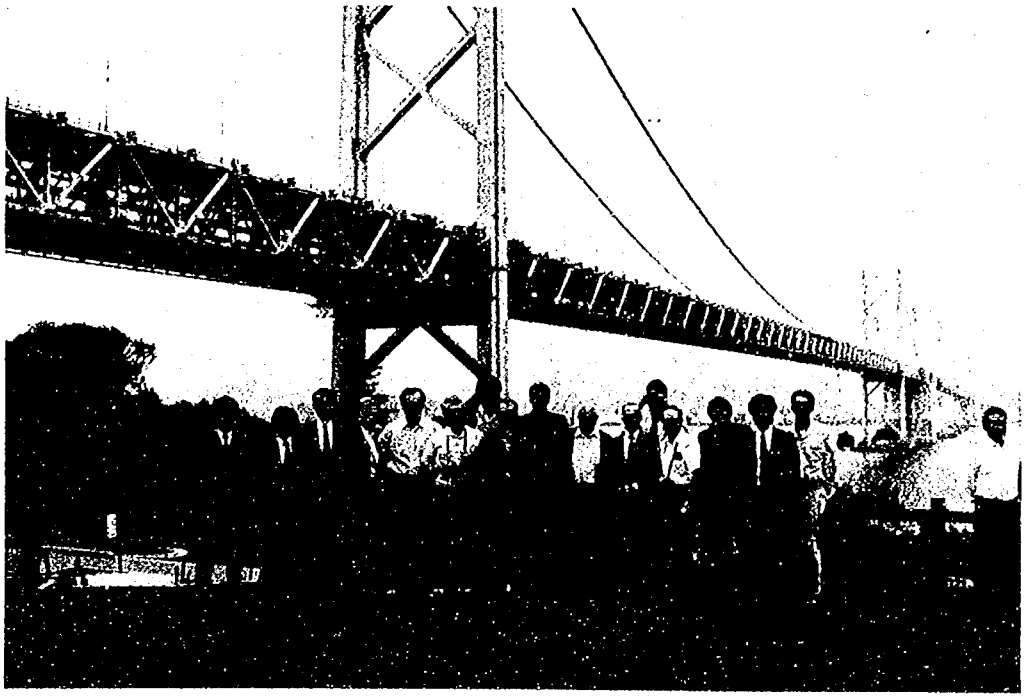


写真－4　関西国際空港（海上基地上）

現場案内までしていただいた。

視察は，児島から坂出まで自動車道で渡り，与島で下り各参加者とも本四架橋の全貌の写真を撮っていた（写真－5）。帰りは，坂出から岡山までＪＲのマンリライナーを使用し，鉄道で本四架橋を渡った。一行は午後の新幹線で東京へ向かった。

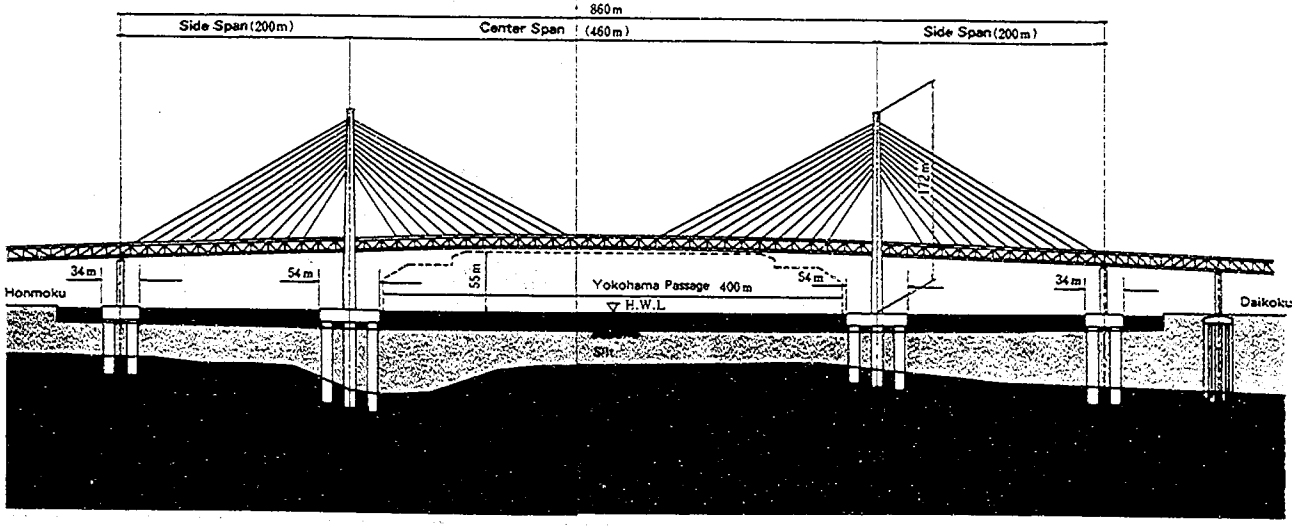
今回の視察旅行は，何の事故もなく，無事終了できた。これもすべて我々を歓迎してくださり，快く現場を案内してくれた首都高速道路公団，阪神高速道路公団，本州四国連絡橋公団，関西国際空港㈱をはじめとする各関係者のおかげと深く感謝しております。改めてお礼申し上げます。



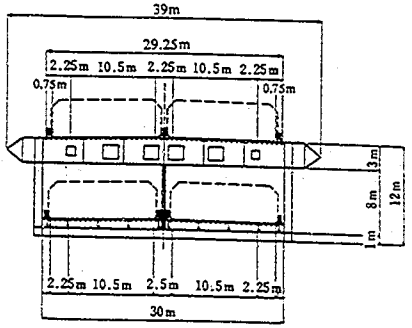
写真－５　本州四国連絡橋

General View

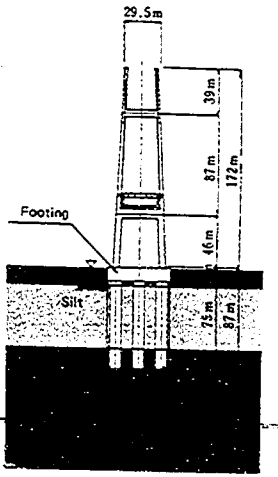
Side View



Cross Section

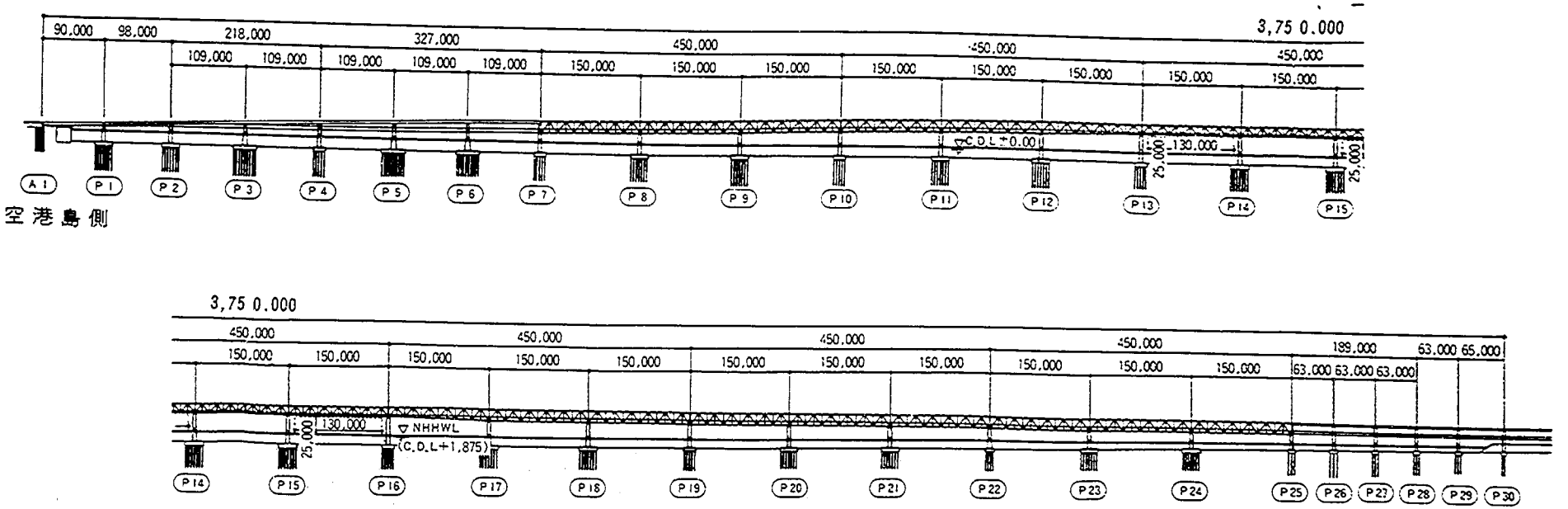


Front View

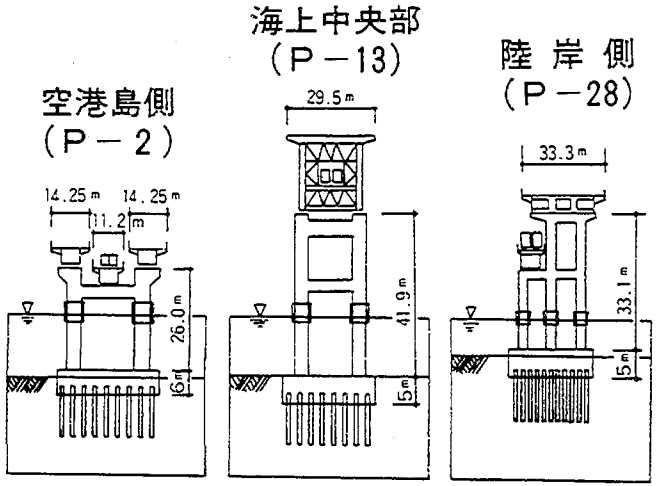


図－1　横 浜 港 横 断 橋

連絡橋一般図



連絡橋断面図



図－2　関西国際空港連絡橋

あ と が き

あ と が き

今回のワークショップは2日間の短期間ではあったが，橋梁の耐風・耐震工学を中心に補修・補強まで幅の広い論文発表と討議が行われた。日米間での橋梁に係る重要な課題に対して最新の情報が交換され，今後の検討の方向が示されたのは誠に意義が大きい。会議参加者からも中味の濃いワークショップだったとの声が聞かれた。

なお，今回のワークショップの開催にあたっては土木研究所構造橋梁部，地震防災部を中心に準備会を設けた。役割分担は以下のとおりである。

事　務　局（橋梁研究室）

全体スケジュールの作成，対外連絡文書作成，プログラム作成，出席者との連絡，空港出迎え

論　文　班（構造研究室）

論文のコピー，ファイル，前刷集の作成

会議運営班（基礎研究室）

会場準備，写真撮影，OHPスライド準備，会場運営，配車，コーヒー，昼食

議事録班（耐震研究室）

議事録とりまとめ，宿舎，レセプション準備，宿舎送迎

視察旅行班（振動研究室）

旅行計画，随行

最後に，視察旅行に際しては，首都高速道路公団，阪神高速道路公団，本州四国連絡橋公団，および関西国際空港㈱の各機関の方々にお世話いただいた。記して感謝の意を表します。

付　属　資　料

(1)　第５回日米橋梁ワークショップ結論(英文)

RESOLUSION OF THE FIFTH JOINT U. S. -JAPAN WORKSHOP ON BRIDGE ENGINEERING STRUCTURAL MONITORING, SAFETY AND NONDESTRUCTIVE EVALUATION

Public Works Research Institute

Tsukuba Science City, Japan

May 9 and 10, 1989

The following resolutions are hereby adopted:

1. The fifth U. S. -Japan Bridge Workshop provided valuable exchange of technical information which was beneficial to the bridge engineering communities in both countries. In view of the importance of cooperative programs on the subject of wind and seismic effects on bridges and on performance, strengthening, structural monitoring, safety, nondestructive evaluation and design innovation of these transportation structures, the continuation of technical cooperation and interaction is considered essential.

2. The Workshop recognizes the importance of continued exchange of personnel, technical information, research data and bridge response data from significant earthquakes and strong winds, and use of available unique research facilities in both countries.

3. The primary purpose of the Workshop is to identify current research needs and to establish priorities for them. Among the objectives of this Workshop are:

3. 1 to enable a first-hand understanding of the unique problems each locality is faced with,

3.2 to coordinate, initiate, and standardize, to a great extent, the research efforts directed toward the better performance and strengthening of bridge structures in both countries,

3.3 to stimulate more collaborative research work in this important area of engineering,

3.4 to facilitate the exchange of technical information and ideas and to promote the broadening of viewpoints for those involved.

And, finally,

3.5 to establish a set of priorities for needed research from a more international viewpoint.

4. The Workshop identifies the following technical topics for future cooperative research programs.

4.1 Dynamic control and seismic isolation of bridge structures including: active and passive control, damping augmentation, experimental studies and application to long-span cable-supported bridges,

4.2 System identification techniques for wind and seismic engineering including: data interpretation studies, development of mathematical models, identification of nonlinear systems, reduced-order models, computational algorithms and optimum sensor locations,

4.3 Non-destructive evaluation techniques including damage detection, expert systems, inspection techniques, structural monitoring, performance evaluation and repair proceedures,

4.4 Experimental and analytical studies on the effects of dynamic soil characteristics, including bridge-soil interaction, on the behavior of bridge structures.

5. It is anticipated that the interaction among the delegates from the United States and Japan during the round-table discussions and the technical study tour will lead to an enhanced exchange of data and innovative ideas, and will also lead to the establishment of cooperative research efforts, both theoretical and experimental, on bridge engineering. Because of the importance, benefits and potential of these Workshops, it is recommended to conduct the 6th bridge workshop, just prior to the 22nd UJNR joint meeting in the U. S. in May 1990, in the Lake Taho area in Nevada. A study-tour will be planned to go to base-isolated bridges, Oakland-Bay and Golden Gate suspension bridges in Northern California as well as the newly constructed freeway in Southern California.

(2) UJNR耐風耐震構造専門部会

第21回合同部会におけるワークショップ報告(英文)

May 18, 1989

Report on U.S.-Japan Bridge Workshop(Task Committee J)

FHWA: Mr. Harold Bosch

Task Committee J has held the U.S.-Japan Workshop five times during the last five years, as one of the cooperative activities of UJNR, to promote the exchange of technical information and the cooperative research in the field of bridge engineering.

The fifth U.S.-Japan Bridge Workshop was held at the Public Works Research Institute in Tsukuba Science City, Japan on May 9 to 10, 1989.

Eleven U.S. and thirty-one Japanese members participated in the Workshop,
and ten U.S. papers and thirteen Japanese papers were presented.

Following the workshop, the four-day study tour was made on May 10 to 13.U.S. members visited the representaive long-span bridges in Japan such as Yokohama Bay Bridge of Metropolitan Expressway Public Corporation, Ajigawa Bridge and Hokko Junction of Hanshin Expressway Public Corporation, Kansai International Access Bridge, and also Akashi Kaikyo Bridge and Kojima-Sakaide Route of Honshu-Shikoku Bridge Authority.

In the workshop, the technical information concerning the following topics on bridge engineering was exchanged.

1)Seismic design
2)Wind-resistant design
3)Design and Construction
4)Maintenance
5)Strengthening and Repairing
6)Non-destructive evaluation
7)Instrumentation and structural monitoring

The following resolutions were adopted in the Fifth U.S.-Japan Bridge Workshop;

1. The Fifth U.S.-Japan Bridge Workshop provided valuable exchange of technical information which was beneficial to the bridge engineering communities in both countries.

In view of the importance of cooperative programs on the subject of wind and seismic effects on bridges and on performance, strengthening, structural monitoring, safety, non-destructive evaluation and design innovation of transportation structures, the continuation of technical cooperation and interaction is considered essential.

2. The Workshop recognizes the importance of continued exchange of personnel, technical information, research data and bridge response data from siginificant earthquakes and strong winds, and use of available unique research facilities in both countries.

Nextly, The workshop identifies the following technical topics for future cooperative research programs.

1. Dynamic control and seismic isolation of bridge structures including: active and passive control, damping augmentation, experimental studies and application to long-span cable-supported bridges.

2. System identification techniques for wind and seismic engineering including: data interpretation studies, development of mathematical models, identification of nonlinear systems, reduced-order model, computational algorithms and optimum sensor locations,

3. Non-destructive evaluation techniques including damage detection, expert systems, inspection techniques, structural monitoring, performance evaluation and repair procedures,

4. Experimental and analytical studies on the effects of dynamic soil characteristics, including bridge-soil interaction, on the behavior of bridge structures.

Finally, The Workshop identifies that the interaction among the delegates from the U.S. and Japan during the round-table discussions and the technical study tour will lead to an enhanced exchange of data and innovation ideas.

And it will also lead to the establishment of cooperative research efforts, both theoretical and experimental, on bridge engineering.

Because of the importance, benefits and potential of these Workshops, The Workshop recommends to the "J" task committee to conduct that the 6-th Bridge Workshop, just prior to the 22-nd UJNR joint meeting in the U.S. in May 1990.

(3) UJNR耐風耐震構造専門部会

第21回合同部会におけるJ部会部会報告(英文)

Report of Task Committee on

(J) WIND AND EARTHQUAKE ENGINEERING FOR TRANSPORTATION SYSTEMS

Date: May 18, 1989

Place: Public Works Research Institute, Ministry of Construction
1-banchi Asahi, Tsukuba-shi, Ibaraki-ken 305, Japan

Attendees: Japan Side -	S. Saeki(Chairman)	(PWRI)
	T. Fujitani	(MRI)
	T. Iwasaki	(PWRI)
	Y. Sasaki	(PWRI)
	M. Fujiwara	(PWRI)
	K. Yokoyama	(PWRI)
	M. Okahara	(PWRI)
	K. Kawashima	(PWRI)
	K. Tokida	(PWRI)
	K. Minosaku(Observer)	(PWRI)
U.S. Side -	H. R. Bosch(Temporary Chairman)	(FHWA)
	A. G. Franklin	(WES)

Following the request in item 8 of the Final Resolutions adopted at the 20-th UJNR Joint Panel Meeting held in Gaithersburg in May, 1988, the "Mission Statement" of this Task Committee was drafted for adoption by the Panel as follows:

[Mission Statement]

1. Objective

The objectives of this Task Committee are to plan, promote, and foster research on the behavior of highway bridges when subjected to wind and seismic forces and to disseminate research results and provide specifications and guidelines based on the task committee's findings. Surface transportation systems for movement of goods and people play a

vital part of commerce and intercourse between people. Highway bridges are especially influenced by the forces of wind and earthquakes because of their open exposure to those forces.

2. Scope-of-Work

The scope of the work is applicable mostly to highway bridges without any limitation on their size and function: such as existing bridges and new bridge designs; whole system of bridges; and/or to single components of a bridge. The mission is performed through:

conducting workshops, exchanging researchers,
developing methods for design evaluations and test procedures,
inspection techniques, rehabilitation and maintenance specifications and policies,
and performing cooperative research programs and other relevant cooperative administrative activities.

3. Accomplishments

o Conducted coordinated research studies on the seismic performance of bridge piers and columns. Details of this work involved determing the performance of reinforced concrete piers and columns subjected to dynamic cyclic loading, performing model tests on the failure of reinforced concrete piers, testing full-scale concrete columns and for the behavior of concrete filled steel tubes.

o Held the fourth bridge workshop in San Diego, U.S. in 1988 and the fifth bridge workshop in Tsukuba, Japan in 1989, dealing with the determination and evaluation of the performance and strengthening of bridge structures, structural monitoring, repairs, safety and non-destructive evaluation. Special attention was given to the seismic and wind loadings of modern cable -stayed bridges, vibration suppression, base isolation and dynamic control techniques.

o Both sides presented technical papers at the UJNR Joint Meeting and participated in technical study tours such as factories, construction sites, and instrumented structures.

4. Planned Accomplishments

o Conduct the 6th bridge workshop just prior to the 22nd Joint Panel

meeting in the U.S.

o Continue the coordinated experimental research study on the seismic performance of bridge piers and columns, and continue emphasis on base isolation.

o Develop a coordinated research study on seismic, aeroelastic, and aerodynamic response of cable-supported bridges with emphasis on cable inspection, vibration and corrosion protection.

o Develop a coordinated research study to compare the seismic design criteria for bridges in JAPAN and the U.S.

o Develop a coordinated research study on seismic response control, system identification techniques, and non-destructive evaluation of bridge structures.

5. Information Exchange

o Exchanged technical reports, research program documentation, construction logs, design plans, and assorted photographs and TV videos.

o Mr. S. Unjoh from PWRI worked in University of Southern California and Mr. Ray Zelinsky from Transportation Bureau of California State worked in PWRI to engage in research studies relating to this Task Committee.

6. Impact

o Greater uniformity was achieved in wind engineering test procedures and modeling, resulting in more efficient solutions to the aerodynamic bridge problem.

o The workshops and study tours in the two countries have facilitated technology transfer, as an example, in the area of cable protection and vibration suppression of cable-stayed bridges.

o With respect to the earthquake protection of bridges, the free exchange of literature, instrumentation technology, and earthquake response data has led to the improvement of design and retrofitting guidelines and to calibration and verification of specifications.

o A set of priorities for research needed from a more international viewpoint were established.

7. Barriers

There are no major technical barriers to achieve the Task Committee mission. However, financial barriers, especially funding needed to participate in workshops and panel meetings and for conducting actual bridge tests and large scale model tests, limit the effectiveness of the work in this Task Committee's work.

(4) UJNR耐風耐震構造専門部会

第21回合同部会におけるJ部会部会報告(和文)

（Ｊ）交通システムの耐風耐震技術に関する作業部会報告

開催日：　１９８９年５月１８日

場所　：　茨城県つくば市旭１番地　　建設省土木研究所

出席者：

日本側	佐伯　彰一（作業部会長）	（土木研究所）
	藤谷　徳之助	（気象研究所）
	岩崎　敏男	（土木研究所）
	佐々木　康	（土木研究所）
	藤原　稔	（土木研究所）
	横山　功一	（土木研究所）
	岡原　美知夫	（土木研究所）
	川島　一彦	（土木研究所）
	常田　賢一	（土木研究所）
	箕作　光一（オブザーバー）	（土木研究所）
米国側	H.R. Bosch（臨時作業部会長）	（運輸省高速道路庁）
	A.G. Franklin	（陸軍局工兵隊水路試験所）

１９８８年５月、米国ゲイサースバークで開催された第２０回合同部会の最終結論第８項に添い、第２１回合同部会において本作業部会の活動内容について討議し、下記の作業部会「活動要約」を取りまとめた。

［活動要約］

１．作業部会の目的

交通システムは、人々の交流及び物資の輸送等において重要な役割を有する。この交通システムの中で、特に道路橋はその建設条件から地震や風の影響を受け易い。こうした点を考慮し、本作業部会では、地震や風に対する道路橋の挙動に関する調査研究を計画、推進し、発展させるとともに、それらの調査研究の成果に基づいて、道路橋の耐震、耐風に関するガイドラインや指針を作成することを目的とする。

２．作業範囲

本作業部会では、諸元と機能の多様性にかかわらず、あらゆる道路橋を主要な対象とし、既設橋の耐震・耐風性および新設橋の耐震・耐風設計に関する事項を調査研究の対

象とする。また、橋梁全体としての耐震・耐風性能およびそれらを構成する橋梁部材の耐震・耐風性能に関する項目を調査研究の対象とする。本作業部会では、これらの調査研究を進めるために、橋梁の設計における数値計算や試験および橋梁の点検・補修補強・維持管理等に関してワークショップ・人事交流・共同研究等を実施するものとする。

3．活動状況

◦橋脚および柱の耐震性能に関して、動的繰返し荷重に対する鉄筋コンクリート橋脚や柱の耐荷性能、鉄筋コンクリート橋脚の破壊に関する模型実験、実物大鉄筋コンクリート柱供試体の実験およびコンクリート充填鋼管柱の耐荷性能についての共同研究を実施した。

◦橋梁の性能監視、補強等に関して、1988年に米国のサンディアゴで第４回橋梁ワークショップを、1989年に日本のつくば市で第５回橋梁ワークショップを開催した。また、これらのワークショップでは、構造物の監視システム、補修方法、安全性評価および非破壊診断技術について討議された。特に、最近の斜張橋の地震・対風応答に係わる振動制御技術、免震技術および動的制御技術について大きな関心が寄せられた。

◦日米両サイドは、ＵＪＮＲ合同部会において数多くの報告を行うとともに、橋梁製作工場、橋梁の建設現場および計測現場等へのスタディツアーを行った。

4．将来計画

◦米国で開催される第２２回ＵＪＮＲ合同部会に先だって、第６回橋梁ワークショップを開催する予定である。

◦橋脚および柱の耐震性能ならびに免震技術に関する共同研究を継続する。

◦吊橋や斜張橋の耐震性能、空力弾性学特性および空気力学的特性、ケーブルの検査技術および振動や腐食の防止対策についての共同研究を推進する。

◦日米双方における橋梁の耐震設計基準の比較のための共同研究を推進する。

◦橋梁の地震応答制御、システム同定技術および非破壊診断技術に関しての共同研究を推進する。

5．情報交換

◦技術報告、研究プログラム、建設計画、設計計画およびこれらに関する写真やビデオを交換した。

◦日本から建設省土木研究所の運上茂樹研究員が米国南カルフォルニア大学において、また米国からカルフォルニア州運輸局のMr. Ray Zelinskyが建設省土木研究所において本

作業部会の調査研究に従事した。

6．主要成果

・耐風に関する調査研究における試験方法やモデルの統一を図り、これにより耐風技術に関する諸問題に対する有効な方策を見出した。

・橋梁ワークショップやスタディツアーの実施により、日米双方における斜張橋のケーブルの防食対策および振動防止対策等に関しての技術交換ができた。

・橋梁の耐震技術に関して、文献、測定技術および地震応答測定データの交換により、設計基準や補修指針の改善が図られた。

・国際的な観点から優先的にその実施が必要とされる研究が明らかになった。

7．その他

本作業部会における調査研究を進めるにあたっては、現在のところ特段の問題点は見あたらない。ただし、合同部会やワークショプへの参加、実橋を対象とした試験や大型モデル供試体を用いた実験の遂行にあたって、これらの予算が不足し、本作業部会の活動が制限される状況にある。

第5回日米橋梁ワークショップ論文集

ＩＳＳＮ 0386－5878
土木研究所資料 第2847号
平成２年１月（1990年）

構造橋梁部長　佐伯彰一

要旨

1989年５月９日，10日の２日間にわたって、筑波研究学園都市にある建設省土木研究所において、第５回日米橋梁ワークショップが開催された。本資料は、同ワークショップに提出された論文，および会議プログラム，討議内容、ワークショップ後に行われた視察旅行の内容をとりまとめたものである。

キーワード：橋梁工学，日米技術協力，耐風工学，耐震工学

郵便はがき

41円切手をはって下さい

305-□□

茨城県つくば市大字旭一番地

建設省土木研究所

構造橋梁部橋梁研究室　御中

No. 43

No. 43

配布先氏名

配布先住所

土木研究所資料第 2847 号　　部

上記のとおり受領しました。

所　　属(住所)

氏　名　　印